



STRUCTURAL HEALTH MONITORING OF LARGE CIVIL ENGINEERING STRUCTURES

HUA-PENG CHEN

WITH CONTRIBUTIONS FROM
YI-QING NI

WILEY Blackwell

Table of Contents

[Cover](#)

[Title Page](#)

[Preface](#)

[Biography](#)

[1 Introduction to Structural Health Monitoring](#)

[1.1 Advances in Structural Health Monitoring Technology](#)

[1.2 Structural Health Monitoring System and Strategy](#)

[1.3 Potential Benefits of SHM in Civil Engineering](#)

[1.4 Challenges and Further Work of SHM](#)

[1.5 Concluding Remarks](#)

[References](#)

[2 Sensors and Sensing Technology for Structural Monitoring](#)

[2.1 Introduction](#)

[2.2 Sensor Types](#)

[2.3 Sensor Measurements in Structural Monitoring](#)

[2.4 Fibre Optic Sensors](#)

[2.5 Wireless Sensors](#)

[2.6 Optimum Sensor Selection and Placement](#)

[2.7 Case Study](#)

[2.8 Concluding Remarks](#)

[References](#)

[3 Data Acquisition, Transmission and Management](#)

[3.1 Introduction](#)

[3.2 Data Acquisition Systems](#)

[3.3 Data Transmission Systems](#)

[3.4 Data Processing Systems](#)

[3.5 Data Management Systems](#)

[3.6 Case Study](#)

[3.7 Concluding Remarks](#)

[References](#)

[4 Structural Damage Identification Techniques](#)

[4.1 Introduction](#)

[4.2 Damage in Structures](#)

[4.3 NonDestructive Testing Techniques](#)

[4.4 Comparison of NDT and SHM](#)

[4.5 Signal Processing for Damage Detection](#)

[4.6 DataBased Versus ModelBased Techniques](#)

[4.7 Development of VibrationBased Methods](#)

[4.8 Concluding Remarks](#)

[References](#)

[5 Modal Analysis of Civil Engineering Structures](#)

[5.1 Introduction](#)

[5.2 Basic Equations for Structural Dynamics](#)

[5.3 InputOutput Modal Identification](#)

[5.4 OutputOnly Modal Identification](#)

[5.5 Correlation Between Test and Calculated Results](#)

[5.6 Mode Shape Expansion and Model Reduction](#)

[5.7 Case Study](#)

[5.8 Concluding Remarks](#)

[References](#)

[6 Finite Element Model Updating](#)

[6.1 Introduction](#)

[6.2 Finite Element Modelling](#)

[6.3 Structural Parameters for Model Updating](#)

[6.4 Sensitivity Based Methods](#)

[6.5 Dynamic Perturbation Method](#)

[6.6 Use of Dynamic Perturbation Method for Model Updating](#)

[6.7 Case Study](#)

[6.8 Concluding Remarks](#)

[References](#)

[7 VibrationBased Damage Identification Methods](#)

[7.1 Introduction](#)

[7.2 Structural Modelling for Damage Identification](#)

[7.3 Methods Using Change of Modal Parameters](#)

[7.4 Methods Using Change of Structural Parameters](#)

[7.5 Pattern Recognition Methods](#)

[7.6 Neural Network Techniques](#)

[7.7 Concluding Remarks](#)

[References](#)

[8 ModelBased Damage Assessment Methods](#)

[8.1 Introduction](#)

[8.2 Characterisation of Damage in Structures](#)

[8.3 Matrix Update Methods](#)

[8.4 Sensitivity Based Methods](#)

[8.5 Damage Assessment Using Dynamic Perturbation Method](#)

[8.6 Numerical Examples](#)

[8.7 Potential Problems in VibrationBased Damage Identification](#)

[8.8 Concluding Remarks](#)

[References](#)

[9 Monitoring Based Reliability Analysis and Damage Prognosis](#)

[9.1 Introduction](#)

[9.2 Usage Monitoring](#)

[9.3 Probabilistic Deterioration Modelling](#)

[9.4 Lifetime Distribution Analysis](#)

[9.5 Structural Reliability Analysis](#)

[9.6 Optimum Maintenance Strategy](#)

[9.7 Case Study](#)

[9.8 Concluding Remarks](#)

[References](#)

[10 Applications of SHM Strategies to Large Civil Structures](#)

[10.1 Introduction](#)

[10.2 SHM System and Damage Identification of a CableStayed Bridge](#)

[10.3 InConstruction Monitoring of a HighRise Building](#)

[10.4 Monitoring of Tunnel Construction Using FBG Sensors](#)

[10.5 Safety Monitoring of Rail Using Acoustic Emission](#)

[10.6 Structural Integrity Monitoring of Water Mains](#)

[10.7 Concluding Remarks](#)

[References](#)

[Index](#)

List of Tables

Chapter 02

[Table 2.1 Typical sensing methods for structural health monitoring.](#)

[Table 2.2 Examples of sensors used for monitoring of structural responses and operation loads.](#)

[Table 2.3 Examples of sensors used for monitoring of environmental factors.](#)

[Table 2.4 Typical physical quantities of structural responses for monitoring.](#)

[Table 2.5 Typical physical and chemical quantities of environmental factors for monitoring.](#)

[Table 2.6 Typical physical quantities of operational loads for monitoring.](#)

[Table 2.7 Typical physical quantities of structural characteristics for monitoring.](#)

Chapter 04

[Table 4.1 Comparison of databased and modelbased damage assessment techniques.](#)

Chapter 05

[Table 5.1 Comparison of identified natural frequencies and damping ratios between the three excitation types \(after Peeters and Ventura 2003\).](#)

[Table 5.2 Identified natural frequencies \(Hz\) of the first eight modes under various wind conditions using the SSIDATA method and the SSICOV method.](#)

[Table 5.3 Modal data identified by outputonly identification methods from ambient vibration data.](#)

Chapter 06

[Table 6.1 Simulated, measured and updated frequencies of the cantilever beam without weighting on initial parameter estimates.](#)

[Table 6.2 Simulated, measured and updated frequencies of the cantilever beam with weighting on initial parameter estimates.](#)

[Table 6.3 Updated natural frequencies at different iteration numbers for model updating using only eight 'tested' frequencies.](#)

[Table 6.4 Updated natural frequencies at different iteration numbers for model updating using three 'tested' incomplete modes.](#)

[Table 6.5 Both stiffness and mass factors adjusted simultaneously using different](#)

[number of 'tested' incomplete modes.](#)

[Table 6.6 Updated natural frequencies of the FE model using eight simulated incomplete modes without noise and with 7% noise level.](#)

[Table 6.7 Comparison of updated natural frequencies of the FE model using six real experimental incomplete modes by different model updating methods.](#)

[Table 6.8 Updated modal properties of the reduced FE model using 10 measured frequencies excluding two torsion modes.](#)

[Table 6.9 Updated modal properties of the reduced FE model using nine measured incomplete modes.](#)

Chapter 07

[Table 7.1 First five frequencies \(Hz\) of the cantilever beam for different model problems.](#)

[Table 7.2 Comparison of measured and computed natural frequencies \(Hz\) of Tsing Ma Bridge.](#)

[Table 7.3 Simulated damage cases of Tsing Ma Bridge.](#)

[Table 7.4 Results of damage location identification using the COMAC method.](#)

[Table 7.5 Results of damage location identification using the ECOMAC method.](#)

[Table 7.6 Results of damage location identification using the mode shape curvature \(MSC\) method.](#)

[Table 7.7 Results of damage location identification using the flexibility matrix method.](#)

[Table 7.8 Results of damage location identification using the strain energy based damage index method.](#)

[Table 7.9 Comparison of different damage identification methods applied to Tsing Ma Bridge.](#)

[Table 7.10 Results of simulated damaged member identification in deck segment No.3 using artificial neural network \(ANN\) with backpropagation \(BP\).](#)

[Table 7.11 Damage location identification results for probabilistic neural network \(PNN\).](#)

Chapter 08

[Table 8.1 Values of damage indicators for cases with loss of bending stiffness capacity at critical locations.](#)

[Table 8.2 First five natural frequencies \(Hz\) for original and damaged structure.](#)

[Table 8.3 First four natural frequencies \(Hz\) and original mode shapes.](#)

[Table 8.4 Geometric and material properties of the structural members of the framed](#)

[building structure.](#)

[Table 8.5 Simulated damage scenarios for the framed building structure.](#)

[Table 8.6 Correlated noise free frequencies \(Hz\) of the original and damaged structure.](#)

[Table 8.7 Simulated damage scenarios for the gravity dam structure.](#)

Chapter 09

[Table 9.1 List of instrumented structural components and monitoring parameters.](#)

Chapter 10

[Table 10.1 Recorded ambient acceleration data samples under different wind conditions.](#)

[Table 10.2 Identified frequencies \(Hz\) of first eight modes under various wind speed conditions.](#)

[Table 10.3 Simulated damage cases for damage detection studies of Ting Kau Bridge.](#)

[Table 10.4 Damage location identification using mode shape curvature index \$Z\$ values.](#)

[Table 10.5 Damage caused frequency change and damage detectability.](#)

[Table 10.6 Summary of correct damage identification using probabilistic neural network \(PNN\) technique.](#)

[Table 10.7 Comparison between identified and predicted natural frequencies \(Hz\).](#)

List of Illustrations

Chapter 01

[Figure 1.1 System architecture and operation diagram of a SHM system for a bridge.](#)

[Figure 1.2 Structural health monitoring strategies for civil engineering structures \(after Frangopol and Messervey 2009\).](#)

[Figure 1.3 Integrated framework for health monitoring and evaluation of civil structures.](#)

[Figure 1.4 SHM strategy for health evaluation and maintenance planning of civil structures.](#)

Chapter 02

[Figure 2.1 Schematic diagram of a typical sensory system, converting measured quantities into analogue or digital signals.](#)

[Figure 2.2 Accelerometers used in vibration monitoring of civil engineering structures.](#)

[Figure 2.3 Global positioning system \(GPS, Leica Geosystems Model 1230\) used in](#)

[construction monitoring of Canton Tower.](#)

[Figure 2.4 Vibrating wire strain gauges \(Geokon Model GK4200\) installed at the inner tube of Canton Tower.](#)

[Figure 2.5 Anemometer \(R.M. Young Model 05103L\) installed on Canton Tower.](#)

[Figure 2.6 Deployment of weighinmotion \(WIM\) sensors on Tsing Ma Bridge.](#)

[Figure 2.7 Instrumentation layout of sensory systems for structural monitoring in Tsing Ma Bridge.](#)

[Figure 2.8 Modular architecture and input/output block diagrams of the monitoring system of Tsing Ma Bridge.](#)

[Figure 2.9 Setup of SOFO interferometric sensor system.](#)

[Figure 2.10 Functional principle of FabryPérot sensors.](#)

[Figure 2.11 Schematic illustration of a fibre Bragg grating \(FBG\) sensor.](#)

[Figure 2.12 Wireless sensors for structural monitoring.](#)

[Figure 2.13 Functional subsystem and block diagrams of wireless sensors \(after Lynch and Loh 2006\).](#)

[Figure 2.14 Photo of Canton Tower.](#)

[Figure 2.15 Vision inspection system of Canton Tower.](#)

[Figure 2.16 Deployment of sensors and data acquisition substations on Canton Tower for inservice monitoring.](#)

[Figure 2.17 Fibre Bragg gratings \(FBG\) sensing system for Canton Tower.](#)

Chapter 03

[Figure 3.1 Schematic layout of a typical data acquisition unit and its associated equipment.](#)

[Figure 3.2 Comparison of wired and wireless configurations of a structural monitoring system \(after Straser et al. 1998\).](#)

[Figure 3.3 Schematic layout of data acquisition and transmission system.](#)

[Figure 3.4 Block diagram of traffic data analysis in DPCS2, combined digital video converter \(DVC\) and dynamic weighinmotion \(DWIM\) data.](#)

[Figure 3.5 Architectural layout of structural health data management system \(SHDMS\) and its interfaces.](#)

[Figure 3.6 Integrated inconstruction and inservice SHM system for Canton Tower.](#)

[Figure 3.7 Integration of SHM and vibration control.](#)

[Figure 3.8 Wireless data transmission.](#)

Chapter 04

[Figure 4.1 Traditional NDT techniques depending on wave types \(after Ettouney and Alampalli 2012\).](#)

[Figure 4.2 Equipment and applications of the guided wave technique.](#)

[Figure 4.3 Schematic diagrams of a laser Doppler vibrometer system.](#)

[Figure 4.4 Schematic diagrams of configuration of global positioning system \(GPS\) components.](#)

[Figure 4.5 Databased and modelbased damage assessment techniques in structural health monitoring strategies \(after Farrar and Lieven 2007\).](#)

Chapter 05

[Figure 5.1 Impact hammer and accelerometers for vibration testing.](#)

[Figure 5.2 A space steel frame structure used for laboratory testing with test equipment.](#)

[Figure 5.3 Laboratory vibration test results for the space steel frame structure.](#)

[Figure 5.4 Experimental modes from laboratory vibration test for the space frame structure.](#)

[Figure 5.5 Fundamental frequency versus hourly average temperature of the Ting Kau cablestayed bridge.](#)

[Figure 5.6 Relative frequencies extracted by various modal identification methods from the ambient vibration data \(after Peeters and Ventura 2003\).](#)

[Figure 5.7 Relative damping ratios extracted by various modal identification methods from the drop weight data \(after Peeters and Ventura 2003\).](#)

[Figure 5.8 Deployment of accelerometers on Ting Kau Bridge.](#)

[Figure 5.9 Stabilisation diagrams for the SSIDATA and the SSICOV output only identification methods for Ting Kau Bridge.](#)

[Figure 5.10 Identified mode shapes of first eight modes for Ting Kau Bridge.](#)

[Figure 5.11 Plane frame structure with possible sensor locations marked with a circle.](#)

[Figure 5.12 Mean cumulative errors in mode shape expansion as a function of noise level in DOF's readings for the frame structure.](#)

[Figure 5.13 Overall orthogonality errors in mode shape expansion as a function of noise level in DOF readings for the frame structure.](#)

[Figure 5.14 Canton Tower: \(a\) full finite element model, \(b\) positions of installed accelerometers, \(c\) reduced order finite element \(FE\) model.](#)

[Figure 5.15 Averaged normalised power spectral densities \(ANPADs\) of the measured acceleration data used for the peak picking \(PP\) method.](#)

[Figure 5.16 Stabilisation diagram of measured acceleration data used for the stochastic subspace identification \(SSI\) method.](#)

[Figure 5.17 Expanded first and fourth bending modes, compared with the modal readings identified from ambient vibration data and the eigenvectors of the reduced finite element model.](#)

Chapter 06

[Figure 6.1 A cantilever beam structure for model updating.](#)

[Figure 6.2 Finite element model of a plane frame structure for model updating.](#)

[Figure 6.3 Finite element model of the laboratory tested space steel frame structure.](#)

[Figure 6.4 Comparison of updated stiffness parameters of the FE model and simulated exact stiffness parameters at integration point level for beams and columns and at element level for braces, information on different number of noise-free incomplete modes used.](#)

[Figure 6.5 Updated stiffness parameters of the reduced FE model using nine measured incomplete modes.](#)

Chapter 07

[Figure 7.1 Possible global structural damage indices for civil engineering structures \(after Catbas and Aktan 2002\).](#)

[Figure 7.2 A cantilever beam used for different modelling problems.](#)

[Figure 7.3 Elevation of Tsing Ma Bridge.](#)

[Figure 7.4 Percentage difference of natural frequencies \(PDNF\) for simulated damage Cases 1.1 and 1.2.](#)

[Figure 7.5 Mode shape curvature \(MSC\) values for damage Case 2.1 using 3 damaged modes.](#)

[Figure 7.6 Flexibility coefficient index values at nodes on deck for damage Case 1.2.](#)

[Figure 7.7 Values of the strain energy based damage index \$\beta_j\$ for damage Case 2.1.](#)

[Figure 7.8 Simulated 'normal' fluctuation of tension force of the cable.](#)

[Figure 7.9 Novelty index evaluated on training and testing data with 5% reduction in cable tension.](#)

[Figure 7.10 Backpropagation \(BP\) neural network with three layers and nodes.](#)

[Figure 7.11 Architecture of a three-layer probabilistic neural network \(PNN\) for damage identification.](#)

[Figure 7.12 Longitudinal frame member numbering in deck segment No.3 and the selected mode shape components marked with arrows.](#)

Chapter 08

[Figure 8.1 Statically indeterminate plane truss structure for damage assessment.](#)

[Figure 8.2 Inverse predictions for the hypothetical damage scenario of the plane truss using the residual force vector method.](#)

[Figure 8.3 Simply supported grid structure \(plane view\).](#)

[Figure 8.4 Inverse damage identification from the sensitivity based method using natural frequencies.](#)

[Figure 8.5 Inverse damage identification using the dynamic perturbation method from 5 damaged frequencies.](#)

[Figure 8.6 Onebay sixbar plane truss structure.](#)

[Figure 8.7 Inverse damage identification using the dynamic perturbation method from incomplete modes.](#)

[Figure 8.8 Finite element model of the framed building structure with element numbering and sensor locations \(marked with ⊗\).](#)

[Figure 8.9 Singular values, ordinary solution coefficients and regularised solution coefficients for inverse damage predictions.](#)

[Figure 8.10 Lcurves for Tikhonov regularisation with noise levels ranging from 1% to 5% in measured DOF readings.](#)

[Figure 8.11 Identification of damage scenario I \(no stiffness in one brace in first storey, i.e. element no. 24\), 10 incomplete noisy damaged modes used.](#)

[Figure 8.12 Identification of damage scenario II \(no stiffness in braces in first storey, i.e. element nos. 22–29\), 7 incomplete noisy damaged modes used.](#)

[Figure 8.13 Gravity dam structure with measured nodes marked with both ■ and ●.](#)

[Figure 8.14 Inverse damage predictions using the dynamic perturbation method for the gravity dam structure.](#)

Chapter 09

[Figure 9.1 Framework for reliability analysis using an SHM strategy \(after Catbas et al. 2008\).](#)

[Figure 9.2 Monitoring of wind velocities, directions and occurrence at tovertop of Tsing Ma Bridge.](#)

[Figure 9.3 Axle load distribution and spectrum from the weighinmotion data.](#)

[Figure 9.4 Gross vehicle weight distribution and spectrum from the weighinmotion data.](#)

[Figure 9.5 Fatigue crack growth curves simulated by the gamma process model and](#)

[predicted by the Paris–Erdogan law.](#)

[Figure 9.6 Probability distribution of time to failure using the gamma process model under different critical thresholds of fatigue crack length \(\$a_{cr}\$ \).](#)

[Figure 9.7 Lifetime distribution \(CDF\) as a function of concrete crack width.](#)

[Figure 9.8 Symptom reliability \(survival function\) by Bayesian updating due to inspection and repair.](#)

[Figure 9.9 Probability density functions \(PDFs\) of resistance effect \$R\$ and load effect \$S\$.](#)

[Figure 9.10 Schematic representation of load processes and resistance deterioration \(after Melchers 1999\).](#)

[Figure 9.11 Structural lifetime \$T^*\$ associated with a target probability of failure \$p_f^*\$.](#)

[Figure 9.12 Deck crosssection CH24662.5 and strain gauge SPTLS16 at Detail H of Tsing Ma Bridge.](#)

[Figure 9.13 Monitoring data of dynamic stresses collected from strain gauge SPTLS16.](#)

[Figure 9.14 Probability of failure and reliability index as a function of fatigue life.](#)

[Figure 9.15 Pareto optimum solution sets with single and double interventions for inspection and maintenance.](#)

[Figure 9.16 Dynamic strain gauges in longitudinal stiffening truss for highway traffic monitoring.](#)

[Figure 9.17 Estimates of railway loading based on strain results in waybeams.](#)

[Figure 9.18 Comparison of measured and designed suspender forces.](#)

[Figure 9.19 Stress history in top chord of outer longitudinal truss \(North\).](#)

[Figure 9.20 Fatigue life estimation for top chord of outer longitudinal truss \(North\).](#)

Chapter 10

[Figure 10.1 Threetower cablestayed Ting Kau Bridge.](#)

[Figure 10.2 Modular architecture of structural monitoring systems for Ting Kau Bridge.](#)

[Figure 10.3 Sensory system of SHM strategy for Ting Kau Bridge.](#)

[Figure 10.4 Threedimensional finite element model of Ting Kau Bridge.](#)

[Figure 10.5 Framework for finite element model updating by measurement data.](#)

[Figure 10.6 New Headquarters of Shenzhen Stock Exchange, a highrise building with a floating platform.](#)

[Figure 10.7 Layout of temporary braces of the highrise building.](#)

[Figure 10.8 Growth of stresses measured in the process of dismantling temporary](#)

[supports.](#)

[Figure 10.9 Comparison of measured and computed stress increments during unloading process.](#)

[Figure 10.10 Wireless monitoring system for the highrise building.](#)

[Figure 10.11 Distribution of accelerometers on the floating platform.](#)

[Figure 10.12 Vertical dynamic response of floating platform at sensor location P9.](#)

[Figure 10.13 Rivercrossing metro tunnel during freezing construction.](#)

[Figure 10.14 Freezing monitoring tube accommodating a FBG sensor.](#)

[Figure 10.15 Deployment locations of FBG sensors in the frozen soils.](#)

[Figure 10.16 Measured temperature time histories during freezing construction.](#)

[Figure 10.17 Deployment of FBG based liquidlevel sensors on subgrade surface of the railway line.](#)

[Figure 10.18 Measured Bragg wavelengths by liquidlevel sensors for estimating subgrade settlement.](#)

[Figure 10.19 Piezoelectric \(PZT\) based acoustic emission sensing system for damage detection of rail turnouts.](#)

[Figure 10.20 Undamaged rail turnouts and arrangement of PZT transducers on railway switch area.](#)

[Figure 10.21 Signals collected from PZT transducer 1 for undamaged rail turnout.](#)

[Figure 10.22 Damaged rail turnout and passage train.](#)

[Figure 10.23 Signals collected from PZT transducer 1 for damaged rail turnout.](#)

[Figure 10.24 Comparisons of power spectrum density \(PSD\) from PZT transducer 1 for undamaged and damaged rail turnout.](#)

[Figure 10.25 Schematic of FBG sensory system for structural integrity monitoring of water mains.](#)

[Figure 10.26 FBG sensors for monitoring water mains.](#)

[Figure 10.27 Distribution of strain, temperature and pressure sensors.](#)

[Figure 10.28 Topology of the sensory system for structural monitoring of water mains.](#)

[Figure 10.29 Correlation of strain and temperature variation at measurement point A with water flow.](#)

[Figure 10.30 Correlation of strain and temperature variation at measurement point A with water cutoff.](#)

[Figure 10.31 Strain and temperature changes at crosssection #35 with water cutoff.](#)

Figure 10.32 Water pressures at the middle of the GRP pipeline with water cutoff.

Figure 10.33 Normalised crosscorrelation between each pair of temperature and strain sensors at crosssection #35, where blue (solid) line for point A; green (dashed) line for point B; red (dotted) line for point C.

Structural Health Monitoring of Large Civil Engineering Structures

HuaPeng Chen
University of Greenwich
UK

With contributions from

YiQing Ni
Hong Kong Polytechnic University
HK

WILEY Blackwell

This edition first published 2018
© 2018 John Wiley & Sons Ltd

All rights reserved. No part of this publication may be reproduced, stored in a retrieval system, or transmitted, in any form or by any means, electronic, mechanical, photocopying, recording or otherwise, except as permitted by law. Advice on how to obtain permission to reuse material from this title is available at <http://www.wiley.com/go/permissions>.

The right of HuaPeng Chen to be identified as the author of the editorial material in this work has been asserted in accordance with law.

Registered Offices

John Wiley & Sons, Inc., 111 River Street, Hoboken, NJ 07030, USA

John Wiley & Sons Ltd, The Atrium, Southern Gate, Chichester, West Sussex, PO19 8SQ, UK

Editorial Office

9600 Garsington Road, Oxford, OX4 2DQ, UK

For details of our global editorial offices, customer services, and more information about Wiley products visit us at www.wiley.com.

Wiley also publishes its books in a variety of electronic formats and by printondemand. Some content that appears in standard print versions of this book may not be available in other formats.

Limit of Liability/Disclaimer of Warranty

While the publisher and authors have used their best efforts in preparing this work, they make no representations or warranties with respect to the accuracy or completeness of the contents of this work and specifically disclaim all warranties, including without limitation any implied warranties of merchantability or fitness for a particular purpose. No warranty may be created or extended by sales representatives, written sales materials or promotional statements for this work. The fact that an organization, website, or product is referred to in this work as a citation and/or potential source of further information does not mean that the publisher and authors endorse the information or services the organization, website, or product may provide or recommendations it may make. This work is sold with the understanding that the publisher is not engaged in rendering professional services. The advice and strategies contained herein may not be suitable for your situation. You should consult with a specialist where appropriate. Further, readers should be aware that websites listed in this work may have changed or disappeared between when this work was written and when it is read. Neither the publisher nor authors shall be liable for any loss of profit or any other commercial damages, including but not limited to special, incidental, consequential, or other damages.

Library of Congress Cataloging in Publication Data

Names: Chen, HuaPeng, author. | Ni, YiQing, contributor.

Title: Structural health monitoring of large civil engineering structures / by HuaPeng Chen ; with contribution from YiQing Ni.

Description: Hoboken, NJ : John Wiley & Sons, 2018. | Includes index. | Identifiers: LCCN 2017042885 (print) | LCCN 2017056352 (ebook) | ISBN 9781119166627 (pdf) | ISBN 9781119166634 (epub) | ISBN 9781119166436 (cloth)

Subjects: LCSH: Structural health monitoring. | Structural analysis (Engineering)

Classification: LCC TA656.6 (ebook) | LCC TA656.6 .C44 2018 (print) | DDC 624.1/71-dc23

LC record available at <https://lcn.loc.gov/2017042885>

Cover design: Wiley

Cover image: © ngkaki/Gettyimages

Preface

Civil engineering structures such as bridges and buildings are typically large and are built with uncertainties. Their behaviour during the construction phase should be monitored to control the quality and safety of the construction processes. After civil structures have been constructed, the construction materials are subjected to degradation over time, leading to a decrease in structural capacity and serviceability. Monitoring during the service phase offers useful information on structural performance under gradual material degradation and expected loads, and also records the structural responses of unexpected sudden overloading. Data collected from real time monitoring can then be used for damage assessment and health evaluation of the civil engineering structures in service. The continuously measured data from the monitoring system can provide the basis for predicting future performance and determining optimum maintenance strategy for the existing structures.

Structural health monitoring (SHM) is a process of inservice damage identification and health evaluation for an engineering structure through an automated monitoring system. SHM uses sensing systems and necessary hardware and software facilities to monitor structural responses and operational conditions of the structure. A typical SHM strategy comprises several key components, including sensors, data acquisition, data transmission, data processing, data management, health evaluation and decision making. Sensing technology and the signal interpretation algorithms are two critical factors in developing successful SHM strategies for large civil engineering structures. Damage assessment methods using vibration measurements such as modal parameters show promise for the health evaluation of the civil structures.

The development of a structural health monitoring strategy requires a multidisciplinary approach involving many fields, such as sensors and sensor networks, signal processing, modal testing, numerical modelling, probabilistic analysis, damage diagnosis and damage prognosis. Each of these topics is a disciplinespecific subject by itself, and is equally important in developing effective SHM strategies. Sensing systems are critical for accurate data acquisition and transmission, and the acquired data is used for signal processing to extract key features sensitive to local damage. Modal testing and analysis is adopted to identify modal parameters from vibration measurements, and the obtained modal data can be used for model updating and damage assessment. Probabilistic approaches are needed for numerical modelling to account for uncertainties, and provide an essential framework for reliability analysis and damage prognosis. The objective of this book is to integrate these topics with the specific focus on developing SHM strategies for large civil engineering structures.

This book aims to explain the principles of the SHM strategy, and so it covers all aspects of sensing system, data processing and analysis, damage assessment and decision making for structural monitoring and health evaluation of large civil engineering structures. The book consists of four major parts. First, sensors and sensing technology and data transmission systems are introduced for monitoring of civil structures. From the data measured from the

monitoring system on the structure, modal analysis techniques are presented to extract modal parameters, which are used to update and validate the associated finite element numerical model. Then, various methods are provided for identifying the existence, location and extent of damage in civil structures using the measured data and their derivatives. Finally, from the continuously monitored data, probabilistic approaches are utilised for deterioration modelling and reliability analysis, giving the basis for decision making. The techniques for the SHM strategy are well explained in a number of examples and are also demonstrated in many real case studies.

This book can be used as the textbook for a graduate level course on structural health monitoring with emphasis on civil engineering structures. Also, the book can be used as a guide for the practising engineers who want to apply SHM techniques in practice. The book is written with an assumption that the reader has a basic engineering background and needs knowledge of little more than undergraduate level mathematics. Furthermore, the book is an invaluable reference for those undertaking research in the areas of structural monitoring and health evaluation of civil engineering structures.

In this book, several real case studies on health monitoring of civil engineering structures, such as Tsing Ma Bridge, Ting Kau Bridge and Canton Tower, are generously contributed by Professor YiQing Ni, The Hong Kong Polytechnic University. These practical applications cover various areas in structural health monitoring technology including sensors and sensing networks, data transmission and processing systems, structural damage identification techniques and usage monitoring systems, which are used as examples in several chapters, such as [Chapter 2](#), [Chapter 3](#), [Chapter 7](#) and [Chapter 10](#). The book would not be complete without these practical examples, thus deepest gratitude must go to Professor YiQing Ni and his colleagues, in particular Professor J.M. Ko, Dr. K.Y. Wong and Dr. X.W. Ye.

Finally, the author is indebted to many people for their direct and indirect assistance in the preparation of this book. The author would like to thank the former and current colleagues, research fellows and PhD students for their support and useful works, particularly Dr. T.L. Huang, Dr. T.S. Maung, Dr. J. Nepal and Mr. C. Zhang. The author deeply thanks his family for their continuous patience and understanding; especially Chengheng Xiao, Helen, Alice and Xuezhong have been the constant supporters.

November 2017

HuaPeng Chen, in London

Biography

HuaPeng Chen is Professor of Civil Engineering, Head of Innovative and Smart Structures at the University of Greenwich, UK. He received his PhD in Structural Engineering from the University of Glasgow, UK. He has been working for over 20 years on structural health monitoring, advanced numerical modelling and structural performance assessment. He is a Chartered Civil Engineer (UK) and a Fellow of the Institution of Civil Engineers (UK).

1 Introduction to Structural Health Monitoring

Structural Health Monitoring (SHM) is a process of inservice health assessment for a structure through an automated monitoring system, and it is a key element of costeffective strategies for conditionbased maintenance. A SHM strategy consists of many important components including sensing network, data processing and analysis, damage assessment and decision making. SHM technology has the great potential to offer significant economic and lifesafety benefits. However, the application of the SHM technology to actual civil engineering structures is still in its infancy, and it requires advancements in various fields due to its multidisciplinary nature. Extensive further works are therefore needed to ensure that infrastructure managers benefit from this emerging technology. This chapter first introduces the development of SHM technology and the framework and strategy of SHM systems. The critical issues and potential benefits of the application of SHM to large civil engineering structures are presented. Finally, the challenges of SHM technologies in civil engineering applications and the required further studies are discussed.

1.1 Advances in Structural Health Monitoring Technology

The structural health monitoring process involves the observation and evaluation of a structure over time using periodically sampled measurements from a sensing system. Structural health monitoring is a popular and growing research field, providing a powerful tool for damage assessment and performance evaluation of engineering structures.

1.1.1 Structural Health in Civil Engineering

Civil infrastructure comprises bridges, buildings, towers, pipelines, tunnels, dams and other types of structures. Their continued safe and economical operation largely depends on proper maintenance and management. In order to evaluate optimal management strategies for existing civil infrastructure, accurate assessment of present and future safety is important and necessary (Ettouney and Alampalli 2012). Maintaining safe and reliable civil infrastructure for daily use is critical to the wellbeing of the society. Thus, structural health can be stated as its current capacity for providing intended level of service in a safe and costeffective manner against the expected hazards during its service life.

Despite the necessary design methodology initially used, civil engineering structures deteriorate with time. This deterioration is due to various reasons, including failure caused by cyclic traffic loads, effects of environmental factors (e.g. steel corrosion, concrete carbonation) and aging in the construction materials. Also, the deterioration can be caused by infrequent extreme events such as earthquakes, hurricanes and floods. Therefore, structural

health will be affected by operational and environmental factors, including normal load conditions, current and future environments and expected hazards during the lifetime. All these factors are variables with uncertainties, so it is difficult to define the structural health in terms of its age and usage and its level of safety to resist severe natural actions. In order to reliably assess structural health and maintain structural safety, continued inservice monitoring of the structure is essential.

Catastrophic structural failures, such as sudden collapse of the I35 highway bridge (NTSB 2008), have highlighted problems associated with aging critical civil infrastructure. Severe natural disasters such as earthquakes and typhoons result in demands for quick condition assessment of civil structures (Brownjohn et al. 2011). Currently, the condition assessment of existing civil infrastructure such as bridges largely depends on visual inspection. This subjective and inaccurate condition assessment methodology has been identified as the most critical technical barrier to effective infrastructure management. For example, condition of bridges is typically expressed in terms of subjective indices on the basis of visual inspection alone. Thus, it is difficult to accurately evaluate structural condition from the inaccurate visual inspection data, even when this may be conducted by experts (Aktan et al. 1998). These issues have driven the research and development on the continuous observation and interpretation of fullscale performance of civil engineering structures during their service life.

Health monitoring applications based on advanced sensors and realtime monitoring for civil infrastructure offer great potential for informed and effective infrastructure management. Health monitoring is necessary for civil engineering structures since they may exhibit premature deterioration, structural damage and performance problems, or they may even have aged beyond their expected design life. Health monitoring can be utilised for tracking the responses of a structure along with inputs, if possible, over a sufficient duration to determine anomalies, to detect deterioration and to assess damage for decision making. Damage assessment methods using measured vibration modal data, such as natural frequencies and mode shapes, show promise for the health evaluation of engineering structures (Bicanic and Chen 1997, Chen 1998). Health monitoring can assess the performance of civil structures in a proactive manner using measured data and data interpretation algorithms, in order to correctly evaluate the current condition and to predict the remaining service life.

1.1.2 Aims of Structural Health Monitoring

Structural health monitoring is defined as the process of implementing a damage identification and health evaluation strategy for engineering structures. SHM uses sensing systems and associated hardware and software facilities to monitor the structural performance and operational environments of engineering structures. SHM involves the observation of a structure over time, using periodically sampled structural response and operational environment measurements from an array of sensors and then the evaluation of the current state and future performance of the structure. For longterm SHM, the output of this process is periodically updated information regarding the capability of the structure to perform its intended function, by considering the inevitable aging and degradation resulting from operational environments (Farrar et al. 2003). Furthermore, SHM is adopted for rapid

condition assessment to provide prompt and reliable information regarding the integrity of the structure after extreme events, such as an earthquake or blast loading.

SHM aims to identify structural damage and evaluate the health of the structure using monitored data. Damage is defined here as changes to the material and/or geometric properties of a structure, which affects the current state and future performance of the structure. The objectives of an SHM strategy can be outlined as the following five levels (Farrar et al. 2009).

- Level I: Damage detection, giving a qualitative indication that damage might be present in the structure
- Level II: Damage localisation, giving information about the probable position of damage
- Level III: Damage classification, giving information about the type of damage
- Level IV: Damage assessment, giving an estimate of the extent of damage
- Level V: Damage prognosis, giving information about the safety of the structure, e.g. estimate of remaining useful life

The level in the order given above represents increasing knowledge of the damage state. A higher level usually requires information available about all lower levels. The first two levels, damage detection and localisation, can be generally achieved using vibration based damage detection methods from structural dynamic response measurements. To identify the type of damage, data from structures with the specific types of damage must be available for correlation with the measured data. Analytical models are usually needed to achieve the fourth and fifth levels, damage assessment and prognosis. In general, these two levels may not be achieved without first identifying the type of damage present. Estimates of the future loading, together with predictive deterioration models, are necessary to accomplish the final level for damage prognosis.

SHM strategies offer useful information for optimising maintenance planning of engineering structures in service. To ensure a reliable operation and to schedule maintenance and repair work in a costeffective manner, it is necessary to continuously monitor and assess the structural performance and to have an accurate estimation of the remaining useful life. Thus, the SHM strategy integrated with lifecycle management is necessary to calibrate structural assessment and predictions, to enable optimal operation and maintenance of engineering structures and, eventually, to operate the structures beyond their original design life.

1.1.3 Development of SHM Methods

Structural damage identification based on changes in the dynamic response of the structure has been practised in a qualitative manner for a long time. The beginnings of this damage detection method as an area of interest to engineers can be traced back as far as the time when tap testing (e.g. on train wheels) for fault detection became common. This field, however, did not really become established in research communities until the 1980s, when much interest was generated in the structural condition of offshore platforms, and later in the health of aerospace structures. Recently, the development of quantifiable SHM methods has been closely linked

with the evolution and cost reductions of digital computing hardware and sensing systems. In conjunction with these developments, SHM has received considerable attention in the technical literature. The details of literature surveys on SHM development can be found in comprehensive reviews by Doebling et al. (1996) and Sohn et al. (2004).

The civil engineering community has investigated vibration based damage identification of bridge structures and buildings since the early 1980s. Modal properties, and the associated quantities derived from these properties, such as mode shape curvature and dynamic flexibility matrix indices, were the primary features used to identify damage in the civil engineering structures. Environmental and operational condition variability (e.g. variation of temperature) presents significant challenges to the health monitoring of the civil structures. The physical size of the civil structures, typically in large scale with numerous components, also presents many practical challenges for vibration based damage assessment. Furthermore, the requirement for realtime structural condition assessment after severe discrete events (e.g. aerodynamic gust loads on long span bridges, earthquake loading on civil infrastructure) is also a major challenge for SHM technology. Regulatory requirements in Asian countries such as in China are driving current research and commercial development of SHM systems for large civil engineering structures (Farrar and Worden 2007). Nowadays, SHM is a popular and still growing research field, which is more and more becoming a focus of the civil engineering community.

Recently, advances have been made in various branches of technology, including sensing instrumentation, signal acquisition and transmission, data processing and analysis and numerical simulation and modelling. These technological advancements enable the required current and historical information of the civil structures to be collected and analysed effectively. SHM strategies take advantage of the technological advancements for accurately evaluating the health of civil structures using realtime monitored data.

1.2 Structural Health Monitoring System and Strategy

A health monitoring system for civil structures often includes observation by sensing systems and the evaluation by data interpretation algorithms. In general, both global and local health monitoring strategies are important for effective damage identification and safety assessment of large civil engineering structures.

1.2.1 SHM System and its Components

The development of successful SHM methods generally depends on two key factors: sensing technology and the associated signal analysis and interpretation algorithms. An SHM system generally consists of many key components, including sensors, data acquisition, data transmission, data processing, data management, health evaluation and decision making. Each of these components is equally important in assessing the health state of a civil structure. The sensing component of the SHM system includes the selection of sensor types, their number and location. The data acquisition component involves selecting the excitation methods, signal

conditioning and data acquisition hardware. The measured data needs to be transmitted by wired or wireless transmission networks. The data processing component typically includes data validation, normalisation, cleansing, fusion and compression. This preprocessed monitoring data is then stored and managed properly. From this data, the health of the structure can be evaluated and then a decision will be made on the basis of the health assessment.

Bridges are major applications of SHM systems due to their largescale and structural complexity. In general, bridge health monitoring process involves the collection and analysis of data for the execution of the following four categories of works:

- *Observation*, e.g. collection, processing, analysis and reporting of all observed (measured and derived) data from the sensory systems
- *Evaluation*, e.g. realtime or near realtime performance analysis of the structure under monitoring, and offtime diagnostic and prognostic analyses of the structure under normal operations or after extreme events
- *Rating*, e.g. ranking and prioritisation of structural components for planning and scheduling of inspection and/or maintenance activities
- *Management*, e.g. systematic storage and fast retrieval of all observation, evaluation and rating data for subsequent interfacing analysis and display

The SHM system architecture of a bridge is generally composed of four key subsystems, as demonstrated in the applications to longspan bridges (Wong and Ni 2009) and as shown in [Figure 1.1](#):

- *Structural health observation system (SHOS)*, devised as an onstructure instrumentation system including sensory system and equipped with appropriate data processing, analysis and reporting software tools
- *Structural health evaluation system (SHES)*, devised as a computation system equipped with relevant preconstructed analytical models to carry load demand analysis and load resistance analysis
- *Structural health rating system (SHRS)*, devised as an analytic database system equipped with relevant customised software tools and databases for evaluating the condition ratings of the structure and its components
- *Structural health data management system (SHDMS)*, devised as a data and information management system for systematic storage and fast retrieval of all data by means of data warehouse platform and data warehouse

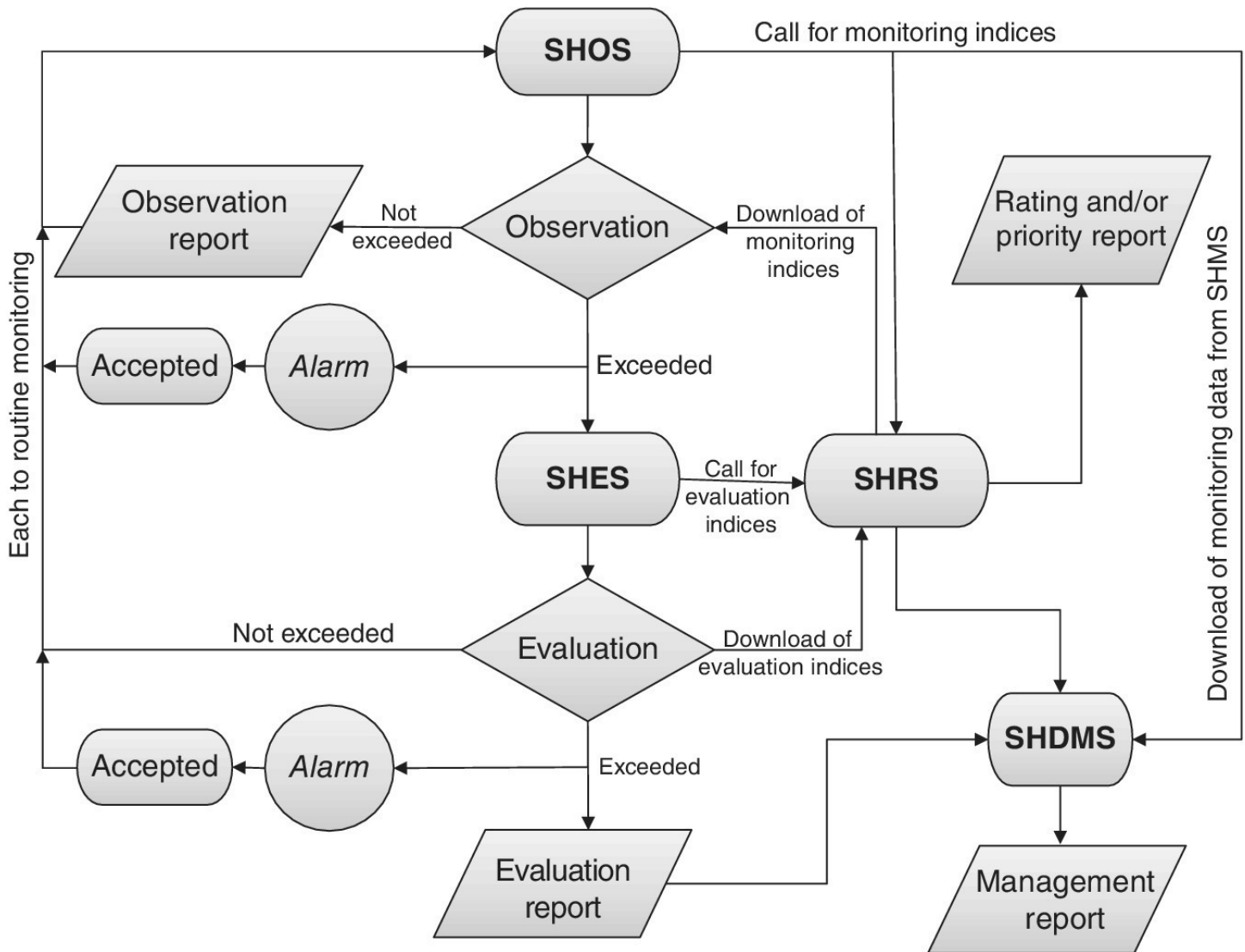


Figure 1.1 System architecture and operation diagram of a SHM system for a bridge.

1.2.2 SHM Strategy and Method

SHM strategies can broadly be categorised into two groups: global and local. In general, both global and local monitoring strategies provide different types of information, and support different types of analysis. [Figure 1.2](#) shows global and local monitoring strategies, the types of information collected and the associated measurement types (Frangopol and Messervey 2009).

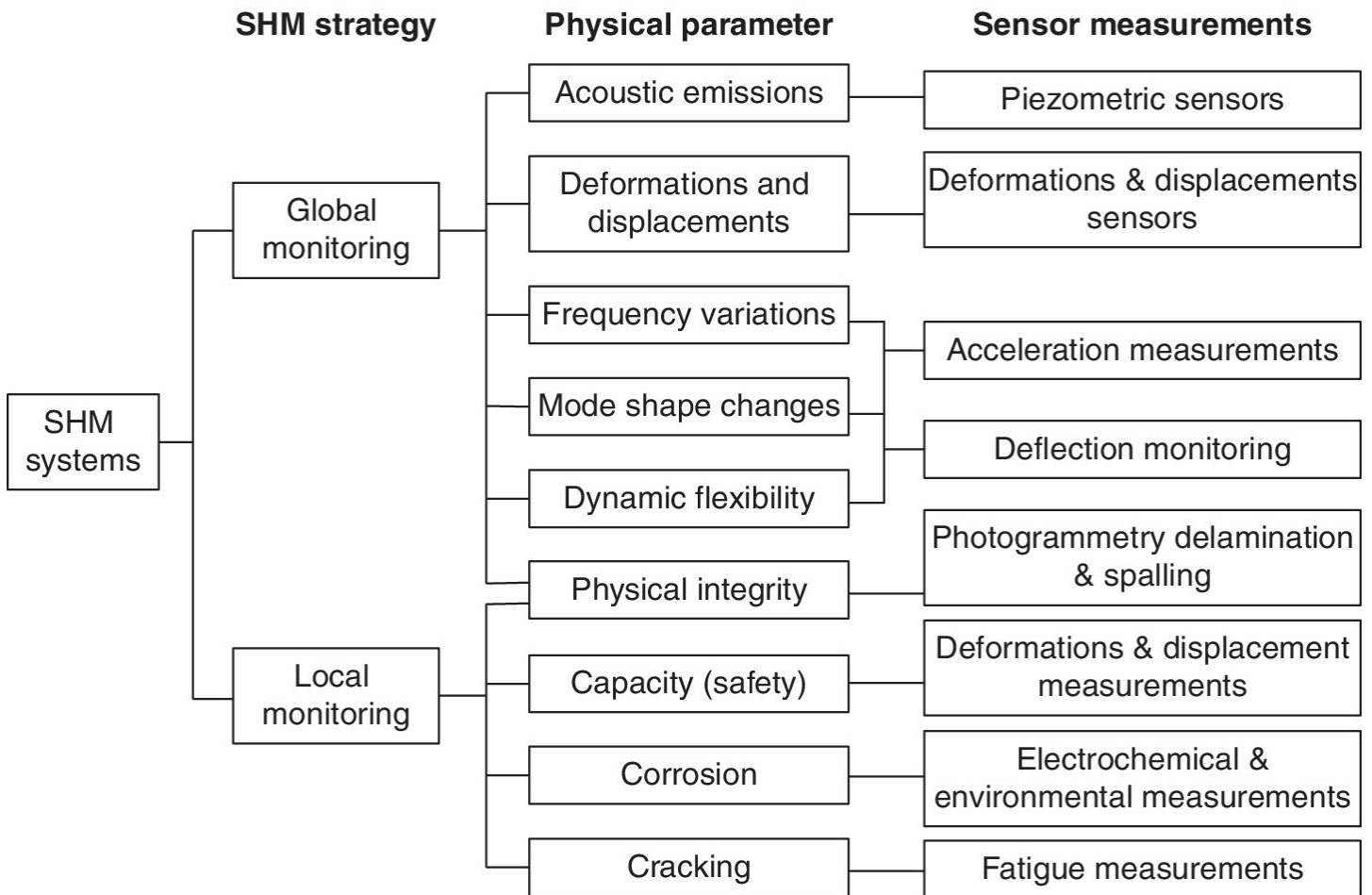


Figure 1.2 Structural health monitoring strategies for civil engineering structures (after Frangopol and Messervey 2009).

Selecting an appropriate monitoring strategy largely depends on the structure concerned, the type of analysis, or both. For example, a global monitoring approach has to be chosen when accessibility to specific parts of the structure is impossible. For a global monitoring system, accelerometers would be an appropriate instrument for measuring the dynamic response (i.e. accelerations) of the structure subjected to forced or ambient vibration. The measured acceleration data can be used for extracting modal parameters such as natural frequencies and mode shapes. This extracted modal data then can be used for updating the structural parameters of the analytical model, or for identifying structural damage using global SHM techniques. However, in the cases when analysing a specific structural failure mechanism at local area such as crack or fatigue, information on the local material and geometrical properties as well as stress state may be needed to assess the structural condition at the local level. Typically, nondestructive testing techniques such as ultrasound could be used to identify the local damage in the structure.

Global monitoring strategies have been the traditional tool used to assess the safety of large civil engineering structures such as bridges. Ideally, by use of measured parameters, health monitoring of civil structures has the ability to identify the location and severity of damage in the structures when damage occurs. However, existing global SHM methods, such as some vibration based damage detection methods, may only determine whether or not damage is

present somewhere in the entire structure. These global methods are important for checking if damage has occurred in the structure. Once damage presence is detected, further examination of the structure to determine the exact location and severity of the damage can be undertaken. Then, local SHM methods, such as guided waves to measure the state of stress or eddy current techniques to locate cracks, are adopted to determine the exact location and extent of the damage. Nondestructive testing, used here as a local SHM method, is often timeconsuming and expensive, and access is not always possible (Chang et al. 2003). Therefore, both global and local SHM strategies are necessary in health monitoring of large civil structures.

1.3 Potential Benefits of SHM in Civil Engineering

Civil engineering structures are typically large and are constructed with uncertainties. Their inservice behaviour is often affected by environmental factors. These issues make SHM strategies in civil engineering a challenge. However, the application of SHM strategies to civil structures will bring many benefits, such as structural safety and cost savings.

1.3.1 Character of SHM in Civil Engineering

Unlike aerospace or automotive structures, civil structures are not built with the same level of precision. In many cases, because of onsite construction constraints and varying ground conditions, the structure may not be constructed according to the archived design. Accuracy of implementation and uncertainty of workmanship are often an issue. Total uniformity of material can never be achieved when concrete materials are used. Furthermore, the behaviour of civil structures is usually affected by environmental factors such as temperature and moisture. For example, the natural frequencies of a bridge are often related to the temperature variation around the bridge due to thermal effects. For health evaluation of civil structures, physical models based on idealised behaviour such as perfect pin or rigid connections can never reflect what is achieved in practice. It is often not possible to obtain the data necessary for building an accurate physical model (Chang et al. 2003). These problems make the health monitoring and evaluation of civil infrastructure a challenge, in particular for modelbased (physicsbased) SHM techniques.

Civil structures deteriorate with time due to operational loads and environmental effects. Structural damage such as fatigue caused by repetitive traffic loads often occurs in the structure. Meanwhile, largescale discrete events such as earthquakes and hurricanes can cause serious structural damage. Typical examples are aerodynamic gust loads on long span bridges and earthquake loading on all types of civil infrastructure. Thus, the following assessment through an SHM strategy would typically be necessary (Karbhari 2009): (a) damage to the structure and changes in the structural resistance, (b) probability of failure or of the structure's performance falling below a certain threshold, (c) evaluation of the severity of damage and the remaining service life.

Vibration based damage identification methods show promise for global damage assessment of large civil structures (Chen and Maung 2014). These damage identification methods can be

broadly divided into two groups: databased and modelbased techniques. Databased techniques adopt measurements directly to assess the current state, but may only be able to detect the existence of damage. Modelbased techniques require a validated initial physical model of the structure (baseline) for locating and assessing damage in the structure (Chen and Bicanic 2000, Chen 2008). Their dependence on baseline data can be an issue in global damage assessment, since environmental effects such as temperature can change the vibration measurements from an undamaged structure. Thus, the environmental effects need to be treated properly in the damage identification process.

Although the field of SHM as applied to civil structures is still in its infancy, it is already demonstrating significant advantages not only in the safety assessment of existing structures but also in paving the way for both a better understanding of structural response and the development of design codes. It is expected that the further development of SHM systems in civil engineering will lead to the establishment of a comprehensive methodology for automated health monitoring of civil structures, so that true condition based inspection and maintenance would become a reality (Karbhari 2009). The integration of advanced sensing networks with the development of effective tools for realtime data analysis provides useful tools for current condition assessment, remaining life prediction and optimal repair planning of civil structures, as illustrated in [Figure 1.3](#). In addition, the use of an appropriately designed SHM system would enable further understanding of structural response through data analysis and interpretation. This would also lead to better and more refined methods of structural design. As a result, all of these would generate innovations in the design and maintenance of civil structures, leading to the development of a modern field of smart civil infrastructure.

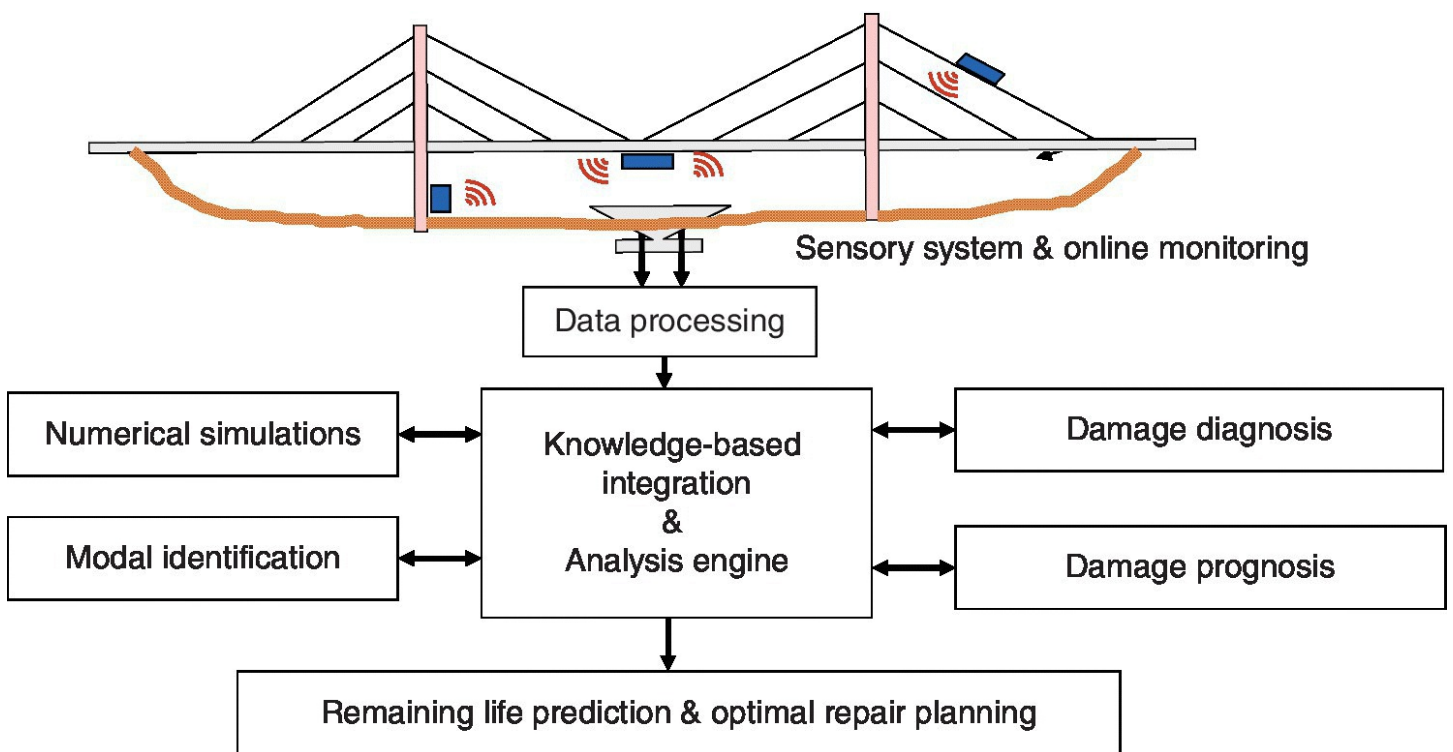


Figure 1.3 Integrated framework for health monitoring and evaluation of civil structures.

1.3.2 Potential Benefits of SHM

Structural health monitoring technologies have the potential to improve the design and management of civil structures in several ways (Frangopol and Messervey 2009, Ko and Ni 2005):

- performance based design can be undertaken by recording sitespecific environmental conditions such as wind, load demands or temperature
- design assumptions and parameters can be validated with the potential benefit of improving design specifications and guidelines for future similar structures
- inspections can be scheduled on an “as needed” basis informed by structurespecific data when indicated by monitoring data
- performance thresholds can be established to provide warning when prescribed limits are violated, such as for anomalies in loading and response
- realtime safety assessment can be carried out during normal operations or immediately after disasters and extreme events
- accuracy of structural assessments can be improved by analysing recorded structural response data
- more accurate information can be used for optimally scheduling maintenance and repair activities, leading to cost savings.

Among these potential benefits, the first and most obvious benefit is increased human safety. Unsurprisingly, the majority of the research on SHM strategies has been motivated by disasters such as bridge collapses. Even at the lowest level of SHM strategies, e.g. detection of damage existence or strength degradation, they can be hugely beneficial if used to provide an early warning for safety issues (Cross et al. 2013). In addition, with an automated SHM system, any inaccessible areas of a structure can be assessed to increase safety, while these areas may have been neglected in a visual inspection routine.

Other arising benefits will come from the policy change that sophisticated SHM systems could generate. Currently, most civil structures undergo routine inspection and maintenance at specific time intervals. For example, bridge inspections in the USA are scheduled every two years. A time based approach to management of civil structures has the implication that any unexpected faults occurring in between scheduled inspections may be ignored and cause danger to life. On the other hand, the set timescales for inspections of civil structures may be unreasonably conservative. If a structure continues to be in good health, the costs of thorough inspections could have been saved. In the case of routine maintenance, where structural components may be replaced even if they are in excellent condition, the economic impact may be even greater. SHM strategies have the ability to solve both sides of this issue, since structural monitoring has the potential to become continuous, and maintenance could become condition based (Cross et al. 2013). Use of condition based maintenance could also reduce the downtime that a structure may undergo for routine and emergency maintenance. This, in turn, would be of economic and environmental benefit.

SHM is an emerging technology that will allow existing time based maintenance policies to

evolve into potentially more cost-effective condition based maintenance strategies. The concept of condition based maintenance is based on the philosophy that SHM on a structure will monitor the structural response and notify the operator that damage has been detected. Life safety and economic benefits associated with such a philosophy will only be realised if the SHM system provides sufficient warning, so that corrective actions can be taken before the damage evolves to a failure level (Farrar and Worden 2007). The tradeoff associated with implementing an SHM system is that it requires a more sophisticated monitoring system to be deployed on the structure and a more robust data analysis procedure to be used for interpreting the measured data.

1.4 Challenges and Further Work of SHM

The development of SHM methods for structural damage identification has now achieved some degree of maturity. However, the application of SHM methods for practical structural health evaluation and condition based maintenance is still in its infancy. Further work is needed to ensure that infrastructure managers benefit from the emerging SHM strategies.

1.4.1 Challenges of SHM in Civil Engineering

Although SHM technology has advanced significantly over the past decade, there are still many significant barriers to the general implementation of SHM systems. The common technical challenges to the adaptation of SHM systems in practice are discussed by Farrar and Lieven (2007) and Farrar et al. (2009), and are summarised as follows.

- The philosophy of vibration based SHM methods is that damage will alter structural parameters such as stiffness of a system, which in turn will alter the measured global dynamic response properties of the system. Although vibration based methods appear promising, their actual application in civil engineering raises many significant technical challenges. The most fundamental challenge for vibration based methods is the fact that damage is typically a local phenomenon. Damage may not significantly influence the lower frequency global structural dynamic response, which is normally measured during system operation.
- Another fundamental challenge for SHM methods is that in many situations feature selection and damage detection must be performed when data from damaged systems is not available. Moreover, the selected feature must be sensitive to small damage sizes, e.g. a fatigue crack at a structural component. Large complex civil structures are usually made up of numerous components, and they may have multiple damage present. An SHM system that is suitable for detecting one type of damage may not be useful for detecting other damage types.
- A significant challenge for SHM systems is to choose properly the required sensing system before field deployment, and to ensure that the sensing system itself will not be damaged in service. The number and location of the sensors need to be optimally determined, and a certain amount of redundancy must be implemented into the sensor network. Sensors need

to be inexpensive and easy to implement, so that they can be attached to existing civil structures with little effort.

- Civil structures in their service life are usually subjected to changing operational and environmental conditions, e.g. temperature and moisture. The varying conditions will generate changes in structural response measurements, which should not be interpreted as indications of damage. For example, temperature variation can affect the stiffness of a civil structure, and moisture variation can influence the mass of concrete and pavements. Thus, these changing operational and environmental conditions must be accounted for during the damage identification process.
- Damage in civil structures can accumulate over a long timescale, which poses significant challenges for an SHM sensing system. This problem generates many practical issues for accurate and repeatable measurements from the sensing system over long periods of time. The sensing system is usually expected to operate for the life of the civil structure, which may be as long as 50 or 100 years. Thus, robust sensing system is needed to perform reliably for lifetime of the structure.
- Finally, there are other nontechnical issues in the applications of SHM technology to actual practice. For example, SHM technology has to provide asset managers with an economic benefit over current maintenance approaches. In the meantime, this technology has to provide regulatory agencies with a significant lifesafety benefit. Furthermore, SHM systems need more effort to be undertaken, owing to its multidisciplinary nature. It requires people with diverse technical expertise and a significant amount of technology integration and validation.

As SHM technology evolves, it is anticipated that the SHM strategies in civil engineering will be used for many purposes, such as to assess structural integrity to normal and extreme loading conditions, to estimate the reliability of the structural system and its components over its lifetime, to predict the remaining service life and to determine the optimal times for inspections and repairs. SHM strategies in actual engineering applications will become a huge challenge for engineers in the coming decades, because of their multidisciplinary and complex nature.

1.4.2 Further Work on SHM for Practical Applications

Although extensive efforts have been made in research on SHM technology, this technology is still in its current embryonic stages of development. For real applications of an SHM strategy, more studies are needed for the health evaluation and maintenance planning of civil structures over their lifetime, as illustrated in [Figure 1.4](#). Further works for the development of effective SHM strategies are discussed in Miyamoto (2009) and Farrar and Lieven (2007), and summarised as follows.

- *Advance of sensing systems with optimised placement of networkable sensors.* More efforts are needed to develop largescale, selforganising and embedded sensing networks for a wide variety of applications. Investigations should focus on developing

cost-effective dense sensing arrays and novel approaches to powering the sensing systems. The number and location of sensors must be optimally determined. Sensors must be properly selected and be sensitive to changes in structural condition caused by damage. The sensing system itself must be more reliable than the structure and its components under monitoring.

- *Advanced signal processing techniques for robust damage identification.* The accurate definition of damage and novel sensitive features (e.g. damage indices) should be developed. These features could be able to distinguish not only the location and the extent of damage but also the types of damage in a structure.
- *Predictive modelling for future loading estimates.* A successful damage prognosis requires the current state assessment and the strength deterioration prediction when subjected to future loading. Future loading should be forecast from the analysis of previous loading histories and reliable predictive modelling techniques.
- *Verification and validation of initial and damage models of a structure.* Reliable identification of the location and extent of damage in a structure largely depends on the quality of the initial physical model of the undamaged structure. Accurate future performance predictions are based on the predictive deterioration model of the structure subjected to cumulative damage over time. Thus, the initial physical model and the predictive damage model must be verified and validated.
- *Reliability analysis for infrastructure management decision making.* From the future loading estimate and the predictive deterioration model, the probability of failure over lifetime can be determined using time-dependent reliability analysis. As a result, the remaining useful life can be estimated, and the optimal maintenance strategy can be determined using lifecycle cost analysis.
- *Need for long-term proof-of-concept studies on SHM systems* . There are very limited long-term SHM investigations performed on actual civil structures. These investigations are difficult to undertake due to their costs and the rapid evolution of sensor technology. However, such investigations are necessary to deal with the environmental and operational variability issues and to develop a methodology for condition based maintenance.

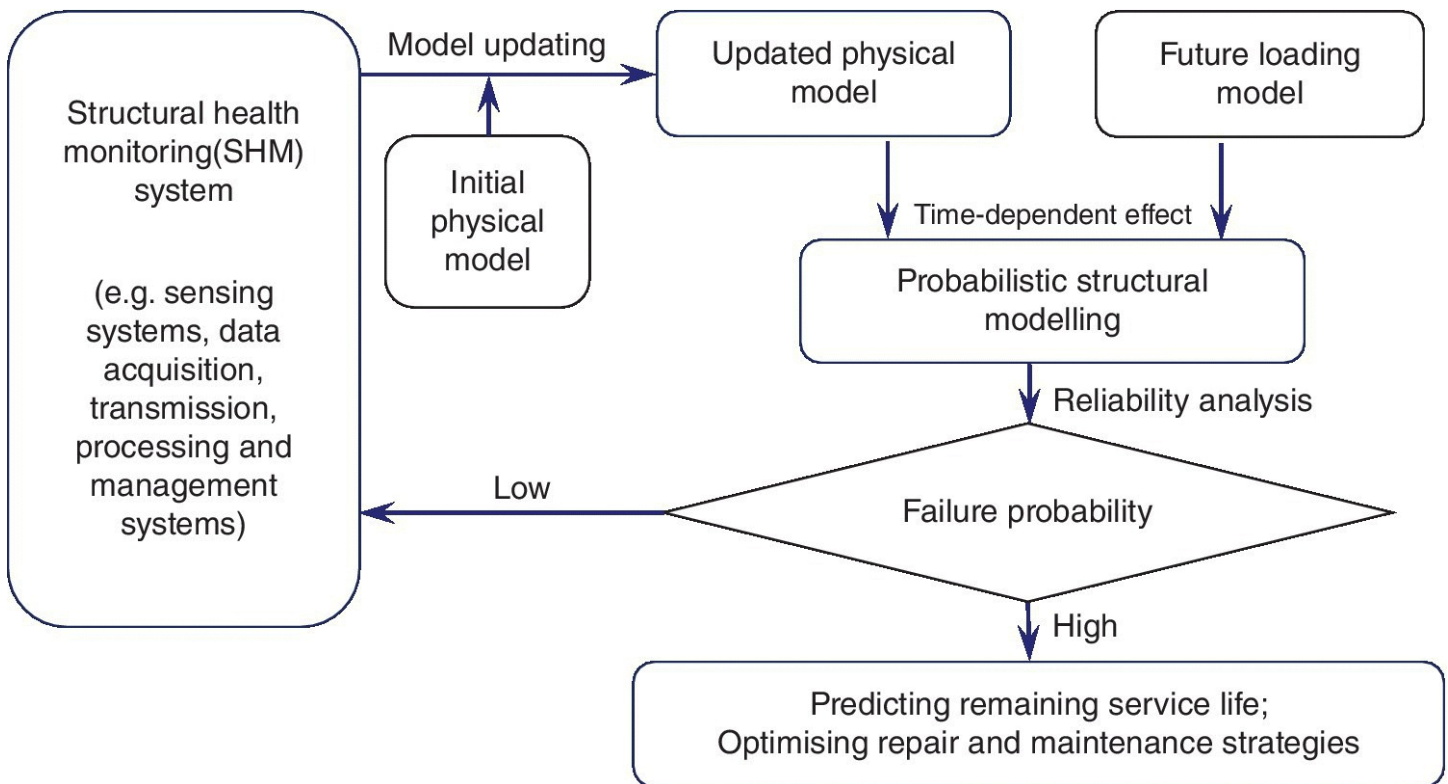


Figure 1.4 SHM strategy for health evaluation and maintenance planning of civil structures.

These topics for further work are currently the main focus of various research efforts by many industries, including civil infrastructure, defence, instrumentation and communication, where multidisciplinary approaches are adopted to advance the current capabilities of SHM strategies.

1.5 Concluding Remarks

The development of robust SHM technology for costeffective infrastructure management has become a major challenge for the engineering community. For a civil structure, it is important and necessary to identify damage in the structure at the earliest possible time. Obviously, SHM technology has the potential to offer tremendous economic and lifesafety benefits. However, there are still limited examples of where SHM technology has made the successful transition from research to practice.

Currently, extensive techniques exist for structural damage assessment, including local non destructive testing techniques and global vibration based damage identification methods. Since all the techniques have their own advantages and disadvantages, there is no general approach that can be used for tackling all kinds of problems in various structures. In general, only damage above a certain size can be detected. It should be noted that a reduction in stiffness does not necessarily mean that there is a decrease in structural strength. The quantification of damage and the prediction of the remaining useful lifetime are definitely the most challenging problems in SHM strategies (Montalvão et al. 2006). Other major challenges of SHM strategies include developing and integrating advanced sensing networks, robust monitoring systems and powerful data processing and analysis algorithms.

Significant future development of an SHM strategy requires multidisciplinary research efforts involving fields such as sensor, signal processing, data telemetry, data interpretation, numerical modelling, probabilistic analysis and computational hardware. In general, these topics are the focus of significant disciplinespecific research efforts. Thus, these technologies must be advanced and integrated with the specific focus of developing SHM strategies. Finally, the problem of global SHM methods is very complex and diverse, and it is difficult to see it being solved in the immediate future. Advancements in SHM will be made in increments, requiring focused and integrated research efforts over long periods of time.

References

- Aktan, A.E., Helmicki, A.J. and Hunt, V.J. (1998) Issues in health monitoring for intelligent infrastructure. *Smart Materials and Structures*7, 674–692.
- Bicanic, N. and Chen, H.P. (1997) Damage identification in framed structures using natural frequencies. *International Journal for Numerical Methods in Engineering*40(23), 4451–4468.
- Brownjohn, J.W.W., De Stefano, A., Xu, Y.L., Wenzel, H. and Aktan, A.E. (2011) Vibration based monitoring of civil infrastructure: challenges and successes. *Journal of Civil Structural Health Monitoring*2(1), 79–95.
- Chang, P.C., Flatau, A. and Liu, S.C. (2003) Health monitoring of civil infrastructure. *Structural Health Monitoring*2(3), 257–67.
- Chen, H.P. (1998) *Structural Damage Identification Using Vibration Modal Data*. PhD thesis Department of Civil Engineering, Glasgow University, UK.
- Chen, H.P. (2008) Application of regularization method to damage detection in plane frame structures from incomplete noisy modal data. *Engineering Structures*30(11), 3219–3227.
- Chen, H.P. and Bicanic, N. (2000) Assessment of damage in continuum structures based on incomplete modal information. *Computers and Structures*74, 559–570.
- Chen, H.P. and Maung, T.S. (2014) Structural damage evolution assessment using regularised time step integration method. *Journal of Sound and Vibration*333(18), 4104–4122.
- Cross, E.J., Worden, K. and Farrar, C.R. (2013). Structural health monitoring for civil infrastructure. *Health Assessment of Engineering Structures: Bridges and Other Infrastructure*, Haldar (ed.), World Scientific Publishing, Singapore.
- Doebling, S.W., Farrar, C.R., Prime, M.B. and Shevitz, D.W. (1996) *Damage Identification and Health Monitoring of Structural and Mechanical Systems from Changes in their Vibration Characteristics: A Literature Review*. Los Alamos National Laboratory report LA 13070MS.

- Ettouney, M.M. and Alampalli, S. (2012) *Infrastructure Health in Civil Engineering*, CRC Press, London.
- Farrar, C.R. and Lieven, N.A.J. (2007) Damage prognosis: the future of structural health monitoring. *Philosophical Transactions of the Royal Society A***365**, 623–632.
- Farrar, C.R. and Worden, K. (2007) An introduction to structural health monitoring. *Philosophical Transactions of the Royal Society A***365**(1851), 303–315.
- Farrar, C.R., Sohn, H., Hemez, F.M., Anderson, M.C., Bement, M.T., Cornwell, P.J., Doebling, S.W., Lieven, N., Robertson A.N. and Schultze J.F. (2003) *Damage Prognosis: Current Status and Future Needs*. Los Alamos National Laboratory report LA14051MS.
- Farrar, C.R., Worden, K. and DulieuBarton, J. (2009) Principles of structural degradation monitoring. *Encyclopaedia of Structural Health Monitoring*, Boller, Chang and Fujino (ed.), John Wiley & Sons, Chichester, UK.
- Frangopol, D.M. and Messervey, T.B. (2009) Maintenance Principles for Civil Structures. *Encyclopaedia of Structural Health Monitoring*, Boller, Chang and Fujino (ed.), John Wiley & Sons, Chichester, UK.
- Karbhari, M.V. (2009) Design principles for civil structures. *Encyclopaedia of Structural Health Monitoring*, Boller, Chang and Fujino (ed.), John Wiley & Sons, Chichester, UK.
- Ko, J.M. and Ni, Y.Q. (2005) Technology developments in structural health monitoring of largescale bridges. *Engineering Structures***27**(12), 1715–1725.
- Miyamoto, A. (2009) *Usage Management of Civil Structures*. *Encyclopaedia of Structural Health Monitoring*, Boller, Chang and Fujino (ed.), John Wiley & Sons, Chichester, UK.
- Montalvão, D., Maia, N.M.M. and Ribeiro, A.M.R. (2006) A review of vibration based structural health monitoring with special emphasis on composite materials. *The Shock and Vibration Digest***38** (4), 1–30.
- National Transportation Safety Board (NTSB) (2008) *Highway Accident Report, Collapse of I35W Highway Bridge, Minneapolis, Minnesota, August 1, 2007*, NTSB/HAR 08/03 PB 2008916203, Notation 7975C.
- Sohn, H., Farrar, C.R., Hemez, F.M., Shunk, D.D., Stinemates, D.W. and Nadler, B.R. (2004) *A Review of Structural Health Monitoring Literature: 1996–2001*. Report LA13976MS. Los Alamos National Laboratory.
- Wong, K.Y. and Ni, Y.Q. (2009) Modular architecture of structural health monitoring system for cablesupported bridges. *Encyclopaedia of Structural Health Monitoring*, Boller, Chang and Fujino (ed.), John Wiley & Sons, Chichester, UK.

2 Sensors and Sensing Technology for Structural Monitoring

2.1 Introduction

Sensors are instruments that detect the state of the system and produce the appropriate information (e.g. structural responses and environmental quantities) for health assessment of civil engineering structures. The sensors are typically used for (a) safety monitoring and active safety control of the structure, (b) usage monitoring such as accumulating strain load data for condition assessment and future design, (c) health monitoring for current state estimate and (d) deterioration monitoring for future performance prediction and optimum maintenance strategy.

There are many types of sensor available for various applications of health monitoring of civil infrastructure. Traditional sensing techniques such as piezoelectric sensors have been extensively used in practice for many decades. Advanced sensing methods such as micro electromechanical systems (MEMS) have become popular in civil engineering applications. Recently, emerging sensing techniques such as fibre optic sensors have shown superior performance compared to traditional sensors. Sensors have to be robust and must operate stably and reliably. The quality of sensors should not be altered by environmental effects such as temperature, humidity and electromagnetic fields. Currently, choosing sensors is mainly a qualitative process based on the expert's judgement. Such a qualitative process has the advantage of simplicity, but it may provide ineffective solutions.

Sensors should be properly selected on the basis of the measurands to be monitored. In order to identify the measurands of structural health monitoring, important issues such as type of the structure, construction materials, environmental conditions and expected damage and degradation phenomena, must be accounted for. In SHM for civil engineering structures, the most common measurands are mechanical (e.g. strain, deformation, displacement, crack opening, stress and load), environmental (e.g. temperature, humidity and pore pressure), and chemical (e.g. corrosion, carbonation, pH and oxidation). A specific measurand can often be monitored by various types of sensor, thus proper selection of sensors is important for a successful SHM strategy.

Recently, a wide range of work using SHM systems based on fibre optic sensing technologies has been carried out on civil engineering structures, e.g. bridges, tunnels, highrise buildings and pipelines. Fibre optic sensors use light as both a transduction and signal transmission mechanism by modulating light parameters, such as phase, polarisation state, intensity and wavelength. Fibre optic sensors offer many advantages, including the capability for embedment in solids (e.g. concrete), wider measuring sensitivity and range, insensitivity to electromagnetic interference, capability for continuous (distributed) sensing and ease of installation (LopezHiguera et al. 2011). In addition, fibre optic sensors can be used for

sensing most needed measurands, such as strain, acceleration, displacement and temperature.

In response to the high costs associated with tethered SHM systems, the use of wireless communication has been investigated for the transfer of data between sensors and the data storage. Such wireless monitoring systems are assembled from lowcost wireless sensors that offer sensing, communication and computing in a single device (Lynch and Loh 2006).

Compared to tethered sensors, wireless sensors have several advantages including limited demands for connecting hardware, capability for higher number of sensors, lower cost per sensor and power sources via innovative methods (e.g. solar, ambient vibration).

The quality of the measurements and thus the quality of SHM achieved largely depends on which sensors are selected and where the sensors are placed on the structure. Although advances continue on innovative sensor systems, there is still considerable uncertainty over deciding on the number of sensors required and their location, in order to obtain adequate information on structural condition. Thus, deciding on an optimal sensor placement is a critical issue in the construction and implementation of an effective monitoring system. An optimal sensor configuration can minimise the number of sensors required, increase accuracy and provide a more robust monitoring system.

This chapter first explores categories of sensors for health monitoring of civil engineering structures. The most common physical and chemical parameters measured in structural monitoring are discussed. To measure these parameters, different types of sensors for the measurements are presented with practical applications. Emerging sensing techniques such as fibre optic sensors and wireless sensors are introduced with real civil engineering applications. Principles for appropriate sensor selection and optimal sensor placement are provided. Finally, a case study is given to show the application of sensors and sensing systems for the health monitoring of a constructed highrise structure.

2.2 Sensor Types

Sensors are one of the most critical components of an SHM strategy, since the quality of the analysis results directly depends on the quality of the data collected. Sensing is a process that produces certain information about the state of a system by interrogating the system (Wong and Ni 2009), as illustrated in [Figure 2.1](#). Sensors can be categorised according to measurand or operating principle. Detailed summaries of various sensors used for structural monitoring can be found from various sources, such as Doebelin 1990, Glisic and Inaudi 2007, Huston 2011, and Reese and Kawahara 1993.

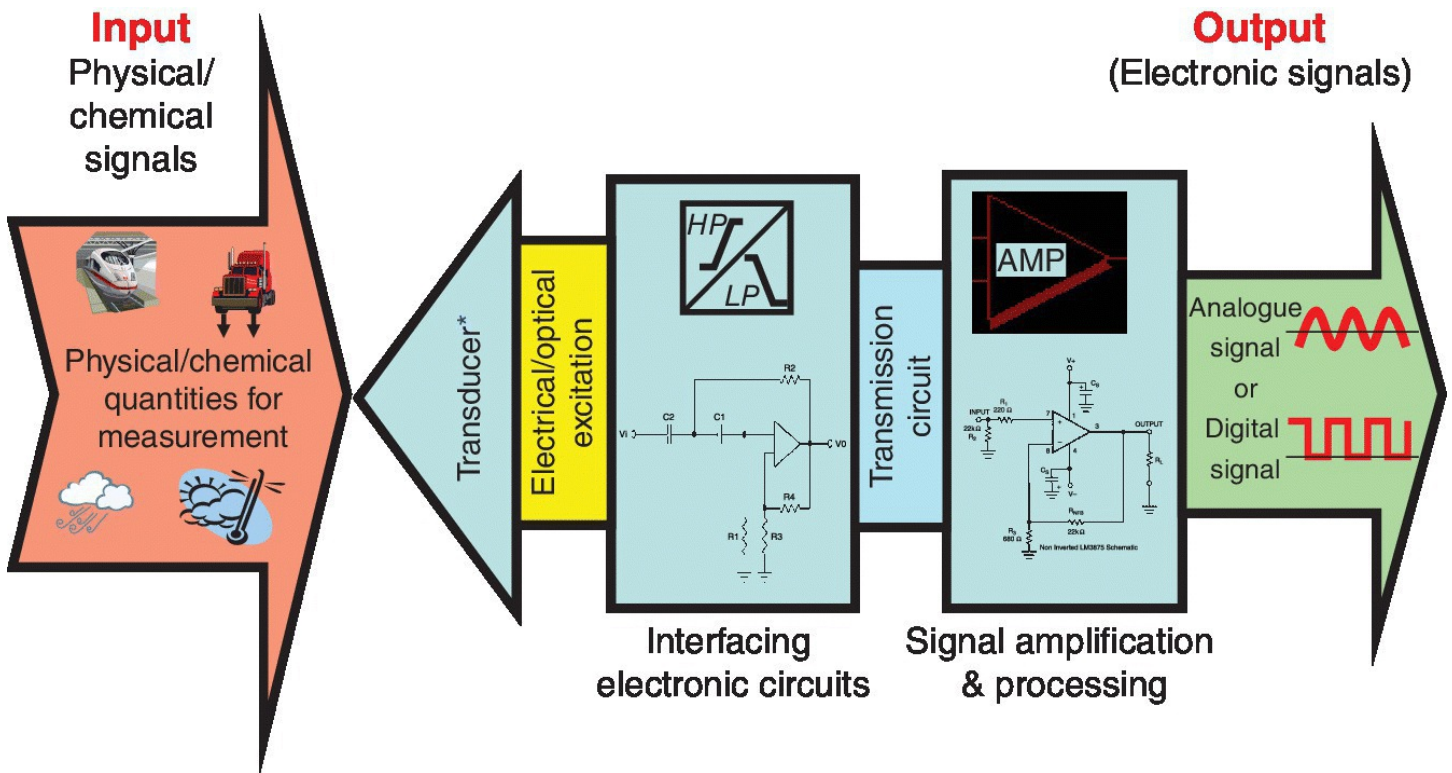


Figure 2.1 Schematic diagram of a typical sensory system, converting measured quantities into analogue or digital signals.

Typical sensing methods for structural monitoring include traditional methods (e.g. ceramics and oxides and electromagnetic), advanced methods (e.g. microelectromechanical and thin/thick film) and emerging techniques (e.g. fibre optic and wireless). [Table 2.1](#) provides typical sensing techniques for SHM applications along with their measurement types, physical principles and reliability issues (Blackshire and Jata 2009).

Table 2.1 Typical sensing methods for structural health monitoring.

Sensor group	Sensor type	Measurement type	Physical principle	Reliability issue
Ceramics and oxides	Piezoelectric	Strain, vibration, ultrasound	Electromechanical	Brittle fracture, disbond
	Pyroelectric	Temperature	Thermoelectric	Brittle fracture, disbond
	Ferroelectric	RFIDs, vibration, temperature	Dipole moment	Brittle fracture, disbond
Electromagnetic	MWM, Foil EC	Cracks, fatigue, corrosion	Dielectric, eddy currents	Electrical short, disbond
Microelectro mechanical	MEMS	Strain, vibration, force	Micromechanical motions	Fracture, wear, short
Thin/thick film	Strain/crack gauges	Strain, crack growth	Electrical resistance	Electrical short, disbond
	Thermocouples	Temperature	Electrical resistance	Oxidation, disbond
	Electrochemical	Corrosivity, chemical	Electrical resistance	Electrical short, disbond
Fibreoptic	EFPI, Bragg grating	Strain, temperature, chemical	Optical reflectance	Brittle fracture, pullout
Wireless	Passive sensor, active sensor	Strain, vibration, force	Sensing interface	Power fault, electrical short

Traditional sensing techniques, such as piezoelectric (PZT) sensors and meandering winding magnetometer (MWM)array sensors, have been proven to be reliable and stable. Such sensors are relatively expensive, and they are typically not integrated with microprocessors. Recently, advanced sensing methods have progressed, such as microelectromechanical systems (MEMS) and thin/thick film. MEMS sensors have the potential to impact a variety of sensing activities, based on their versatility, small size and low cost when manufactured in large numbers. MEMS can be integrated with onboard computing to make these sensors selfcalibrating and selfdiagnosing. The thinfilm strain gauges and corrosivity sensors are useful for structural monitoring. Fibre optic and wireless sensing methods are emerging technology available for practical applications. Distributed fibre optic sensors are capable of

continuous sensing, and cover a large range without loss of accuracy. Wireless sensors are not sensors by their very nature, but rather are autonomous data acquisition nodes. Such sensors can be used to perform their own data interrogation tasks.

In the SHM of civil engineering structures, various types of sensors are often adopted for measuring different types of physical and/or chemical quantities. The key factors considered in the selection a proper type of sensor for monitoring include: type of measurand, type of output signal, type of excitation, measuring range, measuring resolution, measuring accuracy, measuring linearity, sampling rate, environmental operation limits and service life. [Table 2.2](#) provides the examples of some usual factors for selecting sensor types used for monitoring of operation loads and structural responses of civil structures such as bridges (Wong and Ni 2009). [Table 2.3](#) gives the examples of sensor types used for monitoring of environmental factors.

Table 2.2 Examples of sensors used for monitoring of structural responses and operation loads.

Sensor type	Measurand	Measuring range	Measuring accuracy	Resolution	Sampling rate	Excitation /Signal type
Triaxial servotype accelerometer	Acceleration in three orthogonal directions	±30 g	—	1 µg	≥100 Hz	Voltage/ Analogue
Vibration type strain gauge	Strain in concrete	±4000 µε	0.1% of full scale	1 µε	≥20 Hz	Voltage/ Analogue
Load cell	Stress in tendon	100 kN to 10,000 kN	0.25% of full scale	—	≥20 Hz	Voltage/ Analogue
Weldable foil type strain gauge	Stress in structural steel	±3500 µε	0.1% of full scale	1 µε	≥100 Hz	Voltage/ Analogue
Global position system (GPS)	Displacement in three orthogonal directions	—	Horizontal: 3 mm ±0.5 ppm Vertical: 5 mm ±1 ppm	—	≥20 Hz	Voltage/ Digital
Biaxial tiltmeter	Rotation in µ radian	Low gain: ±8000 µ radian High gain: ±800 µ radian	—	±0.1 µ radian	≥20 Hz	Voltage/ Digital
Displacement transducer	Uniaxial displacement	±500 mm	±0.5% of full scale	1 mm	≥20 Hz	Voltage/ Analogue
Dynamic weight in motion station	Axleload; Axlespeed	0.5–20 ton; 5–200 kph	±0.6%; ≥9.0%	—	≥215 Hz	Voltage/ Analogue
High definition video cameras	Image of highway traffic composition	—	—	—	—	Voltage/ Digital

Table 2.3 Examples of sensors used for monitoring of environmental factors.

Sensor type	Measurand	Measuring range	Measuring accuracy	Resolution	Sampling rate	Excit /Sign type

Triaxial ultrasonic type anemometer	Wind speed in three orthogonal direction	0–100 m/s	±1%RMS	0.01 m/s	≥20 Hz	Volta Digit
Ambient temperature and relative humidity sensor	Ambient air temperature	–20 °C to +60 °C	0.1 °C	—	0.02 Hz	Volta Anal
	Relative humidity	0–100%	±2%	0.1%	—	Volta Anal
Temperature inside structural components	Temperature in steel/concrete/pavement section	–40 °C to +60 °C	±0.1 °C	0.01 °C	0.02 Hz	Volta Anal
	Temperature in cable	–40 °C to +200 °C	—	—	Slow	Optic Digit
	Strain in cable	Distributed type (in km)	±100 $\mu\epsilon$	—	Slow	Optic Digit
Electrochemical corrosion cells for embedded steel reinforcement	Corrosion potential	–200 mV to +2000 mV	±0.2 mV	0.2 mV	Slow	Volta Anal
	Corrosion current	–2 mA to +2 mA	±200 nA	200 nA	Slow	Volta Anal
	Concrete resistivity	0 to 7 m Ω	±1 Ω	1 Ω	Slow	Volta Anal
	Linear polarisation resistance	–1 k Ω to +1 k Ω	±1 Ω	1 Ω	Slow	Volta Anal
	Concrete relativity humidity	0–100%	±2%	0.1%	Slow	Volta Anal
	Concrete temperature	–40 °C to +60 °C	±0.1 °C	0.01 °C	Slow	Volta Anal
Electrochemical gas detector	Carbon dioxide	0–5000 ppm	±5% of full scale	±1% of full scale	30 seconds per sample	Volta Digit
	Oxygen	0–25 vol%				
	Chloride	0–3 ppm				
	Hydrogen chloride	0–6 ppm				
	Carbon monoxide	0–150 ppm				

2.3 Sensor Measurements in Structural Monitoring

Sensors are typically chosen according to the measurand – the quantity to be measured. Three

categories of physical and chemical quantities should be considered for measuring in structural monitoring of civil engineering structures: structural responses, environmental quantities and operational quantities.

2.3.1 Structural Responses

The structural responses of civil structures typically include: acceleration; displacement; velocity; strain, stress or force; pressure and tilt.

Acceleration – Accelerometers are sensors that use different principles for measuring accelerations. There is a wide range of different accelerometer types available (Chen and Maung 2014, Wong and Ni 2011), as shown in [Figure 2.2](#). However, many types of accelerometers are not suitable for insitu applications. The main types of accelerometers include:

- piezoelectric accelerometer
- servoaccelerometer
- capacitive accelerometer
- strain gauge accelerometer
- MEMS (capacitive and piezoresistive) accelerometer
- FBG (fibre Bragg grating) accelerometer
- LVDT (linear variable differential transformers) based accelerometer
- laser vibrometer.

(a) Servo-type bi-axial accelerometers of Tsing Ma Bridge



(b) Accelerometer (Tokyo Sokushin Model AS-2000C) of Canton Tower

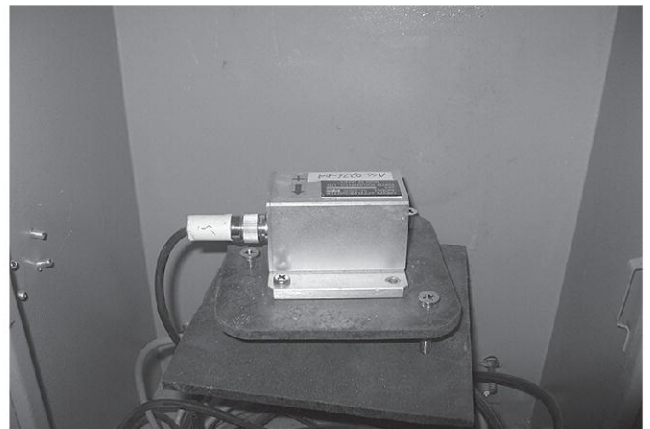


Figure 2.2 Accelerometers used in vibration monitoring of civil engineering structures.

The selection of accelerometers for civil infrastructure applications depends on cost, dynamic range, resolution, noise floor, frequency range, power consumption, cabling requirements and limitations and conditioning requirements (Catbas et al. 2012). During the selection process, the challenging civil structure environments, such as low frequency and low level vibrations,

need to be considered.

Displacement – Structural movements may comprise both dynamic components, caused by seismic, wind and vehicular loading, and quasistatic components, caused by thermal effects, settlement and variation of static loading. Displacements are usually relative values and require definition of a reference datum. They are typically determined with respect to an unloaded or undeformed state. Dynamic displacements related to vibrations can be calculated from accelerations by double integration after highpass filtering. Measurement techniques include conventional survey techniques and advanced methods (Catbas et al. 2012), such as:

- laser and LED devices, e.g. laser Doppler vibrometers (LDVM)
- global positioning system (GPS)
- image tracking via CCD arrays
- surveying and total station
- optical marker tracking
- microwave interferometry, e.g. radar system
- pneumatic system
- contacting displacement measurements, e.g. LVDT.

Laser Doppler vibrometers are useful for bridge dynamic testing for both displacement and velocity measurements. However, LDVMs have limitations to applications for modal testing since they cannot measure multiple locations simultaneously. The global positioning system has been successfully applied for measuring displacements of large civil infrastructure, such as long span bridges, landslides and highrise structures (Ni 2014), as shown [Figure 2.3](#). GPS can offer measurements with an accuracy of a few millimetres at sample rates as high as 20 Hz. GPS is a promising but relatively expensive sensing technology. Alternatively, displacements could be derived from other measurements, such as acceleration, velocity, strain or rotation signals.

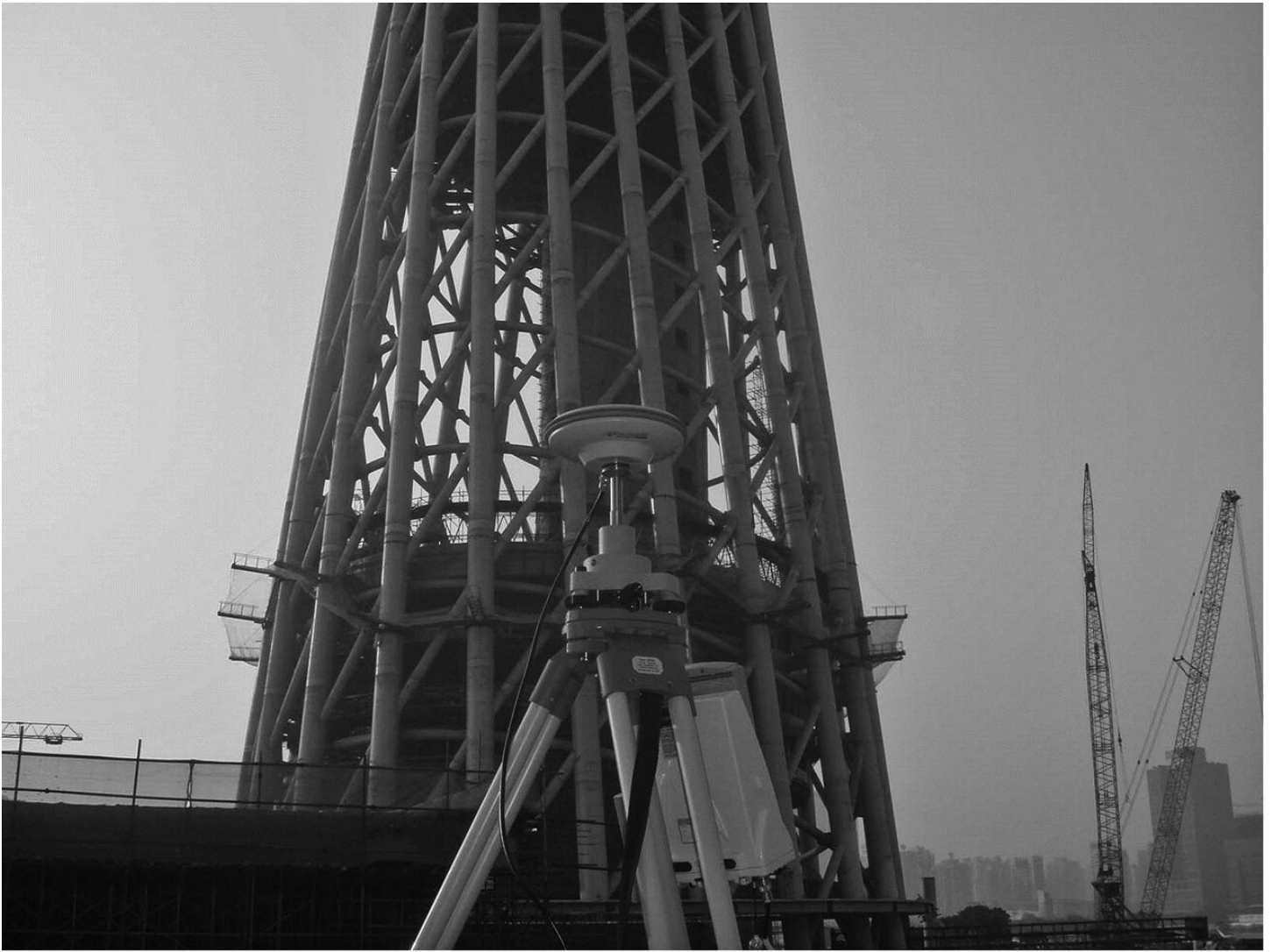


Figure 2.3 Global positioning system (GPS, Leica Geosystems Model 1230) used in construction monitoring of Canton Tower.

Velocity – Velocity measurements are a common feature of seismic studies. LDVMs can measure velocity by Doppler shifting of light frequencies. They are noncontacting and can operate at both short and long ranges, but they are generally expensive and can only measure at a single point at a time. Alternatively, velocities can be measured indirectly by integrating the accelerations measured from LVDT accelerometers.

Strain – Strain gauges are widely used to measure strains in critical structural components, such as girders, rebar and concrete decks. The measured strain data can then be utilised to calculate stresses and evaluate load bearing capacity of the structure. Only differential strain can be measured without knowledge of a baseline value. Due to thermal effects, self temperature compensating type sensors are preferred in the cases with temperature variations. Typical methods used for measuring strains include:

- foil strain gauges or piezoelectric foil gauges
- demountable strain gauges
- strain transducers

- vibrating wire gauges
- fibre optic sensors, e.g. fibre Bragg grating (FBG).

Electrical resistance strain gauges are cheap but often noisy. Vibrating wire strain gauges are popular because of their reliability and repeatability, as shown in [Figure 2.4](#). The fibre optic sensing method is an emerging technology; it can provide integrated, quasidistributed or fully distributed strain measurements.

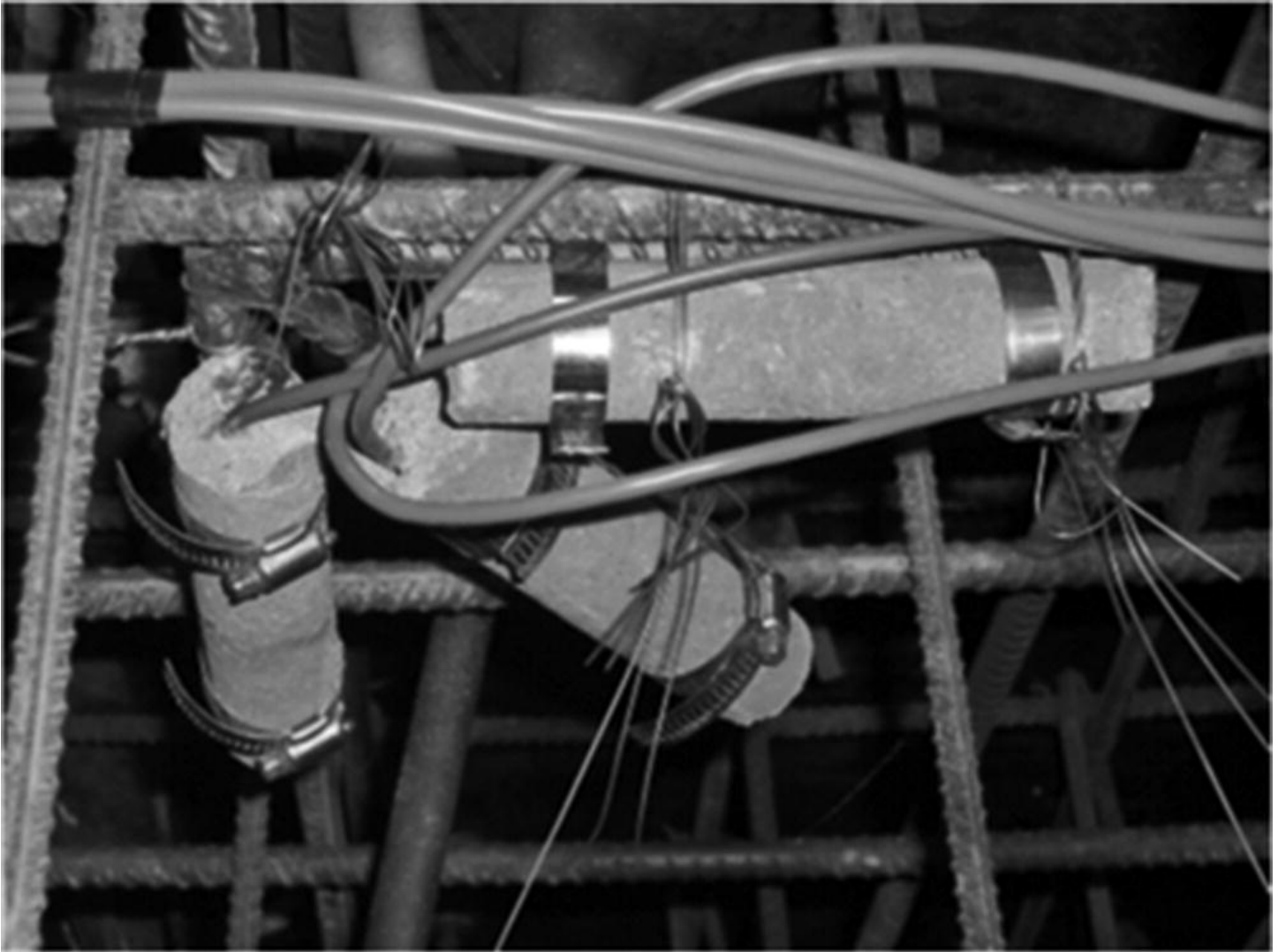


Figure 2.4 Vibrating wire strain gauges (Geokon Model GK4200) installed at the inner tube of Canton Tower.

Stress or force – Direct stress measurement instruments are relatively rare. Vibrating wire stress cells are often used for measurements in tunnel linings, and in concrete boxgirder bridges (Catbas et al. 2012). A form of stress cell using elastomagnetic effects can be used for monitoring of cable forces, such as for posttensioning tendons and stays, main cables and hangers of suspended bridges.

Load cells are mechanical devices for measuring naturally or mechanically induced loads on structures. There are several types of load cells, such as mechanical load cells (hydraulic or pneumatic), strain gauge based load cells (shear beam, ring and pancake and bending beam)

and other load cells (e.g. fibre optic and piezoresistant). Currently, most commonly used load cells are transducers made based on strain gauges and their principles.

Pressure – Pressure measurement technology is similar to force measurement technology, such as by using vibrating wire pressure sensors for static measurements and/or piezoelectric pressure sensors for dynamic measurements, as described in detail in Doebelin (1990). High speed pressure on surfaces can be measured via pressure taps, a standard technology in wind tunnel testing. Static water pressure measurements are common, for example in piezometers for water level measurement (Catbas et al. 2012). Dynamic water pressure measurements are required to understand fluid–structure interactions, particularly for dams.

Tilt – Inclinometers are used to measure inclination (tilt) of structural components due to distress in the system. For example, they are often utilised to assess fixity of bridge girders at supports and to monitor longterm movements of bridge piers, abutments and girders. There are several types of inclinometers, including hydraulically and electrically based. The hydraulic inclinometers are simple, but not suitable for dynamic measurements.

2.3.2 Environmental Quantities

Environmental quantities, such as temperature, wind and corrosion (due to aggressive environments), should be measured during monitoring of civil engineering structures.

Temperature – Temperature measurements are often needed in structural monitoring, since many structural responses and parameters, such as strains, displacements and frequencies, are related to temperature due to thermal effects. There are several methods for measuring temperature, including

- biomaterial temperature sensors
- electrical resistance thermometers
- thermocouple thermometers
- pyroelectric thermometers.

Other types of thermometers include fibre optic temperature sensors and infrared thermometers. Temperature sensors are often installed in other instruments, such as in vibrating wire and fibre optic strain gauges, in order to compensate for thermal effects on instrument performance.

Wind – Various types of anemometer are widely used in fullscale tests of structures, including cupandvane, windmill, propeller and sonic anemometers. Other types include hot wire and laser Doppler anemometers (for wind tunnels) and Doppler sonar for meteorology (Catbas et al. 2012). Cupandvane anemometers are the conventional standard, measuring the horizontal component of wind speed and the compass bearing. Measuring all three components of wind requires devices with propellers along three axes, or sonic anemometers, as shown in [Figure 2.5](#). Technical factors affecting the choice of an anemometer include the number of components resolved and the frequency response. Practical factors include cost, use of moving parts, susceptibility to electromagnetic interference and data output type. For long

term monitoring, reliability should be the main consideration.



Figure 2.5 Anemometer (R.M. Young Model 05103L) installed on Canton Tower.

Corrosion – Steel corrosion affects the durability, serviceability and safety of civil engineering structures, such as bridges. Corrosion is a major problem with bridge structural components, such as stay cables, tendons, steel structural members and the reinforcement in concrete structures. Corrosion measurement methods vary in complexity and size, from use of polarisation resistance to time-domain reflectometry. A popular corrosion measuring method is the half cell technique, owing to its simplicity and ease of implementation. But the method cannot be used for posttensioned construction and often gives localised corrosion rate. Other corrosion measurement techniques include electrochemical techniques, electrical resistance probes, measurement of chloride concentration in concrete and destructive (coring) techniques.

2.3.3 Operational Quantities

Operational quantities include such factors as traffic volume for a bridge and mass loading of an offshore oil platform. Highway traffic loading can be measured by a weigh-in-motion system. [Figure 2.6](#) shows the implementation of dynamic weigh-in-motion stations on Tsing

Ma Bridge (Ni et al. 2015). The information generated from the weighinmotion systems includes the vehicle arrival date and time, bound number, sequence number, lane number, vehicle speed, vehicle class, number of axles, axle weight and axle spacing.

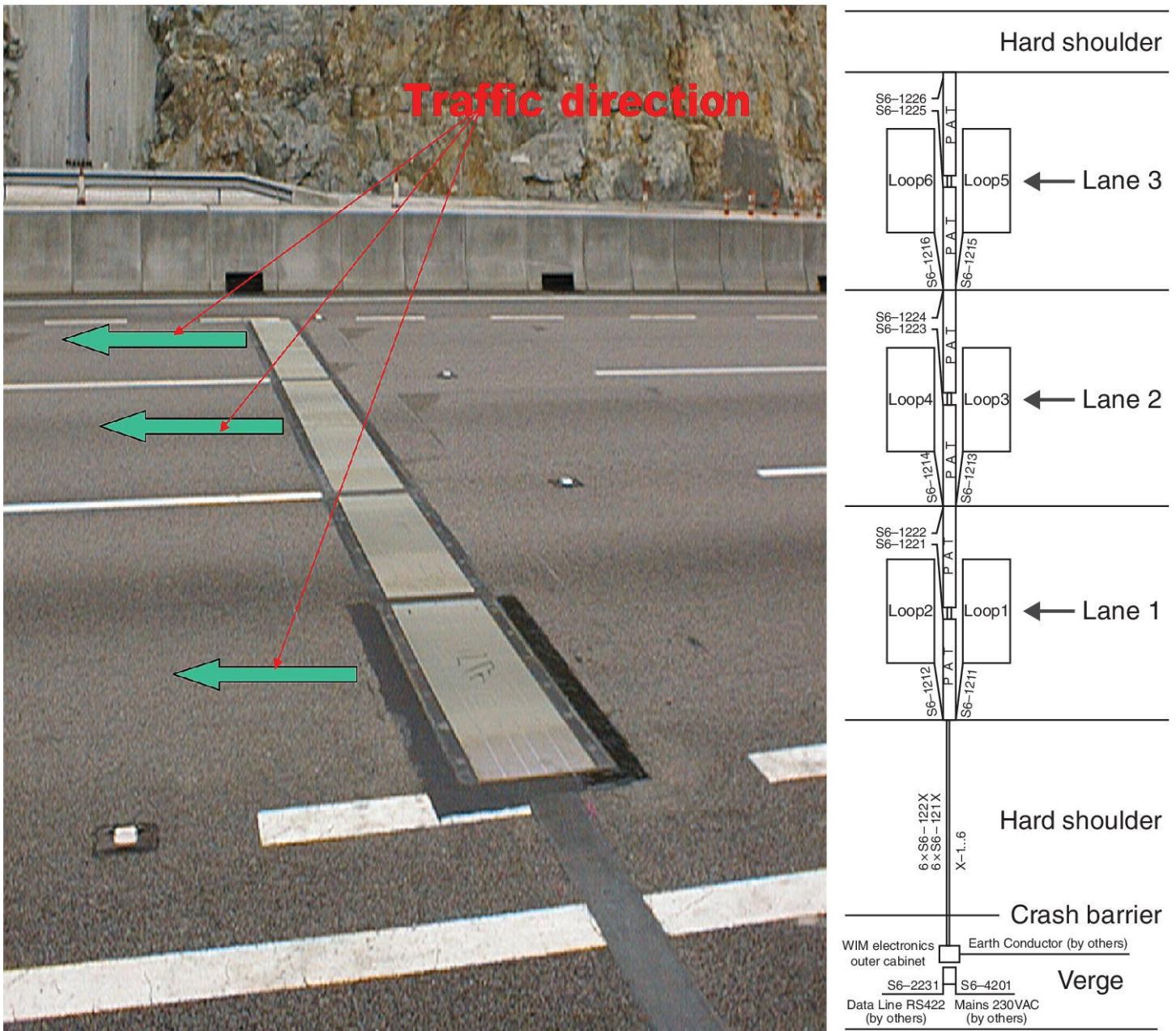


Figure 2.6 Deployment of weighinmotion (WIM) sensors on Tsing Ma Bridge.

2.3.4 Typical Quantities for Bridge Monitoring

The physical and chemical quantities for monitoring of civil engineering structures such as bridges depend on the structural configurations, such as structural arrangement, geometry, materials and site location. For bridges, the physical and chemical quantities for the SHM strategy can be classified into following types, as detailed in Wong and Ni (2009).

- Bridge responses, including the forces in cables, the geometrical profiles in decks, towers and piers, the load or stress histories and the accumulative fatigue damage in instrumented

and key components, and the displacement and stress histories in articulated components. [Table 2.4](#) summarises the details of typical physical quantities for monitoring of structural responses, required monitoring sensory systems and monitoring parameters for a bridge.

- Environmental factors, including wind, temperature, seismic actions, humidity, ship impact, settlement, scouring, corrosion status, etc. [Table 2.5](#) summarises the details of typical physical and chemical quantities for monitoring of environmental factors.
- Operational loads, including highway traffics, railway traffics, ship impacting loads and permanent loads. [Table 2.6](#) summarises the details of typical physical quantities for monitoring of bridge operational loads.
- Bridge characteristics, including the static characteristics (e.g. static influence coefficients, creep or relaxation effects) and the dynamic characteristics (e.g. modal frequencies, mode shapes, modal damping ratios or modal mass participation factors). [Table 2.7](#) summarises the details of typical physical quantities for monitoring of structural characteristics.

Table 2.4 Typical physical quantities of structural responses for monitoring.

Monitoring quantity	Monitoring sensory systems	Monitoring parameters/plots
Cable parameters	<ul style="list-style-type: none"> • Portable servo type accelerometers • Load cells 	<ul style="list-style-type: none"> • Cable frequencies, cable forces • Cable damping ratios and Scruton numbers
Tendon forces	<ul style="list-style-type: none"> • Load cells • Static strain gauges • Electromagnetic gauges (for unbonded tendons) 	<ul style="list-style-type: none"> • Tendon forces • Tendon relaxation
Geometry configuration	<ul style="list-style-type: none"> • GPS and tiltmeters • Level sensing stations • Displacement transducers • Servotype accelerometers • Static strain gauges 	<ul style="list-style-type: none"> • Dynamic monitoring of deformation and stress distribution in global bridge structural system due to instant movements at monitoring locations • Load effects (xy plots) at key/monitoring locations
Stress/force	<ul style="list-style-type: none"> • Dynamic strain 	<ul style="list-style-type: none"> • Stress histories at key/monitoring locations

distribution	<ul style="list-style-type: none"> gauges • Static strain gauges 	<ul style="list-style-type: none"> • Stress/force demand ratios at key/monitoring locations • Principal and VonMises stresses at key/monitoring locations • Strain/stress profiles at key/monitoring sections
Fatigue life estimation	<ul style="list-style-type: none"> • Dynamic strain gauges • Dynamic weigh inmotion stations (bendingplate type) 	<ul style="list-style-type: none"> • Fatigue life estimation due to combined effects of loadinduced fatigue and distortion induced fatigue • Fatigue life estimation due to highway traffic loadeffects
Articulation component responses	<ul style="list-style-type: none"> • Dynamic strain gauges • Displacement transducers • Bearing sensors • Buffer sensors 	<ul style="list-style-type: none"> • Load histories in bearings • Stress demand ratios in bearing • Motion histories in movement joints • Stress and motion histories in buffers

Notes: Static strain gauges should be used for concrete structures; Dynamic strain gauges should be used for steel structures; Dynamic monitoring of deformation and stress distribution must be worked with the finite element model of the global bridge structural system.

Table 2.5 Typical physical and chemical quantities of environmental factors for monitoring.

Monitoring quantity	Monitoring sensory systems	Monitoring parameters/plots
Wind loads	<ul style="list-style-type: none"> • Ultrasonic type anemometers • Propeller type anemometers • Barometers • Precipitation and visibility sensors • Hygrometers 	<ul style="list-style-type: none"> • Wind speeds and wind directions • Wind speeds (mean and gust) and directions • Extreme wind speeds derivation • Terrain factors and wind speed profiles • Wind rose diagrams and wind incidence diagrams • Wind turbulence components and mean wind resultant • Wind turbulence intensities and

		<p>intensity profiles</p> <ul style="list-style-type: none"> • Wind turbulent time and length scales • Wind turbulent spectrum and co spectrum • Wind turbulent horizontal and vertical coherences • Wind responses (xy plots) • Wind transfer functions at key/monitoring locations • Histograms of air pressure, rainfall and humidity
Temperature loads	<ul style="list-style-type: none"> • Temperature sensors for structural steel sections, structural concrete sections, asphalt pavement and air • Thermocouplers or fibre optic sensors for steel cables 	<ul style="list-style-type: none"> • Effective temperatures in typical structural components • Differential temperatures in typical structural components • Air temperatures and asphalt pavement temperatures • Extreme temperatures derivation • Thermal responses in typical structural components • Temperature transfer functions at key/monitoring locations
Seismic and ship impacting loads	<ul style="list-style-type: none"> • Servotype accelerometers 	<ul style="list-style-type: none"> • Response spectra (in terms of acceleration, velocity and displacement) at bases of substructures • Seismic and ship impacting transfer functions at key/monitoring locations
Settlement loads	<ul style="list-style-type: none"> • Settlement sensors/systems • Liquid levelling system 	<ul style="list-style-type: none"> • Settlements at monitoring locations • Derivation of settlement loads on bridge and components

Scouring loads	<ul style="list-style-type: none"> • Scouring sensors/systems 	<ul style="list-style-type: none"> • Speeds and depths of scouring • Derivation of scouring loads at storm and flood conditions
Corrosion status of embedded steel rebar	<ul style="list-style-type: none"> • Corrosion cells • Hygrometers • Temperature sensors • Gas concentration detectors 	<ul style="list-style-type: none"> • Open circuit potentials and corrosion current • Concrete resistance and linear polarization resistance • Relative humidity and temperature in structural concrete • Potential risk of corrosion in structural concrete • Potential risk of crack formation in concrete cover

Note: For avoidance of measuring errors due to wind turbulent flow around the structure, anemometers should be located at ≥ 7.5 m away from the structure.

Table 2.6 Typical physical quantities of operational loads for monitoring.

Monitoring quantity	Monitoring sensory systems	Monitoring parameters/plots
Highway traffic loads	<ul style="list-style-type: none"> • Dynamic weigh-in-motion stations (bending plate type) • Dynamic/static strain gauges • High definition video cameras 	<ul style="list-style-type: none"> • Highway traffic composition in each traffic lane • Highway traffic loading spectrum in each traffic lane • Daily highway traffic characteristics • Highway traffic load effects in key/monitoring locations during traffic jams
Railway traffic loads	<ul style="list-style-type: none"> • Dynamic/static strain gauges • High definition video cameras 	<ul style="list-style-type: none"> • Railway traffic composition at each rail track • Railway traffic loading spectrum at each rail track • Daily railway traffic characteristics

Notes: Static strain gauges should be used for concrete structures; Dynamic strain gauges should be used for steel structures.

Table 2.7 Typical physical quantities of structural characteristics for monitoring.

Monitoring quantity	Monitoring sensory systems	Monitoring parameters/plots
Static influence coefficients	<ul style="list-style-type: none"> • Level sensing stations • GPS and tiltmeters • Dynamic/static strain gauges 	<ul style="list-style-type: none"> • Influence lines (displacement and stress) of each key/monitoring location due to moving traffic loads on each traffic lane or rail track
Global bridge dynamic characteristics	<ul style="list-style-type: none"> • Fixed servo type accelerometer • Portable servotype accelerometers 	<ul style="list-style-type: none"> • Global bridge natural frequencies • Global bridge vibration mode shapes • Global bridge modal damping ratios (derived) • Global bridge modal mass participation factors (derived)

Notes: Static strain gauges should be used for concrete structures; Dynamic strain gauges should be used for steel structures.

2.3.5 Example of an SHM System – a Suspension Bridge (I)

The Tsing Ma Bridge is a twospan suspension bridge carrying both highway and railway traffic. The lengths of the two suspended spans (the main span and the Ma Wan side span) is 1377 m and 352.5 m respectively. The key structural feature of the bridge is the 2160 m continuous spanlength of the steeltrussgirdertype stiffening deck system. The deck system is designed to have two trussactions, namely, the Warren trussaction in the longitudinal direction, and the Vierendeel trussaction in the transverse or lateral direction.

A bridge health monitoring system, called wind and structural health monitoring system (WASHMS), has been installed and operated on the Tsing Ma Bridge since its opening to public traffic in 1997 (Wong and Ni 2011). The monitoring system for Tsing Ma Bridge is composed of a total number of 283 sensors in eight types: anemometers, servotype accelerometers, temperature sensors, weldable foiltype strain gauges (or dynamic strain gauges), global positioning systems, displacement transducers, level sensing stations and dynamic weighinmotion stations. The layout of these sensory systems and their associated data acquisition outstations on the Tsing Ma Bridge are illustrated in [Figure 2.7](#).

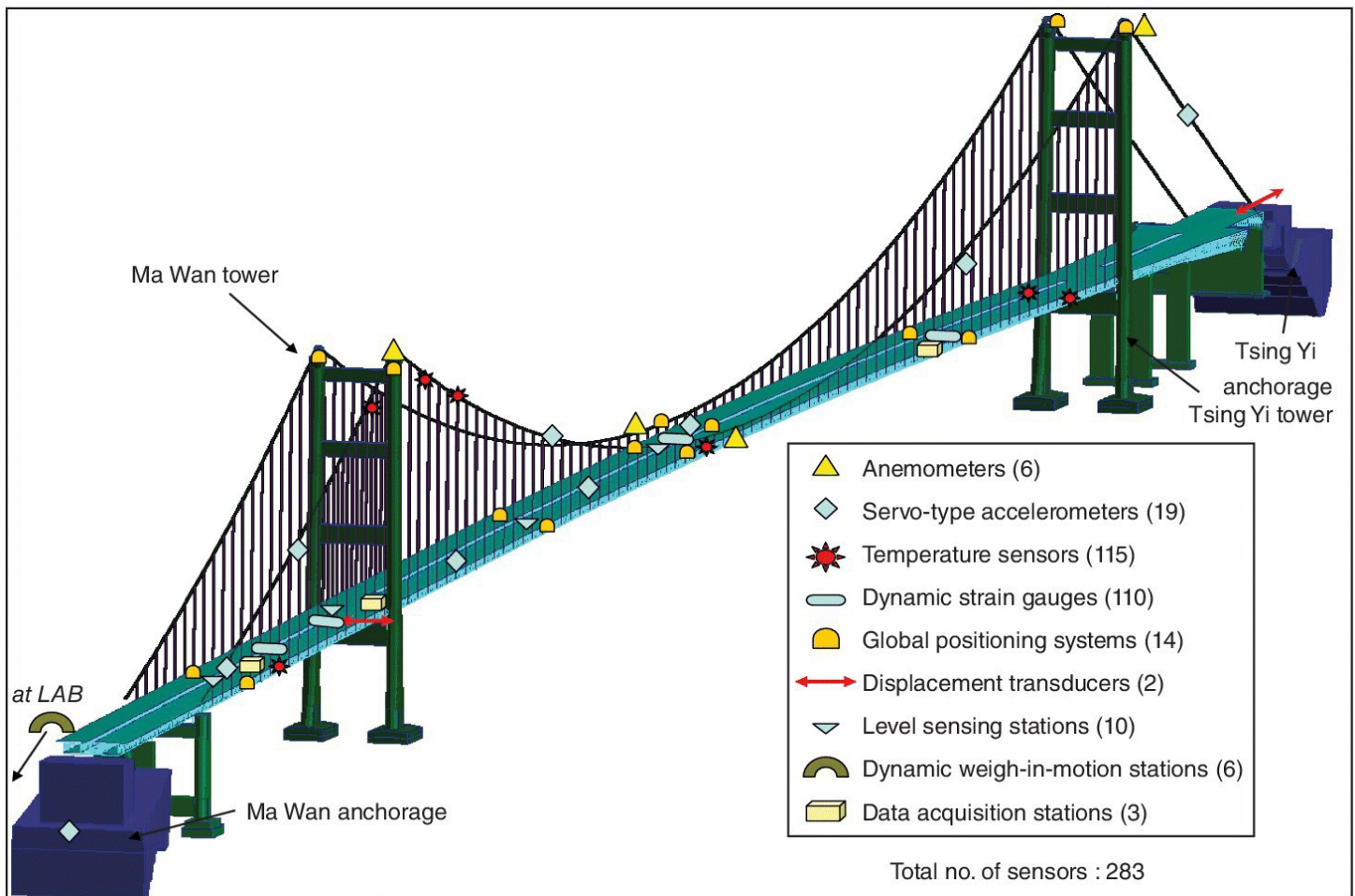


Figure 2.7 Instrumentation layout of sensory systems for structural monitoring in Tsing Ma Bridge.

The structural monitoring system is devised to monitor four major categories of parameters: bridge responses, environments, traffic loads and bridge features. The key monitoring parts include highway traffic load monitoring, railway traffic load monitoring, stress monitoring and fatigue life monitoring. Other parts of the monitoring include wind load, temperature, geometry, global dynamic features, articulation and static influence coefficient. The bridge health monitoring system WASHMS is composed of six integrated modules for monitoring structural condition and evaluating structural deterioration (Wong and Ni 2009), as illustrated in [Figure 2.8](#):

- Module 1 (sensory system), referring to the sensors and their corresponding interfacing units for input signals recorded from various monitoring equipment and sensors, discussed in detail in [Section 2.3.4](#);
- Module 2 (data acquisition and transmission system), composed of data acquisition units and cabling network systems for acquisition, processing, temporary storage and transmission of signals, further discussed in [Sections 3.2.2](#) and [3.3.3](#)
- Module 3 (data processing and control system), referring to hardware and software for executing the functions of system control, system operation display, bridge operation display and postprocessing and analysis of data, further discussed in [Section 3.4.3](#)

- Module 4 (structural health evaluation system), as the core of the bridge monitoring system to provide analysis tools for damage diagnosis and prognosis from the measured and simulated data, further discussed in [Sections 7.3.7, 7.4.4, 7.5.3, 7.6.4, 9.2.4, and 9.5.4](#)
- Module 5 (structural health data management system), composed of a highperformance server, equipped with data management software, and the interfacing platform for the interoperability of data and information, further discussed in [Section 3.5.2](#)
- Module 6 (inspection and maintenance system), composed of a set of portable computers and a toolbox for carrying out the inspection and minor maintenance works on the sensory system, data acquisition units, local and global cabling networks and all display facilities. All information on system design, installation, operation and maintenance is stored and retrieved for references in the computers. The toolbox carries out system inspection activities and minor remedial works in Modules 1 and 2 only.

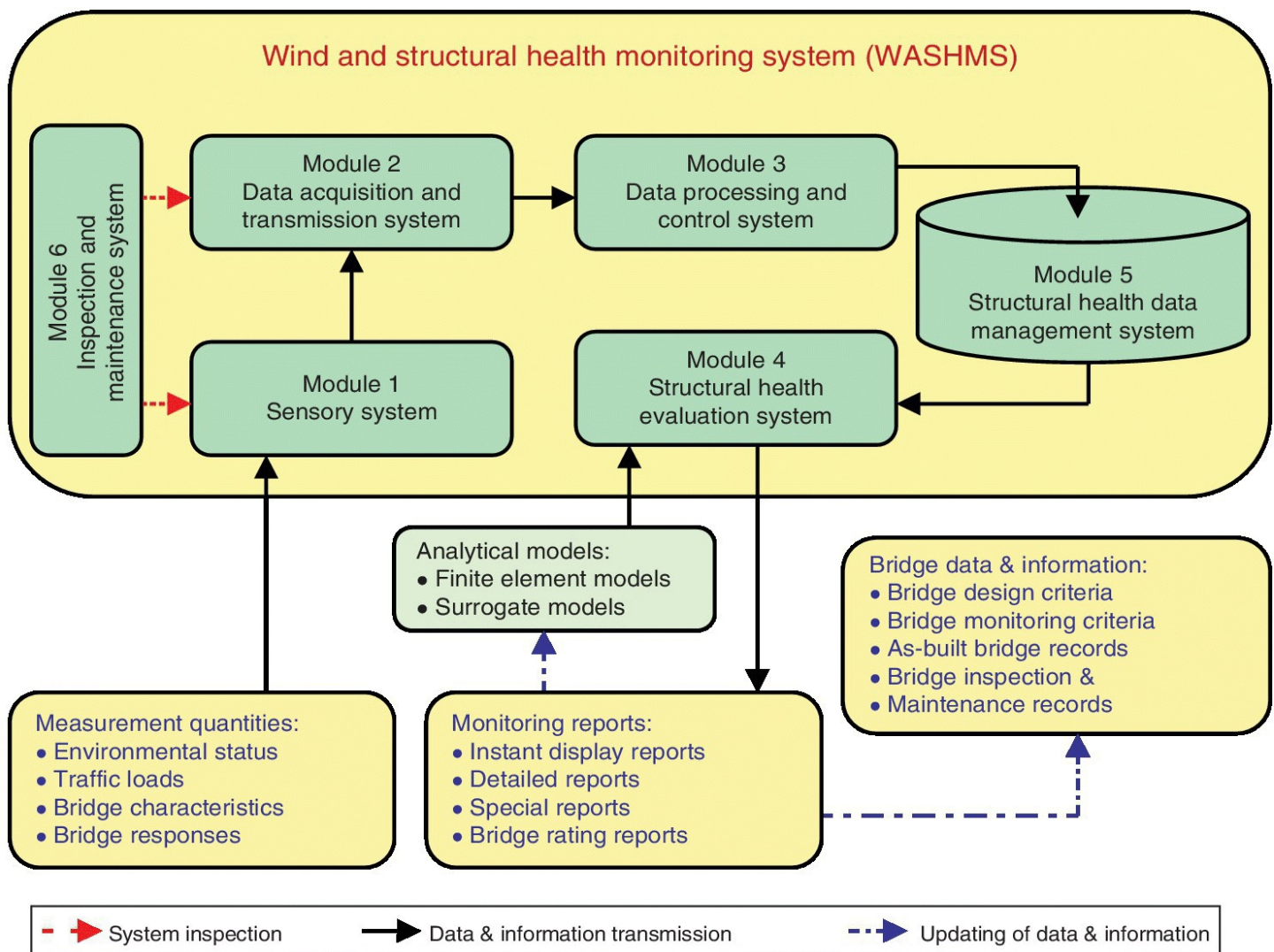


Figure 2.8 Modular architecture and input/output block diagrams of the monitoring system of Tsing Ma Bridge.

The sensory systems (Module 1) used for stress and traffic loads monitoring include: dynamic strain gauges, dynamic weighinmotion stations and servotype accelerometers. These

sensory systems generate three types of timeseries data of strain, acceleration and axle weight and axlespeed, respectively. The systems include three categories (Wong and Ni 2011):

- stiffening deck system stress monitoring, including statistical processing of stress history, stress demand ratios, stress influence coefficients and fatigue life estimation
- traffic loads monitoring, including commercial vehicles spectrum, equivalent standard fatigue vehicle spectrum, accumulated vehicleinduced fatigue damage and train loading estimation
- cable force monitoring, including tension forces in the main suspension cables and suspenders.

2.4 Fibre Optic Sensors

Fibre optic sensors are becoming popular in health monitoring applications for civil infrastructure. Such sensors have many advantages, particularly because of their insensitivity to external perturbations and electromagnetic interference. The principles and detailed descriptions of fibre optic sensors can be found in many books, such as Glisic and Inaudi (2007) and LopezHiguera (2002).

2.4.1 Classification of Fibre Optic Sensors

In general, an optical fibre is a thin flexible strand of dielectric material that is protected mechanically by a polymer coating, which is further protected by a multilayer cable structure designed to protect the fibre from the installation environment. Since glass is inert and resistant to almost all chemicals, even at extreme temperatures, it is ideal for use in harsh environments and is particularly useful for civil engineering applications. Since the light confined in the core of the optical fibres does not interact with any surrounding electromagnetic field, fibre optic sensors are immune to any electromagnetic interferences and are intrinsically safe. The fibre optic sensing technology overcomes most of the limitations encountered in other forms of sensor (Casas and Cruz 2003) and it offers several advantages:

- it is free from corrosion, having longterm stability and allowing continuous monitoring
- it is free from electromagnetic interference, avoiding undesirable noise
- it has an excellent transmission capabilities, allowing remote monitoring
- many measuring points can be multiplexed along a single optical fibre, allowing fully distributed measures
- cabling and sensors are very small and light, making it possible to permanently incorporate them into the structures.

Depending on the spatial distribution of the measurand, fibre optic sensors can be generally classified as point, integrated, quasidistributed and distributed (LopezHiguera et al. 2011).

In principle, fibre optic sensors are based on measuring changes in the physical properties of the guided light. There are four main parameters of the light that can be modulated: phase, polarisation state, intensity and wavelength. Thus, according to the modulated optical parameter, the sensors can be classified in four different categories: interferometric, polarimetric, intensity modulated and spectrometric.

2.4.2 Typical Fibre Optic Sensors in SHM

For structural monitoring of civil infrastructure, typical fibre optic sensors include SOFO interferometric, FabryPérot interferometric, fibre Bragg grating (FBG) and distributed Brillouin and Raman scattering sensors (Glisic and Inaudi 2007).

SOFO interferometric sensors (both static and dynamic systems) are longbase sensors, with a measurement base ranging from 200 mm to 10 m or more. The SOFO system uses low coherence interferometry to measure the length difference between two optical fibres installed on the structure to be monitored (LopezHiguera et al. 2011), as illustrated in [Figure 2.9](#).

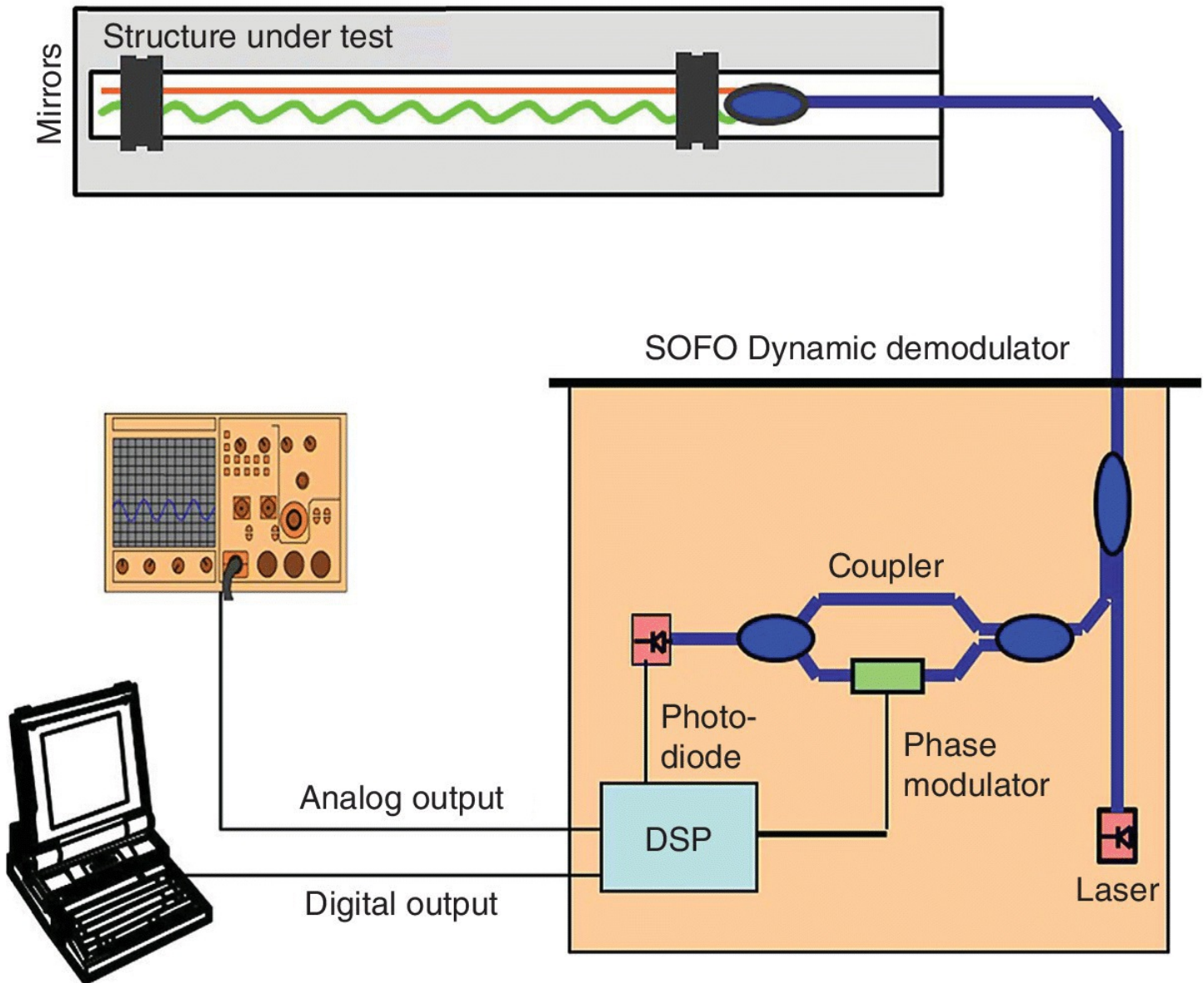


Figure 2.9 Setup of SOFO interferometric sensor system.

(Courtesy of Smartec)

The sensor consists of a pair of singlemode fibres placed in the structure to be monitored. The measurement fibre is pretensioned and mechanically coupled to the structure at two anchorage points, in order to follow its deformations, while the reference fibre is placed loose in the same pipe. The sensors have excellent longterm stability and precision of $\pm 2 \mu\text{m}$ independent of the measurement base. Even a change in the fibre transmission properties does not affect the precision, since the displacement information is encoded in the coherence of the light and not in its intensity. Since the measurement of the length difference between the fibres is absolute, there is no need to maintain a permanent connection between the reading unit and the sensors.

FabryPérot interferometric sensors – FabryPérot (FP) cavities (both passive and active) have been successfully used in sensing applications exploiting measurand-induced changes in one of their cavity parameters. The cavity can be active, for instance integrating a fibre laser

sensor, or passive. An extrinsic FabryPérot interferometer (EFPI) consists of a capillary glass tube containing two partially mirrored optical fibres facing each other, but leaving an air cavity of a few micrometres between them (Glisic and Inaudi 2007, LopezHiguera et al. 2011), as illustrated in [Figure 2.10](#).

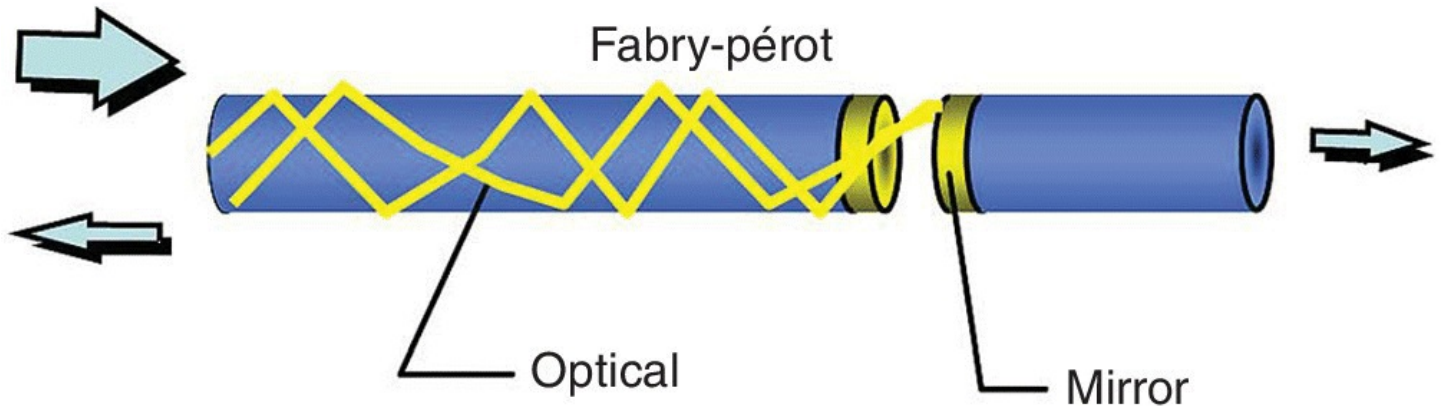


Figure 2.10 Functional principle of FabryPérot sensors.

(Courtesy of Roctest)

When light is launched into one of the fibres, a backreflected interference signal is obtained from the two mirrors. This interference can be demodulated using coherent or lowcoherence techniques to reconstruct the changes in the fibre spacing. Since the two fibres are attached to the capillary tube near its two extremities (with a typical spacing of 10 mm), the gap change will correspond to the average strain variation between the two attachment points. Many sensors based on this principle are currently available for monitoring of civil infrastructure, including piezometers, strain gauges, temperature sensors, pressure sensors and displacement sensors.

Fibre Bragg grating (FBG) sensors – Bragg gratings are periodic alterations in the index of refraction of the fibre core, produced by adequately exposing the fibre to intense ultraviolet light in the region of 244–248 nm, as illustrated in [Figure 2.11](#). The produced gratings typically have a length of about 10 mm. Light at the wavelength corresponding to the grating period will be reflected, while all other wavelengths will pass through the grating undisturbed. The grating period (length) changes with temperature and strain, thus both parameters can be measured through the spectrum of the reflected light. Light traveling down the Bragg grating core that leads to a resonance condition is a special case of the Bragg equation, given by

$$\lambda_B = 2n_{eff}P \quad (2.1)$$

where λ_B is the Bragg wavelength, n_{eff} is the effective refraction index of the fibre core and P is the period of the index modulation. As a consequence of the coupling between the forward and backward propagating modes, a portion of the illuminated light is reflected by the grating while the remainder is transmitted. Both n_{eff} and P depend on temperature and strain, thus the Bragg wavelength is sensitive to both strain and temperature.

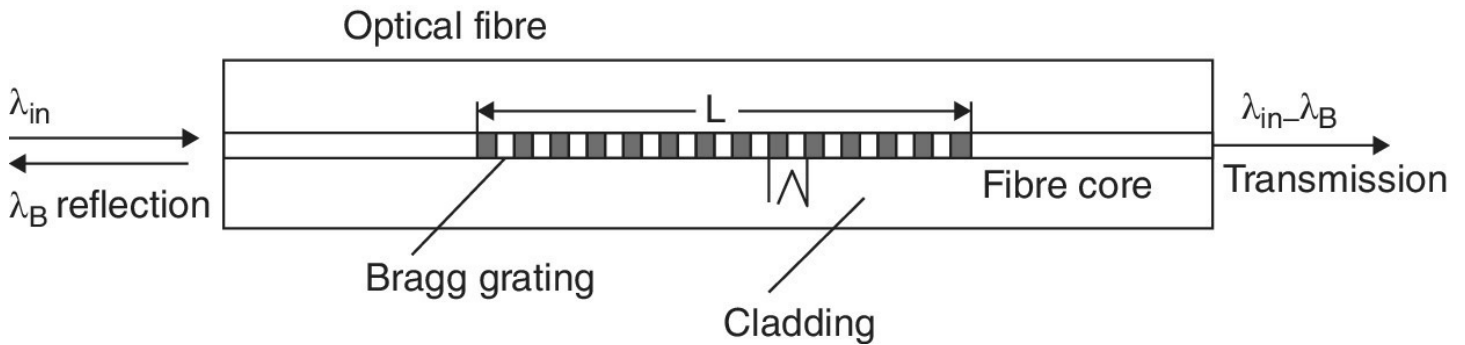


Figure 2.11 Schematic illustration of a fibre Bragg grating (FBG) sensor.

One of the most significant features of an FBG sensor is its selfreferencing capability. It means that no recalibration and/or reinitialisation are needed for this kind of sensor, since the measurands are encoded into the wavelength, which is an absolute parameter. The main benefit with FBG sensors is their multiplexing potential, with several gratings in the same fibre at different locations and tuned to reflect different wavelengths. Accuracy of the order of $1 \mu\epsilon$ and $0.1 \text{ }^\circ\text{C}$ can be achieved with the best demodulators.

Distributed Brillouin and Raman scattering sensors – Brillouin and Raman scattering effects give completely different spectral characteristics, because they are associated with different dynamic inhomogeneities in the silica fibres (LopezHiguera et al. 2011). The Brillouin scattering is a backward process, while the Raman scattering is backward and forward process. If an intense light at a known wavelength is shone into a fibre, a very small amount of the light is scattered back from every location along the fibre itself. Besides the original wavelength (called the Rayleigh component), the scattered light contains components at wavelengths that are higher and lower than the original signal (called the Raman and Brillouin components).

Distributed fibre optic sensors measure physical parameters, in particular strain and temperature, along their whole length. They allow the measurements of thousands of points from a single readout unit. The shifted components contain information on the local properties of the fibre, in particular its strain and temperature. Systems based on Raman scattering typically exhibit temperature accuracy of the order of $\pm 0.1 \text{ }^\circ\text{C}$ and a spatial resolution of 1 m over a measurement range up to 8 km (Catbas et al. 2012). The best Brillouin scattering systems offer a temperature accuracy of $\pm 0.1 \text{ }^\circ\text{C}$, a strain accuracy of $\pm 20 \mu\epsilon$ and a measurement range of 30 km, with a spatial resolution of 1 m.

2.4.3 Fibre Optic Sensors for Structural Monitoring

Fibre optic sensors can be used for monitoring many physical or chemical quantities of civil structures (Glisic and Inaudi 2007). The practical applications of FBG sensors in civil engineering problems such as the SHM of a supertall structure, monitoring of tunnel construction and integrity monitoring of water pipes are discussed in [Sections 2.7.2, 10.4 and 10.6](#), respectively.

Crack monitoring – The current state of many critical concrete structures can be assessed

through the detection and monitoring of cracking in concrete. For example, in concrete bridge decks, crack openings beyond 0.15–0.2 mm will allow excessive penetration of water and chloride ions into the concrete cover, leading to reinforcement corrosion. So far, many optical crack sensors have been developed, such as sensing based on fibre breakage and point sensors, but they may be limited in their applications. Distributed fibre optic sensors can overcome the limitations on the basis of the measurement of the intensity loss due to deformation. They do not require prior knowledge of the crack locations, which is a major advantage over existing crack monitoring techniques (Casas and Cruz 2003). Furthermore, several cracks in concrete can be detected, located and monitored with a single fibre.

Strain monitoring – The commonly used fibre optic sensors for strain sensing include Fabry–Pérot sensors and FBG sensors. The FabryPérot sensing technique has very good accuracy with a maximum resolution of $\pm 0.01 \mu\epsilon$. However, a new calibration is needed every time when the readings are stopped. The FBG technique has less precision with a resolution around $\pm 10 \mu\epsilon$ for standard equipment, but the FBG technique has the advantage of reading absolute values, and thus they are unaffected by interrupted measurements. Many small instruments using FBG sensors have been developed to be embedded into concrete and to monitor the strain. In structural integrity assessment, the strain of the concrete may not be as useful as the strain of the reinforcing bars in the tensioned region of the crosssection. When there are cracks appearing in this region, the concrete releases some stress and the rebar is more strained (Casas and Cruz 2003). Thus, it should be more useful to measure the strain on the reinforcing bars.

Temperature monitoring – FBG sensors have a main limitation of dual sensitivity to temperature and strain. This creates a problem for sensors used for strain monitoring, since temperature variations along the fibre can lead to abnormal strain readings. To tackle the problem, reference gratings are used. Such reference gratings are in thermal contact with the structure, but do not respond to local strain changes. Thus, compensation can be achieved by subtracting the shift of the reference gratings from the shift of the sensing gratings. Many fibre optic sensors are available for temperature monitoring. However, these sensors cannot be embedded, unless a box is used to isolate the sensor from any structural strain.

Corrosion monitoring – Fibre optic sensors were developed to directly monitor the corrosion of the steel reinforcing bars in concrete structures. Some of these sensors are based on the Bragg grating technology which is also used for strain and temperature sensors. The measurements from corrosion monitoring can be read by the same optical system that is used for other types of sensors, such as corrosion, strain and temperature sensors (Casas and Cruz 2003). Fibre optic sensors for corrosion monitoring are based on the concept that the corrosion of reinforcing bars generate an expansive layer of corrosion products at the interface of rebar and the surrounding concrete. Thus, corrosion can be measured from the expansion of the corroded reinforcing bar.

Monitoring of other quantities – Since FBG sensors have many advantages such as low self weight, multiple measuring points, superior performance and better reliability, they can also be used for monitoring other quantities (Casas and Cruz 2003), including inclination of structural

components, vibration of the structure by measuring acceleration, force by using FBG load cells, ice detection on pavements and traffic conditions on bridges.

2.5 Wireless Sensors

Wireless sensors are gaining popularity for monitoring of large civil engineering structures because they are inexpensive and easy to install. Wireless sensors have the ability to collect data in place of traditional cabled sensors, but they do not function as exact replacements. Strictly speaking, wireless sensors are not sensors, but rather are autonomous data acquisition nodes to which traditional sensors (e.g. strain gages or accelerometers) can be attached. Wireless sensors are considered as a platform where mobile computing and wireless communication elements converge with the sensing transducer. Currently, there are a large number of different academic and commercial wireless sensors, as shown in [Figures 2.12\(a\)](#) and (b). A comprehensive review of wireless sensors for structural monitoring is presented in Lynch and Loh (2006).

(a) Commercial wireless accelerometer (BeanDevice® AX-3D Xrange, Courtesy of Beanair).



(b) Academic wireless sensing prototype (after Ni et al. 2011).



[Figure 2.12](#) Wireless sensors for structural monitoring.

2.5.1 Components of Wireless Sensors

Wireless sensors are generally divided into two groups: passive sensors and active sensors. Passive sensors measure a specific physical or chemical quantity by responding passively to the state of the system to be monitored. Passive wireless sensors consist of three functional subsystems: sensing interface, computational core and wireless transceiver. Active sensors, by contrast, generate signals in a controlled manner, and then they sense the response of the system to those signals. An additional subsystem, (an actuation interface) is added in the active sensors to generate the signal (Lynch and Loh 2006), as illustrated in [Figure 2.13](#). Without

wires, wireless sensors require internally stored power for operation. Several power sources can be used in wireless sensing systems, such as conventional batteries, radio frequency identification (RFID), ambient energy sources, such as solar, vibration and thermal.

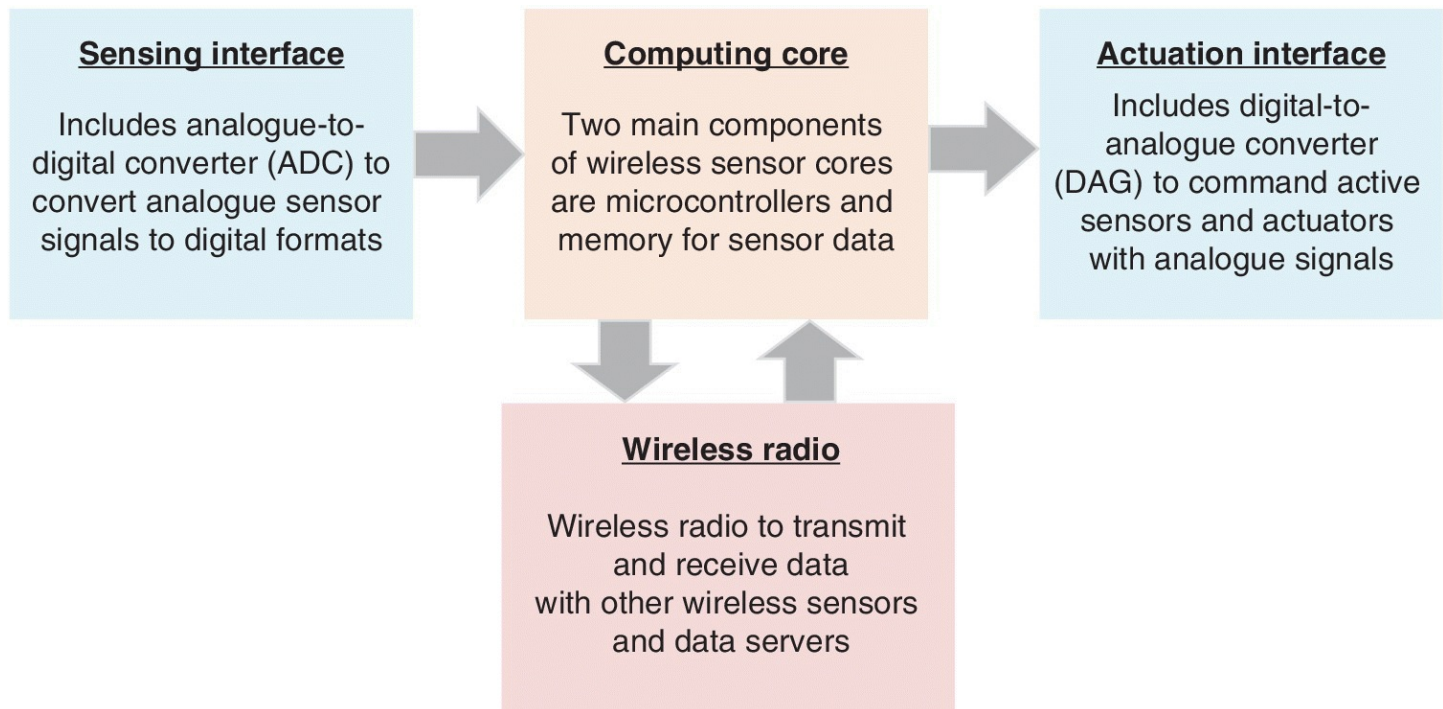


Figure 2.13 Functional subsystem and block diagrams of wireless sensors (after Lynch and Loh 2006).

Wireless sensors contain an interface to which sensing transducers can be connected. The sensing interface is largely responsible for converting the analog output of sensors into a digital representation. Once measurement data has been collected by the sensing interface, the computing core undertakes the local data processing and computational tasks. Then, the computational demands on the central data processing resources are reduced. In order to accomplish these tasks, the computational core is provided by a microcontroller that can store measurement data in random access memory and data interrogation programs in read only memory. In order to have the capability to interact with other wireless sensors and to transfer data to remote data repositories, a wireless transceiver is necessary for both the transmission and reception of data (Lynch and Loh 2006). Finally, an actuation interface provides a wireless sensor with the capability of interacting directly with the physical system. The core element of the actuation interface is the digitaltoanalogue converter (DAC), which converts digital data generated by the microcontroller into a continuous analogue voltage output.

2.5.2 Field Deployment in Civil Infrastructure

The academic wireless sensing prototype shown in [Figure 2.12\(b\)](#) is an integrated wireless monitoring system that supports realtime data acquisition for structural monitoring (Wang et al. 2007). This prototype wireless monitoring system was adopted for exploring the feasibility of wireless sensing technologies in the ambient vibration monitoring of the Canton Tower (Ni et al. 2011) and in construction monitoring of a highrise building (New Headquarters of

Shenzhen Stock Exchange) discussed in [Section 10.3](#). This system incorporates an integrated hardware and software design to implement a simple star topology wireless sensor network. The wireless sensing units are responsible for acquiring sensor output signals, analysing data and transferring data to the base station for storage and further data analysis.

The wireless sensing unit consists of three functional modules: sensing interface, computational core and wireless transceiver. The sensing interface converts analogue sensor signals into a digital format as used in the computational core. The main component of the sensor signal digitisation module is a 4channel, 16bit analoguetodigital (A/D) converter (Texas Instruments ADS8341). The 16bit A/D resolution is sufficient for most applications in civil engineering. The highest sampling rate supported by this A/D converter is 100 kHz. The digitised sensor data is then transferred to the computational core through a high speed serial peripheral interface (SPI) port. Embedded software was developed for the ATmega128 microcontroller to allow the microcontroller to effectively coordinate the various hardware components in the wireless sensing unit. An extensive algorithmic library has also been embedded in the computational core to perform data processing tasks, such as modal analysis and damage detection, on the sensor node itself.

The wireless sensing unit is designed to be operable with two different wireless transceivers: 900 MHz MaxStream 9XCite and 2.4 GHz MaxStream 24XStream. Pin compatibility between these two wireless transceivers makes it possible for the two modules to share the same hardware connection in the wireless unit. This dualtransceiver support offers the wireless sensing unit the opportunity to be used in different regions around the world. This support also allows the sensing unit to have more flexibility in terms of data transfer rate, communication range and power consumption. For example, although the 9XCite transceiver requires less power consumption, it can only be used in the region where the 900 MHz band is for free public usage. For this reason, the 24XStream transceiver operating on the open 2.4 GHz was employed in the applications of structural monitoring of the Canton Tower and the highrise building. Through the associated wireless transceiver, the base station can communicate with the wireless sensing units that are spatially distributed throughout the structure.

2.6 Optimum Sensor Selection and Placement

For effective monitoring of civil structures, selecting the most appropriate sensors and determining an optimal sensor placement are critical issues. An optimal configuration of sensors can reduce the costs, increase accuracy and provide a more robust sensing system.

2.6.1 Factors for Sensor Selection

There are many factors and parameters that affect the selection of appropriate sensors for monitoring of civil structures. The sensor selection largely depends on specific conditions of the structural monitoring. In general, the following factors should be considered in selecting sensors (Ettouney and Alampalli 2012).

- *Objectives of sensing* – Consideration of the objectives is a common and important factor in any SHM project. The objectives can be such as condition assessment, research, validating design assumptions, cost implication and hazardspecific safety.
- *Type of structure* – The type of sensors to be used generally depends on the type of structures to be monitored. Parameters such as material types (e.g. steel, concrete), design life of structure, site location of structure (e.g. underground, below water) have to be considered in sensor selection.
- *Quantities to measure* – The type of physical and chemical quantities for sensing decides the selection of appropriate sensors. For example, strains can be directly measured using strain gauges, while stress can be obtained from the measurements of strain.
- *Sensor physical attributes* – The physical attributes of sensors include size, weight, ruggedness and interaction effects with the structure. These attributes can affect the accuracy of test results.
- *Sensor properties* – The important properties of sensors include bandwidth, sensitivity, range and resolution of sensing. Sensors with a high frequency range tend to be more sensitive to local response, requiring a sensor with a large bandwidth. In general, the sensitivity reduces, as the bandwidth increases. The range of measurements needs to be estimated before sensor selection, and resolution is often coupled with measurement range.
- *Operational environments* – Some sensors are designed for laboratory tests and may not be suitable for field applications under aggressive environments. In harsh operating conditions, proper protection is needed to meet the necessary requirements for sensor operation against hostile conditions, such as low or high temperature, humidity, chloride and acid.
- *Cost* – The total cost for a structural monitoring system includes the costs for sensors, additional hardware, labour, maintenance and expertise for data analysis and report preparation. The total cost also depends on the monitoring time period.
- *Number of sensors and sensor locations* – When deciding on the number and location of sensors, two main considerations are whether or not the sensing system should be optimal and how much redundancy is desired. It is important that the expected damage type gives known, observable and statistically significant effects in features derived from the measured quantities at the chosen sensor locations.

Calibration and stability of sensors are essential for providing accurate measurements. Most sensors are calibrated at a specialised calibration facility. Calibration may generate several important issues, including both precision and flexibility, for example how to calibrate a 32 bit sensor over its entire dynamic range, and how to calibrate a precise sensor versus a coarse sensor (Farrar et al. 2003). Reliability and confidence in the sensors are prime considerations for successful SHM strategies.

2.6.2 Optimal Sensor Placement

In health monitoring of a large civil structure, the number of sensors is typically small when compared with the size and complexity of the structure. Thus, the locations of the sensors need to be determined optimally to ensure quality of damage identification and efficiency in both cost and computation. Successful sensor placement heavily depends on the knowledge and experience of the users. The sensor placement optimisation problem has been investigated in many studies, such as by Meo and Zumpano (2005).

The optimisation problem can be considered as threestep decision process: number of sensors, sensor placement optimisation and performance evaluation (Barthorpe and Worden 2009). Firstly, for example, in vibration testing the number of sensors required cannot be less than the number of mode shapes to be identified, with an upper limit usually applied either by the cost or availability of a testing facility. In practice, more sensors may be used to allow the mode shapes to be visualised (Chen et al. 2012). Then, for the limited number of sensors available, appropriate deployment of these sensors should be chosen, so that a suitable sensor placement performance measure is optimised. Finally, the performance of the chosen sensor sets should be assessed.

Many methods have been proposed to determine the optimum locations for sensor placement. These methods mainly rely on the concept of assessing all the locations of the candidate sensor set against an objective function, and then iteratively deleting those sensors that perform least well, until the required number of measurement locations remain. Typical approaches used in the optimisation problem include:

- effective independence
- average drivingpoint residue
- effective independence drivingpoint residue
- kinetic energy method
- eigenvalue vector product
- mutual information
- information entropy method
- sensitivity based methods.

The details of the above approaches are described in Barthorpe and Worden (2009) and Meo and Zumpano (2005). The solution for the sensor placement optimisation problem can be searched by using the genetic algorithms or combinatorial optimisation algorithms such as ‘ant colony metaphors’.

In practice, other factors should be considered in searching for optimal sensor placement. For example, for bridge structures, appropriate types of sensors will be deployed at key locations where the measured results could be able to carry out the following functions:

- validation of adopted design assumption and design parameters: sensors should be deployed at locations with responses (e.g. strain, stress, displacement) to be sensitive to

damage such as fatigue-induced damage

- monitoring the structural condition and durability performance of the structure at key locations under its in-service conditions
- development of current and future environmental and operational load models for the evaluation of current and future load effects
- validating relevant finite element models for structural health evaluation
- carrying out structural performance assessment of the global structural system
- intercalibration of measurement results from various types of sensory systems.

2.7 Case Study

The Canton Tower in Guangzhou, China, is a supertall tube-in-tube structure with a total height of 618 m, as shown in [Figure 2.14](#). The main tower, 454 m high, is composed of a reinforced concrete inner structure with an elliptical cross-section of 14×17 m and a steel lattice outer structure. The cross-section of the outer structure has a profile of varying oval that decreases from 50×80 m at the ground to the minimum of 20.65×27.5 m at a height of 280 m (waist level), and then increases to 41×55 m at the top of the main tower. There are 37 floors connecting the inner and outer structures. The antenna mast of 164 m high, founded on the top of the main tower, is a steel spatial structure with an octagonal cross-section of 14 m maximum diagonal (Chen and Huang 2012, Ni et al. 2008). The Canton Tower serves multiple functions, including TV and radio transmission, sightseeing and cultural entertainment.

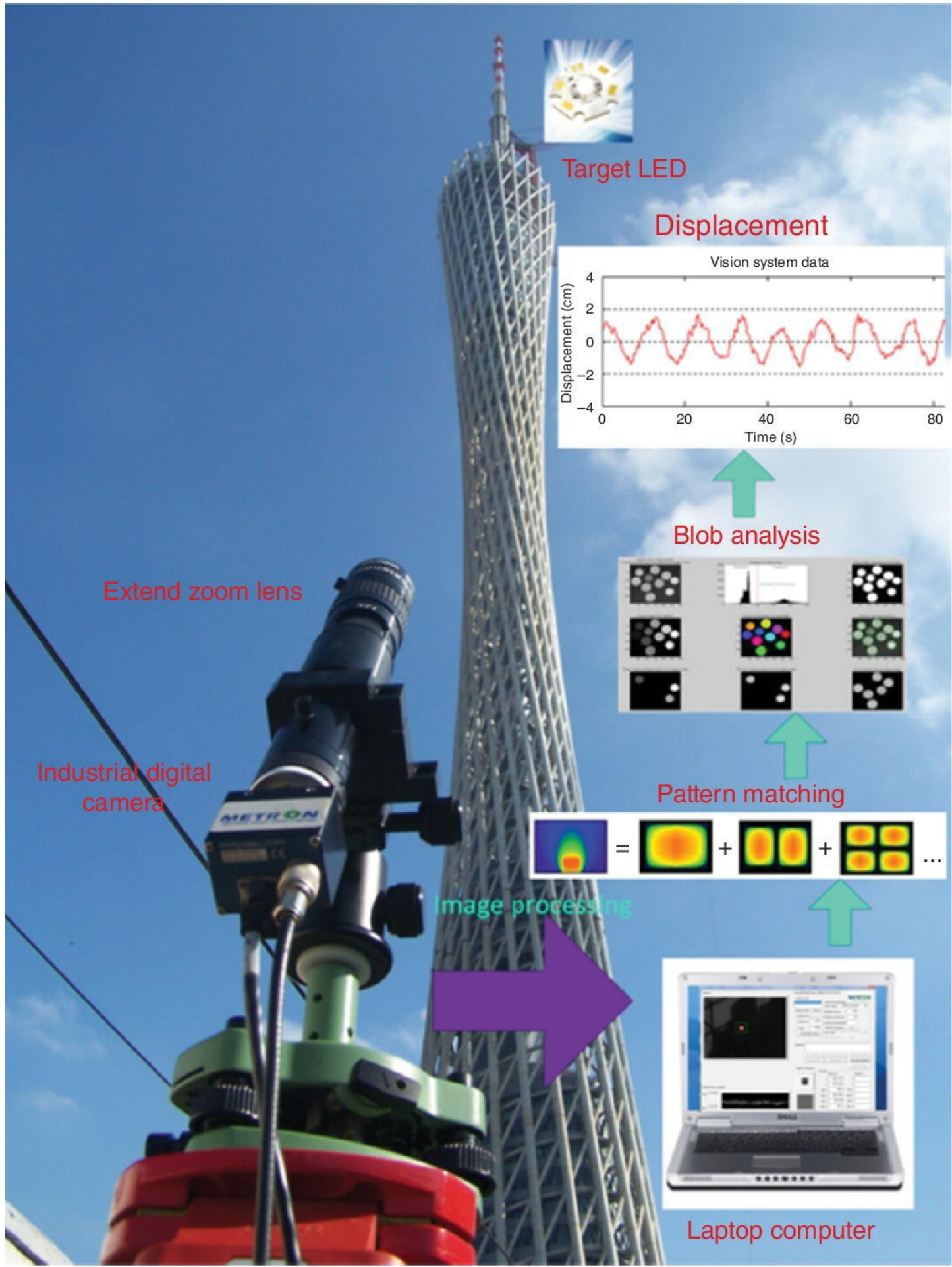


[Figure 2.14](#) Photo of Canton Tower.

2.7.1 Sensors and Sensing System for SHM

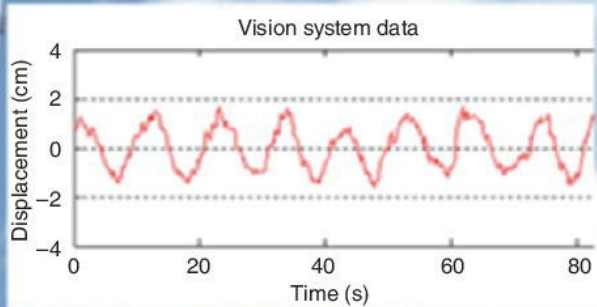
The SHM system for the Canton Tower consists of six modules (Ni et al. 2008, Ni 2014): (a) sensory, (b) data acquisition and transmission, (c) data processing and control, (d) data management, (e) structural health evaluation (f) inspection and maintenance. There are a total number of 16 types of sensors installed on the structure: weather station, total station, anemometer, wind pressure sensor, zenithal telescope, level sensor, tiltmeter, theodolite, global positioning system (GPS), vibrating wire strain gauge, thermometer, accelerometer, seismograph, corrosion sensor, digital video camera and fibre optic sensor. These sensors are deployed for monitoring the three categories of parameters: (a) loading sources, e.g. wind, seismic and thermal, (b) structural responses, e.g. strain, displacement, inclination, acceleration and geometric configuration, (c) environmental effects, e.g. temperature, humidity, rain, air pressure and corrosion.

These various installed sensors offer a platform to explore sensor and data (information) fusion for structural monitoring. In order to calibrate the dynamic displacement measurement data acquired by a GPS system, a visual inspection system, as shown in [Figure 2.15](#), was developed and used together with the GPS system. The visual inspection system is capable of remote longdistance (500–1000 m) dynamic displacement measurement with a sampling frequency 5–60 Hz.



Target LED

Displacement



Blob analysis



Pattern matching

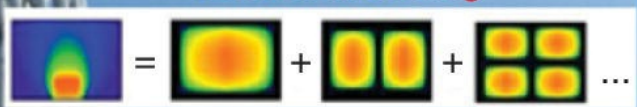


Image processing



Laptop computer

Extend zoom lens

Industrial digital camera

[Figure 2.15](#) Vision inspection system of Canton Tower.

The SHM systems for the Canton Tower are designed for both in-construction monitoring and in-service monitoring. [Figure 2.16](#) illustrates the deployment of sensors and data acquisition substations for in-service monitoring. The in-construction monitoring system has 527 sensors, while the in-service monitoring system has 280 sensors. Thirteen data acquisition substations are employed for in-construction monitoring, while six data acquisition substations are utilised for in-service monitoring. A total of 12 cross-sections have been selected for in-construction monitoring, and a total of five cross-sections have been selected for in-service monitoring. The selected sections are expected to suffer large stresses under certain construction and in-service loadings or to experience an abrupt change in lateral stiffness. These monitoring sections were determined by finite element analysis on the structure at critical construction stages and the completed stage. As shown in [Figure 2.16](#), accelerometers are positioned at many cross-sections to capture complete modal shapes and verify the effectiveness of vibration control devices to be installed.

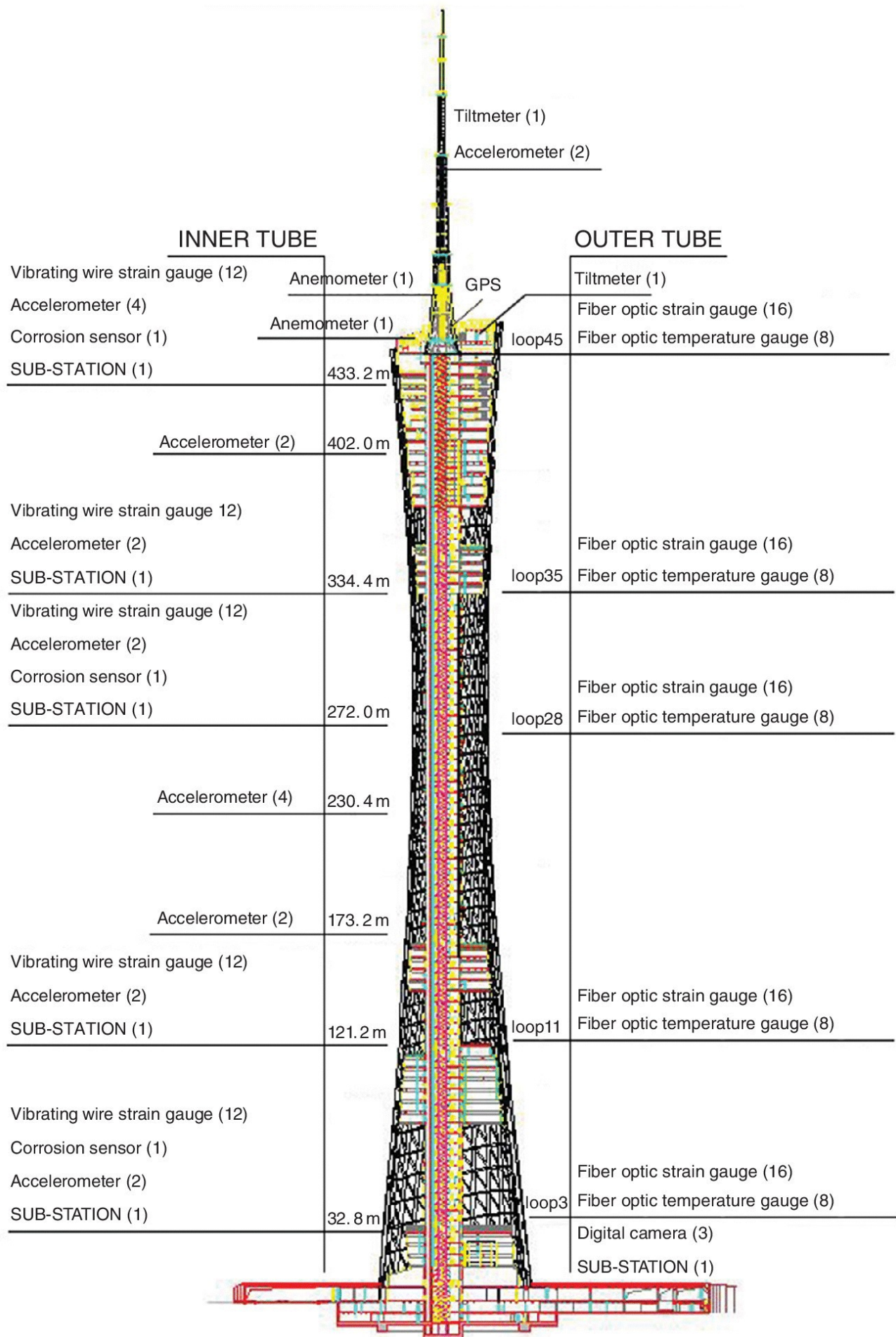


[Figure 2.16](#) Deployment of sensors and data acquisition substations on Canton Tower for in service monitoring.

2.7.2 Installation of FBG Sensors

A fibre optic sensing system based on fibre Bragg gratings (FBGs) is implemented on the Canton Tower to provide longterm, realtime strain and temperature monitoring (Ni et al. 2008, Ni 2014). The FBG sensors designed for inservice monitoring are also deployed in synchronism with the construction progress. The sensing system comprises 120 FBG sensors which can be monitored at speeds of up to 50 samples per second. [Figure 2.17](#) shows the system configuration where five groups of 24 FBG sensors are employed to monitor the outer tube of the structure at different heights. Each group of the 24 sensors is arranged into four sixFBG sensor arrays. Four of the FBGs in each array are allocated for strain measurement and the other two for temperature measurements. Both the FBG strain and temperature sensors employed are specifically designed to cope with the hostile environment outside the tower. Each FBG sensor is attached to 0.8 mm thick SS 302 stainless steel to protect it from handling and to ensure longterm reliability. The steel packaged FBGs permit them to be welded directly onto the structure. The sensing system is designed to measure temperature with an accuracy of 0.1 °C over the temperature range of -40 °C to +120 °C and strain with an accuracy of 1 $\mu\epsilon$ and strain limits of $\pm 2500 \mu\epsilon$.

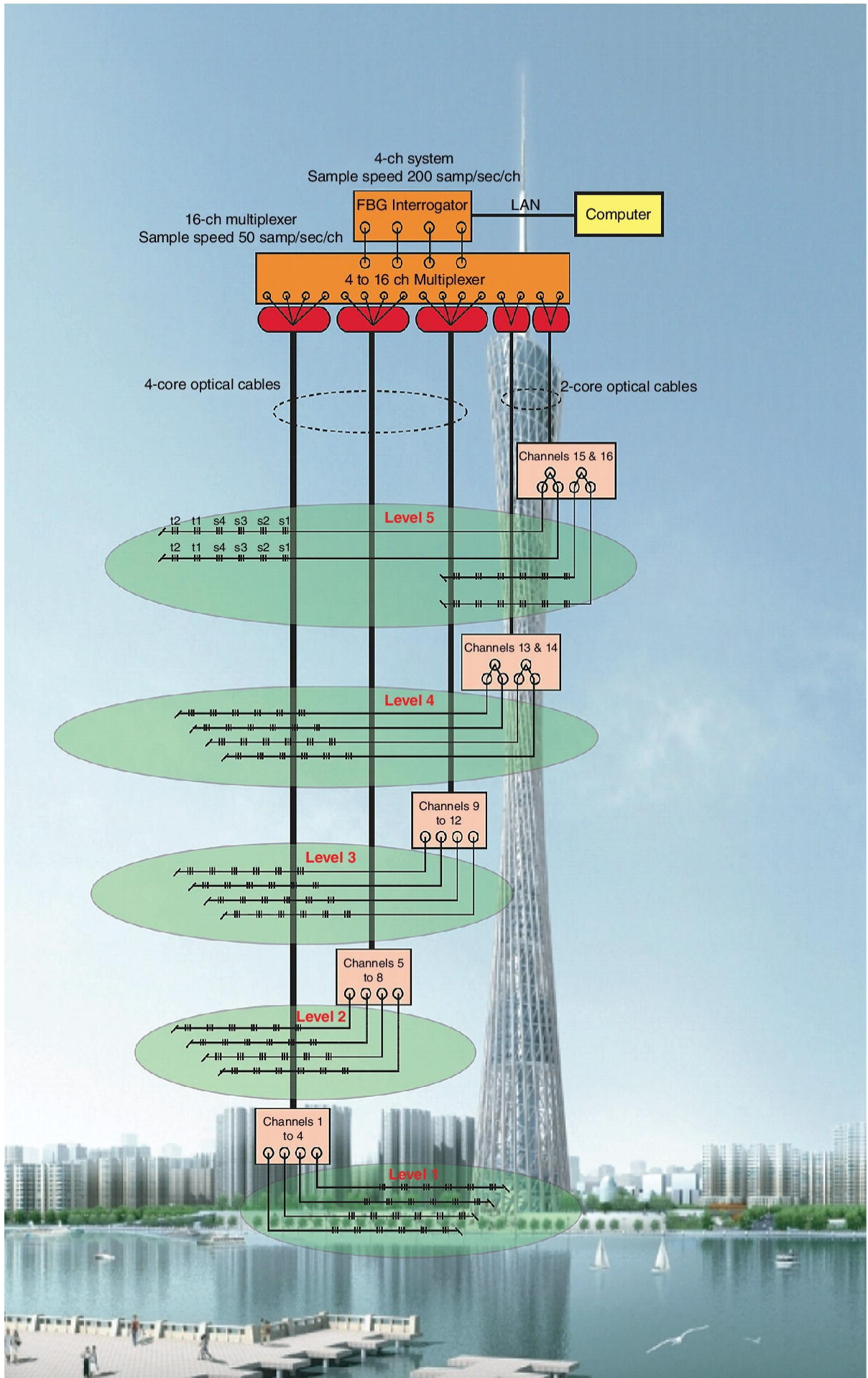


Figure 2.17 Fibre Bragg gratings (FBG) sensing system for Canton Tower.

The FBG interrogation system adopts a wavelength-tunable fibre laser. Its emission wavelength can be tuned at speed of 200 Hz with each cycle covering the entire reflection wavelength of the FBG sensors. The FBG interrogator has a wavelength tuning range of 80 nm. The interrogator has four outputs that are increased to 16 outputs using an optic multiplexer. Each of the 16 channels covers 80 nm but operates at a quarter of the original sampling speed (i.e. 50 Hz). Armoured optic fibres are used to connect all the FBG sensors to the FBG interrogation system. The FBG sensors are secured to a stainless steel tray which also keeps the armoured optic cables in position. During installation, the two metal stubs are welded onto the surface of steel structural members. Then, the FBG sensor tray is placed around the metal stubs before welding the FBG package onto the structure. A metal cover measuring $10 \times 70 \times 140$ mm for protecting the FBG sensor is screwed onto the metal stubs and sealed with a sealant to prevent water seeping into the sensor housing.

2.8 Concluding Remarks

Sensors are an integral and essential component in the SHM system of civil engineering structures. Various types of sensors are normally adopted for measuring different types of physical and chemical quantities. The usual factors considered in selecting a proper type of sensors for monitoring include: type of measurand, type of output signal, type of excitation, measuring range, measuring resolution, measuring accuracy, sampling rate, environmental operation limits and service life. From the installed sensors, physical and chemical quantities that can describe the state of the structure are transmitted to the enduser by sensing networks. These measurable quantities can be structural responses, environmental quantities and operational quantities of the structure concerned. There are several different ways for any given physical or chemical quantity to be measured. When choosing sensors for specific tasks, the sensor properties need to be considered.

Fibre optic sensing technology is attractive in the cases where it offers superior performance, compared to the more proven, conventional sensors offering. Fibre optic sensors offer many advantages, such as improved quality of measurement, better reliability in challenging environments, no recalibration of sensors required, long signal transmission lines and multiple sensors on a single transmission line. Techniques have been developed that allow optical fibres to be bonded onto steel and concrete surfaces, or embedded within concrete, and to monitor internal and external parameters. However, there are several challenging tasks for fibre optic sensing technology, such as to reduce the sensor cross sensitivities, to improve the resolution and the measurement range, to improve the stability in practical applications and to achieve cost-effective sensors through more advanced techniques.

An obvious benefit of wireless sensors is that they are inexpensive to install, since extensive wiring is no longer required between sensors and the data acquisition system. A significant advantage of wireless sensor networks over traditional cable based monitoring systems is the collocation of computational power with the sensing transducer. However, wireless sensors

have limitations that require novel system architectures and modes of operation. The majority of existing wireless sensors are passive devices that only record the response of the structure. In the future, wireless sensors with actuation interfaces should be adopted to offer more powerful techniques for monitoring civil structures.

The selection of appropriate sensors for structural monitoring depends on many parameters and factors, such as operating environment, cost and sensor properties. The basic criteria for selection of sensors include minimal change of the measurand (e.g. resolution, linearity and accuracy), measuring range, type of measurement (e.g. static, dynamic), test duration (e.g. shortterm, longterm), test environment, installation environment and financial resources. Since the number of sensors adopted is often limited, the locations of these sensors need to be selected optimally. Intuitively, sensors should be placed near expected damage locations. In practice, highdensity sensor arrays are required to provide localised information relating to damage, also to provide for redundancy. It is important to ensure that the sensing system is more reliable than the structure being monitored. As the number of sensors increases, the cost, reliability and perhaps power requirements may become significant issues.

References

- Barthorpe, R.J. and Worden, K. (2009) Sensor Placement Optimization. *Encyclopaedia of Structural Health Monitoring*, Boller, Chang and Fujino (ed.), John Wiley & Sons, Chichester, UK.
- Blackshire, J.L. and Jata, K.V. (2009) Integrated sensor durability and reliability. *Encyclopaedia of Structural Health Monitoring*, Boller, Chang and Fujino (ed.), John Wiley & Sons, Chichester, UK.
- Casas, J.R. and Cruz, J.S. (2003) Fibre optic sensors for bridge monitoring, *Journal of Bridge Engineering ASCE*, **8**(6), 362–373.
- Catbas, F.N., KijewskiCorrea, T. and Aktan, A.E. (2012). *Structural Identification of Constructed Facilities: Approaches, Methods, and Technologies for Effective Practice of StId*, ASCE, Reston, VA. USA.
- Chen, H.P. and Huang, T.L. (2012) Updating finite element model using dynamic perturbation method and regularization algorithm. *Smart Structures and Systems***10**(4–5), 427–442.
- Chen, H.P. and Maung, T.S. (2014) Regularised finite element model updating using measured incomplete modal data. *Journal of Sound and Vibration***333**(21), 5566–5582.
- Chen, H.P., Tee, K.F. and Ni, Y.Q. (2012) Mode shape expansion with consideration of analytical modelling errors and modal measurement uncertainty. *Smart Structures and Systems***10**(4–5), 485–499.
- Doebelin, E.O. (1990) *Measurement Systems: Application and Design*, McGrawHill, New York, NY, USA.

- Ettouney, M.M. and Alampalli, S. (2012) *Infrastructure Health in Civil Engineering*, CRC Press, London. UK.
- Farrar, C.R., Sohn, H., Hemez, F.M., Anderson, M.C., Bement, M.T., Cornwell, P.J., Doebling, S.W., Lieven, N., Robertson A.N. and Schultze J.F. (2003) *Damage Prognosis: Current Status and Future Needs*. Los Alamos National Laboratory report LA14051MS.
- Glisic, B. and Inaudi, D. (2007) *Fibre Optic Methods for Structural Health Monitoring*. John Wiley & Sons, Chichester, UK.
- Huston, D. (2011) *Structural Sensing, Health Monitoring and Performance Evaluation*, Taylor and Francis Group, LLC, Boca Raton, FL, USA.
- LopezHiguera, J.M. (ed.). (2002) *Handbook of Optical Fibre Sensing Technology*. John Wiley & Sons, New York, USA.
- LopezHiguera, J.M., Cobo, L.R., Incera, A.Q. and Cobo, A. (2011) Fibre optic sensors in structural health monitoring. *Journal of Lightwave Technology*, **29**(4), 587–608.
- Lynch, J.P. and Loh, K.J. (2006) A summary review of wireless sensors and sensor networks for structural health monitoring. *Shock and Vibration Digest*, **38**(2), 91–128.
- Meo, M. and Zumpano, G. (2005) On the optimal sensor placement techniques for a bridge structure. *Engineering Structures* **27**(10), 1488–1497.
- Ni, Y.Q. (2014) Sensing Solutions for Assessing and Monitoring Supertall Towers. In book: *Sensor Technologies for Civil Infrastructures (Vol. 2): Applications in Structural Health Monitoring*, Wang, Lynch and Sohn (ed.), Woodhead Publishing, Cambridge, UK.
- Ni, Y.Q., Li, B., Lam, K.H., Zhu, D.P., Wang, Y., Lynch, J.P. and Law, K.H. (2011) In construction vibration monitoring of a supertall structure using a longrange wireless sensing system. *Smart Structures and Systems*, **7**(2), 83–102.
- Ni, Y.Q., Wang, Y. W., and Xia, Y.X. (2015) Using weighinmotion data to identify traffic loading on a longspan suspension bridge. *Proceedings of the 7th International Conference on Structural Health Monitoring of Intelligent Infrastructure (SHMII7)* , Turin, Italy.
- Ni, Y.Q., Xia, Y., Lu, Z.R., and Tam, H.Y. (2008) Technological issues in developing structural health monitoring for a supertall structure. *Proceedings of the 3rd World Congress on Engineering Asset Management and Intelligent Maintenance Systems*, Beijing, China.
- Reese, R.T. and Kawahara, W.A. (1993) *Handbook on Structural Testing*, Fairmont Press, Inc., Bethel, CT, USA.
- Wang, Y., Lynch, J.P. and Law, K.H. (2007) A wireless structural health monitoring system with multithreaded sensing devices: design and validation. *Structure and Infrastructure Engineering* **3**(2), 103–120.

Wong, K.Y. and Ni, Y.Q. (2009) Structural health monitoring of cablesupported bridges in Hong Kong. In book: *Structural Health Monitoring of Civil Infrastructure Systems*, Karbhari and Ansari (ed.), Woodhead Publishing, Cambridge, UK.

Wong, K.Y. and Ni, Y.Q. (2011) Structural health monitoring of a suspension bridge. In book: *Monitoring Technologies for Bridge Management*, Bakht and Mufti and Wegner (ed.), Multi Science Publishing, Essex, UK.

3

Data Acquisition, Transmission and Management

3.1 Introduction

Structural health monitoring systems for applications in civil engineering generally consist of some or all of following components (Farrar et al. 2009):

- various sensors measuring specific physical and chemical parameters
- data acquisition units, including signal conditioning devices and analogue to digital (A/D) converters that transform the analogue electrical signal into a digital signal
- networks for data transmission, e.g. wired networks and wireless networks
- processing facilities for data validation, normalisation, cleaning and fusion as well as data analysis and compression
- storage devices to save the acquired data and to manage files
- tools for structural health evolution using the monitored data
- power for the SHM system

The implementation of an SHM system typically starts with designing a modular architecture. First, a sensory system for the SHM framework should be determined. The physical quantities to be measured, the type and number of sensors and the sensor placement need to be decided. Next, the issue of data acquisition should be addressed, such as how often the data should be collected and how to select the resolution and dynamic ranges of the measured quantities. The selection of data acquisition and signal processing devices is application specific, and their costs need to be considered in the decision making process. Then, the measured parameters are transmitted safely by means of wired or wireless transmission systems to central monitoring facilities. This monitored data is processed and analysed for evaluating the health of the structure. Finally, this data is stored and the files are archived in the storage devices.

The SHM systems vary depending upon the specific SHM activity. Traditional SHM systems often have a starlike network where each deployed sensor is connected via long cable networks to a central computer acting as data acquisition and storage device. The installation of such SHM systems tends to be timeconsuming and therefore expensive. In particular, in the case of large and complex civil structures, the sensors may be located far way away from the data acquisition unit, resulting in high installation costs. The costs could be a major problem, limiting broad applications of SHM techniques to largescale civil infrastructure (Bischoff et al. 2009). Recent advances in wireless communication can overcome most of these limitations. With wireless sensor network techniques, the local sensing and processing units can communicate with a centralised processing unit and with each other.

The SHM systems for civil structures are typically designed for continuous, realtime and longterm operation. During operation, massive high dimensional data is acquired and a file based approach is usually adopted in the management of the data. Due to the massive quantity and high dimensionality of the monitoring data, the file based approach often makes the data interrogation slow and timeconsuming. Therefore, it is important for a data management system to have the capability of effective storage, query, visualisation, swap and retrieval of the monitoring data. Recently, the data management system has become an integral component of the SHM framework.

This chapter introduces several key systems in a framework of the structural health monitoring of civil engineering structures. First, data acquisition systems are presented for acquiring various physical and chemical measurements from the installed sensors. The monitored data is then transmitted by data transmission systems. Traditional wire transmission systems and recently developed wireless communication are discussed. The necessary procedures for data processing and analysis before structural health evolution are explored. Data management systems are introduced for effective data storage and file management. These key systems of the structural monitoring framework are demonstrated by their applications to a suspension bridge. Finally, a case study shows the actual application of these key systems to a constructed supertall structure.

3.2 Data Acquisition Systems

Data acquisition is the procedure for converting analogue or digital signals, transmitted from sensors by wired or wireless networks, to digital data. Such data may be permanently stored locally (e.g. on a computer disk drive) or may be processed locally to a reduced quantity of higher level data.

3.2.1 Data Acquisition for Structural Monitoring

In health monitoring of civil structures, a wide range of measurements may be covered, ranging from slowly sampled (static) digital signals to conventional analogue (voltage) signals at varying dynamic sample rates (Catbas et al. 2012, Chen and Maung 2014). For example, capturing day and night variation of static response parameters (e.g. temperature) can be undertaken by sampling as slowly as once per hour. For dynamic signals, sample rates depend on the structure size and frequency range of the external loading. For global response of long span bridges (>500 m) and tall buildings (>200 m) 10 Hz bandwidth should be adequate. This requires sample rates approximately 2.5 times larger to provide room for antialias filtering. For short span highway bridges, bandwidth up to 40 Hz will be sufficient. Seismometers typically are set to 100 Hz bandwidth. General purpose logger systems usually have a pure data acquisition function. This function can be configured to read a wide range of sensor types (e.g. vibrating wire gauges and thermocouples) at slow sample rates, but sometimes with high speed acquisition capabilities. Seismometers and the loggers or interfaces for fibre optics, GPS and other signal types often have limited functionality. Such loggers may be networked and interrogated directly or controlled by a computer.

Reliability and longevity of data acquisition systems requires robust hardware, that is, protection from harsh environments (e.g. dust, overheating and moisture), rugged computers and redundant data storage. In general, upgrade paths may be needed for monitoring systems expected to last a long time (e.g. over a decade). Reliable and clean power supplies with uninterruptible power supply protection have to be provided, as well as communication via high speed broadband links.

3.2.2 Data Acquisition in Bridge Monitoring

In the wind and structural health monitoring system (WASHMS) of the Tsing Ma Bridge discussed in [Section 2.3.5](#), the data acquisition system is a key component of the data acquisition and transmission system (Module 2). The data acquisition system is composed of fixed data acquisition units (DAUs), portable DAUs and digital video converters (DVCs) for collecting respective random and digital video signals. All DAUs and DVCs are PC based equipment. The fixed DAUs and DVCs are permanently installed in the bridge deck and bridge towers for collection and processing of the signals received from sensory system (excluding corrosion cells). The portable DAUs are used to collect signals from portable servotype accelerometers and corrosion cells during ambient vibration measurements and specified field measurement works. [Figure 3.1](#) shows the schematic layout of a typical connection between sensory system, DAU and fibreoptic cable (Wong and Ni 2009a). The major components in the DAU include the peripheral components interconnect (PCI) controller, the signal conditioning device and the analoguetodigital converter. The proper design of these components is the key to obtaining measurement data with high quality.

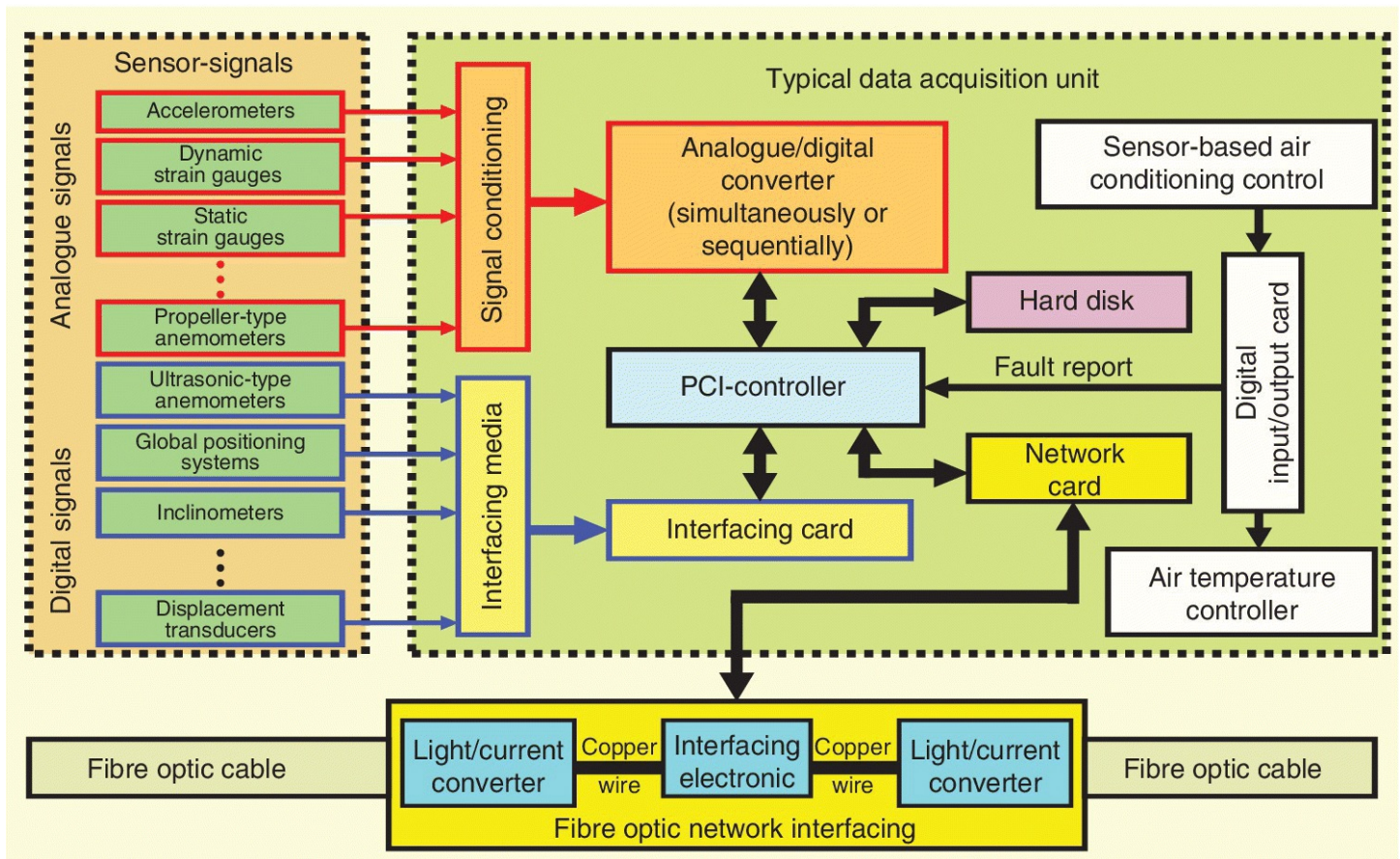


Figure 3.1 Schematic layout of a typical data acquisition unit and its associated equipment.

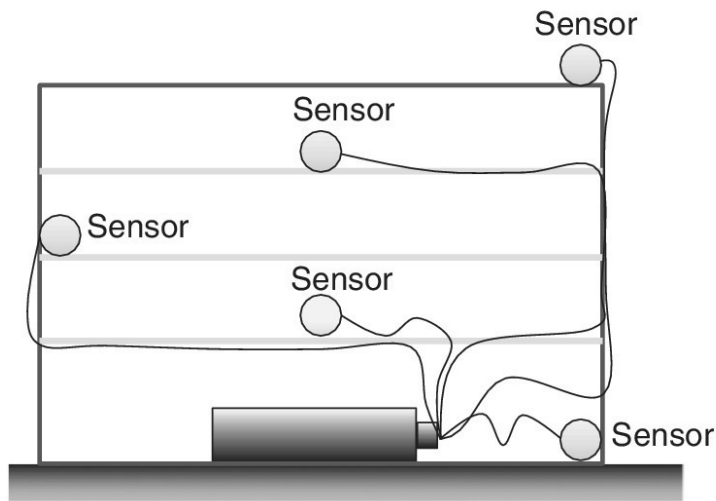
3.3 Data Transmission Systems

Data transmission system is required in the SHM framework to transmit the data, so that the acquired raw data can be transformed into useful information. The selection of the data transmission system largely depends on the specific SHM activities. In general, there are two types of the data transmission systems available: wired and wireless.

3.3.1 Wired Transmission Systems

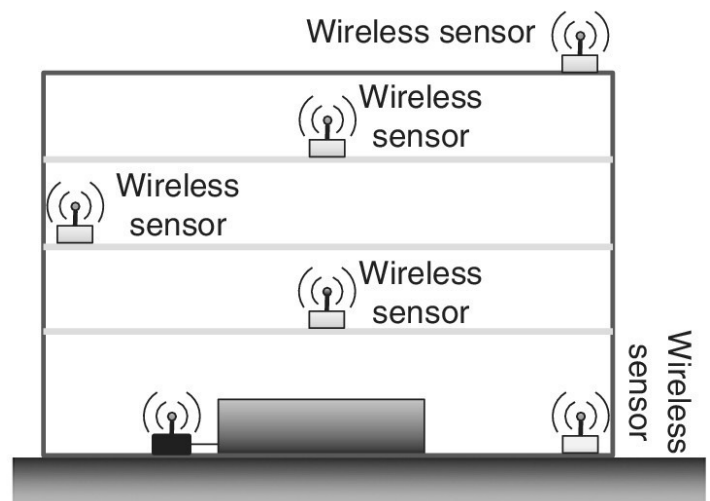
Data transmission using wired technology can telemeter data and transfer power to the sensors over a direct wired connection from the transducer to the central data analysis facility (Straser et al. 1998), as illustrated in [Figure 3.2\(a\)](#). The installed common sensors output analogue signals that are sampled and digitised for use in modern discrete signal processing systems. The distance from the sensors to the data acquisition system can range from 10 to 300 m in practice. As the signal transmission distance becomes longer, the analogue signals become noisier and degrade owing to coupled noise sources near the cable path (Sohn et al. 2004). When the analogue signals arrive at the centralised data acquisition and storage system, the signals will be discretised and then used for extracting the relevant engineering quantities from the data.

(a) Conventional wired monitoring system



Centralised data acquisition and storage

(b) Modular wireless monitoring system



Redundant data storage with wireless modem

Figure 3.2 Comparison of wired and wireless configurations of a structural monitoring system (after Straser et al. 1998).

There are a wide range of commercially available wired systems for generalpurpose data transmissions and for SHM applications. The wired systems for general purpose data transmission can typically interface with a wide variety of transducers and also have the capability to drive actuators. Most wired systems have integrated signal conditioning, data processing and data storage capabilities and runoff of alternating current (AC) power. The wired systems designed to run off batteries typically have a limited number of channels, and they have limited ability to operate for long periods of time (Farrar et al. 2009). Wired systems for temporary and time limited studies, such as forced vibration testing, require robust and foolproof but quickfit connectors.

For permanent SHM applications, cables with appropriate ratings must also be structurally robust (particularly when exposed on wind/rainblown faces of structures) and have the required electrical characteristics of low resistance and shielding of conductors. High quality cables will minimise problems due to electromagnetic interference and crosstalk. Lightning protection is also needed for exposed wiring, sensors and housings, requiring careful arrangements for grounding (avoiding earth loops) and surge suppression. In cases where multiple loggers need to be networked using local area network connections, or where modems and logger are separated, fibre optic links may be required for distances over 100 m (Catbas et al. 2012). Synchronisation of signals from loggers is a major problem for dynamic testing, most usually dealt with by using hardwired analogue connections.

3.3.2 Wireless Transmission Systems

In order to avoid the high costs and limited flexibility associated with wired transmission systems, wireless communication has been used for the transfer of data between sensors and a data repository in structural monitoring systems. Such wireless monitoring systems are

assembled from lowcost wireless sensors that collocate sensing, communication and computing in a single device (Catbas et al. 2012). Wireless communication can tackle the recurring cabling problem of the conventional wired data transmission systems. With the wireless communication and embedded processors, it is possible to move the data acquisition and a portion of data processing towards the wireless sensors. A schematic system architecture view of a wireless monitoring system (Straser et al. 1998) is shown in [Figure 3.2\(b\)](#). A comprehensive review of the applications of wireless sensors and sensor networks for SHM applications is provided in Lynch and Loh (2006).

A wireless sensor network is essentially a computer network comprising several small, intercommunicating computers equipped with one or more sensors (Bischoff et al. 2009). Each small computer represents a sensor node of the network. The communication within the network is established using radio frequency transmission techniques. The sensor nodes usually form a multihop mesh network by establishing communication links to neighbour nodes. Multihop networks offer various advantages when monitoring data has to be transmitted over long distances. Because of the network robustness to sensor node failure and the high power efficiency, multihop networks are attractive for SHM applications. All sensor nodes are equipped with specific sensors selected for the required measurements. These nodes act as data sources, and also act as relaying stations, receiving and forwarding data from adjacent nodes. A base station needs to be selected from particular sensor nodes to aggregate all the data obtained within the network. The base station establishes a communication link to a data logging unit or a remote site, using standard wired or wireless communication technologies such as universal mobile telecommunications system (UMTS) or a wireless local area network (WLAN).

A major concern in using a dense sensor array in SHM systems for civil engineering applications is the problem of providing power to the sensors. In the cases where power can only be provided by direct cable connections, wireless protocols become impractical, since the cabled power link could also be used for the transmission of data. Therefore, micropower generators embedded in the hardware are essential for wireless communication. The problem of localised power generation could be solved by harvesting ambient energy, such as using thermal, vibration, acoustic and solar sources.

3.3.3 Data Transmission in Bridge Monitoring

In the WASHMS of the Tsing Ma Bridge discussed in [Section 2.3.5](#), the data transmission system is another key component of the data acquisition and transmission system (Module 2). The data transmission system includes local cabling network system, global cabling network system and commercial cabling network system. The local cabling network system is composed of two local cabling networks: the fibre optic cabling network for transmission of the signals from global positioning systems and digital video cameras, and the copper cabling network for transmission of the signals from other sensors of the sensory system to data acquisition units (DAUs) for random signals and digital video converters (DVCs) for digital video signals (Wong and Ni 2009a, 2009b), as illustrated in [Figure 3.3](#).

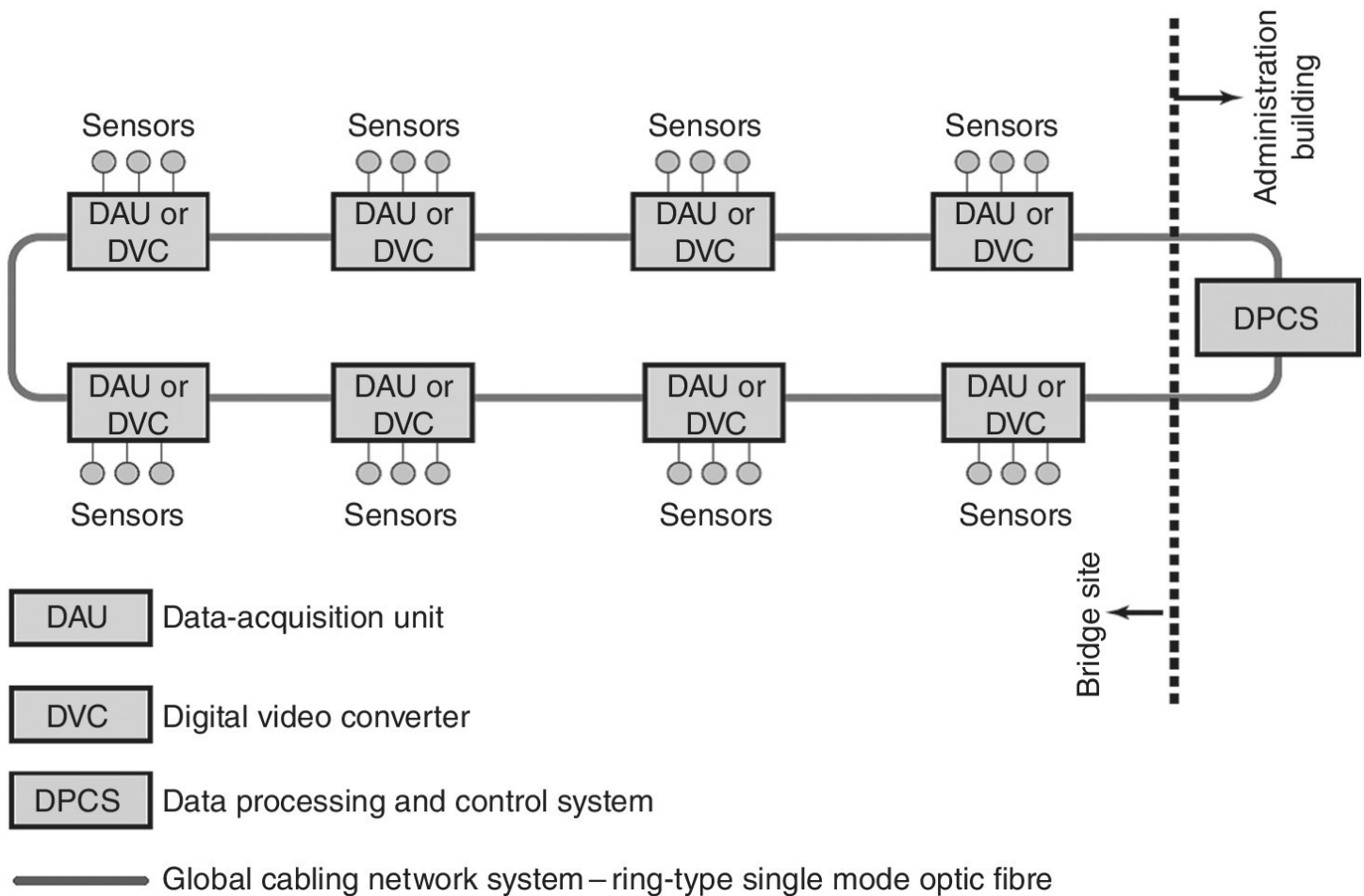


Figure 3.3 Schematic layout of data acquisition and transmission system.

The global cabling network system is composed of two backbone cabling networks: (1) the random signal transmission cabling network for transmission of digitised signals (excluding digital video cameras) from individual DAUs to a data processing and control system (DPCS1) and (2) the digital video signal transmission cabling network for transmission of digital video signals from individual DVCs to another data processing and control system (DPCS2). Both backbone cabling networks are ring-shaped single mode fibreoptic cabling networks with a data transmission capacity of 1 GB/s. The commercial cabling network system is the high speed line with a data transmission rate of not less than 40 MB/s for data communication. The commercial cabling network system is used for data transmission between the bridge monitoring room in the Tsing Yi administration building and the bridge monitoring room in the Tsing Ma control area of the Tsing Ma Bridge.

3.4 Data Processing Systems

Data processing systems are the key and challenging components of the SHM framework. Such systems convert the data acquired from the sensors into information about the state of the structure concerned. The data processing procedure typically includes data preprocessing and data interpretation.

3.4.1 Data PreProcessing for SHM

In SHM systems for civil engineering structures, sensor measurements need to be pre processed before their application to structural condition assessment. The preprocessing procedure includes data validation, normalisation, cleansing and fusion. First of all, the data obtained from sensing devices has to be inspected. The data validation process ensures that the sensor data possesses information relevant to subsequent analyses. For example, measured acceleration data may have anomalies because of electromagnetic interference, and it may have missing values because of disrupted radiofrequency transmission or a constant offset caused by drift (Farrar et al. 2003). Statistical inference techniques such as outlier analysis and novelty detection can be used in this data validation process.

Because data is often measured under varying conditions, the ability to normalise the data becomes critical for the SHM strategy. For example, the measured natural frequencies of a bridge usually vary with change in temperature due to thermal effects. Data normalisation is the process of distinguishing between changes in sensor readings caused by damage and changes caused by varying operational and environmental factors. Typically, data normalisation is accomplished through some combination of sensing system hardware and data processing software (Sohn et al. 2004). However, these hardware and software approaches are not optimal if they are not done in a coupled manner.

Data cleansing is the process of selectively choosing data to accept or reject from the process, for the feature selection for damage identification. The data cleansing process usually depends on knowledge gained by individuals directly associated with the data acquisition (Sohn et al. 2004). For example, manual signal processing techniques such as filtering and decimation can be considered as data cleansing processes applied to data acquired during dynamic tests.

Data fusion is the process of combining information from various sensors in an effort to enhance the reliability of the SHM process. The purpose of data fusion is to integrate data from a number of sensors with the objective of making a more robust and confident decision, compared with a decision made from any one sensor alone. In many cases, data fusion is undertaken in a simple manner, similar to examining relative information between various sensors (Sohn et al. 2004). However, complex analyses of information from sensor arrays may be required in the data fusion process for some cases, such as those provided by artificial neural networks.

3.4.2 Data Analysis and Compression

After data preprocessing, the data can be used for feature extraction and damage identification. Feature extraction is the process of identifying damagesensitive properties, derived from the measured data such as vibration response measurements. The extracted feature has the ability to distinguish between the undamaged and damaged structure. Various methods have been proposed for identifying features for damage identification. Past experience with measured data from a structure, particularly data recorded before and after damaging events, is often the basis for feature selection. Alternatively, numerical simulations of the structural responses of the undamaged and damaged structure can be used for identifying

features. Also, fitting linear or nonlinear, physics based, or nonphysics based models of the structural response to measured data can help identify damagesensitive features.

The implementation of an SHM system in civil engineering structures typically produces a large amount of data. Almost all feature extraction procedures inevitably perform some form of data compression. Data compression is the process of reducing the dimensionality of the data, or the feature extracted from the data, in order to facilitate efficient information storage. In addition, condensation of the data is advantageous and necessary, particularly if many data sets over structural lifetime are compared (Sohn et al. 2004). Data may be acquired from a structure over an extended period of time and in an operational environment, and so reliable data reduction techniques must retain sensitivity of the selected features to the structural changes under varying environmental and operational conditions.

3.4.3 Data Processing in Bridge Monitoring

For the WASHMS of the Tsing Ma Bridge discussed in [Section 2.3.5](#), the data processing and control system (DPCS) refers to the hardware and software for executing the following functions: system control, system operation display, bridge operation display and post processing and analysis of data (Wong and Ni 2009a). This data processing and control system is composed of two subsystems – DPCS1 and DPCS2 – to carry out the processing and control of onedimensional signals and twodimensional signals, respectively.

The system control includes the control of all the operation modes in facilities, including sensory systems, data acquisition units (DAUs), digital video converters (DVCs), cabling network systems and associated display tools, in particular for the functions of data collection, data processing, data archiving and data display, as well as failure or fault reporting. The system operation display includes the display of all the operation modes in the facilities, in particular for displaying and activating the alarming signal. The bridge operation display in DPCS1 and DPCS2 has different functions. The DPCS1 displays the environmental conditions at the bridge site, the operational loads on the bridge and the variation of kinematic quantities; it also activates the alarm signals when the measurands exceed the defined threshold. The DPCS2 displays the traffic flow conditions and characteristics of the bridge, including the near realtime display of overloaded vehicles and overspeeding vehicles.

The postprocessing and analysis of data in DPCS1 and DPCS2 also have different functions. The DPCS1 performs the environmental loads and status derivation, operation loads derivation, bridge features extraction and bridge responses derivation by an unsupervised learning mode of statistical analysis. The DPCS2 performs the image analysis of the selected digital video records and it transfers the analysed results into spreadsheet data formats for subsequent traffic features and potential traffic loadeffect analyses. [Figure 3.4](#) shows the block diagram of data analysis in the DPCS2 (Wong and Ni 2009b), where raw data is acquired from various sensors such as dynamic weighinmotion (DWIM), digital video converter (DVC) and global positioning system (GPS).

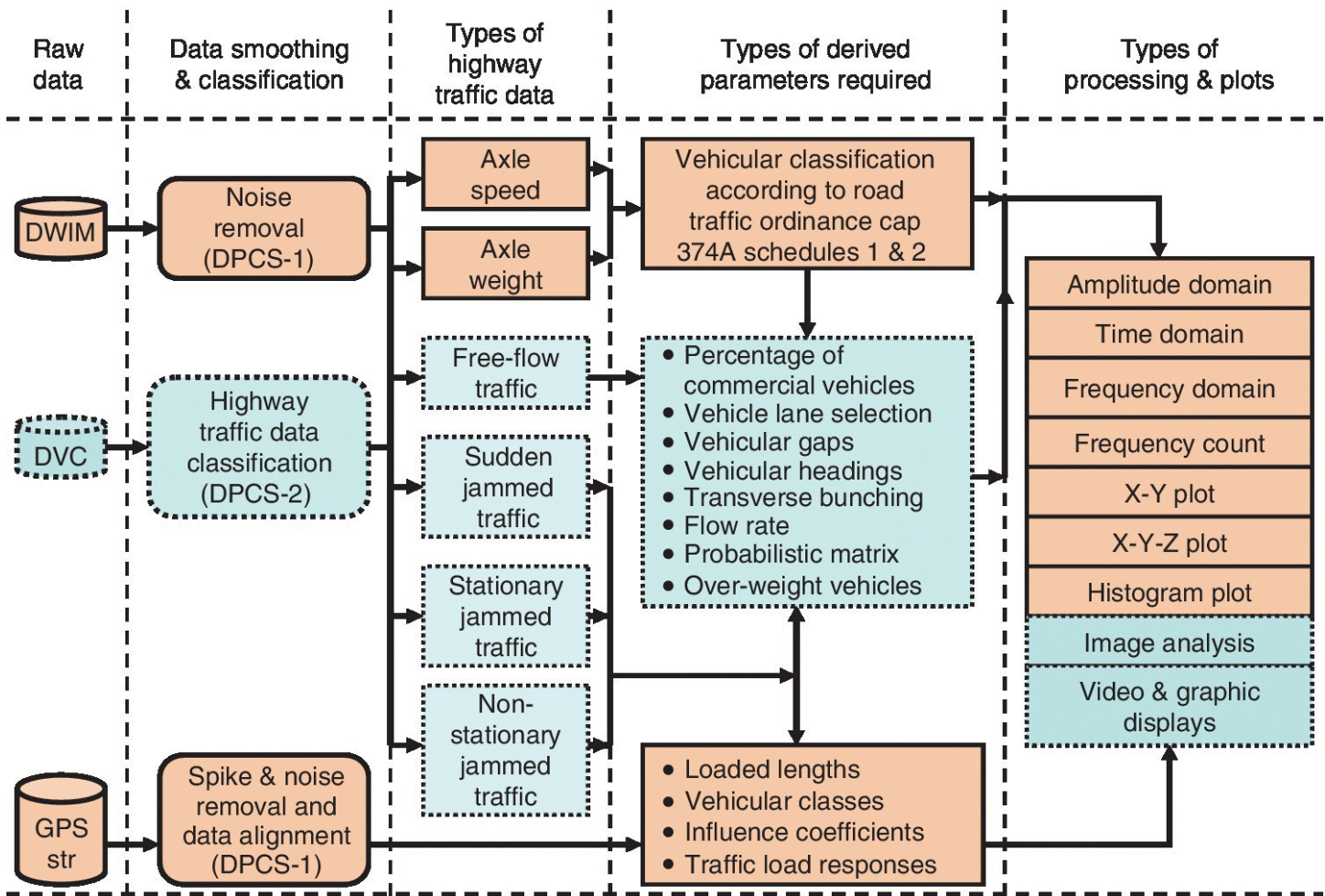


Figure 3.4 Block diagram of traffic data analysis in DPCS2, combined digital video converter (DVC) and dynamic weighinmotion (DWIM) data.

3.5 Data Management Systems

The implementation of sophisticated SHM systems will generate vast amounts of high dimensional data. For the purpose of structural health evaluation, this data must be efficiently assessed and processed. Thus, the collected and generated data has to be managed in an effective manner by the use of data management systems.

3.5.1 Data Storage and File Management

At the final stage, the processed and condensed data needs to be archived and managed properly. The most efficient data storage format is binary files, generated directly by acquisition software. Rather than saving directly to a database, an efficient procedure is to use individual files saved at convenient intervals with dataembedded file names. File sizes for raw data from sensor measurements depend on channel count and sample rate. The disk storage should not be a critical constraint except when dealing with video recordings (Catbas et al. 2012). Use of sensible sample rates will speed up internet transfer and processing.

The raw data typically remains on the local storage systems, and it needs to be accessed and

observed, in order to investigate the behaviour and response of the structure under operational loading and extreme events (e.g. earthquake or hurricane). For shorttime measurements, raw test data has high value for structural condition assessment. Hence, careful and logically organised data archiving is necessary, along with all the records of the testing, including specifications, plans, method statements, notes on sensor configurations and calibrations, photographs, videos and drawings. When the processed results are saved, the version of software used to generate them should also be saved. For raw binary data, a version of reader software and details of the file structure ensure future accessibility.

Large data sets generally require sophisticated storage capabilities to physically store the information and also to access it efficiently (Farrar et al. 2003). Storage and accessibility are therefore important components of the SHM strategy of civil structures. Compression algorithms are often needed to improve the efficiency, so that large data sets can be effectively stored and accessed. For example, data compression can link directly into the pattern recognition and feature extraction technology. Archiving as much as possible the collected and generated data is also critical. Historic data sets have to be available for revisiting for further indepth investigations, if an abnormality is detected in the future. These data sets also can provide useful information about the evolution of structural performance over the life of the structure.

3.5.2 Data Management in Bridge Monitoring

In the WASHMS of the Tsing Ma Bridge discussed in [Section 2.3.5](#), the structural health data management system (SHDMS) has the functions of data storage and management. The data management system is composed of a highperformance server equipped with data management software. This system is the interfacing platform for the interoperability of data and information, so that the efficiency of the fusion of data and information for decision making can be significantly enhanced, as illustrated in [Figure 3.5](#) (Wong and Ni 2009a). The following five major databases are devised for the storage and retrieval of data and information:

- realtime structural health data database (RSHDDB) for all preprocessed time series data obtained from data acquisition units (DAUs)
- statistical and probabilistic analysed data database (SPADDB) for all data generated from signal or data processing and analysis software tools
- finite element analysis data database (FEADDB) for all input and output finite element data generated by finite element solvers
- structural health rating data database (SHRDDB) for all new or updated rating indices (or criteria), generated by the structural health rating system (SHRS)
- structural health evaluation data database (SHEDDB) for all concise historical monitoring and evaluation results and all reports, generated by the structural health evaluation system (SHES)

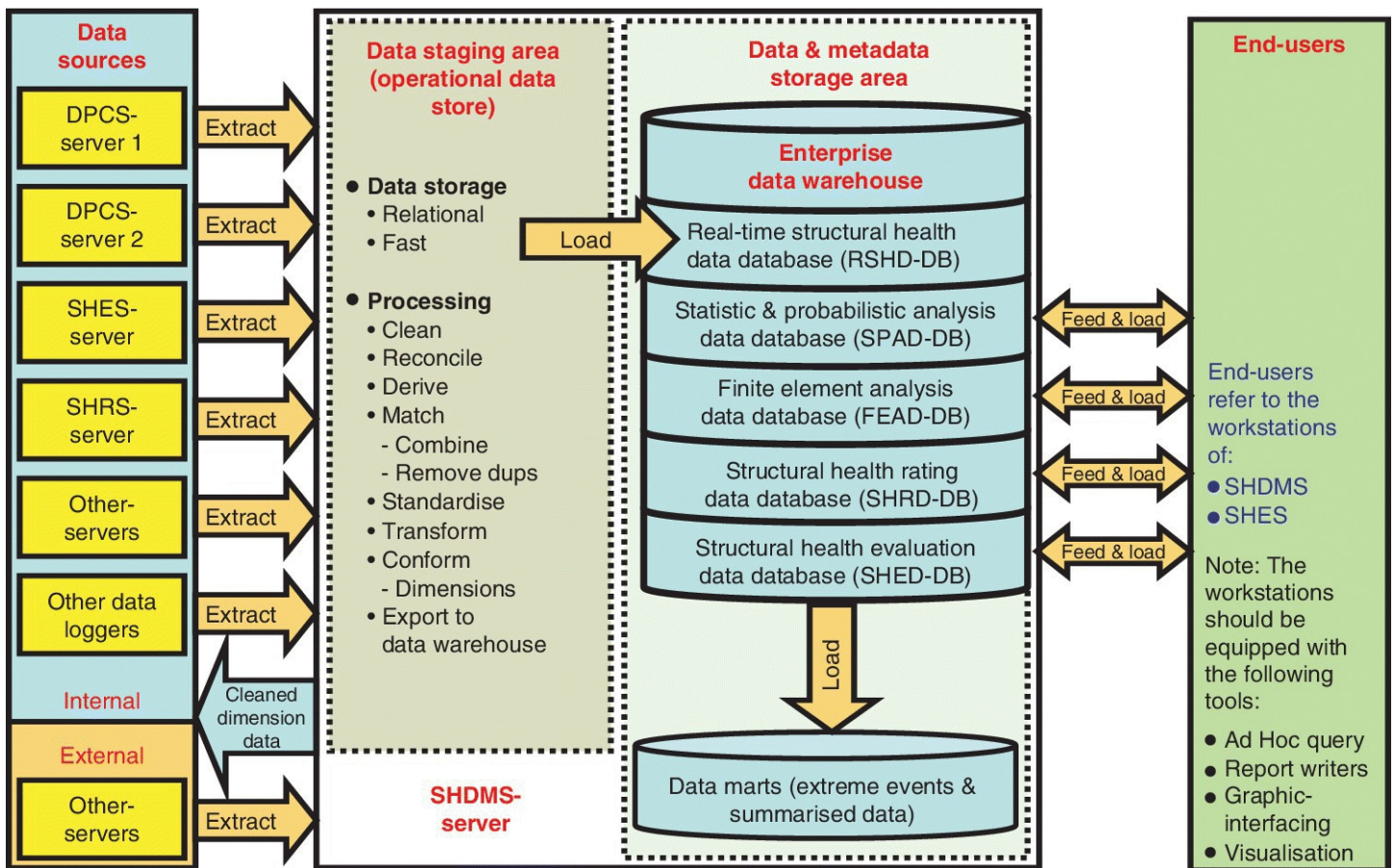


Figure 3.5 Architectural layout of structural health data management system (SHDMS) and its interfaces.

These five databases are manipulated and managed by a data warehouse management system. This system is equipped with online analytical processing tools for integrating a wide range of corporate data into a single repository. From this repository, users or engineers can easily run queries, perform different types of analyses and generate monitoring and evaluation reports. The data warehouse management system in the SHDMS is devised to carry out the following functions:

- systematic cleansing, reconciliation, derivation, matching, standardisation, transformation and conformity of data and information from all data source systems such as data processing and control system (DPCS) servers, SHES servers and SHRS servers
- manipulation of all types of correlation analyses and features extraction plots, by online analytical processing tools and appropriate data mining tools
- creation of data marts, based on the results of the correlation analyses and plots, for the execution of the monitoring and evaluation works, including reporting the current and future environmental and operational loads, reporting the current and future corrosion status, reporting the current and future structural health conditions, planning and scheduling bridge inspection and maintenance activities and updating the bridge rating system and computational models
- forming the centre of data interrogation and metamodelling for bridge damage diagnosis

and prognosis, through the integration of data and information from both measurement and computational systems

3.6 Case Study

The SHM system of the Canton Tower discussed in the case study in [Section 2.7](#) consists of six standard modules (subsystems). The sensory system and data acquisition and transmission system are located in the structure. The data processing and control system, data management system and structural health evaluation system are placed in the monitoring centre room. The inspection and maintenance system is a portable system. The integrated in-construction and in-service sensory system is composed of 16 types of sensors with over 600 sensors (Chen and Tee 2014, Ni 2014, Ni et al. 2011), as discussed in detail in [Section 2.7](#). As illustrated in [Figure 3.6](#), this online SHM system has been devised to possess the following features:

- modular architecture for easy maintenance and upgrade
- lifecycle SHM with the integration of in-construction monitoring and in-service monitoring
- dual function of online health monitoring and realtime feedback control with the integration of SHM and vibration control
- integration with renewable energy technology (solar photovoltaic and wind turbine systems) to monitor the power generation efficiency and operational condition
- innovative sensors and customised design fit for special circumstances
- hybrid tethered and wireless data transmission network customised for harsh operational conditions
- userfriendly graphical user interface for easy operation
- innovative structural health evaluation methodologies catering for structural maintenance and management purposes
- allround protection customised for severe surrounding environment
- remote expert service through the web based data collection around the world
- popularisation of scientific knowledge through a virtual reality system integrated with sightseeing

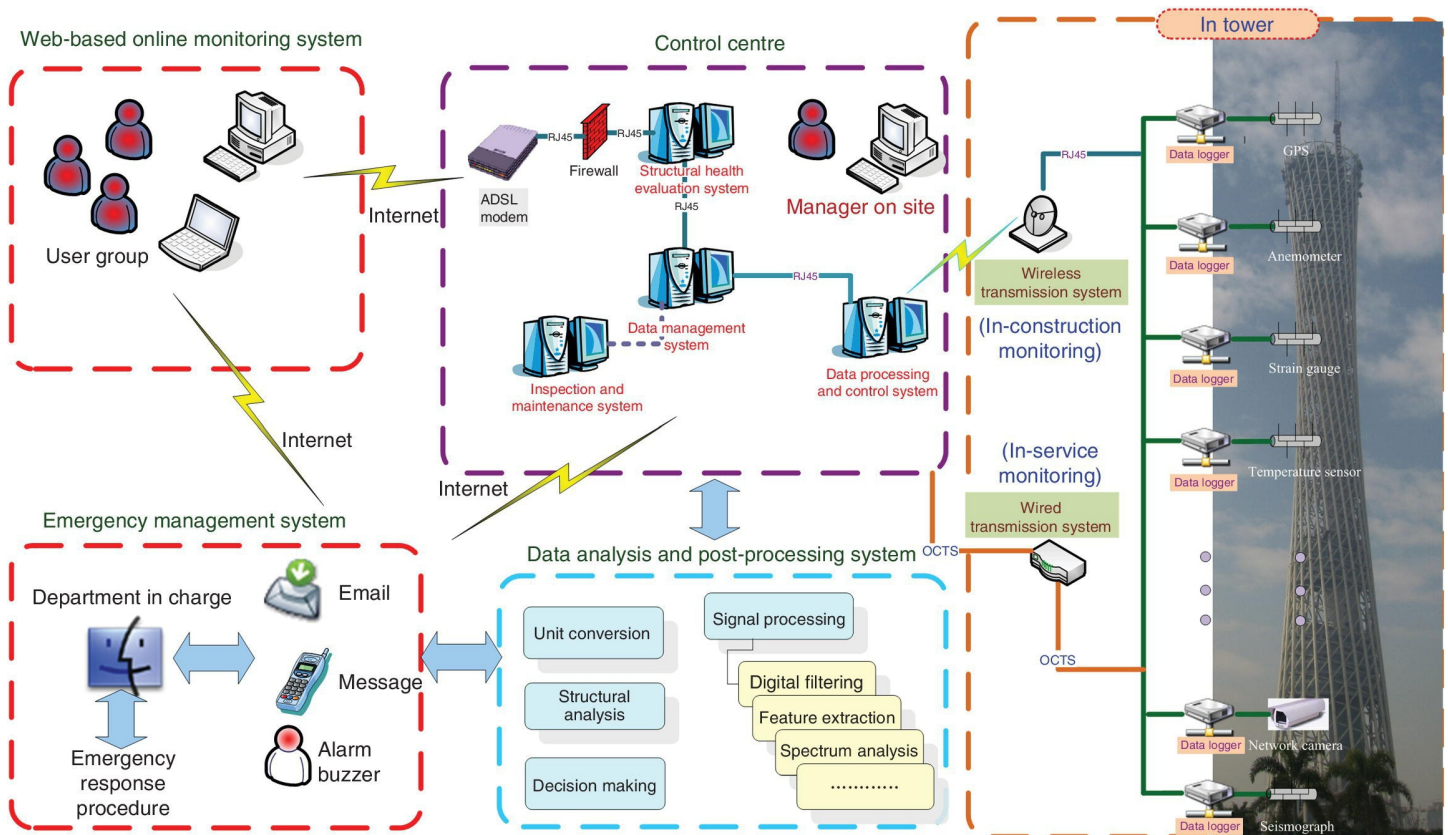
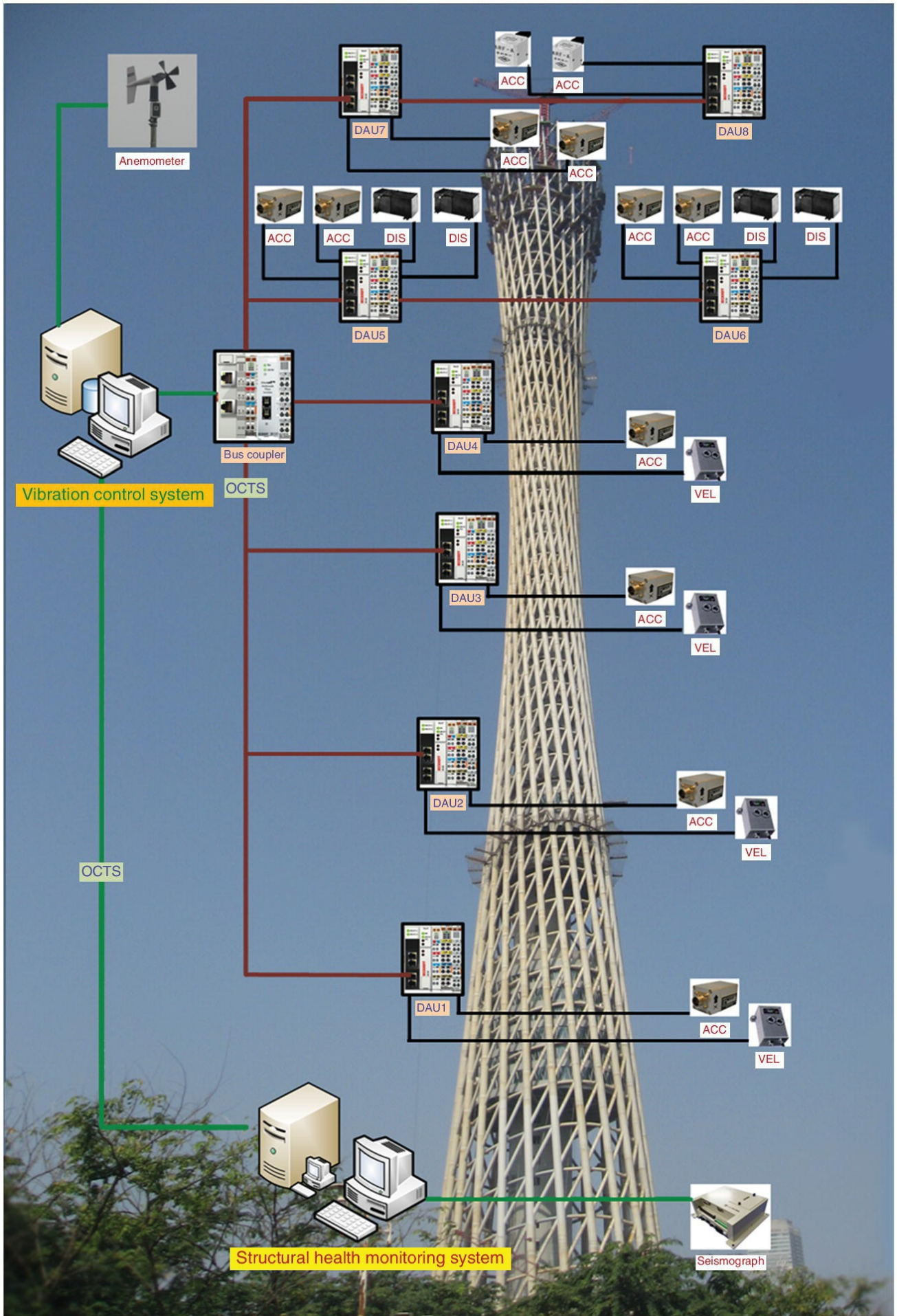


Figure 3.6 Integrated in-construction and inservice SHM system for Canton Tower.

The SHM system has a special function of monitoring and verifying the effectiveness of vibration control devices installed on the structure. It is a unique and interesting practice of SHM. A hybrid control system, consisting of two tuned mass dampers coupled with two active mass dampers, was installed at a floor of 438 m high for mitigating wind-induced vibration of the main tower. To online command the active mass dampers (made from linear motion actuators) it is necessary to establish a structural response feedback system for providing thorough information for realtime vibration control. As illustrated in [Figure 3.7](#), the SHM system has been devised to integrate with the vibration control system, so that reliable and realtime monitoring data can be obtained for feedback vibration control to enhance the control effectiveness.



[Figure 3.7](#) Integration of SHM and vibration control.

The supertall structure provides a unique testbed for investigating the optimal design of sensor network and the technique for longrange wireless monitoring (Ni et al. 2011). A hybrid tethered and wireless data acquisition network in conjunction with 13 data acquisition units (DAUs) during inconstruction monitoring and five DAUs during inservice monitoring has been adopted in the SHM system. Wireless systems have been implemented in the SHM system for both static and dynamic monitoring. As shown in [Figure 3.8](#), the wireless system is operated for synchronous acquisition of strain and temperature data and for realtime data transmission from the DAUs to the site office. The vibration of the structure is monitored mainly by using a wired cabling network, while the wireless system is also adopted in situ for complementary vibration monitoring. The hybrid network enables the verification of the wireless monitoring data.

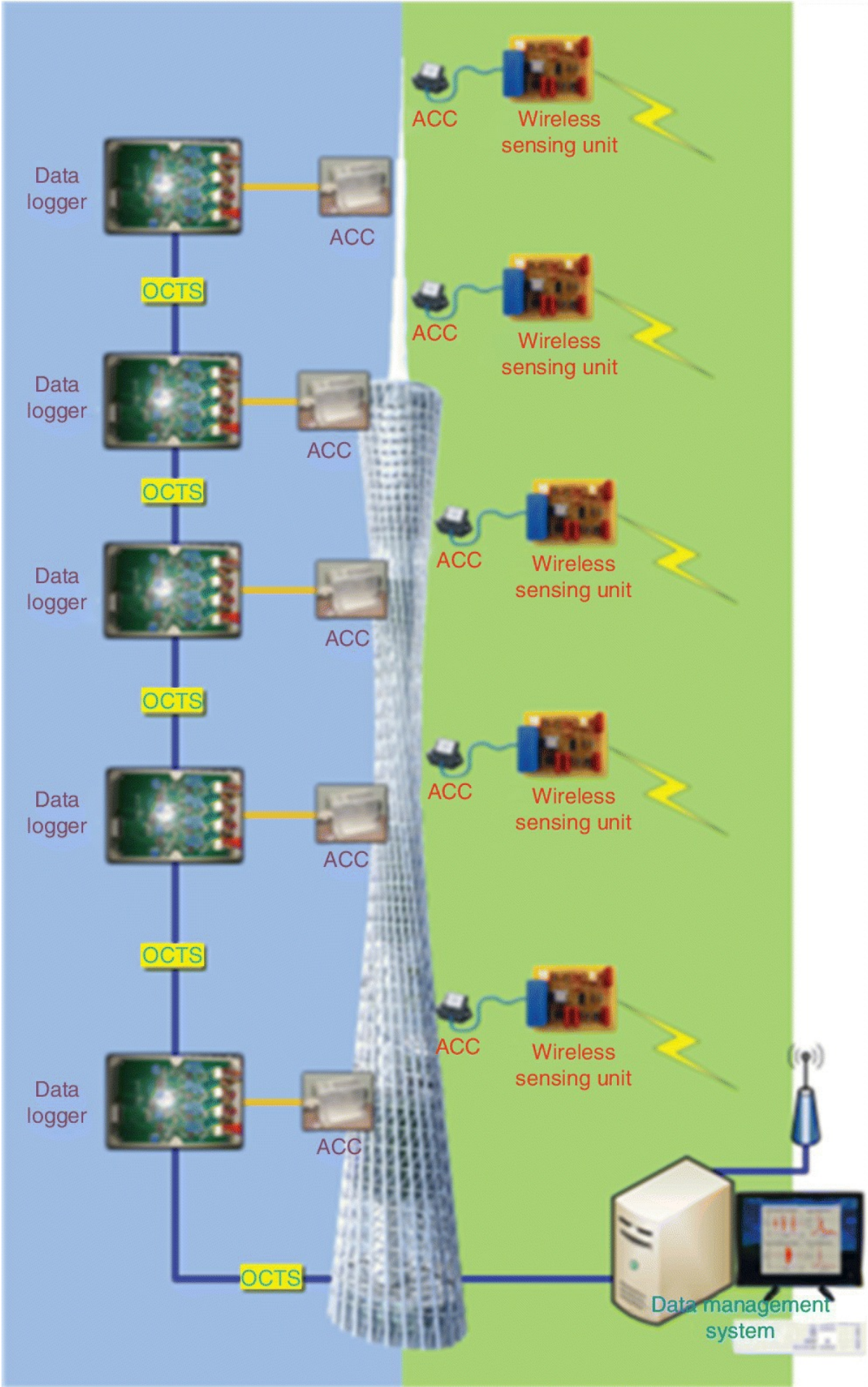


[Figure 3.8](#) Wireless data transmission.

3.7 Concluding Remarks

The health monitoring system for civil engineering applications should be designed using a modular architecture. The architecture of the monitoring system typically includes several modules, such as sensory system, data acquisition system, data transmission system, data processing system, data management system, as well as structural health evolution system. The structural health evolution system is a critical module for damage diagnosis and prognosis, and it will be discussed in detail in following chapters.

The sensory system should be able to monitor properly the health status of civil structures under normal condition and to evaluate structural health after infrequent extreme events. Different types of sensors may be deployed at the key locations and components, such as where large displacements and stresses are expected to occur, so that the measured data can be validated through correlation studies. To ensure data quality, the data acquisition system should have an appropriate hardware configuration, particularly the signal conditioning devices. The performance requirements on the linearity, temperature drift, accuracy, direct current resolution, bandwidth, and so on, of the signal conditioning devices and the data acquisition devices should be identified and quantified. Appropriate customised software systems should be developed and configured to process the measured data in the data formats applicable to SHM strategies.

Depending on the application, data transmission can be accomplished by either wired or wireless systems. Wired systems can offer robust and accurate data transmission for SHM techniques. However, this approach can impose serious limitations on application of an SHM system to a large civil structure, since for such a structure it is highly desirable to have a very large number of sensors. Wired systems also tend to have a limited flexibility in terms of the rearrangement of sensors and scalability. The adoption of wireless sensor network techniques to SHM applications should overcome the drawbacks of wired systems. It has been demonstrated that wireless sensing technologies can be deployed reliably in monitoring the low frequency and low amplitude ambient vibration of the Canton Tower. However, wireless data appears to be more strongly influenced by environmental noise than with a wired system. Potential constraints on wireless systems include maximum range, amount of bandwidth available, energy requirement and susceptibility to electromagnetic interference.

Structural health monitoring and evaluation tasks should be executed through the correlation analyses and feature extractions of the measured, derived and analysed results. These correlation analyses and feature extractions often involve the synchronised processing of two or more data sets. Thus, the use of a data warehouse management system, for managing the storage and retrieval processes of data and information, facilitates the automatic execution of such synchronised data processing and analysis.

References

- Bischoff, R., Meyer, J. and Feltrin, G. (2009) Wireless sensor network platforms. *Encyclopaedia of Structural Health Monitoring*, Boller, Chang and Fujino (ed.), John Wiley & Sons, Chichester, UK.
- Catbas, F.N., KijewskiCorrea, T. and Aktan, A.E. (2012). *Structural Identification of Constructed Facilities: Approaches, Methods, and Technologies for Effective Practice of StId*, ASCE, Reston, VA. USA.
- Chen, H.P. and Maung, T.S. (2014) Regularised finite element model updating using measured incomplete modal data. *Journal of Sound and Vibration* **333**(21), 5566–5582.
- Chen, H.P. and Tee, K.F. (2014) Structural finite element model updating using ambient vibration modal data. *Science China Technological Sciences*, **57**(9), 1677–1688.
- Farrar, C.R., Park, G. and Farinholt, K.M. (2009) Sensor Network Paradigms. *Encyclopaedia of Structural Health Monitoring*, Boller, Chang and Fujino (ed.), John Wiley & Sons, Chichester, UK.
- Farrar, C.R., Sohn, H., Hemez, F.M., Anderson, M.C., Bement, M.T., Cornwell, P.J., Doebling, S.W., Lieven, N., Robertson A.N. and Schultze J.F. (2003) *Damage Prognosis: Current Status and Future Needs*. Los Alamos National Laboratory report LA14051MS.
- Lynch, J.P. and Loh, K.J. (2006) A summary review of wireless sensors and sensor networks for structural health monitoring. *Shock and Vibration Digest*, **38**(2), 91–128.
- Ni, Y.Q. (2014) Sensing Solutions for Assessing and Monitoring Supertall Towers. In book: *Sensor Technologies for Civil Infrastructures (Vol. 2): Applications in Structural Health Monitoring*, Wang, Lynch and Sohn (ed.), Woodhead Publishing, Cambridge, UK.
- Ni, Y.Q., Li, B., Lam, K.H., Zhu, D.P., Wang, Y., Lynch, J.P. and Law, K.H. (2011) In construction vibration monitoring of a supertall structure using a longrange wireless sensing system. *Smart Structures and Systems*, **7**(2), 83–102.
- Sohn, H., Farrar, C.R., Hemez, F.M., Shunk, D.D., Stinemates, D.W. and Nadler, B.R. (2004) *A Review of Structural Health Monitoring Literature: 1996–2001*. Report LA13976MS. Los Alamos National Laboratory.
- Straser, E.G., Kiremidjian, A.S., Meng, T.H., and Redlefsen, L. (1998) A modular, wireless network platform for monitoring structures. *Proceedings of the 16th International Modal Analysis Conference*, California, USA.
- Wong, K.Y. and Ni, Y.Q. (2009a) Modular architecture of structural health monitoring system for cablesupported bridges. *Encyclopaedia of Structural Health Monitoring*, Boller, Chang and Fujino (ed.), John Wiley & Sons, Chichester, UK.

Wong, K.Y. and Ni, Y.Q. (2009b) Structural health monitoring of cablesupported bridges in Hong Kong. In book: *Structural Health Monitoring of Civil Infrastructure Systems*, Karbhari and Ansari (ed.), Woodhead Publishing, Cambridge, UK.

4

Structural Damage Identification Techniques

4.1 Introduction

Damage in civil engineering structures can be represented by a reduction of the structural bearing capacity during their service period. This reduction is usually caused by degradation of materials, structural components or connections due to environmental or loading effects. All loadcarrying civil engineering structures, such as bridges, buildings and offshore platforms, continuously accumulate damage during their service life. Typical types of damage in civil engineering structures include cracks, fatigue, steel corrosion, concrete spalls, scour and deterioration. Undetected damage may lead to structural failure and loss of human life. It is therefore important and necessary to detect damage within a structure and to undertake appropriate repairs as early as possible.

Visual inspection is the most common method of damage detection. However, this method is unreliable for complex civil structures, because critical damage can occur in inaccessible areas or it may be concealed by paint. Visual inspection also cannot provide quantitative assessment for damage in the structure. Very often, loose connections or cracking of structural components can be difficult to detect visually, but can considerably weaken the structural capacity. In order to tackle the shortcomings of visual inspections, nondestructive testing (NDT) techniques have been extensively employed to assess the integrity of a structure (Michaels and Michaels 2006), including acoustic emission, ultrasound, guided (Lamb) waves, thermography, electromagnetic methods, capacitive methods, laser Doppler vibrometer and global positioning system (GPS). However, these NDT techniques differ greatly in their range of applicability, and may only be suitable for damage assessment in local areas. They have certain kinds of limitation in practical applications, particularly for large complex civil engineering structures.

The need for effectively identifying damage in complex civil structures has motivated the development of structural health monitoring methods. Structural health monitoring is an emerging method for assessing the current state and predicting the future performance of existing engineering structures. A comparatively recent development in SHM methods is vibrationbased damage identification. The basic premise of common vibrationbased damage identification methods is that damage in a structure will alter the stiffness, mass or energy dissipation properties of the structure, which in turn will alter the measured dynamic response of the structure (Chen 1998, Farrar and Worden 2007). For example, the method used to monitor the condition of train wheels is much the same today as it was 100 years ago: tapping each wheel with a hammer and listening to its response.

Vibrationbased damage identification methods show great promise for online damage assessment of large civil engineering structures. These methods rely on vibration

measurements, such as accelerations of a structure, which are associated with damage in the structure (Montalvão et al. 2006). From this vibration measurement data, signal processing techniques, such as Fourier transforms, wavelet transforms and Hilbert–Huang transform, can be employed to directly detect structural damage. Alternatively, modelbased techniques, based on a structural model or modal model, can be adopted for identifying the location and extent of the structural damage. By using vibrationbased methods, damage can be identified in a global sense, even when the location of damage is inaccessible and not known. Although their successful application has been developed recently, the damage assessment of large complex civil engineering structures, such as bridges and buildings, still remains a challenging task in practice for civil engineers.

This chapter first classifies types of damage in civil engineering structures. Traditional non destructive testing techniques are introduced for detecting damage in structures. The nature of various NDT techniques and their application to civil engineering practices are discussed. Then, the recently developed SHM methods for damage identification of civil engineering structures are reviewed. NDT techniques and SHM methods are compared for structural damage identification in practice. For SHM methods, two types of damage identification approaches are further discussed: databased and modelbased. Typical databased approaches such as signal processing techniques are presented for structural damage detection. Finally, the philosophy and development of vibrationbased damage identification in civil engineering applications is discussed.

4.2 Damage in Structures

Damage can be defined in general terms as changes introduced into a system that adversely affect its current or future performance. Here, the main focus is the study of damage identification in civil engineering structures. Thus, the definition of damage is limited to any deviation in the geometric or material properties of a structure, which has an adverse effect on current or future performance of the structure, such as undesirable stresses, displacements or vibrations of the structure. These deviations may develop due to a variety of causes such as:

- failure of the material, i.e. corrosion, fatigue, plasticity and cracking
- flaws, voids, cracks and weak spots caused during manufacture
- loss of structural connections, i.e. loose bolts and broken welds
- improper assembly or misfits during construction.

Damages in civil engineering structures vary, depending on the cause of the damage. The causes of damage can be operational factors and/or environmental factors. The common types of damage include material cracks, degradation of material properties, change in geometric properties or loss of structural strength. Location of damage can be almost anywhere in the structure, and is associated with the cause of the damage. The extent of damage can range from the microscopic scale to the global scale. The severity of damage can be a minor effect or a severe effect on structural safety (Ettouney and Alampalli 2012). In the damage assessment

process, the key damage parameters, such as the cause, type, location, extent and severity, need to be determined.

Damage can accumulate incrementally over long periods of time, such as fatigue or corrosion. Damage can also result from unexpected discrete events, such as fire or earthquake. Damage usually starts at the material level (Farrar and Worden 2007). As the damage grows, it reaches a point where it affects the structural performance, eventually to an unacceptable point to the user (i.e. failure). If a structure has sustained damage, and the damage remains undetected, the damage could progressively increase until the structure fails. In order to detect damage at an early stage, appropriate damage identification methods should be selected, on the basis of technical issues (e.g. damage size, failure modes, temporal and spatial considerations), utility (e.g. size of equipment, simplicity, labour needs, health and safety) and cost–benefit.

Since damage in a structure is a change in an initial state, damage can be identified in two different methodologies: directly by inspection or through a comparison between a baseline (undamaged) state and a changed state. Methods for direct damage detection include most conventional NDT techniques. NDT techniques do not require a baseline, and they are usually carried out offline in a local manner after the damage has been located. Thus, the NDT techniques are primarily used for damage characterisation and as a severity check when there is a priori knowledge of the damage location.

Another damage identification methodology is based on the change in structural state. This methodology often involves a comparison between two different states of the structural system – an initial (undamaged) state and a changed state – so as to quantify the difference between the two states due to the damage. For civil infrastructure, damage in a structure will cause changes in the geometric or material properties of the structure, for example, a structural crack (stiffness change), bridge pillar silting (boundary condition change), counterweight balancing loss (mass change) or looseness in a bolted joint (connectivity change). These changes between initial and current state can be used to assess the damage in the structure. This concept is often used in health evaluation of the structure from monitored data.

4.3 NonDestructive Testing Techniques

Traditional nondestructive testing techniques have been extensively employed for detecting damage in engineering structures, as discussed in the book by Heller (2001). These NDT techniques give the effective damage detection results in local areas, in particular when the approximate damaged location is known. There are many NDT techniques available, and different methods target different ranges of the wave spectrum (Ettouney and Alampalli 2012), as illustrated in [Figure 4.1](#). And the NDT techniques reside in various frequency ranges, since the frequency is inversely proportional to the wavelength. For example, ultrasound locates in the lower wave frequency range, and thermography targets the infrared frequency range. The penetrating radiation of Xrays is at much higher frequency range. By using the properties of these waves, damage in a structure can be detected by observing the interaction of different wave types and the structure concerned.

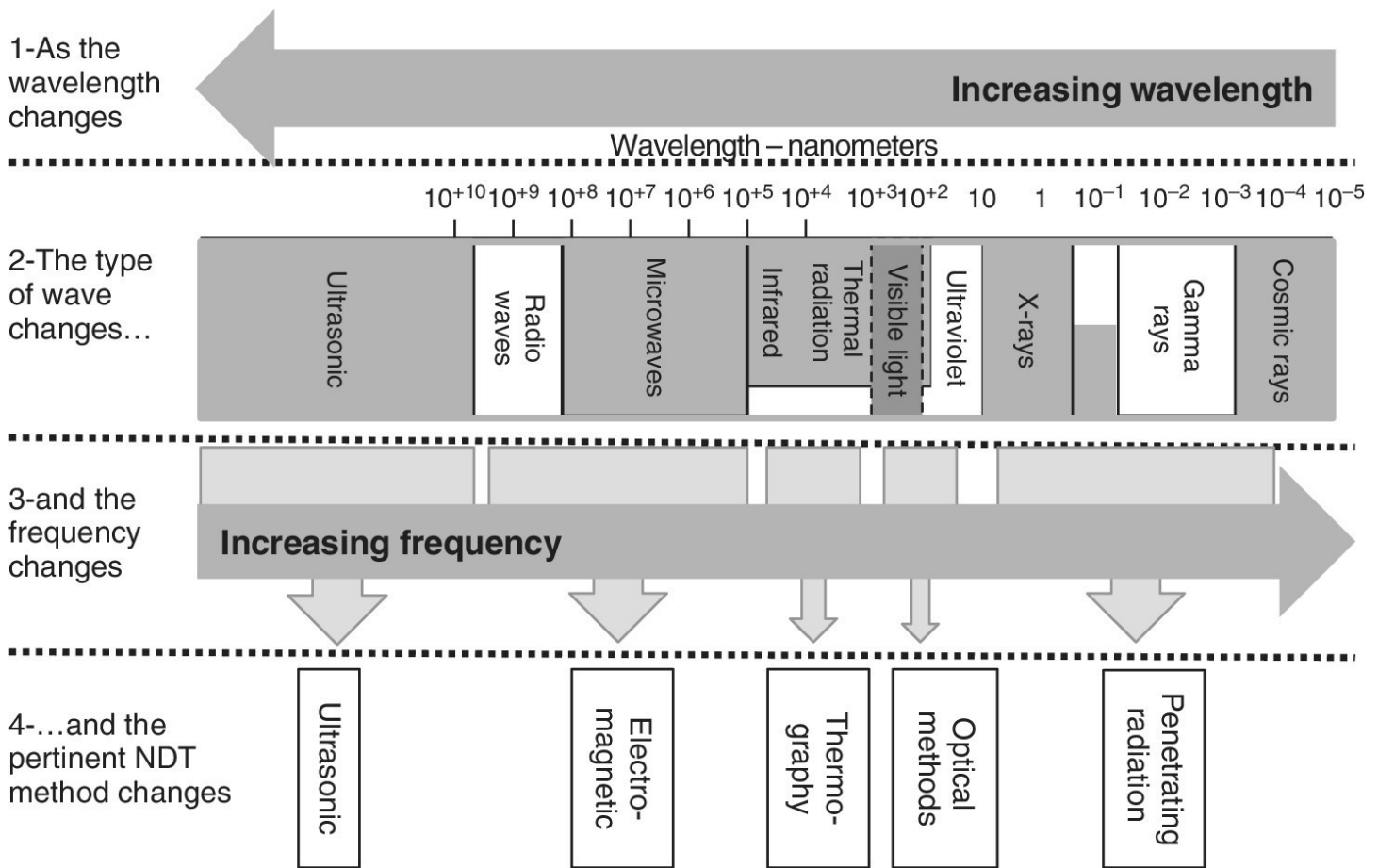


Figure 4.1 Traditional NDT techniques depending on wave types (after Ettouney and Alampalli 2012).

4.3.1 Acoustic Emission

Acoustic emission (AE) is initially used to investigate the physical parameters and damage mechanisms of materials. Acoustic emission can also be utilised as an NDT technique. The philosophy of AE is that damage events in a material or structure create stress waves propagating throughout the structure. These stress waves are called acoustic emission with a frequency range typically from 20 kHz to 1.0 MHz. The properties of these stress waves depend on the nature of structural damage and the properties of the structure. By analysing the measured acoustic emission signals, structural damage can be detected and the state of the structure can be estimated.

Acoustic emission is a passive NDT method, and depends on the propagation of damage signals. Processes, such as cracking, deformation, impacts and crushing, all produce localised transient changes in stored elastic energy with a broad spectral content (Ciang et al. 2008). A typical source of an AE wave within a material is the appearance of a crack from an initial defect when a preexisting crack grows. Acoustic emission is initiated when energy is released from a local source due to these processes within a material or structure. Thus, this technique makes it possible to detect the crack growth in real time. There are several important properties of AE signals, including amplitude, frequency content and rate of decay. The most common sensor type used in monitoring stress waves in materials is based on a surface

mounted piezoelectric crystal. When high accuracy of damage evaluation is needed, the number of sensors must be increased, and subsequently the amount of data output to the signal processing system is also increased.

Acoustic emission testing has been used extensively in various civil engineering structures, including bridges, tunnels, dams, pipelines and nuclear structures. The AE method is very powerful in detecting any damage mode up to the microscale. However, since acoustic emission energy can be extremely small, this can be a severe limitation, especially when used in an in situ structural monitoring where the background noise can interfere with the AE signals. Also, this method is less capable of damage characterisation and further damage evaluation. For realtime health monitoring of civil structures, damage detection that is based on wave speed in a complex structure may not be the most effective method, since the wave speed in a structure is a function of the geometric and material parameters of the structure. An inservice structural neural system can be used to improve the damage evaluation capability of the AE method (Kirikera et al. 2007). The passive structural neural system has high sensitivity to damage and simple instrumentation of the monitoring system.

4.3.2 Ultrasound

Ultrasound is a well established and very popular NDT technique for investigating the inner structure in a solid test object. The basic principle of the technique is that as an ultrasonic wave propagates through the object, the wave changes its form through reflection, refraction and scattering (Ettouney and Alampalli 2012). In ultrasound scanning, a transmitter transfers ultrasound waves into the material and its signal is collected by a receiver, once the transmitter has passed through the material. The transmitter and receiver can be simply placed on opposite surfaces of the material. Then, the signals collected by the receiver can be processed and the damage in the test object can be detected.

There are various ultrasonic testing methods available for practical applications, such as impact echo, pulse echo, sonic vibration, guided waves and laser based ultrasound. Although the frequency range of ultrasound is similar to acoustic emission, ultrasound is very different from acoustic emission. The ultrasound technique is an active method, and it generates sound signals and monitors the interaction of the signals with the test objects. Ultrasound scanning typically reveals planar cracks oriented perpendicular to the direction of sound wave propagation. The transmit time and amplitude of the ultrasound are often obtained. The transmit time can be used to identify the location of the defect relative to the position of the transducers, while the transmit amplitude can be used to assess the extent of the defect. Damage of size as small as a few millimetres can be detected using ultrasonic testing.

Ultrasonic testing has proved its effectiveness in a variety of applications to civil engineering structures, such as condition assessment of bridge decks, concrete evaluation for locating voids and discontinuities and properties estimation of structural geometries and materials. In practice, it is important to choose appropriate ultrasound methods for damage detection and condition assessment. In general, higher resolution of frequency sampling is only possible with lower resolution of time sampling, and vice versa. In the cases for large civil structures such

as bridges, the low frequency but long distance ultrasound methods may be more suitable for damage assessment. Damage localisation using ultrasound methods may be inaccurate for complex structures. The recently developed ultrasound propagation imaging technique can be very promising. When a laser is used as both transmitter and receiver, the technique can be used as a remote in-service SHM for large structures. Recently, acoustic wavefield imaging has been proposed for damage detection (Michaels and Michaels 2006). Since this technology provides a scanned movie or snapshots, it can provide easy explanations on the wave propagation mechanism and the interaction of the wavefield with damage in the structure.

4.3.3 Guided (Lamb) Waves

Guided wave (GW) testing has emerged as a very prominent option among ultrasound methods. The guided wave is widely acknowledged as one of the most encouraging tools for estimating the location, severity and type of damage in a structure (Lowe et al. 1998). Guided waves are defined as stress waves forced to follow a path defined by the material boundaries of the structure (Raghavan and Cesnik 2007). The critical elements of the guided wave technique for damage detection include transducers, signal processing methodology and arrangement of the transducer network to scan the structure. Guided waves are excited and received in a structure using transducers for structural damage assessment (Niu et al. 2017). [Figure 4.2](#) shows the equipment and applications of the guided wave technique developed by the Teletest of TWI for structural integrity assessment of pipelines. Guided waves have also shown suitability for applications in the field of SHM, since they have an online sensor and actuator network to assess the state of a structure during operation. The actuator and sensor pair in GW testing has a large coverage area, requiring fewer units distributed over the structure.

(a) Low frequency flaw detector and ruggedised personal computer.



(b) Testing a 24-inch foam insulated pipe of a sleeved road crossing.



Figure 4.2 Equipment and applications of the guided wave technique.

(Courtesy of Teletest, TWI)

Lamb waves are an important class of guided waves, and they can propagate in a solid plate with free surfaces. Lamb waves, combinations of longitudinal and shear modes, are available in a thin plate, and their propagation characteristics vary with entry angle, excitation and

structural geometry. These waves can be actively excited and collected by a variety of means, including ultrasonic probe, laser, piezoelectric element, interdigital transducer and optical fibre (Su et al. 2006). Lamb wave based damage detection is essentially subject to interpretation of the captured wave signals. Problems often arise in the extraction of key features useful for damage detection from the collected signals. These problems include contamination by diverse noise, interference from natural structural vibration, confusion of multiple modes and bulkiness of sampled data. An appropriate Lamb mode for damage detection should have useful features, such as nondispersion, low attenuation, high sensitivity, easy excitability and good detectability. To effectively detect damage in a structure using Lamb waves, many signal processing techniques have been proposed, including time series analysis, frequency analysis and integrated timefrequency analysis.

Guided waves are attractive in NDT applications because of their superior range and versatile theoretical background. These waves can travel over a long distance, and thus a broad area can be quickly examined. GW based damage detection methods offer many advantages, including:

- dependence of the stress and strain distribution on frequency, allowing the mode selection best fitted to specific damage type
- ability to inspect large structures while retaining coating and insulation
- ability to follow complex shaped structures
- ability to inspect the entire crosssectional area of a structure
- excellent sensitivity to multiple defects with high precision of identification.

Some applications for relatively small scale civil structures have been examined for GW damage detection with promising results. Since civil engineering structures are generally large and complex, in situ actuators have to provide high actuation stresses to cover a reasonable area (Su et al. 2006). For largescale civil structures such as bridge decks, impact can be used to generate a highenergy pulse and high penetration of the stress waves.

4.3.4 Thermography

Thermal imaging is a subsurface defect detection method, based on temperature differences measured on the investigated surface during monitoring by using infrared sensors or cameras (Ciang et al. 2008). Since heat flow is associated with material properties, it is possible to detect material damage by monitoring how heat flows. Thermal imaging methods can be categorised into two groups in terms of the thermal excitation approach used: passive and active. The passive method is used to investigate materials with a different temperature from ambient. This method is not commonly used in damage detection in civil engineering structures. By contrast, the active approach uses an external source, such as optical flash lamps or heat lamps, to induce relevant thermal contrasts on the test subject (Stanley 1997). One of typical active thermal imaging methods is the thermoelastic stress method based on the thermo elastic effect.

Thermography has shown great promise in the field of NDT for civil engineering structures.

These methods can be used for assessing various defects in civil infrastructure, such as fatigue, reinforcement corrosion and seismic damage. Thermal imaging needs only low load magnitudes, and it can be utilised to validate stress distributions predicted by finite element model at the initial stage and to detect the spread of damage during failure. Thermal imaging damage detection can be a local technique or a global technique, because this method is able to assess the damage from a single or fullfield measurement in image form, depending on camera resolution. However, the thermal excitation method is the main problem with thermal imaging methods. Passive excitation can be used, but it is limited to abnormal electrical components that produce excess heat during operation. Active excitation is expensive and it is labour intensive to excite the structure on site. Recently, a heat source, such as a halogen lamp or ultrasound generated by contact transducers and noncontact pulsed laser, have been used to tackle the problem based on the mechanical loading. This method, particularly the non contact ultrasoundinduced thermography, is potentially promising for inservice SHM in the future.

4.3.5 Electromagnetic Methods

Electromagnetic methods use the interaction between the electromagnetic flux and waves and the flaws in the test material (Ettouney and Alampalli 2012). Typical electromagnetic methods in practice include eddy current, static magnetic field, magnetic particle and microwave techniques. These techniques are able to detect surface or subsurface flaws with size less than 1 mm. Among these methods, eddy current and microwave techniques can be used for insitu automated testing, without requiring pretest and posttest preparations. Static magnetic field techniques detect flaws by measuring magnetic field perturbations, while microwave techniques can detect interior damage by measuring electromagnetic wave reflection to indicate damage states. All electromagnetic methods can detect fatigue cracks and earthquake damage in metals. Microwave techniques can detect even more types of damage, such as reinforcement corrosion, scour and bridge security. The optimal method depends on geometry and size of the expected damage, and should be chosen by careful decision making analysis.

Eddy current is a popular NDT method for inspecting surface or near surface flaws of conductive materials. It is also used to detect material properties, such as conductivity, corrosion and permeability. A basic eddy current system often consists of a coil that is excited by an alternating current. When a flaw occurs in the material, the flaw will cause a variation in the eddy current flow, leading to modification of the second magnetic field. By observing this modification, damage detection and localisation become possible. Eddy current techniques offer many advantages, including simple and accurate surface defect detection and high efficiency in metallic materials. However, some a priori knowledge of damage location is required for effective use of the eddy current technique.

Electromagnetic methods can be used in many ways in structural damage detection. Most of these methods can only be applied to conductive materials, such as metals, depending on the type of test, and they are limited to detecting surface or nearsurface flaws. They are suitable for direct sensing and require close proximity, thus their usefulness in remote sensing applications for SHM is limited.

4.3.6 Capacitive Methods

Capacitive methods are based on electromagnetic techniques, and they were initially used for assessing water content in civil engineering materials such as concrete, masonry and soils (Balageas et al. 2006). This technique uses two or more electrodes on the surface of materials, and then applies a voltage between them. This system forms a capacitor, and the changes in capacitance indicate internal constituents, such as material properties and moisture content. Owing to its simplicity, the system can be designed to meet special requirements in applications. Capacitive methods are particularly useful for assessing concrete materials and structures, including measurement of moisture content in cover concrete and diagnosis of external posttensioned steel cables. These methods are also well suited to monitoring the health of historic buildings by analysing the water content measurements collected from the system. Capacitive methods have the potential to make continuous measurements on large area of civil engineering structures. These measurements, together with an online localisation system, enable the detection of variations in capacitance associated with local defects, which eventually provides information about the location and size of defects.

To improve damage diagnosis of civil engineering structures, capacitive methods can be used with other NDT techniques, such as ultrasound, ground penetrating radar (GPR) and the impact echo technique (Dérobert et al. 2008). Electromagnetic waves of capacitive methods and GPR are sensitive to the water and chloride contents, potentially to porosity, while ultrasonic waves are more sensitive to mechanical properties and porosity, even if they are affected by changes in water content in concrete. A combination of different techniques, based on the propagation of waves of different nature (GPR and impact echo) and different frequency range (capacitive technique and GPR), reduces the uncertainty of damage evaluation. This integrated method is useful for damage assessment of civil engineering structures, in particular concrete structures.

4.3.7 Laser Doppler Vibrometer

The laser Doppler vibrometer (LDV) is a noncontact velocity transducer, based on the analysis of the Doppler effect on a laser beam emerging from a solid surface (Martarelli et al. 2001). In order to apply this method to damage detection, an approach using modal properties can be employed, by assuming that damage will cause detectable changes in the modal properties. These measurements can then be used to extract modal parameters such as natural frequencies and mode shapes. The obtained modal parameters give essential information for structural damage assessment. Comparing these parameters allows the location and extent of damage in the structure to be determined by using vibrationbased damage identification methods to be discussed in [Chapters 7](#) and [8](#). [Figure 4.3](#) illustrates the system of a laser Doppler vibrometer for structural damage detection (Siringoringo and Fujino 2006).

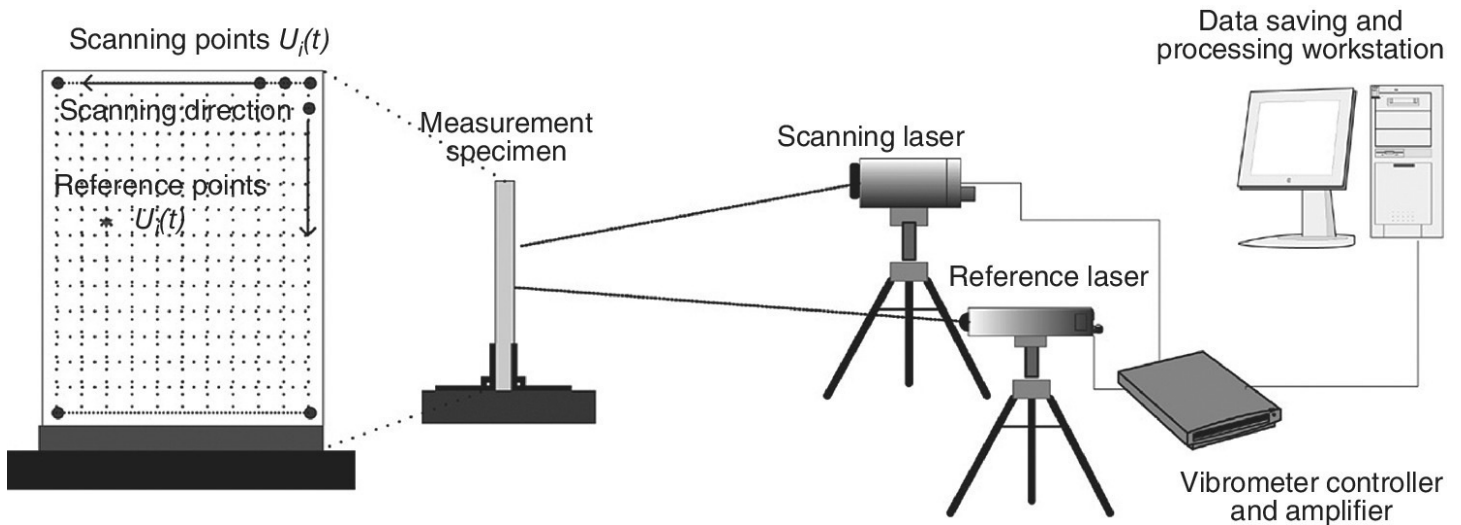


Figure 4.3 Schematic diagrams of a laser Doppler vibrometer system.

(Courtesy of Siringoringo and Fujino 2006)

The use of scanning LDV as a vibration transducer has many advantages, such as high sensitivity and noncontact capabilities (Ciang et al. 2008). Scanning LDV provides a high spatial resolution of measurement, so as to avoid using a massive number of transducers. Also, this technique allows measurement of test objects that are inaccessible by conventional transducers. These features can improve the quality and efficiency of modal testing. Scanning LDV can identify the location of damage on a structure by using changes of operational deflection shapes obtained from measurements. This technique can offer very accurate results for detecting damage, because of the use of the operational response of the structure.

The laser Doppler vibrometer is very promising, since the method has a high spatial resolution of measurement. It is a noncontact method and thus is easy to implement in practice. For practical applications, the LDV based structural condition assessment should operate under ambient excitation. This type of excitation is more attractive since it allows modal analysis to be performed under service condition of the structure and does not require any artificial excitors (Siringoringo and Fujino 2006). From operational modal data measurements, the method can be used with most vibrationbased damage identification methods. When laser pulse excitation is used, the method has the potential for a remote health monitoring strategy of civil structures in service. However, the laser Doppler vibrometer is still uneconomic for civil engineering applications.

4.3.8 Global Positioning System

Global positioning system technology is an emerging tool that can measure directly both static and dynamic responses (Yi et al. 2013). GPS is a satellitebased positioning system that allows users in the field to determine their location without the need to transmit and hence identify their position. GPS technology can provide relative displacements measured at rates of 20 Hz and even higher up to 100 Hz. The accuracy of dynamic displacement measurements using GPS is at a subcentimetre to millimetre level and at a maximum distance from the reference GPS receivers to the structure receivers of up to 30 km. These provide a great

opportunity to monitor the displacement or deflection behaviour of large civil engineering structures in real time under ambient loading conditions.

A GPS system generally consists of three components: satellites orbiting the Earth, control and monitoring stations on Earth and GPS receivers owned by the users (KijewskiCorrea et al. 2006), as illustrated in [Figure 4.4](#). GPS surveying techniques can be static, faststatic or realtime kinematic. Kinematic GPS enables the rover to be dynamic, hence allowing the instantaneous position of a moving platform to be obtained at precise times in three dimensions. The outcome of using kinematic GPS is that the position of any point at any time can be recorded (Brown et al. 2006). GPS techniques have several major advantages, including

- line of sight is not required
- one base unit can serve several rovers
- the data can be collected and downloaded directly to a webbased system for remote interrogation
- the technique can be used where access is difficult.

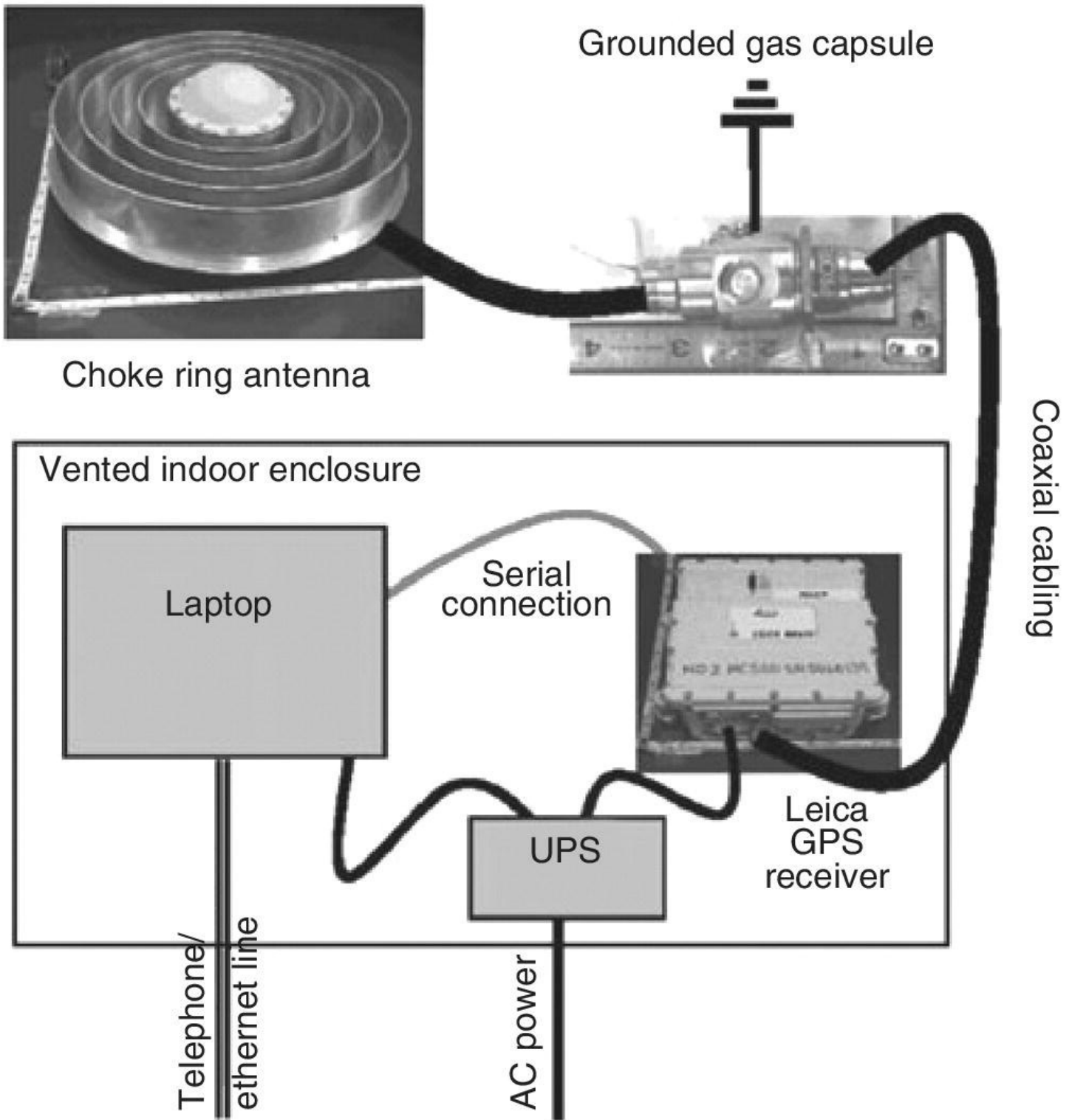


Figure 4.4 Schematic diagrams of configuration of global positioning system (GPS) components.

(Courtesy of KijewskiCorrea et al. 2006)

Although GPS offers many advantages, there are still some issues to be solved before practical applications, such as determining the lower limit of measurable deflection amplitude, reducing capital cost of testing, modifying antenna type to be minimally intrusive and understanding the limitations of constellation geometry (Brown et al. 2006). Thus, an integrated sensor system,

consisting of GPS receivers, accelerometers, displacement transducers or even groundbased pseudosatellite (pseudolite) transmitters, should be developed to increase the accuracy, reliability and productivity of the overall monitoring system. The GPS technology will continue to evolve and become more costeffective, such that insitu monitoring will become a powerful tool for assessing the performance of large civil engineering structures.

4.3.9 Visual Inspection

Visual inspection is the simplest and most straightforward NDT method. Visual inspection is based on observing the condition of a structure visually and attempting to detect its current state, according to personal experience and available guidelines. In order to reduce costs and time, visual inspection should be an integral part of any NDT project (Ettouney and Alampalli 2012). Visual inspection has many advantages, including being very simple and quick, able to apply remotely and suitable for local to global inspection. However, the inspection is qualitative and may require special equipment for access.

4.4 Comparison of NDT and SHM

Nondestructive testing provides a wide range of powerful techniques for detecting damage and assessing conditions for civil engineering structures. NDT techniques have been in use and in continuous development for a long time. The use of these techniques has been successful in condition evaluation of civil engineering structures such as bridges (Ettouney and Alampalli 2012). These techniques are complementary and beneficial tools for health monitoring of civil infrastructure.

SHM is an emerging method for realtime health evolution of engineering structures using monitored data. SHM can provide more information about current state estimate and future performance prediction of a structure, so as to make appropriate decisions for effective management of the structure. SHM methods consists of key components, such as sensing network, system identification, damage diagnosis and damage prognosis. SHM methods are very different from NDT techniques in many respects.

In the area of sensing network, sensing technology of NDT techniques is well established and very advanced. A single type of sensor is typically used in NDT techniques. Operations of NDT techniques are usually manual and relatively simple. NDT techniques are generally localised in nature, and they generally require a priori knowledge of the location of damage in a structure. By contrast, SHM methods often use various types of sensors, and their sensing network can be automated through advanced data transmission systems such as wireless communications. SHM methods can cover large areas, and a priori knowledge of damage location is not needed, which is particularly suited for large civil engineering structures. SHM methods undertake continuous monitoring and offer valuable information for assessing the state of a structure in service. However, advanced and reliable sensing technology for SHM methods, such as wireless sensing, is still in development for implementation to large civil engineering structures.

System identification approaches are not very useful for NDT techniques, since these approaches identify global structural behaviour rather than behaviour in a local area. However, system identification approaches are an essential part of most SHM methods, and they are well developed for evaluating structural and/or modal parameters from ambient measurements. System identification approaches have been implemented to many SHM methods in civil structures.

In damage diagnosis, NDT techniques can provide localised identification of damage sites, when the type and region of damage is available before identification. The global structural information and analytical model are not required for these techniques because of their localised nature. NDT techniques often need relatively simple computational algorithms, and provide high reliability for the characteristics of the damage. By contrast, SHM methods can offer global identification of damage in a structure. The damage identification by SHM methods often requires more information about the geometry and material properties of the structure, which is often not easy and straightforward. The identification procedure of SHM methods may need extensive computational efforts. Reliable and efficient algorithms for damage identification based on SHM are still in development.

Damage prognosis provides informed decision making for civil infrastructure management. NDT techniques can evaluate localised damage accurately, thus they provide reliability at local area or at structural component level. Due to their localised nature, the reliability of the overall structural system may not be obtained, and thus the consequences of global failure are not addressed. Due to the short time event of NDT, stochastic modelling of structural capacity and loading conditions is usually not possible, but SHM methods can assess the performance of the structural system due to their global nature. SHM methods can give information for stochastic modelling on the basis of continuous monitored data, which is useful for reliability analysis of the structural system. Based on the evolution of models (e.g. strength deterioration and future loading models) from SHM methods, time-dependent reliability of the structure can be determined, which can be used for optimising the maintenance strategy of existing civil engineering structures.

4.5 Signal Processing for Damage Detection

Most structural damage detection methods are based on measuring and analysing time signals collected from sensors. Such time signals can be input signals, such as earthquakes, wind pressures or blast pressures, or output signals, such as accelerations, strains or displacements. Signals can be broadly divided into two types according to signal property: stationary and nonstationary. Stationary signals do not change their characteristics with time, while nonstationary signals change their characteristics. Most signals acting on civil infrastructure are nonstationary, such as earthquakes and wind. If signals are analysed in the frequency domain by transforming from the time domain, the damage identification process is often more effective (Ettouney and Alampalli 2012). Therefore, signal processing methods, typically Fourier based transforms, wavelet transforms and Hilbert–Huang transform, are required for structural damage detection.

4.5.1 Fourier Based Transforms

A time signal can be represented in the frequency domain by various Fourier transforms. The details of these methods can be found in the comprehensive review by Boashash (2003). When any time signal $x(t)$ over time t is available, the most popular forward and inverse continuous Fourier transforms (FT) can be expressed, respectively, as

$$FT(\omega) = \int_{-\infty}^{\infty} x(t)e^{-j\omega t} dt, x(t) = \frac{1}{2\pi} \int_{-\infty}^{\infty} FT(\omega)e^{j\omega t} d\omega \quad (4.1)$$

where ω is the angular frequency and $j = \sqrt{-1}$. $FT(\omega)$ is necessarily complex, and a plot of the amplitude of this function against frequency represents the frequency content of the time signal. From [Equation \(4.1\)](#), the discrete Fourier transform is obtained by representing the continuous Fourier transforms in terms of summations.

The Fourier transforms have many advantages, such as being applicable to various problems, well understood and explicit inverse transforms. However, their major disadvantage is that the Fourier transform spectra do not reveal any information regarding the time dependency of frequency content of the signal. Thus, the Fourier transforms are not applicable for non stationary signals, such as wind and earthquake signals, or nonlinear problems. Another limitation of the Fourier transforms is the loss of temporal information of frequency content. To avoid this limitation, the timeFourier transforms are introduced by using a window function. However, the timeFourier transforms are still not applicable for nonstationary or non linear problems.

4.5.2 Wavelet Transforms

To address the issues in the Fourier transforms, wavelet transforms have been developed for effective signal processing, as described in detail in Graps (1995). The wavelet transforms are a tool that can cut data, functions or operators into different frequency components with a resolution matched to its scale (Daubechies 1988). The forward and inverse continuous wavelet transform (WT) for a time signal $x(t)$ are defined, respectively, as

$$WT(s, \tau) = \int x(t)\psi(s, \tau, t) dt, x(t) = \iint WT(s, \tau)\psi(s, \tau, t) ds d\tau \quad (4.2)$$

The basic function (wavelet function) $\psi(s, \tau, t)$ includes a scaling variable (s) and a translation variable (τ), expressed as

$$\psi(s, \tau, t) = \frac{1}{\sqrt{s}}\psi\left(\frac{t - \tau}{s}\right) \quad (4.3)$$

The scaling factor controls the amplitude of the wavelet function, and the translation factor controls the location of the wavelet function on the time scale. As the scaling factor changes, the effective width of the wavelet function changes. Unlike Fourier transforms, wavelet

transforms can be designed to meet the requirements of particular problems.

The wavelet transforms enable the study of time history in terms of its frequency content in signal processing. Although the windowed Fourier transforms could provide the time location by windowing the signal, the window lengths are always the same, regardless of the frequency components. By contrast, the wavelet transforms allow multiple time resolutions, depending on the frequency components (Ettouney and Alampalli 2012). They can give high accuracy in numerical differentiation as well as flexible implementation of boundary conditions. The wavelet transforms offer many advantages: (a) they are well developed, (b) inverse transforms exist, (c) both continuous and discrete forms exist, (d) they do not have limits on frequency and time resolutions, (e) they are suitable for nonstationary and nonlinear problems.

Wavelet analysis is very suited to analysing nonstationary signal, so it can be used as a feasible method for processing a signal to construct the intended feature index of structural damage. Wavelet analysis has various applications in structural damage detection, including singular signal detection, signal/noise separation, frequency band analysis and so on. The spectrum graph obtained using wavelet transforms can indicate the damage existence directly. In the review by Yan et al. (2007), a study was undertaken based on the wavelet transforms for structural damage detection. By comparing the discrete wavelet transforms of two sets of vibration signals from the undamaged and damaged structure in the space domain, both the presence and the location of the damage can be detected. Numerical results show that even a minor localised defect can induce significant changes in the wavelet coefficients of the vibration signals.

Another wavelet based approach was proposed to locate damage in civil engineering structures, on the basis of the acceleration time history responses (Zabel 2005). By use of the Haar mother wavelet, the first level fast wavelet decomposition of the measurements was applied for both the undamaged and damaged prestressed reinforced concrete frame structure. The sensitive feature is defined as the standard deviation of the error between the reconstructed signal and the actual measured signal. This method does not require the knowledge of the excitation mechanism, since it is entirely based on the measured responses. However, wavelet transforms have several limitations in structural damage identification, such as low accuracy in damage localisation, and difficulty in quantification of damage in complex structures.

4.5.3 Hilbert–Huang Transform

The Hilbert–Huang transform (HHT) has become a popular method for signal processing. In contrast to other common transforms, such as Fourier transforms, HHT is an empirical approach that can be applied to a data set, as discussed in detail in Huang and Shen (2014). This approach is based on the Hilbert transform, which is defined, for an arbitrary time signal $x(t)$ with the Cauchy principal value P , as

$$\hat{x}(t) = \frac{1}{\pi} P \int_{-\infty}^{+\infty} \frac{x(\tau)}{t - \tau} d\tau \quad (4.4)$$

HHT is the result of the Hilbert spectral analysis and the empirical mode decomposition; it uses empirical mode decomposition to decompose a signal into so-called intrinsic mode functions with a trend. Then HHT applies Hilbert spectral analysis to the intrinsic mode functions to obtain instantaneous frequency data. The HHT keeps the characteristics of the varying frequency, since the signal is decomposed in the time domain, and the length of the intrinsic mode functions is the same as the original signal. This is a great advantage of HHT since realworld signals usually have multiple causes happening in different time intervals. HHT offers many advantages, such as being applicable to nonstationary signals or non-linear problems, able to produce more physically meaningful results than other transforms, and able to produce adequate frequency and time resolution to the problem concerned within the time and frequency ranges of interest.

HHT is very useful for nonstationary, nonzero mean and nonlinear real signals. It makes an empirical mode decomposition of the time signal into narrow band components with zero mean. These components do not have a specific analytical representation, but each component can be associated with a physical meaning. These components can be related to the mode shapes of dynamic structural systems and therefore the existence of damage.

HHT has been used in damage detection in civil engineering structures with many successful applications (Montalvão et al. 2006). From the results of its application to the ASCE benchmark problem for SHM, HHT is able to identify the modal data, such as natural frequencies, damping ratios and mode shapes, as well as the stiffness matrix with reasonable accuracy. Damage can then be detected by comparing the stiffness of each floor before and after introducing damage. Simulation results show that HHT can detect the assumed damage with good accuracy. Furthermore, fast Fourier transforms have been used for nonlinear and nonstationary data processing to characterise damage in civil structures such as structural members and pile foundations. The HHT analysis showed a more significant frequency downshift than the Fourier based approaches for measurements near the damage location.

An experimental investigation of the applicability of the empirical mode decomposition has been undertaken for identifying structural damage caused by a sudden change of structural stiffness (Yan et al. 2007). Empirical mode decomposition is then applied to measured time histories to identify the damage occurring time instant and the damage location for various test cases. By comparing identified results with measured ones, the damage occurring time instants could be accurately detected in terms of damage spikes extracted directly from the measurement data. The damage location could be determined by the spatial distribution of the spikes along the structure.

4.5.4 Comparison of Various Transforms

Fourier based transforms are well-established methods. They have been extensively used in earthquake engineering, although earthquake signals are nonstationary. Fourier based transforms can lose either frequency resolution at low frequency or time resolution at high frequency. They are not applicable to nonstationary and nonlinear problems.

Wavelet transforms avoid the shortcomings of the Fourier based transforms, and they do not

have the limitation on frequency or time resolution. The wavelet transforms are able to apply to nonstationary signals and nonlinear systems. They can be used for analysing potential nonstationary and nonlinear responses to give indication of damage in a structure. However, the wavelet transforms are not adaptive.

HHT has all the advantages of the wavelet transforms. Also, HHT has the property of adaptivity, which can produce more physically meaningful results and provide adequate frequency and time resolution. It can be used for processing nonstationary signals and for detecting damage in nonlinear structural systems.

4.6 DataBased Versus ModelBased Techniques

Structural damage assessment techniques can generally be classified as either databased or modelbased. These two types are complementary, and a combination of both will usually be applied, since one is more appropriate than the other in different contexts. The applications of databased and modelbased techniques in an SHM strategy are discussed in Farrar and Lieven (2007) and illustrated in [Figure 4.5](#).

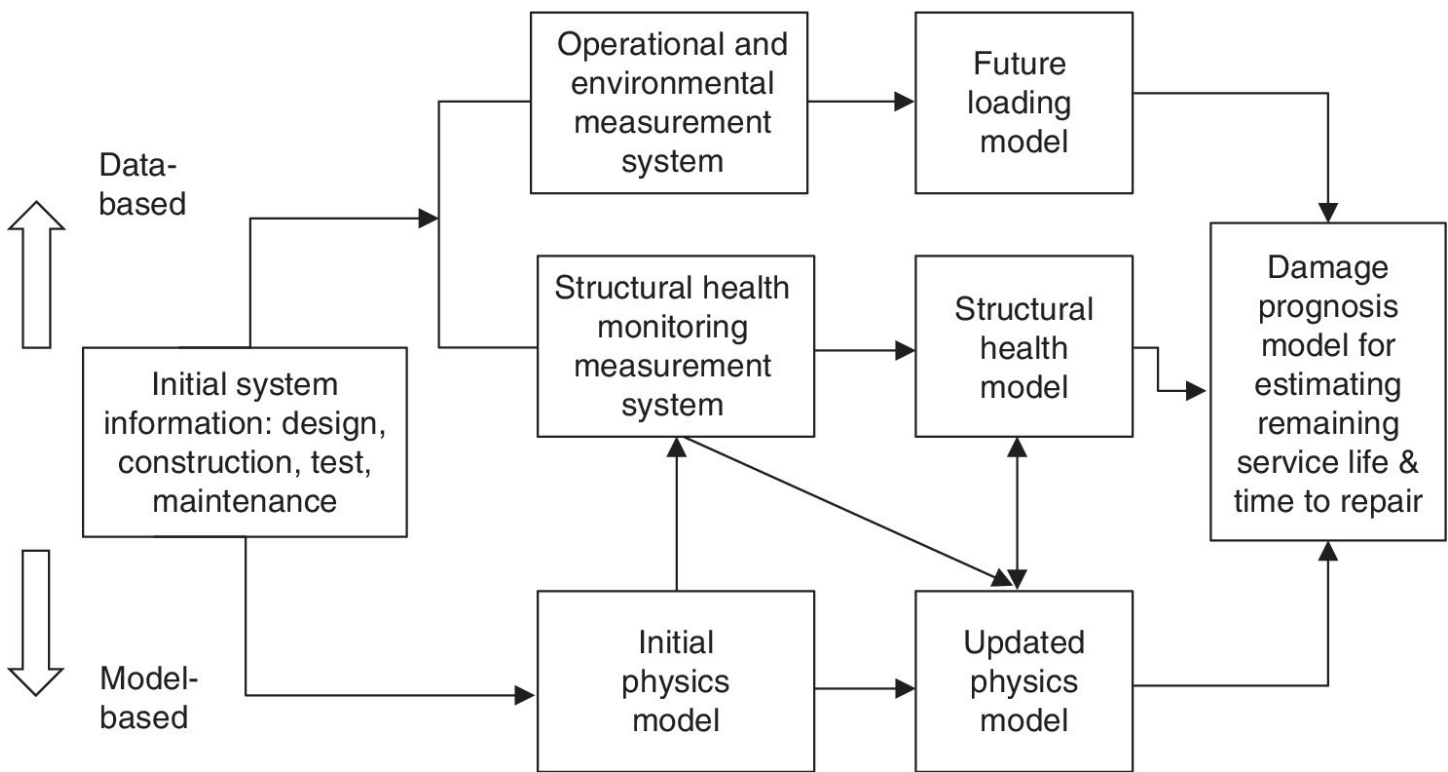


Figure 4.5 Databased and modelbased damage assessment techniques in structural health monitoring strategies (after Farrar and Lieven 2007).

Databased techniques are based on previous measurements from the system to assess the current damage state. Such techniques are typically performed by means of some sort of pattern recognition method. They do not require the development and use of a behaviour model of the system. Since they are much easier to implement, they have the potential to be used on a large number of structures. These techniques have a primary goal of detecting anomalies in structural

behaviour. The anomalies are detected as a difference in measurements with respect to measurements recorded during a previous period. The databased methodology is completely data driven in the sense that the evolution of the data is estimated without information on the physical processes. Examples of the datadriven models include autoregressive models and rational polynomial models. These models typically consist of many approaches, such as anomaly detection and data processing, data reduction and representation, and feature extraction (Catbas et al. 2012). Therefore databased techniques can indicate a change in the presence of new loading conditions or system configurations such as damage in a structure. However, databased techniques will perform poorly when trying to classify the nature of the change such as development of the damage.

On the other hand, modelbased (or physicsbased) techniques are especially useful for predicting system responses to new loading conditions and/or new system configurations (damage states). One type of commonly used physical model in structural damage assessment is the structural model (e.g. finite element model). Structural models are typically initially constructed from design and test data. The initial structural models have to be calibrated using measurements on the real structure. In contrast to the databased techniques used for direct data interpretation, structural models are formulated to explicitly represent the underlying physics of the structural system, such as boundary and continuity conditions, equilibrium and kinematics. These models can be used to explicitly simulate structural behaviour under various critical loading conditions. Thus, such models can diagnose the causes of changes in behaviour, and they identify how such changes may impact the performance of the overall system (Catbas et al. 2012). Currently, the most commonly employed structural models in damage identification for civil engineering structures are finite element models. These provide structural connectivity and property information in the form of elemental force–displacement relationships and material constitutive properties. The finite element models can be updated using continuously monitored data, so as to produce the evolution of structural models with time. Therefore, future performance of the structure as well as remaining service life can be predicated through model evolution and probabilistic analysis.

Another type of physical model commonly used in structural damage identification is the modal model. This consists of modal parameters, i.e. modal frequencies, mode shapes and modal damping ratios. The modal model is different from the structural model, since the modal model does not contain specific information about the structural connectivity or the geometric distribution of mass, structural damping and stiffness. Since the modal parameters describe the resonant spatial and temporal behaviour of the structure, the modal models may be more convenient for the expression of the structural behaviour.

Compared to direct data interpretation of databased techniques, modelbased techniques can provide more useful information in structural health monitoring strategies, such as damage evolution, structural reliability analysis, remaining useful life estimate and optimal repair planning. However, modelbased techniques are typically more computationally intensive than databased techniques. The details of advantages and disadvantages of these two types of damage assessment techniques are given in Catbas et al. (2012) and summarised in [Table 4.1](#). Typically, the balance between databased techniques and modelbased techniques will

depend on the amount of relevant data available and the level of confidence in the predictive accuracy of the modelbased models.

Table 4.1 Comparison of databased and modelbased damage assessment techniques.

Type	Application	Advantage	Disadvantage
<p>Databased damage assessment (Direct signal analysis)</p>	<p>Most appropriate when</p> <ul style="list-style-type: none"> • many structures need to be monitored • there is time for training the system • it is difficult to construct structural or modal models 	<ul style="list-style-type: none"> • No modelling costs • May not need for damage scenarios • Many options for signal analysis • Incremental training can track damage accumulation • Good for longterm use on structures for early detection of situations requiring modelbased interpretation 	<ul style="list-style-type: none"> • Physical interpretation of the signal may be difficult • Weak support for decisions on rehabilitation and repair • Indirect guidance for structural management activities • Cannot be used to justify replacement avoidance
<p>Modelbased damage assessment (Structural or modal models)</p>	<p>Most appropriate when</p> <ul style="list-style-type: none"> • design model is not accurate • structure has strategic importance • damage is suspected • damage evolution is needed • there are needs to predict future performance 	<ul style="list-style-type: none"> • Interpretation is easy when links between measurements and potential causes are explicit • Effects of changes in loading and usage can be predicted • Guidance for further inspection and measurement • Consequences of future damage can be estimated • Support for planning rehabilitation and repair • Help make better decision in maintenance 	<ul style="list-style-type: none"> • Modelling is expensive and time consuming • Errors in models and in measurements can lead to identification of the wrong model • Large numbers of candidate models are hard to manage • Identification of the right model could require several interpretation – measurement cycles • Complex structures with many elements have combinatorial challenges

4.7 Development of VibrationBased Methods

For large and complex civil engineering structures, it is very difficult to accurately identify damage using local damage detection methods such as NDT techniques. In order to identify damage in these civil structures, a global methodology called vibrationbased damage identification has been developed during the past two decades. Vibrationbased methods are among the earliest and most common damage detection methods used, principally because they are simple to implement on any size structure (Ciang et al. 2008). In the process of vibration based methods, structures can be excited by ambient energy, an external shaker or embedded actuators. Then, accelerometers can be used to monitor the dynamic response of the structure. The basic principle behind this methodology is that modal parameters (i.e. frequencies, mode shapes and modal damping) are functions of the physical properties of the structure (i.e. mass, stiffness and structural damping) (Chen 1998). Structural damage reduces the stiffness of the structure and then alters its modal parameters. Therefore, measurement and monitoring of vibration responses should theoretically permit the identification of both the location and severity of the structural damage (Chen 2005).

Vibrationbased damage identification methods show great promise, in particular in the application to remote damage identification for large civil engineering structures. These methods offer many advantages (Humar et al. 2006), including

- location of the damage is not required to be known a priori
- sensors required to measure the vibration responses are not necessary to be placed in the vicinity of the damage, since the modal parameters are global properties
- just a limited number of sensors can provide sufficient information to locate the damage and assess its severity, even in a large and complex civil structure
- vibration measurements do not require the use of bulky equipment, and can be collected under ambient environments using advanced sensing systems on the structure.

However, in practice, there are several limitations associated with vibrationbased damage identification methods, as summarised below.

- *Low sensitivity to damage.* Modal parameters may not be very sensitive to local damage, although they are associated with local damage in a structure. Damage in a structure typically is a local phenomenon. Local response is captured by higher frequency modes, whereas lower frequency modes tend to capture the global response of the structure and are less sensitive to local changes in the structure. Consequently, the change in modal parameters caused by local damage may be difficult to identify, unless the damage is very severe or the measurements are very accurate.
- *Incomplete nature of the measured modal parameters.* A real civil structure typically possesses a large number of degrees of freedom and hence a large number of frequencies and mode shapes. However, the higher frequencies and mode shapes are very difficult to measure accurately in practice. In addition, due to limited sensors available, only limited

number of degrees of freedom can be measured, leading to incomplete mode shapes. Measurement errors and mode truncation and incomplete mode shapes introduce errors in damage identification, may lead to unreliable predictions.

- *Complexity of the damage identification algorithms.* Structural damage identification can be considered as an inverse problem, which is often illconditioned and has a non unique solution. Sophisticated computational techniques have to be employed to obtain the most appropriate damage identification solution.
- *Effect of factors other than damage.* For civil structures, global vibration responses are often affected by environmental and operational factors other than structural damage, such as thermal effects caused by temperature variation, varying moisture, variation of loading conditions and change in boundary conditions.

Therefore, further investigations have to be carried out to address the difficulties associated with the practical applications of vibrationbased damage identification methods, including

- construction and extraction of sufficiently sensitive feature index from structural vibration responses for local damage
- optimisation of the position and number of sensors to provide the necessary information for accurate predictions of structural damage
- development of reliable damage identification methods through multidisciplinary approaches
- full understanding and reduction of the effects of environmental and nonlinear factors on damage identification.

4.8 Concluding Remarks

Damage in a civil engineering structure may come from various sources, such as failure of materials, defects during manufacturing, loss of structural connections and misfits during construction. Nondestructive testing techniques have been widely applied to civil engineering structures for detection of structural damage. NDT techniques typically include acoustic emission, ultrasound, guided waves, thermography, electromagnetic methods, capacitive methods, laser Doppler vibrometer, global positioning system, and visual inspection. Application of these techniques requires a priori knowledge of the possible damage sites and access to such sites. Thus, NDT techniques are generally localised in nature, and only suitable for detection of local damage. The results obtained from the NDT techniques are often inconclusive or difficult to interpret.

In contrast to the NDT techniques, SHM methods avoid the limitation of NDT and provide a methodology for global identification of damage in a structure. SHM methods offer many advantages, such as global nature, limited sensors needed, online monitoring, model calibration and updating, and performance predictions. The SHM strategy is useful for damage diagnosis and prognosis of large complex civil engineering structures in practice.

The signals measured and collected from SHM systems have to be properly analysed for structural damage detection. Typical signal processing methods include Fourier based transforms, wavelet transforms and the Hilbert–Huang transform. Fourier based transforms are straightforward, but cannot be used for nonstationary or nonlinear problems. Wavelet and Hilbert–Huang transforms are powerful tools for signal processing, well suited for damage detection in nonstationary or nonlinear problems.

Damage in a structure can be assessed by either databased or modelbased techniques. Databased methods adopt historic measurements to assess the current state of the structure. Such methods do not require physical models of the structure for damage assessment, but they are often unable to provide quantitative information on the development of the damage. On the other hand, modelbased methods use models that are constructed from structural properties or modal properties. On the basis of continuous monitoring on a structure, modelbased methods offer useful information for effective infrastructure management, such as predictive damage evolution, remaining life estimate and optimum repair planning.

Vibrationbased damage identification methods show great promise for onorbit, remote damage assessment of large civil engineering structures. Such methods can offer information on the location and quantification of damage in a structure, when vibration measurements are used with system identification algorithms. A structural model of the undamaged structure, usually correlated with test data of the undamaged structure, is adopted with vibration measurements from the damaged structure in the damage identification process. The vibrationbased damage identification methods are in principle similar to the verification of structural properties in specific locations (often referred to as model updating). From continuous monitoring, the damage evolution of the structure can be used for timedependent reliability analysis, future performance predictions and risk and cost balanced maintenance strategy.

References

Balageas, D., Fritzen, C.P. and Guemes, A. (2006) *Structural Health Monitoring*. ISTE Ltd. London, UK.

Boashash, B. (2003) *Time–Frequency Signal Analysis and Processing: A Comprehensive Reference*. Elsevier, Amsterdam, The Netherlands.

Brown, C.J., Roberts, G.W. and Meng, X. (2006) Developments in the use of GPS for bridge monitoring. *Proceedings of the Institution of Civil Engineers, Bridge Engineering* **159**(3), 117–119.

Catbas, F.N., KijewskiCorrea, T. and Aktan, A.E. (2012). *Structural Identification of Constructed Facilities: Approaches, Methods, and Technologies for Effective Practice of StId* , ASCE, Reston, VA. USA.

Chen, H.P. (1998) *Structural Damage Identification Using Vibration Modal Data*. PhD thesis Department of Civil Engineering, Glasgow University, UK.

- Chen, H.P. (2005) Nonlinear perturbation theory for structural dynamic systems. *AIAA Journal***43**(11), 2412–2421.
- Ciang, C.C., Lee, J.R. and Bang, H.J. (2008) Structural health monitoring for a wind turbine system: a review of damage detection methods. *Measurement Science and Technology***19**, 1–20.
- Daubechies, I. (1988) Orthonormal bases of compactly supported wavelets. *Communications on Pure and Applied Mathematics***41**, 909–96.
- Dérobot, X., Iaquina, J., Klysz, G. and Balayssac, J.P. (2008) Use of capacitive and GPR techniques for nondestructive evaluation of cover concrete. *NDT & E International***41**, 44–52.
- Ettouney, M.M. and Alampalli, S. (2012) *Infrastructure Health in Civil Engineering*, CRC Press, London. UK.
- Farrar, C.R. and Lieven, N.A.J. (2007) Damage prognosis: the future of structural health monitoring. *Philosophical Transactions of the Royal Society A***365**, 623–632.
- Farrar, C.R. and Worden, K. (2007) An introduction to structural health monitoring. *Philosophical Transactions of the Royal Society A***365**(1851), 303–315.
- Graps, A. (1995) An Introduction to wavelets. *IEEE Computing in Science & Engineering***2**, 50–61.
- Heller, C.J. (2001) *Handbook of NonDestructive Evaluation*. McGrawHill, New York, NY, USA.
- Huang, N. and Shen, S. (2014) *Hilbert–Huang Transform and Its Applications*. Second edition, Interdisciplinary Mathematical Sciences, Vol. **16**, World Scientific Publishing, Singapore.
- Humar, J., Bagchi, A. and Xu, H. (2006) Performance of vibrationbased techniques for the identification of structural damage. *Structural Health Monitoring***5**(3), 215–241.
- KijewskiCorrea, T., Kareem, A. and Kochly, M. (2006) Experimental verification and full scale deployment of global positioning systems to monitor the dynamic response of tall buildings. *Journal of Structural Engineering ASCE***132**(8), 1242–1253.
- Kirikera, G.R., Shinde, V., Schulz, M.J., Ghoshal, A., Sundaresan, M. and Allemang, R. (2007) Damage localisation in composite and metallic structures using a structural neural system and simulated acoustic emissions. *Mechanical Systems and Signal Processing***21**, 280–97.
- Lowe, M.J.S., Alleyne, D.N. and Cawley, P. (1998) Defect detection in pipes using guided waves. *Ultrasonics***36**, 147–154.
- Martarelli, M., Revel, G.M. and Santolini, C. (2001) Automated modal analysis by scanning

laser vibrometry problems and uncertainties associated with the scanning system calibration *Mechanical Systems and Signal Processing***15**, 581–601.

Michaels, T.E. and Michaels, J.E. (2006) Application of acoustic wavefield imaging to non contact ultrasonic inspection of bonded components. *Review of Progress in Quantitative Nondestructive Evaluation***25**, 1484–1491.

Montalvão, D., Maia, N.M.M. and Ribeiro, A.M.R. (2006) A review of vibration based structural health monitoring with special emphasis on composite materials. *The Shock and Vibration Digest***38**(4), 1–30.

Niu, X., Chen, H.P. and Marques, H.R. (2017) Coupled piezoelectric transducer array optimization through simulation techniques for guided wave testing of cylindrical structures. *Proceedings of the 8th ECCOMAS Thematic Conference on Smart Structures and Materials (SMART 2017)*, Madrid, Spain.

Raghavan, A. and Cesnik, C.E.S. (2007) Review of guided wave structural health monitoring. *The Shock and Vibration Digest***39**, 91–114.

Siringoringo, D.M. and Fujino, Y. (2006) Experimental study of laser Doppler vibrometer and ambient vibration for vibration based damage detection. *Engineering Structures***28**, 1803–1815.

Stanley, P. (1997) Applications and potential of thermoelastic stress analysis. *Journal of Materials Processing Technology***64**, 359–70.

Su, Z., Ye, L. and Lu, Y. (2006) Guided Lamb waves for identification of damage in composite structures: A review. *Journal of Sound and Vibration***295**, 753–80.

Yan, Y., Cheng, L., Wu, Z. and Yam, L. (2007) Development in vibration based structural damage detection technique. *Mechanical Systems and Signal Processing***21**(5), 2198–2211.

Yi, T.H., Li, H.N. and Gu, M. (2013) Recent research and applications of GPS based monitoring technology for highrise structures. *Structural Control and Health Monitoring***20**(5), 649–670.

Zabel, V. (2005) A wavelet based approach for damage detection on civil engineering structures. *Proceedings of the 23rd International Modal Analysis Conference (IMAC XXIII)*, Orlando, Florida, USA.

5 Modal Analysis of Civil Engineering Structures

5.1 Introduction

The design and construction of large civil engineering structures, such as longspan bridges and highrise buildings has become increasingly popular. This demands the development of reliable experimental tools for the accurate identification of the most relevant dynamic modal properties: natural frequencies, mode shapes and damping ratios. Such modal identification tools can provide reliable data to support the validation of finite element models used at the design stage (Cunha and Caetano 2006, Cunha et al. 2001). These tools also offer updated information to support identification of damage in civil engineering structures through structural health monitoring strategies.

The modal properties of a civil engineering structure should be determined in normal operational conditions to represent the real dynamic response of the structure. There are generally two groups to identify the modal properties: the inputoutput identification methods and the outputonly identification methods. The inputoutput methods need both the input forces (excitation) and output measurements (response) to identify the modal parameters. These methods have been developed in either frequency domain or time domain, such as rational fraction polynomial (RFP), polyreference frequency domain (PRFD), Ibrahim time domain (ITD), and eigensystem realisation algorithm (ERA), as discussed in detail in Ewins (2000), Heylen et al. (1995) and Maia et al. (1997).

The outputonly identification methods, also called operational modal analysis (OMA), are a useful tool for identifying modal properties of a structure, since they only need the response measurements of the structure in operational condition under ambient excitation. Typical outputonly methods include the frequency domain techniques, e.g. the peakpicking (PP) and the complex mode indication function (CMIF) (Peeters and Ventura 2003), and the time domain techniques, e.g. the Ibrahim time domain (ITD), the covariancedriven stochastic subspace identification (SSICOV) and the datadriven stochastic subspace identification (SSIDATA) (Van Overschee and De Moor 1996). These outputonly identification methods have been successfully applied to many real civil engineering structures such as the Ting Kau Bridge (Ni et al. 2005) and the Canton Tower (Chen et al. 2012).

The identified modal parameters have to be checked with the associated analytical model or finite element model using various criteria. These criteria include the modal assurance criterion (MAC), orthogonality checks and the coordinate modal assurance criterion (COMAC) (Friswell and Mottershead 1995). Owing to the limited number of sensors available in practice, the identified mode shapes of the tested structure are usually incomplete. To overcome this problem, mode shape expansion or model reduction should be considered to eliminate the requirement of complete measurements of the actual tested structure. Traditional

mode shape expansion methods involve a model reduction transformation matrix as an expansion mechanism to obtain the unmeasured mode shape components. Recently, the perturbed force approach has provided more accurate estimates for mode shape expansion, particularly in the cases with limited modal data measurements, large modelling errors and severe measurement noise (Chen 2010).

This chapter reviews structural dynamic testing and modal analysis of civil engineering structures under controlled forces or in ambient conditions. Two main groups of modal parameter identification methods either in frequency domain or in time domain are discussed: input/output and output only. These methods are compared for evaluating the performance for modal parameter identification under various conditions. The identified modal parameters of the tested structure are then correlated with the associated analytical model using various criteria. Because of the incompleteness of measured modal data, mode shape expansion methods or model reduction methods are introduced for correlation studies and model validations. Finally, a real case of a supertall structure is studied for modal parameter identification and mode shape expansion using ambient vibration measurements.

5.2 Basic Equations for Structural Dynamics

The equation of motion for the linear damped forced vibration of a structural dynamic system with a total number of N degrees of freedom (DOFs) can be expressed as

$$\mathbf{M}\ddot{\mathbf{u}} + \mathbf{C}\dot{\mathbf{u}} + \mathbf{K}\mathbf{u} = \mathbf{f}(t) \quad (5.1)$$

where $\mathbf{f}(t)$ is external force vector applied to the system over time t . Dynamic responses \mathbf{u} , $\dot{\mathbf{u}}$ and $\ddot{\mathbf{u}}$ are nodal displacement, velocity and acceleration vectors associated with time t of the system, respectively. Structural parameters \mathbf{M} , \mathbf{C} and \mathbf{K} are the $N \times N$ global mass, damping and stiffness matrices of the dynamic system, respectively. To simplify calculations, the damping matrix \mathbf{C} may be assumed to be proportional to a combination of the corresponding mass and stiffness matrices, expressed as

$$\mathbf{C} = c_m \mathbf{M} + c_k \mathbf{K} \quad (5.2)$$

in which c_m and c_k are proportionality constants associated with the mass and stiffness of the structural systems, respectively. In the cases without the presence of external force $\mathbf{f}(t)$, it becomes free vibration and then the equation of motion [Equation \(5.1\)](#) is rewritten as

$$\mathbf{M}\ddot{\mathbf{u}} + \mathbf{C}\dot{\mathbf{u}} + \mathbf{K}\mathbf{u} = \mathbf{0} \quad (5.3)$$

The characteristic equation, using Laplace operator s , is expressed as

$$s^2 \mathbf{M} + s \mathbf{C} + \mathbf{K} = \mathbf{0} \quad (5.4)$$

The basic [Equations \(5.3\)](#) and [\(5.4\)](#) are often adopted in modal identification procedures.

5.2.1 Modal Solution

For a nontrivial solution of the equation of motion of free vibration in [Equation \(5.3\)](#), assumes that the displacement response is harmonic with a frequency of ω :

$$\mathbf{u} = \boldsymbol{\phi} e^{j\omega t} \quad (5.5)$$

where $j = \sqrt{-1}$ and $\boldsymbol{\phi}$ is a modal vector. By using the assumed displacement, [Equation \(5.3\)](#) becomes

$$\left(-\omega^2 \mathbf{M} + j\omega \mathbf{C} + \mathbf{K}\right) \boldsymbol{\phi} = \mathbf{0} \quad (5.6)$$

The above is a quadratic eigenvalue problem with a total number of N complex conjugate pairs of eigensolutions of eigenvalue ω and eigenvector $\boldsymbol{\phi}$ in general. By using the eigensolution, the displacement of the structural dynamic system can now be expanded into the series

$$\mathbf{u} = \sum_i A_i \boldsymbol{\phi}_i e^{j\omega_i t} \quad (5.7)$$

The eigenvalues are obtained in complex conjugate pairs for viscous damping as

$$\lambda_i, \bar{\lambda}_i = -\zeta_i \omega_i \pm j\omega_i \sqrt{1 - \zeta_i^2} \quad (5.8)$$

where the overbar indicates the complex conjugate, and ζ_i is the i th viscous damping ratio. From this equation, the natural frequency and the modal damping can be determined.

For an undamped structural dynamic system $\mathbf{C} = \mathbf{0}$, the eigenvalue problem in [Equation \(5.6\)](#) is simplified as

$$\left(\mathbf{K} - \lambda_i \mathbf{M}\right) \boldsymbol{\phi}_i = \mathbf{0} \quad (5.9)$$

where $\lambda_i = \omega_i^2$ and $\boldsymbol{\phi}_i$ are the i th eigenvalue and the corresponding eigenvector for the free vibration system, respectively. The eigensolution of a total number of N eigenvalues and eigenvectors is real, since both stiffness and mass matrices are symmetric. The eigenvalues and the corresponding eigenvectors of the free vibration system can be obtained from finite element dynamic analysis by solving the eigenproblem in [Equation \(5.9\)](#). These eigenvectors are linearly independent, and often mass normalised in the following form

$$\boldsymbol{\phi}_i^T \mathbf{M} \boldsymbol{\phi}_i = 1 \text{ and } \boldsymbol{\phi}_k^T \mathbf{M} \boldsymbol{\phi}_i = 0 \text{ if } k \neq i \quad (5.10)$$

where superscript T denotes the transpose of a vector or matrix quantity throughout the book. As a result, the structural stiffness matrix has orthogonality relations as

$$\boldsymbol{\phi}_i^T \mathbf{K} \boldsymbol{\phi}_i = \lambda_i \text{ and } \boldsymbol{\phi}_k^T \mathbf{K} \boldsymbol{\phi}_i = 0 \text{ if } k \neq i \quad (5.11)$$

The above orthogonality relations can be used for assessing the quality of the measured modal data such as natural frequencies and mode shapes.

5.2.2 Frequency Response Function

In forced harmonic vibration with the external force $\mathbf{f}e^{j\omega t}$ of a driving frequency ω , the equation of motion in [Equation \(5.1\)](#) becomes

$$\left(-\omega^2\mathbf{M} + j\omega\mathbf{C} + \mathbf{K}\right)\mathbf{y} = \mathbf{f} \quad (5.12)$$

where the \mathbf{y} is the harmonic displacement vector, obtained from

$$\mathbf{y} = \mathbf{H}(\omega)\mathbf{f} \quad (5.13)$$

in which

$$\mathbf{H}(\omega) = \left(-\omega^2\mathbf{M} + j\omega\mathbf{C} + \mathbf{K}\right)^{-1} \quad (5.14)$$

The matrix $\mathbf{H}(\omega)$ is named as frequency response function (FRF). Its components $h_{pq}(\omega)$ represent the harmonic displacement of the p th degree of freedom due to unit harmonic force in the direction of the q th degree of freedom. Physically, the FRF represents the dynamic flexibility of the structural system. The numerical FRFs can be obtained from the calculated modal data such as natural frequencies ω_i , mode shape vector ϕ_i and damping ratio ζ :

$$\mathbf{H}(\omega) = \sum_{i=1}^N \frac{\phi_i\phi_i^T}{\left(\omega_i^2 - \omega^2 + 2j\zeta\omega_i\omega\right)} \quad (5.15)$$

For frequency domain analyses, the dynamic stiffness $\mathbf{Z}(\omega)$ can be defined as

$$\mathbf{Z}(\omega) = \mathbf{H}(\omega)^{-1} = \left(-\omega^2\mathbf{M} + j\omega\mathbf{C} + \mathbf{K}\right) \quad (5.16)$$

In structural dynamic testing, FRFs are obtained by measuring the system responses at different locations during experiments due to harmonic external forces, and then they can be used in modal identification.

5.3 InputOutput Modal Identification

In dynamic test of a structure, input sources are the places where the structure is excited by an external force, and output stations are the locations where the structural response is measured (Avitabile 2001, Friswell and Mottershead 1995). There are several input and output combinations, such as single input source and single output station (SISO), single input source and multiple output stations (SIMO), multiple input sources and single output station (MISO)

and multiple input sources and multiple output stations (MIMO). The output measurements, together with the input data, are then adopted for modal identification of the tested structure. In practice, the inputoutput modal identification techniques have been well established to accurately identify the modal parameters of engineering structures, such as natural frequencies, mode shapes and damping ratios.

5.3.1 Equipment and Test Procedure

In modal testing, the frequency response functions (FRFs) are constructed from the relationship between the applied external force and the corresponding response at several pairs of points on the structure. The construction of FRFs needs a set of modal testing facilities, including structural excitation, data acquisition and signal processing, as described in Cunha and Caetano (2006) and Ewins (2000).

Small and medium size civil engineering structures can be excited by an impulse hammer, as shown in [Figure 5.1](#)(a). The impulse hammer has the advantage of providing a wideband input to stimulate different modes of vibration. However, it has some disadvantages, such as lack of energy to excite some relevant modes of vibration. Alternatively, large electrodynamic shakers can be utilised to generate a large variety of input signals (random, multisine, etc.) with controlled frequencies and amplitudes. The shakers are capable of exciting structures in a lower frequency range and higher frequency resolution. By applying sinusoidal forces on a structure, resonance frequencies can be excited and identified, together with a direct identification of mode shapes.

(a) Impulse hammer



(b) Installed accelerometer sensors

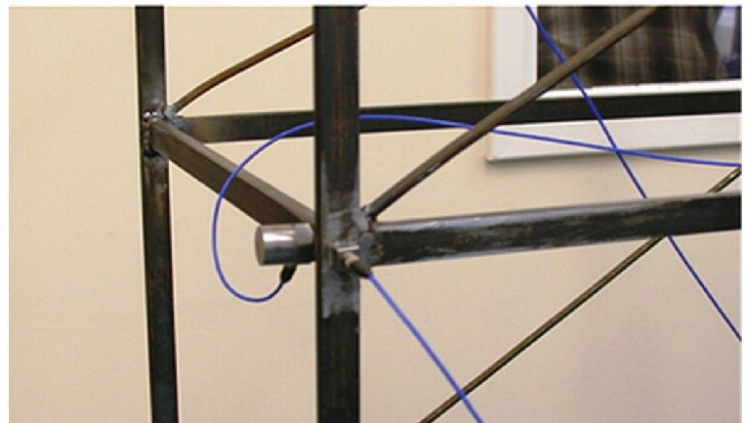


Figure 5.1 Impact hammer and accelerometers for vibration testing.

Large civil engineering structures can be excited by using heavy excitation equipment, such as an eccentric mass vibrator. The vibrator generates sinusoidal forces with variable frequency and amplitude for structural dynamic testing. However, the equipment has some drawbacks including low force amplitude induced at low frequencies. To overcome the drawbacks, a servohydraulic shaker can be used to provide a wideband excitation over the most interesting frequency range for large civil engineering structures.

The dynamic response of the tested structure is typically measured with accelerometers, such

as piezoelectric or forcebalance, as indicated in [Figure 5.1\(b\)](#). Piezoelectric accelerometers do not need a power supply and operate well over a wide frequency range. However, they may not be suitable for low frequency applications. In contrast, forcebalance accelerometers can be used for low frequency response cases. The electrical signals generated by these sensors are often low and need to be amplified by conditioning units. The data acquisition and storage require the use of an analogue-to-digital (A/D) converter in the measurement system. The measured acceleration time-history can be multiplied by appropriate time windows to reduce leakage effects. Finally, frequency response functions are obtained using estimators from the input forces and acceleration measurements. Appropriate software may be required for efficient evaluation of FRFs for analysis and signal processing.

5.3.2 Modal Identification Techniques

Many techniques are available for input-output modal identification, on the basis of either estimates of a set of FRFs or the corresponding impulse response functions (Ljung 1999). The impulse response functions (IRFs) are obtained through the inverse Fourier transform. These techniques can be classified according to various factors, such as domain of application (time or frequency), type of formulation (indirect or direct), number of modes analysed (single DOF or multi DOF) and number of inputs and type of estimates (SISO, SIMO, MISO, MIMO). These techniques generally require some fitting between measured and theoretical functions to identify modal parameters.

5.3.2.1 Frequency Domain Techniques

The frequency domain techniques are based on the FRF estimates obtained from the modal testing. For a simple single DOF system, typical frequency domain methods, such as peak amplitude, curve fit and inverse methods, perform the fit between a measured FRF and a theoretical FRF of the single DOF system in the vicinity of each resonant frequency. For more complex multiple DOF systems, typical frequency domain methods include rational fraction polynomial (RFP), complex exponential frequency domain (CEFD) and polyreference frequency domain (PRFD). Details of these frequency domain techniques are discussed in Maia et al. (1997). These techniques carry out a global fit between measured and theoretical FRFs for a wide range of frequencies. The frequency domain techniques have drawbacks in the frequency resolution of spectral estimates and leakage errors in the estimates.

5.3.2.2 Time Domain Techniques

To avoid the drawbacks in the frequency domain techniques, time domain methods can provide better results when a large frequency range or a large number of modes exist in the data. The time domain techniques are either direct, such as autoregressive moving average (ARMA) or indirect, such as polyreference complex exponential (PRCE), Ibrahim time domain (ITD) and eigensystem realisation algorithm (ERA). All these methods are described in detail by Maia et al. (1997).

5.3.3 Example for Modal Identification – a Steel Space Frame (I)

In the laboratory vibration testing for a space steel frame structure shown in [Figure 5.2](#), a total number of 16 uniaxial accelerometers are placed at the beam-column joints to measure translational accelerations. These sensors are used to record the response of the frame structure excited by the impulse hammer. A supersoft rubber tip is attached to the hammer to broaden the impulse on the structure in order to better excite lower frequency modes. The dynamic response data is acquired by using five signal processing modules with fourchannel 24bit AC/DC input modules and a data acquisition chassis. The data is then collected by Labview Signalexpress software.

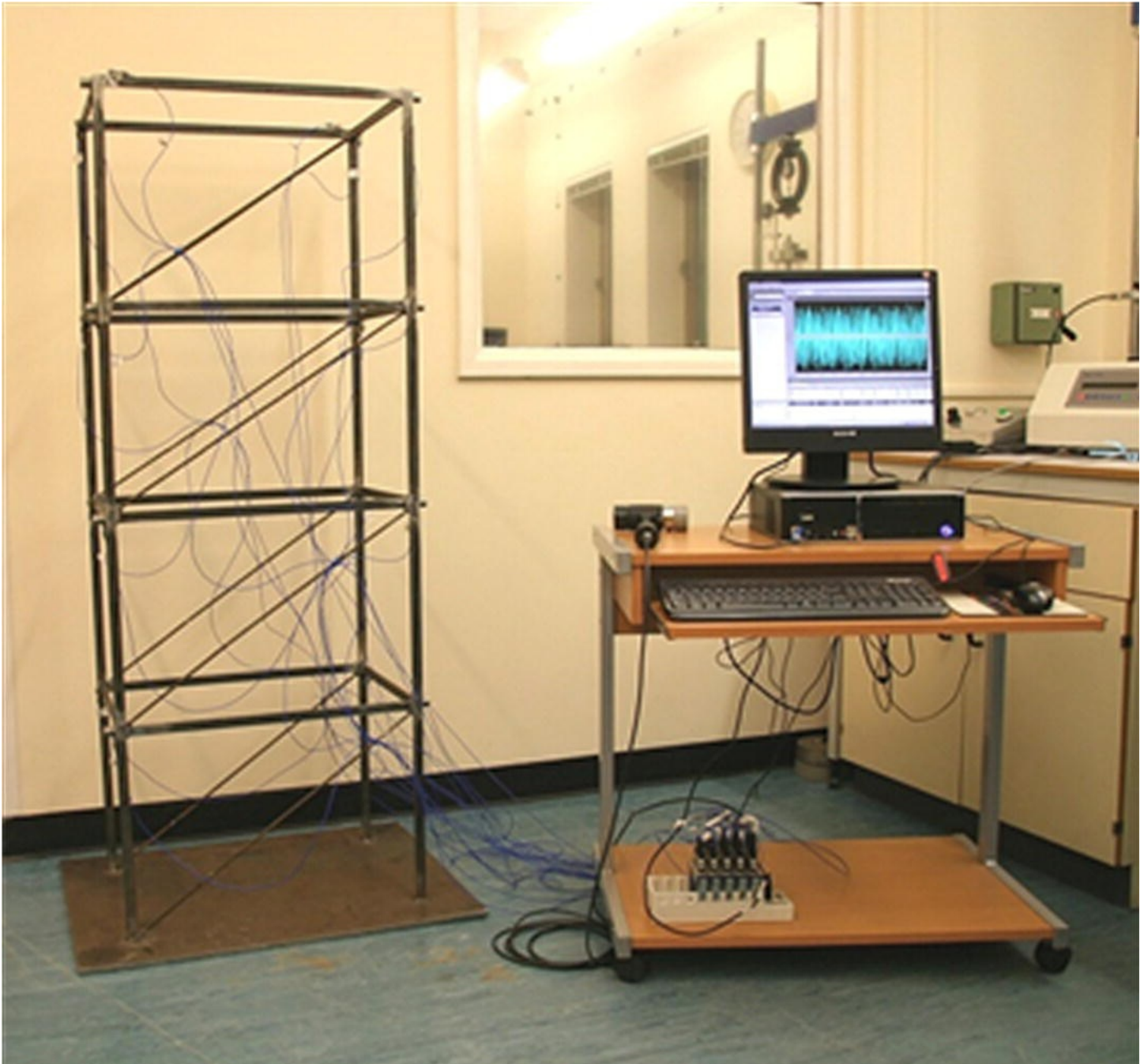
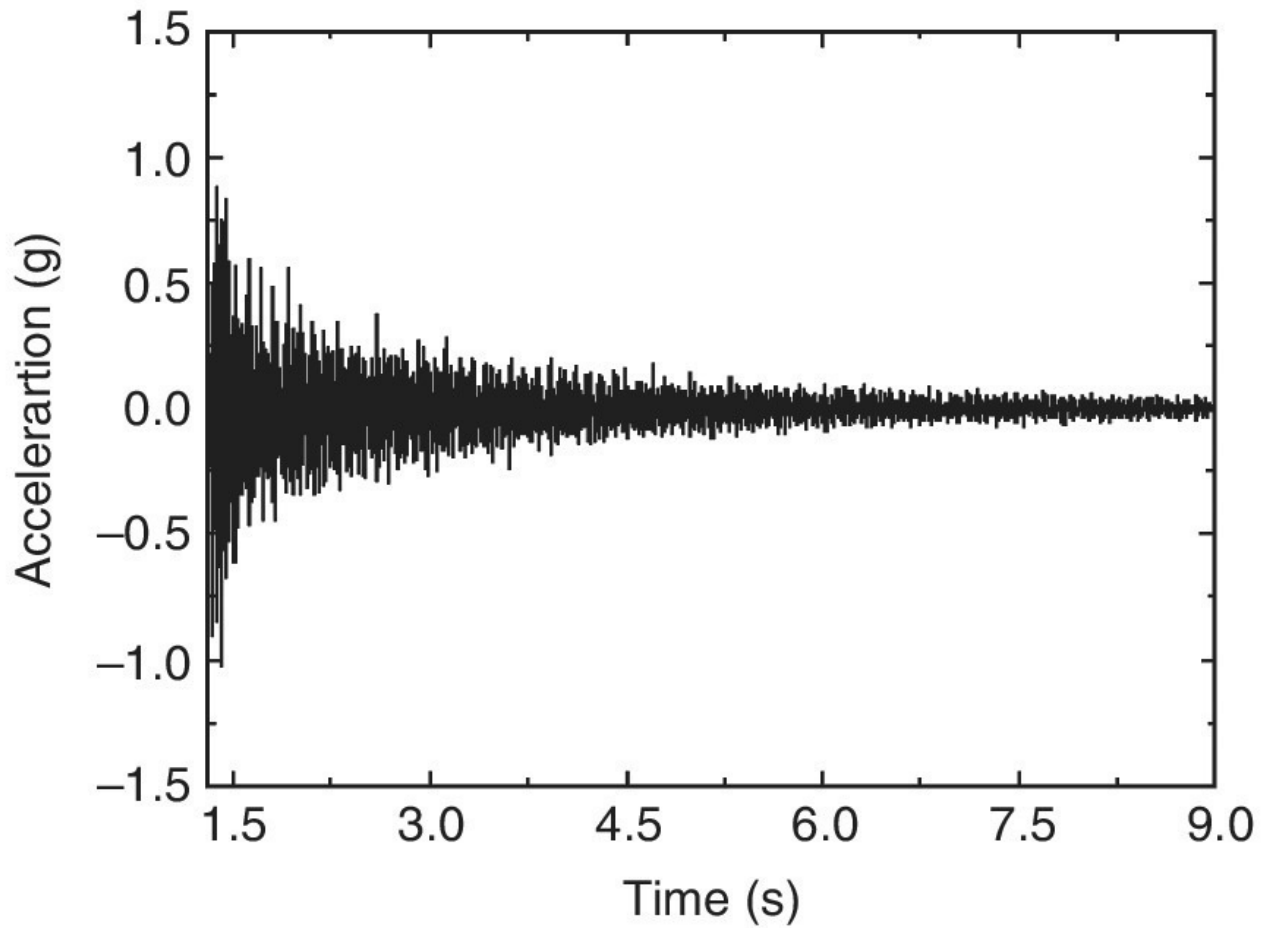


Figure 5.2A A space steel frame structure used for laboratory testing with test equipment.

The single input and multiple output (SIMO) test procedure is utilised for the vibration testing of the frame structure. Curve fitting is employed on a reference set of FRFs to extract modal

parameters by using ME'Scope VES modal analysis software. The recorded typical acceleration measurements and the identified natural frequencies for the laboratory tested frame structure are shown in [Figures 5.3\(a\)](#) and (b).

(a) Acceleration measurements at a beam-column joint



(b) Frequency response function (FRF) and identified frequencies

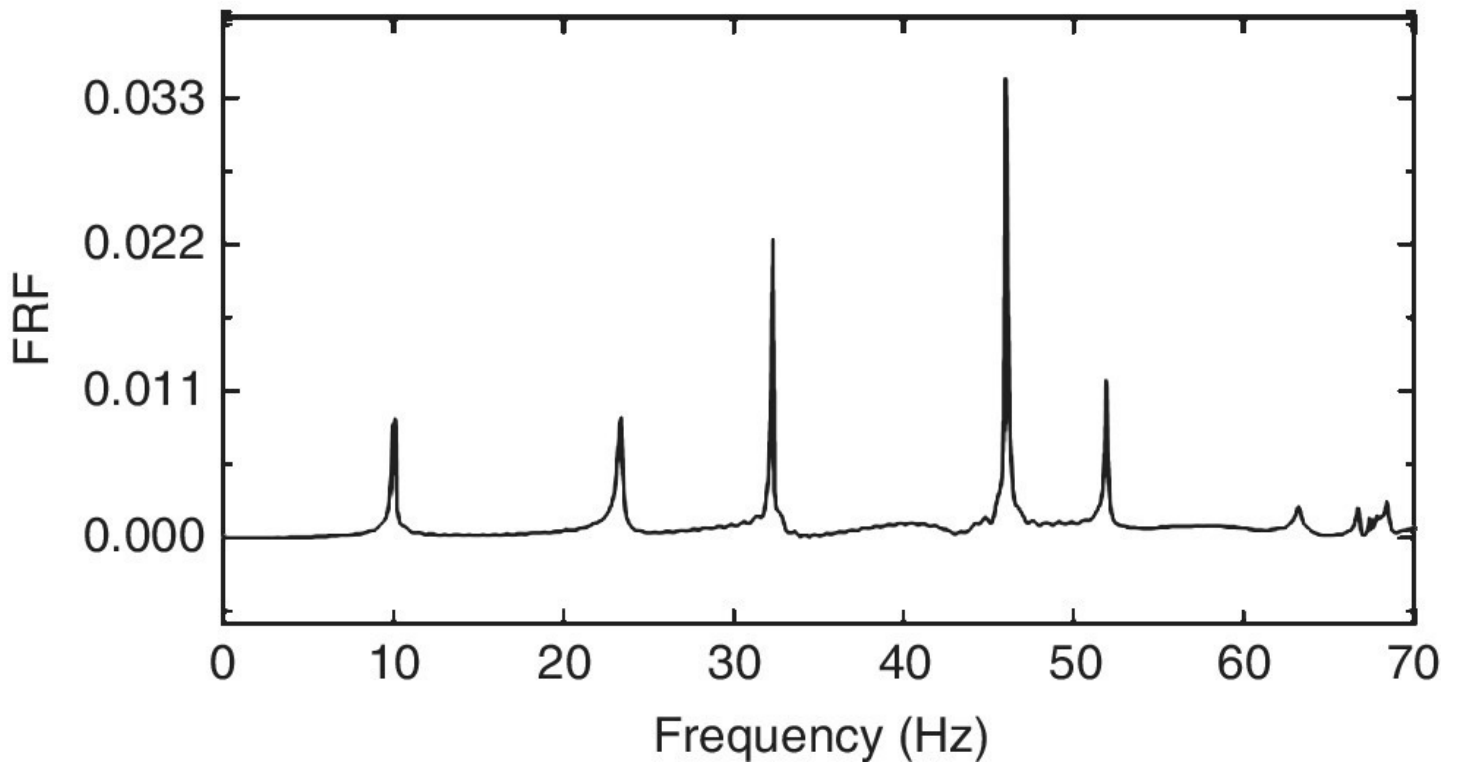


Figure 5.3 Laboratory vibration test results for the space steel frame structure.

The first three measured frequencies and the corresponding mode shapes for the laboratory tested structure are shown in **Figure 5.4**. Among these three identified modes, there are two bending modes with respect to the weak axis (first and third modes) and one torsion mode (second mode).

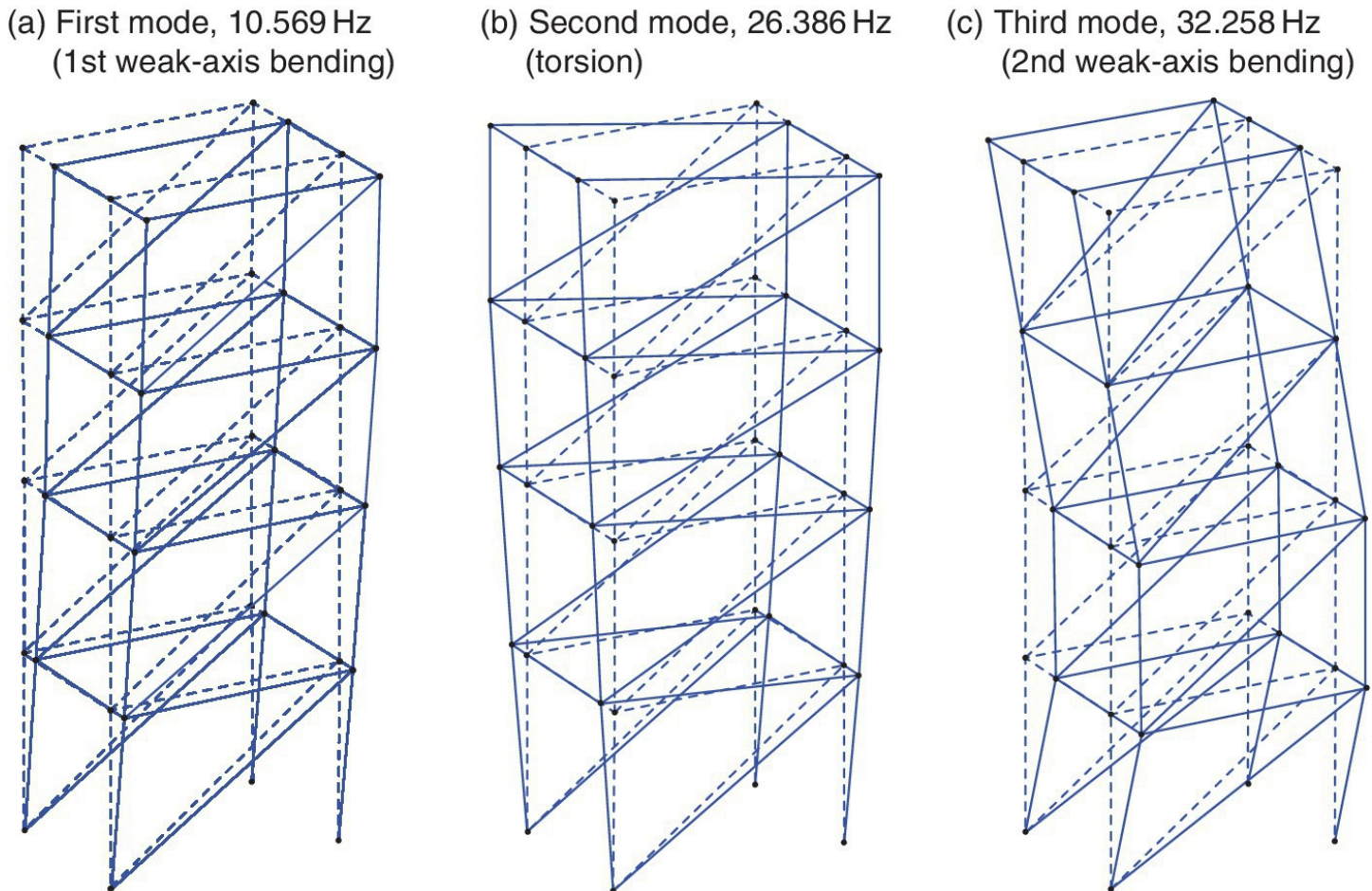


Figure 5.4 Experimental modes from laboratory vibration test for the space frame structure.

5.4 OutputOnly Modal Identification

The main problem associated with forced vibration tests on large civil engineering structures is the difficulty in exciting the interested low frequency modes with sufficient energy and in a controlled manner. Existing exciters such as impact hammers and shakers may not be suitable for use with large civil structures such as longspan bridges and highrise buildings. Thus, outputonly modal identification, also known as operational modal analysis (OMA), is required to accurately identify the modal properties of large structures at the construction stage or during their service life without interruption of normal operation (Hermans and Van der Auweraer 1999, Heylen et al. 1995).

5.4.1 Equipment and Test Procedure

Forcebalance accelerometers are often used for dynamic response induced by ambient excitations such as wind and traffic. In the vibration tests, the structural ambient response such as acceleration is captured by a few reference sensors at fixed places and with a set of sensors at different measurement points along the structure. The number of sensors and their locations need to be optimised to characterise appropriately the shape of the most relevant modes of vibration. The optimised sensor array should be able to provide maximum information for the applications of modal data, such as finite element model updating and vibrationbased structural damage identification.

Forcebalance accelerometers need sufficient power supply, and their analogue signals are usually transmitted to a data acquisition system with an A/D conversion card. The data acquisition and processing systems are required to collect and analyse the data measured from ambient vibration tests. The use of long electrical cables in the outputonly modal identification tests in large civil structures is timeconsuming. Wireless systems have therefore been developed to avoid this problem and to provide more effective signal transmission.

5.4.2 Operational Modal Identification Techniques

Ambient excitation usually provides multiple inputs and a wideband frequency content (Bendat and Piersol 1993, Brincker et al. 2000). Due to the lack of knowledge of the input, the output only modal identification techniques assume that the excitation input does not contain any information – it is a zeromean Gaussian white noise. The assumption of white noise is not too strict in practical applications. The outputonly techniques will work well in the cases where the input spectrum is quite flat. As a result of the lack of knowledge of the input, the estimated mode shapes cannot be scaled to unity modal mass. The outputonly modal identification methods are broadly classified as two groups: nonparametric methods essentially developed in the frequency domain and parametric methods in the timedomain. The details of the outputonly modal identification techniques are provided in Peeters and De Roeck (2001) and Peeters and Ventura (2003).

5.4.2.1 FrequencyDomain Methods

Nonparametric frequencydomain methods use either FRFs or output spectrum for output only modal parameter estimation (Peeters and Ventura 2003). Typical frequencydomain methods are described as follows.

Peakpicking (PP) method: The PP method is the basic frequency domain method to estimate the modal parameters of a structure. This method is named after its key step – the identification of the natural frequencies at the peaks of the FRF plot. In cases with low damping and well separated frequencies, the output power spectrum matrix S_y near a frequency ω_i can be approximated by

$$S_y(j\omega_i) \approx \alpha_i \mathbf{v}_i \mathbf{v}_i^H \quad (5.17)$$

where α_i is a scale factor, \mathbf{v}_i is the i th mode shape and superscript H represents the complex conjugate transpose of a matrix or vector. The basic assumptions of low damping and well separated frequencies in the PP method has significant influence on operational modal identification. The selection of the frequencies can be subjective if the spectrum peaks are not very clear. Despite these disadvantages, the PP method has been successfully applied to many civil engineering cases due to its simple implementation and its effectiveness.

Complex mode indication function (CMIF) method: The CMIF method uses the singular value decomposition (SVD) of the spectrum matrix:

$$\mathbf{S}_y(j\omega) = \mathbf{U}(j\omega)\mathbf{\Sigma}(j\omega)\mathbf{U}^T(j\omega) \quad (5.18)$$

where \mathbf{U} is a complex unitary matrix containing the singular vectors as its columns. The diagonal matrix $\mathbf{\Sigma}$ contains the real positive singular values in descending order. This method is based on the diagonalisation of the spectral density matrix and on the fact that the spectrum matrix evaluated at a certain frequency is only determined by a few modes. The CMIF method may be considered as an SVD extension of the PP method.

Rational fraction polynomial (RFP) method: The RFP method is a basic modal parameter estimation method and was extended to the multiple input case by Van der Auweraer and Leuridan (1987). It is found that the FRF matrix can be parameterised as an RFP model:

$$\mathbf{H}(j\omega) = \left[(j\omega)^p \boldsymbol{\beta}_p + (j\omega)^{p-1} \boldsymbol{\beta}_{p-1} + \dots + \boldsymbol{\beta}_0 \right] \left[(j\omega)^p \mathbf{I} + (j\omega)^{p-1} \boldsymbol{\alpha}_{p-1} + \dots + \boldsymbol{\alpha}_0 \right]^{-1} \quad (5.19)$$

where $\boldsymbol{\alpha}_i$ are the denominator matrix coefficients and $\boldsymbol{\beta}_i$ are the numerator matrix coefficients. The polynomial order p is related to the number of modes. These matrix coefficients can be estimated from FRF measurements, and then are used for estimating the modal parameters.

5.4.2.2 TimeDomain Methods

Timedomain methods adopt an appropriate mathematical model to idealise the dynamic structural behaviour, e.g. timediscrete or statespace stochastic models, for the outputonly modal identification (Peeters and De Roeck 2001). Typical timedomain methods include Ibrahim timedomain (ITD), covariancedriven stochastic subspace identification (SSI COV), and datadriven stochastic subspace identification (SSIDATA).

Ibrahim timedomain (ITD) method: The ITD method was originally proposed for identifying the modal parameters from free decay responses, and then to a polyreference IRF (impulse response function)driven modal parameter estimation method (Ibrahim and Mikulcic 1977). The IRF is obtained as the inverse Fourier transforms of the FRF. The ITD method aims to compute the complex eigensolutions: complex eigenvalues and associated complex eigenvectors. From the obtained complex eigenvalues, the natural frequencies and modal damping can be estimated.

Covariancedriven stochastic subspace identification (SSICOV) method: The SSICOV

method deals with the stochastic realisation problem, that is, the identification of a stochastic statespace model from outputonly data. Stochastic realisation relies on a fundamental property of stochastic statespace systems. Theoretically, the system order can be determined by inspecting the number of nonzero singular values of the block Toeplitz matrix (Peeters and De Roeck 1999). A stabilisation diagram can be effectively constructed by computing the singular value decomposition of the covariance Toeplitz matrix. The constructed stabilisation diagram is then employed to obtain a good model for modal analysis applications, by identifying a whole set of models with different order. However, in practice, the estimated covariance Toeplitz matrix is considerably affected by noise, typically caused by modelling inaccuracies by a statespace model, measurement noise by the sensing system, computational errors and the finite amount of data.

Datadriven stochastic subspace identification (SSIDATA) method: As opposed to the SSICOV method, the SSIDATA method avoids the computation of covariances between the outputs (Van Overschee and De Moor 1996). This is replaced by projecting the row space of future outputs into the row space of past outputs. Thus the SSIDATA method directly works with the measured time histories, without requiring IRFs conversion or output covariances. It has been shown that the datadriven algorithms outperform an optimal version of the eigensystem realisation algorithms (ERA). The SSIDATA method has many successful practical applications for outputonly modal analysis.

5.4.3 Damping Estimation

In structural dynamics and modal testing problems, the precise mechanisms of damping are not well understood. In general, the viscous damping assumption does not match exactly the real damping characteristics of the structures. The modal damping ratios increase gradually with levels of oscillation (Cunha and Caetano 2006, Brincker et al. 2001). Thus there is a major problem in the accurate identification of modal damping ratios due to the considerably larger scatter associated with various natural frequency and mode shape estimates. In many practical situations, a free vibration test may be performed to effectively identify the modal damping ratios. For example, for longspan slender bridges, the technique with a drop weight is particularly useful, since the knowledge of certain damping ratios is critical for assessing aeroelastic instability problems.

5.4.4 Effect of Temperature on Modal Data

Large civil engineering structures such as bridges are exposed directly to ambient environments, such as traffic, humidity, wind and temperature, during their service lifetime. The operational environments such as temperature may affect the modal parameters of the structures due to thermal effects. To investigate the effect of temperature on natural frequencies, a study was carried out for the Ting Kau cablestayed bridge using longterm monitoring data (Ni et al. 2005). From the measured modes, the values of natural frequencies reduce slightly with increase in ambient temperature, although the variation of natural frequencies is fairly small. The relationship between frequencies and temperature is not simply linear and actually is highly dispersed, as indicated in [Figure 5.5](#).

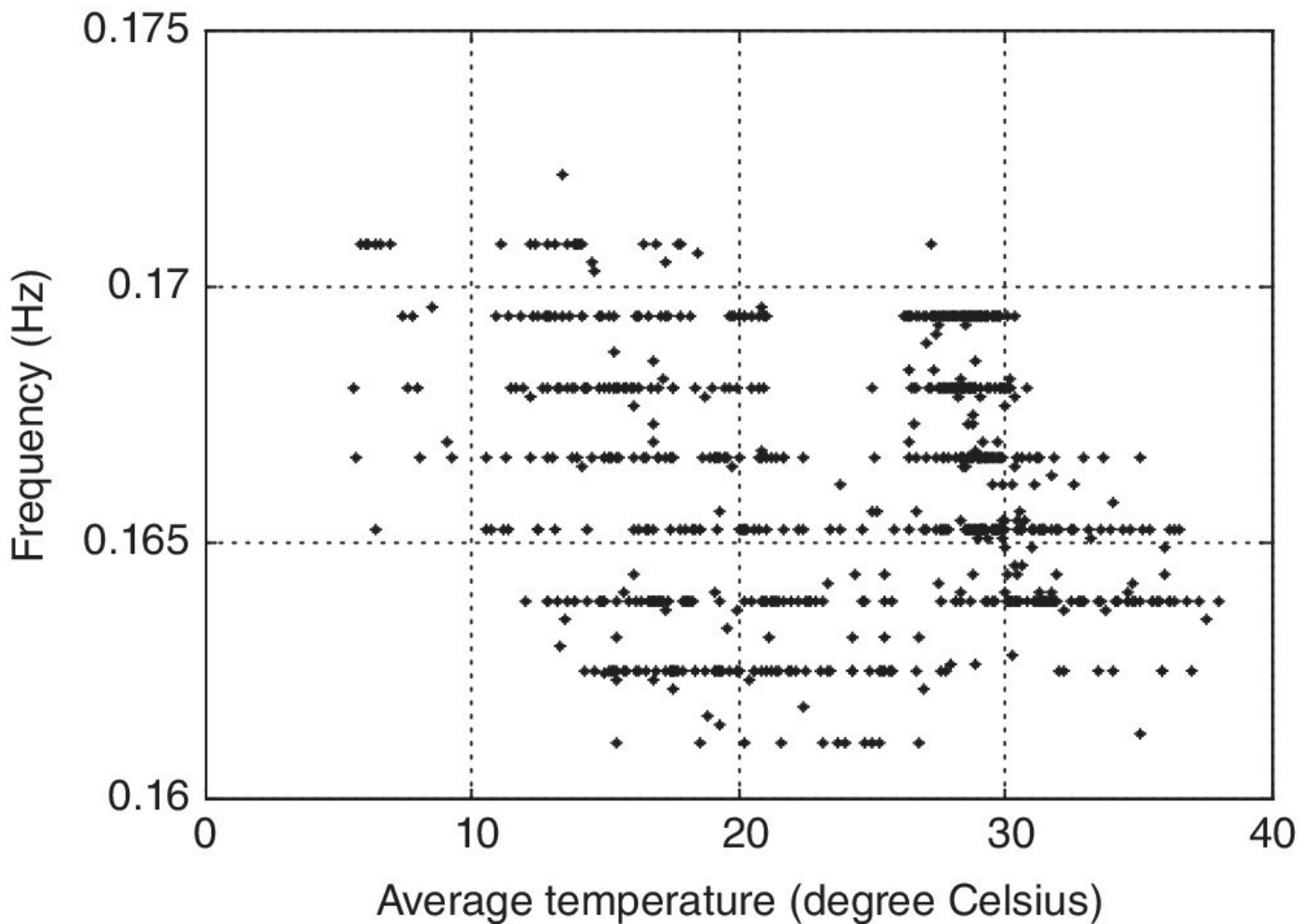


Figure 5.5 Fundamental frequency versus hourly average temperature of the Ting Kau cable stayed bridge.

Temperature is the critical source causing variability of modal parameters such as natural frequencies. The variations of natural frequencies caused by change in temperature may reach 5–10% for bridges. In general, natural frequencies of dynamic structural systems decrease as structural or ambient temperature increases. The thermal effects on the associated mode shapes are usually relatively smaller and can be neglected. This is also confirmed by other studies, such as in the case studies by Xia et al. (2012).

5.4.5 Comparison of Methods

A comparative study on the performance of various modal identification techniques was undertaken for operational modal analysis (Peeters and Ventura 2003). The Z24Bridge, a classical posttensioned concrete box girder bridge, is used in their comparative study. The bridge was excited by controlled external forces and by ambient sources, respectively. Two shakers were used for the controlled shaker tests: one on a sidespan and another at mid span. A drop weight was also used to excite the bridge to stimulate the free vibration of the structure. The ambient excitation sources acting on the bridge were typically wind and traffic on the highway.

The differences in the identified natural frequencies between the excitation types are generally small, as summarised in [Table 5.1](#). This discrepancy may be caused by the temperature changes during the measurement period. On the other hand, the damping ratios identified from the three excitation types appear very consistent with consideration of their higher uncertainty.

Table 5.1 Comparison of identified natural frequencies and damping ratios between the three excitation types (after Peeters and Ventura 2003).

Mode No.	Natural frequencies (Hz)			Damping ratios (%)		
	Shaker	Drop weight	Ambient	Shaker	Drop weight	Ambient
1	3.87	3.85	3.86	0.9	0.8	0.9
2	4.82	4.81	4.90	1.7	1.6	1.4
3	9.77	9.74	9.77	1.5	1.7	1.3
4	10.5	10.4	10.3	1.6	1.8	1.4
5	12.4	12.2	12.5	3.1	3.8	2.5
6	13.2	13.2	13.2	4.6	4.1	3.0
7	17.2	16.9	—	5.0	4.9	—
8	19.3	19.2	19.0	2.5	2.3	2.0

The performance of the selected output-only identification methods for frequency identification using ambient data is rather different, as indicated in [Figure 5.6](#). The peak picking (PP) method identifies the first six frequencies well with good estimates. The complex mode indication function (CMIF) method gives reasonable estimates for the first five frequencies. The rational fraction polynomial (RFP) method can only identify the first three frequencies. The stochastic subspace identification (SSI) methods provide the best results for frequency identification. For all identification methods, lower frequencies – say the first three modes – can be identified from ambient vibration data. Some higher frequencies failed to be identified because these modes are not so well excited. Stochastic subspace identification (SSI) methods perform well since they can deal with noisy data.

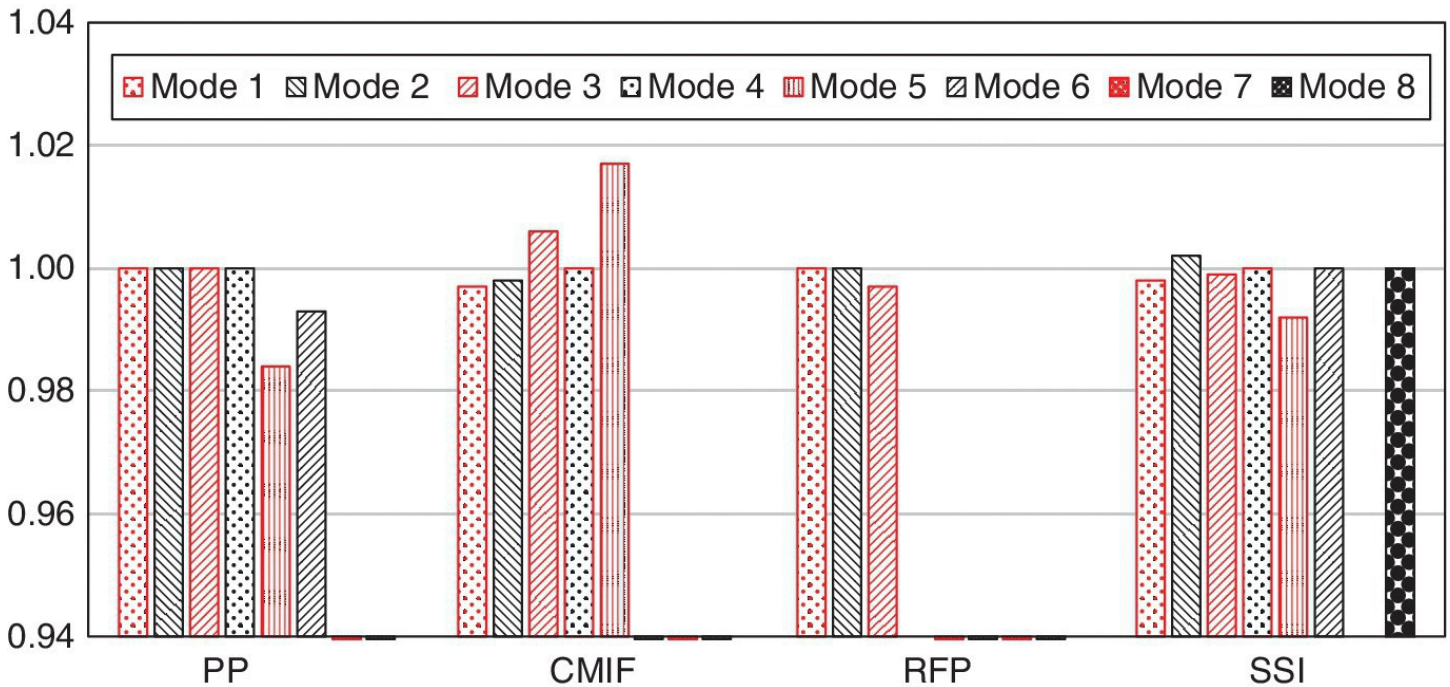


Figure 5.6 Relative frequencies extracted by various modal identification methods from the ambient vibration data (after Peeters and Ventura 2003).

The results of damping ratios from the drop weight data are diverse and depend on the modal identification methods used, as shown in [Figure 5.7](#). The variations of estimated damping ratios between the identification methods are much greater than those of frequencies due to higher uncertainty in damping ratio estimation. The Ibrahim timedomain (ITD) method gives the lowest values of damping ratios. Again, the stochastic subspace identification (SSI) methods provide the best estimates for damping ratios.

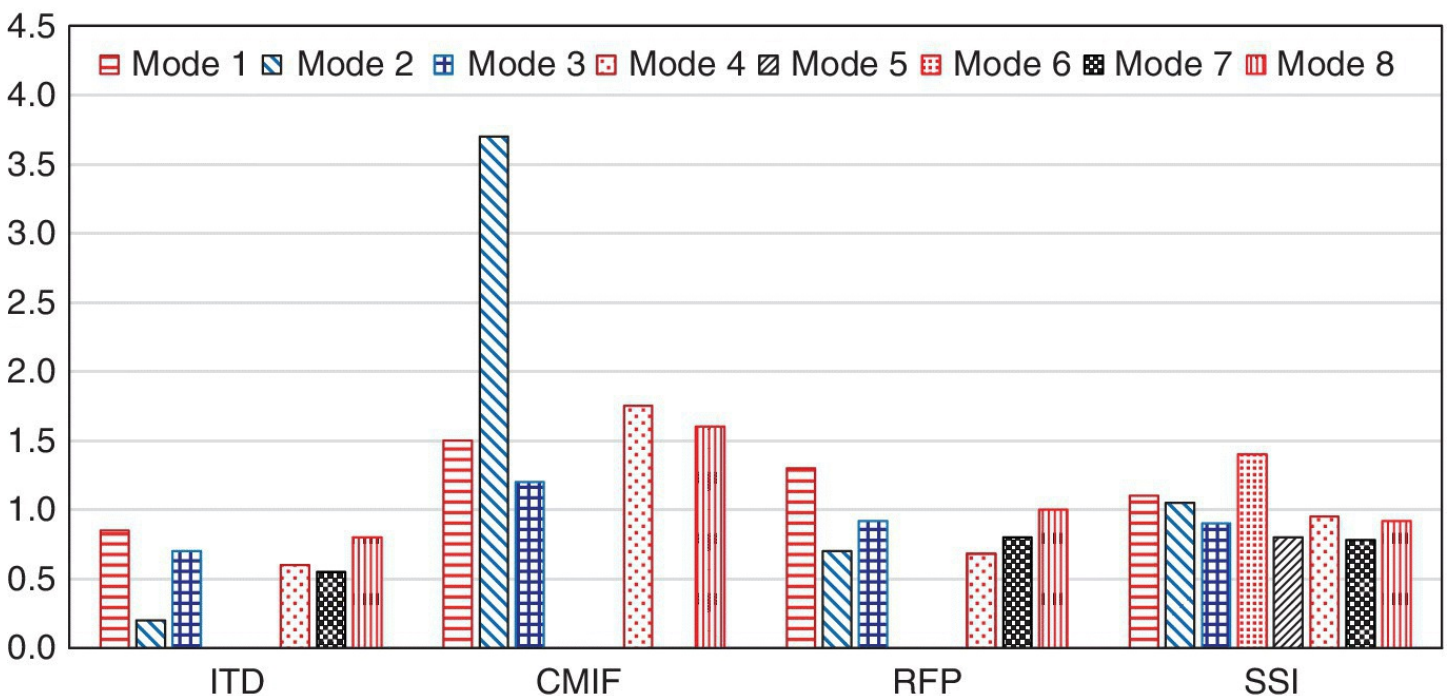


Figure 5.7 Relative damping ratios extracted by various modal identification methods from the drop weight data (after Peeters and Ventura 2003).

5.4.6 Example for Modal Identification – a CableStayed Bridge

The Ting Kau Bridge is a threetower cablestayed bridge in Hong Kong. Details of the bridge and its health monitoring strategy will be discussed in [Section 10.2](#). In the bridge health monitoring system, there are a total of 24 uniaxial accelerometers installed at eight sections (B, D, E, G, J, L, M, O) of the bridge deck (Ni et al. 2015), as shown in [Figure 5.8](#). The accelerometers that are installed on the two sides of the bridge deck measure the vertical accelerations, while the accelerometers installed along the middle of the bridge deck collect the transverse acceleration measurements. The sampling frequency of these accelerometers is 25.6 Hz.

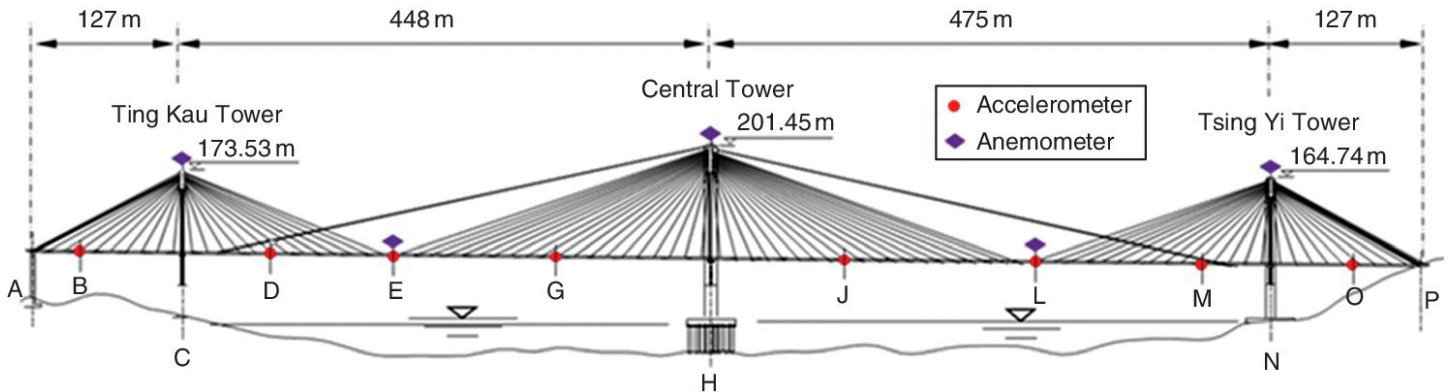
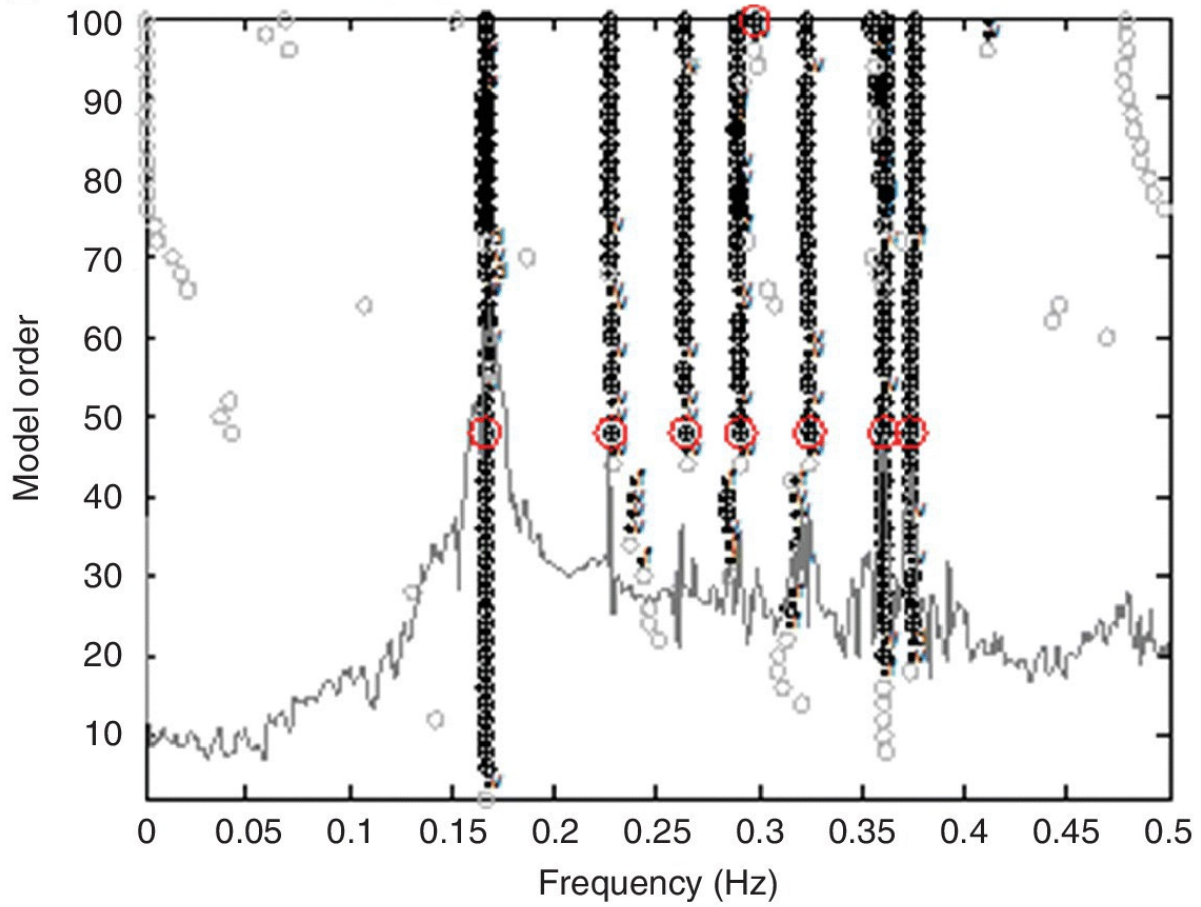


Figure 5.8 Deployment of accelerometers on Ting Kau Bridge.

Two timedomain modal identification methods – datadriven stochastic subspace identification (SSIDATA) and covariancedriven stochastic subspace identification (SSICOV) – are employed to extract modal properties, such as natural frequencies and mode shapes, from the collected acceleration measurements under strong wind conditions. The stabilisation diagrams for the SSIDATA method and the SSICOV method, as shown in [Figure 5.9](#), are constructed to identify natural frequencies, together with the associated mode shapes and damping ratios. The first eight frequencies are clearly indicated on both stabilisation diagrams.

(a) Results from the SSI-DATA.



(b) Results from the SSI-COV

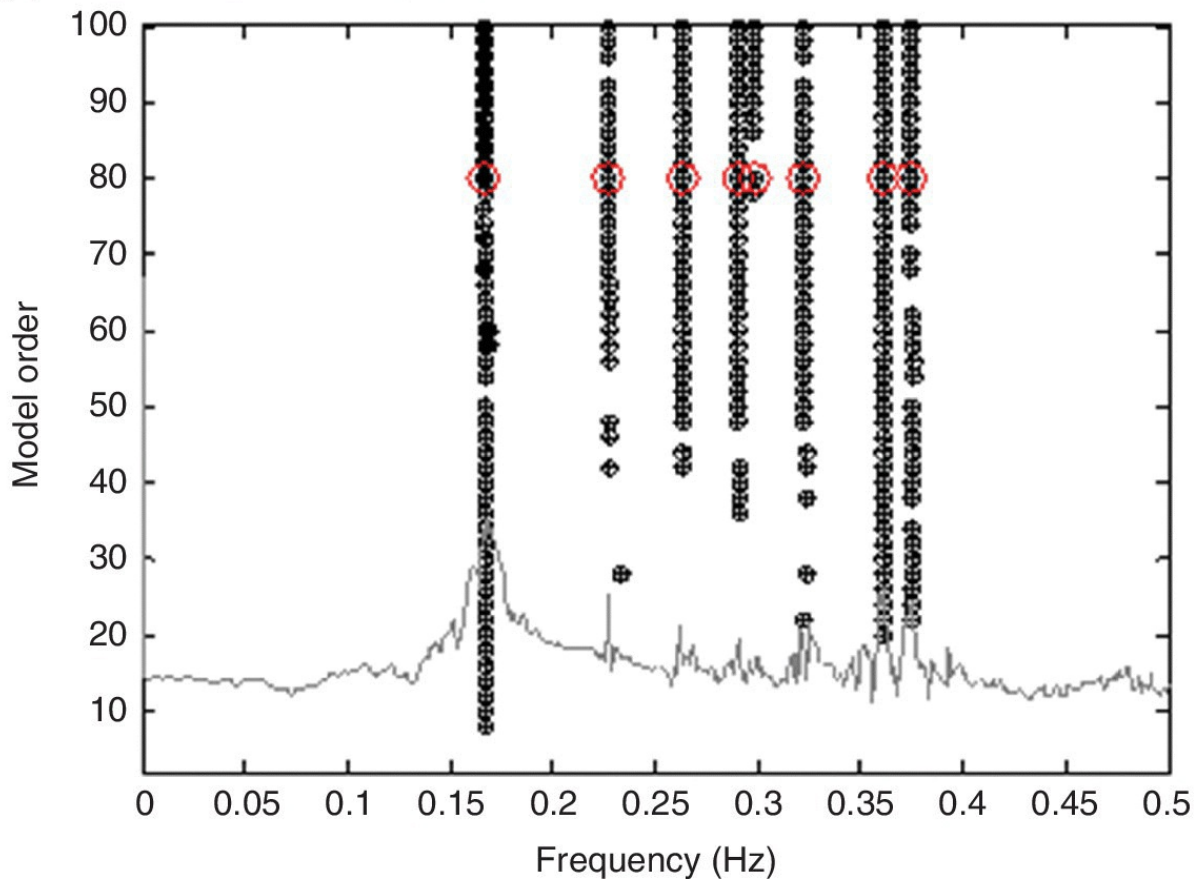


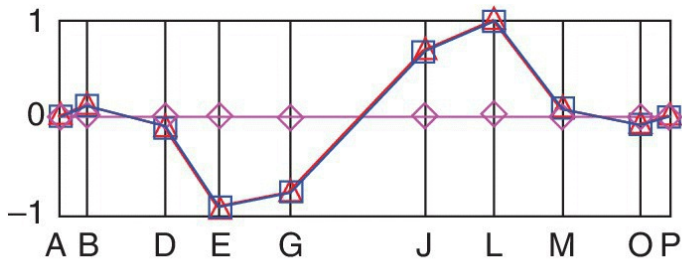
Figure 5.9 Stabilisation diagrams for the SSIDATA and the SSICOV output only identification methods for Ting Kau Bridge.

The influence of ambient excitations, such as wind conditions, on modal identification is investigated using monitored data (Huang and Chen 2017). [Table 5.2](#) summarises the identified first eight natural frequencies under various strong wind conditions (S7S10 with wind speeds of 12.11–15.91 m/s). The results are very close to each other for different wind conditions. The difference in the estimates of the frequencies identified from the SSIDATA method and the SSICOV method is small. Both identification methods give reliable and consistent results for frequency estimates from various ambient vibration measurements.

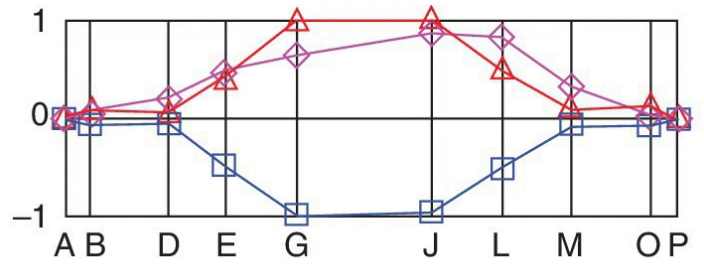
Table 5.2 Identified natural frequencies (Hz) of the first eight modes under various wind conditions using the SSIDATA method and the SSICOV method.

Mode No.	SSIDATA				SSICOV			
	S7	S8	S9	S10	S7	S8	S9	S10
1	0.167	0.164	0.164	0.164	0.166	0.164	0.165	0.166
2	0.228	0.228	0.227	0.227	0.227	0.227	0.227	0.226
3	0.264	0.264	0.260	0.260	0.263	0.264	0.259	0.260
4	0.291	0.292	0.287	0.287	0.290	0.293	0.287	0.289
5	0.298	0.301	0.297	0.297	0.298	0.301	0.297	0.302
6	0.324	0.324	0.319	0.319	0.322	0.323	0.319	0.317
7	0.361	0.361	0.358	0.358	0.361	0.361	0.358	0.359
8	0.374	0.374	0.375	0.374	0.374	0.372	0.374	0.373

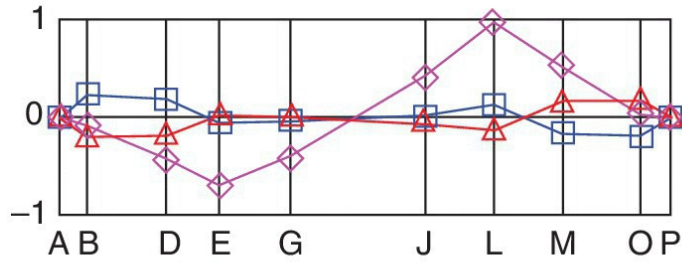
The mode shapes of the first eight modes are extracted from ambient vibration measurements under strong wind conditions, as plotted in [Figure 5.10](#). The modal responses obtained from vertical accelerometers on the two sides of the bridge deck are plotted with lines with square and triangle symbols, while the modal responses obtained from transverse accelerometers along the middle of the bridge deck are plotted with lines with diamond symbols.



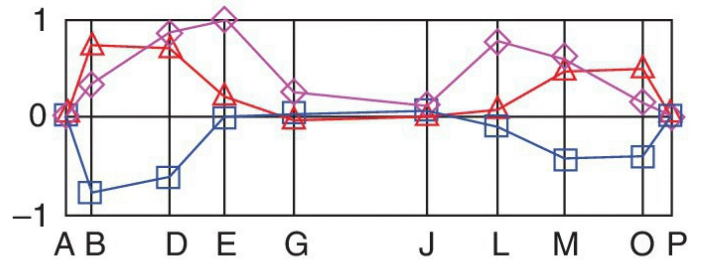
First mode (0.164 Hz), predominantly vertical mode



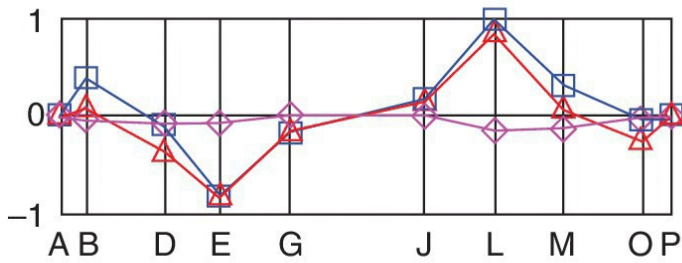
Second mode (0.227 Hz), coupled torsional & lateral mode



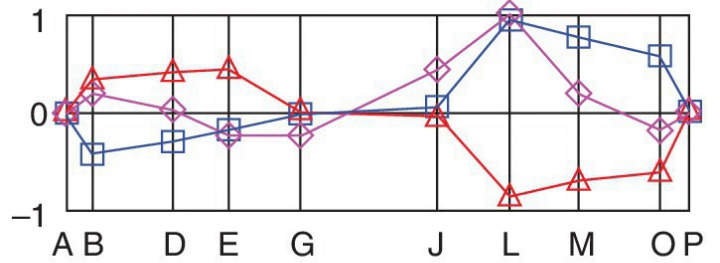
Third mode (0.264 Hz), predominantly vertical mode



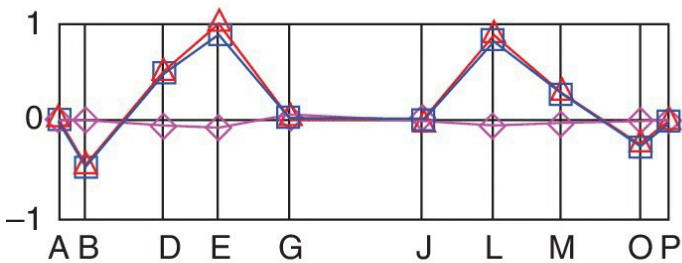
Fourth mode (0.290 Hz), coupled torsional & lateral mode



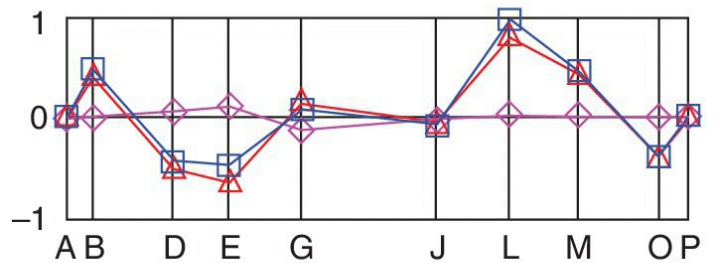
Fifth mode (0.298 Hz), predominantly vertical mode



Sixth mode (0.324 Hz), coupled torsional & lateral mode



Seventh mode (0.361 Hz), predominantly vertical mode



Eighth mode (0.372 Hz), predominantly vertical mode

Figure 5.10 Identified mode shapes of first eight modes for Ting Kau Bridge.

5.5 Correlation Between Test and Calculated Results

The experimental results for the tested structure need to be compared with the calculated results usually predicted by the finite element (FE) model. Difficulties arise in the comparison

since the number of sensors adopted for the dynamic test is typically less than the number of degrees of freedom (DOFs) generated by the associated FE numerical model. Due to noise in measurements and errors in FE modelling, there may be considerable discrepancy between the test results and the numerical predictions.

5.5.1 Modal Assurance Criterion

The modal data obtained from experiments, such as natural frequencies and mode shapes, must be paired with those predicted by the associated FE model. The mode pairing must be undertaken before correlation studies, FE model updating and structural damage identification. The modal assurance criterion is widely used for pairing experimental modes with the associated calculated modes.

In structural dynamic testing, measured modal data about the natural frequency $\hat{\omega}_i$ and mode shape readings $\hat{\Psi}_i$ of the tested structure can be extracted from vibration measurements. The measured mode shapes, with dimension of N_s , where N_s is the total number of effective sensors installed, are usually incomplete with reference to the FE model typically having a large number of DOFs. The measured modes should be paired to the calculated eigenvectors of dimension N_s (restricted to the same dimensions as $\hat{\Psi}_i$), Φ_k^a . The modal assurance criterion (MAC) between the measured mode shape $\hat{\Psi}_i$ and the associated calculated mode shape Φ_k^a is defined as

$$MAC(\Phi_k^a, \hat{\Psi}_i) = \frac{|\Phi_k^{aT} \hat{\Psi}_i|^2}{|\Phi_k^{aT} \Phi_k^a| |\hat{\Psi}_i^T \hat{\Psi}_i|} \quad (5.20)$$

The value of the MAC ranges from 0 to 1. Large MAC factors indicate a high degree of similarity between two mode shapes, and small MAC factors represent little or even no correlation between two vectors. If all measured and calculated modes are paired to each other, then the MAC matrix is obtained. This matrix should have values close to unity at the diagonal, and values close to zero elsewhere.

The MAC may be modified by using a weighting matrix, such as a mass matrix, rewritten as

$$MAC^*(\Phi_k^a, \hat{\Psi}_i) = \frac{|\Phi_k^{aT} \mathbf{M} \hat{\Psi}_i|^2}{|\Phi_k^{aT} \mathbf{M} \Phi_k^a| |\hat{\Psi}_i^T \mathbf{M} \hat{\Psi}_i|} \quad (5.21)$$

From the orthogonality of eigenvectors with respect to the mass matrix, the modified MAC matrix should have values of zero for the offdiagonal entries, when the measured and calculated modes are identical. The modified MAC may not give much improved results in the cases when the measured modes are not close to the calculated ones.

5.5.2 Orthogonality Checks

The calculated eigenvectors from the FE model are often normalised with respect to the mass matrix, thus the orthogonality of the eigenvectors with respect to stiffness matrix is expressed as

$$\Phi^T \mathbf{M} \Phi = \mathbf{I} \quad \text{and} \quad \Phi^T \mathbf{K} \Phi = \Lambda \quad (5.22)$$

where Φ is the matrix of eigenvectors, \mathbf{I} is the identity matrix and Λ is the diagonal matrix of eigenvalues.

The orthogonality performance criteria are introduced to measure the cross orthogonality of the measured mode shapes with respect to the mass and stiffness (Chen and Maung 2014). The average mass and stiffness orthogonality errors for a total number of Nm measured modes are defined, respectively, as

$$E_M = \frac{1}{\frac{1}{2} Nm(Nm-1)} \sum_{i=1}^{Nm} \sum_{j=i+1}^{Nm} \left(\frac{\hat{m}_{ij}^2}{\hat{m}_{ii} \hat{m}_{jj}} \right)^{1/2} \quad \text{and} \quad E_K = \frac{1}{\frac{1}{2} Nm(Nm-1)} \sum_{i=1}^{Nm} \sum_{j=i+1}^{Nm} \left(\frac{\hat{k}_{ij}^2}{\hat{k}_{ii} \hat{k}_{jj}} \right)^{1/2} \quad (5.23)$$

where coefficients \hat{m}_{ij} and \hat{k}_{ij} are defined as

$$\hat{m}_{ij} = \hat{\psi}_i^T \mathbf{M} \hat{\psi}_j \quad \text{and} \quad \hat{k}_{ij} = \hat{\psi}_i^T \mathbf{K} \hat{\psi}_j \quad (5.24)$$

Two problems arise in the use of orthogonality checks: measurements of complex modes and incompleteness of the measured modes. The incompleteness is due to the limited sensors installed in collecting measurements. Therefore, the mass and stiffness matrices need to be reduced by model reduction techniques, or the measured modes need to be expanded by mode shape expansion techniques.

5.5.3 Modal Scale Factor

The measured mode shapes are often mass normalised, as given in [Equation \(5.22\)](#). However, the mass normalised mode shape is not unique since it may have a different sign (phase shift 180°). Thus to compare the measured and calculated mode shapes a consistent scalar is required. Assume that the i th measured mode shape $\hat{\psi}_i$ is scaled by a modal scale factor (MSF) with respect to the i th calculated eigenvector ϕ_i^a restricted to the same dimensions as $\hat{\psi}_i$. The i th scaled measured mode shape $\hat{\phi}_i^a$ with the MSF is expressed as

$$\hat{\phi}_i^a = MSF_i \cdot \hat{\psi}_i \quad (5.25)$$

The MSF for the i th measured mode shape is defined as

$$MSF_i = \frac{|\phi_i^{aT} \hat{\psi}_i|}{|\hat{\psi}_i^T \hat{\psi}_i|} = \frac{|\hat{\psi}_i^T \phi_i^a|}{|\hat{\psi}_i^T \hat{\psi}_i|} \quad (5.26)$$

Similarly, a weighted MSF for the i th measured mode shape using mass matrix \mathbf{M} is defined as

$$MSF_i^* = \frac{|\phi_i^{aT} \mathbf{M} \hat{\psi}_i|}{|\hat{\psi}_i^T \mathbf{M} \hat{\psi}_i|} = \frac{|\hat{\psi}_i^T \mathbf{M} \phi_i^a|}{|\hat{\psi}_i^T \mathbf{M} \hat{\psi}_i|} \quad (5.27)$$

The modal scale factor can be used to ensure that the measured incomplete mode shapes of the actual tested structure are close to the corresponding part of the FE numerical eigenvectors.

5.5.4 Coordinate Modal Assurance Criterion

When using the modal assurance criterion, it may be difficult to compare modes, when the modes have close frequencies and are measured at limited sensor places. An extension of the MAC is the coordinate modal assurance criterion (COMAC). The COMAC attempts to identify which measured DOFs contribute negatively to a low value of MAC. The COMAC is calculated over a set of mode pairs ϕ_m and ψ_m . For each DOF, for example the k th DOF, the COMAC is calculated by summing over total Nm paired modal vectors, defined as

$$COMAC_k = \frac{\sum_{m=1}^{Nm} (\phi_{m,k} \psi_{m,k})^2}{\sum_{m=1}^{Nm} (\phi_{m,k} \phi_{m,k}) \sum_{m=1}^{Nm} (\psi_{m,k} \psi_{m,k})} \quad (5.28)$$

A COMAC value of unity indicates good correlation. Note that the above equation assumes that there is a match for every mode shape in the two sets. Only those modes that match between the two sets are included in the calculation.

5.6 Mode Shape Expansion and Model Reduction

One major problem arises in the correlation study between the tested results and the analytical model or finite element (FE) numerical model. In general, the calculated mode shapes obtained from the finite element numerical model contain a full set of degrees of freedom (DOFs) of the numerical model. The measured data set of a dynamic test, however, is usually incomplete and only exists at the DOFs associated with the test points, because the measurements are often taken at a limited set of locations in selected coordinate directions. In many structural dynamics applications such as vibrationbased model updating and damage identification, it is desirable to expand the reduced experimental data set onto the associated full finite element coordinate set. The alternative would be a model reduction process that destroys the original sparse pattern in mass and stiffness matrices and propagates modelling errors or structural

damage all over the reduced mass and/or stiffness matrices.

5.6.1 General Expansion and Reduction Methods

For a dynamic structural system, the full set of analytical DOFs can be divided into two complementary sets: the measured DOFs at the test points and the remaining unmeasured DOFs (Chen 2010). The characteristic equation for an N DOFs dynamic system with global stiffness matrix \mathbf{K} and mass matrix \mathbf{M} , expressed in [Equation \(5.9\)](#), can be rewritten in a partitioned form as

$$\begin{bmatrix} \mathbf{K}^{aa} & \mathbf{K}^{au} \\ \mathbf{K}^{ua} & \mathbf{K}^{uu} \end{bmatrix} \begin{Bmatrix} \boldsymbol{\phi}_i^a \\ \boldsymbol{\phi}_i^u \end{Bmatrix} - \omega_i^2 \begin{bmatrix} \mathbf{M}^{aa} & \mathbf{M}^{au} \\ \mathbf{M}^{ua} & \mathbf{M}^{uu} \end{bmatrix} \begin{Bmatrix} \boldsymbol{\phi}_i^a \\ \boldsymbol{\phi}_i^u \end{Bmatrix} = \begin{Bmatrix} \mathbf{0} \\ \mathbf{0} \end{Bmatrix} \quad (5.29)$$

where subscripts a and u denote the measured and unmeasured DOFs, respectively. From the second equation of the partitioned set, the unmeasured part of the mode shape can be obtained from

$$\boldsymbol{\phi}_i^u = -[\mathbf{K}^{uu} - \omega_i^2 \mathbf{M}^{uu}]^{-1} [\mathbf{K}^{ua} - \omega_i^2 \mathbf{M}^{ua}] \boldsymbol{\phi}_i^a \quad (5.30)$$

Consequently, the i th expanded mode shape with full set of DOFs, comprising the measured part $\boldsymbol{\phi}_i^a$ and unmeasured part $\boldsymbol{\phi}_i^u$, is expressed as

$$\boldsymbol{\phi}_i = \begin{Bmatrix} \boldsymbol{\phi}_i^a \\ \boldsymbol{\phi}_i^u \end{Bmatrix} = \mathbf{T} \boldsymbol{\phi}_i^a \quad (5.31)$$

where \mathbf{T} is the transformation matrix between the reduced set of measured DOFs and the full set of DOFs, depending on the expansion methods adopted.

The static expansion method (Guyan 1965) is based on the static stiffness by neglecting the inertial forces at the unmeasured DOFs. The static transformation matrix \mathbf{T}_s is given by

$$\mathbf{T}_s = \begin{bmatrix} \mathbf{I} \\ -\mathbf{K}^{uu-1} \mathbf{K}^{ua} \end{bmatrix} \quad (5.32)$$

The Guyan static method may give accurate mode shape expansion estimates only when there are sufficient DOFs to represent the mass inertia of the actual tested dynamic system.

The dynamic expansion method (Kidder 1973) is the same as the static expansion method, except that the inertial forces at the unmeasured DOFs are included in the expansion process at a particular frequency. The dynamic transformation matrix \mathbf{T}_d is given by

$$\mathbf{T}_d = \begin{bmatrix} \mathbf{I} \\ -[\mathbf{K}^{uu} - \omega_i^2 \mathbf{M}^{uu}]^{-1} [\mathbf{K}^{ua} - \omega_i^2 \mathbf{M}^{ua}] \end{bmatrix} \quad (5.33)$$

The system equivalent reduction expansion process (SEREP) is not directly related to the stiffness and mass of the analytical model, and depends on analytical mode shapes to develop the mapping between the full set of analytical DOFs and the reduced set of measured DOFs (O'Callahan et al. 1989). In the cases where the number of measured DOFs is greater than the number of modes of the tested structure, the SEREP transformation matrix \mathbf{T}_u is expressed as

$$\mathbf{T}_u = \begin{Bmatrix} \phi^a \\ \phi^u \end{Bmatrix} \left[\phi^{aT} \phi^a \right]^{-1} \phi^{aT} \quad (5.34)$$

In the SEREP expansion process, the initial displacements at the measured DOFs may be modified. The SEREP method could produce poor expansion estimates if the experimental mode shapes are not correlated well with the corresponding analytical mode shapes, which often happens in the cases with large modelling errors in the analytical model.

For model reduction, the expansion processes can be inverted to reduce the analytical model to the measured DOFs. By eliminating the displacements at unknown DOFs, the reduced structural parameter matrices – e.g. stiffness matrix \mathbf{K}_{red} , mass matrix \mathbf{M}_{red} and damping matrix \mathbf{C}_{red} – can be written, respectively, as

$$\mathbf{K}_{red} = \mathbf{T}^T \mathbf{K} \mathbf{T}, \mathbf{M}_{red} = \mathbf{T}^T \mathbf{M} \mathbf{T} \text{ and } \mathbf{C}_{red} = \mathbf{T}^T \mathbf{C} \mathbf{T} \quad (5.35)$$

The transformation matrix \mathbf{T} depends on the model reduction methods adopted. The transformation matrix \mathbf{T}_s , \mathbf{T}_d or \mathbf{T}_u is used for the static, the dynamic or the SEREP model reduction, respectively.

The general expansion and reduction methods discussed above are often used to expand the measured incomplete mode shapes in structural dynamic applications. However, these methods do not consider the discrepancy between the analytical model and the actual tested structure, since only the structural or modal parameters associated with the analytical model are utilised in the expansion and reduction processes. In addition, the modal data at the measured DOFs are directly adopted for mode shape expansion, and the influence of measurement uncertainty cannot be reduced.

5.6.2 Perturbed Force Approach

In structural dynamic applications, the analytical model (or FE numerical model) usually has uncertainties in modelling the associated actual tested structural dynamic system. The analytical model uncertainties are mainly related to the unknown perturbations of stiffness and mass between the analytical model and the tested system. In order to include the modelling errors in the analytical model and reduce the influence of noise in measured modal data, a

perturbed force approach for expanding mode shapes is proposed in the study by Chen (2010). The perturbed force approach is based on the dynamic perturbation method (Chen 2005), as discussed in detail in [Section 6.5](#). The approach has been successfully applied to the mode shape expansion of the Canton Tower (Chen et al. 2012). The perturbed force approach takes the perturbed force vector containing modelling errors as basic parameters, which can be obtained from modal data measurements, and then applies it to predicting the unmeasured part of the expanded mode shapes.

Define a perturbed force vector for the i th mode of the tested dynamic system, associated with the unknown perturbations of stiffness ($\Delta\mathbf{K}$) and mass ($\Delta\mathbf{M}$), as

$$\mathbf{r}_i = (\Delta\mathbf{K} - \hat{\omega}_i^2 \Delta\mathbf{M}) \hat{\phi}_i \quad (5.36)$$

where $\hat{\omega}_i$ and $\hat{\phi}_i$ are the i th natural frequency and the corresponding mode shape for the tested system, respectively. The perturbed force vector \mathbf{r}_i becomes zero if both $\Delta\mathbf{K}$ and $\Delta\mathbf{M}$ are equal to zero, that is, no structural modelling errors exist in the analytical model. The relation between the perturbed force vector \mathbf{r}_i and the mode shape of the tested dynamic system $\hat{\phi}_i$ is expressed as

$$\sum_{k=1}^N \frac{\phi_k^T \mathbf{r}_i}{(\hat{\omega}_i^2 - \omega_k^2)} \phi_k = \hat{\phi}_i \quad (5.37)$$

In modal testing, modal information about the natural frequency $\hat{\omega}_i$ and limited number of measured DOF's readings $\hat{\psi}_i$ of dimension N_s can be extracted. In order to make the measured mode shapes close to the corresponding part of the analytical mode shapes ϕ_i^a , the incomplete measured mode shapes $\hat{\psi}_i$ need to be scaled with the modal scale factor (MSF) defined in [Equation \(5.25\)](#), giving the scaled known mode shape $\hat{\phi}_i^a$.

From [Equation \(5.37\)](#), the perturbed force vector for the i th experimental mode can be directly calculated from

$$\mathbf{r}_i = \mathbf{S}_i^+ \hat{\phi}_i^a \quad \text{and} \quad \mathbf{S}_i^+ = \mathbf{S}_i^T [\mathbf{S}_i \mathbf{S}_i^T]^{-1} \quad (5.38)$$

where \mathbf{S}_i^+ is the Moore–Penrose pseudoinverse of matrix \mathbf{S}_i , and \mathbf{S}_i is the sensitivity coefficient matrix of dimension $N_s \times N$ for the i th experimental mode, defined as

$$\mathbf{S}_i = \sum_{k=1}^N \frac{\phi_k^a \phi_k^T}{(\hat{\omega}_i^2 - \omega_k^2)} \quad (5.39)$$

Due to the inevitable noise in modal data measurements, the solution of the perturbed force

vector obtained from the Moore–Penrose pseudoinverse in [Equation \(5.38\)](#) may not be stable. In order to reduce the influence of noise in modal data measurements on the performance of mode shape expansion, a regularisation method is now employed to obtain reasonable solutions for the perturbed force vector. The Tikhonov regularised solution for a continuous regularisation parameter α (Tikhonov and Arsenin 1977), replacing the Moore–Penrose pseudoinverse, is given in terms of the regularisation parameter α as

$$\mathbf{r}_i(\alpha) = \mathbf{S}_i^\#(\alpha) \hat{\boldsymbol{\phi}}_i^a \text{ and } \mathbf{S}_i^\#(\alpha) = (\mathbf{S}_i^T \mathbf{S}_i + \alpha^2 \mathbf{I})^{-1} \mathbf{S}_i^T \quad (5.40)$$

where \mathbf{I} is the identity matrix and $\mathbf{S}_i^\#(\alpha)$ is the influence matrix associated with the Tikhonov regularisation parameter α . This regularisation parameter can be determined using Lcurve criterion (Hansen and O’Leary 1993). Details about the Tikhonov regularisation method are discussed in [Section 6.5.2](#), and its applications to the mode shape expansion are provided in the study by Chen (2010).

Consequently, the i th full experimental mode shape, comprising the measured part $\hat{\boldsymbol{\phi}}_i^a$ and the unmeasured part $\hat{\boldsymbol{\phi}}_i^u$, can be obtained from

$$\hat{\boldsymbol{\phi}}_i = \begin{Bmatrix} \hat{\boldsymbol{\phi}}_i^a \\ \hat{\boldsymbol{\phi}}_i^u \end{Bmatrix} = \mathbf{T}_p^i \hat{\boldsymbol{\phi}}_i^a \quad (5.41)$$

where the regularised transformation matrix \mathbf{T}_p^i of the perturbed force approach for the i th mode shape expansion is defined as

$$\mathbf{T}_p^i = \begin{bmatrix} \mathbf{I} \\ \sum_{k=1}^N \frac{\boldsymbol{\phi}_k^u \boldsymbol{\phi}_k^T \mathbf{S}_i^\#(\alpha)}{(\hat{\omega}_i^2 - \omega_k^2)} \end{bmatrix} \quad (5.42)$$

The transformation matrix depends on the individual experimental mode to be expanded, since it includes the associated experimental natural frequency $\hat{\omega}_i$.

5.6.3 Comparison of Methods

A plane frame structure shown in [Figure 5.11](#) is used for comparing the general mode expansion methods with the perturbed force approach (Chen 2010). The frame structure has a total number of 28 conventional beam elements with axial deformations and a total number of 81 DOFs. The structure has section properties of area $A = 9.20 \times 10^{-3} \text{ m}^2$ and moment of inertia $I = 4.52 \times 10^{-6} \text{ m}^4$ as well as material properties of Young’s modulus $E = 7.20 \times 10^{10} \text{ N/m}^2$ and density $\rho = 2700 \text{ kg/m}^3$. It is assumed that the actual tested frame structure has perturbations of stiffness of +15% and mass of –10% at elements 1–16 for the columns, and additional

perturbations of stiffness of -10% and mass of $+10\%$ at elements 17–28 for the beams. The incomplete mode shapes of the tested structure are assumed to be obtained from the possible sensor locations measuring only translational DOFs, as indicated in [Figure 5.11](#). The noise in modal data measurements is simulated by corrupting the ideal modal data with additive standard normally distributed errors at different levels.

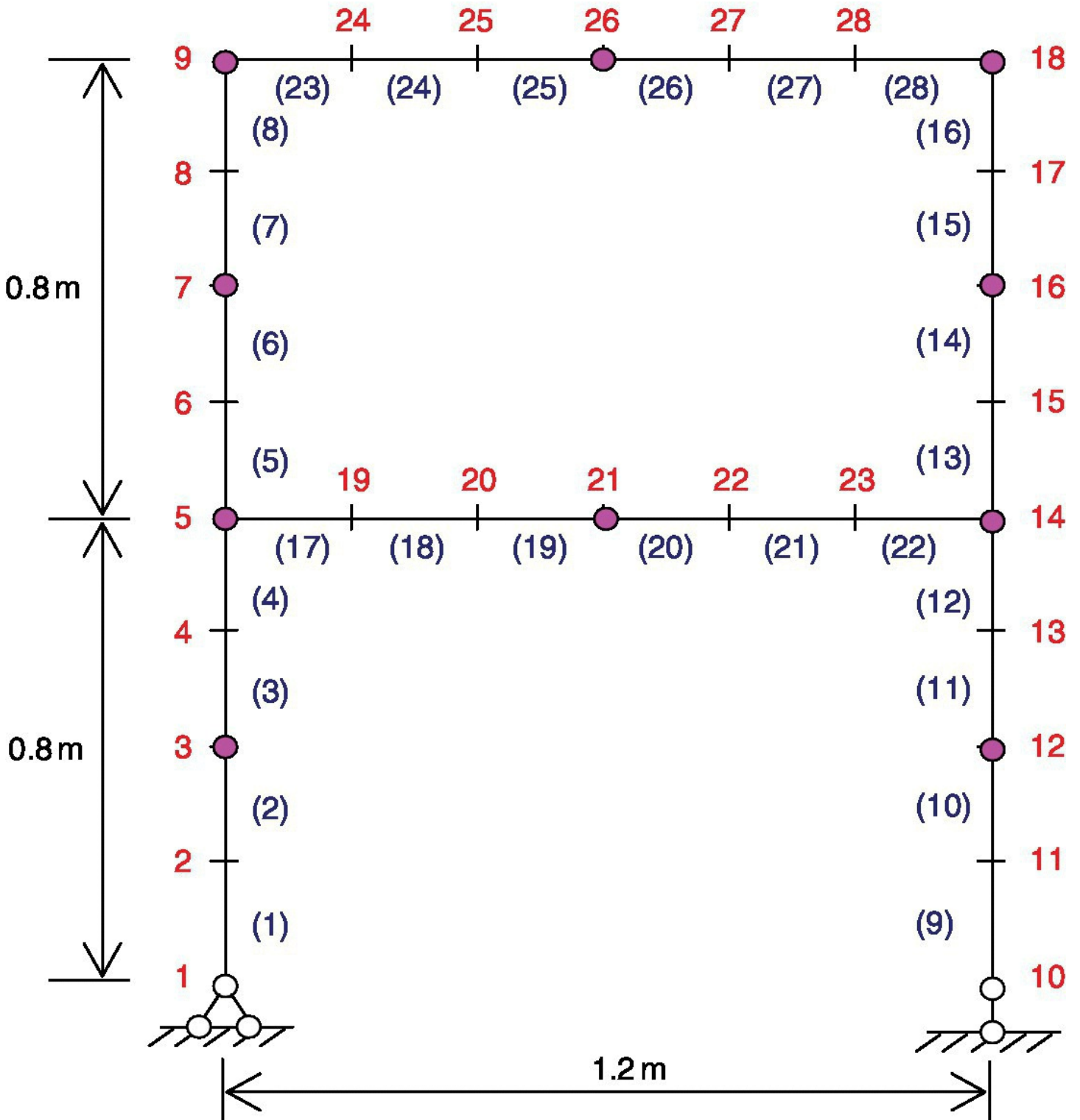


Figure 5.11 Plane frame structure with possible sensor locations marked with a circle.

The results from the general mode expansion methods and the perturbed force approach are

summarised in [Figures 5.12](#) and [5.13](#). The mean cumulative errors and the overall orthogonality errors, defined in [Chen \(2010\)](#), for the first 10 expanded modes are plotted as a function of simulated noise level. The static method has the overall worst performance, and fails to produce acceptable mode shape expansion estimates. The SEREP method is the most sensitive approach to the noise level in measured DOF readings, generating significant mean cumulative errors and overall orthogonality errors as noise level increases. The dynamic method yields substantial mean cumulative errors and overall orthogonality errors even in the cases with low noise levels. The perturbed force approach is capable of expanding mode shapes to a greater level of accuracy than the general mode expansion methods, giving mean cumulative error of 12.8% and overall orthogonality error of 4.2%, even in the case when the noise level reaches 10%.

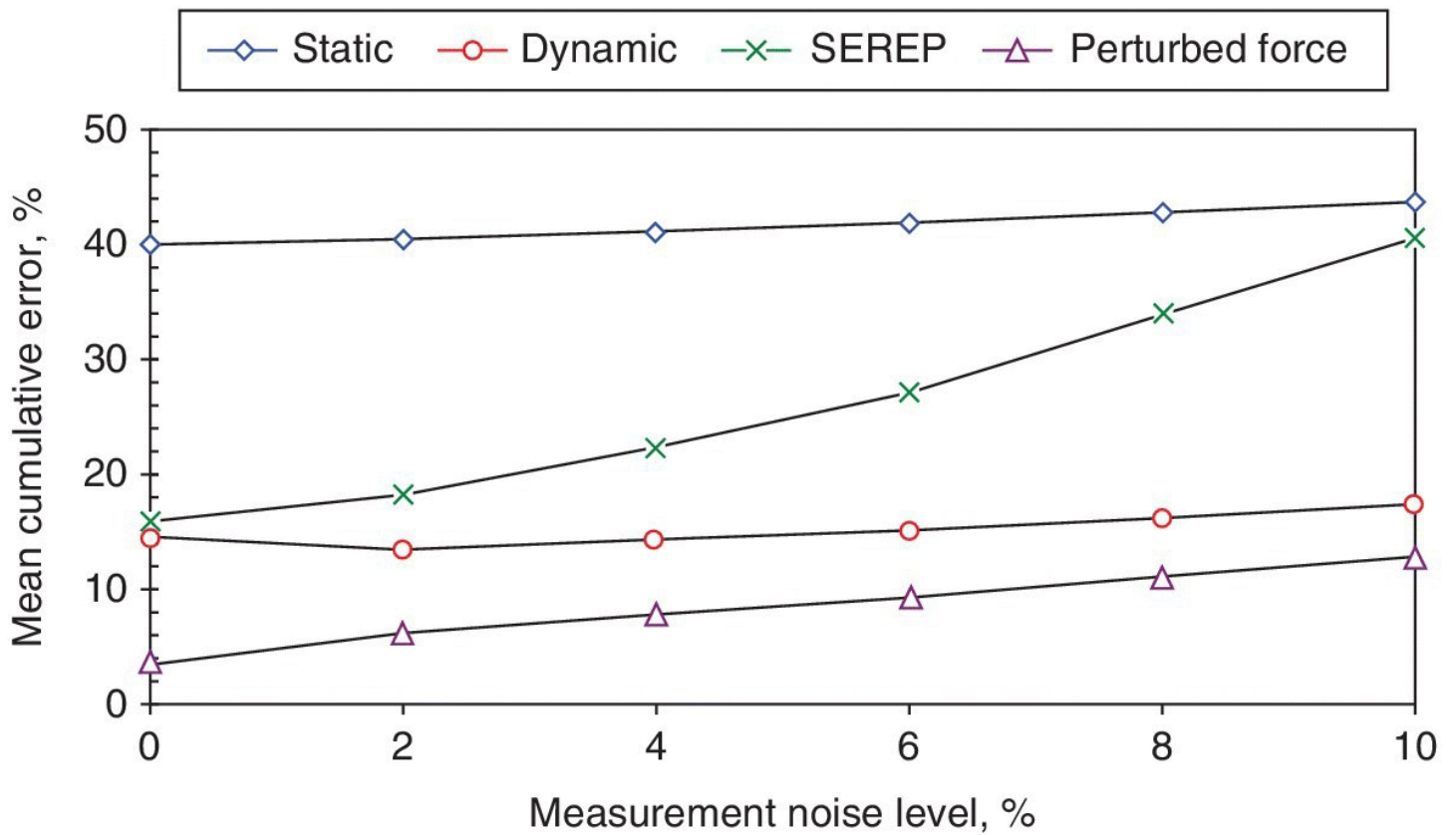


Figure 5.12 Mean cumulative errors in mode shape expansion as a function of noise level in DOF's readings for the frame structure.

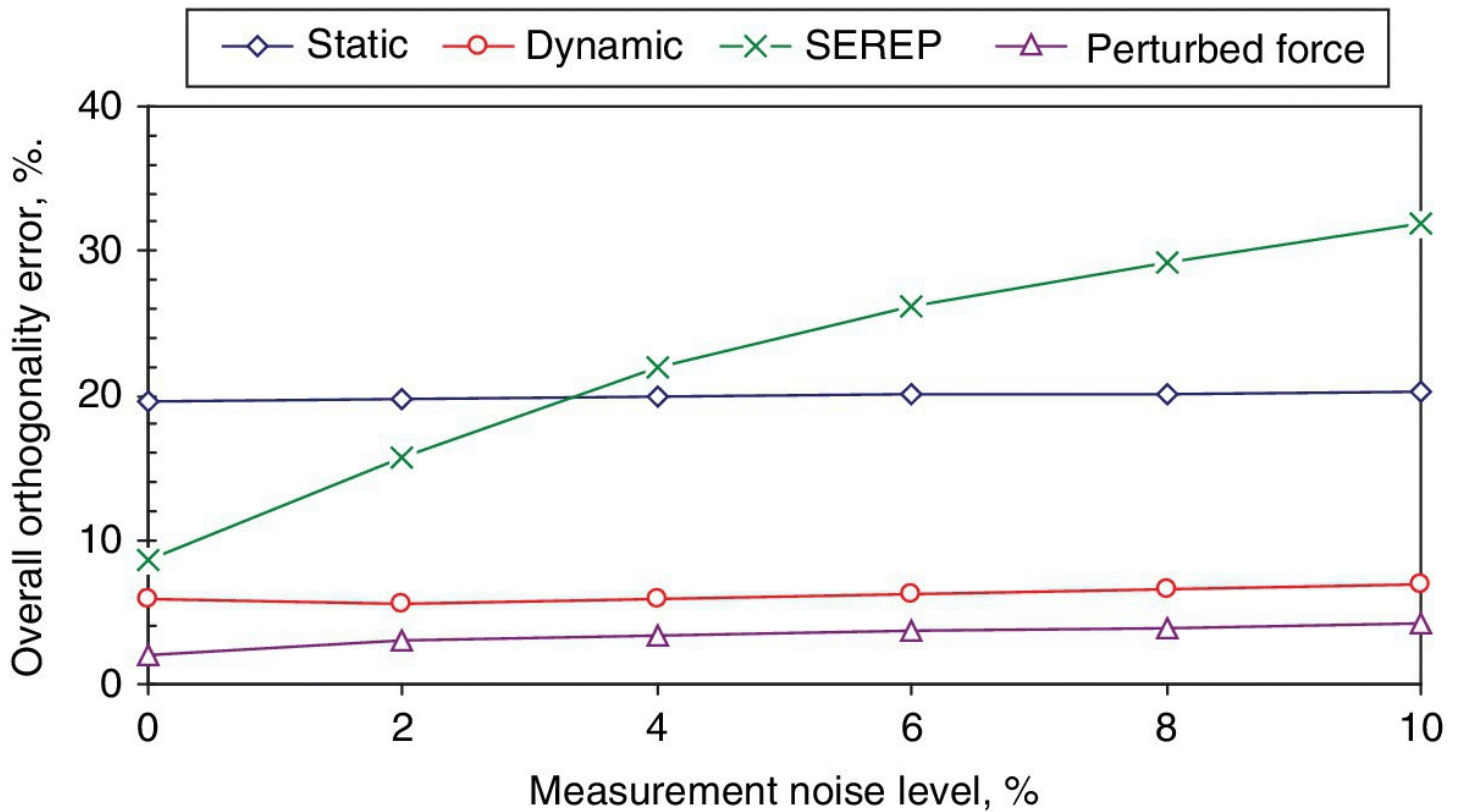
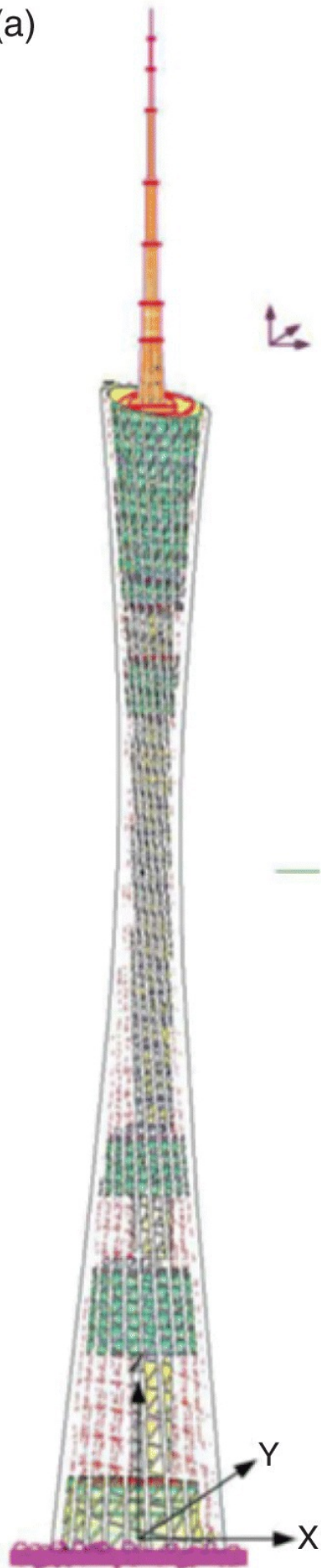


Figure 5.13 Overall orthogonality errors in mode shape expansion as a function of noise level in DOF readings for the frame structure.

5.7 Case Study

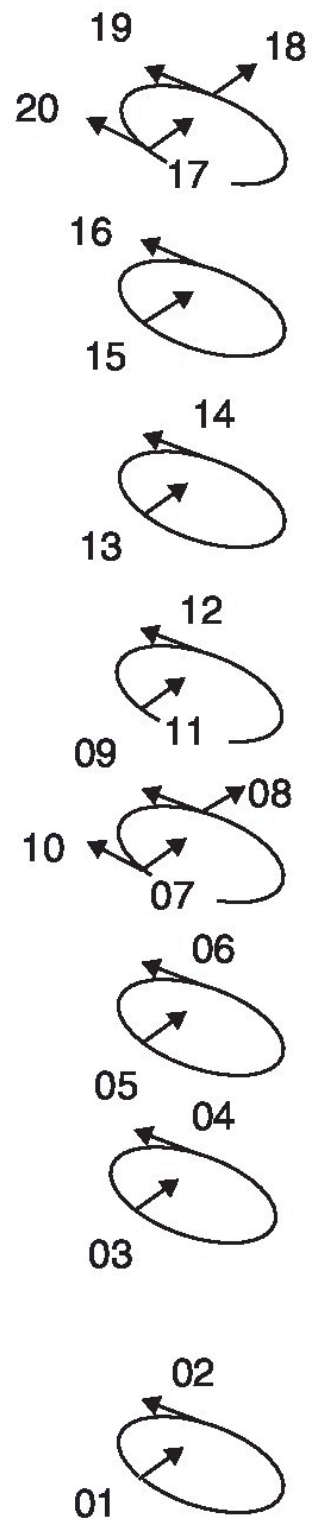
The constructed supertall structure Canton Tower, as discussed in the case studies in [Sections 2.7](#) and [3.6](#), is employed here for the case study on the output-only modal identification and mode shape expansion, as shown in [Figure 5.14](#). In order to obtain the operational modal properties of the tower, 20 uniaxial accelerometers were installed at eight different levels, as shown in [Figure 5.14\(b\)](#). Four uniaxial accelerometers were placed in the 4th and 8th floors, and two uniaxial accelerometers were equipped in each of the remaining six floors. The field ambient vibration measurement data can then be collected through the installed SHM system. In order to undertake structural health monitoring and associated studies, a reduced three-dimensional (3D) beam model shown in [Figure 5.14\(c\)](#) was established on the basis of the complex 3D full finite element model shown in [Figure 5.14\(a\)](#) (Ni et al. 2012). For this case study, the monitoring data recorded from 18:00 on 19 January to 18:00 on 20 January 2010 with a sampling frequency of 50 Hz by the SHM system are used.

(a)



(b)

Accelerometer
direction and
channel label



(c)

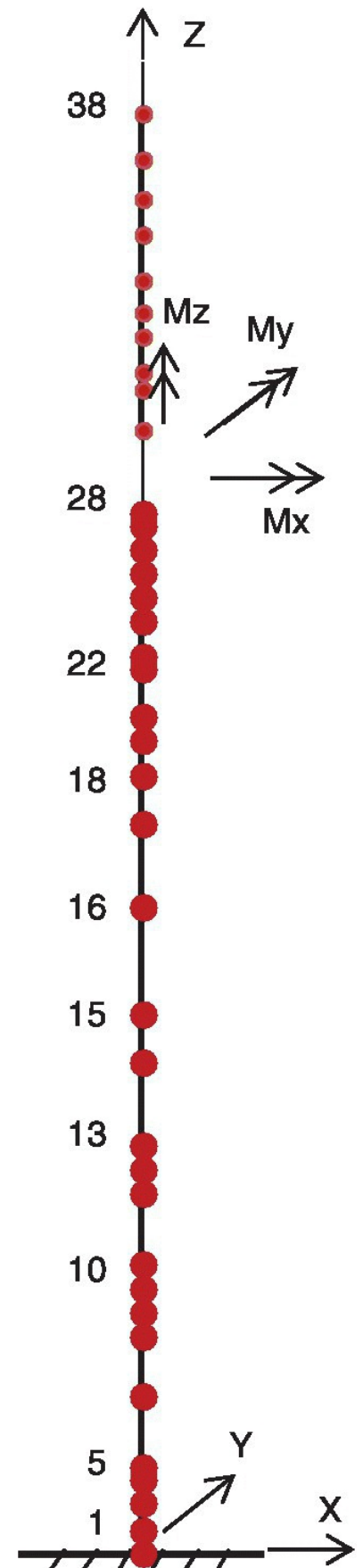


Figure 5.14 Canton Tower: (a) full finite element model, (b) positions of installed accelerometers, (c) reduced order finite element (FE) model.

5.7.1 Operational Modal Analysis

First, the simple output only modal identification technique, the peak picking (PP) method, is used to extract modal properties such as natural frequencies from the recorded ambient vibration measurements. The peak picking method is a frequency domain based technique. This method is often used for operational modal identification in civil engineering practice from ambient vibration measurements due to its simple implementation and fast processing speed. A practical implementation of the PP method can be realised by the averaged normalised power spectral densities (ANPSDs) in order to obtain a global picture of frequencies. The ANPSDs are calculated by converting the acceleration measurements to the frequency domain by a discrete Fourier transform and then by averaging the individual power spectral densities. As a result, the natural frequencies could be simply determined from the observation of the peaks on the graphs of the ANPSDs, as shown in [Figure 5.15](#). The PP method, however, can only provide the operational deflection shapes and is unable to produce mode shapes.

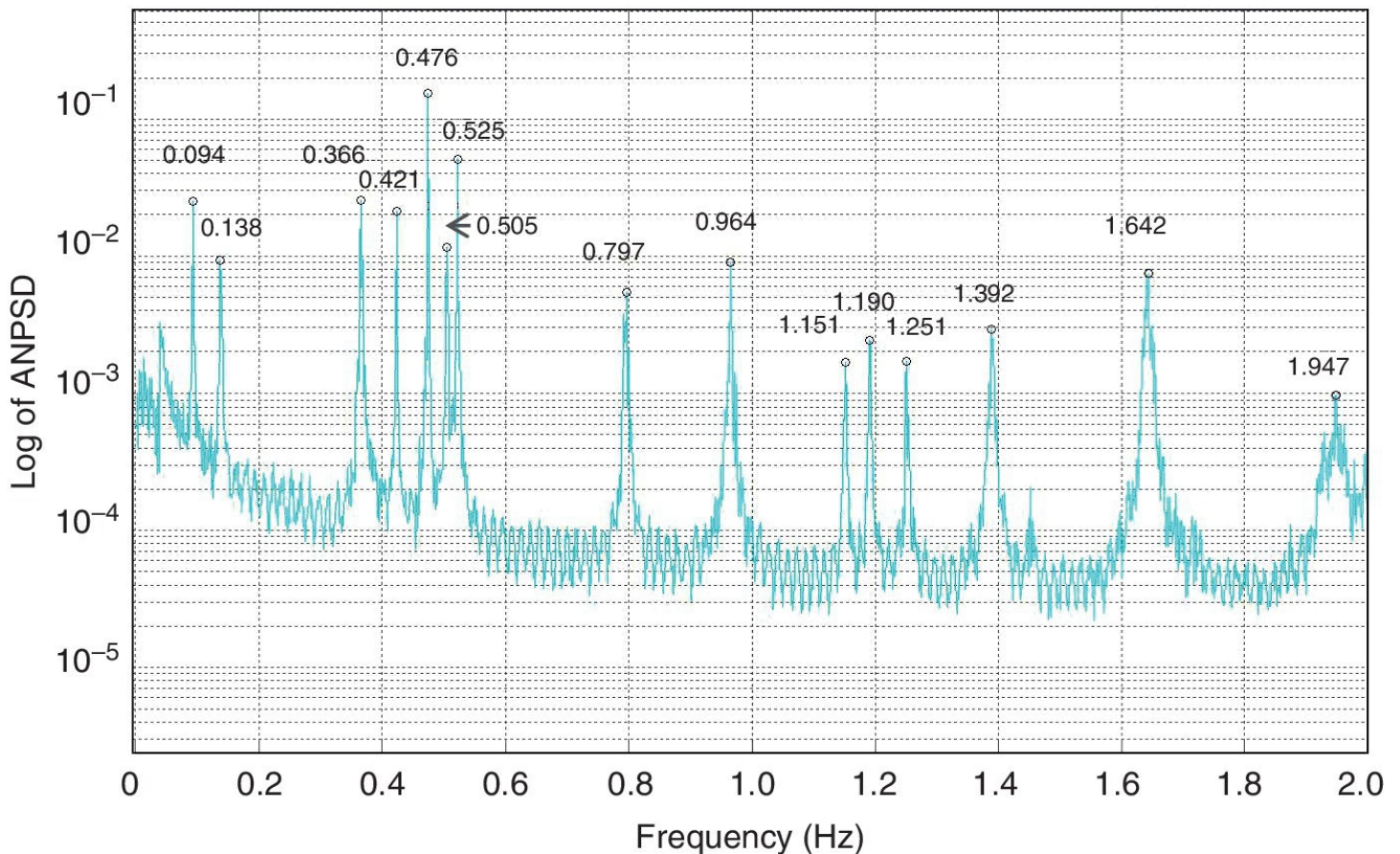


Figure 5.15 Averaged normalised power spectral densities (ANPADs) of the measured acceleration data used for the peak picking (PP) method.

The sophisticated stochastic subspace identification (SSI) method is now used to extract modal

properties such as frequencies, damping ratios and mode shapes from the recorded ambient vibration measurements. This method is a time-domain method and directly works with time dependent data, without requiring the conversions of the measured data into correlations or spectra. The SSI method identifies the statespace matrices on the basis of the measurements by using robust numerical techniques, such as singular value decomposition. Once the mathematical description of the structure (the statespace model) is determined, it is straightforward to extract natural frequencies from the stabilisation diagram, as shown in [Figure 5.16](#), and also to produce the associated damping ratios and mode shapes.

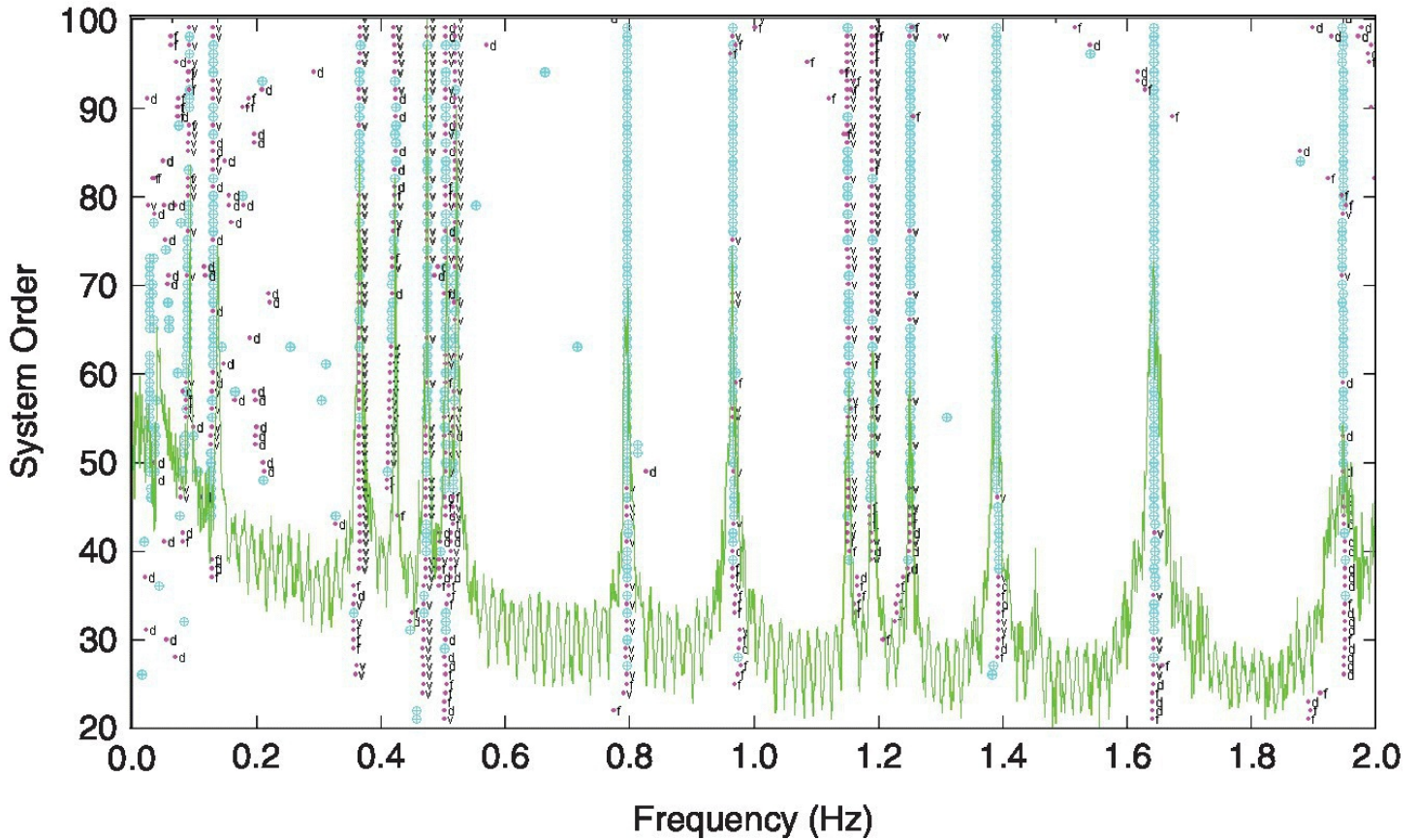


Figure 5.16 Stabilisation diagram of measured acceleration data used for the stochastic subspace identification (SSI) method.

The modal properties identified by the PP method and the SSI method are summarised in [Table 5.3](#). The frequencies identified by the SSI method are very close to those from the PP method. The MAC diagonal values, computed from the incomplete mode shapes identified by the SSI method and the calculated eigenvectors restricting to the same DOFs, indicate good correlation between the identified and calculated modes, except for two torsion modes: 6th and 12th. The difference between the frequencies identified from the ambient vibration measurements and those predicted by finite element model is relatively large, with the largest relative error in the fundamental frequency. The significant difference between the measured and calculated frequencies requires an updating of the finite element model of the supertall structure.

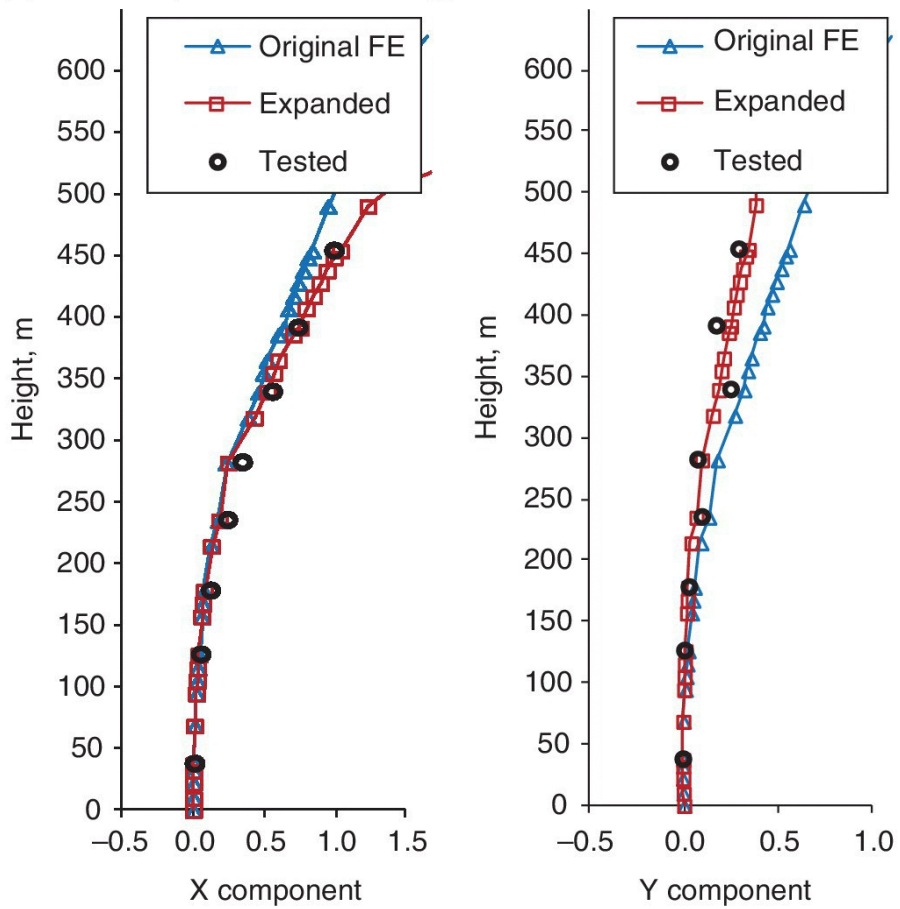
Table 5.3 Modal data identified by output-only identification methods from ambient vibration data.

Mode	PP method (Hz)	SSI method (Hz)	FE model (Hz)	Damping (%)	MAC value	Mode description
1	0.094	0.090	0.111	2.97	0.904	Shortaxis bending
2	0.138	0.131	0.159	6.18	0.938	Longaxis bending
3	0.366	0.366	0.347	0.24	0.888	Shortaxis bending
4	0.421	0.422	0.369	—	0.888	Longaxis bending
5	0.476	0.474	0.400	0.07	0.869	Shortaxis bending
6	0.505	0.504	0.462	0.38	0.104	Torsion
7	0.525	0.520	0.487	0.07	0.783	Long and shortaxis bending
8	0.797	0.796	0.738	0.20	0.797	Shortaxis bending
9	0.964	0.966	0.904	0.33	0.771	Longaxis bending
10	1.151	1.151	0.997	0.10	0.701	Shortaxis bending
11	1.190	1.191	1.037	0.03	0.753	Longaxis bending
12	1.251	1.251	1.121	0.16	0.161	Torsion
13	1.392	1.390	1.245	0.35	0.793	Coupled bending and torsion
14	1.642	1.643	1.504	0.25	0.623	Coupled bending and torsion
15	1.947	1.946	1.726	0.59	0.609	Coupled bending and torsion

5.7.2 Mode Shape Expansion

The operational modal data of the Canton Tower – e.g. natural frequencies and incomplete mode shapes identified by the SSI method – are now adopted for the mode shape expansion. The reduced 3D beam model shown in [Figure 5.14\(c\)](#) is used for the analytical model in the mode expansion process. The perturbed force approach with Tikhonov regularisation incorporating the Lcurve criterion is adopted to reduce the noise effects. The first and fourth bending modes are considered for the regularised model shape expansion, as shown in [Figure 5.17](#).

(a) Mode 1 (short-axis bending).



(b) Mode 4 (long-axis bending).

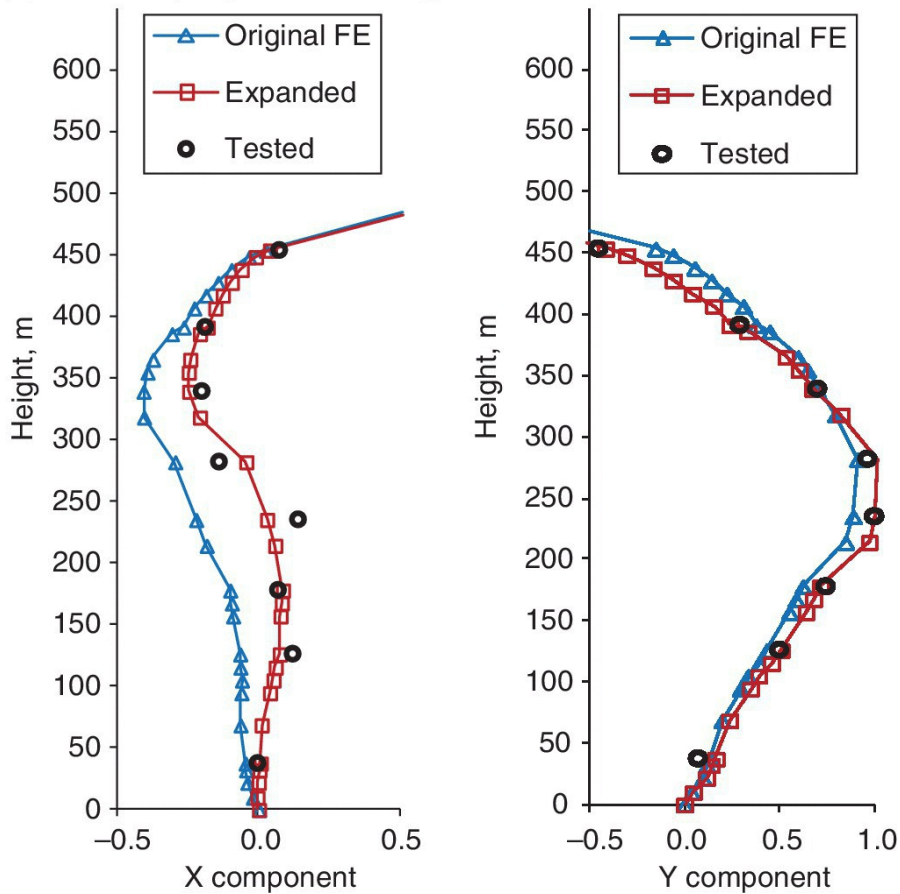


Figure 5.17 Expanded first and fourth bending modes, compared with the modal readings identified from ambient vibration data and the eigenvectors of the reduced finite element model.

The perturbed force approach provides optimised and smooth estimates of mode shape expansion, without simply reproducing the measured DOF readings for the known part of the complete mode shape concerned. The results of expanded mode shapes obtained by the perturbed force approach are then compared with the results calculated from the reduced order finite element model and the modal data identified from the ambient vibration measurements. The expanded mode shapes correlate very well with the corresponding original analytical eigenvectors. They also have better correlation with the measured incomplete mode shapes after the expansion.

5.8 Concluding Remarks

Modal data of civil engineering structures can be identified from the vibration measurements generated by controlled forces or ambient sources through the installed SHM system. Civil engineering structures are typically large in size and generally have low natural frequencies. If a structure has low frequency modes (e.g. below 1 Hz), it may be difficult to excite the structure by an external force, such as a shaker. The use of controlled excitation is only applicable when the generated response surpasses the inevitably exciting ambient responses. For very large civil structures, such as longspan bridges and highrise buildings, the use of controlled excitation becomes almost impossible. These large structures could be excited by other excitation types, such as a drop weight or ambient sources. Ambient sources, however, may not excite well the high frequency modes of the structures.

The accelerations of a civil structure associated with ambient excitations are typically very small, and they can vary considerably due to the operational and environmental conditions. The accurate identification of operational modal data then becomes a challenge to the sensing networks and identification algorithms. The outputonly modal identification methods are a powerful tool for accurate identification of modal data under normal operational conditions. The stochastic subspace identification methods are reliable with noise effects and generally give good estimates of operational modal data from ambient vibration measurements. If only ambient vibration measurements are available, the stabilisation diagram is very useful and provides objective selections of natural frequencies, since it does not need to find often unclear peaks in the spectrum or frequencydomain singular value plots. The outputonly methods are unable to provide the massnormalised mode shapes from ambient excitations. To obtain the correct scale of the measured mode shapes, the controlled force has to be known.

The identified modal data of the tested structures must be checked against the analytical model (or finite element numerical model) by correlation studies. In finite element model updating or structural damage identification procedures, the expansions of measured mode shapes are often required to match the full DOFs of the analytical model. The general mode shape expansion methods may not perform well when discrepancies between the analytical model and tested

results are large. The perturbed force approach is capable of successfully expanding mode shapes for the actual complex structure and produces reliable expansion estimates, where large modelling errors in the analytical model may exist and only limited DOF measurements are available. The perturbed force approach gives optimised and smooth expansion estimates in the least squares sense, and reduces the influence of measurement uncertainties in the expansion processes. Each mode shape can be expanded independently, and the expanded results only depend on the corresponding measured frequency and DOF readings of the tested structure. The results from the case study on the Canton Tower demonstrate that the perturbed force approach gives accurate estimates of mode shape expansion for the measured incomplete modal data.

References

- Avitabile, P. (2001). Experimental modal analysis: a simple nonmathematical presentation. *Sound and Vibration* **35**(1), 20–31.
- Bendat, J.S. and Piersol, A.G. (1993) *Engineering Applications of Correlation and Spectral Analysis*. Second Edition, John Wiley & Sons, New York, USA.
- Brincker, R., Ventura, C. and Andersen, P. (2001) Damping estimation by frequency domain decomposition. *Proceedings of the 19th International Modal Analysis Conference*, Kissimmee, Florida, FL, USA.
- Brincker, R., Zhang, L. and Andersen, P. (2000) Modal identification from ambient responses using frequency domain decomposition. *Proceedings of the 18th International Modal Analysis Conference*, San Antonio, TX, USA.
- Chen, H.P. (2005) Nonlinear perturbation theory for structural dynamic systems. *AIAA Journal* **43**(11), 2412–2421.
- Chen, H.P. (2010) Mode shape expansion using perturbed force approach. *Journal of Sound and Vibration* **329**(8), 1177–1190.
- Chen, H.P. and Maung, T.S. (2014) Regularised finite element model updating using measured incomplete modal data. *Journal of Sound and Vibration* **333**(21), 5566–5582.
- Chen, H.P., Tee, K.F. and Ni, Y.Q. (2012) Mode shape expansion with consideration of analytical modelling errors and modal measurement uncertainty. *Smart Structures and Systems* **10**(45), 485–499.
- Cunha, A. and Caetano, E. (2006) Experimental modal analysis of civil engineering structures. *Sound and Vibration* **40**(6), 12–16.
- Cunha, A., Caetano, E. and Delgado, R. (2001) Dynamic tests on a large cablestayed bridge – an efficient approach. *Journal Bridge Engineering ASCE* **6**(1), 54–62.

- Ewins, D.J. (2000) *Modal Testing: Theory, Practice and Application*. Research Studies Press, Baldock, Hertfordshire, UK.
- Friswell, M.I. and Mottershead, J.E. (1995) *Finite Element Model Updating in Structural Dynamics*. Kluwer Academic Publishers, Dordrecht, The Netherlands.
- Guyan, R. (1965) Reduction of stiffness and mass matrices. *AIAA Journal***3**(2), 380–387.
- Hansen, P.C. and O’Leary, D.P. (1993) The use of the Lcurve in the regularisation of discrete illposed problems. *SIAM Journal on Scientific Computing***14**(6), 1487–1503.
- Hermans, L. and Van der Auweraer, H. (1999) Modal testing and analysis of structures under operational conditions: industrial applications. *Mechanical Systems and Signal Processing***13**(2), 193–216.
- Heylen, W., Lammens, S. and Sas, P. (1995) *Modal Analysis Theory and Testing*, Department of Mechanical Engineering, Katholieke Universiteit Leuven, Belgium.
- Huang, T.L. and Chen, H.P. (2017) Mode identifiability of a cablestayed bridge using modal contribution index. *Smart Structures and Systems*, in press.
- Ibrahim, S.R. and Mikulcik, E.C. (1977) A method for the direct identification of vibration parameters from the free response. *The Shock and Vibration Bulletin***47**, 183–198.
- Kidder, R.L. (1973) Reduction of structural frequency equations. *AIAA Journal***11**(6), 892.
- Ljung, L. (1999) *System Identification: Theory for the User*. Second Edition, PrenticeHall, Upper Saddle River, NJ, USA.
- Maia, N.M.M., Silva, J.M.M., He, J., Lieven, N.A.J., Lin, R.M., Skingle, G.W., To, W.M. and Urgueira, A.P.V. (1997) *Theoretical and Experimental Modal Analysis*. Research Studies Press, Taunton, Somerset, UK.
- Ni, Y.Q., Hua, X.G., Fan, K.Q. and Ko, J.M. (2005) Correlating modal properties with temperature using longterm monitoring data and support vector machine technique. *Engineering Structures***27**, 1762–1773.
- Ni, Y.Q., Wang, Y.W. and Xia, Y.X. (2015). Investigation of mode identifiability of a cable stayed bridge: comparison from ambient vibration responses and from typhooninduced dynamic responses. *Smart Structures and Systems*, **15**(2), 447–468.
- Ni, Y.Q., Xia, Y., Lin, W., Chen, W.H. and Ko, J.M. (2012). SHM benchmark for highrise structures: a reducedorder finite element model and field measurement data. *Smart Structures and Systems*, **10**(45), 411–426.
- O’Callahan, J.C., Avitabile, P. and Riemer, R. (1989) System equivalent reduction expansion process, *Proceedings of the 7th International Modal Analysis Conference*, Las Vegas, Nevada, USA.

- Peeters B. and De Roeck, G. (1999) Reference based stochastic subspace identification for output only modal analysis. *Mechanical Systems and Signal Processing***13**, 855–878.
- Peeters, B. and De Roeck, G. (2001) Stochastic system identification for operational modal analysis: a review. *Journal of Dynamic Systems, Measurement, and Control ASME***123** (4), 659–667.
- Peeters, B. and Ventura, C.E. (2003) Comparative study of modal analysis techniques for bridge dynamic characteristics. *Mechanical Systems and Signal Processing***17**(5), 965–988.
- Tikhonov, A.N. and Arsenin, V.Y. (1977) *Solutions of illposed problems* . John Wiley & Sons, New York, USA.
- Van der Auweraer, H. and Leuridan, J. (1987) Multiple input orthogonal polynomial parameter estimation. *Mechanical Systems and Signal Processing***1**, 259–272.
- Van Overschee, P. and De Moor, B. (1996) *Subspace Identification for Linear Systems: Theory Implementation Applications* . Kluwer Academic Publishers, Dordrecht, The Netherlands.
- Xia, Y., Chen, B., Weng, S., Ni, Y.Q. and Xu, Y.L. (2012) Temperature effect on vibration properties of civil structures: a literature review and case studies. *Journal of Civil Structural Health Monitoring***2**, 29–46.

6

Finite Element Model Updating

6.1 Introduction

The finite element (FE) method is a powerful tool for structural design and analysis in civil engineering practices. The FE method can also be used for many other applications, including predicting static and dynamic structural behaviour in service. Furthermore, after appropriate experimental validation, FE models can provide essential baseline information that can subsequently be compared with information obtained from longterm monitoring systems to detect structural damage and forecast future performance (Doebeling et al. 1996). In general, the FE model of an actual structure is constructed on the basis of highly idealised engineering design and construction, which may not fully represent all physical aspects of the actual structure. As a result, a significant discrepancy may exist between the predictions by the FE model and the measurements on the actual tested structure. This problem arises not only from the modelling errors caused by simplified assumptions for complex structures, but also from the parameter estimation errors due to the uncertainties in material and geometric properties. In order to minimise the discrepancy and to maximise the correlation between the FE model and the actual tested structure, structural model updating methods are often utilised to adjust the FE model by using the measured modal data of the actual structure.

Many investigations have been undertaken on FE model updating using vibration measurements over the past decades (Mottershead and Friswell 1993, Friswell and Mottershead 1995). Existing model updating methods can be broadly classified into two major groups: direct methods and iterative methods. The direct methods directly update the elements of stiffness and mass matrices and are a onestep procedure (Friswell et al. 1998, Kabe 1985). These methods allow the updated analytical model to reproduce measured vibration modal data, but there is no guarantee that the updated model truly represents the physical properties of the actual structure concerned. On the other hand, the iterative parameter updating methods adopt the sensitivity of the parameters to update the analytical model (Link 1999, Modak et al. 2002, Mottershead et al. 2011). Such methods set the errors between the analytical and measured data as an objective function, and attempt to minimise the chosen objective function by adjusting the preselected set of physical parameters of the analytical model in question. Compared with the direct methods, the iterative methods, such as sensitivity based methods and dynamic perturbation method, are more popular since they can be implemented conveniently in existing FE codes (Chen and Maung 2014, Farhat and Hemez 1993). Furthermore, there is a readily available physical explanation for each structural updating parameter, which is typically associated with the element stiffness and mass of the analytical model.

The sensitivity based methods are probably the most successful approach with many

applications to the model updating problems. For a sensitivity based updating approach, its performance largely depends on the selections of an objective function and constraints, structural updating parameters and optimization techniques (Brownjohn and Xia 2000). The objective function can be taken as the residuals between the measured modal data and the associated predictions from the initial FE model, for example the difference in frequencies and mode shape measurements. The selection of structural parameters to be updated requires considerable physical insight into the tested structure so as to correctly characterise the physical properties at local level, for example at connections of structural elements (Palmonella et al. 2005). Bayesian updating procedures can be adopted for reducing the influence of uncertainties in structural parameters and vibration measurements, and for improving the correlation between the tested structure and its associated FE model (Simoen et al. 2013). Advanced global optimisation techniques such as simulated annealing method and genetic algorithm, combined with sensitivity analyses, are powerful tools. These techniques are often employed to obtain globally optimised structural updating parameters for complex structural systems in order to avoid local optimal solutions. However, the sensitivity analysis and optimisation techniques used in the sensitivity based model updating procedures might not perform well since they require significant computational efforts in the model updating process. These problems arise particularly in the cases when the number of the chosen structural parameters to be updated is large and the discrepancy between the initial FE model and the actual tested structure is significant.

The dynamic perturbation method can directly adopt measured incomplete modal data for evaluating the chosen structural updating parameters (Chen 1998, Chen and Maung 2014). This method is based on the exact relationship between the perturbation in structural parameters and the measured modal data of the tested structure. This method therefore does not require the sensitivity analysis and the construction of an objective function. An iterative solution procedure is then used to estimate the chosen structural updating parameters in the least squares sense, without requiring an optimisation technique. This method has been successfully applied for updating FE models of the constructed complex structures, such as the supertall structure Canton Tower (Chen and Huang 2012, Chen and Tee 2014).

This chapter presents various methods for finite element model updating to improve the correlation between the measurements of the tested structure and the predictions of the finite element model. Problems in finite element modelling, such as construction of finite element models and errors in modelling, are discussed. Parameters to be updated are studied so as to be chosen at the appropriate level to reflect the physical behaviour of the structure. The popular sensitivity based methods are introduced for model updating, by minimising the difference between the output measurements and the finite element predictions. The effective dynamic perturbation method avoids limitations in sensitivity based methods, requiring only limited information on incomplete modal data for reliable model updating. Finally, case study on model updating of an actual supertall structure is presented.

6.2 Finite Element Modelling

The finite element method is useful for many applications in engineering practice, such as structural analysis and structural behaviour predictions. The FE model is generally established on the basis of the details of the design and construction of the associated actual engineering structure. In FE modelling processes, a structure is modelled by the assemblage of small pieces, called finite elements. The FE model, however, may not fully represent all the physical and geometrical aspects of the actually built structure.

6.2.1 Stiffness and Mass Matrices

In the finite element method, a mathematical model is discretised by dividing it into a mesh of finite elements. Thus a fully continuous field over a structure is represented by a piecewise continuous field. A continuum problem usually has an infinite number of unknowns. FE discretisation procedures reduce the problem to a finite number of unknowns. Thus, the global stiffness matrix \mathbf{K} and mass matrix \mathbf{M} of the FE model can be obtained by assembling the element stiffness matrix of a total number of NE elements within the structure:

$$\mathbf{K} = \sum_{e=1}^{NE} \mathbf{K}_e \quad \text{and} \quad \mathbf{M} = \sum_{e=1}^{NE} \mathbf{M}_e \quad (6.1)$$

where \mathbf{K}_e and \mathbf{M}_e are the e th element stiffness and mass matrices, respectively, associated with element type and size and material properties. The element stiffness and mass matrices of the e th element with a volume of V_e can be calculated by a general form:

$$\mathbf{K}_e = \int_{V_e} \mathbf{B}^T \mathbf{D} \mathbf{B} dv \quad \text{and} \quad \mathbf{M}_e = \int_{V_e} \rho \mathbf{N}^T \mathbf{N} dv \quad (6.2)$$

where ρ indicates mass density, \mathbf{B} is strain matrix representing the relationship between the strains and the displacements, consisting of the first derivatives of the shape function matrix \mathbf{N} , and \mathbf{D} is the material matrix representing the relationship between the stresses and strains.

For a conventional beam, the element stiffness and mass matrices of the beam with cross sectional area A , bending stiffness EI and element length l can be expressed as

$$\mathbf{K}_e = \int_l EI \mathbf{B}^T(x) \mathbf{B}(x) dx \quad \text{and} \quad \mathbf{M}_e = \int_l \rho A \mathbf{N}^T(x) \mathbf{N}(x) dx \quad (6.3)$$

where $\mathbf{B}(x)$ now contains terms consisting of the second derivatives of the shape function $\mathbf{N}(x)$ with respect to x .

The basic equations for structural dynamic analyses using FE methods were described in [Section 5.2](#). The details of the FE methods can be found in the book by Zienkiewicz and Taylor (1977).

6.2.2 Finite Element Modelling Error

Finite element procedures are useful for the analysis and design of complex civil engineering

structures. Their practical applications, however, often suggest considerable discrepancy between FE predictions and test results (Chen and Huang 2012). Relative to reality, two sources of error are introduced in finite element modelling: discretisation errors and modelling errors. Discretisation errors can be reduced by using more elements. Modelling errors can be reduced by improving the FE model, using a model updating procedure. It should be noted that only some types of modelling errors can be adjusted correctly by changing the values of the chosen updating parameters, as discussed in Mottershead et al. (2011). The model updating process can correct certain errors in FE models, including

- material parameters such as Young's modulus or mass density
- crosssectional properties of beams such as area and second moments of inertia
- shell or plate thicknesses
- spring stiffness or nonstructural mass, etc.

Other errors related to the mathematical representations of the FE models may not be corrected by typical model updating processes, including

- idealisation errors resulting from the assumptions made to characterise the mechanical behaviour of the physical structure, e.g. erroneous modelling of boundary conditions, erroneous modelling of joints, simplifications of the structure or a nonlinear structure assumed to behave linearly
- discretisation errors introduced by FE methods, e.g. discretisation errors caused by too coarse finite element meshes, truncation errors in order reduction methods or poor convergence.

In order to predict the structural response correctly, all types of modelling errors should be minimised to give a reliable structural analysis. If the finite element model is not properly adjusted, the updated model may not be useful for predicting the system behaviour beyond the frequency range used in the updating, although it may be able to reproduce the used test data (Mottershead et al. 2011). The quality of the updated finite element model can be evaluated in the following steps:

- accessing idealisation and numerical method errors before parameter updating
- selecting appropriate parameters for model updating
- correlating analytical model predictions and test results
- reassessing model quality after parameter updating, such as assessment of structural behaviour under various load conditions, system behaviour beyond the frequency range or effects of structural modifications.

6.3 Structural Parameters for Model Updating

In structural model updating procedures, system parameters to be updated, such as parameters for material and geometric properties, are selected to reflect the updating of structural

parameters, such as stiffness matrix and/or mass matrix. The parameters for updating should be justified by physical understanding of the tested structure, and they should have a direct physical meaning. When selecting these updating parameters, the test data should be sensitive to small changes in these updating parameters. Difficult features, such as joints and boundary conditions, may be represented more or less sensitively by choosing different types of parameters (Mottershead et al. 2011). In general, structural stiffness is more difficult to model than mass, thus errors in stiffness modelling are more responsible for inaccurate predictions than mass. Joints and boundary conditions are particularly difficult to model accurately. Damping is in many respects a special case, and it is even more difficult to obtain its accurate estimate.

6.3.1 Updating Parameters for Framed Structures

The parameters for model updating could be material properties, geometric properties and nondimensional scalar multipliers applied at element level or at integration point level. Since the stiffness modelling plays a more important role in model updating, parameters in stiffness updating are mainly concerned, while mass could be treated in a similar way.

6.3.1.1 Updating Stiffness and Mass at Element Level

In the cases where structural updating parameters are chosen at element level, such as for bar or truss elements, the change in element stiffness matrix $\Delta\mathbf{K}_e$ and the change in element mass matrix $\Delta\mathbf{M}_e$ can be expressed, respectively, by

$$\Delta\mathbf{K}_e = \hat{\mathbf{K}}_e - \mathbf{K}_e = \alpha_e \mathbf{K}_e \quad (6.4a)$$

$$\Delta\mathbf{M}_e = \hat{\mathbf{M}}_e - \mathbf{M}_e = \beta_e \mathbf{M}_e \quad (6.4b)$$

where α_e is a nondimensional scalar multiplier for stiffness updating characterised at element level and \mathbf{K}_e and $\hat{\mathbf{K}}_e$ are the e th element stiffness matrices for the initial FE model and the actual structure, respectively. Similarly, β_e is a nondimensional scalar multiplier for mass updating characterised at element level and \mathbf{M}_e and $\hat{\mathbf{M}}_e$ are the e th element mass matrices for the initial FE model and the actual structure, respectively.

6.3.1.2 Updating Stiffness at Integration Point Level

For framed structures, it is difficult to accurately model beam–column joints in the FE modelling, and the stiffness at the joints is often estimated with uncertainty. In order to effectively update the bending stiffness at the ends of beam and column elements, the element stiffness matrix is now calculated from an integral form. The element stiffness matrix excluding axial stiffness for a conventional plane beam with bending stiffness EI and element length l , as described in [Equation \(6.3\)](#), is rewritten here as

$$\mathbf{K}_e^b = \int_{-1}^1 EI \mathbf{b}^T(\xi) \mathbf{b}(\xi) \frac{l}{2} d\xi \quad (6.5)$$

where the dimensionless natural coordinate ξ related to longitudinal beam axis \bar{x} is defined as $\xi = 2\bar{x}/l - 1$, and row vector $\mathbf{b}(\xi)$ is defined as $\mathbf{b}(\xi) = \frac{1}{l^2} [6\xi, (3\xi - 1)l, -6\xi, (3\xi + 1)l]$.

By using the threepoint Newton–Cotes integration rule (Stoer and Bulirsch 1980), the element stiffness matrix in [Equation \(6.5\)](#) is now calculated from the sum of the contributions of integration points in the middle and at both ends of the element (Chen and Maung 2014):

$$\mathbf{K}_e^b = \sum_{r=1}^{Nr} \mathbf{K}_r^b, \quad \text{where} \quad \mathbf{K}_r^b = \frac{l}{2} w_r (EI)_r \mathbf{b}^T(\xi_r) \mathbf{b}(\xi_r) \quad (6.6)$$

in which index r denotes the integration points in the middle and at both ends of the element, where $\xi_r = 0$ and $\xi_r = \pm 1$, respectively, and Nr represents the total number of integration points. Weight coefficients w_r for the threepoint Newton–Cotes integration rule in the middle and at both ends are $w_r = 4/3$ and $w_r = 1/3$, respectively, and $(EI)_r$ represents bending stiffness at integration points, i.e. in the middle and at both ends of the structural element. The change in element stiffness matrix $\Delta \mathbf{K}_e^b$ between the element stiffness of actual structure $\hat{\mathbf{K}}_e^b$ and the element stiffness of the initial FE model \mathbf{K}_e^b for the beam element is given by

$$\Delta \mathbf{K}_e^b = \hat{\mathbf{K}}_e^b - \mathbf{K}_e^b = \sum_{r=1}^{Nr} \alpha_r \mathbf{K}_r^b \quad (6.7)$$

where α_r is a nondimensional scalar multiplier for stiffness updating characterised at integration point level.

For space beam elements, the same method described above with similar formulas to [Equation \(6.5\)](#) is used to obtain the change in element stiffness matrices related to axial deformation and torsion. Here, the elastic stiffness EA and torsion stiffness GJ should be adopted in the associated element stiffness matrices with consideration of axial deformation and torsion, respectively.

6.3.1.3 Updating Material and Sectional Properties

The most common material property parameters for framed structures are Young's modulus and mass density, since the element stiffness and mass matrices have a linear relation to Young's modulus and mass density, respectively. Use of material properties and crosssectional dimensions is powerful for model updating, since they often apply throughout a finite element mesh with the same material and sectional properties for framed structures. Thus a small change in material properties and crosssectional dimensions often cause a considerable change in modal parameters such as natural frequencies.

6.3.1.4 Updating Joints and Boundary Conditions

For framed structures, joints and boundary conditions are difficult to represent accurately in FE modelling, for example rigid assumption for flexible joints and fixed assumption for spring boundaries. The problem of introducing flexibility into joints and boundaries assumed to be rigid or fixed can be dealt with in many ways, in order to improve the dynamic behaviour of the model and its physical usefulness (Mottershead et al. 2011). One of useful approaches is to make use of offset finite element nodes and to use the offset dimensions to correct the finite element model.

6.3.2 Updating Parameters for Continuum Structures

For continuum structures, the parameters adopted for updating the FE model can be mass density, plate thicknesses and the thicknesses and dimensions of thinwalled sections. Very often, nondimensional scaler multipliers are also used as updating parameters of continuum structures. Parameters for updating stiffness and mass matrices can be chosen at element level, as described in [Equation \(6.4\)](#).

In order to update stiffness locally, stiffness updating parameters can be chosen at integration point (Gauss point) level, and change in element stiffness matrix is expressed as

$$\Delta \mathbf{K}_e = \sum_{g=1}^{NG} \alpha_g \mathbf{K}_g \quad (6.8)$$

where α_g is a nondimensional scaler multiplier for stiffness updating characterised at integration points of continuum structures, \mathbf{K}_g is the contribution of the g th integration point to the element stiffness matrix and NG denotes the total number of integration points adopted in a structural element.

Finally, by considering changes in element stiffness matrix $\Delta \mathbf{K}_e$, the changes of global stiffness and mass matrices between the actual structure and the initial FE model can be expressed in a general form, respectively, as

$$\Delta \mathbf{K} = \sum_{e=1}^{NE} \Delta \mathbf{K}_e = \sum_{j=1}^{N\alpha} \alpha_j \mathbf{K}_j \quad (6.9a)$$

$$\Delta \mathbf{M} = \sum_{e=1}^{NE} \Delta \mathbf{M}_e = \sum_{m=1}^{N\beta} \beta_m \mathbf{M}_m \quad (6.9b)$$

where NE denotes the total number of elements within the structure, $N\alpha$ and $N\beta$ represent the total number of stiffness and mass updating parameters adopted in calculations, respectively, α_j and β_m are the stiffness and mass updating parameters characterised at element level or integration point level, respectively, and \mathbf{K}_j and \mathbf{M}_m are the j th and m th contributions

associated with the corresponding structural updating parameters to the global stiffness and mass matrices, respectively.

6.4 Sensitivity Based Methods

Sensitivity based methods for model updating use the measurable outputs of the tested structure, for example natural frequencies, mode shapes, displacements and frequency response functions. Such methods are based on the use of a truncated Taylor series of the measurable outputs as a function of the unknown updating parameters, since the relationship between the measurable outputs and the updating parameters is typically nonlinear (Mottershead et al. 2011). On the basis of the linearisation, the updating parameters associated with the FE model are then corrected to bring the measurable outputs of FE model closer to the corresponding test results.

6.4.1 Sensitivity Matrix

A Taylor series of expansion truncated after the linear term gives

$$\delta \mathbf{z}(\mathbf{p}) = \mathbf{z}_m - \mathbf{z}(\mathbf{p}) \approx \mathbf{z}_m - \mathbf{z}_a - \mathbf{S} \delta \mathbf{p} \quad (6.10)$$

where $\delta \mathbf{z}$ is residual, assumed to be small for updating parameters \mathbf{p} in the vicinity of \mathbf{p}_a , $\delta \mathbf{p} = \mathbf{p} - \mathbf{p}_a$ is change of updating parameters and \mathbf{z}_m and $\mathbf{z}_a = \mathbf{z}(\mathbf{p}_a)$ are the measured outputs and the corresponding analytically predicted outputs, respectively. The sensitivity matrix \mathbf{S} contains the first derivative of the outputs $\mathbf{z}(\mathbf{p})$ with respect to the updating parameters \mathbf{p} :

$$\mathbf{S} = \{s_{ij}\} = \frac{\partial z_i(p_j)}{\partial p_j} \quad (6.11)$$

where $i = 1, 2, \dots, Nq$ represents the output data point, and $j = 1, 2, \dots, Np$ is the parameter index. The sensitivity matrix \mathbf{S} is calculated at the current value of the updating parameters $\mathbf{P} = \mathbf{P}_a$. Due to its complexity, the sensitivity matrix \mathbf{S} may be obtained from numerical approximations by the simple procedure of perturbing the updating parameters in turn by a suitably small quantity, and then calculating numerically the change in the predicted outputs. Computing the sensitivity coefficients s_{ij} by numerical methods needs intensive computational efforts. For natural frequencies and mode shapes, the sensitivity matrix can be given by the analytical approach.

6.4.1.1 Sensitivity of Eigenvalue

Natural frequencies are often chosen as the outputs in updating FE models. Here, the eigenvalue is defined as the square of the natural frequency: $\lambda_i = \omega_i^2$. The measured eigenvalues must be paired with the calculated eigenvalues of the initial FE model by using the modal assurance criterion, as defined in [Equation \(5.20\)](#). The sensitivity coefficients are

determined analytically from the derivative of the i th eigenvalue λ_i with respect to the j th updating parameter p_j (Fox and Kapoor 1968), giving

$$s_{ij} = \frac{\partial \lambda_i(p_j)}{\partial p_j} = \boldsymbol{\phi}_i^T \left(\frac{\partial \mathbf{K}}{\partial p_j} - \lambda_i \frac{\partial \mathbf{M}}{\partial p_j} \right) \boldsymbol{\phi}_i \quad (6.12)$$

The expression is easy to calculate and requires only the i th eigenvalue and eigenvector of the initial FE model.

6.4.1.2 Sensitivity of Eigenvector

For the cases where mode shape readings are taken as the outputs, the residual is the difference between the measured incomplete mode shapes restricted to readings of degrees of freedom (DOFs) at the location of sensors and the FE calculated modes shapes at the same coordinates. Since the number of measured DOFs is generally much less than the number of finite element DOFs, it is essential that either the measured incomplete mode shapes are expanded to full model size or the FE full model is reduced to the number of measured DOFs, as discussed in [Section 5.6](#). The FE calculated and experimental mode shapes must be normalised in the same way, for example with respect to the mass.

Eigenvector derivatives are more difficult to calculate. The method given by Fox and Kapoor (1968), by expressing the eigenvector derivative as a linear combination of all the eigenvectors, is widely used due to its simplicity of implementation:

$$s_{ij} = \frac{\partial \boldsymbol{\phi}_i(p_j)}{\partial p_j} = -\frac{1}{2} \boldsymbol{\phi}_i^T \frac{\partial \mathbf{M}}{\partial p_j} \boldsymbol{\phi}_i \boldsymbol{\phi}_i + \sum_{l=1, l \neq i}^N \frac{1}{(\lambda_i - \lambda_l)} \left[\boldsymbol{\phi}_i^T \left(\frac{\partial \mathbf{K}}{\partial p_j} - \lambda_i \frac{\partial \mathbf{M}}{\partial p_j} \right) \boldsymbol{\phi}_l \right] \boldsymbol{\phi}_l \quad (6.13)$$

Convergence problems may arise for neighbouring eigenvalues $\lambda_i \approx \lambda_l$. Other methods for calculating eigenvector derivatives are also available in Friswell and Mottershead (1995).

6.4.1.3 Sensitivity of Input Force

The input force residual is generated by substituting the measured displacements \mathbf{x}_m into the equation of motion (Mottershead et al. 2011). The j th column of the sensitivity coefficients is then obtained from the first derivative of the input force vector \mathbf{f} with respect to the j th updating parameter p_j :

$$\mathbf{s}_j = \frac{\partial \mathbf{f}(p_j)}{\partial p_j} = \left[\frac{\partial \mathbf{K}}{\partial p_j} + i\omega \frac{\partial \mathbf{C}}{\partial p_j} - \omega^2 \frac{\partial \mathbf{M}}{\partial p_j} \right] \mathbf{x}_m \quad (6.14)$$

where ω is the excitation frequency and $i = \sqrt{-1}$. The stiffness matrix \mathbf{K} , damping matrix \mathbf{C} and mass matrix \mathbf{M} need to be reduced to the measured DOFs using model reduction methods. In order to reduce the influence caused by random measurement noise and systematic errors due

to model reduction, an approach by weighting the force residual using matrix $\mathbf{H}(\omega_f, \mathbf{p}_0)$ is introduced. Here, $\mathbf{H}(\omega_f, \mathbf{p}_0)$ is the frequency response function matrix of the initial FE model at selected frequencies ω_f . The j th column of the sensitivity coefficients associated with the weighted force is given by

$$\mathbf{s}_j = \frac{\partial \mathbf{x}(p_j)}{\partial p_j} = \mathbf{H}(\omega_f, \mathbf{p}_0) \left[\frac{\partial \mathbf{K}}{\partial p_j} + i\omega \frac{\partial \mathbf{C}}{\partial p_j} - \omega^2 \frac{\partial \mathbf{M}}{\partial p_j} \right] \mathbf{x}_m \quad (6.15)$$

in which the frequency response function matrix at the measured DOFs expressed by modal data from the initial model $\mathbf{p} = \mathbf{p}_0$, by assuming modal damping or proportional damping ζ_f , is calculated from

$$\mathbf{H}(\omega_f, \mathbf{p}_0) = \sum_{k=1}^N \frac{\boldsymbol{\phi}_k \boldsymbol{\phi}_k^T}{\left(\omega_k^2 - \omega_f^2 + 2i\zeta_f \omega_k \omega_f \right)} \Big|_{\mathbf{p}=\mathbf{p}_0} \quad (6.16)$$

The force residual and the pseudoresponse technique have been investigated in many studies (e.g. Imregun et al. 1995), with respect to the bias and illconditioning problems as well as the optimal choice of the excitation frequencies.

6.4.2 Direct Parameter Estimation

In parameter estimation, the residual described in [Equation \(6.10\)](#) has to be defined. Optimum parameters are then sought to reproduce the FE calculated outputs as closely as possible to the corresponding measured data. The objective for the optimisation problem is defined to minimise the weighted residual norm

$$J(\mathbf{p}) = \delta \mathbf{z}(\mathbf{p})^T \mathbf{W}_z \delta \mathbf{z}(\mathbf{p}) \quad (6.17)$$

where the positive definite symmetric weighting matrix \mathbf{W}_z is adopted to account for the importance of each individual term in the residual vector (Mottershead et al. 2011), often taken as diagonal matrix $\mathbf{W}_z = \left[\text{diag}(\mathbf{z}_m) \right]^{-2}$.

In parameter updating, the number of output measurements should be made larger than the number of updating parameters ($N_q > N_p$), leading to overdetermined equation systems. In this case, the weighted residual norm $J(\mathbf{p})$ is minimised by the weighted least squares technique to give an improved parameter estimate:

$$\delta \mathbf{p} = \left[\mathbf{S}^T \mathbf{W}_z \mathbf{S} \right]^{-1} \mathbf{S}^T \mathbf{W}_z \delta \mathbf{z} \quad (6.18)$$

The updating parameters and output measurements should be scaled to improve the conditioning of matrix inversion. Since the equation system is generally illconditioned and is

significantly affected by the noise in output measurements, a sort of regularisation method is introduced to give better estimate for parameters, by modifying the objective function defined in [Equation \(6.17\)](#) as

$$J(\mathbf{p}) = \delta \mathbf{z}(\mathbf{p})^T \mathbf{W}_z \delta \mathbf{z}(\mathbf{p}) + \alpha^2 \delta \mathbf{p}^T \mathbf{W}_p \delta \mathbf{p} \quad (6.19)$$

where α is regularisation parameter to be determined. The parameter weighting matrix \mathbf{W}_p should be chosen to reflect the uncertainty in the initial parameter estimates, and to allow the parameter changes to be constrained according to their sensitivity (Link 1999), given as

$$\mathbf{W}_p = \frac{\text{mean}(\text{diag}[\mathbf{S}^T \mathbf{W}_z \mathbf{S}])}{\text{mean}(\text{diag}[\mathbf{S}^T \mathbf{W}_z \mathbf{S}]^{-1})} [\mathbf{S}^T \mathbf{W}_z \mathbf{S}]^{-1} \quad (6.20)$$

When the parameter weighting matrix $\mathbf{W}_p = \mathbf{I}$, it becomes the classical Tikhonov regularisation for solving illconditioned equation systems (Tikhonov and Arsenin 1977). A regularised parameter estimate is then obtained by minimising the objective function in [Equation \(6.19\)](#), as

$$\delta \mathbf{p} = [\mathbf{S}^T \mathbf{W}_z \mathbf{S} + \alpha^2 \mathbf{W}_p]^{-1} \mathbf{S}^T \mathbf{W}_z \delta \mathbf{z} \quad (6.21)$$

The regularisation parameter α can be estimated by using the Lcurve criterion (Hansen and O'Leary 1993), which provides a balance between the measurement residual and the parameter change. The optimum value of the regularisation parameter is taken at the point with maximum curvature at the corner of the loglog plot of the Lcurve. The details of the Tikhonov regularisation method and the Lcurve criterion are discussed in [Section 6.5.2](#).

Since the relationship between the parameters and the measurements is generally nonlinear, an iterative procedure is required for estimating parameters with possible associated convergence problems. During the iterative procedure, the optimum regularisation parameter evaluated at the first iteration may be retained. The FE model is then evaluated at every iteration. If the change in parameters between successive iterations is sufficiently small, a satisfactory estimate of the parameters can be obtained for the FE model updating.

6.4.3 Residual Minimisation Methods

The finite element model updating problems can also be solved by directly using optimisation techniques by minimising the residual between the tested data and the finite element predictions. In modal testing, modal data about the natural frequency $\hat{\omega}_i$ and mode shape readings $\hat{\Psi}_i$ of the tested structure can be extracted from vibration measurements by modal analysis techniques. The measured incomplete mode shapes $\hat{\Psi}_i$ with dimension of N_s are usually incomplete with reference to the FE model. The measured mode shapes are paired to the FE calculated eigenvectors restricted to the same dimensions, by using the modal assurance

criterion (MAC) defined in [Equation \(5.20\)](#).

In order to ensure that the measured incomplete mode shapes are close to the corresponding part of the original FE calculated eigenvectors ϕ_i^a , the measured DOF readings $\hat{\psi}_i$ are scaled by a modal scale factor (MSF_i) described in [Equation \(5.25\)](#). When a total number of Nm measured modes are available, the objective function can be chosen as

$$J(\mathbf{p}) = \sum_{i=1}^{Nm} w_{\omega,i} \left(\frac{\hat{\omega}_i - \omega_i(\mathbf{p})}{\hat{\omega}_i} \right)^2 + \sum_{i=1}^{Nm} w_{\phi,i} \left\| MSF_i \hat{\psi}_i - \phi_i^a(\mathbf{p}) \right\|^2 \quad (6.22)$$

The first term in the objective function minimises the residual between the measured and the FE calculated natural frequencies, and the second term minimises directly the residual between the measured and the FE calculated mode shapes (Balageas et al. 2006). Both terms are weighted by individual weighting coefficients, w_{ω} and w_{ϕ} , respectively.

In some model updating applications, the above objective function can be revised as

$$J(\mathbf{p}) = \sum_{i=1}^{Nm} w_{\omega,i} \left(\frac{\hat{\omega}_i - \omega_i(\mathbf{p})}{\hat{\omega}_i} \right)^2 + \sum_{i=1}^{Nm} w_{\phi,i} \left[1 - MAC_i(\phi_i^a(\mathbf{p}), \hat{\psi}_i) \right]^2 \quad (6.23)$$

Here, the second term maximises the correlation between the measured and the FE calculated mode shapes by minimising the difference between the MAC factors and unity. The MAC values do not compare the mode shape components between two modal vectors.

The residual minimisation methods allow the inclusion of linear and nonlinear inequality constraints on the parameters. In order to ensure physical significance for the updating parameters and avoid physically impossible updating parameter values, the lower and upper bounds for the parameter values may be applied. When a parameter reaches its allowable extreme values during iterative model updating, the parameter becomes ineffective during the rest of the procedure. The convergence of the iterative procedure may not achieve satisfactory requirements when parameter bounds are imposed (Brownjohn and Xia 2000). A tradeoff between physically acceptable parameter values and the convergence level is then necessary.

6.4.4 Example for Model Updating – a Cantilever Beam

An experimental cantilever beam is used here to show the applications of sensitivity based model updating methods, as discussed in detail in Friswell and Mottershead (1995). The beam flexibly clamped at its end is made from aluminium alloy, with a cantilevered length of 700 mm. The joint at the clamped end is modelled using a translational spring and a rotational spring. The analytical model of the experimental beam consists of seven beam elements of equal length, as illustrated in [Figure 6.1](#). Three parameters are chosen for the model updating: flexural rigidity of the beam EI with an estimate of $EI = 450 \text{ Nm}^2$, translational spring stiffness k_t with an estimate of $k_t = 30 \text{ MNm}^{-1}$, and rotational spring stiffness k_r with an estimate of $k_r =$

150 kNmrad⁻¹.



Figure 6.1 A cantilever beam structure for model updating.

[Table 6.1](#) gives the first six measured natural frequencies and the corresponding simulated natural frequencies, as well as the MAC values between the measured and the corresponding simulated modes. The average absolute error for the first six simulated natural frequencies with respect to the measured values is 4.46%. Four measured frequencies are used in the updating procedure given in [Equation \(6.18\)](#), and are weighted with a standard deviation of 0.25% for the first two frequencies and 0.5 % for the next two frequencies. After updating, the average absolute error of the adjusted first six frequencies is reduced to a value of 2.73%.

Table 6.1 Simulated, measured and updated frequencies of the cantilever beam without weighting on initial parameter estimates.

Mode	Simulated (Hz)	Measured (Hz)	Error (%)	MAC	Updated (Hz)	Error (%)
1	38.60	37.51 [#]	2.91	1.000	39.09	4.21
2	240.3	246.2 [#]	-2.40	0.998	250.0	1.54
3	656.7	662.3 [#]	-0.85	0.999	685.7	3.53
4	1228	1287 [#]	-4.58	0.983	1273	-1.09
5	1927	2087	-7.67	0.916	2011	-3.64
6	2825	3083	-8.37	0.769	3011	-2.34
Average absolute error (%)			4.46			2.73

[#] Frequencies used for model updating.

A systematic error may exist in the analytical model, since the analytical model is significantly different from the tested beam. This error may cause poor performance of the model updating procedure. Now the initial parameter estimates are weighted on the basis of the estimated standard deviation of 1% for EI , 100% for k_t and 100% for k_r . [Table 6.2](#) summarises the results obtained for [Equation \(6.21\)](#). Here, the average absolute error of the first six frequencies is further reduced to a value of 1.52%. The updated frequencies are closer to the measured frequencies than those in the case where no weighting is applied to the initial parameter estimates.

Table 6.2 Simulated, measured and updated frequencies of the cantilever beam with weighting on initial parameter estimates.

Mode	Simulated (Hz)	Measured (Hz)	Error (%)	MAC	Updated (Hz)	Error (%)
1	38.60	37.51 [#]	2.91	1.000	37.83	0.85
2	240.3	246.2 [#]	-2.40	0.998	241.6	-1.87
3	656.7	662.3 [#]	-0.85	0.999	674.1	1.78
4	1228	1287 [#]	-4.58	0.983	1290	0.23
5	1927	2087	-7.67	0.916	2055	-1.53
6	2825	3083	-8.37	0.769	2996	-2.82
Average absolute error (%)			4.46			1.52

[#] Frequencies used for model updating.

6.5 Dynamic Perturbation Method

Linear or firstorder approximations are typically considered in modal sensitivity analyses, which work well when the difference between the predictions by the FE model and the outputs of the actual structure is relatively small. However, in the cases where such difference is sufficiently large, the linear or firstorder approximations may be inappropriate. Therefore, an exact relationship between the perturbation of structural parameters and the perturbation of the associated modal parameters is required. This exact relationship can then be used for various applications, such as structural reanalyses, eigendata modification, model updating and damage identification (Chen 2005). In the inverse problems for parameter estimation, such as model updating and damage identification, the generated governing equation system is typically illconditioned. Thus, some sort of regularisation of the illconditioned problems is necessary to reduce the influence of noise in measured modal data.

6.5.1 Governing Equations

Assume that \mathbf{K} and \mathbf{M} are, respectively, the global stiffness matrix ($N \times N$) and the global mass matrix ($N \times N$) for the original dynamic structural system, and λ_i and ϕ_i are the i th eigenvalue and the corresponding eigenvector for the original structure, respectively. Suppose that the perturbations of stiffness matrix and mass matrix are defined as $\Delta\mathbf{K}$ and $\Delta\mathbf{M}$, respectively. The stiffness matrix and mass matrix for the modified structural system, therefore, can be written as

$$\hat{\mathbf{K}} = \mathbf{K} + \Delta\mathbf{K}, \quad \hat{\mathbf{M}} = \mathbf{M} + \Delta\mathbf{M} \quad (6.24)$$

Meanwhile, the perturbations of the i th eigenvalue and the corresponding eigenvector, which are caused by the perturbations of stiffness matrix and mass matrix, are defined as $\Delta\lambda_i$ and $\Delta\phi_i$, respectively. The eigenvectors for both the original and modified structural system are linearly

independent, since the stiffness and mass matrices are symmetric. The i th eigenvalue and the corresponding eigenvector for the modified structural system are

$$\hat{\lambda}_i = \lambda_i + \Delta\lambda_i, \quad \hat{\phi}_i = \phi_i + \Delta\phi_i \quad (6.25)$$

It is assumed that the eigenvectors of the original structural system are mass normalised. From the characteristic equations for the original and modified structural dynamic system, as described in [Equation \(5.9\)](#), the governing equations for the modified structural dynamic system are given in the study by Chen (1998), rewritten here as

$$\phi_i^T [\Delta\mathbf{K} - (\lambda_i + \Delta\lambda_i)\Delta\mathbf{M}] (\phi_i + \Delta\phi_i) - \Delta\lambda_i \phi_i^T \mathbf{M} (\phi_i + \Delta\phi_i) = 0 \quad (6.26a)$$

$$\phi_k^T [\Delta\mathbf{K} - (\lambda_i + \Delta\lambda_i)\Delta\mathbf{M}] (\phi_i + \Delta\phi_i) - (\lambda_i + \Delta\lambda_i - \lambda_k) \phi_k^T \mathbf{M} (\phi_i + \Delta\phi_i) = 0 \quad (6.26b)$$

where $k \neq i$. In order to ensure the uniqueness of an eigenvector of the modified structural system, the modified eigenvector is mass normalised in the form

$$\phi_i^T \mathbf{M} \hat{\phi}_i = \phi_i^T \mathbf{M} (\phi_i + \Delta\phi_i) = 1 \quad (6.27)$$

By use of the above formulation, [Equations \(6.26\)](#) can be rewritten as

$$\phi_i^T [\Delta\mathbf{K} - (\lambda_i + \Delta\lambda_i)\Delta\mathbf{M}] (\phi_i + \Delta\phi_i) - \Delta\lambda_i = 0 \quad (6.28a)$$

$$\phi_k^T [\Delta\mathbf{K} - (\lambda_i + \Delta\lambda_i)\Delta\mathbf{M}] (\phi_i + \Delta\phi_i) - (\lambda_i + \Delta\lambda_i - \lambda_k) C_{ik} = 0 \quad (6.28b)$$

where the mode participation factors C_{ik} are defined as

$$C_{ik} = \phi_k^T \mathbf{M} \Delta\phi_i \quad \text{where } k \neq i \quad (6.29a)$$

$$\text{or } C_{ik} = \phi_k^T \mathbf{M} \hat{\phi}_i \quad \text{where } C_{ii} = 1 \quad (6.29b)$$

Premultiplying [Equation \(6.29a\)](#) by ϕ_k , then summing up equations from 1 to N and using the mass normalisation of the original eigenvectors and the assumption of linearly independent eigenvectors of the original system, gives

$$\Delta\phi_i = \sum_{k=1, k \neq i}^N C_{ik} \phi_k \quad (6.30)$$

It is found that the perturbation of an eigenvector of a structural system can be expressed as the linear combination of the original eigenvectors except the corresponding original one. From

[Equation \(6.28b\)](#), the mode participation factors C_{ik} can be expressed by

$$C_{ik} = \frac{\phi_k^T [\Delta \mathbf{K} - (\lambda_i + \Delta \lambda_i) \Delta \mathbf{M}] (\phi_i + \Delta \phi_i)}{(\lambda_i + \Delta \lambda_i) - \lambda_k} \quad (6.31)$$

From [Equation \(6.31\)](#), [Equation \(6.30\)](#) is rewritten as

$$\sum_{k=1, k \neq i}^N \frac{\phi_k^T [\Delta \mathbf{K} - (\lambda_i + \Delta \lambda_i) \Delta \mathbf{M}] (\phi_i + \Delta \phi_i)}{(\lambda_i + \Delta \lambda_i) - \lambda_k} \phi_k - \Delta \phi_i = 0 \quad (6.32)$$

The governing equations of the nonlinear dynamic perturbation method, given in [Equations \(6.28a\)](#) and [\(6.32\)](#), represent the exact relationship between the perturbation of structural parameters and the perturbation of modal parameters. It should be noted that the Taylor series expansion procedure is not employed and information about the derivatives of eigenvalues or eigenvectors is not required to develop the theory.

When the perturbation of structural parameters is small enough, only the first order approximation may be sufficient. The set of nonlinear [Equation \(6.28a\)](#) and [Equation \(6.32\)](#) can then be simplified to linear relationship in the form

$$\Delta \lambda_i = \phi_i^T [\Delta \mathbf{K} - \lambda_i \Delta \mathbf{M}] \phi_i \quad (6.33a)$$

$$\Delta \phi_i = \sum_{k=1, k \neq i}^N \frac{\phi_k^T [\Delta \mathbf{K} - \lambda_i \Delta \mathbf{M}] \phi_i}{\lambda_i - \lambda_k} \phi_k \quad (6.33b)$$

The preceding linear relationship is very commonly utilised for sensitivity analysis, model updating and damage identification. Note that the set of linear equations might be insufficient if relatively large perturbation of structural parameters is present.

When the perturbation of structural parameters, $\Delta \mathbf{K}$ and $\Delta \mathbf{M}$, is known, the perturbation of modal parameters, $\Delta \lambda_i$ and $\Delta \phi_i$, can be computed using the nonlinear dynamic perturbation method (Chen 2006). This is considered as a forward problem here. Note that information on the modal parameters of the modified system is not required during the evaluation of the perturbation of modal parameters.

When the perturbation of modal parameters, $\Delta \lambda_i$ and $\Delta \phi_i$, is known, the perturbation of structural parameters, $\Delta \mathbf{K}$ and $\Delta \mathbf{M}$, can also be inversely determined using the nonlinear dynamic perturbation method. This is considered as an inverse problem here. Different procedures are developed for model updating (Chen and Maung 2014) and damage identification (Chen and Bicanic 2010), depending on information about modal data available.

System parameters, such as coefficients of stiffness or the mass matrix as well as parameters for material properties and geometric properties, can be employed to represent the

perturbation of structural parameters, such as the change in stiffness matrix and/or mass matrix. Such system parameters characterising either at a matrix coefficient level, an integration point level, an element level or at a subsystem level can be utilised for model updating and damage identification.

6.5.2 Regularised Solution Procedure

In the inverse problems for parameter estimation, e.g. model updating and damage identification, a system of linear equations is often generated from the dynamic perturbation governing equations to be solved for the parameters. This system may be determined, underdetermined or overdetermined, depending on the size of the measured modal data. The system of linear equations is expressed in a general and simple form as

$$\mathbf{A}_{NM \times ND} \mathbf{x}_{ND} = \mathbf{b}_{NM} \quad (6.34)$$

where \mathbf{A} is an $NM \times ND$ matrix consisting of known sensitivity coefficients, \mathbf{x} is a column vector containing a total number of ND unknown parameters (e.g. updating parameters or damage indicators) and \mathbf{b} is a column vector containing a total number of NM modal parameter measurements. Without loss of generality it is assumed that $NM \geq ND$, the method, however, can also be applied when NM is considerably smaller than ND . The singular value decomposition (SVD) of matrix \mathbf{A} can be expressed in the form

$$\mathbf{A}_{NM \times ND} = \mathbf{U}_{NM \times NM} \mathbf{\Sigma}_{NM \times ND} \mathbf{V}_{ND \times ND} = \sum_{j=1}^{ND} \sigma_j \mathbf{u}_j \mathbf{v}_j^T \quad (6.35)$$

where $\mathbf{\Sigma}$ is the diagonal matrix of singular values σ_j that are nonnegative and nonincreasing numbers, i.e. $\sigma_1 \geq \sigma_2 \geq \dots \geq \sigma_{ND} \geq 0$. \mathbf{U} and \mathbf{V} are the matrices of orthonormal left and right vectors \mathbf{u}_j and \mathbf{v}_j , respectively. The ordinary least squares solution to [Equation \(6.34\)](#) can then be expressed as a singular value expansion

$$\mathbf{x} = \sum_{j=1}^{ND} \frac{\mathbf{u}_j^T \mathbf{b}}{\sigma_j} \mathbf{v}_j \quad (6.36)$$

In the inverse parameter estimation, the system of linear equations in [Equation \(6.34\)](#) is typically illconditioned, because the singular values of the sensitivity coefficient matrix \mathbf{A} decay gradually to zero and the ratio between the largest and the smallest nonzero singular values is usually large (Chen and Bicanic 2010).

Hence, some sort of regularisation of the illconditioned problem is required to filter out the contributions of the inevitable noise in \mathbf{b} consisting of measured modal data. One of the most commonly used regularisation methods utilising a continuous regularisation parameter is Tikhonov regularisation. This regularisation method replaces the original operation with a betterconditioned but related one, and produces a regularised solution to the original problem (Tikhonov and Arsenin 1977). The Tikhonov regularised solution is given in terms of

the SVD by

$$\mathbf{x}_\alpha = \sum_{j=1}^{ND} f_j(\alpha) \frac{\mathbf{u}_j^T \mathbf{b}}{\sigma_j} \mathbf{v}_j \quad (6.37)$$

where $f_j(\alpha)$ are the Tikhonov filter factors, which depend on singular values σ_j and regularisation parameter α through the expression

$$f_j(\alpha) = \frac{\sigma_j^2}{\sigma_j^2 + \alpha^2} \approx \begin{cases} 1, & \text{if } \sigma_j \gg \alpha \\ \frac{\sigma_j^2}{\alpha^2}, & \text{if } \sigma_j \ll \alpha \end{cases} \quad (6.38)$$

A stable solution can then be obtained, since the Tikhonov regularised solution coefficients $f_j |\mathbf{u}_j^T \mathbf{b}| / \sigma_j$ gradually damp out as singular values decrease. The filter factors f_j gradually filter out the contributions to \mathbf{x}_α associated with the small singular values, while the contributions associated with the large singular values are almost unaffected.

The regularisation parameter α needs to be properly chosen in order to filter out enough noise, without losing too much information in the regularised solution. The Lcurve criterion has been proven to be a robust and useful method for choosing a regularisation parameter in many problems (Hansen and O'Leary 1993). This criterion does not require the a priori knowledge of noise in the measured data. The Lcurve is a plot in loglog scale of the corresponding values of the residual and solution norms as a function of the regularisation parameter α , defined, respectively, in terms of the SVD as

$$\rho(\alpha) = \|\mathbf{A}\mathbf{x}_\alpha - \mathbf{b}\|_2^2 = \sum_{j=1}^{ND} \left[(1 - f_j(\alpha)) \mathbf{u}_j^T \mathbf{b} \right]^2 \quad (6.39a)$$

$$\eta(\alpha) = \|\mathbf{x}_\alpha\|_2^2 = \sum_{j=1}^{ND} \left[f_j(\alpha) \frac{\mathbf{u}_j^T \mathbf{b}}{\sigma_j} \right]^2 \quad (6.39b)$$

The Lcurves basically consist of the flat and the steep parts. The flat part corresponds to the regularised solutions where the regularisation parameter is too large and the solution is dominated by regularisation errors. The steep part corresponds to the solutions where the regularisation parameter is too small and the solution is dominated by perturbation errors, i.e. noise in the measured modal data \mathbf{b} . The balance between the two errors must occur near the Lcurve's corner, where the curvature of the Lcurve approximately has a maximum value.

Considering the definition in [Equation \(6.39\)](#), the curvature of the Lcurve $\kappa(\alpha)$ as a function of α can be expressed by

$$\kappa(\alpha) = \frac{2\eta\rho (\alpha^2\eta'\rho + 2\alpha\eta\rho + \alpha^4\eta\eta')}{\eta' (\alpha^4\eta^2 + \rho^2)^{3/2}} \quad (6.40)$$

where η' denotes the first derivative of η with respect to α . A onedimensional optimisation procedure is utilised to determine the optimum regularisation parameter α , corresponding to the maximum curvature. The same optimum regularisation parameter may be adopted to obtain the regularised solutions to [Equation \(6.37\)](#) during an iterative procedure, because the change of the sensitivity coefficient matrix for different iterations is small.

6.6 Use of Dynamic Perturbation Method for Model Updating

The sensitivity based methods for structural model updating may not perform properly when either the number of the chosen updating parameters is large or a model refinement with relatively large modifications of structural parameters is required. The dynamic perturbation method discussed in [Section 6.5](#), providing the exact relationship between the perturbation of structural parameters and the perturbation of modal parameters, is used here for updating FE models.

6.6.1 Use of Frequencies Only

Assume that information about a total number of Nm measured natural frequencies is available from vibration testing of the actual structure. The measured frequency $\hat{\omega}_i$ is then paired to the FE calculated natural frequency by using the modal assurance criterion defined in [Equation \(5.20\)](#). From the dynamic perturbation method, the exact relationship between the change in structural parameters and the measured frequencies of the tested structure, given in [Equation \(6.28a\)](#), is expressed here as

$$\phi_i^T (\Delta\mathbf{K} - \hat{\omega}_i^2 \Delta\mathbf{M}) \hat{\phi}_i - (\hat{\omega}_i^2 - \omega_i^2) = 0 \quad (6.41)$$

From [Equations \(6.25\)](#) and [\(6.30\)](#), the eigenvectors of the tested structure with dimension of N can be expressed as a linear combination of the FE calculated eigenvectors

$$\hat{\phi}_i = \sum_{k=1}^N C_{ik} \phi_k \quad (6.42)$$

where mode participation factors C_{ik} defined in [Equation \(6.31\)](#) are rewritten as

$$C_{ik} = \frac{1}{(\hat{\omega}_i^2 - \omega_k^2)} \left[\phi_k^T (\Delta\mathbf{K} - \hat{\omega}_i^2 \Delta\mathbf{M}) \hat{\phi}_i \right] \quad (6.43)$$

By using the changes of global stiffness and mass matrices between the tested structure and FE

model given in [Equation \(6.9\)](#), the governing equation in [Equation \(6.41\)](#) is rewritten as

$$\sum_{j=1}^{N\alpha} \hat{\phi}_i^T \mathbf{K}_j \hat{\phi}_i \alpha_j - \hat{\omega}_i^2 \sum_{m=1}^{N\beta} \hat{\phi}_i^T \mathbf{M}_m \hat{\phi}_i \beta_m - (\hat{\omega}_i^2 - \omega_i^2) = 0 \quad (6.44)$$

Similarly, the mode participation factors C_{ik} are rewritten as

$$C_{ik} = \frac{1}{(\hat{\omega}_i^2 - \omega_k^2)} \left[\sum_{j=1}^{N\alpha} \hat{\phi}_k^T \mathbf{K}_j \hat{\phi}_i \alpha_j - \hat{\omega}_i^2 \sum_{m=1}^{N\beta} \hat{\phi}_k^T \mathbf{M}_m \hat{\phi}_i \beta_m \right] \quad (6.45)$$

Define the sensitivity coefficients associated with eigenmodes and structural parameters in a general form as

$$\hat{a}_{iji} = \hat{\phi}_i^T \mathbf{K}_j \hat{\phi}_i, \quad \hat{b}_{imi} = \hat{\phi}_i^T \mathbf{M}_m \hat{\phi}_i \quad (6.46a)$$

$$a_{kjl} = \hat{\phi}_k^T \mathbf{K}_j \hat{\phi}_l, \quad b_{kml} = \hat{\phi}_k^T \mathbf{M}_m \hat{\phi}_l \quad (6.46b)$$

By using [Equation \(6.42\)](#), the governing equation in [Equations \(6.44\)](#) and [\(6.45\)](#) are now rewritten, respectively, as

$$\sum_{j=1}^{N\alpha} \hat{a}_{iji} \alpha_j - \hat{\omega}_i^2 \sum_{m=1}^{N\beta} \hat{b}_{imi} \beta_m = (\hat{\omega}_i^2 - \omega_i^2) \quad (6.47a)$$

$$C_{ik} = \frac{1}{(\hat{\omega}_i^2 - \omega_k^2)} \sum_{l=1}^N \left[\sum_{j=1}^{N\alpha} a_{kjl} \alpha_j - \hat{\omega}_i^2 \sum_{m=1}^{N\beta} b_{kml} \beta_m \right] C_{il} \quad (6.47b)$$

Because of the coupled governing equations, an iterative solution procedure is required to solve for the updating parameters α_j and β_m . The iterative solution procedure is initiated by assuming that the initial mode participation factors are zero, i.e. $C_{ik}^{(0)} = 0$ where $k \neq i$. The initial sensitivity coefficient $\hat{a}_{iji}^{(0)}$ is calculated from [Equation \(6.46a\)](#) by using the known $C_{ik}^{(0)}$. The first approximation for the updating parameters, $\alpha_j^{(1)}$ and $\beta_m^{(1)}$, can then be obtained from the governing equations [Equation \(6.47a\)](#), which now become a set of linear equations because of the known $\hat{a}_{iji}^{(0)}$. The Tikhonov regularisation algorithm incorporating the Lcurve criterion method for determining the regularisation parameter, as described in [Section 6.5.2](#), is applied to find a reliable solution. After the estimate of updating parameters $\alpha_j^{(1)}$ and $\beta_m^{(1)}$ are obtained, the next approximations for $C_{ik}^{(1)}$ can then be calculated from [Equation \(6.47b\)](#). Consequently, the set of governing equations is used recursively to compute further approximations for $\alpha_j^{(n)}$ and $\beta_m^{(n)}$ as well as $C_{ik}^{(n)}$. The above recursive process is repeated

until the convergence for updating parameters $\alpha_j^{(n)}$ and $\beta_m^{(n)}$ is achieved, often after only a few iterations.

6.6.2 Use of Incomplete Modes

From modal testing, modal data about natural frequencies $\hat{\omega}_i$ and incomplete mode shapes $\hat{\Psi}_i$ with dimension of N_s can be identified from vibration measurements. The measured incomplete mode shapes are then paired to the associated FE calculated eigenvectors ϕ_k^a , by using the modal assurance criterion defined in [Equation \(5.20\)](#). The measured DOF readings $\hat{\Psi}_i$ are scaled by the modal scale factor (MSF_i) defined in [Equation \(5.25\)](#), giving the scaled modal measurement vector $\hat{\Phi}_i^a$ of dimension N_s , i.e. $\hat{\Phi}_i^a = MSF_i \cdot \hat{\Psi}_i$.

The unmeasured part of the experimental mode shapes can be expressed as a linear combination of the original FE calculated eigenvectors, as expressed in [Equation \(6.42\)](#). The remaining $(N - N_s)$ unmeasured components $\hat{\Phi}_i^u$ are then calculated from

$$\hat{\Phi}_i^u = \phi_i^u + \sum_{k=1, k \neq i}^N C_{ik} \phi_k^u \quad (6.48)$$

where ϕ_k^u is original FE eigenvector corresponding to the entries of the unmeasured components. The mode participation factors C_{ik} are defined in [Equation \(6.43\)](#). Thus, the i th complete mode shape of the tested structure, consisting of the measured components and the remaining calculated components, is given by

$$\hat{\Phi}_i = \hat{\Phi}_i^a + \hat{\Phi}_i^u = \varphi_i^a + \sum_{k=1, k \neq i}^N C_{ik} \phi_k^u \quad (6.49)$$

where φ_i^a is a known vector of dimension N , defined as

$$\varphi_i^a = MSF_i \cdot \hat{\Psi}_i + \phi_i^u \quad (6.50)$$

From the dynamic perturbation method in [Equation \(6.32\)](#) and using [Equation \(6.28a\)](#), the exact relationship between the change in structural parameters and the modal properties of the tested structure is expressed as

$$\sum_{k=1}^N \frac{\phi_k}{(\hat{\omega}_i^2 - \omega_k^2)} [\phi_k^T (\Delta K - \hat{\omega}_i^2 \Delta M) \hat{\Phi}_i] - \hat{\Phi}_i = 0 \quad (6.51)$$

By using the constructed eigenvector in [Equation \(6.49\)](#), [Equation \(6.51\)](#) is now restricted to the dimension for the measured components and becomes

$$\sum_{k=1}^N \frac{\phi_k^T \Delta \mathbf{K} \left(\varphi_i^a + \sum_{l=1, l \neq i}^N C_{il} \phi_l^u \right)}{(\hat{\omega}_i^2 - \omega_k^2)} \phi_k^a - \hat{\omega}_i^2 \sum_{k=1}^N \frac{\phi_k^T \Delta \mathbf{M} \left(\varphi_i^a + \sum_{l=1, l \neq i}^N C_{il} \phi_l^u \right)}{(\hat{\omega}_i^2 - \omega_k^2)} \phi_k^a - \hat{\phi}_i^a = 0 \quad (6.52)$$

Similarly, from [Equation \(6.43\)](#) the mode participation factors C_{ik} are rewritten as

$$C_{ik} = \frac{1}{(\hat{\omega}_i^2 - \omega_k^2)} \left[\phi_k^T \Delta \mathbf{K} \left(\varphi_i^a + \sum_{l=1, l \neq i}^N C_{il} \phi_l^u \right) - \hat{\omega}_i^2 \phi_k^T \Delta \mathbf{M} \left(\varphi_i^a + \sum_{l=1, l \neq i}^N C_{il} \phi_l^u \right) \right] \quad (6.53)$$

The governing equations in [Equation \(6.52\)](#) represent the exact relationship between the change in structural parameters to be updated and the mode shape readings of the tested structure. These equations avoid the approximations and complexity in most existing eigensensitivity based methods for model updating, without requiring eigensolution derivatives.

6.6.2.1 Iterative Solution Method

The changes of global stiffness and mass matrices in [Equation \(6.9\)](#) are now used in [Equations \(6.52\)](#) and [\(6.53\)](#). To minimise the computational effort, the sensitivity coefficients associated with the known eigenmodes and structural parameters in the governing equation, [Equation \(6.52\)](#), are defined in a general form as

$$\mathbf{p}_{jii}^a = \sum_{k=1}^N \frac{\phi_k^T \mathbf{K}_j \varphi_i^a}{\hat{\omega}_i^2 - \omega_k^2} \phi_k^a, \quad \mathbf{p}_{jil}^u = \sum_{k=1}^N \frac{\phi_k^T \mathbf{K}_j \phi_l^u}{\hat{\omega}_i^2 - \omega_k^2} \phi_k^a \quad (6.54a)$$

$$\mathbf{q}_{mii}^a = \sum_{k=1}^N \frac{\phi_k^T \mathbf{M}_m \varphi_i^a}{\hat{\omega}_i^2 - \omega_k^2} \phi_k^a, \quad \mathbf{q}_{mil}^u = \sum_{k=1}^N \frac{\phi_k^T \mathbf{M}_m \phi_l^u}{\hat{\omega}_i^2 - \omega_k^2} \phi_k^a \quad (6.54b)$$

thus, the governing equation, [Equation \(6.52\)](#), for the i th measured mode is rewritten as

$$\sum_{j=1}^{N\alpha} \left[\mathbf{p}_{jii}^a + \sum_{k=1, k \neq i}^N \mathbf{p}_{jik}^u C_{ij} \right] \alpha_i - \hat{\omega}_i^2 \sum_{m=1}^{N\beta} \left[\mathbf{q}_{mii}^a + \sum_{k=1, k \neq i}^N \mathbf{q}_{mik}^u C_{ij} \right] \beta_m - \hat{\phi}_i^a = 0 \quad (6.55)$$

Similarly, define the sensitivity coefficients associated with the known eigenmodes and structural parameters in [Equation \(6.53\)](#) in a general form as

$$g_{kji}^a = \phi_k^T \mathbf{K}_j \varphi_i^a, \quad g_{kjl}^u = \phi_k^T \mathbf{K}_j \phi_l^u \quad (6.56a)$$

$$h_{kmi}^a = \phi_k^T \mathbf{M}_m \varphi_i^a, \quad h_{kml}^u = \phi_k^T \mathbf{M}_m \phi_l^u \quad (6.56b)$$

the mode participation factors C_{ik} for the i th measured incomplete mode shape in [Equation](#)

(6.53) are thus expressed as

$$C_{ik} = \frac{1}{(\hat{\omega}_i^2 - \omega_k^2)} \left[\sum_{j=1}^{N\alpha} \left(g_{kji}^a + \sum_{l=1, l \neq i}^N g_{kjl}^u C_{il} \right) \alpha_j - \hat{\omega}_i^2 \sum_{m=1}^{N\beta} \left(h_{kmi}^a + \sum_{l=1, l \neq i}^N h_{kml}^u C_{il} \right) \beta_m \right] \quad (6.57)$$

On the basis of the governing equations (6.55) and (6.57) developed above, an iterative solution procedure is required to solve for a total number of $ND (= N\alpha + N\beta)$ structural updating parameters α_j and β_m . It is assumed that a total number of Nm experimental modes are measured from a total number of Ns sensors installed on the tested structure. The governing equation (6.55) should be used for the total number of Nm measured modes to generate a total number of $NM (= Nm \times Ns)$ equations available, in order to find a solution for a total number of ND structural updating parameters. An iterative solution procedure, similar to the procedure for the use of only frequencies for model updating discussed in Section 6.6.1, is required for finding the structural updating parameters α_j and β_m .

6.6.2.2 Simplified Direct Solution Method

In order to avoid the iterative solution procedure in model updating, the mode participation factors C_{ik} are simply estimated from Equations (6.29b) and (6.49), by using the mass normalisation and ignoring the small unknown term in Equation (6.49), as

$$\tilde{C}_{ik} = \phi_k^T \mathbf{M} \phi_i^a \quad (6.58)$$

By replacing the mode participation factors C_{ik} in Equation (6.55) with the estimated \tilde{C}_{ik} , the governing equations for the i th measured mode are rewritten in a set of linear equations as

$$\sum_{j=1}^{N\alpha} \left[\mathbf{p}_{jii}^a + \sum_{k=1, k \neq i}^N \tilde{C}_{ik} \mathbf{p}_{jik}^u \right] \alpha_j - \hat{\omega}_i^2 \sum_{m=1}^{N\beta} \left[\mathbf{q}_{mii}^a + \sum_{k=1, k \neq i}^N \tilde{C}_{ik} \mathbf{q}_{mik}^u \right] \beta_m - \hat{\phi}_i^a = 0 \quad (6.59)$$

Consequently, the structural updating parameters α_j and β_m are now directly obtained by solving the set of linear governing equations (6.59), and no iterative procedure is needed.

6.6.3 Example for Model Updating – a Plane Frame

A symmetric plane frame illustrated in Figure 6.2 is adopted for FE model updating using the dynamic perturbation method by use of natural frequencies only and incomplete modes, respectively. In order to avoid problems associated with structural symmetry, a non symmetric element mesh with 18 elements, 18 nodes and a total of 48 DOFs is generated. All structural members have the same material and geometric properties with Young's modulus $E = 2.1 \times 10^{11}$ N/m², density $\rho = 7800$ kg/m³, crosssectional area $A = 0.092$ m², and second moment of area $I = 4.52 \times 10^{-5}$ m⁴. The geometry of the structure and element numbering are shown in Figure 6.2. A hypothetical set of sensors are placed at nodes 3, 5, 7, 9 and 11–14,

and only translation modal readings are measured. It is assumed that stiffness values at elements 3, 11 and 16 are modified by factors +50%, -30%, and +20% for the simulated 'tested' structure, respectively. A FE dynamic analysis is then performed for both the original FE model and the 'tested' structure to calculate the original FE and 'measured' modal data, i.e. natural frequencies and incomplete mode shapes.

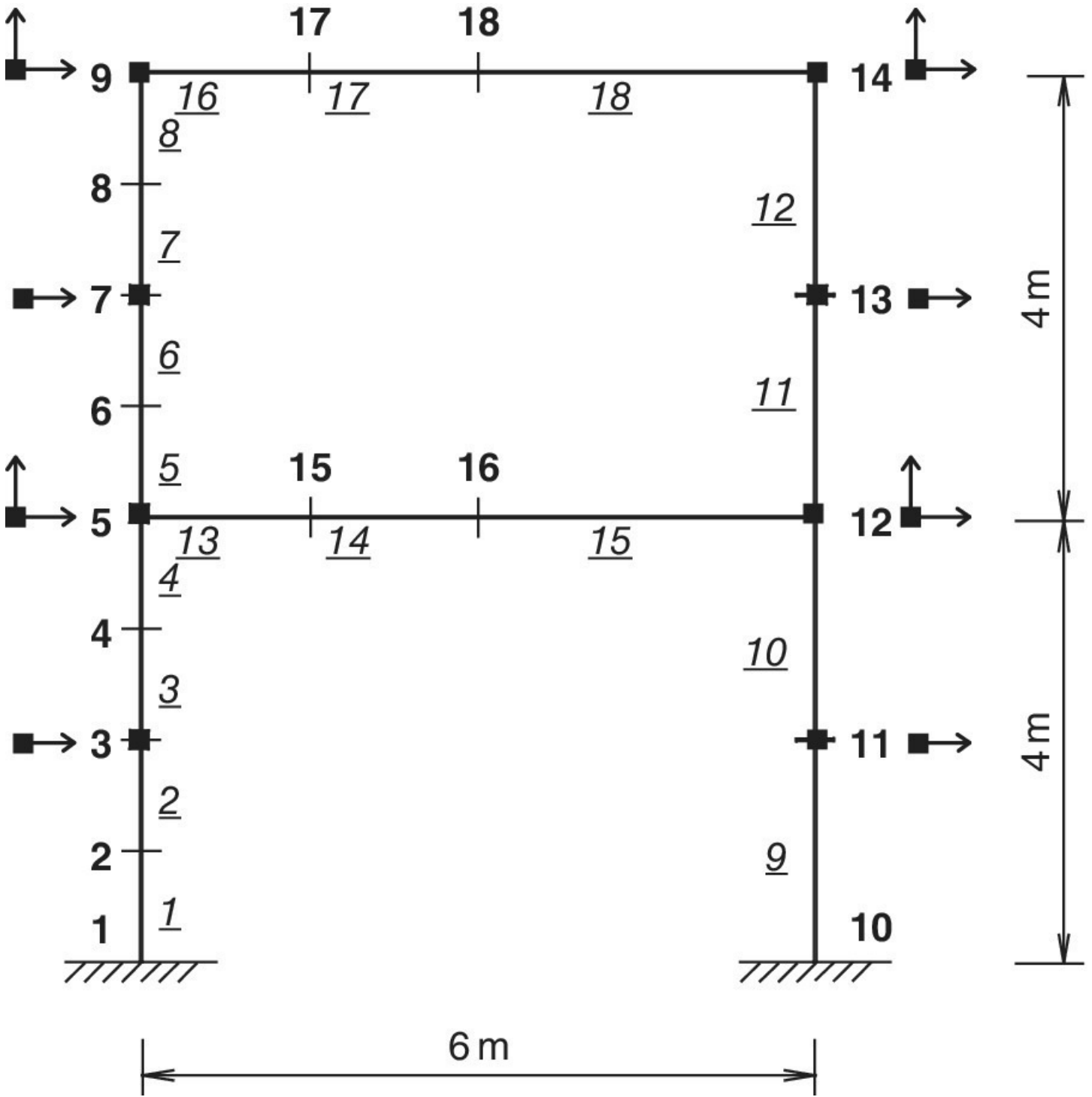


Figure 6.2 Finite element model of a plane frame structure for model updating.

Table 6.3 shows the adjusted natural frequencies at different iteration numbers using the dynamic perturbation method. The information about only eight 'tested' natural frequencies is

employed to update the original FE model. The results show that the convergence of the iterative solution procedure for model updating is achieved rapidly. The first eight adjusted natural frequencies are in excellent agreement with the exact solutions. The other natural frequency estimates are closer to the exact solutions, compared to the results from the first order approximation method under the heading of first iteration.

Table 6.3 Updated natural frequencies at different iteration numbers for model updating using only eight ‘tested’ frequencies.

Original frequencies (Hz)	Updated frequencies (Hz)			Tested exact ^b	MAC value
	First iteration	Second iteration	Fifth iteration		
1.4096	1.4062	1.4074	1.4074	1.4074	1.0000
4.7367	4.7958	4.8031	4.8024	4.8024	0.9990
7.2662	7.2607	7.2709	7.2706	7.2706	0.9992
9.0017	9.0515	9.0605	9.0599	9.0599	0.9975
16.5695	16.6250	16.6849	16.6851	16.6852	0.9485
19.0584	19.0589	19.1079	19.1003	19.1003	0.9475
23.7686	24.2738	24.3031	24.2984	24.2985	0.9917
24.8744	24.0807	24.1633	24.1620	24.1619	0.9775
31.1452	31.0702	31.0542	31.0471	30.9663	0.9904
32.5375	32.7893	32.8204	32.8064	32.8360	0.9878
50.9666	51.3042	51.3628	51.3394	51.2520	0.9843
61.3211	60.6836	60.8501	60.8391	61.0721	0.9666
64.4138	65.0944	65.0988	65.0533	64.8405	0.9498
74.7171	72.7126	72.9228	72.9089	72.6380	0.9483
84.5668	85.1241	85.2344	85.1871	85.3921	0.9063
$D\alpha\beta^a$	1.23E + 0	2.50E – 01	1.79E – 03	/	/

^a Absolute error for updating parameters

^b Italic values of tested exact frequencies are used for model updating

Table 6.4 shows the updated natural frequencies obtained from incomplete modal data using the dynamic perturbation method. Three incomplete ‘measured’ modes (modes 1, 2 and 3) with DOF readings measured at the hypothetical set of sensors are used for the model updating. The iterative solution procedure converges very quickly, achieving the converged results after only five iterations. From the results, the updated natural frequencies are very accurate when compared with the exact solution. The first order approximation method, giving the results under the heading of first iteration, may not be sufficiently appropriate for model updating in

this case.

Table 6.4 Updated natural frequencies at different iteration numbers for model updating using three ‘tested’ incomplete modes.

Original frequencies (Hz)	Updated frequencies (Hz)			Tested exact ^b	MAC value
	First iteration	Second iteration	Fifth iteration		
1.4096	1.4055	1.4071	1.4074	1.4074	1.0000
4.7367	4.7737	4.8020	4.8024	4.8024	0.9990
7.2662	7.2409	7.2724	7.2706	7.2706	0.9992
9.0017	9.0142	9.0647	9.0599	9.0599	0.9975
16.5695	16.5499	16.7183	16.6852	16.6852	0.9485
19.0584	18.9513	19.1244	19.1004	19.1003	0.9475
23.7686	24.2469	24.3260	24.2986	24.2985	0.9917
24.8744	23.9801	24.2612	24.1617	24.1619	0.9775
31.1452	30.7421	31.0416	30.9663	30.9663	0.9904
32.5375	32.6977	32.8205	32.8359	32.8360	0.9878
50.9666	50.9483	51.3226	51.2521	51.2520	0.9843
61.3211	60.7231	61.3023	61.0724	61.0721	0.9666
64.4138	64.3805	64.8695	64.8402	64.8405	0.9498
74.7171	71.6284	72.9868	72.6377	72.6380	0.9483
84.5668	84.7122	85.4616	85.3914	85.3921	0.9063
$D\alpha\beta^a$	1.65E + 00	8.08E – 01	4.40E – 03	/	/

^a Absolute error for updating parameters;

^b Incomplete modes with italic values are used for model updating.

Furthermore, both stiffness and mass can be adjusted at the same time, using the dynamic perturbation method, as summarised in [Table 6.5](#). It is assumed that the original stiffness and mass for each element have factors of unity, respectively. Both stiffness and mass values at elements 3, 5, 8, 9, 11 and 16 are modified for the ‘tested’ structure by factors of +30%, –10%, +10%, –10%, –20% and +10%, respectively. A total number of four and six ‘tested’ incomplete modes with DOF readings measured at the assumed sensor set are employed to update the modified model, respectively. From the results, both stiffness and mass are adjusted correctly by using information about only six ‘tested’ incomplete modes.

Table 6.5 Both stiffness and mass factors adjusted simultaneously using different number of ‘tested’ incomplete modes.

Element			Adjusted structural parameters					
	‘Tested’		Four modes		Six modes		Exact	
	Stiffness	Mass	Stiffness	Mass	Stiffness	Mass	Stiffness	Mass
1	1.00	1.00	0.99	0.99	0.99	1.00	1.00	1.00
2	1.00	1.00	0.97	0.92	0.99	0.99	1.00	1.00
3	1.30	1.30	1.01	1.06	0.99	0.99	1.00	1.00
4	1.00	1.00	1.00	0.96	0.99	0.99	1.00	1.00
5	0.90	0.90	0.99	0.88	0.99	0.99	1.00	1.00
6	1.00	1.00	0.98	1.02	0.99	0.99	1.00	1.00
7	1.00	1.00	1.00	1.03	0.99	0.99	1.00	1.00
8	1.10	1.10	0.99	0.94	0.99	0.99	1.00	1.00
9	0.90	0.90	0.99	0.93	0.99	0.99	1.00	1.00
10	1.00	1.00	1.00	1.03	0.99	0.99	1.00	1.00
11	0.80	0.80	0.99	0.98	0.99	0.99	1.00	1.00
12	1.00	1.00	1.00	1.01	0.99	0.99	1.00	1.00
13	1.00	1.00	1.00	1.03	0.99	0.99	1.00	1.00
14	1.00	1.00	1.01	0.98	0.99	0.99	1.00	1.00
15	1.00	1.00	0.99	1.01	0.99	0.99	1.00	1.00
16	1.10	1.10	1.00	0.99	0.99	0.99	1.00	1.00
17	1.00	1.00	1.01	1.00	0.99	0.99	1.00	1.00
18	1.00	1.00	0.99	1.00	0.99	0.99	1.00	1.00

6.6.4 Example for Model Updating – a Steel Space Frame (II)

The laboratory tested space steel frame structure, as discussed in [Section 5.3.3](#) and shown in [Figure 5.2](#), is now used for structural model updating. The FE model to be updated is constructed by modelling the experimental frame structure with the geometric dimensions and the node and element numbering, as shown in [Figure 6.3](#). The FE model has 20 nodes and 40 elements with a total number of 96 DOFs. The column and beam elements have the same rectangular crosssection with dimensions of 20 mm × 10 mm. The brace elements have an identical circular crosssection with diameter of 6 mm. The material properties of Young’s modulus $E = 2.0 \times 10^{11}$ N/m² and density $\rho = 7850$ kg/m³ are adopted in calculations for all beam, column and brace elements. Details of the modal testing of the space steel frame structure are discussed in [Section 5.3.3](#).

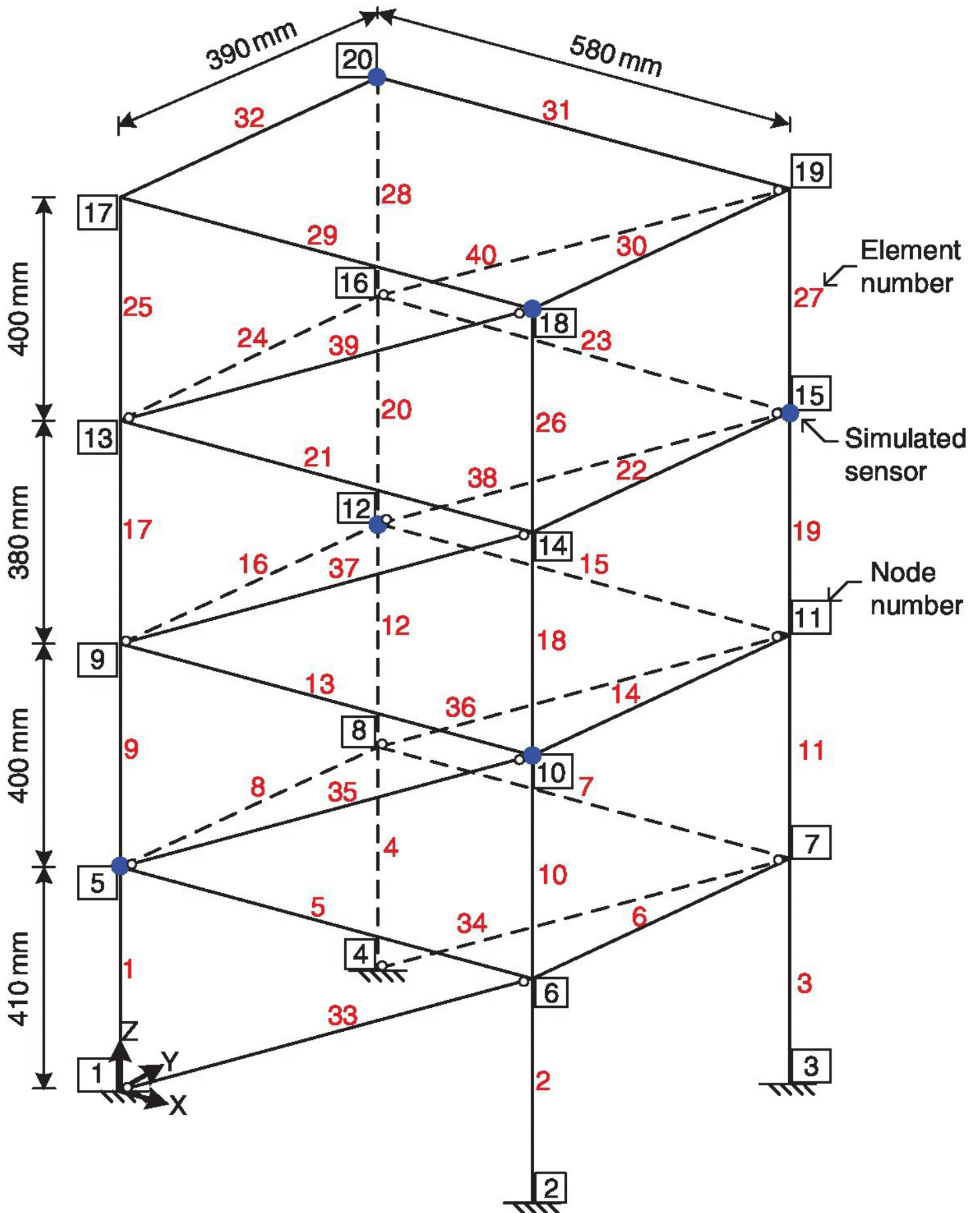


Figure 6.3 Finite element model of the laboratory tested space steel frame structure.

In the FE model, the diagonal brace members are assumed to be pinjointed at both ends due to limited flexural stiffness at the joints, and therefore primarily subjected to axial force. The connections of the beams and columns at the associated joints are modelled as rigid joints to sustain bending moments. In order to update the physical properties at specific locations in individual structural components, structural updating parameters associated with bending stiffness (e.g. EI) are chosen to characterise the physical properties at critical point level for beams and columns, i.e. at both ends and in the middle, and at element level for braces. A total number of 104 stiffness updating parameters are introduced for updating the initial FE model, i.e. 48 for columns, 48 for beams and 8 for braces. The updating of mass is not considered here due to its relatively higher accuracy.

In the numerical simulation investigations, the stiffness changes to be updated are simulated at different structural elements with various updating levels, i.e. -50% change at both ends of column elements 2, 3, 18 and 19, -10% change at both ends of beam elements 6 and 22 and -30% change in brace elements 34 and 38. Here, the ‘measured’ exact modal data, i.e. natural frequencies and the corresponding incomplete mode shapes, are obtained from FE dynamic analysis for the simulated ‘tested’ structure, namely by solving the characteristic equations for the ‘tested’ structure with assumed stiffness changes. The first eight natural frequencies for the initial FE model and the simulated ‘tested’ structure are listed in [Table 6.6](#), with an average frequency absolute error of 6.569%. The ‘measured’ incomplete mode shapes are constructed by the DOF translational modal readings in only X and Y directions at six nodes, i.e. nodes 5, 10, 12, 15, 18 and 20, with a total number of 12 measurements for each individual mode, as shown in [Figure 6.3](#).

Table 6.6 Updated natural frequencies of the FE model using eight simulated incomplete modes without noise and with 7% noise level.

Mode	FE (Hz)	Exact (Hz)	Error (%)	Noisefree		7% noise level	
				Updated (Hz)	Error (%)	Updated (Hz)	Error (%)
1	10.3552	9.4554	9.517	9.4553	-0.001	9.4378	-0.186
2	25.9380	25.1115	3.291	25.1116	0.001	25.1028	-0.035
3	31.7608	28.0390	13.273	28.0410	0.007	28.1050	0.235
4	45.2475	42.4984	6.469	42.4973	-0.003	42.4491	-0.116
5	51.8179	50.4929	2.624	50.4915	-0.003	50.5029	0.020
6	65.5716	63.5167	3.235	63.5168	0.000	63.4860	-0.048
7	70.6418	65.0895	8.530	65.0884	-0.002	65.3023	0.327
8	72.1780	68.3407	5.615	68.3569	0.024	68.4744	0.196
Average error E_ω (%)			6.569		0.005		0.150

The initial FE model is adjusted through the dynamic perturbation method by using the

simulated ‘measured’ incomplete modal data, as given in [Table 6.6](#). Information about eight incomplete modes without noise and with 7% noise level, respectively, is utilised for evaluating the total number of 104 chosen stiffness updating parameters from the corresponding total number of 96 equations available. The updated frequencies are in excellent agreement with the simulated exact values, with average absolute errors of only 0.005% for the case without noise and of 0.150% for the case with 7% noise level, respectively.

In order to investigate the accuracy of the updated structural parameters, results for updated stiffness parameters are then compared with the simulated exact values, as shown in [Figure 6.4](#). Information about different numbers of noise-free incomplete modes is employed in the model updating predictions, using six modes, eight modes and ten modes, respectively. From the results, the adjusted stiffness factors are in good agreement with the simulated exact values at the critical points of beams and columns (2, 3, 6, 18, 19, 22) and in braces (34, 38). The results show that information about six incomplete modes is sufficient to provide correct predictions of structural model updating by using the dynamic perturbation method.

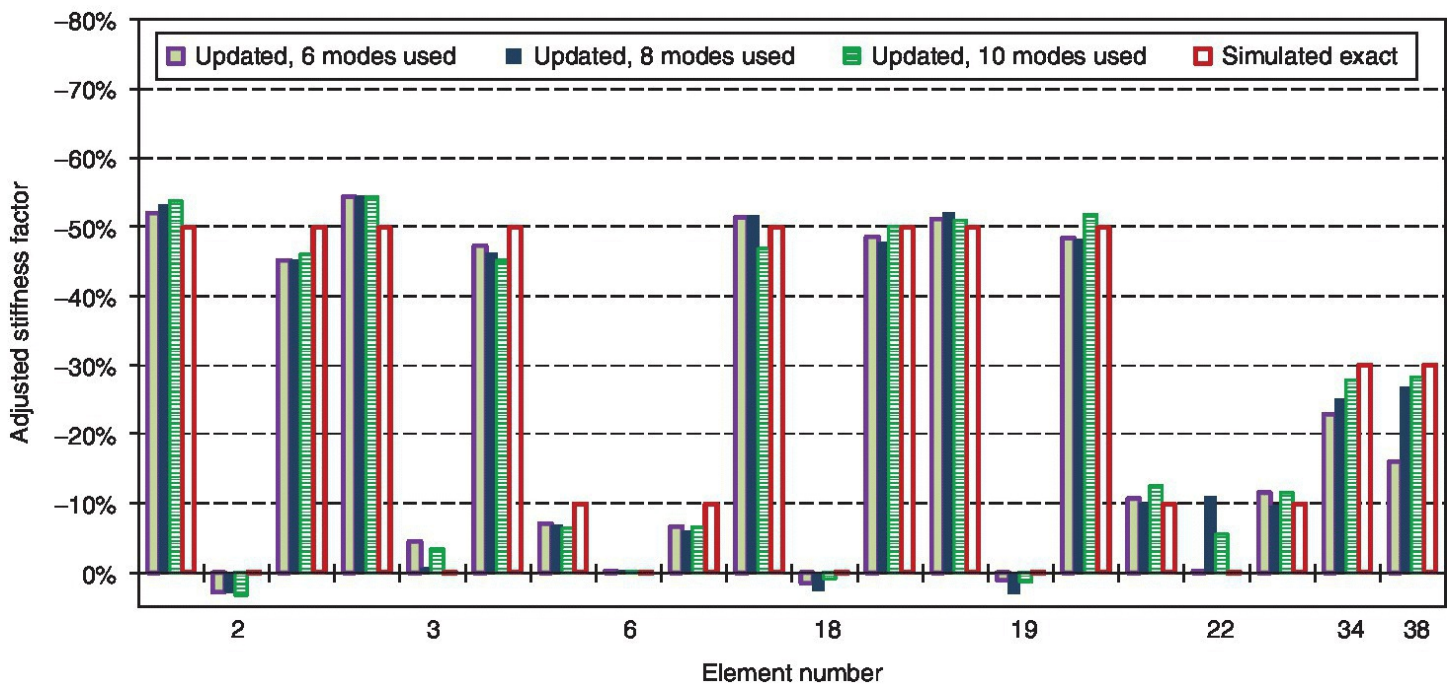


Figure 6.4 Comparison of updated stiffness parameters of the FE model and simulated exact stiffness parameters at integration point level for beams and columns and at element level for braces, information on different number of noise-free incomplete modes used.

Now, the real modal data measurements from the laboratory vibration testing, as discussed in [Section 5.3.3](#), are used for updating the initial FE model shown in [Figure 6.3](#). [Table 6.7](#) shows the updated natural frequencies from six experimental incomplete modes by using different model updating methods, i.e. the sensitivity based method, the simplified direct dynamic perturbation method and the iterative dynamic perturbation method. For the sensitivity based method, the average frequency absolute error is reduced from an initial value of 1.178% to a value of 0.339% after updating. The simplified direct method and the iterative method give very close results with updated average frequency absolute errors of 0.109% and 0.072%,

respectively, which are better than those obtained by the sensitivity based method.

Table 6.7 Comparison of updated natural frequencies of the FE model using six real experimental incomplete modes by different model updating methods.

Mode				Sensitivity		Direct		Iterative	
	FE (Hz)	Measured (Hz)	Error (%)	Updated (Hz)	Error (%)	Updated (Hz)	Error (%)	Updated (Hz)	Error (%)
1	10.3552	10.569	-2.022	10.495	-0.697	10.544	-0.240	10.551	-0.173
2	25.9380	26.386	-1.698	26.189	-0.746	26.386	0.000	26.389	0.010
3	31.7608	32.258	-1.541	32.416	0.490	32.203	-0.173	32.225	-0.101
4	45.2475	46.018	-1.674	45.993	-0.054	45.948	-0.153	45.972	-0.099
5	51.8179	51.847	-0.056	51.836	-0.022	51.821	-0.051	51.834	-0.026
6	65.5716	65.522	0.076	65.506	-0.024	65.550	0.043	65.535	0.020
Average absolute error (%)			1.178		0.339		0.109		0.072

6.7 Case Study

The constructed supertall structure Canton Tower, as described in the case study in [Section 5.7](#), is adopted again for structural model updating using measured modal data. Since the full scale 3D FE model shown in [Figure 5.14\(a\)](#) has a large number of elements and DOFs, an equivalent reducedorder FE model shown in [Figure 5.14\(c\)](#) is used for FE model updating and structural health monitoring (Ni et al. 2012). In the reduced FE model, the tower is modelled as a cantilever beam with 37 beam elements and 38 nodes: 27 elements for the main tower and 10 elements for the upper mast (Chen and Huang 2012, Chen and Tee 2014). The vertical displacement of the structure is ignored in the reduced FE model, giving a total number of five DOFs for each node, i.e. two horizontal translational DOFs and three rotational DOFs. Therefore, each beam element has 10 DOFs and the reduced FE model has a total of 185 DOFs with a fixed end at the base.

A finite element analysis is performed to calculate the natural frequencies and mode shapes for the reducedorder FE model. The operational modal data identified from the ambient vibration measurements by the SSI technique, given in [Table 5.3](#), is adopted for model updating. [Table 6.8](#) shows that the difference between the frequencies identified from the ambient vibration measurements and those from FE model is relatively large, with the largest relative error in the fundamental natural frequency. The modal assurance criterion (MAC) diagonal values, determined from the measured incomplete mode shapes and the FE calculated eigenvectors restricting to the same DOFs, indicate good correlations between the measured and calculated modes, except two torsion modes: 6th and 12th modes.

Table 6.8 Updated modal properties of the reduced FE model using 10 measured frequencies excluding two torsion modes.

Mode	Tested frequency (Hz)	Before updating			After updating			
		FE frequency (Hz)	Difference (%)	MAC value	FE frequency (Hz)	Difference (%)	MAC with tested	MAC with FE
1	0.090	0.111	23.81	0.904	0.093	3.76%	0.773	0.937
2	0.131	0.159	21.19	0.938	0.142	8.14%	0.824	0.936
3	0.366	0.347	-5.17	0.888	0.367	0.19%	0.881	0.996
4	0.422	0.369	-12.50	0.888	0.402	-4.71%	0.917	0.998
5	0.474	0.400	-15.59	0.869	0.428	-9.66%	0.844	0.998
6	0.504	0.462	—	—	—	—	—	—
7	0.520	0.487	-6.31	0.783	0.506	-2.69%	0.892	0.995
8	0.796	0.738	-7.21	0.797	0.781	-1.80%	0.832	0.997
9	0.966	0.904	-6.44	0.771	0.940	-2.65%	0.832	0.996
10	1.151	0.997	-13.34	0.701	1.004	-12.72%	0.683	0.999
11	1.191	1.037	-12.86	0.753	1.055	-11.42%	0.810	0.998
12	1.251	1.121	—	—	—	—	—	—
		Average	12.44%*	0.829#		5.77%*	0.829#	0.985#

* Average of the absolute values of difference in frequencies.

Average of MAC values excluding two torsion modes.

The significant difference between the measured and FE calculated frequencies indicates that there are modelling errors in the reduced FE model and measurement uncertainty from the recorded vibration data. This significant difference requires an updating of the finite element model. Here, a total number of 37 structural stiffness parameters are adopted for updating the reduced FE model for the Canton Tower. A total number of 20 DOF readings are available for each measured mode shape. The updating of mass is not considered due to its relatively higher accuracy.

Table 6.8 summarises the results for the updated modal properties of the reduced FE model by using the dynamic perturbation method. A total number of 10 measured frequencies are used for model updating. The average of the absolute values of the difference in frequencies reduces from 12.44% before updating to 5.77% after updating. The obtained high MAC diagonal values indicate that the updated mode shapes match well the original FE calculated eigenvectors and experimental mode shapes as well.

Table 6.9 lists the updated modal properties of the reduced FE model by using nine measured incomplete modes. The results show that the updated frequencies are much closer to the

frequencies identified from vibration measurements, reducing the average frequency absolute error from 11.83% initially to 4.29% after updating. The obtained MAC diagonal values indicate that the updated mode shapes correlate well with the initial modes of the FE model and also have good correlation with the modes identified from field measurements.

Table 6.9 Updated modal properties of the reduced FE model using nine measured incomplete modes.

Mode	Tested frequency (Hz)	Before updating			After updating			
		FE frequency (Hz)	Difference (%)	MAC value	FE frequency (Hz)	Difference (%)	MAC with tested	MAC with FE
1	0.090	0.111	23.81	0.904	0.085	-5.56%	0.712	0.973
2	0.131	0.159	21.19	0.938	0.136	3.82%	0.595	0.945
3	0.366	0.347	-5.17	0.888	0.368	0.55%	0.986	0.837
4	0.422	0.369	-12.50	0.888	0.402	-4.74%	0.996	0.958
5	0.474	0.400	-15.59	0.869	0.428	-9.70%	0.997	0.851
6	0.504	0.462	-8.33	—	0.461	-8.53%	0.718	—
7	0.520	0.487	-6.31	0.783	0.512	-1.54%	0.962	0.874
8	0.796	0.738	-7.21	0.797	0.783	-1.63%	0.971	0.818
9	0.966	0.904	-6.44	0.771	0.941	-2.59%	0.959	0.857
		Average	11.83%*	0.829#		4.29%*	0.877#	0.889#

* Average of the absolute values of difference in frequencies.

Average of MAC values.

Figure 6.5 indicates the results for the updated stiffness parameters of the reduced FE model using nine measured incomplete modes. The values of stiffness updating parameters are relatively small, ranging from -8.93% to 13.24% with an average of the absolute values of 3.80%. These results appear reasonable in practice, since only relatively small stiffness modifications in the wellconstructed initial FE model are required to minimise significant differences between the FE calculated and the identified modal data.

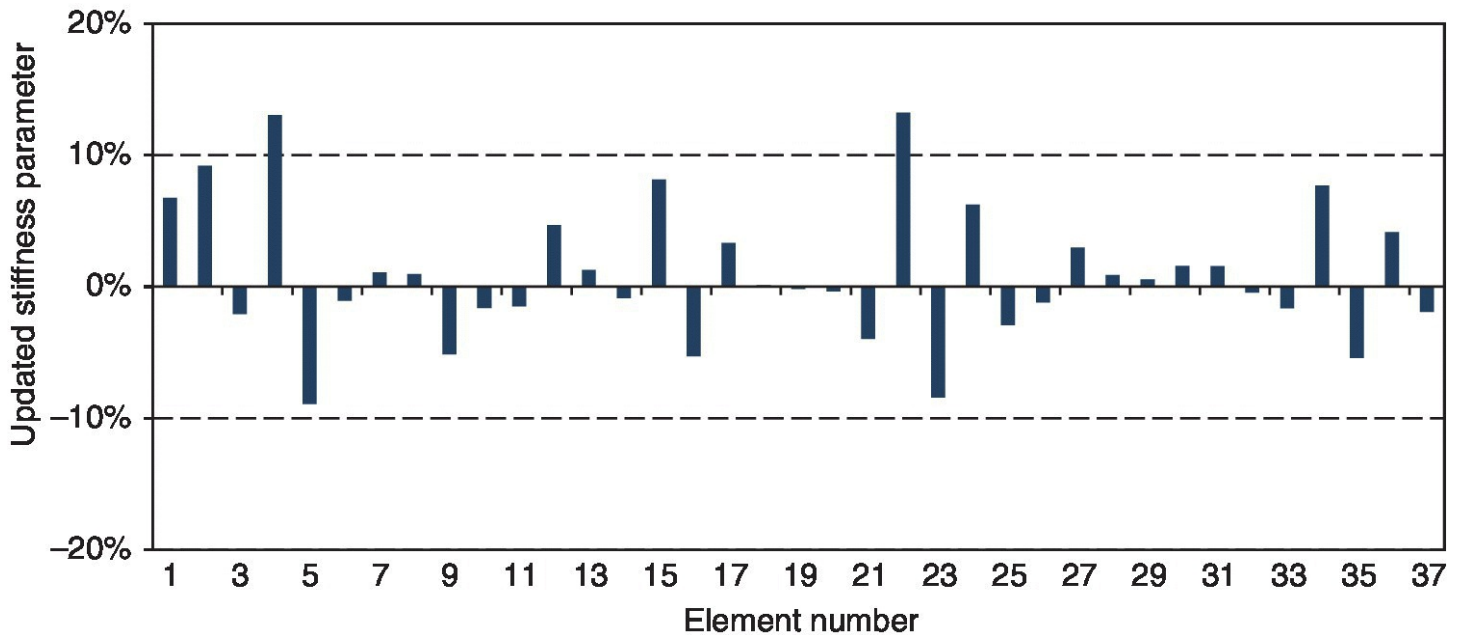


Figure 6.5 Updated stiffness parameters of the reduced FE model using nine measured incomplete modes.

6.8 Concluding Remarks

Model updating methods aim to improve the correlation between the measured data and the results predicted by the finite element model. A model updating procedure can adjust certain errors in finite element modelling, such as material properties, cross-sectional properties and plate thickness. The parameters for model updating may be chosen at local level by using non dimensional scalar multipliers. Owing to inevitable noise in output measurements and errors in finite element modelling, a regularisation method, such as the Tikhonov regularisation algorithm incorporating the Lcurve criterion, is often required to give reliable estimates for the updating parameters.

Sensitivity based methods are the most commonly used method in practice. In these methods, the measured outputs, such as frequencies and mode shapes, are adopted for updating the initial finite element model. The sensitivity based methods allow a wide choice of the parameters for model updating and the measured outputs to be weighted. Calculating the sensitivity of measurements with respect to parameters is computationally intensive, and only the approximations of the sensitivity may be obtained. Since the sensitivity is generally non linear functions of the parameters, an iterative procedure is necessary with possible associated convergence problems to solve for the selected parameters.

The dynamic perturbation method overcomes some limitations in the sensitivity based methods. This method is based on the exact relationship between the perturbation of structural parameters and the modal properties of the actual tested structure. The dynamic perturbation method directly adopts the measured incomplete modal data, and does not require mode shape expansion or model reduction in the model updating processes. Thus, this method needs much less computational effort to estimate the updating parameters. The method provides optimised

solutions for model updating in the least squares sense without requiring optimisation techniques. Also, the method offers reliable estimates of structural updating parameters, even in the cases where relatively large modifications in structural parameters and/or in modal properties exist between the finite element model and the tested structure.

Recently, various techniques have been developed for updating finite element models. The full field measurements of vibration mode shapes, obtained from scanning laser velocimetry (Stanbridge et al. 2004) and digital image processing (Wang, et al. 2009), have been used for model updating. A Bayesian probabilistic framework for robust finite element model updating has been proposed, which is capable of identifying multiple nonunique solutions (Beck and Katafygiotis 1998, Simoen et al. 2013). Furthermore, time-domain data and nonlinear frequency response function measurements have been utilised for nonlinear model updating, such as updating the linear and nonlinear parameters of a beam with a cubic stiffness at one end (Meyer and Link 2003). These new methods improve the algorithms and procedures for updating finite element models. After the finite element model is updated and validated using real measurements, this model can then be used as the baseline model of the intact structure for damage identification.

References

- Balageas, D., Fritzen, C.P. and Guemes, A. (2006) *Structural Health Monitoring*. ISTE Ltd. London, UK.
- Beck, J.L and Katafygiotis, L.S. (1998) Updating models and their uncertainties I: Bayesian statistical framework. *Journal Engineering Mechanics ASCE***124**(4), 455–61.
- Brownjohn, J.M.W. and Xia, P.Q. (2000) Dynamic assessment of curved cablestayed bridge by model updating. *Journal of Structural Engineering ASCE***126** (2), 252–260.
- Chen, H.P. (1998) *Structural Damage Identification Using Vibration Modal Data*. PhD thesis Department of Civil Engineering, Glasgow University, UK.
- Chen, H.P. (2005) Nonlinear perturbation theory for structural dynamic systems. *AIAA Journal***43**(11), 2412–2421.
- Chen, H.P. (2006) Efficient methods for determining modal parameters of dynamic structures with large modifications. *Journal of Sound and Vibration***298** (1–2), 462–470.
- Chen, H.P. and Bicanic, N. (2010) Identification of structural damage in buildings using iterative procedure and regularisation method. *Engineering Computations***27**(8), 930–950.
- Chen, H.P. and Huang, T.L. (2012) Updating finite element model using dynamic perturbation method and regularization algorithm. *Smart Structures and Systems***10**(4–5), 427–442.
- Chen, H.P. and Maung, T.S. (2014) Regularised finite element model updating using measured incomplete modal data. *Journal of Sound and Vibration***333**(21), 5566–5582.

- Chen, H.P. and Tee, K.F. (2014) Structural finite element model updating using ambient vibration modal data. *Science China Technological Sciences***57**(9), 1677–1688.
- Doebbling, S.W., Farrar, C.R., Prime, M.B. and Shevitz, D.W. (1996) *Damage Identification and Health Monitoring of Structural and Mechanical Systems from Changes in their Vibration Characteristics: A Literature Review*. Los Alamos National Laboratory report LA 13070MS.
- Farhat, C. and Hemez, F.M. (1993) Updating finite element dynamic models using an element byelement sensitivity methodology. *AIAA Journal***31**(9), 1702–1711.
- Fox, R.L. and Kapoor, M.P. (1968) Rates of changes of eigenvalues and eigenvectors. *AIAA Journal***6**(12), 2426–2429.
- Friswell, M.I. and Mottershead, J.E. (1995) *Finite Element Model Updating in Structural Dynamics*. Kluwer Academic Publishers, Dordrecht, The Netherlands.
- Friswell, M.I., Inman, D.J. and Pilkey, D.F. (1998) Direct updating of damping and stiffness. *AIAA Journal***36**(3), 491–493.
- Hansen, P.C. and O’Leary, D.P. (1993) The use of the Lcurve in the regularisation of discrete illposed problems. *SIAM Journal on Scientific Computing***14**(6), 1487–1503.
- Kabe, A.M. (1985) Stiffness matrix adjustment using modal data. *AIAA Journal***23**(9), 1431–1436.
- Link, M. (1999) Updating of analytical models – Review of numerical procedures and application aspects. *Proceedings of Structural Dynamics Forum SD2000*, Los Alamos, USA.
- Imregun, M., Visser, W.J. and Ewins, D.J. (1995) Finite element model updating using frequency response function data I: Theory and initial investigation. *Mechanical Systems and Signal Processing***9**(2), 187–202.
- Meyer, S. and Link, M. (2003) Modelling and updating of local nonlinearities using frequency response residuals. *Mechanical Systems and Signal Processing***17**(1), 219–226.
- Modak, S.V., Kundra, T.K. and Nakra, B.C. (2002) Comparative study of model updating methods using simulated experimental data. *Computers and Structures***80**, 437–447.
- Mottershead, J.E. and Friswell, M.I. (1993) Model updating in structural dynamics: a survey. *Journal of Sound and Vibration***167**(3), 347–375.
- Mottershead, J.E., Link, M. and Friswell, M.I. (2011) The sensitivity method in finite element model updating: A tutorial. *Mechanical Systems and Signal Processing***24**, 2275–2296.
- Ni, Y.Q., Xia, Y., Lin, W., Chen, W.H. and Ko, J.M. (2012). SHM benchmark for highrise structures: a reducedorder finite element model and field measurement data. *Smart Structures and Systems***10**(4–5), 411–426.

- Palmonella, M., Friswell, M.I., Mottershead, J.E. and Lees, A.W. (2005) Finite element models of spot welds in structural dynamics: review and updating. *Computers and Structures***83**, 648–661.
- Simoen, E. Papadimitriou, C. and Lombaert, G. (2013) On prediction error correlation in Bayesian model updating. *Journal of Sound and Vibration***332**(18), 4136–4152.
- Stanbridge, A., Martarelli, M. and Ewins, D. (2004) Measuring area vibration mode shapes with a continuous scan LDV. *Measurement***35**, 181–189.
- Stoer, J. and Bulirsch, R. *Introduction to Numerical Analysis*, SpringerVerlag, New York, USA.
- Tikhonov, A.N. and Arsenin, V.Y. (1977) *Solutions of illposed problems*. John Wiley & Sons, New York, USA.
- Wang, W., Mottershead, J.E. and Mares, C. (2009) Vibration mode shape recognition using image processing. *Journal of Sound and Vibration***326**(3–5), 909–938.
- Zienkiewicz, O.C. and Taylor, R.L. (1977) *The Finite Element Method*. McGrawHill, London, UK.

7

VibrationBased Damage Identification Methods

7.1 Introduction

Structural damage identification is important for assessing the condition of civil engineering structures in service and for determining effective maintenance plans of the structures. Among the existing damage identification methods, the most commonly used for identifying damage in engineering structures is the vibrationbased method. Vibrationbased damage identification methods were initially investigated in mechanical, aerospace and offshore engineering. These methods have received increasing interest in civil engineering over the past two decades. The underlying principle behind these methods is that the vibration signature – e.g. modal parameters or frequency response functions – is a sensitive indicator of structural physical integrity. When damage occurs in a structure, structural parameters, such as stiffness, flexibility and strain energy, will be changed, and consequently modal parameters, such as natural frequency, mode shape and damping, will also be changed (Chen 1998, Chen and Maung 2014a, Doebling et al. 1996, Yan et al. 2007). As a result, both change in structural parameters and change in modal parameters can be used as damage indicators for identifying damage in a structure.

Modal parameters can be obtained from vibration measurements of the structure concerned through modal testing and analysis. The obtained modal parameters are associated with change in structural parameters, such as reduction of stiffness, due to damage in a structure. It is therefore natural to use the measured change in dynamic behaviour for the identification of structural damage. By use of the vibrationbased methods, damage can be identified in a global sense, even when the location of damage is inaccessible. The damage identification methods using measured natural frequencies are attractive, since frequencies can be easily measured at a single point on the structure and are independent of the position selected (Bicanic and Chen 1997). Frequencies are less contaminated with measurement errors and easier to extract. However, use of change in frequencies alone may not be sufficient for accurate structural damage identification. Information on other measured vibration data, such as mode shapes, frequency response functions and modal strains, is often further needed for the identification of damage location. In general, the measured frequencies are usually more accurate than the mode shapes, but the mode shapes are more sensitive to local damage.

Damage identification methods using change of structural parameters are based on the philosophy that damage in a structure causes decrease in structural stiffness or increase in structural flexibility. On the basis of the relationship between the structural parameters and the modal parameters, the damage in the structure can be identified using the measured vibration modal data. In addition, the strain energy of a structure such as a beam will change when damage occurs in the structure. The change of strain energy can therefore be adopted for

damage identification using the vibration modal data or strain measurements.

The applications of neural networks have attracted increasing attention due to their capabilities such as pattern recognition, classification and function approximation. Statistical pattern recognition deals with the discovery of regularities in the measured data and subsequent actions such as classification (Staszewski and Worden 2009). A robust damage detection method must be capable of recognising patterns in the observed response or modal parameters of the structure with local damage. This capability is generally within the scope of the pattern matching capabilities of neural networks. Therefore, neural networks show promise for structural damage detection. Typical methods for detecting damage in civil engineering structures include novelty detection, backpropagation neural network, and probabilistic neural networks.

This chapter offers a comprehensive and updated review on various methods for detecting and localising damage in a structure using measured vibration modal data. First, proper structural modelling is discussed for damage identification to accurately represent the behaviour of a structure and to characterise damage in the structure. Depending on the selected damage indicators, two commonly used types of damage identification methods are discussed. One type uses the change of modal parameters and their derivatives, such as natural frequencies, mode shapes and their curvatures, frequency response functions and modal strain energy. Another type of method uses the change of structural parameters, such as flexibility matrix, strain energy and modal strain. Finally, advanced computational methods such as pattern recognition and neural networks are introduced for damage identification in civil structures.

7.2 Structural Modelling for Damage Identification

The damage model for structural damage identification may be simple or complex, depending on the type of structure (Lam et al. 1998, Worden and Friswell 2009). For example, a cracked beam may be modelled as a reduction in stiffness in a large finite element model. Alternatively, a very detailed model may be used for modelling the cracked beam from fracture mechanics. Constructing a damage model often depends on the requirements of the damage identification procedure and the quality of the measured data. Only a coarse model of the damage may be identified when vibration modal measurements of the lower frequency modes are adopted. For complex civil engineering structures, the equivalent continuum technique (Stubbs et al. 1990) and the substructuring technique (Hajela and Soeiro 1990) may be used for modelling a structure with damage. The equivalent continuum technique may generate large modelling errors and mask the individual member with damage. The traditional substructuring technique is a feasible approach to decrease the model dimension and to reduce the system parameters. The substructure where damage occurs needs to be small enough to obtain accurate damage location. For civil infrastructure, possible global structural damage indices can be adopted for structural health monitoring (Catbas and Aktan 2002), as shown in [Figure 7.1](#).

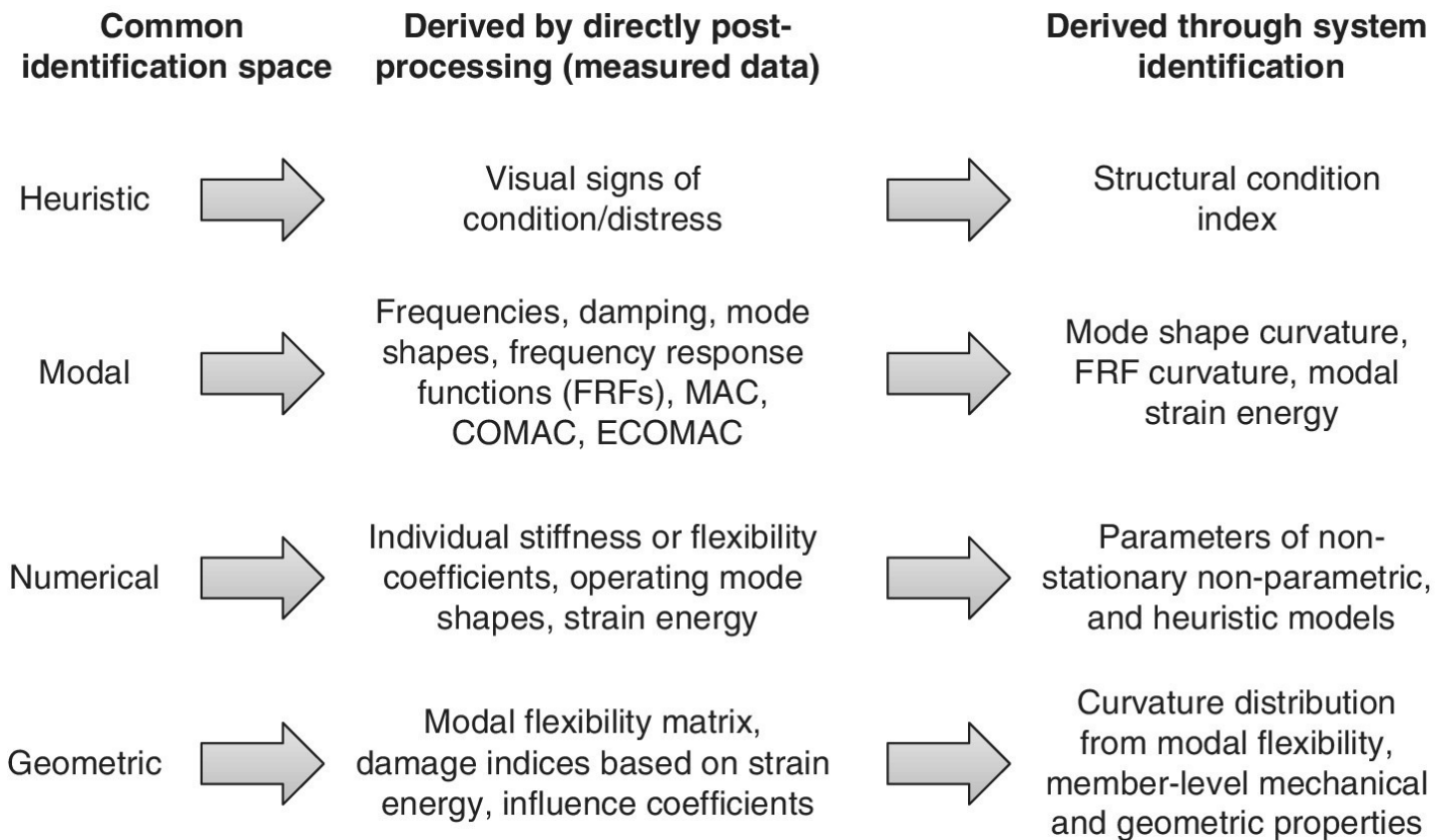


Figure 7.1 Possible global structural damage indices for civil engineering structures (after Catbas and Aktan 2002).

For large civil infrastructure such as cablesupported bridges, global modal parameters may be insensitive to damage that has occurred in some local structural members. As a result, problems can arise in identifying the damage in these structural members using modal parameters. For heavily redundant structures, a priori classification of structural members in terms of their sensitivity degrees to damage can exclude the redundant physical parameters from the system variables. Meanwhile, a priori evaluation of the sensitivities of different modes to damage is helpful for selecting appropriate modes for damage identification. Such information can be obtained through modal sensitivity analysis of the structural model. It requires the model to be accurate enough, so that the modal sensitivity with respect to any individual structural member can be directly calculated. Therefore, the structural model needs to be validated through a model updating procedure before damage detection (Chen and Huang 2012, Chen and Maung 2014b, Friswell and Mottershead 1995).

For large civil engineering structures, finite element (FE) modelling based on direct assembly of all critical structural components will involve a huge number of degrees of freedom (DOFs) and thus become computationally demanding. This also results in a critical problem that the number of the finite element model DOFs is much greater than the number of DOFs measured in modal testing. To proceed with incomplete modal data, a model reduction or mode shape expansion technique is often required (Chen 2010, Chen et al. 2012). When the measured DOFs are far less than the finite element model DOFs, both techniques will seriously degrade the damage detection capability. Also, a structural model with excessive DOFs results in an

inverse problem for damage identification with time-consuming and ill-conditioning issues.

To obtain accurate structural damage identification results, structural modelling should satisfy the following requirements: (a) the computed modal parameters predicted by the structural model are well correlated with the measured data from the intact structure, (b) modal parameter uncertainty due to modelling errors is less than modal parameter changes caused by actual damage, (c) the size of the finite element model is appropriate so that the number of the model DOFs is not significantly larger than that of measured DOFs in the modal testing, (d) the structural model is accurate enough not to mask the damage location in the modelling process.

A simple example of a cantilever beam, as shown in [Figure 7.2](#), is employed to compare various structural modelling approaches. The beam has dimensions of 5.0 m in length, 0.5 m in width and height. It has material properties of elastic modulus $E = 3.2 \times 10^{10} \text{ N/m}^2$, Poisson's ratio $\nu = 0.15$ and density $\rho = 2400 \text{ kg/m}^3$. The structure can be modelled with different approaches, e.g. onedimensional conventional or Timoshenko beam problem, two dimensional plate stress or plate bending problem and threedimensional solid problem.

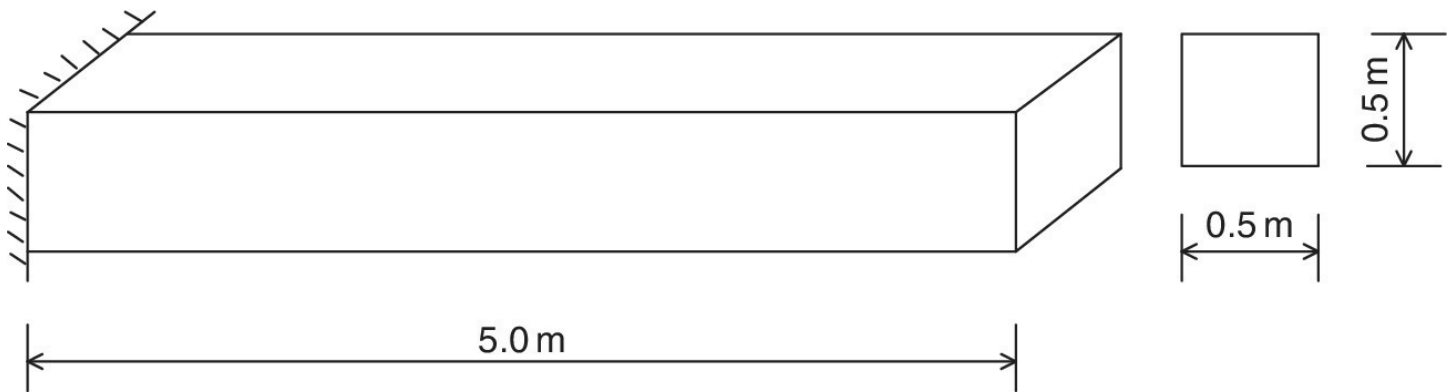


Figure 7.2 A cantilever beam used for different modelling problems.

Structural dynamic analysis and damage identification for these model problems can be performed using the corresponding types of elements. For the onedimensional beam model problem, the used finite elements include conventional beam elements with explicit or numerically integrated stiffness or Timoshenko beam elements. Meanwhile, plane stress elements or plate bending elements are used for the twodimensional continuum model problem. Solid brick elements are used for the threedimensional model problem. A finite element analysis was performed to calculate modal parameters for the cantilever beam problem. The first five natural frequencies of the structure for different model problems are listed in [Table 7.1](#). From the results, there are some differences in the calculated natural frequencies between the various structural modelling approaches. These systematic type errors in structural modelling should be minimised in damage identification. This can be achieved by selecting an appropriate structural model for damage detection, and a model updating procedure should be used to validate the structural model.

Table 7.1 First five frequencies (Hz) of the cantilever beam for different model problems.

Problem idealisation	Element type	Original mode				
		1	2	3	4	5
1D Beam	Explicit	11.7968	73.9319	207.0575	406.0334	672.2537
	Integrated	11.7968	73.9319	207.0578	406.0374	672.2820
	Timoshenko	11.7139	70.5350	186.7041	341.3871	524.4700
2D	Plane stress	11.7401	71.0200	182.6583	189.1143	348.1219
Continuum	Plate bending	11.7263	70.5867	114.8138	186.7733	341.3830
3D Solid	Solid brick	11.7565	71.1085	120.3859	182.7632	189.3234

7.3 Methods Using Change of Modal Parameters

Modal parameters, such as natural frequencies and mode shapes, are global properties of a structural dynamic system. The change in modal parameters can indicate the presence of structural damage associated with structural parameters, such as stiffness and mass. The damage identification methods based on change of modal parameters do not require the measurements at or near the damage location. Such methods assume that structural damage can be identified by comparing the current modal measurements with those for the undamaged state (DCSE 1998a). Any measured change in modal parameters is assumed to be caused by damage in the structure only, by ignoring the effects of other factors such as change in environmental conditions.

7.3.1 Natural Frequencies

In modal testing, natural frequencies are easy to measure and are independent of the measurement location. Since change in stiffness due to damage in a structure, whether local or distributed, causes change in natural frequencies of the structure, the presence of structural damage can then be detected simply by using change in natural frequencies. The sensitivity of natural frequencies ($\Delta\omega_i^2$) to change in stiffness matrix ($\Delta\mathbf{K}$) is expressed in (Cawley and Adams 1979) by

$$\Delta\omega_i^2 = \hat{\omega}_i^2 - \omega_i^2 = \frac{\phi_i^T \Delta\mathbf{K} \phi_i}{\phi_i^T \mathbf{M} \phi_i} \quad (7.1)$$

where $\hat{\omega}_i$ and ω_i are the i th natural frequency of the damaged and undamaged structure, respectively, ϕ_i is the i th mode shape of the undamaged structure and \mathbf{M} is the global mass matrix. It is assumed that the structural damage causes a negligible changes in the mass and in the mode shapes. When damage occurs at a single location, e.g. at the e th element, from Equation (6.9a), the change in stiffness matrix $\Delta\mathbf{K}$ is rewritten as

$$\Delta \mathbf{K} = \alpha_e \mathbf{K}_e \quad (7.2)$$

where α_e is a nondimensional coefficient for the e th element stiffness matrix, and \mathbf{K}_e is the e th element stiffness matrix of the undamaged structure expanded in full DOFs. From [Equation \(7.2\)](#), the sensitivity equation [Equation \(7.1\)](#) is rewritten as

$$\Delta \omega_i^2 = \alpha_e \frac{\phi_i^T \mathbf{K}_e \phi_i}{\phi_i^T \mathbf{M} \phi_i} \quad (7.3)$$

This equation indicates the relationship between the shift in natural frequency and the structural damage at the e th element, on the basis of the modal information of the undamaged structure. Assuming that the mode shapes of the undamaged structure are mass normalised, leads to the following sensitivity equation

$$\alpha_e = \frac{\Delta \omega_i^2}{\phi_i^T \mathbf{K}_e \phi_i} \quad (7.4)$$

This method is only applicable to singledamage cases due to its assumptions. For symmetric structures, the identification by this method in the case of single damage may result in two or more possible damage locations. In such situations, several pairs of modes must be used in order to define the damage position uniquely or to reduce the number of possible locations to the minimum dictated by symmetry. When some insensitive modes are included in the mode pairs, the identification for the damage location may result in erroneous results. The improvement can be achieved only after eliminating these unfavourable modes from the analysis.

Structural damage at single location can also be detected by the damage location assurance criterion (DLAC) using the frequency changes in a number of modes (Williams et al. 1997). The DLAC for location j is defined, using a correlation criterion similar to the modal assurance criterion, as

$$DLAC(j) = \frac{|\Delta \hat{\omega}^T \delta \omega_j|^2}{(\Delta \hat{\omega}^T \Delta \hat{\omega}) \cdot (\delta \omega_j^T \delta \omega_j)} \quad (7.5)$$

where $\Delta \hat{\omega}$ is the vector of measured natural frequency changes and $\delta \omega_j$ is the analytical frequency change vector with the assumed damage at location j . Given an analytical or finite element model, $\delta \omega_j$ and then $DLAC(j)$ can be computed for all possible damage locations. DLAC values range from 0 to 1, with 0 indicating no correlation and 1 indicating an exact match between the patterns of frequency change. The location j giving the highest DLAC value indicates the predicted damage location.

7.3.2 Direct Mode Shape Comparison

Measurements of the mode shape of a civil engineering structure require sufficient spatial sensor resolution. Mode shape changes are found to be rather sensitive to damage in a structure, in particular, when higher order modes are adopted. Mode shape changes have the capability of directly providing damage location information (Carden and Fanning 2004). The commonly used methods to compare two sets of mode shapes include the modal assurance criterion (MAC) and the coordinate modal assurance criterion (COMAC).

The MAC can be used to detect the existence and the location of structural faults (Wolff and Richardson 1989), defined here as

$$MAC(\phi_i^u, \phi_j^d) = \frac{|\phi_i^{uT} \phi_j^d|^2}{|\phi_i^{uT} \phi_i^u| |\phi_j^{dT} \phi_j^d|} \quad (7.6)$$

in which ϕ_i^u is the i th mode shape of the structure before damage, and ϕ_j^d is the j th mode shape of the structure after damage. The superscripts u and d denote the undamaged and damaged states, respectively.

The MAC is a scale quantity ranging from 0 to 1, representing the degree of correlation between two sets of mode shapes: 1 for perfectly correlated and 0 for completely uncorrelated. Low MAC values close to zero indicate possible damage. This approach is simple and straightforward, but is based on the intuitive assumption that change in mode shapes at the DOFs near a damaged location are relatively larger than others far away from the damaged location. This assumption, however, is not necessarily true. Sufficient sensors must be used to ensure that the MAC value is a meaningful indicator of the mode shape correlation.

The COMAC is a pointwise measure of the difference between two sets of mode shapes with a value ranging from 0 to 1. The COMAC spatially correlates two sets of mode shapes and identifies the DOFs with maximum disagreement between the mode pair (Lieven and Ewins 1988). When applied to damage localisation, the COMAC can be defined as

$$COMAC(j) = \frac{\sum_{i=1}^{Nm} [\phi_i^u(j) \phi_i^d(j)]^2}{\sum_{i=1}^{Nm} [\phi_i^u(j) \phi_i^u(j)] \sum_{i=1}^{Nm} [\phi_i^d(j) \phi_i^d(j)]} \quad (7.7)$$

where $\phi_i^u(j)$ and $\phi_i^d(j)$ are the i th mode shape of the undamaged and damaged structure at location j , respectively, and Nm is the number of selected modes. The DOF with low value of the COMAC indicates a possible damage location.

The enhanced coordinate modal assurance criterion (ECOMAC) is another index used to check the spatial correlation between two sets of mode shapes (Hunt 1992). The ECOMAC is defined as

$$ECOMAC(j) = \frac{1}{2Nm} \sum_{i=1}^{Nm} |\phi_i^u(j) - \phi_i^d(j)| \quad (7.8)$$

A high value of the ECOMAC indicates very little correlation between the mode pair. A low value of ECOMAC indicates very high correlation. Therefore, the degree of freedom with a high ECOMAC value indicates the possible damage location, when the ECOMAC is applied to two sets of mode shapes in the undamaged and damaged states.

7.3.3 Mode Shape Curvature

The use of mode shape curvatures in damage detection is based on the assumption that the changes in the curvatures of mode shapes are highly localised in the damaged region. This mode shape curvature is often calculated from the displacement mode shapes using a central difference approximation. The change in mode shape curvature then can be used to detect and locate damage in a structure (Pandey et al. 1991). For the i th mode, the mode shape curvatures of the undamaged and damaged structure at location j are defined, respectively, as

$$C_i^u(j) = \left[\phi_i^u(j+1) - 2\phi_i^u(j) + \phi_i^u(j-1) \right] / \Delta l^2 \quad (7.9a)$$

$$C_i^d(j) = \left[\phi_i^d(j+1) - 2\phi_i^d(j) + \phi_i^d(j-1) \right] / \Delta l^2 \quad (7.9b)$$

where $\phi_i(j-1)$, $\phi_i(j)$ and $\phi_i(j+1)$ are the mode shape values of the i th mode at the $(j-1)$ th, j th and $(j+1)$ th nodes, respectively, and Δl is the distance between two nodes.

The modal curvature change rate index for the i th mode is now defined as

$$\beta_i(j) = \frac{|C_i^u(j) - C_i^d(j)|}{\sum_j |C_i^u(j) - C_i^d(j)|} \quad (7.10)$$

When a total number of Nm modes are used for damage detection, the mode shape curvature (MSC) damage index is defined as the average of the mode curvature change rates for the total Nm modes:

$$MSC(j) = \frac{1}{Nm} \sum_{i=1}^{Nm} \beta_i(j) \quad (7.11)$$

The changes in the curvature of mode shapes are localised near the damaged zone. Such changes are much smaller outside the damaged region, whereas the changes in the displacements of mode shapes are not localised to the damaged zone. This characteristic of the curvature of mode shapes is useful in locating the region of damage. The change in the mode shape curvature increases with increasing size of the damage. Mode shapes and their

derivatives have been widely used for structural damage identification with many successful applications. The methods based on mode shapes and their derivatives are more sensitive to damage than those based on change in natural frequencies. However, the problem of measuring mode shapes for damage detection is the requirement of a complicated test procedure for sufficient spatial measurement resolution. The required measurement resolution could be achieved by the use of a scanning laser Doppler vibrometer. This equipment allows for a dense grid of measurements.

7.3.4 Damping

The introduction of damage in a structure will usually cause changes in the damping capacity of the structure. From the experiments of a beam by Rytter (1993), the modal damping ratios of the cantilevers are extremely sensitive to even small cracks. However, the changes in damping are highly dependent on several additional factors, such as temperature, load history and treatment during manufacturing. Such factors make damping an impracticable candidate to be used to detect damage in a structure. In addition, the possibility of using modal damping ratios for damage detection in connection with the performance of vibration monitoring on bridges was studied by Alampalli et al. (1992). Repetitive tests performed on a model of a composite bridge deck show that the modal damping ratios are very sensitive to environmental conditions, such as temperature. This clearly makes it difficult to use modal damping ratios for damage detection.

7.3.5 Frequency Response Function Curvature

The change of a frequency response function (FRF) caused by structural damage can be used for damage detection. Significant slope and curvature differences are found whenever a crack is introduced, especially near the natural frequency range. The FRF based damage identification methods include FRF based mode shape, FRF based mode shape curvature and FRF based damage index (Montalvão et al. 2006). These methods are equivalent to the mode shape detection methods, but using FRFs instead of mode shapes.

The FRF curvature method is based only on the measured data, without requiring any modal extraction. This method includes all frequencies in the measurement range and not just the modal frequencies. The method uses FRF data at different locations along the structure (Maia et al. 2003). For the chosen frequency range ω , the absolute difference in the FRF curvatures $\Delta h_{ij}''$ between the damaged and undamaged structure is defined as

$$\Delta h_{ij}'' = \sum_{\omega} |h_{ij}^{d''} - h_{ij}^{u''}| \quad (7.12)$$

where h_{ij}^d and h_{ij}^u are the FRFs at location i for an applied force at place j of the damaged and undamaged structure, respectively. This method generally performs well, although false damage indications remain a problem. Improvements could be made in various ways, such as in the interpolation process, in the method of calculating the maximum occurrences, and in

applying statistics to the results.

From the studies on the FRF curvature method, some useful conclusions are made by Sampaio et al. (1999) and summarised by Montalvão et al. (2006). This method works well for a range before the first antiresonance or resonance frequency. This is because the difference between the curvatures of the damaged and undamaged structure becomes less significant for wider frequency ranges. This is the case when the curvature difference is compared with the amplitude difference arising from the resonances' frequency shift caused by the loss of stiffness. The method is not very sensitive to noise, and the position of the exciting force may not have a significant influence. When compared with the mode shape curvature method, the FRF curvature method has better overall performance, although the mode shape curvature method produces better results for higherorder modes.

Antiresonance frequencies can also be used for damage detection and localisation. When the resonance peaks are defined by the system poles, the antiresonances are different from each individual FRF. The sensitivities of the antiresonances can be expressed by the sensitivities of natural frequencies and mode shapes (Mottershead 1998). These sensitivities are significantly influenced by the modes with frequencies closest to zero. The results from a cantilever model show that as the point of measurement gets closer to the location of the defect, fewer and fewer antiresonances are shifted from their original values until one gets to the location of the defect (Afolabi, 1987). At this location, all the antiresonances are exactly as they were in the undamaged state.

7.3.6 Modal Strain Energy

When a particular dynamic mode keeps a significant amount of strain energy in a particular structural load path, the modal data of the mode will be much more sensitive to changes in the load path. Changes in modal strain energy can therefore be utilised as a useful indicator for the damage identification. The modal strain energy distribution in the structural elements can be calculated using the measured mode shapes (Carrasco et al. 1997). The modal strain energy of the j th element with element stiffness matrix \mathbf{K}_j in the i th mode $\boldsymbol{\phi}_i$ is computed from

$$U_{ij} = \frac{1}{2} \boldsymbol{\phi}_i^T \mathbf{K}_j \boldsymbol{\phi}_i \quad (7.13)$$

The weighted difference in energy distribution between the undamaged and damaged structure is given by

$$\Delta \tilde{U}_{ij} = (U_{ij}^u - U_{ij}^d) U_{ij}^u \quad (7.14)$$

Implementation of the weighted modal strain energy has a potential to blur noise effects by assigning large weights to the sensitive elements and small weights to the insensitive elements. The weighted modal strain energy differences are then lumped into the connecting nodes of the elements to provide indications of the damage location. The identification results of the tested space truss structure show that this technique is able to locate the damage with significant

amount, but may be unable to detect the small damage.

The extent of damage in structural elements can be estimated by an element damage factor, defined as

$$\alpha_{ij} = \frac{U_{ij}^u}{U_{ij}^d} - 1 = \frac{\phi_i^{uT} \mathbf{K}_j \phi_i^u}{\phi_i^{dT} \mathbf{K}_j \phi_i^d} - 1 \quad (7.15)$$

where α_{ij} is a damage factor that estimates the damage for the j th element using the i th mode. This factor may take values ranging from -1 to infinity, where negative values indicate potential damage. The formulation gives a meaningful indication, only when the elements have some strain energy content in the undamaged and damaged states.

In addition to the measured mode shapes, timedomain responses can be adopted directly for identifying the location of damage in a structure. When timedomain responses are obtained in a set of measurement points, the mean strain energy for a specified time interval is calculated for each individual structural element (Choi and Stubbs 2004). The obtained mean strain energy is then used to construct a damage index representing the ratio of the stiffness parameters of the undamaged and damaged structure:

$$\beta_j = \frac{\sum_{i=1}^{Nt} \mathbf{V}_i^{uT} \mathbf{K} \mathbf{V}_i^u}{\sum_{i=1}^{Nt} \mathbf{V}_i^{dT} \mathbf{K} \mathbf{V}_i^d} \cdot \frac{\left(\sum_{i=1}^{Nt} \mathbf{V}_i^{dT} C_j \mathbf{V}_i^d + \sum_{i=1}^{Nt} \mathbf{V}_i^{dT} \mathbf{K} \mathbf{V}_i^d \right)}{\left(\sum_{i=1}^{Nt} \mathbf{V}_i^{uT} C_j \mathbf{V}_i^u + \sum_{i=1}^{Nt} \mathbf{V}_i^{uT} \mathbf{K} \mathbf{V}_i^u \right)} \quad (7.16)$$

in which β_j is the damage index for the j th element, Nt is the total number of sampling points, \mathbf{V}_i^u and \mathbf{V}_i^d are the displacement configuration vectors at time t_i for the undamaged and damaged states, respectively, and C_j is the geometric portion of the contribution of the j th element to the global stiffness matrix \mathbf{K} . The defined damage index can identify the locations of damage in a structure by using a classification algorithm. The classification algorithm is based on the assumption that the normalised damage index is a random variable with a normal distribution. After the possible locations of damage are identified, the associated damage extent can be estimated. The quality of this damage identification method depends on the balance between lowering the significance level for damage localisation and increasing the number of false positives.

7.3.7 Example for Damage Localisation – a Suspension Bridge (II)

The Tsing Ma Bridge is a doubledeck suspension bridge in Hong Kong. A structural health monitoring system has been installed on the bridge, as described in [Section 2.3.5](#). The bridge carries two threelane carriageways on the upper deck and twin railway tracks and two single emergency road lanes on the lower deck (Ni et al. 2000). Structurally, it consists of about

20,000 components, as illustrated in [Figure 7.3](#), including the longitudinal trusses, Vierendeel cross frames, deck plates, plan bracings, rail waybeams, tower beams and columns, main cables, hangers, piers, saddles, anchorages and supporting bearings (Wang et al. 2000). A precise threedimensional finite element model of the Tsing Ma Bridge was developed for accurate damage simulation studies. In this finite element model, the spatial configuration of the original structure completely remains and the stiffness contribution of all individual structural components is independently described. Therefore, damage occurring in any structural component at the element level can be accurately simulated in the model.

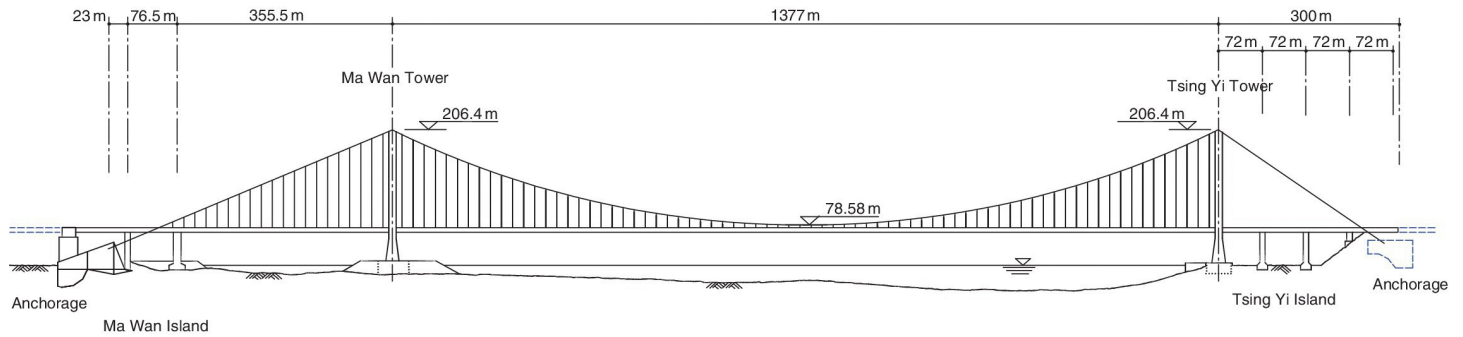


Figure 7.3 Elevation of Tsing Ma Bridge.

The finite element model is validated by using the measured modal data obtained from the on line monitoring system. [Table 7.2](#) gives a comparison between the measured and computed natural frequencies for the first four lateral, vertical and torsional modes, where the measurement data was monitored after the bridge was open for operation (Lau et al. 1999). The vibration modes of the bridge include global and local modes. Most global modes are threedimensional and have coupled components in three directions, especially the lateral bending and torsional modes.

Table 7.2 Comparison of measured and computed natural frequencies (Hz) of Tsing Ma Bridge.

Mode type	Mode order	Measured (Hz)	Computed (Hz)	Difference (%)
Predominantly lateral mode	1st	0.070	0.0686	-2.00
	2nd	0.170	0.1611	-5.24
	3rd	0.254	0.2546	0.24
	4th	0.301	0.2820	-6.34
Predominantly vertical mode	1st	0.114	0.1154	1.23
	2nd	0.133	0.1420	6.75
	3rd	0.187	0.1836	-1.82
	4th	0.249	0.2350	-5.62
Predominantly torsional mode	1st	0.270	0.2584	-4.30
	2nd	0.324	0.3014	-6.97
	3rd	0.486	0.4942	1.69
	4th	0.587	0.5660	-3.58

Three damage scenarios with a total of six cases are simulated, as listed in [Table 7.3](#), where x and z represent the longitudinal and lateral coordinates, respectively, with the origin in the middle of the main span. Scenario 1 simulates the damage of bearings between the Ma Wan tower and deck. Scenario 2 simulates the damage of deck members near the Ma Wan tower. Scenario 3 simulates the damage of hangers in the middle of the main span. Damage to structural elements is modelled by assuming a 98% reduction in member stiffness, but no change in mass. The ‘measured’ modal data for the damaged structure is then obtained from finite element dynamic analysis.

Table 7.3 Simulated damage cases of Tsing Ma Bridge.

Case No.	Damaged member(s)	Location
Case 1.1	one vertical bearing	$x = -688.5 \text{ m}, z = -13.0 \text{ m}$
Case 1.2	one side bearing	$x = -688.5 \text{ m}, z = -15.35 \text{ m}$
Case 2.1	one top chord	$x = -643.5 \sim -639.0 \text{ m}, z = -13.0 \text{ m}$
Case 2.2	one diagonal chord	$x = -643.5 \sim -639.0 \text{ m}, z = -13.0 \text{ m}$
Case 2.3	one bottom chord	$x = -643.5 \sim -639.0 \text{ m}, z = -13.0 \text{ m}$
Case 3	two hangers	$x = \pm 9.0 \text{ m}, z = -18.0 \text{ m}$

The main span deck of the bridge is divided into 76 segments. It is assumed that there is only one measurement point in a segment, thus a total of 76 DOF coordinate measurements are

available for the damage identification. In order to evaluate the influence of the number of measured modes on the damage identification performance, the modal parameters of the first three modes, first five modes and first eight modes are used for the damage identification simulation studies, respectively. To investigate the sensitivity of natural frequencies to the simulated damage scenarios, the percentage difference of natural frequencies (PDNF) between the intact and damaged structure for the i th mode is defined as

$$PDNF_i = (\omega_i^d - \omega_i^u) / \omega_i^u \quad (7.17)$$

where ω_i^u and ω_i^d are the natural frequencies of the i th mode of the undamaged and damaged structure, respectively.

The values of the percentage difference of natural frequencies for damage Cases 1.1 and 1.2 are calculated and shown in [Figure 7.4](#) (Wang et al. 2000). From the results, the frequency change patterns for Cases 1.1 and 1.2 are completely different, although the damage locations of these two cases are the same. Therefore, frequency change patterns depend on damage types in the structure, and can be used for the damage classification.

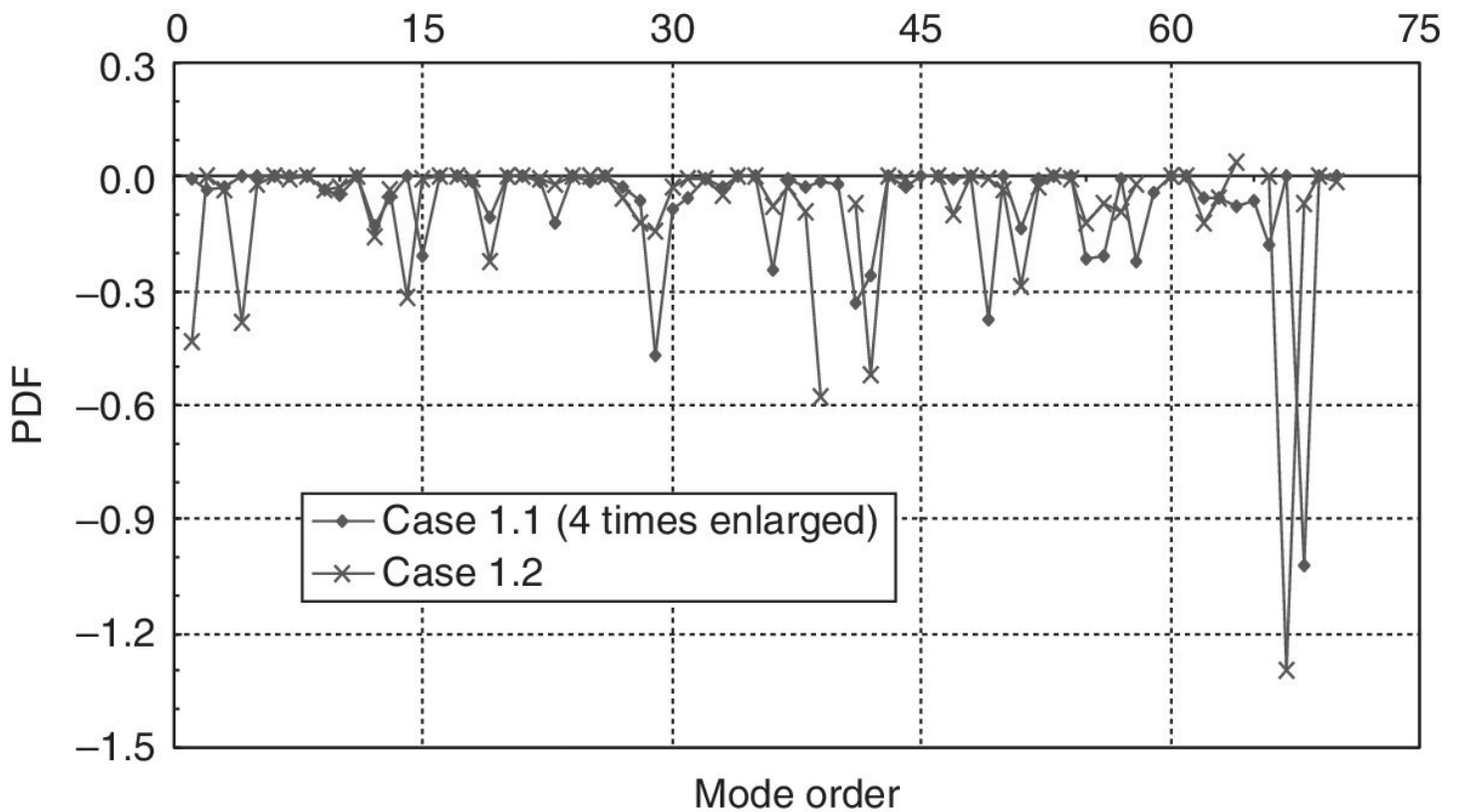


Figure 7.4 Percentage difference of natural frequencies (PDNF) for simulated damage Cases 1.1 and 1.2.

The coordinate modal assurance criterion (COMAC) method is adopted for detecting and localising the assumed damage scenarios. The COMAC spatially correlates two sets of simulated damaged mode shapes, and identifies the degree(s) of freedom with maximum disagreement between the mode pair. The damage location identification results from the

COMAC method are given in [Table 7.4](#) (Wang et al. 2001). From the results, damage Cases 2.1, 2.2 and 2.3 can be identified, where one chord is assumed to be damaged, when three, five or eight simulated damaged modes are used in the calculations. Damage Cases 1.1, 1.2 and 3, where bearing or hangers are assumed to be damaged, cannot be detected from the COMAC method.

Table 7.4 Results of damage location identification using the COMAC method.

Case No.	True damaged segment(s)	Identified damage segment(s)		
		3 modes	5 modes	8 modes
Case 1.1	1	0	0	0
Case 1.2	1	0	0	0
Case 2.1	between 2 & 3	2	2	2
Case 2.2	between 2 & 3	3	3	3
Case 2.3	between 2 & 3	3	3	3
Case 3	38, 39	0	0	0

Note: '0' denotes no damage identified.

The enhanced coordinate modal assurance criteria (ECOMAC) method is an alternative index used to check the spatial correlation between two sets of simulated damaged mode shapes. When the ECOMAC is applied to two sets of mode shapes obtained in undamaged and damaged states, respectively, the degree of freedom with a high ECOMAC value indicates the damage location. [Table 7.5](#) shows the damage location identification results from the ECOMAC method. Similarly, damage Cases 2.1, 2.2 and 2.3 can be identified from the ECOMAC method, while damage Cases 1.1, 1.2 and 3 cannot be detected.

Table 7.5 Results of damage location identification using the ECOMAC method.

Case No.	True damaged segment(s)	Identified damage segment(s)		
		3 modes	5 modes	8 modes
Case 1.1	1	0	0	0
Case 1.2	1	0	0	0
Case 2.1	between 2 & 3	3	3	3
Case 2.2	between 2 & 3	3	3	3
Case 2.3	between 2 & 3	3	3	3
Case 3	38, 39	0	0	0

Note: '0' denotes no damage identified.

The change in mode shape curvature (MSC) is now used to locate the assumed damage scenarios in the structure. [Table 7.6](#) lists the damage location identification results from the MSC method. It is found that the MSC damage index performs better than the COMAC and

ECOMAC indices. All the damage cases are detected. The damage locations are correctly identified or identified with false positives. [Figure 7.5](#) shows the diagram of the MSC value versus segment number for damage Case 2.1 by use of the first three simulated damaged modes (Wang et al. 2001). It is obvious that a significant MSC value exists at segment 3, indicating correctly the damage location for the assumed damage Case 2.1.

Table 7.6 Results of damage location identification using the mode shape curvature (MSC) method.

Case No.	True damaged segment(s)	Identified damage segment(s)		
		3 modes	5 modes	8 modes
Case 1.1	1	1	1	1
Case 1.2	1	1	1	1
Case 2.1	between 2 & 3	3	3	3
Case 2.2	between 2 & 3	2, 3	2, 3	2, 3
Case 2.3	between 2 & 3	3	3	3
Case 3	38, 39	37, 38, 39, 40	37, 38, 39, 40	37, 38, 39, 40

Note: '0' denotes no damage identified.

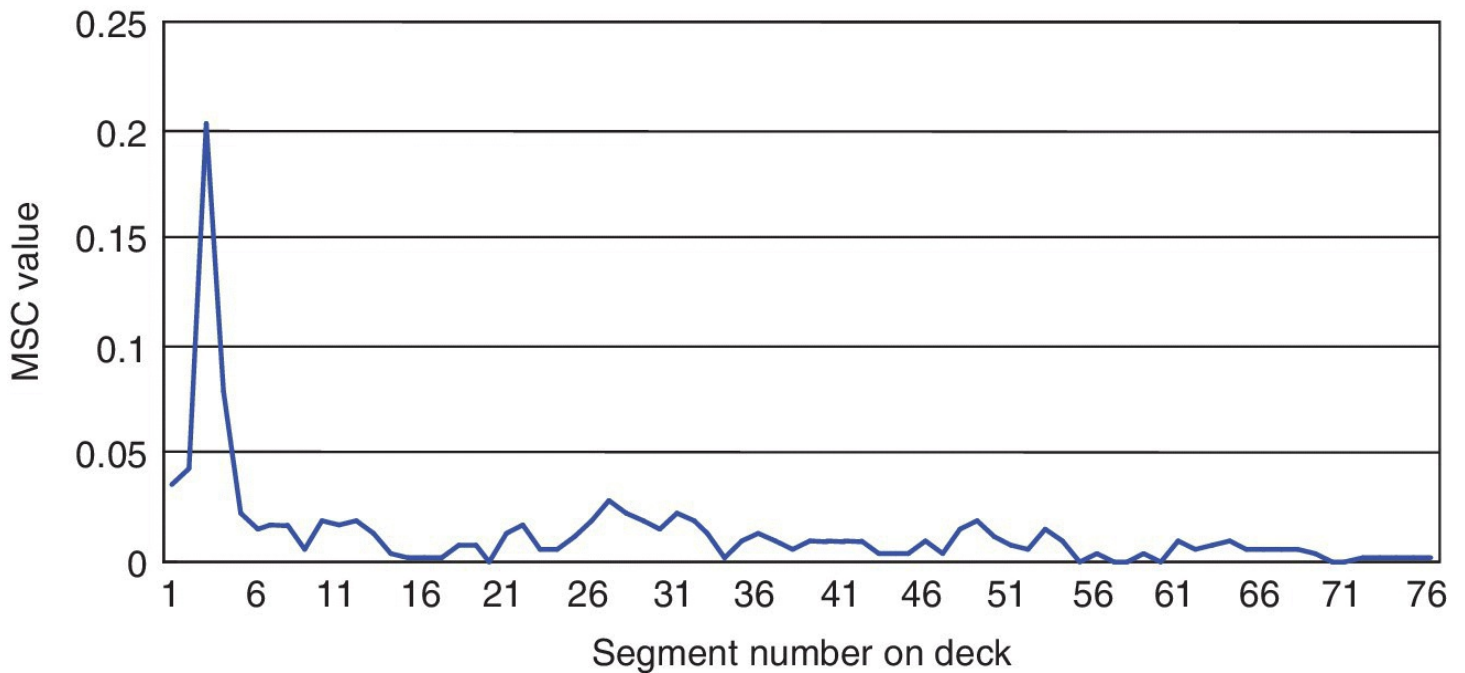


Figure 7.5 Mode shape curvature (MSC) values for damage Case 2.1 using 3 damaged modes.

7.4 Methods Using Change of Structural Parameters

Damage identification methods using vibration measurements are based on the fact that damage in a structure causes a reduction in stiffness or an increase in flexibility, leading to change in modal parameters of the damaged structure. Structural parameters such as stiffness, flexibility

and strain energy can be estimated by using modal measurements such as natural frequencies, mode shapes and modal strain (DCSE 1998a). From this relationship, structural damage can be identified from the change of structural parameters.

7.4.1 Flexibility Matrix

Compared with estimating the change in stiffness matrix, it may be more straightforward to estimate the change in flexibility matrix. The method based on the flexibility matrix does not require the development of an analytical model of the structure under investigation. The identification of damage in a structure is performed directly using the experimental modal data (Pandey and Biswas 1994). From the modal data, the flexibility matrix \mathbf{F} is defined as

$$\mathbf{F} = \mathbf{\Phi} \mathbf{\Lambda}^{-1} \mathbf{\Phi}^T = \sum_{i=1}^N \frac{1}{\omega_i^2} \boldsymbol{\phi}_i \boldsymbol{\phi}_i^T \quad (7.18)$$

where $\mathbf{\Phi}$ is the mass normalised mode shape matrix containing $\boldsymbol{\phi}_i$ and $\mathbf{\Lambda}$ is the eigenvalue diagonal matrix containing frequencies $\lambda_i = \omega_i^2$. The modal contribution to the stiffness matrix increases as the frequency increases. To obtain an accurate estimate of the stiffness experimentally, the high frequency modes have to be measured. By contrast, the modal contribution to the flexibility matrix decreases as the frequency increases, that is, the flexibility matrix converges rapidly with increasing values of frequency. From a few of the lower frequency modes, a good estimate of the flexibility matrix can be made.

Damage in a structure reduces the stiffness of the structure. Since flexibility is the inverse of stiffness, reduction of the stiffness should increase the flexibility of the structure. If the modal parameters of the structure are measured at both intact and damaged states, the flexibility matrix \mathbf{F} for the two states can be obtained. Each column of the flexibility matrix \mathbf{F} represents a set of nodal displacements due to a unit force at one of the DOFs. Change in the flexibility matrix $\Delta\mathbf{F}$ can be obtained from

$$\Delta\mathbf{F} = \mathbf{F}^u - \mathbf{F}^d \quad (7.19)$$

where \mathbf{F}^u and \mathbf{F}^d are the flexibility matrices for the undamaged and damaged states, respectively. If only the first Nm modes are measured, the undamaged and damaged flexibility matrices can be estimated, respectively, from

$$\mathbf{F}^u = \sum_{i=1}^{Nm} \frac{1}{\omega_i^{u^2}} \boldsymbol{\phi}_i^u \boldsymbol{\phi}_i^{u^T}, \quad \mathbf{F}^d = \sum_{i=1}^{Nm} \frac{1}{\omega_i^{d^2}} \boldsymbol{\phi}_i^d \boldsymbol{\phi}_i^{d^T} \quad (7.20)$$

For each DOF j , let $\delta \tilde{f}_j$ be the maximum absolute value of the elements in the j th column of $\Delta\mathbf{F}$ with entries δf_{ij} :

$$\delta \tilde{f}_j = \max_i |\delta f_{ij}| = \max_i |f_{ij}^u - f_{ij}^d| \quad (7.21)$$

To detect and locate damage in a structure, the quantity $\delta \tilde{f}_j$ is used as a measure of the change of flexibility for each measurement location. Similar to the mode shape curvature method, the flexibility matrix method does not require an analytical model in the damage identification process. However, the measured mode shapes used in calculations of flexibility matrix must be mass normalised, which means that the mass matrix must be known. Furthermore, when the mode shapes are incomplete with limited readings at DOFs, the mass needs to be lumped only along the measured DOFs, or the mass matrix must be reduced to a size same as the number of the measured DOFs. Model reduction methods such as the Guyan static method, as discussed in [Section 5.6.1](#), may be used for the model reduction.

Experimental verification of the flexibility matrix method for detecting and locating damage was carried out by Pandey and Biswas (1995). Three wideflange steel beams were tested in the laboratory. Damage was created by cutting through the beam using a saw. Modal tests were undertaken to obtain the natural frequencies and mode shapes for both the intact and damaged beam. The measured natural frequencies and mode shapes of the lowest three modes were used in evaluating the flexibility matrix change. Different damage cases were examined. To locate damage limited to the flange of the beam, it was found that measurements taken in the transverse direction are more sensitive than those taken in the vertical direction. From the numerical studies for a bridge girder (Humar et al. 2006), the flexibility matrix method is not always successful, although the method can identify the location of damage in some cases, particularly when damage is located at one site.

On the basis of the change of flexibility matrix, an approach using the damage locating vector (DLV) is proposed by Bernal (2002). The DLV approach is a technique for mapping changes in flexibility to the spatial distribution of damage. Its principle is based on the fact that the null space of the change in flexibility provides vectors leading to stress fields with zero over the damaged site, when treated as loads on the structure. The main idea is to calculate a set of load vectors \mathbf{L} , and the vectors have properties of inducing stress fields whose magnitude is identically zero over the damaged elements. The null space of the change in flexibility contains vectors that lead to identical displacements at the measured coordinates in the undamaged and damaged states. By using the flexibility matrices in the undamaged and damaged states, the identical displacement condition is expressed as

$$(\mathbf{F}^u - \mathbf{F}^d)\mathbf{L} = \Delta\mathbf{F}\mathbf{L} = \mathbf{0} \quad (7.22)$$

This formulation indicates that the load vector \mathbf{L} generates identical displacements, when applied to the undamaged and damaged structure:

$$\mathbf{F}^u\mathbf{L} = \mathbf{F}^d\mathbf{L} \quad (7.23)$$

Although differences exist at local elements in the undamaged and damaged states due to damage, identical displacements for the two states can be obtained by choosing a specific load vector. The DLV localisation is performed by calculating the null space of $\Delta\mathbf{F}$, treating the obtained vectors as static loads on the structure, and then identifying the damage as the

intersection of the regions of zero stress. In practice, the null space and the zero stress region should be defined using a small value in the presence of approximations and truncations. When \mathbf{F}^u and \mathbf{F}^d are rank deficient and their null space have a nonzero intersection, the load vectors \mathbf{L} are not damage locating vectors and then damage cannot be identified (Bernal 2002). A sufficient condition for rank deficiency is that the number of identified modes is smaller than the number of sensors adopted for the test.

7.4.2 Strain Energy Based Damage Index

For beam type structures, a damage index is proposed in the studies by Stubbs et al. (1995) and Cornwell et al. (1999), on the basis of the comparison of modal strain energy before and after damage. Consider a linear elastic beam with NE elements. Damage in the beam causes reduction of the flexural rigidity at the damage site. Information about the lowest Nm modes is available for both the undamaged and damaged structure. To determine mode shape amplitudes at locations between sensors, the modes shapes can be interpolated with a cubic polynomial. Modal curvatures can then be calculated by the measured displacement mode shapes, as discussed in [Section 7.3.3](#). The modal strain energy of a conventional beam associated with the i th mode shape is defined as

$$U_i = \frac{1}{2} \int_l (EI) [\phi_i''(x)]^2 dx \quad (7.24)$$

where EI is the flexural rigidity, l is the length of the beam, and $\phi_i''(x)$ represents modal curvature of the i th mode. The contribution of the j th element with length of δl to the modal strain energy is calculated by

$$U_{ij} = \frac{1}{2} \int_{\delta l} (EI)_j [\phi_i''(x)]^2 dx \quad (7.25)$$

The fraction of modal strain energy contributed by the j th element is

$$F_{ij} = \frac{U_{ij}}{U_i} = \frac{\int_{\delta l} (EI)_j [\phi_i''(x)]^2 dx}{\int_l (EI) [\phi_i''(x)]^2 dx} \quad (7.26)$$

Assuming that the elements are small enough, and flexural rigidity is constant on the elements of the beam, gives

$$F_{ij} = \frac{(EI)_j}{(EI)} \cdot \frac{\int_l [\phi_i''(x)]^2 dx}{\int_l [\phi_i''(x)]^2 dx} = \frac{(EI)_j}{(EI)} f_{ij} \quad (7.27)$$

where coefficient f_{ij} is related to the mode shape curvature. This formulation is then applied to both the undamaged and damaged structure. Assume that only the j th element is damaged, the flexural rigidity over the beam is constant and remains unchanged after damage. Thus, the fractions of modal strain energy are very close to each other before and after damage, i.e.

$F_{ij}^u \approx F_{ij}^d$, leading to

$$\beta_{ij} = \frac{(EI)_j^u}{(EI)_j^d} = \frac{f_{ij}^d}{f_{ij}^u} \quad (7.28)$$

The quantity β_{ij} is the strain energy based damage index associated with the j th element in the i th mode. The damage index increases as the flexural rigidity decreases due to damage. To avoid potential problems due to very small values of the denominator, the definition of the strain energy based damage indicator is revised as

$$\beta_{ij} = \frac{(f_{ij}^d + 1)}{(f_{ij}^u + 1)} \quad (7.29)$$

In the case with a total of Nm modes available, the definition of the strain energy based damage index for the j th element becomes

$$\beta_j = \frac{\sum_{i=1}^{Nm} f_{ij}^d + 1}{\sum_{i=1}^{Nm} f_{ij}^u + 1} \quad (7.30)$$

Statistical methods are then used to examine changes in this index and to associate these changes with possible damage locations. A normal distribution is fitted to the damage indices, and values falling two or more standard deviations from the mean are assumed to be the most likely location of damage (Worden and Friswell 2009). If the statistics are estimated from the values of the damage index on the damaged structure, the threshold is equivalent to using an inclusive discordancy measure to detect outliers of the index.

The strain energy based damage index method discussed above for a beam can be extended to general structure types. The total strain energy of a structure in the i th mode, by using [Equation \(6.1\)](#), is calculated from

$$\tilde{U}_i = \phi_i^T \mathbf{K} \phi_i = \sum_{j=1}^{NE} \phi_i^T \mathbf{K}_j \phi_i \quad (7.31)$$

where \mathbf{K}_j is the element stiffness matrix of the j th element. Similarly, the strain energy of the j th element in the i th mode is obtained from

$$\tilde{U}_{ij} = \phi_i^T \mathbf{K}_j \phi_i \quad (7.32)$$

Thus, the fraction of modal strain energy contributed by the j th element is written as

$$\tilde{F}_{ij} = \frac{\tilde{U}_{ij}}{\tilde{U}_i} = \frac{\phi_i^T \mathbf{K}_j \phi_i}{\phi_i^T \mathbf{K} \phi_i} \quad (7.33)$$

The j th element stiffness matrix for the undamaged and damaged structure can be expressed, respectively, as

$$\mathbf{K}_j^u = E_j^u \mathbf{K}_{j0}, \mathbf{K}_j^d = E_j^d \mathbf{K}_{j0} \quad (7.34)$$

where the scalars E_j^u and E_j^d are parameters representing the material stiffness properties of the j th undamaged and damaged element of the structure, and the matrix \mathbf{K}_{j0} involves only geometric quantities. Again, by assuming that the fraction of modal strain energy before damage is very close to that after damage, i.e. $F_{ij}^u \approx F_{ij}^d$, the strain energy based damage index is now defined as

$$\beta_{ij} = \frac{E_j^u}{E_j^d} = \frac{\phi_i^{d^T} \mathbf{K}_{j0} \phi_i^d \tilde{U}_i^u}{\phi_i^{u^T} \mathbf{K}_{j0} \phi_i^u \tilde{U}_i^d} = \frac{f_{ij}^d}{f_{ij}^u} \quad (7.35)$$

in which coefficients f_{ij}^u and f_{ij}^d are defined, respectively, as

$$f_{ij}^u = (\phi_i^{u^T} \mathbf{K}_{j0} \phi_i^u) / \tilde{U}_i^u, f_{ij}^d = (\phi_i^{d^T} \mathbf{K}_{j0} \phi_i^d) / \tilde{U}_i^d \quad (7.36)$$

The strain energy based damage index for a general structure type is then very similar to the damage index for a beam type structure, given in [Equation \(7.28\)](#).

7.4.3 Modal StrainBased Damage Index

Strain measurements can be directly adopted for damage localisation, as discussed by Serna and Stubbs (1996). With the development of fibre optics, it will be economically feasible to instrument structures with fibre optical strain gauges to collect modal strain measurements. Considering a linear, undamaged, skeletal structure with total NE elements, the modal strain energy of the j th element in the i th mode is defined as

$$U_{ij} = E_j \varepsilon_{ij}^2 V_j \quad (7.37)$$

where E_j and V_j are elastic modulus and volume of the j th element, respectively, and ε_{ij} is the modal strain of the j th element in the i th mode. The total strain energy for total NE elements in the i th mode is given by

$$U_i = \sum_{j=1}^{NE} E_j \varepsilon_{ij}^2 V_j \quad (7.38)$$

The fraction of strain energy contributed by the j th element in the i th mode is defined as

$$F_{ij} = \frac{U_{ij}}{U_i} = \frac{E_j \varepsilon_{ij}^2 V_j}{\sum_{j=1}^{NE} E_j \varepsilon_{ij}^2 V_j} \quad (7.39)$$

From this formulation, the fractions of strain energy for the undamaged and damaged structure are then calculated by using the undamaged and damaged modal strain measurements, respectively. The undamaged and damaged fractions of strain energy, F_{ij}^u and F_{ij}^d , have the relationship

$$F_{ij}^d = F_{ij}^u + dF_{ij} \quad (7.40)$$

where dF_{ij} is associated with the change in the fraction of strain energy of the j th member in the i th mode. Assuming that the structure is damaged at a single location j and the resulting change in F_{ij} is only a function of E_j , a firstorder approximation of dF_{ij} can be obtained from

$$dF_{ij} = \frac{E_j^u - E_j^d}{E_j^u} F_{ij}^u \quad (7.41)$$

By using [Equations \(7.39\)](#) and [\(7.41\)](#) and from [Equation \(7.40\)](#), the modal strainbased damage indicator β_{ij} at the j th element in the i th mode is defined as

$$\beta_{ij} = \frac{E_j^d}{E_j^u} = \frac{1}{2} \frac{(\varepsilon_{ij}^d)^2}{(\varepsilon_{ij}^u)^2} \cdot \frac{U_i^u}{U_i^d} + \frac{1}{2} \quad (7.42)$$

Here again, to avoid possible problems due to nearzero values of the denominator, the definition of the modal strainbased damage indicator is redefined as

$$\beta_{ij} = \frac{((\varepsilon_{ij}^d)^2 + 1)}{((\varepsilon_{ij}^u)^2 + 1)} \quad (7.43)$$

This formulation represents the change in stiffness property at a specific location in terms of measurable undamaged and damage modal strains. When several strain modes are available, the damage indicator β_{ij} is normalised for each mode by

$$z_{ij} = (\beta_{ij} - \mu_{\beta_{ij}}) / \sigma_{\beta_{ij}} \quad (7.44)$$

where $\mu_{\beta_{ij}}$ and $\sigma_{\beta_{ij}}$ are the mean and standard deviation of the sample values of the damage indicator. Damage location is then identified by looking at the magnitude of the normalised damage indicators for all elements. The effectiveness of this formulation is demonstrated on a numerical example of a twodimensional truss (Serna and Stubbs 1996).

7.4.4 Example for Damage Localisation – a Suspension Bridge (III)

The Tsing Ma Bridge discussed in [Section 7.3.7](#) is used again here to check the effectiveness of the damage identification methods based on change of structural parameters. Here, the flexibility matrix method and the strain energy based damage index method are utilised for the location identification of the simulated damage scenarios in the bridge, as summarised in [Table 7.3](#).

The flexibility matrices of the undamaged and damaged structure can be estimated by using only the natural frequencies and massnormalised mode shapes of a few loworder modes. [Table 7.7](#) shows the damage location identification results from the flexibility matrix method. It is found that the damage Cases 2.1, 2.2 and 2.3 can be identified, even when three simulated damaged modes are used. However, damage Cases 1.1, 1.2 Case 3 are difficult to detect except for Cases 1.1 and 1.2 using eight simulated damaged modes.

Table 7.7 Results of damage location identification using the flexibility matrix method.

Case No. True damagedsegment(s)		Identified damage segment(s)		
		3 modes	5 modes	8 modes
Case 1.1	1	0	0	1
Case 1.2	1	0	0	1
Case 2.1	between 2 & 3	2	2	2
Case 2.2	between 2 & 3	3	3	3
Case 2.3	between 2 & 3	3	3	3
Case 3	38, 39	0	0	0

Note: '0' denotes no damage identified.

The results of flexibility matrix index values for damage Case 1.2 are plotted in [Figure 7.6](#) using the first eight simulated damaged global mode shape measurements of the left frame (Wang et al. 2001). The true damage of Case 1.2 is at the left side of the deck. The flexibility matrix index values evaluated on the left frame correctly indicate the damage location, for

example at segment 1.

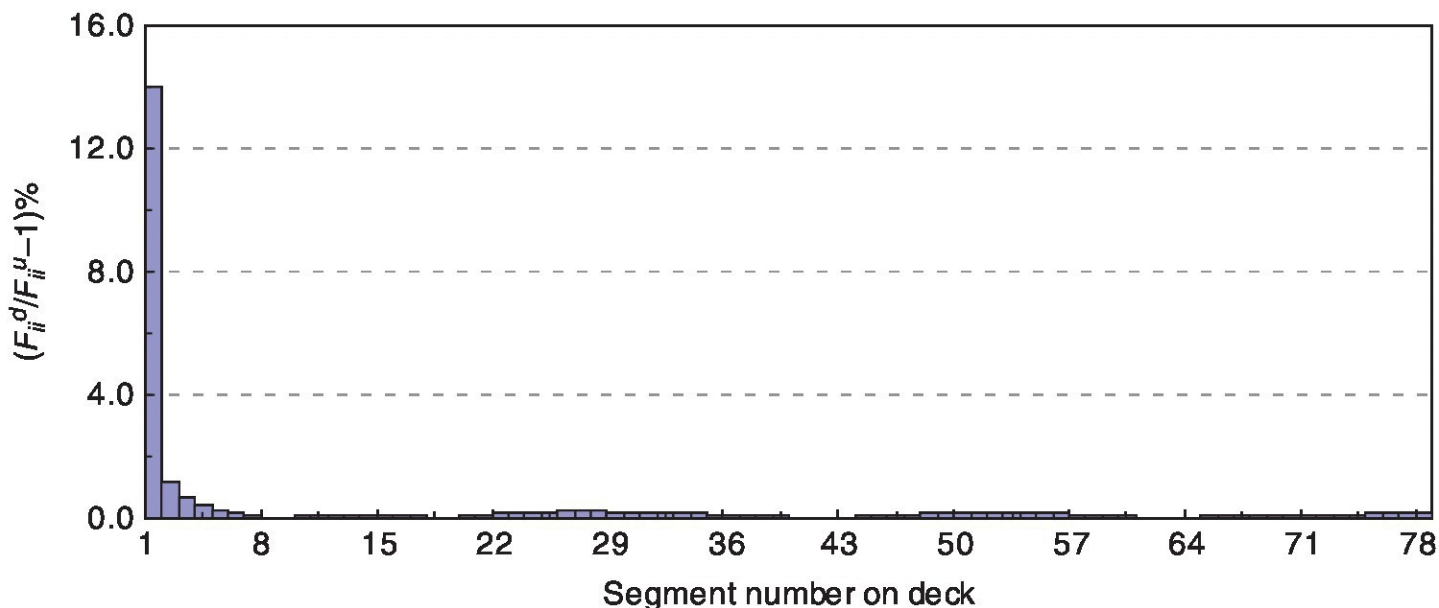


Figure 7.6 Flexibility coefficient index values at nodes on deck for damage Case 1.2.

Finally, the strain energy based damage index method is used for identifying the location of the assumed damage cases. [Table 7.8](#) summarises the damage location identification results from the strain energy based damage index. It is observed that this damage index method performs well for the damage identification of the all six assumed damage scenarios. All the damage locations are correctly identified or identified near the actual position(s). [Figure 7.7](#) shows the diagram of the strain energy based damage index value versus segment number for damage Case 2.1 by use of the first three simulated damaged modes. The results correctly indicate the damage location at the second segment.

Table 7.8 Results of damage location identification using the strain energy based damage index method.

Case No.	True damage segment(s)	Identified damage segment(s)		
		3 modes	5 modes	8 modes
Case 1.1	1	1	1	1
Case 1.2	1	1	1	1
Case 2.1	between 2 & 3	2	2	2
Case 2.2	between 2 & 3	2	2	2
Case 2.3	between 2 & 3	2	2	2
Case 3	38, 39	36, 37, 38, 39	36, 37, 38, 39	36, 37, 38, 39

Note: '0' denotes no damage identified.

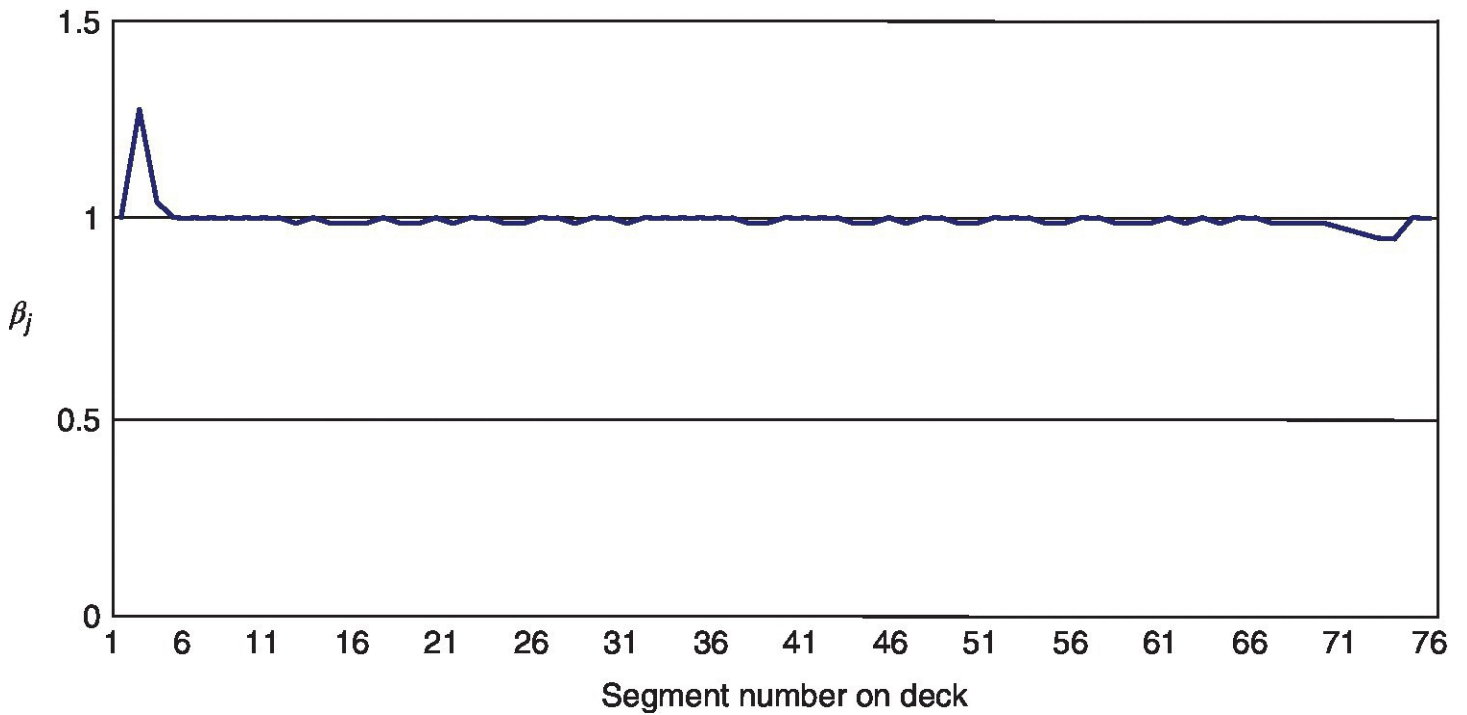


Figure 7.7 Values of the strain energy based damage index β_j for damage Case 2.1.

In order to evaluate various damage location identification methods, [Table 7.9](#) summarises their identification performance in application to the Tsing Ma Bridge. First three simulated damaged modes are used in calculations for damage location identification. From the results, the COMAC and ECOMAC methods are not suitable for damage localisation of this bridge. The mode shape curvature, flexibility matrix and strain energy based damage index methods are appropriate for the identification of damage on deck members. The mode shape curvature and strain energy based damage index methods are better at identifying the damage on bearings and hangers. The simulation studies also show that the mode shape curvature, flexibility matrix and strain energy based damage index methods perform well, even if only relatively sparse modal measurements are available.

Table 7.9 Comparison of different damage identification methods applied to Tsing Ma Bridge.

Method	Case 1.1	Case 1.2	Case 2.1	Case 2.2	Case 2.3	Case 3
COMAC						
ECOMAC						
Mode shape curvature						
Flexibility matrix						
Strain energy based damage index						

Damage located; Damage located with false positives; Damage not located.

7.5 Pattern Recognition Methods

The vibrationbased damage detection problem could be fundamentally one of pattern recognitions (Sohn et al. 2001, 2004). The pattern recognition methods are nonmodelbased damage detection methods and do not require the physical model of the structure concerned. Patterns are usually obtained through features from signal processing, and they are assumed to represent different damage conditions in damage detection. Many pattern recognition methods have been developed for indicating whether a structure is undamaged or damaged. Among these methods, the novelty detection algorithm is often used for detecting the occurrence of damage in a structure.

7.5.1 Stochastic Pattern Recognition

Statistical pattern recognition assigns the features obtained from signal processing to different classes using statistical density functions (Staszewski and Worden 2009). In general, the features extracted from measurements for damage detection are also random variables. Therefore, classifier design should be carried out within a statistical framework, such as statistical pattern recognition, which can consider situations that classes will sometimes overlap, that is, a given set of features may or may not detect damage. Statistical pattern recognition can provide critical information for decision making, that is, it can give a probability for damage diagnosis.

On the basis of the extracted features, the statistical modelling can be undertaken by either parametric estimation or nonparametric estimation. In parametric estimation, the statistical distribution of the features is assumed in advance, and the associated parameters of the assumed distribution are estimated from the given features. On the other hand, nonparametric estimation techniques do not apply unnecessary constraints to the data and leave the data to define its own distribution. The nonparametric estimation approach is more useful when a large amount of training data is available. The nonparametric approach may fail to estimate correctly the distribution of data when only a limited amount of data is available.

Statistical pattern recognition forms a part of machine learning. Machine learning theory deals with three main problems: classification, regression and density estimation. Machine learning algorithms can be classified as two major groups: unsupervised learning and supervised learning. Unsupervised learning involves characterising a set on the basis of measurements, while supervised learning requires examples of input and output data for an assumed relationship, so that associations might be learned, and errors might be corrected. These machine learning algorithms are useful tools for damage detection, since it is often impossible to acquire sufficient data covering the various possible damage states. In general, novelty detection can be undertaken in an unsupervised context.

Novelty detection involves the identification of any deviations in measured data, by comparing with data measured under normal operating conditions. In general, features derived from measurements on a structure in its undamaged state have a distribution with an associated mean and variance. If damage occurs in the structure, then there may be a change in the mean, the variance or both. Statistical process control provides a framework for monitoring the distribution of the features and for detecting new data that is inconsistent with the past, that is,

outlier analysis. If all other variables can be eliminated, then a change in the statistical distribution characteristics of the features will indicate damage in the structure (Carden and Fanning 2004). Statistical pattern recognition techniques do not require the construction of a correlated analytical model, which can be a timeconsuming and difficult task. These techniques are suitable for data sets obtained from ambient excitations, for example, traffic or wind loading on a bridge structure. However, statistical pattern recognition has a major disadvantage, probably limited to detection of damage, rather than location and quantification.

7.5.2 Novelty Detection

The object of novelty detection is to establish whether a new pattern differs from previously obtained patterns in some significant respect. This can be realised by using an auto associative memory neural network. An autoassociative network can be a multilayer feedforward perceptron with ‘bottleneck’ hidden layer(s). This network is trained to reproduce at the output layer, while the patterns are presented at the input layer. Thus, the output layer must have the same number of the input nodes. However, the input values will not be perfectly reconstructed in the output. Since the patterns are passed through hidden layers that have fewer nodes than the input layer, the network is forced to learn just the significant prevailing features of the patterns. The central hidden layer, acting as a bottleneck, generates an internal representation that compresses redundancies in the input pattern, while retaining important information to the output.

When the autoassociative network is used for anomaly detection or damage alarming, a series of measurement data of the healthy structure under normal conditions is required to train the network (DCSE 1998b). No information on the structural model is needed. After the network is trained, the input data presented on training is passed again into the trained network to yield an output data set. The difference between the input and output vectors is then measured using a form of distance function, called a novelty index. In the testing phase, a new series of measurement data obtained later from the same structure (damaged or undamaged) is passed into the above network to form a novelty index sequence. If this sequence deviates from the novelty index sequence of the training phase, the occurrence of damage is detected.

In the training phase, a series of measured modal data of the healthy (intact) structure, $\mathbf{z} = \{z_1 \ z_2 \ \dots \ z_M\}^T$, is used as input to the network. The output $\mathbf{y} = \{y_1 \ y_2 \ \dots \ y_M\}^T$ of the network is set as

$$y_i = (z_i - m_i)\kappa + m_i \quad \text{where } i = 1, 2, \dots, M \quad (7.45)$$

where κ is a positive constant and m_i is the mean of the i th element z_i of the input vector \mathbf{z} over the training data. It is worth noting that training the network needs only the measurement data of the healthy structure. After performing the training, the input pattern \mathbf{z} presented on training is fed again into the trained network to yield output pattern $\hat{\mathbf{y}}$, and the novelty index sequence for the training phase $\beta(\mathbf{y})$ is obtained in terms of the Euclidean norm as

$$\beta(\mathbf{y}) = \|\hat{\mathbf{y}} - \mathbf{y}\| \quad (7.46)$$

In the testing phase, a new series of modal data, $\mathbf{z}_t = \{z_{1t} z_{2t} \dots z_{Mt}\}^T$, is measured from the same structure (damaged or undamaged), and is then passed into the above trained network to yield output $\hat{\mathbf{y}}_t$. The corresponding novelty index for the testing set is then obtained by

$$\beta(\mathbf{y}_t) = \|\hat{\mathbf{y}}_t - \mathbf{y}_t\| \quad (7.47)$$

where $\mathbf{y}_t = \{y_{1t} y_{2t} \dots y_{Mt}\}^T$ is the vector with its i th element

$$y_{it} = (z_{it} - m_i)\kappa + m_i \quad (7.48)$$

If the testing novelty index sequence deviates from the training novelty index sequence, the occurrence of damage is flagged. If the two sequences are indistinguishable, no damage is signalled. In order to quantitatively determine whether damage occurs, a threshold δ_β is introduced. It is estimated from the training data and is defined as

$$\delta_\beta = \mu_\beta + 4\sigma_\beta \quad (7.49)$$

where μ_β and σ_β are the mean and standard deviation of the testing novelty index sequence over the training data, respectively.

7.5.3 Example for Damage Detection – a Suspension Bridge (IV)

The Tsing Ma Bridge, as described in [Section 2.3.5](#) and [Section 7.3.7](#), is used again for a case study on damage detection using the pattern recognition method. Here, the novelty detection algorithm is adopted for the numerical simulations of detecting the damage occurrence in the bridge (DCSE 1999). The neural network based novelty filtering technique is applied for the anomaly (cable tension reduction) detection of the Tsing Yi side span free cables. It is assumed that the true horizontal tension forces of the cables without tension reduction are 405.838×10^6 N. The natural frequencies of the cables corresponding to the true tension forces are computed from an accurate finite element method, by taking into account the cable bending stiffness and the sagextensibility. These computed frequencies can be considered as the deterministic measured modal data of the intact cables.

Due to the measurement noise and the structural uncertainty under ambient fluctuation (e.g. travelling of train and vehicle, wind attack and temperature influence), the measured modal data of a healthy structure under normal operating conditions varies from time to time within a certain threshold. The variation in measured natural frequencies usually follows a normal random distribution (Sohn and Law 1997). The measurement data with random disturbances is generated by adding to the true cable tension forces with a normally distributed random sequence with zero mean and 0.05 variance. [Figure 7.8](#) shows the corresponding ‘normal’ fluctuation of the tension force of the cable after corrupted with the random noise. The added noise corresponds to about $\pm 15\%$ maximum error. The natural frequencies of the first three in

plane and outofplane modes of the cables corresponding to the tension force sequences with 'normal' fluctuation are then computed. These sequences are considered as noise corrupted measurement data of the healthy cables to train an autoassociative network for anomaly detection.

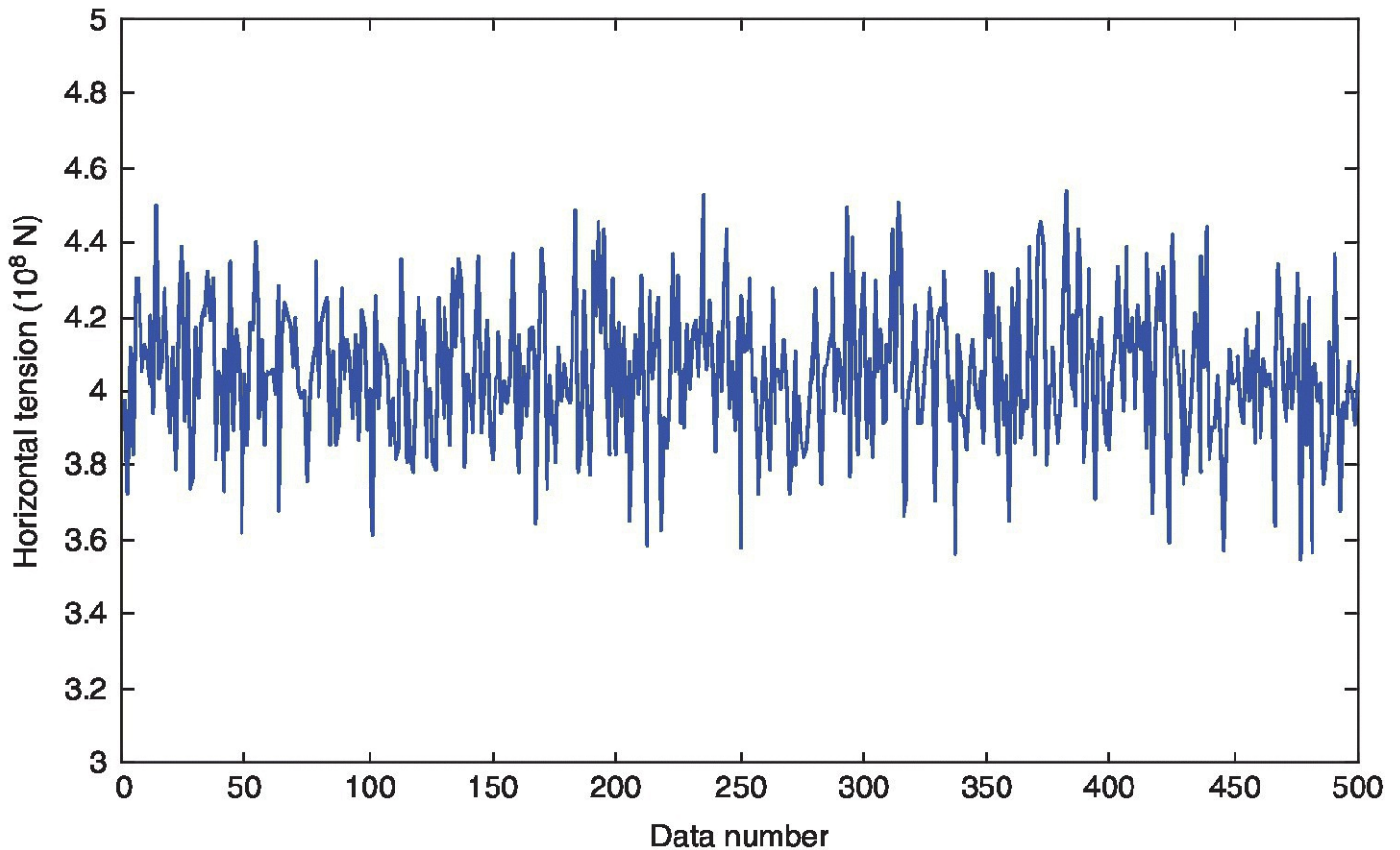


Figure 7.8 Simulated 'normal' fluctuation of tension force of the cable.

A fourlayer feedforward perceptron network with 'bottleneck' internal layers is designed as a novelty filter. This neural network has a node structure 128812. The activation functions are taken as the tangentsigmoid function between the second layer and the third layer. The linear transfer function is adopted for the activation functions between the input layer and the second layer as well as between the third layer and the output layer. The network is trained using the backpropagation algorithm.

The novelty index, similar to the definition in Worden (1997), is adopted for damage detection in the cable. The novelty index sequence in the training phase is plotted in [Figure 7.9](#), corresponding to the former 500 data (DCSE 1999). The fluctuation in the novelty index sequence for the training set reflects the measurement noise and uncertainty of ambient environments under normal conditions of the healthy cables. In order to test the ability of the trained network for anomaly detection, the cable tension is reduced by 5% to simulate an abnormal condition of the cable. By adding to the reduced tension force with a normally distributed random sequence with the same variance of 0.05, the noisecorrupted 'measured' natural frequency data of the cable corresponding to the abnormal condition is generated. The natural frequencies of the cable are obtained and each data sequence is taken with 300 items of

data.

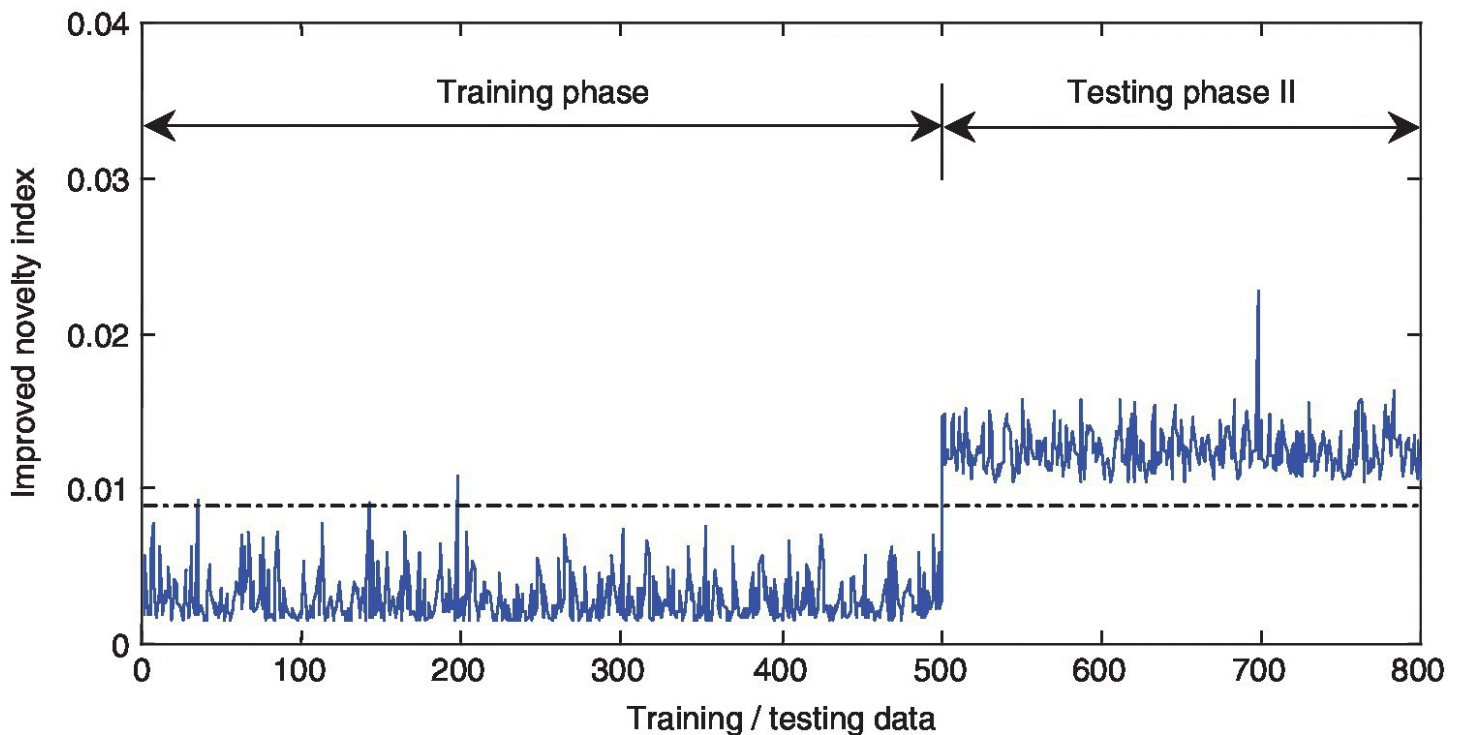


Figure 7.9 Novelty index evaluated on training and testing data with 5% reduction in cable tension.

The novelty index sequence in the testing phase associated with the abnormal state is also shown in [Figure 7.9](#), corresponding to the latter 300 data items. The dashed line represents the threshold ($\delta_{\beta} = 0.008979$). From the results, the novelty index values are greater than the predefined threshold. The novelty index sequence in the testing phase deviates significantly from the sequence in the training phase, clearly signalling the anomaly. Therefore, the novelty index is able to detect the anomaly caused by only 5% reduction in the cable tension, while the measured natural frequencies are corrupted with random noise of 0.05 variance.

7.6 Neural Network Techniques

Artificial neural networks (ANNs) were originally developed to simulate the function of the human brain or neural system. Subsequently, they have been widely applied to various fields ranging from biology to many areas of engineering. Although the neural network technique is not specifically designed for damage detection, its pattern matching capability makes it suitable to be used as a tool for damage detection. A neural network is an assembly of a large number of highly interconnected simple processing units, called neurons. The connections between the neurons have numerical values that represent the strength of these connections called weights. Knowledge is stored in the form of a collection of connection strengths. Neural networks are capable of selforganisation and knowledge acquisition (learning). This usually involves modifying connection weights via a learning rule. Many types of neural networks have been proposed by changing the network topology, node characteristics and the learning

procedures (Cherkassky and Mulier 2007, Hagan et al. 1996, Specht 1996). In general, neural networks are particularly applicable to complex problems where a significant database of information is available, but where it is difficult to specify an explicit algorithm.

7.6.1 BackPropagation Neural Network

The artificial neural network with backpropagation (BP) learning algorithm is frequently used in pattern identifications (Rumelhart and McClelland 1986). The nodes in back propagation neural networks are arranged in layers. Each neural network has an input layer, an output layer and a number of hidden layers. [Figure 7.10](#) shows a typical backpropagation network with three layers (one hidden layer), where LA is the input layer with N_i nodes, LB is the hidden layer with N_h nodes and LC is the output layer with N_o nodes (DCSE 1998b). The presence of hidden nodes allows these networks to represent and compute more complicated associations between patterns. Propagation takes place in a feedforward manner, from input layer to output layer. No communication is permitted between the nodes within a layer, but the nodes in each layer may send their output to nodes in the next layer. Associated with each connection is a numerical value that is the weight of the connection.

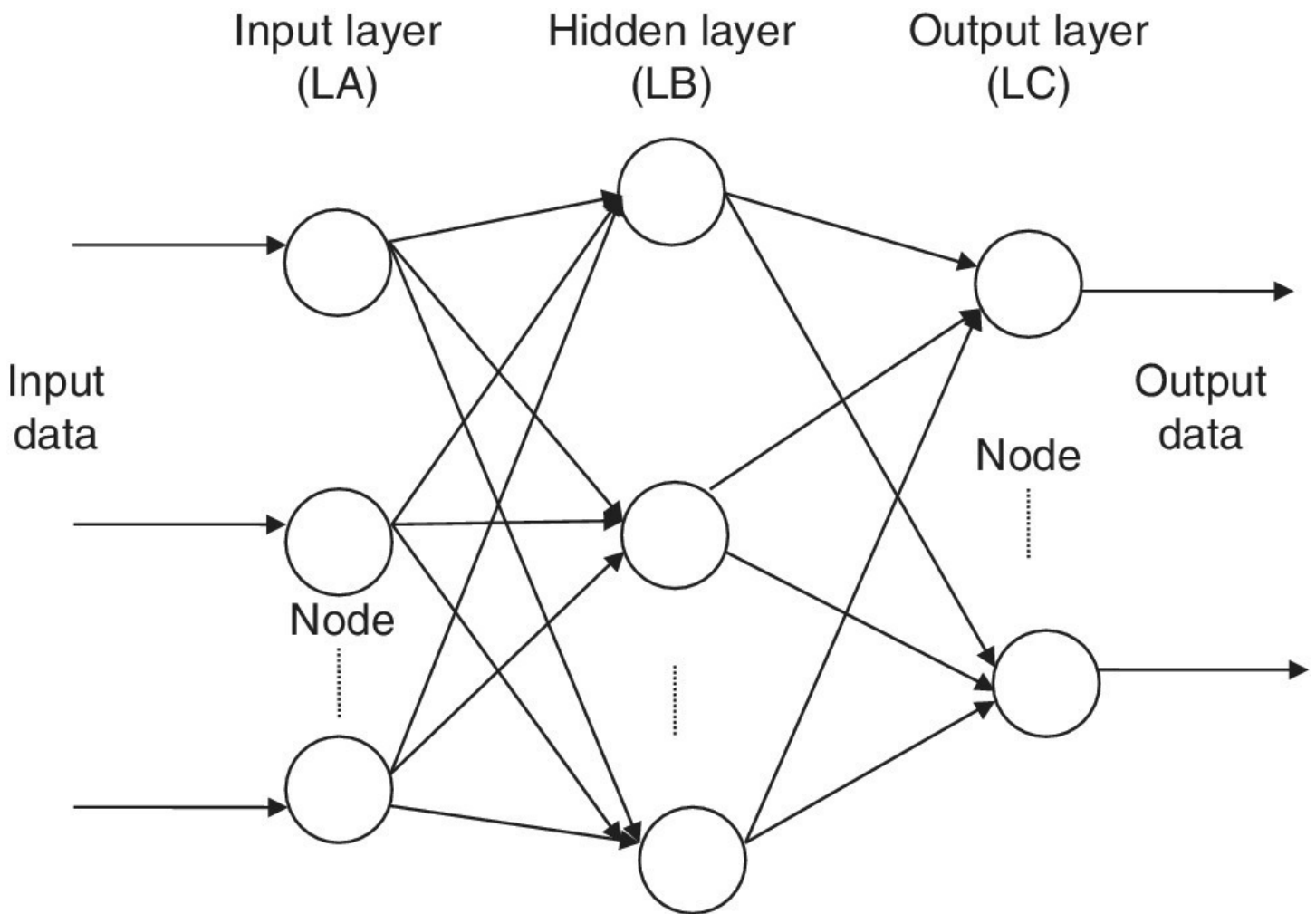


Figure 7.10 Backpropagation (BP) neural network with three layers and nodes.

Assume that a_i is an input of the input nodes, b_r is the output of a hidden node, c_j is an output of

the output nodes, w_{ir} is a connection weight from input node i to hidden node r , v_{rj} is a connection weight from hidden node r to output node j and t_r , θ_j are thresholds of hidden node r and output node j , respectively. The output functions of hidden node and output node are given, respectively, by

$$b_r = f\left(\sum_{i=1}^{N_i} w_{ir} a_i + t_r\right), \quad c_j = f\left(\sum_{r=1}^{N_h} v_{rj} b_r + \theta_j\right) \quad (7.50)$$

where i ranges from 1 to N_i , r ranges from 1 to N_h , j ranges from 1 to N_o and $f(\cdot)$ is the sigmoidal function $f(x) = (1 + e^{-x})^{-1}$.

The connection weights are developed during training of the neural network. At the beginning of a training process, the connection weights are assigned to initial guesses that are generally random values. As samples are presented during the training, the connection weights are modified according to the learning algorithm. At the successful completion of training when the iterative process has converged, the collection of connection weights captures and stores the knowledge and the information present in the samples used in the training. Such a trained neural network is then ready to be used. When an input pattern is provided, a feedforward computation results in an output pattern. This is the result of the generalisation and synthesis of what the network has learned and stored in its connection weights.

The training (i.e. supervised learning) of a multilayer backpropagation neural network is an iterative process. Each step involves the determination of an error associated with each node and then the modification of weights on the connections coming into that node. Each presentation of one training case and subsequent modification of connection weights is called a cycle. Each cycle includes three substeps: (a) forward computation, for the training case to be learned, the network is presented with the input pattern and then propagates the activation through processing nodes, (b) computation of errors between output and expectation and (c) backpropagation of errors. The weights of connections are modified through the gradient descent on the total error in a given training case. A set of cycles, consisting of one cycle for each training case, is called an epoch. The training process for networks may require several hundreds or thousands of epochs for all of the training cases to be learned within a specified error tolerance.

7.6.2 Input Parameters and PreProcessing

The backpropagation neural network has an input layer, several hidden layers and an output layer (DCSE 1998b). The training of the backpropagation neural network requires an iterative process, and an improved backpropagation learning algorithm can be adopted (Hagan et al. 1996). In the applications of neural networks to damage identification, the input vector to the neural network consists of a set of modal parameter measurements, and the output layer is composed of the nodes indicating the damaged location and potential damage quantification.

The neural networks are typically designed with their input vectors in terms of the three types

of data: natural frequencies, mode shapes and transfer functions. Also, the combined modal parameters can be adopted as input vector to the backpropagation neural network for identifying damage in a structure. Use of the combined modal parameters has the following advantages: (a) they can be derived using only natural frequencies and a few modal components, (b) they are higher tolerant of modelling error and less sensitive to measurement noise than natural frequencies and mode shapes, (c) they can be designed as being dependent on only damage location or on both damage location and damage quantification.

The input vector to the backpropagation neural network for damage identification can be expressed as

$$\{\mathbf{Input}\} = \left\{ NFCR_1 \ NFCR_2 \ \dots \ NFCR_{Nf} \ \mathbf{NDSI}_1 \ \mathbf{NDSI}_2 \ \dots \ \mathbf{NDSI}_{Ns} \right\} \quad (7.51)$$

where $NFCR_i$ is the normalised natural frequency change rate of the i th selected mode, defined as

$$NFCR_i = \frac{FFC_i}{\sum_{j=1}^{Nf} FFC_j} \quad \text{where } i = 1, 2, \dots, Nf \quad (7.52)$$

in which Nf is the total number of selected natural frequencies and FFC_i is the percentage frequency change of the i th mode between the undamaged and damaged structure, defined as

$$FFC_i = \frac{(\omega_i^u - \omega_i^d)}{\omega_i^u} \times 100\% \quad (7.53)$$

in which ω_i^u and ω_i^d are the natural frequencies of the i th mode in undamaged and damaged states, respectively. The normalised damage signature index \mathbf{NDSI}_i is defined as

$$\mathbf{NDSI}_i = \frac{\mathbf{DSI}_i}{\sum_{j=1}^{Ns} |\mathbf{DSI}_j|} \quad \text{where } i = 1, 2, \dots, Ns \quad (7.54)$$

where the damage signature index \mathbf{DSI}_i is calculated from

$$\mathbf{DSI}_i = (\phi_i^u - \phi_i^d) / (\omega_i^{u2} - \omega_i^{d2}) \quad (7.55)$$

in which ϕ_i^u and ϕ_i^d are the mode shapes of the i th mode in undamaged and damaged states, respectively, and they may be incomplete.

The output vector of the neural network has the form

$$\{\text{Output}\} = \{d_1 \ d_2 \ \dots \ d_i \ \dots \ d_{Nd}\} \quad (7.56)$$

where Nd is the number of possible damaged members concerned and d_i ($i = 1, 2, \dots, Nd$) represents the percentage damage extent occurring at the i th member.

7.6.3 Probabilistic Neural Network

The probabilistic neural network (PNN) performs the Bayesian decision analysis with the Parzen windows estimator cast into an artificial neural network framework (Specht 1996). When applied to damage identification, the probabilistic neural network uses data from the undamaged and damaged system to determine whether a new measurement of unknown source comes from the undamaged class or the damaged class. Since the probabilistic neural network directly casts the probability density functions (PDFs) of training samples in the network, the network configuration is convenient for dealing with the noisy measurement data for damage identification. A main feature of the probabilistic neural network is that it can explicitly accommodate the noise characteristic as neuroweights in the trained network.

[Figure 7.11](#) shows a threelayer probabilistic neural network to be used for damage location identification (Ni 2014). The network consists of input (distribution) layer, pattern layer and summation layer. An input vector $\mathbf{a} = \{a_1 a_2 \dots a_i \dots a_{NM}\}^T$ to be classified is applied to the neurons of the distribution layer, where the neurons just supply the same input values to all the pattern units. The input vector consists of NM modal parameters (natural frequencies, mode shapes or their combination). For the purpose of damage localisation, the combined modal parameters discussed in [Section 7.6.2](#) are adopted for the input parameters. In the pattern layer, there are a total number of Np pattern classes, each representing a possible damage location. The number of pattern classes depends on a specific structure.

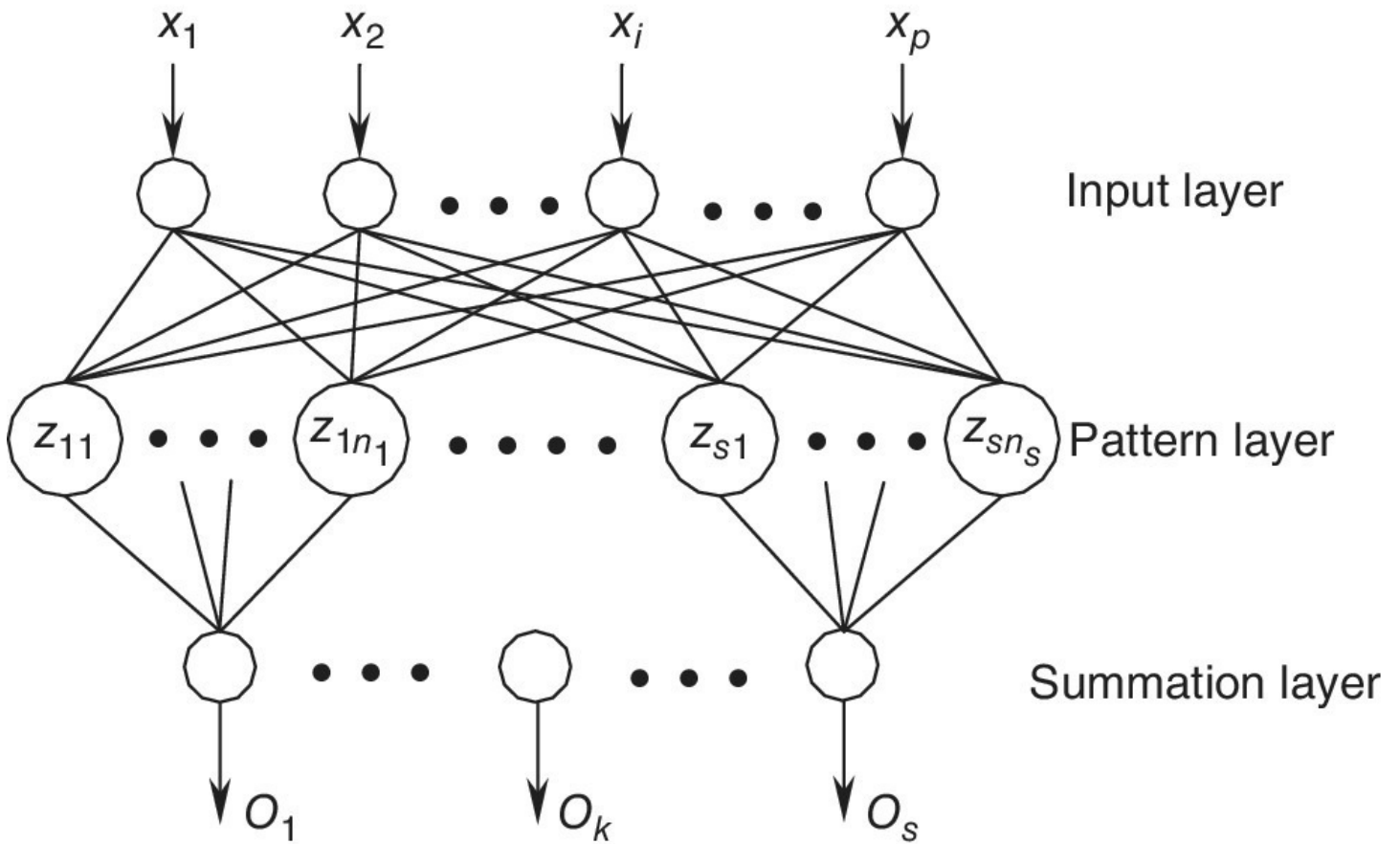


Figure 7.11 Architecture of a three-layer probabilistic neural network (PNN) for damage identification.

Each neuron in the pattern layer forms a dot product of the input vector \mathbf{a} with a weight vector \mathbf{w}_j of a given class, $b_j = \mathbf{a} \cdot \mathbf{w}_j$. The neuron then performs a nonlinear operation on b_j before the output to the summation layer. The activation function used here is $g(b_j) = \exp[(b_j - 1)/\sigma^2]$, where σ is a smoothing parameter. In the summation layer, each neuron receives all pattern layer outputs associated with a given class. For instance, the output of the summation layer neuron corresponding to the class k is expressed as

$$f_k(\mathbf{a}) = \sum_j b_{kj} = \sum_j \exp\left[\frac{(\mathbf{a} \cdot \mathbf{w}_{kj} - 1)}{\sigma^2}\right] \quad (7.57)$$

From this formulation, the kernel density estimators for probability density functions have been cast into the probabilistic neural network by setting the network weight vectors as the corresponding training vectors. The configured probabilistic neural network provides the outputs in the summation layer, that is, estimates for each pattern class at the test vector point. The pattern class with the largest probability density function implies the class of the current test vector, and thereby indicates the damage location with maximum likelihood.

7.6.4 Example for Damage Localisation – a Suspension Bridge (V)

The Tsing Ma Bridge described in [Section 2.3.5](#) and [Section 7.3.7](#) is used here to identify

structural damage using neural networks. [Figure 7.12](#) illustrates the numbering of members in the left longitudinal frame of deck segment No.3 and the selected mode shape components (DCSE 1999). In the network training, the damage is simulated by removing each member in turn. Four damage cases with the damage locations at the members 5, 11, 12 and 16, respectively, and two damage extents for each case, i.e. 50% reduction and 80% reduction of Young's modulus value, are considered in the damage identification simulations.

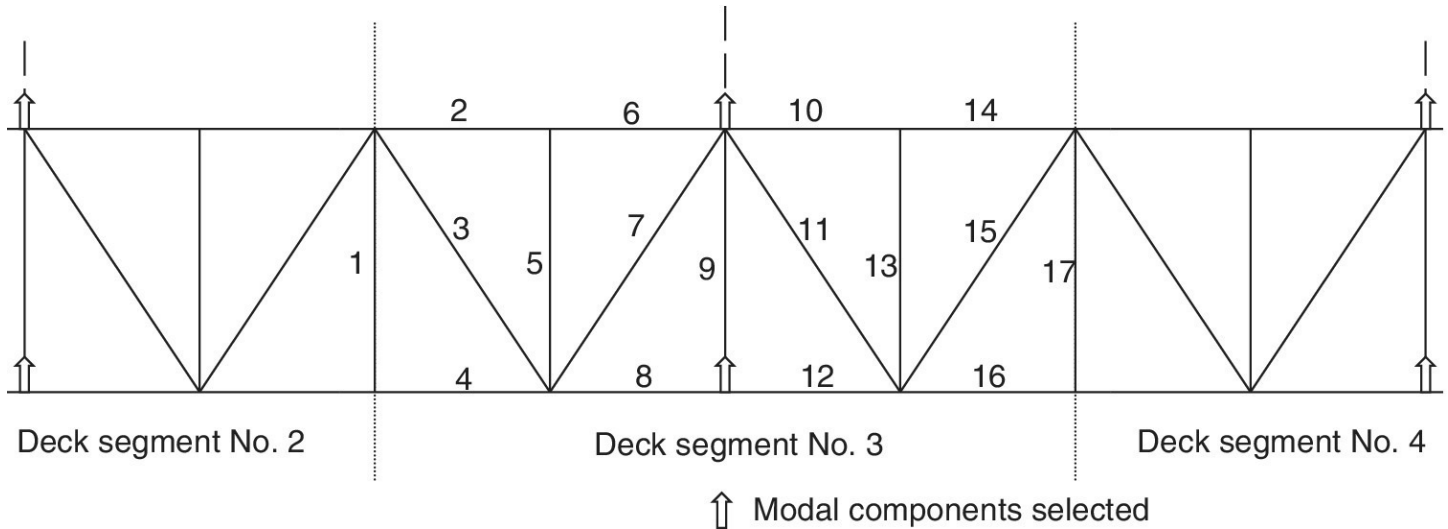


Figure 7.12 Longitudinal frame member numbering in deck segment No.3 and the selected mode shape components marked with arrows.

The artificial neural network with backpropagation learning algorithm is adopted to identify the damaged members in the deck segment. The combined parameters are taken as input vector to the artificial neural network. The natural frequencies of the first 15 global modes and the selected six mode shape components of the second mode are used to construct the input vector of the network. Therefore, there are a total of 21 input nodes in this network. The network is configured with 17 output nodes and one hidden layer consisting of 30 nodes. The network has the output vector consisting of 17 elements, indicating the damage information of the 17 structural members shown in [Figure 7.12](#).

After completing the training of the network, the testing samples of the four damage cases with two different damage sizes are fed into the network. The outputs of the network are listed in [Table 7.10](#) (DCSE 1999). From the results, the damage of members 11, 12 and 16 with the extent of 80% is correctly identified, while damage of member 5 is identified as the damage of both members 5 and 7. For the damage with the extent of 50%, only the damage of members 12 and 16 is correctly identified. The damage of members 5 and 11 is identified as damage at both members 5 and 7 and as damage at both members 11 and 15, respectively. From the results, the backpropagation neural networks require only limited modal data measured at the damage region, and can identify specific damaged member and estimate the damage extent if the damage degree is sufficiently severe. When a structural member is damaged to an insufficient extent, the damage may not be detected using the neural networks.

Table 7.10 Results of simulated damaged member identification in deck segment No.3 using artificial neural network (ANN) with backpropagation (BP).

Frame member	Damaged member (Damage extent)							
	11 (80%)	12 (80%)	5 (80%)	16 (80%)	11 (50%)	12 (50%)	5 (50%)	16 (50%)
1	0.000	0.000	0.000	0.001	0.000	0.005	0.001	0.041
2	0.000	0.000	0.000	0.000	0.000	0.000	0.000	0.000
3	0.000	0.000	0.000	0.000	0.000	0.000	0.000	0.000
4	0.000	0.000	0.000	0.000	0.000	0.000	0.000	0.000
5	0.000	0.000	0.380	0.000	0.000	0.000	0.739	0.000
6	0.002	0.000	0.000	0.000	0.000	0.000	0.000	0.000
7	0.000	0.000	0.999	0.000	0.000	0.000	1.000	0.000
8	0.000	0.001	0.000	0.000	0.000	0.000	0.000	0.000
9	0.000	0.000	0.000	0.000	0.000	0.000	0.000	0.000
10	0.000	0.000	0.000	0.000	0.000	0.000	0.000	0.000
11	0.999	0.000	0.000	0.000	0.288	0.000	0.000	0.000
12	0.000	1.000	0.000	0.001	0.000	1.000	0.000	0.163
13	0.000	0.000	0.000	0.000	0.008	0.000	0.000	0.000
14	0.000	0.000	0.000	0.000	0.000	0.000	0.000	0.000
15	0.000	0.000	0.002	0.000	0.966	0.000	0.002	0.000
16	0.000	0.000	0.000	0.998	0.000	0.000	0.000	0.976
17	0.000	0.003	0.000	0.000	0.000	0.030	0.000	0.000

Now, the probabilistic neural network is used for the simulated damage location identification for the Tsing Ma Bridge deck. The bridge main span comprises a total of 76 deck units, as shown in [Figure 7.3](#). For damage localisation, the main span deck is divided into 16 segments, each including four or five deck units, as shown in [Table 7.11](#) (DCSE 1999). The damage in the deck members within the same segment is classified as one pattern class. As a result, there are a total number of 16 pattern classes. The modal parameters are then taken to construct the input vector, that is, the natural frequency change ratios of the first four modes, and the three translational components of the first mode shape at the 16 nodes of specific deck units (units 2, 7, 12, 17, 22, 27, 32, 36, 41, 45, 50, 55, 60, 65, 70 and 75), namely one node for each selected unit.

Table 7.11 Damage location identification results for probabilistic neural network (PNN).

Pattern class No.	Deck units involved	Training samples		Testing samples		Number of correct localisation		
		Location	Data length	Location	Data length	$\epsilon = 0.10\%$	$\epsilon = 0.06\%$	$\epsilon = 0.02\%$
1	1–4	2,4	50 × 2	3	500	302	483	478
2	5–9	7,8	50 × 2	6	500	168	339	470
3	10–14	10,12	50 × 2	11	500	366	489	500
4	15–19	15,17	50 × 2	16	500	246	467	500
5	20–24	20,22	50 × 2	21	500	485	464	500
6	25–29	25,27	50 × 2	26	500	354	486	500
7	30–34	30,32	50 × 2	31	500	480	498	500
8	35–38	36,38	50 × 2	37	500	405	472	500
9	39–42	39,41	50 × 2	40	500	323	350	485
10	43–47	43,45	50 × 2	44	500	364	432	500
11	48–52	48,50	50 × 2	49	500	415	477	500
12	53–57	53,55	50 × 2	54	500	436	491	500
13	58–62	58,60	50 × 2	59	500	349	463	500
14	63–67	63,65	50 × 2	64	500	251	395	498
15	68–72	68,70	50 × 2	69	500	463	442	500
16	73–76	73,75	50 × 2	74	500	493	479	500
Overall identification accuracy ratio						73.75%	90.34%	99.14%

In order to obtain the training vectors, for each pattern class two damage scenarios, with the damage within the same segment but different units, are introduced in the finite element model of the bridge. The corresponding modal parameters are then calculated. Each set of the computed modal parameters is added with a random sequence to form the training vectors. A total 50 sets of modal parameters are randomly generated for each damage scenario. The noisepolluted training vectors of all pattern classes are entered as weights between the distribution (input) and pattern layers. The probabilistic neural network for damage localisation is then configured (trained). A new input vector (test vector), consisting of measured modal data of unknown source, is presented. In the summation layer, the configured probabilistic neural network outputs the probability density function estimates for each pattern class at the test vector point. Finally, the damaged deck segment is identified by the pattern class with the largest value of the probability density functions.

The test vectors are produced in a similar way to obtaining the training samples. A total of 16 damage scenarios, with one for each deck segment (pattern class), are examined in the testing

phase. The testing damage scenario for each pattern class is incurred at a deck unit different from the training damage scenarios. The modal parameters, when incurring damage at each deck segment in turn, are calculated and then polluted with various random noise to obtain the 'measured' test vectors. The noise levels are simulated at $\varepsilon = 0.10\%$, 0.06% and 0.02% . For each testing damage scenario, a total 500 sets of noisecorrupted test vectors are generated. [Table 7.11](#) summarises the damage location identification results under different noise levels. The integral numbers under various noise levels of the table show the number (times) of correct identification, out of 500 tests for each damage scenario. The identification accuracy is defined as the ratio of the total number of correct identifications to the total test number. The overall identification accuracy value is 73.75% when the noise level $\varepsilon = 0.10\%$, 90.34% when $\varepsilon = 0.06\%$ and 99.14% when $\varepsilon = 0.02\%$, respectively.

As expected, the identification accuracy decreases with the increase of the noise level corrupted in the training and test samples. Only when the noise level is low (e.g. $\varepsilon < 0.05\%$), can the deck damage be localised with a high confidence (i.e. the probability of identifiability greater than 95%). This is mainly due to the low modal sensitivity of the bridge to the deck member damage.

7.7 Concluding Remarks

Many of the methods proposed for structural damage identification are often examined using simulated data, and they are able to cope very well with assumed random noise. Although such numerical simulations are important for assessing the overall performance of damage detection techniques, just using simulations is not sufficient for practical applications. Thus, it is necessary to fully test the techniques on actual engineering structures using real measured data. Before using a damage identification procedure, an accurate structural model, validated by real measurements, is usually required for modelbased damage identification using vibration modal measurements. This is a key aspect for quality of structural damage identification results.

Structural damage identification methods that use changes of modal parameters are attractive. Only limited information on measured modal data, such as natural frequencies and incomplete mode shapes, is required to identify damage in a structure. Change in natural frequencies alone may not provide enough information for the identification of damage in complex engineering structures. For example, in the case of symmetric structures, the change in natural frequencies due to damage at two symmetric locations is exactly the same. The measured mode shape (or frequency response function, modal strain energy, etc.) information is then further required for accurate damage detection and localisation. However, in modal testing, the errors in the measured mode shapes are typically greater than the errors in the measured natural frequencies. Since the measured mode shapes are often incomplete, it is difficult to directly adopt the incomplete modal data in many damage identification methods.

Damage identification methods using change of structural parameters can provide useful information on the location identification of damage in a structure. The flexibility matrix

method takes advantage of the fact that the flexibility matrix can be estimated with higher accuracy, by using only a few lower frequency modes extracted from vibration measurements. However, damage localisation from the observed change in flexibility matrix is not direct or straightforward. By contrast, the methods using strain modal properties utilise the fact that structural damage is followed by stress and strain redistributions. Studies show that the strain energy based damage index method is a powerful tool for damage localisation identification. However, the measurements of full strain modes may be impractical and not feasible for large civil engineering structures. Recent developments in the field of fibre optics suggest that it may be economically feasible to instrument complex structures with fibre optic strain gauges.

Pattern recognition methods identify structural damage by matching the measured and numerically predicted damage characteristics. The database of patterns is often generated by analysing large amounts of data and various damage scenarios, which is timeconsuming. With the help of the advances in neural networks, it is becoming feasible to tackle the problems of damage identification. Instead of identifying the damage information through a reconstruction of the system on the basis of the dynamic characteristics, the neural networks map the dynamic characteristics to the damage information directly. A technique combining pattern recognition and neural networks tends to be promising for damage identification of largescale civil engineering structures.

The damage identification methods discussed in this chapter can provide information on the detection and possible location estimation of damage in a structure, but it may be difficult to accurately quantify the extent of the damage in the structure. Although some successful applications have been reported, structural damage assessment, in terms of location and extent identification of large civil engineering structures such as bridges and buildings, remains a challenging task for civil engineers. Therefore, effective methods for identifying both the location and extent of damage in a large civil structure are needed for accurate damage assessment and reliable damage prognosis.

References

- Afolabi, D. (1987) An antiresonance technique for detecting structural damage. *Proceedings of the 5th International Modal Analysis Conference*, London, UK.
- Alampalli, S., Fu, G. and Aziz, I.A. (1992) Modal analysis as a bridge inspection tool. *Proceedings of the 10th International Modal Analysis Conference*, San Diego, California, USA.
- Bernal, D. (2002) Load vectors for damage localization. *Journal of Engineering Mechanics ASCE***128**(1), 7–14.
- Bicanic, N. and Chen, H.P. (1997) Damage identification in framed structures using natural frequencies. *International Journal for Numerical Methods in Engineering***40**(23), 4451–4468.

- Carden, E.P. and Fanning, P. (2004) Vibration based conditioning monitoring: a review. *Structural Health Monitoring***3**, 355–377.
- Carrasco, C.J., Osegueda, R.A., Ferregut, C.M. and Grygier, M. (1997) Damage localization in a space truss model using modal strain energy. *Proceedings of the 15th International Modal Analysis Conference*, Orlando, Florida, USA.
- Catbas, F.N. and Aktan, A.E. (2002) Condition and damage assessment: issues and some promising indices. *Journal of Structural Engineering ASCE***128**(8), 1026–1036.
- Cawley, P. and Adams, R.D. (1979) The location of defects in structures from measurements of natural frequencies. *Journal of Strain Analysis***14**, 49–57.
- Chen, H.P. (1998) *Structural Damage Identification Using Vibration Modal Data*. PhD thesis Department of Civil Engineering, Glasgow University, UK.
- Chen, H.P. (2010) Mode shape expansion using perturbed force approach. *Journal of Sound and Vibration***329**(8), 1177–1190.
- Chen, H.P. and Huang, T.L. (2012) Updating finite element model using dynamic perturbation method and regularization algorithm. *Smart Structures and Systems***10**(45), 427–442.
- Chen, H.P. and Maung, T.S. (2014a) Structural damage evolution assessment using regularised time step integration method. *Journal of Sound and Vibration***333**(18), 4104–4122.
- Chen, H.P. and Maung, T.S. (2014b) Regularised finite element model updating using measured incomplete modal data. *Journal of Sound and Vibration***333**(21), 5566–5582.
- Chen, H.P., Tee, K.F. and Ni, Y.Q. (2012) Mode shape expansion with consideration of analytical modelling errors and modal measurement uncertainty. *Smart Structures and Systems***10**(45), 485–499.
- Cherkassky, V. and Mulier, F. (2007) *Learning from Data, Concepts, Theory and Methods*. 2nd Edition, John Wiley & Sons, New Jersey, USA.
- Choi, S. and Stubbs, N. (2004) Damage identification in structures using the timedomain response. *Journal of Sound and Vibration***275**, 577–590.
- Cornwell, P., Doebling, S.W. and Farrar, C.R. (1999) Application of the strain energy damage detection method to platelike structures. *Journal of Sound and Vibration***224**, 359–374.
- Department of Civil and Structural Engineering (DCSE) (1998a) Literature Review on VibrationBased Structural Damage Detection. Report No. 1, The Hong Kong Polytechnic University.
- Department of Civil and Structural Engineering (DCSE) (1998b) Assessment Strategy of Possible Structural Damage in the Tsing Ma Bridge, Kap Shui Mun Bridge and Ting Kau Bridge. Report No. 2, The Hong Kong Polytechnic University.

- Department of Civil and Structural Engineering (DCSE) (1999) Damage Detection Simulation for the Tsing Ma Suspension Bridge. Report No. 4(a), The Hong Kong Polytechnic University.
- Doebbling, S.W., Farrar, C.R., Prime, M.B. and Shevitz, D.W. (1996) *Damage Identification and Health Monitoring of Structural and Mechanical Systems from Changes in their Vibration Characteristics: A Literature Review*. Los Alamos National Laboratory report LA 13070MS.
- Friswell, M.I. and Mottershead, J.E. (1995) *Finite Element Model Updating in Structural Dynamics*. Kluwer Academic Publishers, Dordrecht, The Netherlands.
- Hagan, M.T., Demuth, H.B. and Beale, M. (1996) *Neural Network Design*. PWS Publishing Company, Boston, USA.
- Hajela, P. and Soeiro, F.J. (1990) Structural damage detection based on static and modal analysis. *AIAA Journal***28**, 1110–1115.
- Humar, J., Bagchi, A. and Xu, H. (2006) Performance of vibrationbased techniques for the identification of structural damage. *Structural Health Monitoring***5**(3), 215–241.
- Hunt D.L. (1992). Application of an enhanced coordinate modal assurance criterion. *Proceedings of the 10th International Modal Analysis Conference*, San Diego, California, USA.
- Lam, H.F., Ko, J.M. and Wong, C.W. (1998) Localization of damaged structural connections based on experimental modal and sensitivity analysis. *Journal of Sound and Vibration***210**, 91–115.
- Lau, C.K., Mak, W.P., Wong, K.Y., Chan, W.Y., Man, K.L. and Wong, K.F. (1999) Structural performance measurements and design parameter validation for Tsing Ma Suspension Bridge. In book: *Advances in Steel Structures*, ICASS'99, Chan and Teng (eds.), 487–496.
- Lieven N.A.J. and Ewins D.J. (1988). Spatial correlation of mode shapes, the coordinate modal assurance criterion (COMAC). *Proceedings of the 6th International Modal Analysis Conference*, Vol. 1, Kissimmee, Florida, USA.
- Maia, N.M.M., Silva, J.M.M., Almas, E.A.M. and Sampaio, R.P.C (2003) Damage detection in structures: from mode shape to frequency response function methods. *Mechanical Systems and Signal Processing***17**, 489–498.
- Montalvão, D., Maia, N.M.M. and Ribeiro, A.M.R. (2006) A review of vibrationbased structural health monitoring with special emphasis on composite materials. *The Shock and Vibration Digest***38**(4), 1–30.
- Mottershead, J.E. (1998) On the zeros of structural frequency response functions and their sensitivities. *Mechanical Systems and Signal Processing***12**, 591–598.
- Ni, Y.Q. (2014) Structural health monitoring of cablesupported bridges based on vibration

measurements. *Proceedings of the 9th International Conference on Structural Dynamics*, Porto, Portugal.

Ni, Y.Q., Wang, B.S. and Ko, J.M. (2000) Simulation studies of damage location in Tsing Ma Bridge deck. *Proceedings of the SPIE's Fifth International Symposium on Nondestructive Evaluation and Health Monitoring of Aging Infrastructure*, Newport Beach, California, USA.

Pandey, A.K. and Biswas, M. (1994) Damage detection in structures using changes in flexibility. *Journal of Sound and Vibration***169**, 3–17.

Pandey, A.K. and Biswas, M. (1995) Experimental verification of flexibility difference method for locating damage in structures. *Journal of Sound and Vibration***184**, 311–328.

Pandey, A.K., Biswas, M. and Samman, M.M. (1991). Damage detection from changes in curvature mode shapes. *Journal of Sound and Vibration***145**, 321–332.

Rumelhart, D. and McClelland, J. (1986) *Parallel Distributed Processing: Explorations in the Microstructure of Cognition*. MIT Press, Cambridge MA, USA.

Rytter, A. (1993) *Vibrational Based Inspection of Civil Engineering Structures*. Fracture and Dynamics, University of Aalborg, Denmark.

Sampaio, R.P.C., Maia, N.M.M. and Silva, J.M.M. (1999) Damage detection using the frequency response function curvature method. *Journal of Sound and Vibration***226**, 1029–1042.

Serna, O.R. and Stubbs, N. (1996) Nondestructive damage evaluation in complex structures using modal strain parameters. *Smart Structures and Materials, Smart Systems for Bridges, Structures, and Highways, SPIE*, **2719**, 192–200.

Sohn, H. and Law, K.H. (1997) A Bayesian probabilistic approach for structure damage detection. *Earthquake Engineering and Structural Dynamics***26**, 1259–1281.

Sohn, H., Farrar, C.R., Hemez, F.M., Shunk, D.D., Stinemates, D.W. and Nadler, B.R. (2004) *A Review of Structural Health Monitoring Literature: 1996–2001*. Report LA13976MS. Los Alamos National Laboratory.

Sohn, H., Farrar, C.R., Hunter, N.F. and Worden, K. (2001) Structural health monitoring using statistical pattern recognition techniques. *Journal of Dynamic Systems Measurements and Control ASME***123**(4), 706–711.

Specht, D.F. (1996) Probabilistic neural networks and general regression neural networks. *Fuzzy Logic and Neural Network Handbook*, Chen (ed.), McGrawHill, New York, USA.

Staszewski, W.J. and Worden, K. (2009) Signal processing for damage detection. *Encyclopaedia of Structural Health Monitoring*, Boller, Chang and Fujino (ed.), John Wiley & Sons, Chichester, UK.

Stubbs, N., Broome, T.H. and Osegueda, R. (1990) Nondestructive construction error detection in large space structures. *AIAA Journal***28**, 146–152.

Stubbs, N., Kim, J.T. and Farrar, C.R. (1995). Field verification of a nondestructive damage localization and severity estimation algorithm. *Proceedings of the 13th International Modal Analysis Conference*, Nashville, Tennessee, USA.

Wang, B.S., Liang, X.B., Ni, Y.Q. and Ko, J.M. (2001). Comparative study of damage indices for longspan bridges. *Proceedings of the 19th International Modal Analysis Conference*, Kissimmee, Florida, USA.

Wang, J.Y., Ko, J.M. and Ni, Y.Q. (2000). Modal sensitivity analysis of Tsing Ma Bridge for structural damage detection. *Nondestructive Evaluation of Highways, Utilities, and Pipelines IV*, Aktan and Gosselin (ed.), SPIE Vol. 3995, 300–311.

Williams, E.J., Messina, A. and Payne, B.S. (1997). A frequencychange correlation approach to damage detection. *Proceedings of the 15th International Modal Analysis Conference*, Orlando, Florida, USA.

Wolff, T. and Richardson, M. (1989) Fault detection in structures from changes in their modal parameters. *Proceedings of the 7th International Modal Analysis Conference*, Las Vegas, Nevada, USA.

Worden, K. (1997) Structural fault detection using a novelty measure. *Journal of Sound and Vibration***201**, 85–101.

Worden, K. and Friswell, M.I. (2009) Modalvibrationbased damage identification. *Encyclopaedia of Structural Health Monitoring*, Boller, Chang and Fujino (ed.), John Wiley & Sons, Chichester, UK.

Yan, Y., Cheng, L., Wu, Z. and Yam, L. (2007) Development in vibrationbased structural damage detection technique. *Mechanical Systems and Signal Processing***21**(5), 2198–2211.

8

ModelBased Damage Assessment Methods

8.1 Introduction

Structural damage assessment methods based on vibration measurements show great promise, because such methods allow for quick and global damage identification at a relatively low cost after a severe loading event such as an earthquake or a hurricane. These methods rely on the fact that any change in stiffness caused by damage in a structure leads to change in modal parameters of the structure, such as natural frequencies and mode shapes (Chen 1998, Doebling et al. 1996, Sohn et al. 2004). For accurate assessment of damage in a structure, the location and extent of damage in the structure need to be identified. Thus, modelbased methods are usually required for assessing structural damage, on the basis of the associated model (e.g. baseline) for the undamaged structure. Before a damage assessment procedure, the structural parameters (e.g. stiffness and mass) of the initial baseline model have to be updated and validated by the correlation study between the analytical model (or finite element numerical model) and tested results through a model updating procedure (Friswell and Mottershead 1995).

Characterisation of local damage in a structure is a critical issue for successful assessment of damage in a structure. Damage indicators should be properly chosen to characterise local damage in a framed or continuum structure, and they should be capable of reflecting both the location and severity of the damage in individual structural components or in specific locations (Chen 2008). Very often, Young's modulus is chosen as a damage indicator, which works well for truss elements and continuums. However, for a beam or column element, it may be inappropriate to choose Young's modulus as a damage indicator. For example, in the cases where the connection at a beam-column joint is loosened, the axial stiffness remain keep unchanged along the element while the bending stiffness is lost at the joint. Thus, appropriate damage indicators should be adopted to characterise the changes of axial stiffness and bending stiffness at detailed level, respectively.

The matrix update methods rely on the principle that the change of stiffness due to damage in a structure can be estimated from the measured modal parameters of the damaged structure. Typical matrix updating methods include the residual force vector method (Ricles and Kosmatka 1992), the minimum rank update method (Zimmerman and Kaouk 1994) and the optimal matrix updating method (Ewins 2000). These methods can directly use the measured modal parameters of the damaged structure, such as natural frequencies and complete mode shapes, and they can provide simple algorithms for information on the damage location and quantification, with less computational effort.

In sensitivity based methods, change of modal parameters caused by damage in a structure is approximated by the firstorder Taylor series expansion with respect to physical parameters

(Mottershead et al. 2011, Zhao and DeWolf 1999). Modal parameters measured on the damaged structure are adopted in the approximated sensitivity equations for assessing the location and extent of damage in the structure. The sensitivity based methods are most commonly used in vibrationbased damage identification, and they are able to offer correct results for damage assessment when damage is relatively small. The sensitivity based methods may not perform well, in the cases where the change of structural stiffness due to damage and/or the change of modal parameters before and after damage is large due to their being a firstorder approximation.

Problems often arise in practical applications of many vibrationbased damage assessment methods to large civil engineering structures. In modal testing of civil structures, only limited information on measured modal data is usually extracted, due to the limitation of accessibility, cost and techniques available. Also, errors in vibration measurements are inevitable in reality. Thus, practical methods for damage assessment have to accurately identify the location and extent of damage in an engineering structure using limited modal measurements with uncertainty. The dynamic perturbation method provides the exact relationship between the change in stiffness due to damage and the vibration modal data of the damaged structure (Chen 2005, Chen and Bicanic 2006). Thus, the approximations in sensitivity analysis caused by utilising the firstorder Taylor series expansion are avoided. The dynamic perturbation method can directly adopt the incomplete mode shape measurements, without requiring a mode shape expansion or model reduction process. From numerical examples, the dynamic perturbation method is able to provide a reliable estimate of the location and extent of damage in both framed and continuum structures, requiring only limited noisy modal data.

This chapter presents advanced methods for inversely localising and quantifying damage in a structure using measured vibration modal data. Appropriate characterisation of damage in a structure at local level is introduced to reflect both the location and extent of damage in the structure. Matrix update methods based on directly updating structural stiffness are reviewed. Sensitivity based methods using the sensitivity of modal parameters to damage in a structure are discussed. The dynamic perturbation method is further explored for assessing the location and extent of damage in large engineering structures. This method is then examined by numerical examples on identifying the location and extent of damage in a framed building structure and a continuum structure. Finally, potential problems in vibrationbased damage identification methods are discussed.

8.2 Characterisation of Damage in Structures

Characterisation of damage in a structure is one of the key aspects of a modelbased damage assessment method. The success of damage assessment largely relies on the quality of the damage model used, since inverse methods for damage identification are based on the selected damage model. The selection of damage model depends on the type of structure and the damage mechanism, which is often represented by a reduction of stiffness at the damage site. For vibrationbased structural damage assessment, damage indicators need to be chosen to properly characterise the change in stiffness due to damage. These damage indicators have to

be capable of not only identifying the specific location of damage in the structure but also predicting the severity of the damage. For accurate damage assessment, different types of damage indicators are required for different types of structures, such as for framed structures and continuum structures.

8.2.1 Damage in Framed Structures

Structural damage that causes change in stiffness of framed structures can be characterised at element level or at critical point level.

8.2.1.1 Damage Characterisation at Element Level

Framed structures typically comprise various types of structural components, such as truss, brace, beam and column members. Thus, the change in element stiffness matrix $\Delta\mathbf{K}_e$ for a structural member can be expressed by

$$\Delta\mathbf{K}_e = \hat{\mathbf{K}}_e - \mathbf{K}_e = d_e\mathbf{K}_e \quad (8.1)$$

where \mathbf{K}_e and $\hat{\mathbf{K}}_e$ are the e th element stiffness matrices for the original (undamaged) and damaged structure, respectively, and d_e is a damage indicator characterised at element level. A negative value of d_e , ranging from 0% to -100%, indicates the reduction of the element stiffness caused by structural damage. When $d_e = 0\%$, the e th element is undamaged. When $d_e = -100\%$, the stiffness of the e th element is completely lost.

In finite element modelling of framed structures, different finite element types can be used for modelling the structural members. For a truss or brace member, a bar (truss) element can be adopted and its damage indicator is defined as

$$d_t = \frac{(EA)^d - EA}{EA} \quad (8.2)$$

where EA and $(EA)^d$ represent the axial stiffness for the original and damaged element, respectively, the superscript d denoting the quantity associated with the damaged structure. The defined damage indicator can also be used for damage in a beam or column associated with reduction of axial stiffness.

For a beam or column member, a conventional beam element is employed, and the damage indicator associated with reduction of bending stiffness is defined as

$$d_b = \frac{(EI)^d - EI}{EI} \quad (8.3)$$

where EI and $(EI)^d$ are the bending stiffness for the original and damaged element, respectively.

8.2.1.2 Damage Characterisation at Critical Point Level

For a beam or column element, structural damage often occurs at critical locations, such as a loosened connection developed at a joint or hinge formed near the middle of the element. In order to consider the bending stiffness contributions from critical locations, and to characterise local damage at these critical locations, the element stiffness matrix for a beam or column member is now calculated from an integral form (Chen 2008, Chen and Bicanic 2010). The threepoint Newton–Cotes integration rule (Stoer and Bulirsch 1980) is adopted for the numerical integration at these critical points. For a conventional beam element with bending stiffness EI and element length l , the element stiffness matrix associated with bending stiffness can be expressed as

$$\mathbf{K}_c = \mathbf{K}_p^{(g)} + \mathbf{K}_p^{(o)} + \mathbf{K}_p^{(h)} \quad (8.4)$$

where $\mathbf{K}_p^{(g)}$, $\mathbf{K}_p^{(o)}$ and $\mathbf{K}_p^{(h)}$ represent the contributions of critical points (an end g , the middle o and another end h) to the element stiffness matrix, respectively, defined as

$$\mathbf{K}_p^{(g)} = w_g (EI)_g \mathbf{K}_l^{(g)}, \quad \mathbf{K}_p^{(o)} = w_o (EI)_o \mathbf{K}_l^{(o)} \quad \text{and} \quad \mathbf{K}_p^{(h)} = w_h (EI)_h \mathbf{K}_l^{(h)} \quad (8.5)$$

in which weight coefficients are $w_g = 1/3$, $w_o = 4/3$ and $w_h = 1/3$, and $(EI)_g$, $(EI)_o$ and $(EI)_h$ are bending stiffness at critical points g , o and h , respectively, and $\mathbf{K}_l^{(g)}$, $\mathbf{K}_l^{(o)}$ and $\mathbf{K}_l^{(h)}$ are geometrical matrices only related to element length l at integration points g , o and h , respectively (Chen 2008). The damage indicators, $d_p^{(g)}$, $d_p^{(o)}$ and $d_p^{(h)}$, characterising at critical points g , o and h for a beam element are defined in a general form

$$d_p^{(r)} = \frac{w_r^d (EI)_r^d - w_r (EI)_r}{w_r (EI)_r} \quad (8.6)$$

where r represents critical points g , o and h , respectively. Consequently, the change of the element stiffness matrix for a beam element is expressed as

$$\Delta \mathbf{K}_c = d_p^{(g)} \mathbf{K}_p^{(g)} + d_p^{(o)} \mathbf{K}_p^{(o)} + d_p^{(h)} \mathbf{K}_p^{(h)} \quad (8.7)$$

In the cases where a hinge exists at a critical location, such as a hinge at an end or in the middle of the element, the damage indicators can be evaluated by comparing the element stiffness matrix for the structural member having a hinge with that for the intact member, as summarised in [Table 8.1](#). When all damage indicators for a beam element are identical, i.e. $d_b = d_p^{(g)} = d_p^{(o)} = d_p^{(h)}$, [Equation \(8.7\)](#) becomes the special case when damage is characterised at element level given in [Equation \(8.3\)](#).

Table 8.1 Values of damage indicators for cases with loss of bending stiffness capacity at critical locations.

	Damage indicator, $d_p^{(r)}$		
	$d_p^{(g)}$	$d_p^{(o)}$	$d_p^{(h)}$
Undamaged	0%	0%	0%
Hinge at end g	-150%	0%	0%
Hinge at middle o	0%	-150%	0%
Hinge at end h	0%	0%	-150%

The change of global stiffness matrix, after considering [Equations \(8.1\)](#) and [\(8.7\)](#), is computed from the sum of all changes of element stiffness matrices over all structural members of the frame structure, including truss, brace, beam and column members, that is

$$\Delta \mathbf{K} = \sum_{e=1}^{Nt} \Delta \mathbf{K}_e + \sum_{c=1}^{Np} \Delta \mathbf{K}_c = \sum_{j=1}^{NF} d_j \mathbf{K}_j \quad (8.8)$$

where \mathbf{K}_j and d_j represent the original element stiffness matrix of a structural element and its corresponding damage indicator, or the original stiffness contribution of a critical point and its corresponding damage indicator, and $NF (= Nt + Np)$ represents the total number of damage indicators, depending on the total numbers of stiffness contributions at element level Nt and at critical point level Np .

8.2.2 Damage in Continuum Structures

Damage in continuum structures can also be characterised at element level or at integration point level for structural damage assessment.

8.2.2.1 Damage Characterisation at Element Level

Occurrence of damage in continuum structures causes a local change in stiffness. The change of element stiffness matrix $\Delta \mathbf{K}_e$ due to damage in a continuum structure can be expressed in [Equation \(8.1\)](#). Here, \mathbf{K}_e is the e th element stiffness matrix for the original continuum structure defined in [Equation \(6.2\)](#) and d_e is a damage indicator of the continuum structure characterised at element level.

8.2.2.2 Damage Characterisation at Integration Point Level

The element stiffness matrix of a continuum structure defined in [Equation \(6.2\)](#) is usually computed from numerical integration

$$\mathbf{K}_e = \int_{V_e} \mathbf{B}^T \mathbf{D} \mathbf{B} dv = \sum_{j=1}^{Ng} \mathbf{K}_j^{(g)} \quad (8.9)$$

where Ng denotes the total number of integration points (Gauss points) in a structural element and $\mathbf{K}_j^{(g)}$ is the contribution of the Gauss integration point j to the element stiffness matrix.

In general, the effects of damage on structural stiffness can be represented by locally reducing the Young's modulus. Without a loss of generality, a scalar damage model is assumed (Chen and Bicanic 2000). Thus, the change of stiffness matrix of the continuum structure due to damage is expressed in a simple form

$$\Delta \mathbf{K} = \sum_{j=1}^{NG} d_j \mathbf{K}_j^{(g)} \quad (8.10)$$

where NG is the total number of Gauss integration points within the whole continuum structure and d_j is the damage indicator of the continuum structure for the j th integration point and ranges from 0 to -1.

In summary, for both framed and continuum structures, the change of stiffness matrix $\Delta \mathbf{K}$ caused by structural damage, given in [Equations \(8.8\)](#) and [\(8.10\)](#), can be written in a general form for damage assessment as

$$\Delta \mathbf{K} = \sum_{j=1}^{ND} d_j \mathbf{K}_j \quad (8.11)$$

where \mathbf{K}_j is the contribution of the j th element or integration point to the global stiffness matrix; the relevant damage indicator d_j characterises either at element or integration point level and ND is the total number of the selected damage indicators. The damage indicator d_j is sufficient to provide information about not only the location of damage, but also the extent of damage in a structure. For example, in the context of damage identification, structural damage is present for any nonzero damage indicator d_j . In terms of the damage location, the j th element or integration point is considered as damaged if the damage indicator d_j is not equal to zero. For the damage quantification, the extent of structural damage at the j th element or integration point is determined by the magnitude of the damage indicator d_j . Consequently, damage in a structure can be detected, located and quantified when the damage indicator d_j is determined.

For structural damage identification, it may be assumed that the global mass matrix keeps unchanged before and after damage, that is $\Delta \mathbf{M} = 0$, because the change of mass caused by structural damage can usually be ignored in real engineering applications.

8.3 Matrix Update Methods

Matrix update methods provide the updated stiffness of a structure using the vibration modal measurements on the damaged structure. The updated stiffness can give information about the location and extent of the damage in the structure.

8.3.1 Residual Force Vector Method

It is assumed that an initial baseline model is available for the undamaged structure through a model updating process. The validated model of the undamaged structure has structural parameters: stiffness \mathbf{K} , damping \mathbf{C} and mass \mathbf{M} , as well as modal parameters: the i th eigenvalue $\lambda_i (= \omega_i^2)$ and the corresponding mode shape ϕ_i . The eigenvalue equation for the undamaged structure without considering damping is expressed as

$$(\mathbf{K} - \lambda_i \mathbf{M}) \phi_i = 0 \quad (8.12)$$

A postdamage experimental modal testing is performed on the structure to measure the i th eigenvalue $\hat{\lambda}_i (= \hat{\omega}_i^2)$ and mode shapes $\hat{\phi}_i$ of the damaged structure. Similarly, for the damaged structure the eigenvalue equation is written as

$$(\hat{\mathbf{K}} - \hat{\lambda}_i \hat{\mathbf{M}}) \hat{\phi}_i = 0 \quad (8.13)$$

where $\hat{\mathbf{K}}$ and $\hat{\mathbf{M}}$ are the stiffness and mass matrices associated with the damaged structure. As a result of the damage, the changes of stiffness and mass matrices $\Delta\mathbf{K}$ and $\Delta\mathbf{M}$ are expressed, respectively, as

$$\Delta\mathbf{K} = \hat{\mathbf{K}} - \mathbf{K} \quad \text{and} \quad \Delta\mathbf{M} = \hat{\mathbf{M}} - \mathbf{M} \quad (8.14)$$

Substituting [Equation \(8.14\)](#) into [Equation \(8.13\)](#) and rearranging, leads to the definition of the residual force vector for the i th mode (Ricles and Kosmatka 1992) as

$$\mathbf{r}_i = -(\Delta\mathbf{K} - \hat{\lambda}_i \Delta\mathbf{M}) \hat{\phi}_i = (\mathbf{K} - \hat{\lambda}_i \mathbf{M}) \hat{\phi}_i \quad (8.15)$$

The righthand side of the above equation is known, when the natural frequencies and mode shapes of the damaged structure are measured. The residual force vector \mathbf{r}_i can be tested to check whether its values are different from zero, and the damage location can be identified from the position of nonzero entries in the vector. The residual force vector should be calculated for different measured modes.

After the damaged elements are identified, it is possible to express the change in stiffness $\Delta\mathbf{K}$ as the weighted sum of the stiffness matrices of the damaged elements by using the change of stiffness matrix expressed in a general form in [Equation \(8.11\)](#). Assuming no change in the mass, i.e. $\Delta\mathbf{M} = \mathbf{0}$, [Equation \(8.15\)](#) is rewritten as

$$\left[\sum_{j=1}^{ND} \mathbf{K}_j \right] \hat{\mathbf{d}} = -\mathbf{r}_i \quad \text{or} \quad \mathbf{S}_i \mathbf{d} = -\mathbf{r}_i \quad (8.16)$$

When more than one mode is utilised for structural damage identification, the columns of known coefficient matrix \mathbf{S}_i associated with the additional modes may be added below those corresponding to the previous modes. The known vector \mathbf{r}_i may be expanded in a similar manner. [Equation \(8.16\)](#) or its expanded form can be solved for damage indicators d_j by using the regularised solution procedure for inverse problems discussed in [Section 6.5.2](#).

The residual force vector method may not be able to provide good estimates in the damage location and quantification identification, when noise exists in the measured modal data. This problem arises due to the fact that the update with the noisy mode shapes has smeared the stiffness change over the whole stiffness matrix. One possible solution to this problem can be provided by the minimum rank update method.

8.3.2 Minimum Rank Update Method

The residual force vector method may give poor results since the effect of the damage is smeared across the residuals due to measurement uncertainty. To tackle the problem, Zimmerman and Kaouk (1994) proposed a minimum rank update method to enforce locality within the perturbation matrix. This method is based on a generalised minimum rank perturbation theory. By ignoring the change in mass due to structural damage, the residuals \mathbf{R} are expressed in a matrix form

$$\mathbf{R} = \mathbf{K}\hat{\Phi} - \mathbf{M}\hat{\Phi}\hat{\Lambda} = -\Delta\mathbf{K}\hat{\Phi} \quad (8.17)$$

where $\hat{\Lambda}$ is a diagonal matrix of the measured eigenvalues and $\hat{\Phi}$ is the measured mode shape matrix. When \mathbf{R} is of full column rank, the perturbation to the original stiffness matrix due to damage is given by

$$\Delta\mathbf{K} = -\mathbf{R}(\mathbf{R}^T \hat{\Phi})^{-1} \mathbf{R}^T \quad (8.18)$$

It has been proven that the matrix $\Delta\mathbf{K}$ is symmetric, if the measured eigenvectors are mass orthogonal. In addition, when the matrix \mathbf{R} is not of full rank, the corresponding submatrices of \mathbf{R} and $\hat{\Phi}$, which have the same rank as \mathbf{R} , can be used in calculating the change in stiffness $\Delta\mathbf{K}$. The matrix $\Delta\mathbf{K}$ is independent of the submatrices used if the eigenvectors are mass orthogonal. With the knowledge of the location of damage, the rank of the true perturbation matrix $\Delta\mathbf{K}$ can be found by adding the rank of the element stiffness matrix of the damaged members. Finally, the extent of damage at the damaged elements can be derived from the significant nonzero elements of the perturbation matrix $\Delta\mathbf{K}$.

To improve the damage location and extent estimate, many practical techniques have been proposed (Zimmerman et al. 1995). These techniques allow engineering insight and judgement to be incorporated into the minimum rank perturbation algorithm. These damage assessment

techniques include: (a) use of angle damage vectors, (b) mode number selection, (c) damage vector and eigenvector filtering techniques to minimise the effect of measurement noise, (d) rank estimation algorithms and (e) filtering of dynamic residual decomposition among various structural matrices (mass and/or stiffness) when multiple structural matrices are being updated. The minimum rank update method in conjunction with engineering insight and judgement improves the procedure to the point where it is a practical tool for realworld problems.

8.3.3 Optimal Matrix Updating Method

The change of stiffness matrix can provide the indication of damage in a structure, since structural damage causes the reduction of stiffness matrix. The change in stiffness matrix $\Delta\mathbf{K}$ due to damage can be directly estimated (Ewins 2000) from

$$\Delta\mathbf{K} = \mathbf{K}_{red} (\mathbf{K}^{-1} - \hat{\mathbf{K}}^{-1}) \mathbf{K}_{red} = \mathbf{K}_{red} (\mathbf{F} - \hat{\mathbf{F}}) \mathbf{K}_{red} \quad (8.19)$$

where \mathbf{K}_{red} represents the condensed stiffness matrix, reduced from the undamaged analytical stiffness matrix \mathbf{K} to the measured degrees of freedom (DOFs) using mode reduction methods such as the Guyan static method, as described in [Section 5.6.1](#). The flexibility matrices \mathbf{F} and $\hat{\mathbf{F}}$ are calculated using the measured incomplete modes for the undamaged and damaged structure by using [Equation \(7.18\)](#).

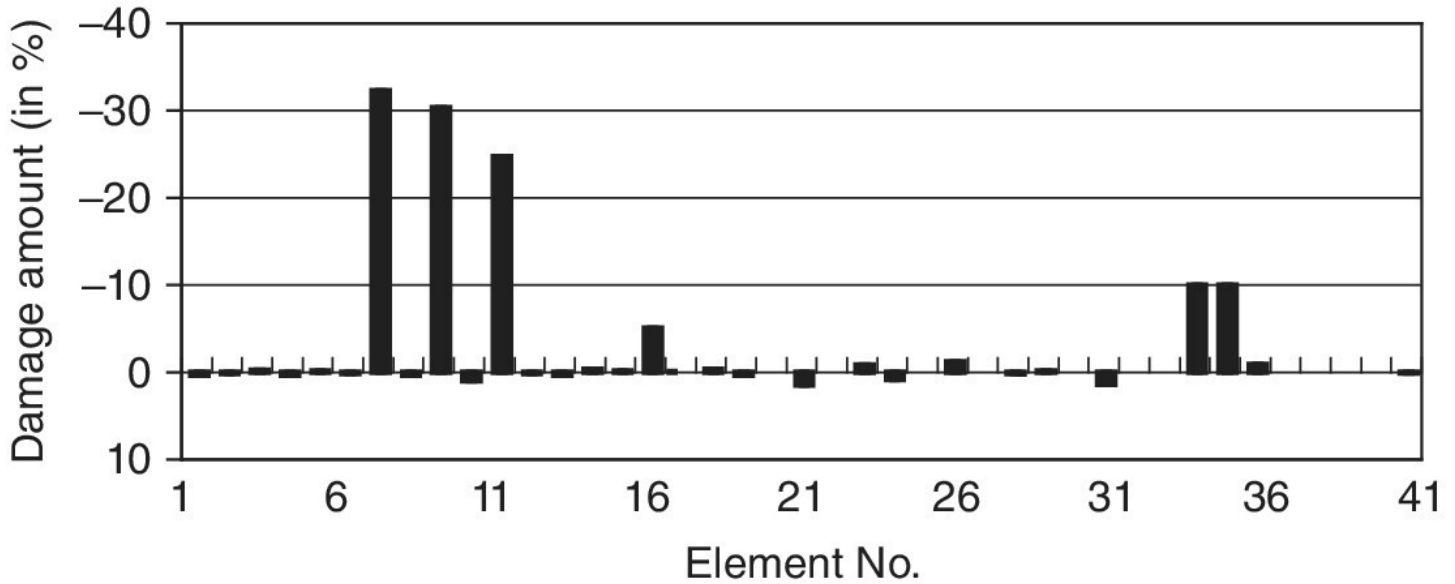
To compare the undamaged analytical model and damaged test structure for damage identification, they must have the same number of DOFs. Due to limited instrumentation, typically the number of measured DOFs is significantly less than the number of DOFs adopted in the analytical model. The model reduction or mode shape expansion technique is usually used for this purpose. While expansion of the measured mode shapes to the order of the analytical model would provide a clearer location of structural damage, the resulting size of the optimisation problem may lead to numerically computational difficulties. In consideration of this, a hybrid reduction or expansion approach was developed by selecting an intermediate DOFs set. This DOF set is small enough for computational efficiency but large enough to describe the physical model with sufficient detail to identify the damage. Through this approach the undamaged analytical model is reduced and the measured mode shapes are expanded to have the same order.

The optimal matrix updating method is then implemented to adjust the undamaged analytical stiffness matrix using the measured modal parameters. This method aims to match the test frequencies and mode shapes by solving a constrained optimisation problem under necessary constraints. The change of stiffness matrix $\Delta\mathbf{K}$ can then be expressed (Kim and Bartkowicz 1993) as

$$\Delta\mathbf{K} = \mathbf{M}\hat{\Phi}\hat{\Phi}^T \mathbf{K}\hat{\Phi}\hat{\Phi}^T \mathbf{M} + \mathbf{M}\hat{\Phi}\hat{\Lambda}\hat{\Phi}^T \mathbf{M} - \mathbf{K}\hat{\Phi}\hat{\Phi}^T \mathbf{M} - \mathbf{M}\hat{\Phi}\hat{\Phi}^T \mathbf{K} \quad (8.20)$$

This change of stiffness matrix is unique, and is the only minimum solution of the optimisation problem. By checking the entries in the change of stiffness matrix $\Delta\mathbf{K}$, the location and extent of structural damage can be identified. Since the change of stiffness matrix often loses sparsity,

(a) Only damaged mode 2 used



(b) Both damaged modes 2 and 3 used

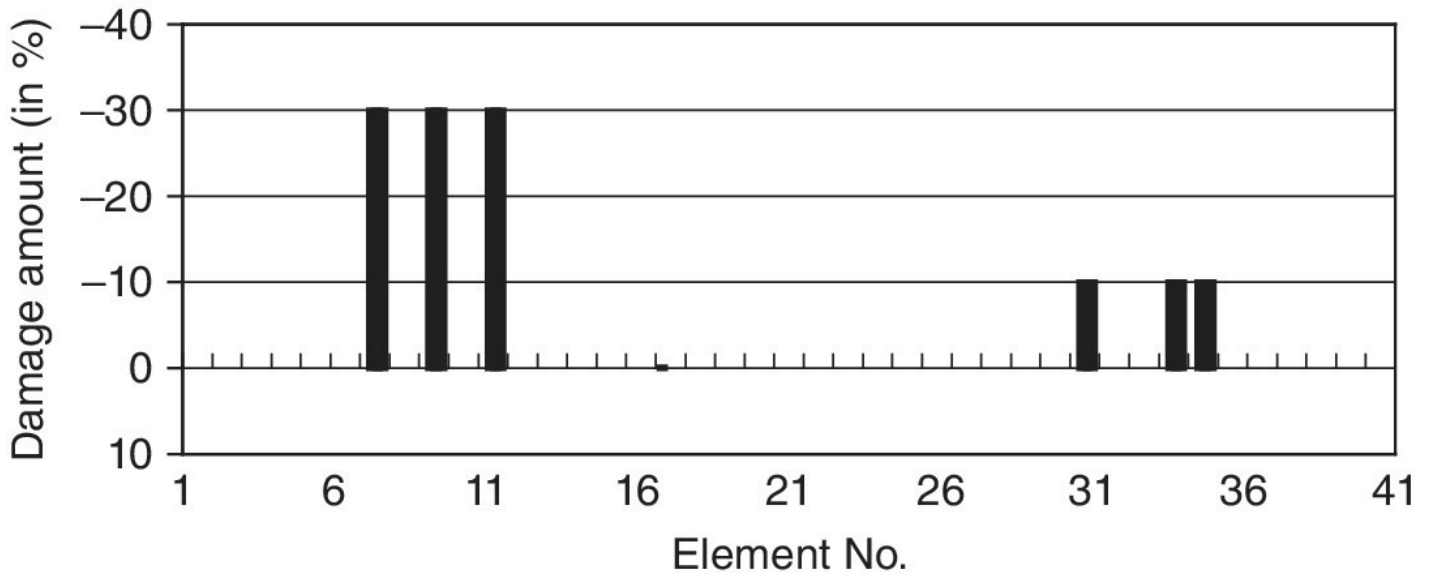


Figure 8.2 Inverse predictions for the hypothetical damage scenario of the plane truss using the residual force vector method.

8.4 Sensitivity Based Methods

Sensitivity based methods rely on the fact that the change of modal parameters – such as natural frequencies, mode shapes and frequency response functions – due to damage in a structure can be approximately expressed by a truncated Taylor series in terms of physical parameters (e.g. damage indicators). If there are sufficient measurements, and a set of damage indicators is properly selected, then the location and quantification of the damage can be identified.

8.4.1 EigenParameter Sensitivity Method

The eigenparameter sensitivities, such as sensitivities of eigenvalues and eigenvectors, are given in Fox and Kapoor (1968) and discussed in [Section 6.4.1](#). The eigenvalue sensitivity is calculated from the derivative of the i th eigenvalue $\lambda_i (= \omega_i^2)$ with respect to the j th physical parameter, as given in [Equation \(6.12\)](#). The eigenvector sensitivity is expressed as a linear combination of the eigenvectors of the structural system, as expressed in [Equation \(6.13\)](#). [Equations \(6.12\)](#) and [\(6.13\)](#) describe the relationships between the derivatives of eigen parameters (e.g. natural frequencies and mode shapes) and the derivatives of the stiffness and mass of the structure due to change of physical parameters (Zhao and DeWolf 1999). Thus, the change of the i th eigenvalue and eigenvector due to structural damage can be approximated by the firstorder Taylor series expansion

$$\Delta\lambda_i = \sum_{j=1}^{ND} \frac{\partial\lambda_i(d_j)}{\partial d_j} \Delta d_j \quad \text{and} \quad \Delta\phi_i = \sum_{j=1}^{ND} \frac{\partial\phi_i(d_j)}{\partial d_j} \Delta d_j \quad (8.21)$$

where Δd_j represents the change in damage indicators, equivalent to damage indicators $d_j = \Delta d_j$ if the original structure is not damaged. The sensitivity equations for Nm modes and a set of ND damage indicators are written in a matrix form as

$$\mathbf{S}_\lambda \mathbf{d} = \Delta\lambda \quad \text{and} \quad \mathbf{S}_\phi \mathbf{d} = \Delta\phi \quad (8.22)$$

where sensitivity matrices and the change of eigenparameter vectors are defined as

$$\mathbf{S}_\lambda = \begin{bmatrix} \partial\lambda_1 / \partial d_1 & \partial\lambda_1 / \partial d_2 & \cdots & \partial\lambda_1 / \partial d_{ND} \\ \partial\lambda_2 / \partial d_1 & \partial\lambda_2 / \partial d_2 & \cdots & \partial\lambda_2 / \partial d_{ND} \\ \vdots & \vdots & \cdots & \vdots \\ \partial\lambda_{Nm} / \partial d_1 & \partial\lambda_{Nm} / \partial d_2 & \cdots & \partial\lambda_{Nm} / \partial d_{ND} \end{bmatrix}, \quad \Delta\lambda = \begin{Bmatrix} \Delta\lambda_1 \\ \Delta\lambda_2 \\ \vdots \\ \Delta\lambda_{Nm} \end{Bmatrix} \quad (8.23a)$$

$$\mathbf{S}_\phi = \begin{bmatrix} \partial\phi_1 / \partial d_1 & \partial\phi_1 / \partial d_2 & \cdots & \partial\phi_1 / \partial d_{ND} \\ \partial\phi_2 / \partial d_1 & \partial\phi_2 / \partial d_2 & \cdots & \partial\phi_2 / \partial d_{ND} \\ \vdots & \vdots & \cdots & \vdots \\ \partial\phi_{Nm} / \partial d_1 & \partial\phi_{Nm} / \partial d_2 & \cdots & \partial\phi_{Nm} / \partial d_{ND} \end{bmatrix}, \quad \Delta\phi = \begin{Bmatrix} \Delta\phi_1 \\ \Delta\phi_2 \\ \vdots \\ \Delta\phi_{Nm} \end{Bmatrix} \quad (8.23b)$$

The derivatives of the stiffness and mass matrices of the structure due to structural damage, $\frac{\partial\mathbf{K}}{\partial d_j}$ and $\frac{\partial\mathbf{M}}{\partial d_j}$, can be determined from the characterisation of structural damage, as discussed in [Section 8.2](#). The changes of the i th natural frequency and mode shape are expressed as $\Delta\lambda_i = \hat{\lambda}_i - \lambda_i$ and $\Delta\phi_i = \hat{\phi}_i - \phi_i$, respectively.

Finally, the damage indicators $\mathbf{d} = \{d_1 \quad d_2 \quad \dots \quad d_{ND}\}^T$ can be evaluated from the sensitivity equations in [Equation \(8.22\)](#). The eigenparameters of the damaged and undamaged structure must be paired by using the modal assurance criterion (MAC) defined in [Equation \(5.20\)](#). In modal testing of civil engineering structures, natural frequencies can be measured more accurately than mode shapes, and they are often preferably used for damage identification. To reduce the influence of noise in measurements, a regularised solution procedure, as described in [Section 6.5.2](#), should be adopted for finding reliable solution of damage indicators.

8.4.2 FRF Sensitivity Method

There are some major advantages of using the frequency response functions (FRFs) data, compared with modal data, such as natural frequencies and mode shapes (Carden and Fanning 2004). Modal data can be contaminated by modal extraction errors in addition to measurement noise, since they are derived data sets. A modal data set is typically incomplete and extracted from a very limited range near resonance. On the other hand, the FRF can provide much more information on structural damage in a desired frequency range. As discussed in [Section 5.2.2](#), the change of the FRF matrix can be given by using a linear Taylor series expansion with respect to damage indicator d_j :

$$\Delta \mathbf{H}(\omega) = \hat{\mathbf{H}}(\omega) - \mathbf{H}(\omega) = \sum_{j=1}^{ND} \frac{\partial \mathbf{H}(\omega)}{\partial d_j} \Delta d_j \quad (8.24)$$

where $\hat{\mathbf{H}}(\omega)$ and $\mathbf{H}(\omega)$ are FRF matrices of the damaged and undamaged structure, respectively. From the relation in [Equation \(5.16\)](#), i.e. $\mathbf{Z}(\omega)\mathbf{H}(\omega) = \mathbf{I}$, and applying the differentiation to the relation, gives

$$\frac{\partial \mathbf{H}(\omega)}{\partial d_j} = -\mathbf{Z}(\omega)^{-1} \frac{\partial \mathbf{Z}(\omega)}{\partial d_j} \mathbf{H}(\omega) = -\mathbf{H}(\omega) \frac{\partial \mathbf{Z}(\omega)}{\partial d_j} \mathbf{H}(\omega) \quad (8.25)$$

where the derivative of dynamic stiffness matrix with respect to damage indicator is given as

$$\frac{\partial \mathbf{Z}(\omega)}{\partial d_j} = \left(-\omega^2 \frac{\partial \mathbf{M}}{\partial d_j} + j\omega \frac{\partial \mathbf{C}}{\partial d_j} + \frac{\partial \mathbf{K}}{\partial d_j} \right) \quad (8.26)$$

From [Equation \(8.25\)](#), the sensitivity equation for FRFs in [Equation \(8.24\)](#) is rewritten as

$$\sum_{j=1}^{ND} \mathbf{S}_j(\omega) d_j = \Delta \mathbf{H}(\omega) \quad (8.27)$$

where damage indicators $d_j = \Delta d_j$ by assuming no damage in the original structure, and the sensitivity matrix is defined as

$$\mathbf{S}_j(\omega) = -\mathbf{H}(\omega) \frac{\partial \mathbf{Z}(\omega)}{\partial d_j} \mathbf{H}(\omega) \quad (8.28)$$

The above firstorder approximation is based on the assumption that small change in the damage indicators cause small change in the FRFs. The firstorder approximation becomes critical when the FRF values are close to resonance. In the special cases of slightly damped systems, the shift of the frequencies may lead to significant deviation of the FRFs, since the peaks of the FRFs reach very large values (Balageas et al. 2006). To tackle this problem, the sensitivity matrix in [Equation \(8.28\)](#) can be revised as

$$\mathbf{S}_j(\omega) = -\mathbf{H}(\omega) \frac{\partial \mathbf{Z}(\omega)}{\partial d_j} \hat{\mathbf{H}}(\omega) \quad (8.29)$$

where $\hat{\mathbf{H}}(\omega)$ is used to replace the $\mathbf{H}(\omega)$ on the right side of [Equation \(8.28\)](#).

On the basis of the sensitivity [equation \(8.27\)](#), structural damage can be identified by using a leastsquares method or a regularised solution procedure, as discussed in [Section 6.5.2](#). In the FRF sensitivity method, the measured data at all DOFs is assumed to be available under the excitation, which is not feasible in practice. Therefore, the unknown DOFs of the damaged structure should be determined by an expansion of the measured DOFs, such as static or dynamic expansions, as discussed in [Section 5.6](#). The best identification results are obtained at lower frequency ranges. In the case of small damages, the errors are the main influence in the damage identification quality, whereas for large damages the incompleteness of measurements becomes the most important factor. Damage identification directly using FRFs may not be able to offer significant advantages over those using the extracted modal data, since the direct use of FRFs in damage identification causes the error to be spread throughout the stiffness matrix. However, when modes are closely spaced, the direct use of FRF data could offer an advantage over modal data.

8.4.3 Example for Damage Assessment – a Grid Structure

A simple grid structure illustrated in [Figure 8.3](#) is employed for inverse structural damage identification by the sensitivity based method using damaged natural frequencies. The structure, which is simply supported at each of the outer corner points, has five structural members, four nodes and nine DOFs. All structural members have the same material properties with Young's modulus $E = 2.1 \times 10^{11}$ N/m², Poisson's ratio $\nu = 0.3$ and density $\rho = 7800$ kg/m³. They have the same crosssection area $A = 0.0045$ m², second moment of area $I = 4.25 \times 10^{-6}$ m⁴ and torsional constant $J = 8.50 \times 10^{-6}$ m⁴. The geometry of the structure with outer dimensions of 3 m, 4 m and 5 m, and the element numbering is shown in [Figure 8.3](#).

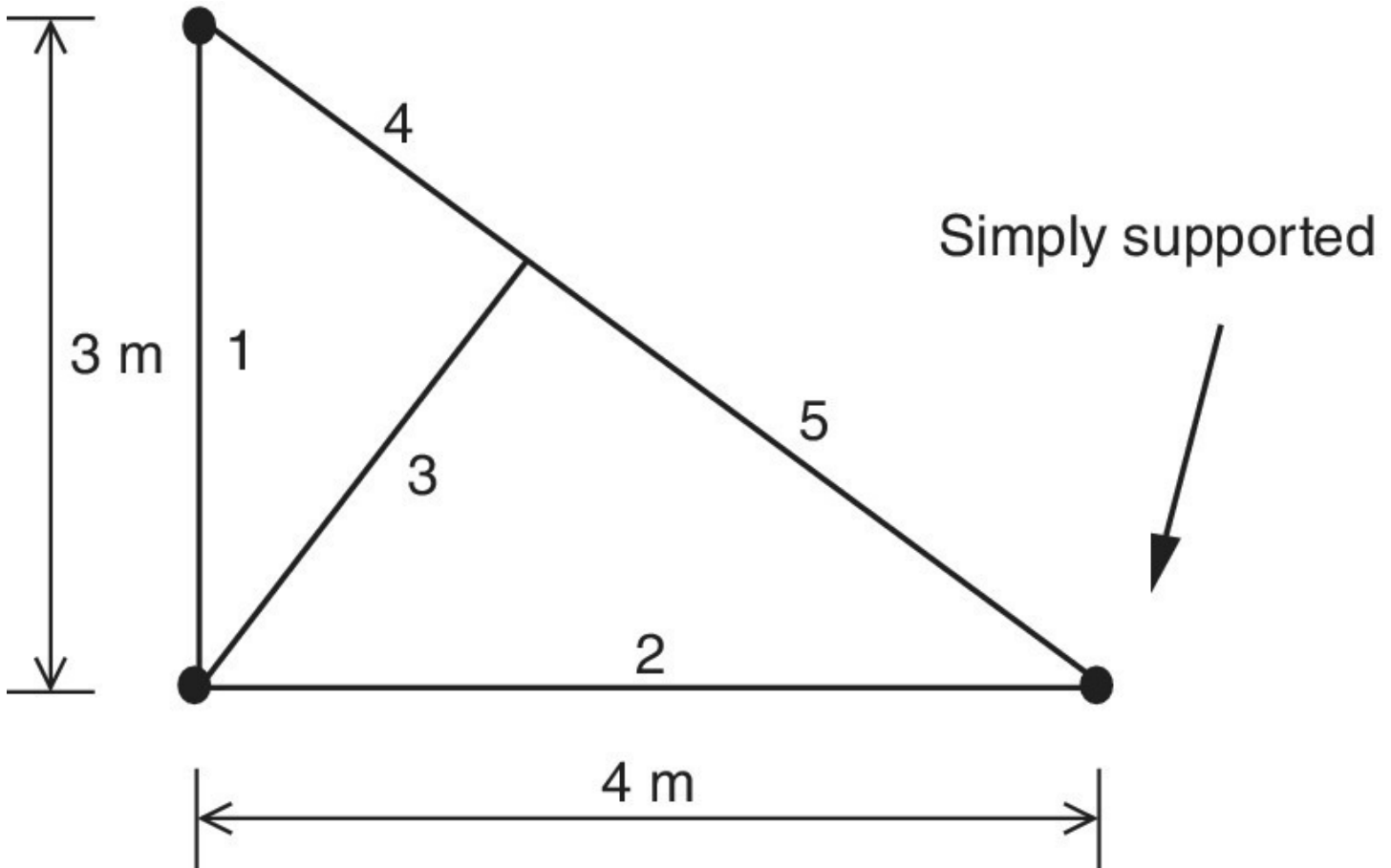


Figure 8.3 Simply supported grid structure (plane view).

A hypothetical damage scenario is induced by reducing the Young's modulus in different elements with different magnitudes, i.e. 0% at element 1, -5% at element 2, -10% at element 3, -15% at element 4, and -20% at element 5. A finite element analysis is performed for both the original and the damaged states to calculate natural frequencies. The first five natural frequencies for the original and damaged structure are listed in [Table 8.2](#).

Table 8.2 First five natural frequencies (Hz) for original and damaged structure.

Mode	1	2	3	4	5
Original	5.7189	14.0371	21.6589	28.3530	46.5395
Damaged	5.3127	13.4261	20.9949	26.3554	44.0490

The sensitivity method is utilised to inversely identify the location and extent of the hypothetical damage. The first five damaged natural frequencies are used for the damage identification. From the results shown in [Figure 8.4](#), the sensitivity based method can provide a reasonable estimate of the location and extent of the hypothetical damage for the grid structure.

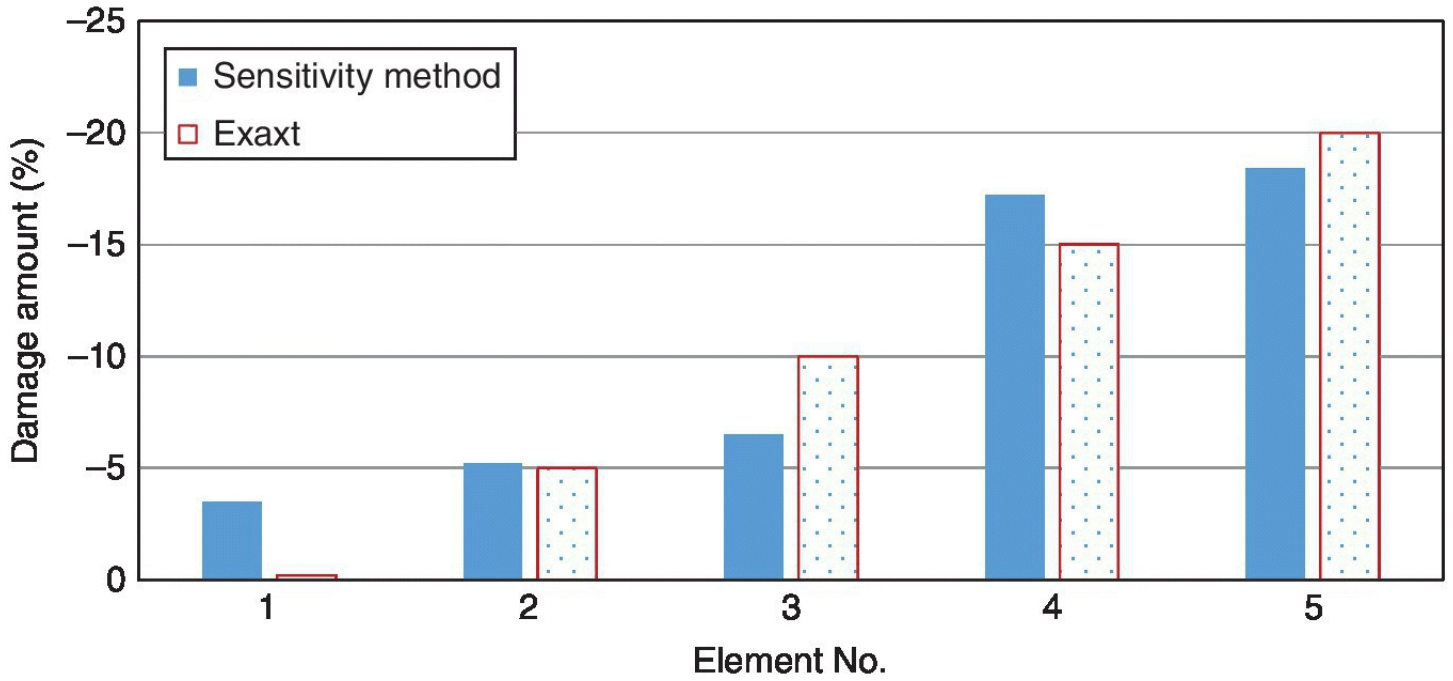


Figure 8.4 Inverse damage identification from the sensitivity based method using natural frequencies.

8.5 Damage Assessment Using Dynamic Perturbation Method

For large civil engineering structures, the sensitivity methods based on the firstorder Taylor series expansion may not be able to provide accurate identification of damage location and quantification. To tackle this problem, the dynamic perturbation method (Chen 2005), as discussed in [Section 6.5](#), is then adopted for structural damage assessment, since this method gives an exact relationship between the perturbation of structural parameters caused by damage and the perturbation of the associated modal parameters.

8.5.1 Use of Frequencies Only

Consider the cases where only a total number of Nm measured natural frequencies of the damaged structure are available. By using the change in eigenvalue $\Delta\lambda_i = \hat{\omega}_i^2 - \omega_i^2$ and ignoring change in mass due to damage $\Delta\mathbf{M} = 0$, the governing [equation \(6.28a\)](#) is rewritten as

$$\phi_i^T \Delta\mathbf{K}(\phi_i + \Delta\phi_i) - (\hat{\omega}_i^2 - \omega_i^2) = 0 \quad (8.30)$$

From [Equation \(6.30\)](#), the change of the i th eigenvector is rewritten as

$$\Delta\phi_i = \sum_{k=1, k \neq i}^{NC} C_{ik} \phi_k \quad (8.31)$$

When k is large enough, the terms with subscripts greater than k can be neglected. Therefore, N can be suitably replaced by NC , denoting the number of the original eigenvectors available (Bicanic and Chen 1997). The mode participation factors C_{ik} are obtained from [Equation \(6.31\)](#), rewritten as

$$C_{ik} = \frac{1}{\left(\hat{\omega}_i^2 - \omega_k^2 - \phi_k^T \Delta \mathbf{K} \phi_k\right)} \left[\phi_k^T \Delta \mathbf{K} \phi_i + \sum_{l=1, l \neq i, k}^{NC} \phi_k^T \Delta \mathbf{K} \phi_l C_{il} \right] \quad (8.32)$$

Considering the change in stiffness caused by damage in a structure given in [Equation \(8.11\)](#), the set of nonlinear [Equation \(8.30\)](#) and [Equation \(8.32\)](#) can be expressed as

$$\sum_{j=1}^{ND} a_{iji} d_j + \sum_{j=1}^{ND} \sum_{l=1, l \neq i}^{NC} a_{ijl} C_{il} d_j - \left(\hat{\omega}_i^2 - \omega_i^2\right) = 0 \quad (8.33)$$

$$C_{ik} = \frac{1}{\left(\hat{\omega}_i^2 - \omega_k^2 - \sum_{j=1}^{ND} a_{kjk} d_j\right)} \left[\sum_{j=1}^{ND} a_{kji} d_j + \sum_{j=1}^{ND} \sum_{l=1, l \neq i, k}^{NC} a_{kjl} d_j C_{il} \right] \quad (8.34)$$

where a_{iji} , a_{ijl} , a_{kji} and a_{kjl} are the eigenmode stiffness sensitivity coefficients, defined in a general form as

$$a_{kjl} = \phi_k^T \mathbf{K}_j \phi_l \quad (8.35)$$

An iterative computational procedure is required to solve for the structural damage indicators d_j and the mode participation factors C_{ik} using the above formulations. First, the initial mode participation factors C_{ik} are assumed to be zero. A first approximation for the damage indicators d_j is then obtained from [Equation \(8.33\)](#). Depending on the total number of damaged frequencies available Nm (number of equations) and the total number of damage indicators present ND (number of unknowns), the sensitivity coefficient matrix in [Equation \(8.33\)](#) may not be square. In order to find a solution for what is, in general, an illconditioned system, the regularised solution procedure discussed in [Section 6.5.2](#) is employed to estimate the damage indicators d_j . After the initial damage indicators d_j are obtained, the next approximation for the mode participation factors C_{ik} can be calculated from [Equation \(8.34\)](#). Consequently, [Equations \(8.33\)](#) and [\(8.34\)](#) are used recursively to compute further approximations for d_j as well as C_{ik} . The above recursive process is repeated until the convergence for damage indicators d_j is achieved.

8.5.2 Use of Incomplete Modes

In modal testing for a civil engineering structure, only a limited number of lower order

natural frequencies can typically be identified from recorded vibration measurements. The limited information on the frequencies of the damaged structure may not be sufficient to correctly assess damage in the structure. Thus, to accurately identify the location and evaluate the severity of damage, it is important to directly utilise the measured incomplete mode shape readings of the damaged structure, in the process of damage location and quantification identification.

Consider that the information about a total of N_s ($<N$) DOF readings of the i th mode shape for the damaged structure $\hat{\Psi}_i^a$ is available. The measured incomplete mode shapes $\hat{\Psi}_i^a$ must be paired to the mode shapes of the original structure restrained to measured DOFs, i.e. ϕ_i^a , by using the modal assurance criterion defined in [Equation \(5.20\)](#). The measured DOF readings $\hat{\Psi}_i^a$ have to be scaled by the modal scale factor (MSF_i) defined in [Equation \(5.26\)](#), giving the scaled modal measurement vector $\hat{\phi}_i^a = MSF_i \cdot \hat{\Psi}_i^a$. The mode scale factor MSF_i has to be updated for each iteration (if an iterative procedure is required), since $\hat{\phi}_i^a$ must be scaled in such a way as to be close to the corresponding remaining unknown components. Consequently, the i th complete eigenvector for the damaged structure $\hat{\phi}_i$ is obtained from the known vector $\phi_i^a = \hat{\phi}_i^a + \phi_i^u$ and the change of unknown components $\Delta\phi_i^u$, expressed in [Equation \(6.49\)](#) and rewritten as

$$\hat{\phi}_i = \phi_i^a + \sum_{l=1, l \neq i}^{NC} C_{il} \phi_l^u \quad (8.36)$$

By combining the dynamic perturbation governing equations in [Equation \(6.32\)](#) and [Equation \(6.28a\)](#), and ignoring change in mass due to damage $\Delta\mathbf{M} = 0$, the exact relationship between the change in stiffness caused by damage and the measured mode shape readings of the damaged structure is expressed as

$$\sum_{k=1}^N \frac{\phi_k}{(\hat{\omega}_i^2 - \omega_i^2)} \phi_k^T \Delta\mathbf{K} \hat{\phi}_i - \hat{\phi}_i = 0 \quad (8.37)$$

From the constructed complete eigenvector of the damaged structure in [Equation \(8.36\)](#), [Equation \(8.37\)](#) is now restricted to the dimension for the measured components and becomes

$$\sum_{k=1}^N \frac{\phi_k^a}{(\hat{\omega}_i^2 - \omega_i^2)} \left[\phi_k^T \Delta\mathbf{K} \left(\phi_i^a + \sum_{l=1, l \neq i}^{NC} C_{il} \phi_l^u \right) \right] - \hat{\phi}_i^a = 0 \quad (8.38)$$

When a total number of Nm modes with N_s DOF readings each are measured on the damaged structure, the proceeding formulation comprises a total of NM ($= Nm \times N_s$) equations. This formulation is also suitable for special cases that all DOF readings for the damaged structure are available ($N_s = N$), that is, the damaged mode shapes are complete.

By using the change in stiffness caused by structural damage given in [Equation \(8.11\)](#), the governing equation [Equation \(8.38\)](#) is rewritten as

$$\sum_{j=1}^{ND} \mathbf{p}_{jii}^a d_j + \sum_{j=1}^{ND} \sum_{l=1, l \neq i}^{NC} \mathbf{p}_{jil}^u C_{il} d_j - \hat{\phi}_i^a = 0 \quad (8.39)$$

where the eigenmode stiffness sensitivity vectors \mathbf{p}_{jii}^a and \mathbf{p}_{jil}^u are defined in [Equation \(6.54a\)](#). The recursive relation for computing the mode participation factor C_{ik} , defined in [Equation \(6.31\)](#), is expressed as

$$C_{ik} = \frac{1}{(\hat{\omega}_i^2 - \omega_i^2)} \left[\sum_{j=1}^{ND} g_{kji}^a d_j + \sum_{j=1}^{ND} \sum_{l=1, l \neq i}^{NC} g_{kjl}^u d_j C_{il} \right] \quad (8.40)$$

where g_{kji}^a and g_{kjl}^u are the eigenmode stiffness sensitivity coefficients, defined in [Equation \(6.56a\)](#).

The set of nonlinear governing equations – i.e. [Equation \(8.39\)](#) and [Equation \(8.40\)](#) – forms a basis for an iterative solution procedure to solve for damage indicators d_j . Similarly, the initial mode participation factors C_{ik} are assumed to be equal to zero. A first estimate for the damage indicators d_j is then obtained from [Equation \(8.39\)](#). Here again, the regularised solution procedure discussed in [Section 6.5.2](#) is employed to estimate the damage indicators. The next estimate for the mode participation factors C_{ik} is obtained from [Equation \(8.40\)](#). Therefore, [Equations \(8.39\)](#) and [\(8.40\)](#) are utilised recursively to compute further estimate for d_j as well as C_{ik} , until the condition of convergence for d_j is satisfied.

8.5.3 Examples for Damage Assessment – Simple Framed Structures

The dynamic perturbation method is now used to inversely assess the assumed damage in two simple framed structures, i.e. a grid structure and a plane truss.

8.5.3.1 Damage Assessment of a Grid Structure Using Frequencies Only

The simple grid structure, as discussed in [Section 8.4.3](#) and illustrated in [Figure 8.3](#), is used for the inverse damage identification by the dynamic perturbation method using frequencies only. A damage scenario is assumed by reducing the Young's modulus: no damage in element 1, –5% in element 2, –10% in element 3, –15% in element 4 and –20% in element 5. The natural frequencies for the original and damaged structure, calculated by the finite element analysis, are listed in [Table 8.2](#).

The information about five damaged frequencies is now used to determine inversely the location and amount of the assumed damage by the dynamic perturbation method. The convergence performance of structural damage parameters for the iterative procedure is shown in [Figure 8.5](#). The iterative solution procedure achieves convergence after only a few

iterations. Both the location and extent of the assumed damage are exactly identified using five damaged natural frequencies, since the number of damaged natural frequencies used in damage identification equals the number of structural damage parameters.

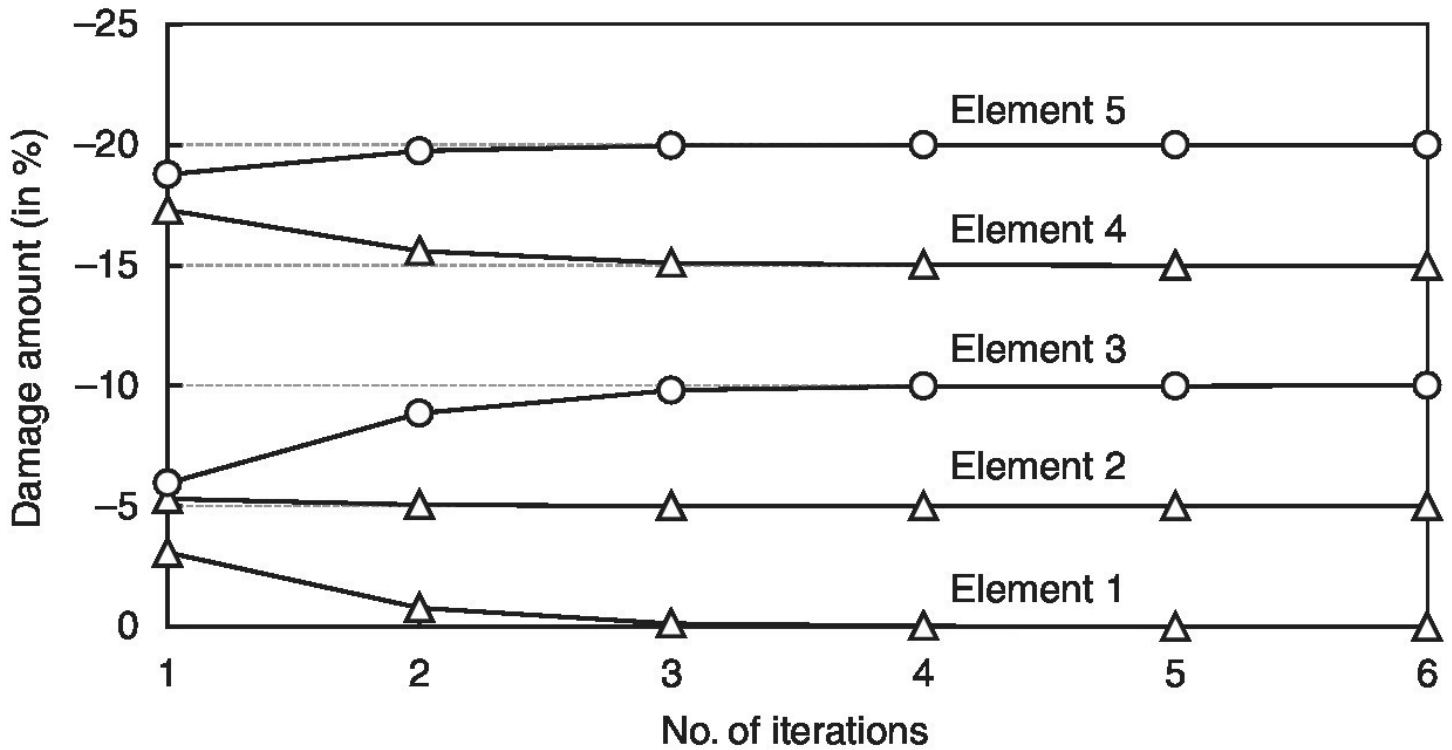


Figure 8.5 Inverse damage identification using the dynamic perturbation method from 5 damaged frequencies.

8.5.3.2 Damage Assessment of a Plane Truss Using Incomplete Modes

A onebay sixbar truss shown in [Figure 8.6](#) is adopted for the inverse damage location and quantification identification from incomplete modes using the dynamic perturbation method. The truss has six structural members, four nodes and five DOFs. All structural members have the identical properties with Young's modulus $E = 2.1 \times 10^{11} \text{ N/m}^2$, density $\rho = 7800 \text{ kg/m}^3$ and cross-sectional area $A = 0.0004 \text{ m}^2$. The geometry of the truss model and the element numbering are also shown in [Figure 8.6](#).

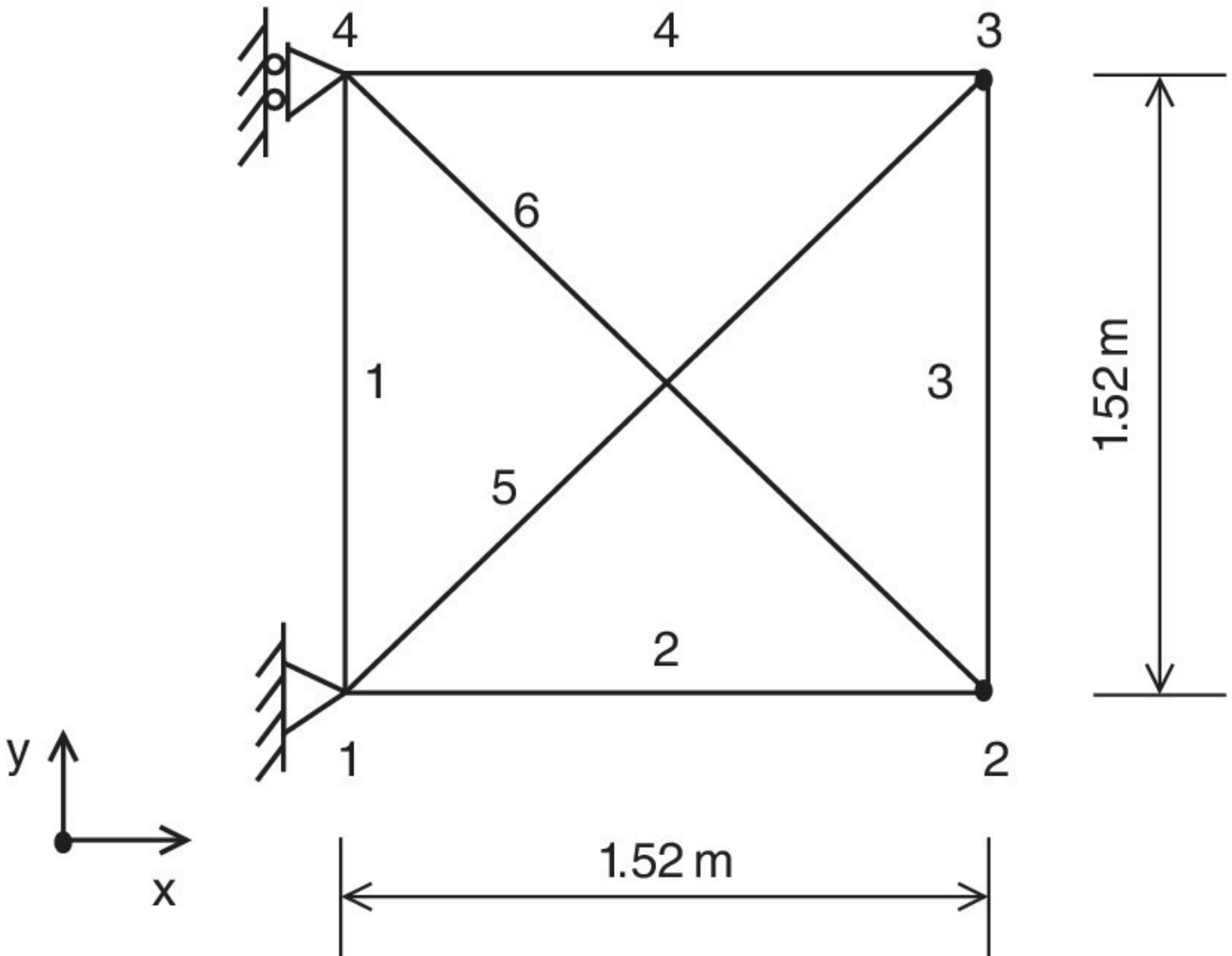
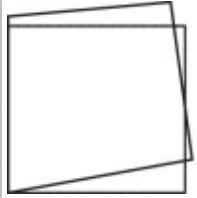
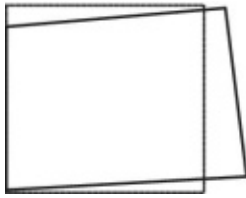
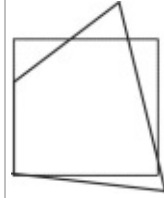
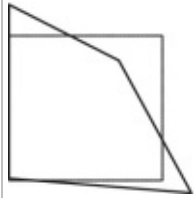


Figure 8.6 Onebay sixbar plane truss structure.

A hypothetical damage scenario is simulated with the reduced Young's modulus in three truss elements: -10% in element 2, -20% in element 3, and -30% in element 5. A finite element analysis was performed for both the original and the damaged states to calculate natural frequencies and the corresponding mode shapes. The first four natural frequencies for the original and damaged structure, together with the corresponding mode shapes for the original structure, are given in [Table 8.3](#). In addition, a set of selected sensor positions is assumed, i.e. at nodes 2 and 3, and the set of incomplete damaged mode shapes is composed of DOF readings for each individual mode, as summarised in [Table 8.3](#).

Table 8.3 First four natural frequencies (Hz) and original mode shapes.

Mode	1	2	3	4
Original frequency	214.47	509.73	570.35	719.64
Damaged frequency	205.94	491.00	557.52	680.18
Measured DOF	2 - y, 3 - x	—	2 - y	2 - y, 3 - x,y
Original mode shape				

The information about the set of incomplete damaged modal data is used to inversely identify the location and amount of the hypothetical structural damage. The convergence performance of structural damage indicators for the iterative solution procedure is shown in [Figure 8.7](#). The dynamic perturbation method using incomplete modes is able to accurately identify the location and extent of the damage using limited incomplete mode shape readings, and achieves convergence after only a few iterations.

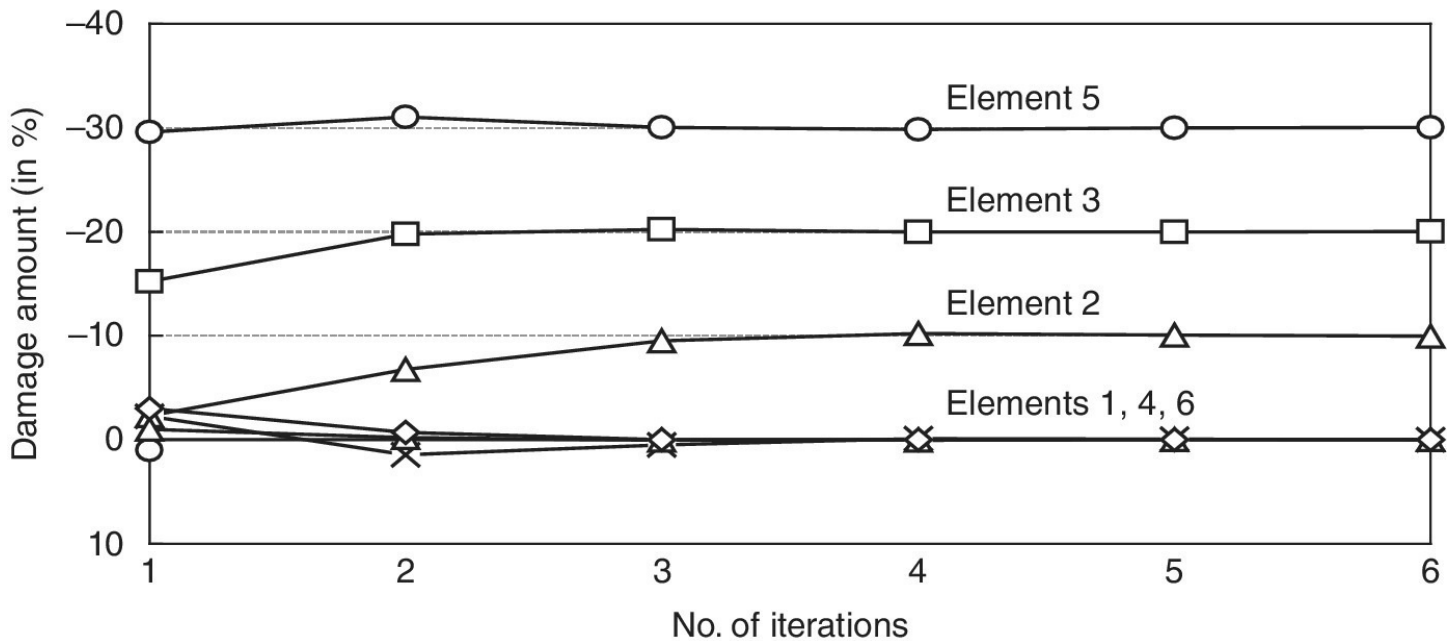


Figure 8.7 Inverse damage identification using the dynamic perturbation method from incomplete modes.

8.6 Numerical Examples

Two numerical examples – a framed building structure and a gravity dam structure, – are used for the location and quantification identification of damage in the structures using the dynamic perturbation method.

8.6.1 Framed Building Structure

The framed building model, as described in the study by Johnson et al. 2004, is adopted for the inverse damage location and quantification identification using the dynamic perturbation method. The structure concerned is a fourstorey, twobay by twobay laboratory scale model structure, comprising beam and column elements with diagonal bracing elements on each storey. The structure has a $2.5\text{ m} \times 2.5\text{ m}$ plan and is 3.6 m tall. A diagram of the finite element model of the structure with node and element numbering is shown in [Figure 8.8](#). The lengths and sectional and material properties of structural members adopted in calculations are listed in [Table 8.4](#). In addition to the selfweight of the structural members, there are floor slab masses on each floor, i.e. 3200 kg slabs on the first floor, 2400 kg slabs on each of the second and third floors and 1750 kg slabs on the top floor.

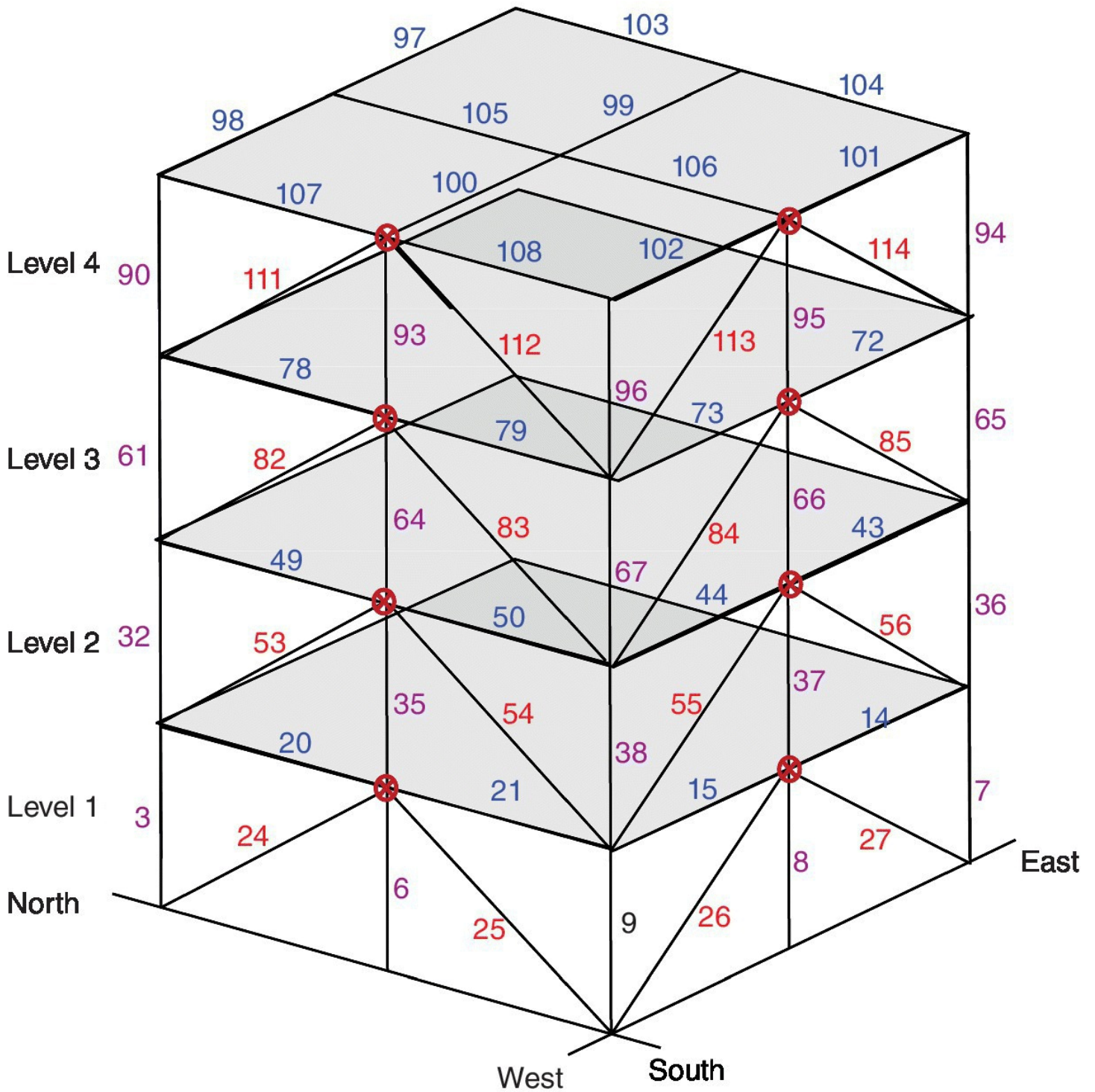


Figure 8.8 Finite element model of the framed building structure with element numbering and sensor locations (marked with ⊗).

Table 8.4 Geometric and material properties of the structural members of the framed building structure.

Property	Columns	Floor beams	Braces
Length L (m)	0.90	1.25	1.54
Crosssectional area A (m ²)	1.133×10^{-3}	1.430×10^{-3}	0.141×10^{-3}
Moment of inertia I – strong direction (m ⁴)	1.970×10^{-6}	1.220×10^{-6}	—
– weak direction (m ⁴)	0.664×10^{-6}	0.249×10^{-6}	—
Torsion constant J (m ⁴)	8.01×10^{-9}	38.2×10^{-9}	—
Young's modulus E (Pa)	2.0×10^{11}	2.0×10^{11}	2.0×10^{11}
Shear modulus G (Pa)	$E/2.6$	$E/2.6$	$E/2.6$
Density ρ (kg/m ³)	7800	7800	7800

A finite element model with 120 DOFs shown in [Figure 8.8](#) is utilised to avoid the difficulty in assessing structural damage at local level arising from the reduced shear building model. The finite element model is developed by allowing outofplane motion and rotations, but the floor nodes are restrained to have the same inplane motion and rotation. In order to identify the specific location of damage in individual structural elements, the damage indicators are chosen to characterise structural damage at element level for braces and at critical point level for beams and columns, respectively. A total of 284 damage indicators are employed for damage assessment: 32 for braces, 144 for beams and 108 for columns. The finite element model adopted for damage identification is assumed to be validated before damage, and then considered as the baseline for damage identification. Two simulated damage scenarios are defined in the inverse damage identification problem by reducing the stiffness of braces at various locations, as summarised in [Table 8.5](#).

Table 8.5 Simulated damage scenarios for the framed building structure.

Damage scenario	Damage description	Element No.	Damage amount
Scenario I	No stiffness in one brace on the west side in the first storey	24	-100%
Scenario II	No stiffness in the braces of the first storey	22–29	-100%

The first 12 noise free natural frequencies of the original and damaged structure are obtained from the finite element analysis, as summarised in [Table 8.6](#). A total of 16 sensors at the sides on each floor measuring only at translational DOF readings are considered, as shown in [Figure 8.8](#). The dynamic modal data measurements with errors of the damaged structure are assumed to have been obtained by corrupting the ideal finite element modal data of the damaged structure with a certain level of errors.

Table 8.6 Correlated noise free frequencies (Hz) of the original and damaged structure.

Dominant motion direction	Undamaged	Damage scenario I	Damage scenario II
North y	8.0943	7.6072	4.9393
East x	8.4076	8.4075	6.5679
Torsion θ	13.9100	13.5651	8.9281
North y	22.3162	21.3250	18.2046
East x	23.9701	23.9700	20.8446
North y	35.3625	34.8551	33.7878
Torsion θ	38.9607	38.3516	32.5279
East x	39.6233	39.5665	37.8477
North y	46.2751	46.1910	45.9293
East x	55.3773	55.3766	54.8760
Torsion θ	61.1045	60.7193	58.4037
Torsion θ	80.8070	80.7021	80.1132

In the inverse predictions of structural damage using the dynamic perturbation method, the system of governing [equations \(8.39\)](#) is typically illconditioned. Thus, a regularised solution procedure, as described in [Section 6.5.2](#), is required. [Figure 8.9](#) indicates the singular values of the sensitivity coefficient matrix, ordinary solution coefficients and regularised solution coefficients for the inverse predictions of damage scenario I for the framed building structure. The singular values range from 2.61 to 1.38×10^{-7} , and the ratio between the largest and the smallest singular values is extremely large. The ordinary solution coefficients increase significantly as the singular values decrease, which makes the solutions for the damage indicators unstable. However, the Tikhonov regularised solution coefficients (Tikhonov and Arsenin 1977) gradually damp out with decrease in the singular values, giving stable solutions for the unknowns.

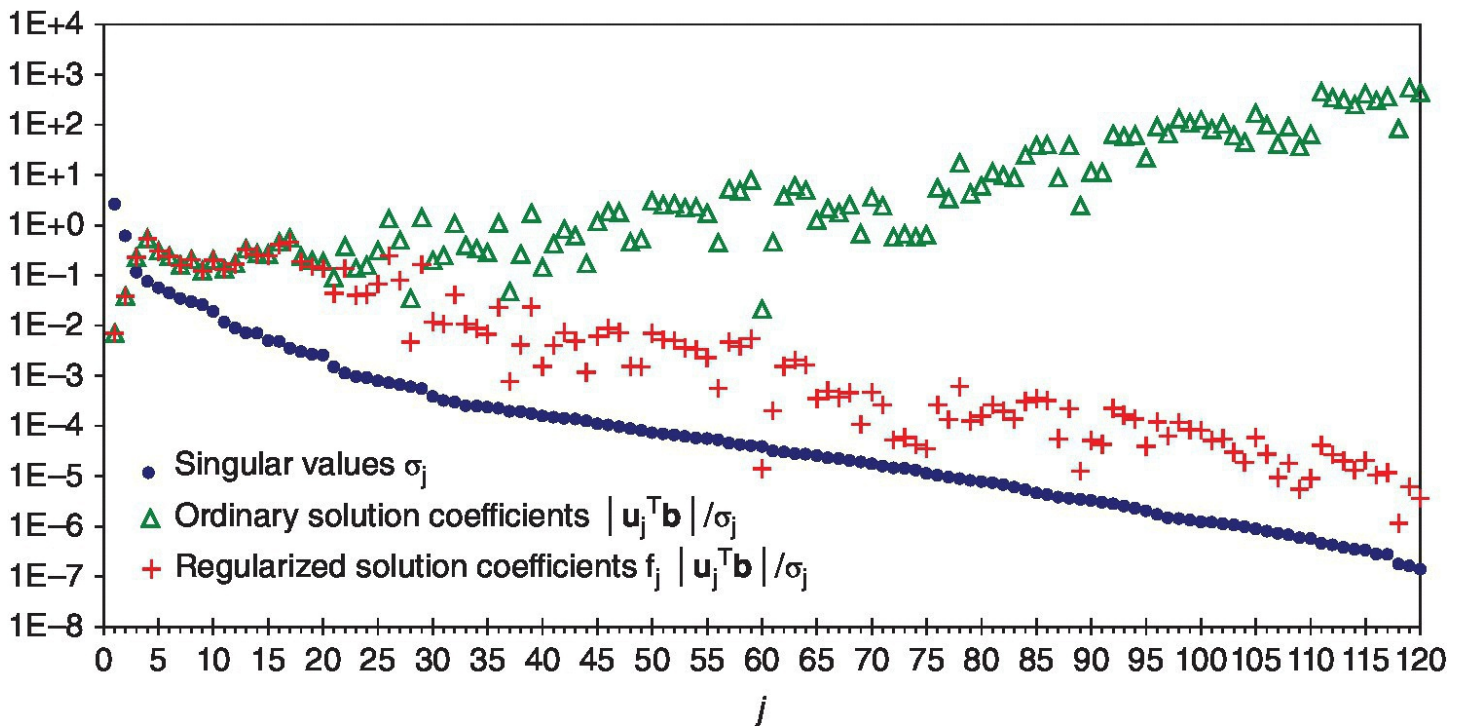


Figure 8.9 Singular values, ordinary solution coefficients and regularised solution coefficients for inverse damage predictions.

[Figure 8.10](#) shows the Lcurves associated with the Tikhonov regularisation discussed in [Section 6.5.2](#) to evaluate regularisation parameters (Hansen and O’Leary 1993). The levels of noise in frequencies of 0.3% and in mode shapes of 1–5% are considered in calculations. The values of regularisation parameter increase as the level of noise in the measured DOF readings increases. This indicates that more regularisation is imposed on the solution, and information on the measured data is gradually lost with the increase of noise level. The flat parts for various noise levels appear very close to each other, where the regularisation parameters are relatively large.

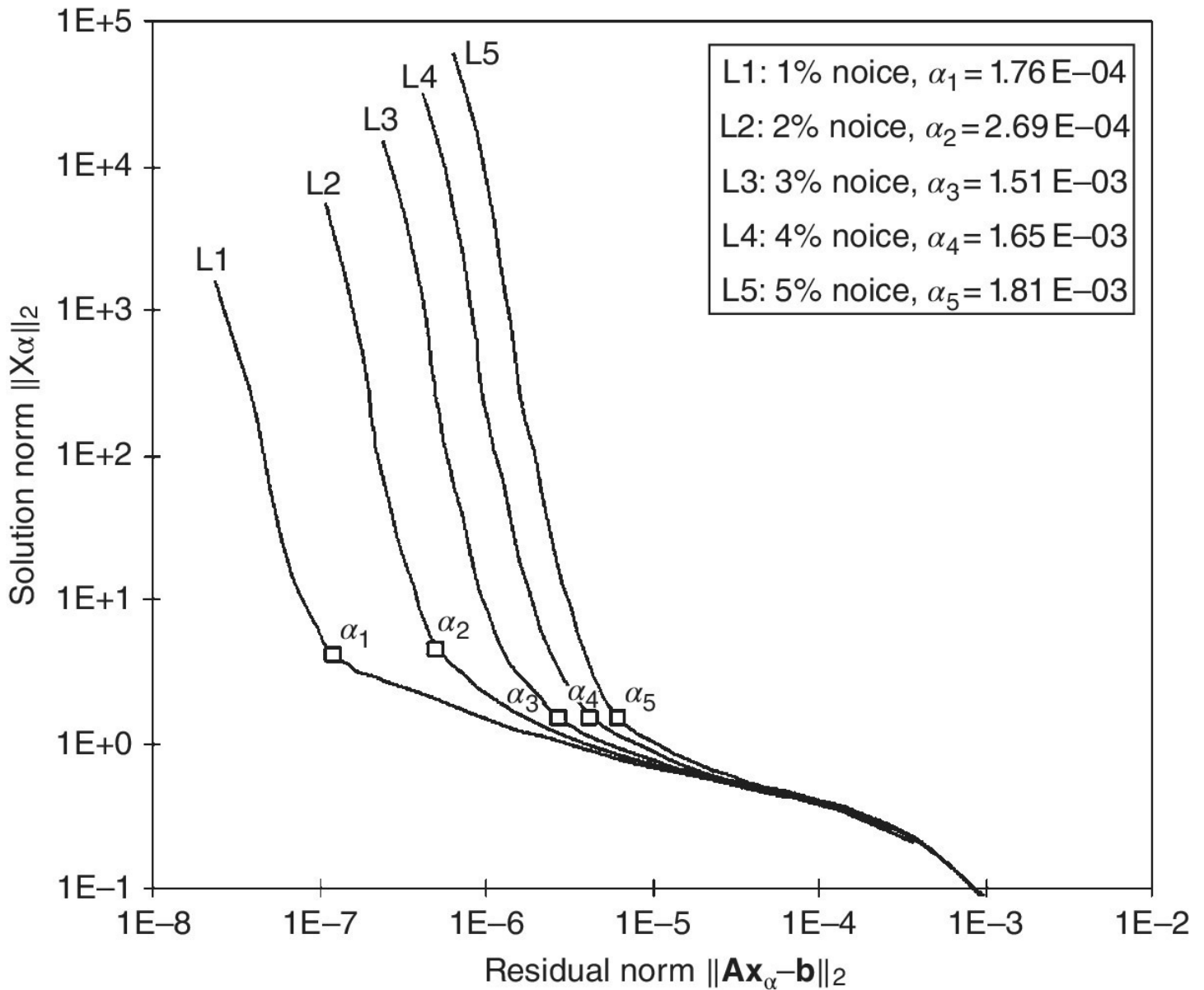


Figure 8.10 Lcurves for Tikhonov regularisation with noise levels ranging from 1% to 5% in measured DOF readings.

In the inverse identification of the assumed damage scenarios I and II, the simulated measurement errors are normally distributed with standard deviations (noise levels) of 0.3% for natural frequencies (maximum error about $\pm 0.9\%$) and 3% for DOF readings of mode shapes (maximum error about $\pm 9\%$). In damage scenario I, stiffness in a single brace in the first storey is completely lost. This damage corresponds to a value of -100% for the selected damage indicator of the damaged brace in the first storey. Information on a total number of 10 incomplete noisy damaged modes is employed for the inverse damage location and quantification identification. The results given in [Figure 8.11](#) show that the actually damaged brace, together with another brace on the same side (west side) in the first storey, is identified. The actual amount of damage is spread closely in these two braces on the same side in the first storey due to the symmetry of the framed building structure.

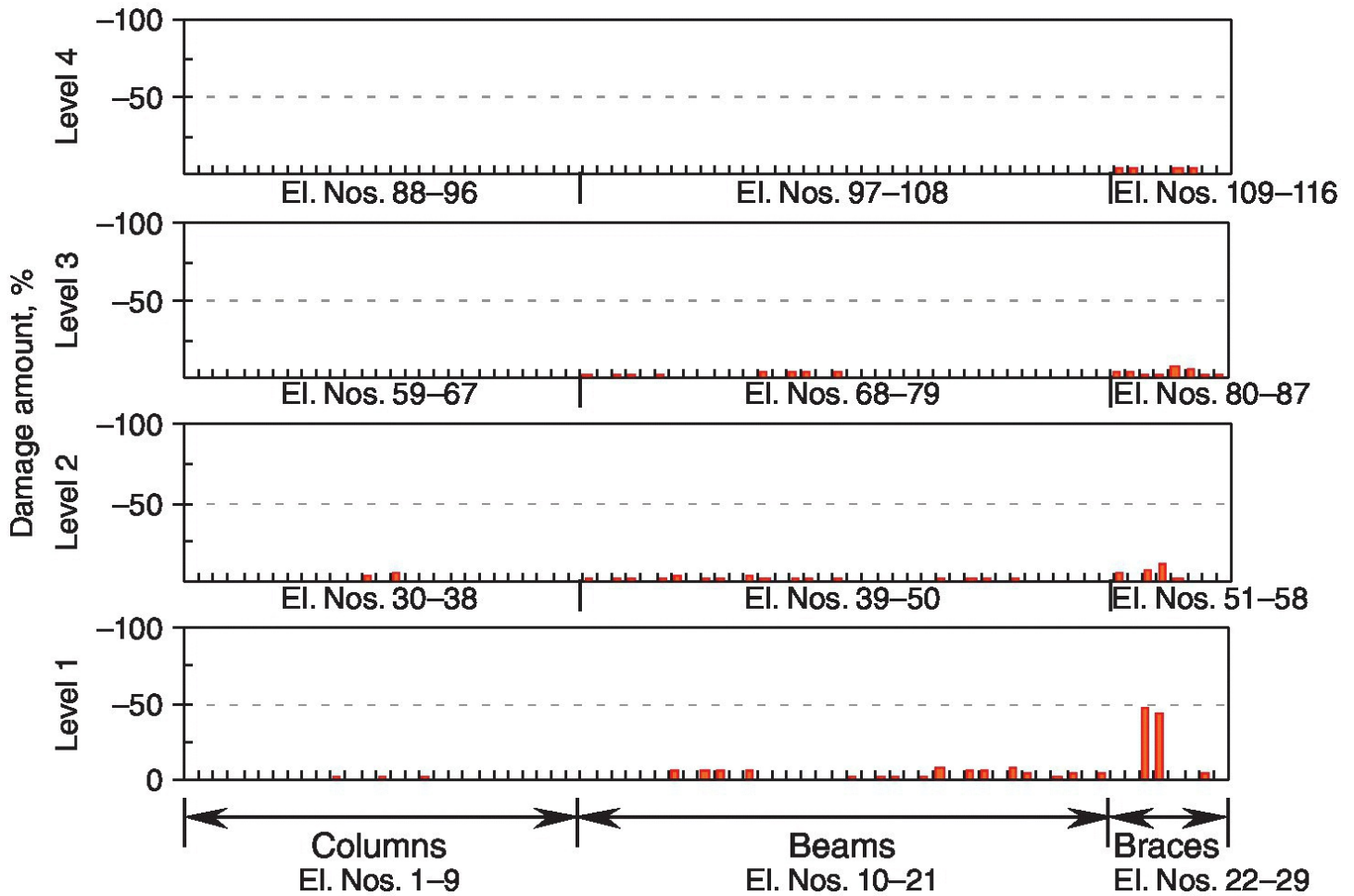


Figure 8.11 Identification of damage scenario I (no stiffness in one brace in first storey, i.e. element no. 24), 10 incomplete noisy damaged modes used.

The assessment of damage scenario II involves the complete loss of stiffness in the braces in the first storey. Information on seven incomplete noisy modes of the damaged structure is employed to inversely identify the assumed damage. The results in [Figure 8.12](#) indicate that the actual location of the damage is correctly identified and the extent of the damage is slightly lower than, but very close to, the actual stiffness loss. Note that structural damage in this damage scenario is extremely severe in real situations, and causes large reduction in stiffness in the first storey and consequently significant reduction in natural frequencies, as shown in [Table 8.6](#). Again, the dynamic perturbation method is capable of providing reliable predictions of the severe damage using limited modal data measurements with realistic errors.

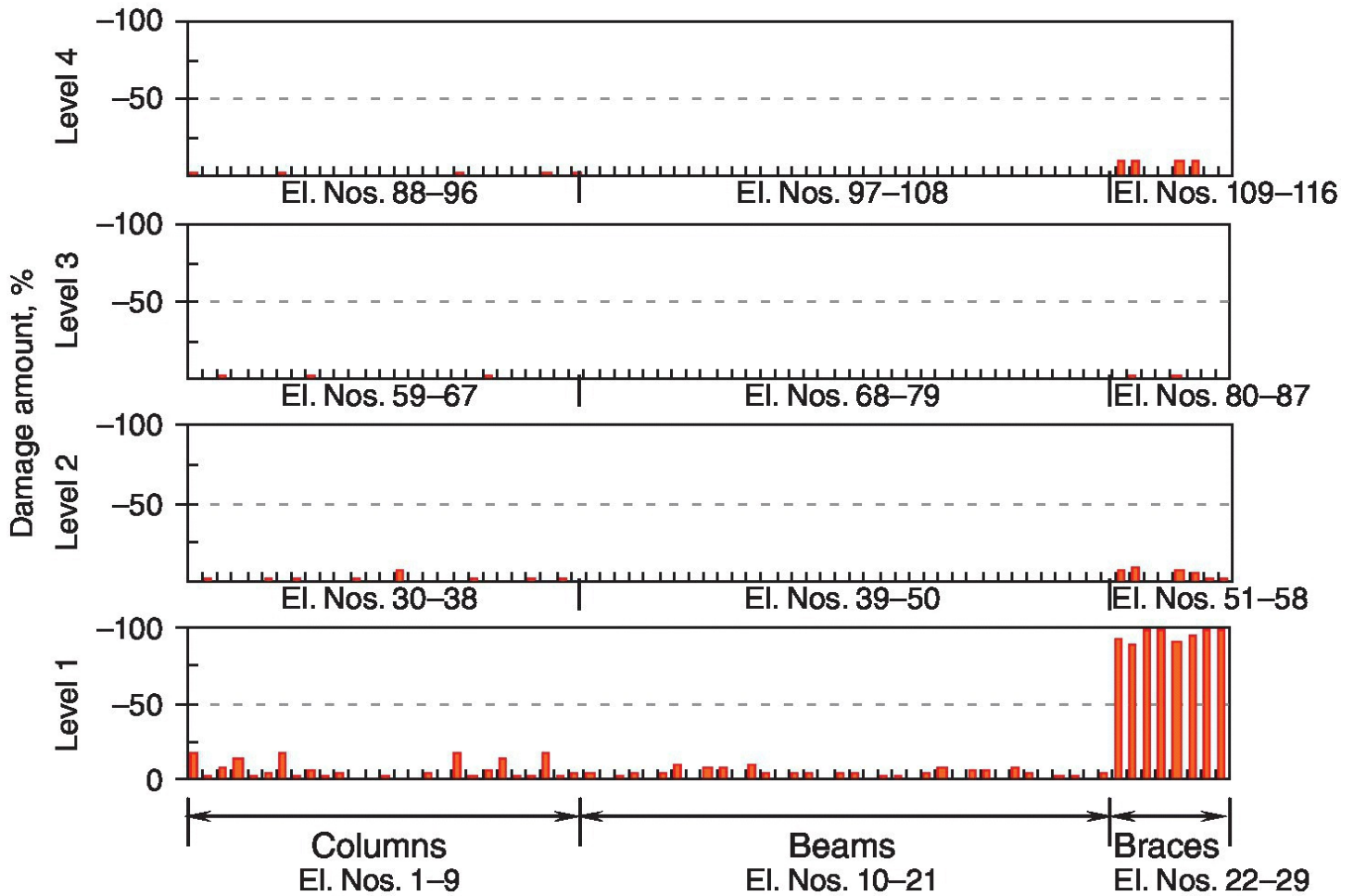


Figure 8.12 Identification of damage scenario II (no stiffness in braces in first storey, i.e. element nos. 22–29), 7 incomplete noisy damaged modes used.

8.6.2 Gravity Dam Structure

A gravity dam structure shown in [Figure 8.13](#) is used for the inverse damage location and quantification identification for the continuum structure by the dynamic perturbation method. A finite element mesh with 248node isoparametric plane strain elements is generated, giving a total of 186 DOFs. Four Gauss integration points are considered for each element in calculations of the element stiffness. A total of 96 damage indicators characterising damage at all the Gauss integration points is employed for the inverse damage identification. All Gauss points have the same material properties with elastic modulus $E = 2.8 \times 10^{10} \text{ N/m}^2$, Poisson's ratio $\nu = 0.15$ and density $\rho = 2400 \text{ kg/m}^3$.

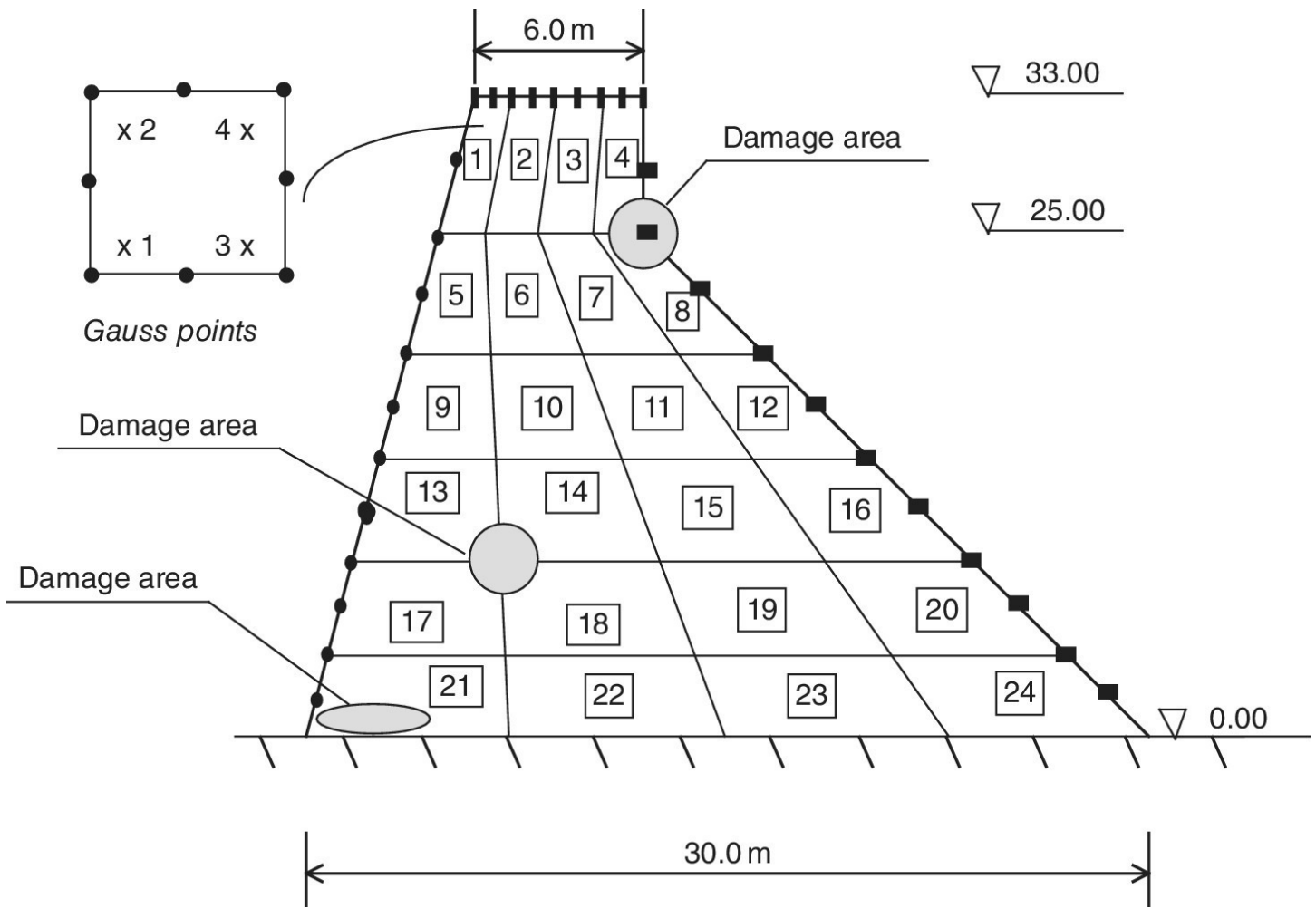


Figure 8.13 Gravity dam structure with measured nodes marked with both ■ and ●.

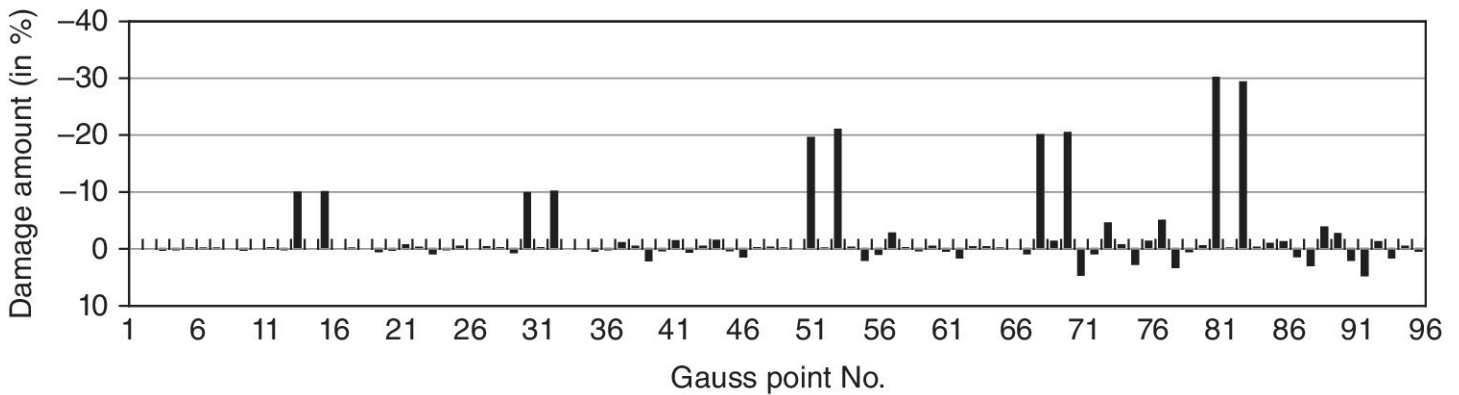
A hypothetical damage scenario for the gravity dam structure is introduced in [Table 8.7](#), where damage occurs at a total number of 10 Gauss points within seven elements with different damage magnitudes. The geometry of the structure, element and Gauss point numbering, hypothetical damage areas, as well as measured locations are shown in [Figure 8.13](#). The modal data with free noise calculated from the finite element analysis for the undamaged structure and the simulated damaged structure is then used for inverse damage assessment.

Table 8.7 Simulated damage scenarios for the gravity dam structure.

Element No	4	8	13	14	17	18	21
Gauss point No	13, 15	30, 32	51	53	68	70	81, 83
Damage amount	-10%	-10%	-20%	-20%	-20%	-20%	-30%

The results shown in [Figures 8.14\(a\)](#) and (b) are inverse damage predictions using information about two different incomplete damaged mode shapes with DOF readings measured at the various locations. The assumed structural damage is determined correctly by using a combination of two incomplete damaged modes. The predictions of structural damage become excellent using the dynamic perturbation method, when information about incomplete damaged modes 2 and 4 is used.

(a) Incomplete damaged modes 1 and 3 used.



(b) Incomplete damaged modes 2 and 4 used.

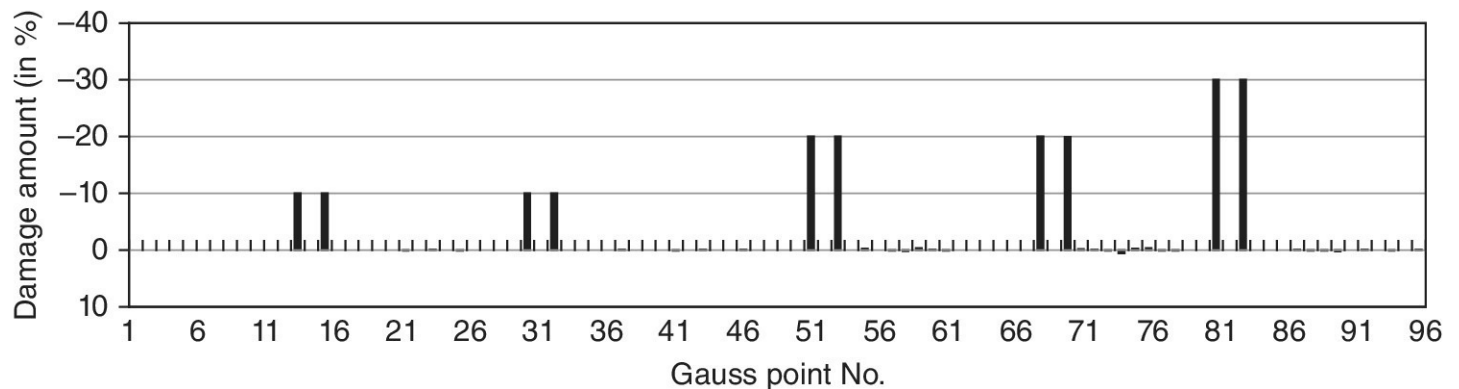


Figure 8.14 Inverse damage predictions using the dynamic perturbation method for the gravity dam structure.

8.7 Potential Problems in VibrationBased Damage Identification

Extensive research on structural damage identification methods has been undertaken in the past a couple of decades. Most widely studied damage identification methods are vibrationbased, and these methods use the measured changes in dynamic features (mainly modal parameters) to evaluate changes in structural parameters that may indicate structural damage or degradation. Although successful applications have been developed during recent years, damage assessment of large civil engineering structures, such as buildings and bridges, remains a challenging task for civil engineers. The primary sources of difficulty include measurement noise, modelling errors, uncertainty of ambient conditions, insensitivity of modal properties to local damage, incompleteness of measured data and lack of practical identification methodologies. These problems are discussed in detail in Worden and Friswell (2009) and are outlined and further extended as follows.

8.7.1 Finite Element Model and Experimental Data

Most damage identification methods such as modelbased methods require a validated finite

element model as the baseline of the structure before damage. For large civil engineering structures like cablesupported bridges, it is extremely difficult to construct a damage detectionoriented structural model. The structural model should meet following points: (a) the calculated modal parameters predicted by the model are well correlated with the measured data from the structure before damage, (b) modal uncertainty due to modelling error is less than modal parameter change caused by actual damage, (c) the size of the finite element model is adequate so that the number of the model DOFs is not extremely larger than that of measured DOFs in modal testing, (d) the model is accurate enough not to blur the damage location in the modelling process.

For large civil engineering structures, the number of DOFs measured is typically much smaller than the number of the finite element model DOFs due to instrumentation limitations, resulting in incomplete set of modal data. To obtain a one-to-one correspondence between the measured and finite element DOFs, a model reduction or modal expansion technique must be used. Both the techniques are used at the expense of losing accuracy. The damage identification capability of many methods will be degraded when using expanded mode shapes or a reduced model. While expansion of measured mode shapes to the order of finite element model would provide a clearer location of structural damage, the errors induced by the expansion process may overshadow damage information contained in the measurements. On the other hand, reduction of the finite element model to the size of the measured DOFs results in the reduced model, which may no longer adequately describe the physical model in sufficient detail to locate the damage. A smearing effect on modelling errors is introduced by the model reduction. Model reduction techniques can also destroy the connectivity information that is important for damage detection. Recently, a perturbed force approach was developed for reliable mode shape expansion. More advanced techniques of matching between the finite element and experimental modal orders are required.

8.7.2 Effect of Modelling and Measurement Errors

There are always errors in the measured data and in the finite element model. These errors unavoidably affect all of the algorithms for structural damage identification. If the real measurements on the damaged structure are adopted for damage identification, the damage identification methods will have great difficulty in distinguishing between the actual damage sites and the location of errors in the original finite element model. If parameters such as damage indicators are not properly selected to consider the undamaged finite element model errors, then this will cause a systematic error between the finite element model and the measured data. Damage identification methods generally have considerable difficulty with systematic errors.

Two approaches can be used to tackle this problem (Worden and Friswell 2009). The first is to update the finite element model of the undamaged structure to produce a reliable finite element model. The quality of the damage identification critically relies on the correctness of updated finite element model. In general, the updated model is validated using a control set of data not used for the model updating. The second utilises differences between the damaged and undamaged response data in damage identification methods. This will remove some error in

the undamaged model of the structure that also exists in the damaged structure. This approach assumes the structure remaining unchanged between the two sets of measurements, except for the damage.

Many of the methods proposed for damage identification are tested on numerical simulations. For successful practical applications, these methods need to be tested on both simulated and real data. The numerical simulations are able to fully examine the damage identification methods, since the effect of errors can be fully investigated and the results are predictable. Simply adding random noise to the finite element model and then using the same model to identify the simulated damage may not be enough. It is critical that systematic type errors are considered in the numerical simulations. Typical approaches for this include the consideration of finite element discretisation errors, different damage mechanisms for generating measurements and for damage identification and change of boundary conditions. Also, a probabilistic framework can be used to deal with modelling errors and measurement noise. On the basis of the uncertainty in numerical modelling and measured data, the uncertainty of the identified damage location and extent could be estimated.

8.7.3 Effect of Environmental Factors

Civil engineering structures are usually subjected to varying environmental conditions such as temperature, humidity and wind. These environmental factors have an effect on operational modal parameters of the structures, and thus cause problems on vibrationbased damage identification. Typical environmental effects are demonstrated by highway bridges, especially those constructed using concrete. For example, temperature changes can cause a significant change in the stiffness properties of a concrete bridge, and it is difficult to predict the effects of temperature from measured data. Also, highway bridges are highly damped with low natural frequencies and are difficult to excite. The frequency resolution in the experimental data is often quite low, leading to considerable difficulties in detecting small frequency changes due to damage in the structure. Therefore, damage identification has considerable problems with modal parameter changes due to environmental factors.

Problems also arise in vibrationbased damage identification when operational mode parameters influenced by environmental factors are used. For practical implementation and reliable performance of the damage identification algorithms, it is important to characterise normal variability of modal parameters due to environmental conditions and to distinguish such normal variability from abnormal changes in modal parameters caused by structural damage. When the effects of normal environmental changes are well understood or quantified, it is possible to achieve reliable and accurate damage identification through incorporating the environmental effect models into the damage detection algorithms in either a statistical or deterministic way.

8.7.4 Frequency Range and Damage Detectability

The range of frequencies used in damage identification has a great influence on the resolution of the results (Worden and Friswell 2009). The advantage in using low frequency vibration

data is that the low frequency modes are generally global, requiring fewer sensors in testing. The problem with low frequency modes is that the spatial wavelengths of the modes are often large, much larger than the damage size. This makes it very difficult to identify small but critical damage in a large civil engineering structure. High frequency excitation generates very local modes, which are able to accurately locate damage, but only very close to the sensor and actuator locations. Also, it is very difficult to estimate accurate modes at these high frequency ranges, and changes in the dynamic response are often utilised for damage identification. Many advanced signal processing algorithms were proposed to interpret experimental data and detect structural damage (Duan et al. 2007, Sohn et al. 2004).

For large civil engineering structures such as bridges, they typically comprise various structural components of different materials. As a result, damage in some structural components mainly affects the modal parameters of higherorder modes, leaving the damage undetected, if only the lower order modes are monitored. However, higherorder mode information is difficult to acquire accurately due to measurement noise, limited bandwidth of the excitation and digitisation capacity. Since the mode shape of a higher frequency mode typically becomes more localised to a particular region of the structure, the frequency response functions will reflect the local modal characteristics, if both the excitation and response points locate in the region. Thus, a combination of global modal data and local frequency response functions could enable the identification of damage in individual structural components.

In general, some modes are more damage sensitive than others. Also, the measurement error existing in certain observed mode may be larger than the error in other modes. Using modes that are not highly affected by damage will only introduce their associated measurement noise in the damage identification process. It is possible that there are some observed modes that are not sensitive to damage and contaminated with relatively high measurement error. When these modes are included in damage identification, the identification results may become unreliable. It is desirable to develop theoretical or empirical procedures that can exclude the damage insensitive modes from the observed modal parameters before the damage identification process. A technique based on the modal sensitivity analysis and modal assurance criterion check seems to be suitable for this purpose.

8.7.5 Damage Diagnosis and Prognosis

The ultimate goal of an SHM strategy is to assess the current state and to predict future performance of engineering structures concerned. The philosophy of damage identification using measured vibration data is based on the assumption that the damage in a structure will change the stiffness of the structure. In some cases, there is a significant difference between strength and stiffness. It is very difficult to evaluate structural reliability and the remaining useful life by using the results from vibrationbased damage identification (Worden and Friswell 2009). Take prestressed concrete highway bridges as an example. Loss of prestressing in the reinforcement may have no significant effect in the stiffness of the concrete structure, but it could cause the structure failure due to loss of compressive stress in the concrete. The dynamic properties depend on structural parameters such as stiffness, thus the modal measurements of the concrete bridge change very little until it collapses. In general, the

prediction of future performance of a civil engineering structure requires an identification of the damage present, an assessment of the probable future loads, an accurate deterioration model and the associated structure failure modes. Although this process is very difficult, the use of inverse damage identification methods, such as the dynamic perturbation method, to generate a physically meaningful model evolution offers a route to damage prognosis.

The development of SHM methods for the identification of damage occurrence, location and severity has now achieved some degree of maturity. However, the application of this monitoring data for determining the inspection, maintenance and management of existing civil engineering structures is still in its infancy. Currently, there is a gap between SHM technology and asset inspection, maintenance and management exercises. This impedes asset managers from benefiting from the SHM system. In practice, asset managers want to get answers to the serviceability and reliability issues from the monitoring data. For example, has the load capacity or resistance of the structure changed? What is the probability of failure of the structural members and the whole structure? Indicators of these performance issues are needed to enable the asset managers to optimally allocate resources towards inspection, maintenance and rehabilitation of the structures.

8.8 Concluding Remarks

Many methods are discussed for the identification of both the location and severity of structural damage at local level in large civil engineering structures. Appropriate damage indicators are chosen to be sensitive to changes in stiffness due to local damage in a framed structure or continuum structure. The selected damage indicators can be characterised at element level for trusses and braces, at critical point level for beams and columns of framed structures, and at Gauss integration point level for continuum structures.

Matrix update methods, such as residual force vector method, minimum rank update method and optimal matrix updating method, are able to identify both the location and extent of damage in a structure. The residual force vector method is a workable method for identifying damage, but it requires a complete set of mode shapes, which may not be possible for large structures. The minimum rank update method gives damage information from the significant nonzero elements of the stiffness matrix perturbation. Some engineering judgement may be incorporated into the method to improve the damage location and extent estimate. The optimal matrix updating method minimises a given cost function subject to certain constraints, directly giving the change in stiffness matrix caused by damage. However, incomplete measured modal data causes difficulties for the matrix update methods during the damage identification process, thus a model reduction or modal expansion technique must be employed.

In the sensitivity based methods for damage assessment, the derivatives of modal parameters with respect to structural parameters are analysed to form a sensitivity matrix. This provides the firstorder relationship between the changes in structural parameters and the changes in modal parameters. As a result, the changes in the structural parameters due to the damage can be determined using the residual of the modal data between the undamaged and damaged

structure. However, the first order approximation of the eigenparameter sensitivity equations may not perform well, when damage in a structure is relatively large. Also, the computations of the sensitivity coefficients are time consuming in the cases with a large number of damage indicators present.

The damage identification methods directly using measured frequency response functions (FRFs) are particularly suitable for structures with closely spaced modes. As modal parameters are indirectly measured test data, they could be contaminated by measurement errors as well as modal extraction errors and provide less information than FRF data. The damage identification method using FRFs can avoid the disadvantage of most modal parameter based methods that require completeness of measured mode shapes. However, the FRF based method requires measurements of both response and excitation signals. In addition, the accuracy of damage identification results produced by the FRF based damage identification method depends heavily on the selected frequency range. If improper frequency points are adopted, the measurement errors may seriously affect the damage identification results.

The dynamic perturbation method is based on the exact relationship between the change in stiffness due to damage in a structure and the vibration modal data of the damaged structure. This method can directly adopt the incomplete modal measurements for damage identification, without requiring model reduction or mode shape expansion techniques. Only a limited number of vibration modal data measurements with uncertainty are sufficient to identify correctly structural damage in numerical simulations, which is potentially useful for assessing damage in large civil engineering structures. A regularisation algorithm, such as the Tikhonov regularisation method incorporating the Lcurve criterion, can be implemented in the method to provide stable solutions for the damage indicators. The dynamic perturbation method is capable of identifying the location of local damage as well as estimating its magnitude, including small damage, multiple damage and weakened beam-column joints of framed structures. This method needs to be examined, using real monitored data for reliable damage assessment of existing large civil engineering structures.

References

Balageas, D., Fritzen, C.P. and Guemes, A. (2006) *Structural Health Monitoring*. ISTE Ltd. London, UK.

Bicanic, N. and Chen, H.P. (1997) Damage identification in framed structures using natural frequencies. *International Journal for Numerical Methods in Engineering* **40**(23), 4451–4468.

Carden, E.P. and Fanning, P. (2004) Vibration based conditioning monitoring: a review. *Structural Health Monitoring* **3**, 355–377.

Chen, H.P. (1998) *Structural Damage Identification Using Vibration Modal Data*. PhD thesis Department of Civil Engineering, Glasgow University, UK.

- Chen, H.P. (2005) Nonlinear perturbation theory for structural dynamic systems. *AIAA Journal***43**(11), 2412–2421.
- Chen, H.P. (2008) Application of regularization method to damage detection in plane frame structures from incomplete noisy modal data. *Engineering Structures***30**(11), 3219–3227.
- Chen, H.P. and Bicanic, N. (2000) Assessment of damage in continuum structures based on incomplete modal information. *Computers and Structures***74**, 559–570.
- Chen, H.P. and Bicanic, N. (2006) Inverse damage prediction in structures using nonlinear dynamic perturbation theory. *Computational Mechanics***37**(5), 455–467.
- Chen, H.P. and Bicanic, N. (2010) Identification of structural damage in buildings using iterative procedure and regularisation method. *Engineering Computations***27**(8), 930–950.
- Doebling, S.W., Farrar, C.R., Prime, M.B. and Shevitz, D.W. (1996) *Damage Identification and Health Monitoring of Structural and Mechanical Systems from Changes in their Vibration Characteristics: A Literature Review*. Los Alamos National Laboratory report LA 13070MS.
- Duan, Z., Yan, G., Ou, J. and Spencer, B.F. (2007) Damage detection in ambient vibration using proportional flexibility matrix with incomplete measured DOFs. *Structural Control and Health Monitoring***14**(2), 186–196.
- Ewins, D.J. (2000) *Modal Testing: Theory, Practice and Application*. Research Studies Press, Baldock, Hertfordshire, UK.
- Fox, R.L. and Kapoor, M.P. (1968) Rates of changes of eigenvalues and eigenvectors. *AIAA Journal***6**(12), 2426–2429.
- Friswell, M.I. and Mottershead, J.E. (1995) *Finite Element Model Updating in Structural Dynamics*. Kluwer Academic Publishers, Dordrecht, The Netherlands.
- Hansen, P.C. and O’Leary, D.P. (1993) The use of the Lcurve in the regularisation of discrete illposed problems. *SIAM Journal on Scientific Computing***14**(6), 1487–1503.
- Johnson, E.A., Lam, H.F., Katafygiotis, L.S. and Beck, J.L. (2004) Phase I IASCASCE structural health monitoring benchmark problem using simulated data. *Journal of Engineering Mechanics ASCE***130**(1), 3–15.
- Kim, H.M. and Bartkowicz, T.J. (1993) Damage detection and health monitoring of large space structures. *Journal of Sound and Vibration***27**(6), 12–17.
- Mottershead, J.E., Link, M. and Friswell, M.I. (2011) The sensitivity method in finite element model updating: A tutorial. *Mechanical Systems and Signal Processing***24**, 2275–2296.
- Ricles, J.M. and Kosmatka, J.B. (1992) Damage detection in elastic structures using vibratory residual forces and weighted sensitivity. *AIAA Journal***30**, 2310–2316.

Sohn, H., Farrar, C.R., Hemez, F.M., Shunk, D.D., Stinemates, D.W. and Nadler, B.R. (2004) *A Review of Structural Health Monitoring Literature: 1996–2001*. Report LA13976MS. Los Alamos National Laboratory.

Stoer, J. and Bulirsch, R. (1980) *Introduction to Numerical Analysis*, SpringerVerlag, New York, USA.

Tikhonov, A.N. and Arsenin, V.Y. (1977) *Solutions of illposed problems* . John Wiley & Sons, New York, USA.

Worden, K. and Friswell, M.I. (2009) Modalvibrationbased damage identification. *Encyclopaedia of Structural Health Monitoring*, Boller, Chang and Fujino (ed.), John Wiley & Sons, Chichester, UK.

Zhao, J. and DeWolf, J.T. (1999) Sensitivity study for vibrational parameters used in damage detection. *Journal of Structural Engineering***125**(4), 410–416.

Zimmerman, D.C. and Kaouk, M. (1994) Structural damage detection using a minimum rank update theory. *Journal of Vibration and Acoustics ASME***116**, 222–231.

Zimmerman, D.C., Kaouk, M. and Simmermacher, T. (1995) Structural health monitoring using vibration measurements and engineering insight. *Journal of Vibration and Acoustics ASME***115**, 214–221.

9 Monitoring Based Reliability Analysis and Damage Prognosis

9.1 Introduction

Recently, civil infrastructure management philosophy has changed considerably, thanks to the development and applications of structural health monitoring (SHM) technology. This technology has the potential to improve the management of existing civil engineering structures in many ways: (a) the accuracy of structural performance assessment can be improved by analysing the monitored structural response data and environmental conditions, (b) inspections can be scheduled effectively on the basis of structurespecific monitoring data, (c) deterioration of structural performance over time can be modelled and calibrated using monitoring data to reduce uncertainties, (d) timevariant reliability can be assessed, using monitored load conditions and predictive deterioration models, (e) as a result of timevariant reliability analysis, the risk and a costbalanced maintenance strategy can be determined using advanced optimisation techniques.

For civil engineering structures, two types of failure are often identified: structural failure and condition failure. Structural failure can be the collapse of a structure due to insufficient resistance, whereas condition failure represents that a certain predetermined failure level has been exceeded due to deterioration. Condition failure is defined as the event at which a structure fails to meet its main functional requirements. Structures usually do not fail due to physical failure, but due to condition failure. Thus, inspections and monitoring must be undertaken to ensure that condition failure will be detected at an early stage, and proper maintenance actions may be necessary to be taken to prevent failure of the structure.

Although condition assessment based on SHM data is a critical step in the management of civil engineering structures, predicting future performance provides an essential basis for the cost effective scheduling of inspections, maintenance, repairs and replacements. In general, the resistance of a structure decreases over time as the structure deteriorates and the load demand may increase. This will lead to a decrease in structural reliability and an increase in the probability of failure of the structure over time. A timely repair will then be necessary to reduce the risk of structural failure, whereas the resources for the repair should be minimised. In performance assessment and management of existing civil structures, the SHM strategy offers useful data for model validation, reliability analysis and informed decision making (Catbas et al. 2008), as shown in [Figure 9.1](#).

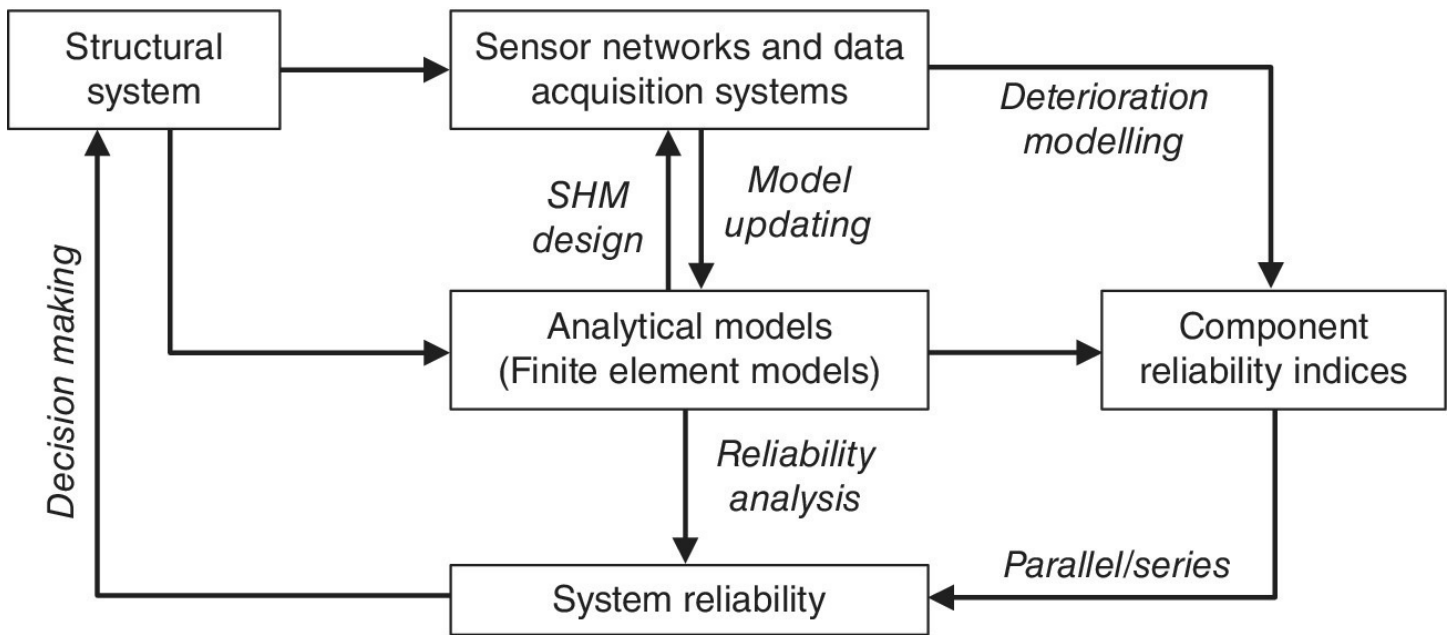


Figure 9.1 Framework for reliability analysis using an SHM strategy (after Catbas et al. 2008).

Civil engineering structures deteriorate over time, and the deterioration needs to be properly modelled using probabilistic approaches with consideration of uncertainties. Due to the uncertainties in material and geometrical properties, in the physical models of the deterioration process, a probabilistic measure of the timevariant structural performance is necessary for realistic results. Also, the evolution over time of the aleatoric and epistemic uncertainty effects has to be properly considered. Although aleatoric uncertainty cannot be reduced, epistemic uncertainty related to incomplete information could be effectively minimised by improving accuracy of predictive models using inspection and monitored data. Lifetime distributions take into account the combined effect of all the uncertainties on a structure by using explicit lifetime models, such as the failure rate function, Markov process, gamma process and Weibull model. As a result, the condition of a structure can be evaluated from the lifetime distribution, accounting for time to failure of the structure as a random variable.

Structural reliability analysis based on limit states associated with failure modes of a civil structure has to take into account the effects of deterioration processes, timevariant loadings and maintenance and repair interventions over the entire lifecycle. The probability of failure of a civil structure during its service life largely relies on the load and resistance effects, as well as their changes with time. Numerical methods are often required to estimate the probability of failure of the structure over time and the calculated probability of failure may convert into the corresponding reliability index for practical purposes. From the results of timevariant reliability analysis, the remaining useful life of the structure can be estimated. Furthermore, the timevariant reliability assessment integrated with lifecycle cost analysis supports decision making processes for optimal planning of the maintenance and repair of the existing civil structure. To ensure a reliable operation and to schedule maintenance and repair actions in a costeffective manner, it is important and necessary to continuously monitor and assess the performance of the structure during its service life.

This chapter explores advances in the fields of usage monitoring, probabilistic deterioration modelling, reliability assessment and optimal maintenance strategy of existing civil engineering structures. First, usage monitoring such as load and environmental condition monitoring of a civil structure in service is discussed. From the monitored data, several probabilistic approaches are presented for stochastic deterioration modelling with uncertainty. Lifetime distributions representing probability of condition failure are obtained from various stochastic processes or predictive models, such as the Markov process, gamma process and Weibull model. Timevariant reliability associated with limit states of the structure is assessed by various methods with consideration of changes in loads and resistances over time. Several techniques are offered for determining an optimal maintenance strategy through time variant reliability analysis and lifecycle cost analysis. Finally, a case study on usage monitoring and fatigue reliability assessment of a suspension bridge is discussed.

9.2 Usage Monitoring

Usage monitoring is the process of acquiring operational loading data from a civil engineering structure in service. The usage monitoring includes measures of loads (e.g. traffic loads on bridges) and environmental conditions (e.g. temperature and moisture). Loads due to the intended use as well as environmental actions (e.g. wind, waves and earthquakes) are usually sitespecific, and may not agree with the design values used. With data from monitoring site specific loads, models can be developed and utilised for performance assessment of the structure. Load effects to the structure due to extreme load events, such as special traffic, extreme wind and earthquakes, can be recorded and evaluated. Moreover, environmental factors often cause the deterioration of structural capacity over time (Rücker et al. 2006a). On the basis of monitoring of loads and environmental conditions, physical properties of the structure are updated over time, and then future deterioration of the structural capacity can be predicted.

9.2.1 Lifecycle Monitoring

Civil engineering structures such as bridges should be monitored over the whole life span during various phases, such as construction and service stages and maintenance periods. Construction is a very delicate phase in the lifetime of a civil structure. For prefabricated structures, a monitoring system is useful for deformation control, stress control at critical locations, stability control and optimisation between two successive segments. For concrete structures, since material properties such as strength change through aging at the early stage, thermal and deformation monitoring systems are needed. It is important to know whether or not the required values have been achieved and maintained during construction. Defects (e.g. premature cracking) arising during construction may have serious consequences on structural performance during the service life. The monitoring data provides useful information for further understanding of the structure's real behaviour. This leads to better estimates of real structural performance and more appropriate remedial actions. Important information obtained through monitoring during construction includes

- estimation of hardening time of concrete, to estimate the time when shrinkage stresses are initially generated
- deformation measurements during the early age of concrete to estimate selfstressing and the risk of premature cracking
- deformation monitoring of cables in prestressed structures to adjust prestressing forces of the cables
- monitoring of foundation settlement to understand the origins of built-in stresses
- damage caused by unusual loads such as floods, hurricanes or earthquakes during construction, affecting the ultimate performance of structures
- optimal adjustment of structural position during erection
- knowledge improvement and recalibration of design methods.

The monitoring system installed on a civil structure during the construction phase can be further used for monitoring the structure during the whole service life. Since civil structures are usually inspected many times during their service, it is cost-effective to install the monitoring system for continuous measurements from the beginning (Miyamoto 2009). The monitoring system is also useful for quality control of structural strengthening during the repair periods and for calibration of finite element models during field tests.

The service phase is the most important period in the life of civil engineering structures. Monitoring during the service phase is necessary, in particular for large civil structures in seismic areas. During the service phase, the construction materials are subjected to degradation over time. The degradation of materials is generally caused by mechanical factors, such as fatigue loading and unexpected loads (e.g. earthquakes) and physicochemical factors, such as steel corrosion and concrete carbonation. As a result of material degradation, the capacity and durability of the structure decrease. Monitoring during service offers information on structural behaviour under expected loads, and also records the effects of unexpected overloading. Data collected by monitoring can be used for damage identification, evaluation of safety and determination of the remaining useful life of the structure. Early damage identification is particularly important for appropriate and timely repairs. Late detection of damage causes either an increase in repair costs or closedown or even collapse of the structure (Miyamoto 2009). The continuously measured data from the monitoring system can be utilised for assessing current state and forecasting future performance of the structure. Perhaps the best use of structural monitoring in the assessment of civil engineering structures is the study of long-term data trends.

9.2.2 Load Monitoring and Evaluation

Loads can be classified into two types according to their effects: static and dynamic loads. For a civil engineering structure, static loads include selfweight of the structure and its components, prestress, construction loads, traffic and transportation loads, etc. The effects of the static loads can be measured by deformations of the structure (e.g. strains and

displacements). Dynamic loads can be such as human excited loads, traffic loads, wind loads, earthquake loads, collision loads or explosion loads. The effects of these dynamic loads correspond in magnitudes and dynamic properties with the loads as well as with the structure. Measurements of dynamic response include vibration velocities and accelerations.

Loads should be determined from monitoring according to their magnitude, frequency, character and temporal and spatial distributions. Extensive information on loads can be collected with a continuous monitoring. When only load exceedance is recorded, inactive monitoring can be activated with trigger signals based on the predefined threshold values. For monitoring slowly variable quantities like static loads, a brief monitoring in regular intervals is often sufficient. Also, an eventdependent monitoring is applicable where the inactive monitoring is controlled by load independent values. The measurements of loads from long term monitoring provide many useful applications (Rücker et al. 2006b), including

- measurement based permanent observation of traffic loads (e.g. traffic intensity density and vehicle weight)
- statistics about the long term trend of increase and decrease of traffic loads
- determination of load collectives and dynamic factors by recording of acting loads, depending on type, location, amplitude, duration and frequency
- improvement of load models and estimates of the extreme value with a fixed probability.

Traffic loads on a civil structure possess static and dynamic components. Traffic loads have local and global effects on the strain of structural components. They cannot be measured directly, but can be determined computationally with validated load models. In addition, information on the traffic flow, such as driving speed and distance of vehicles, is important. The effects of traffic flow are studied in a statistical sense, thus it provides data for the validation of realistic load models or for the determination of extreme loads.

Traffic loads acting on bridges can be computed from measured strains. The computational procedure requires calibration functions representing the structural performance (e.g. influence line). In general, the influence line can be determined with proof loading or in numerical ways. The determined global load values are classified on the basis of the weight of the passing vehicles on each lane. The frequency is calculated for each loading class afterwards.

Axle loads and axle configurations of moving vehicles can be investigated with weighin motion systems. By use of weighinmotion systems, the axle load measurement results of actual traffic are overlaid with dynamic components due to the vibrations of the vehicles. These results can lead to misrepresentation of statistics of traffic loads. Load measurements with weighinmotion systems are more accurate for dense slowmoving traffic.

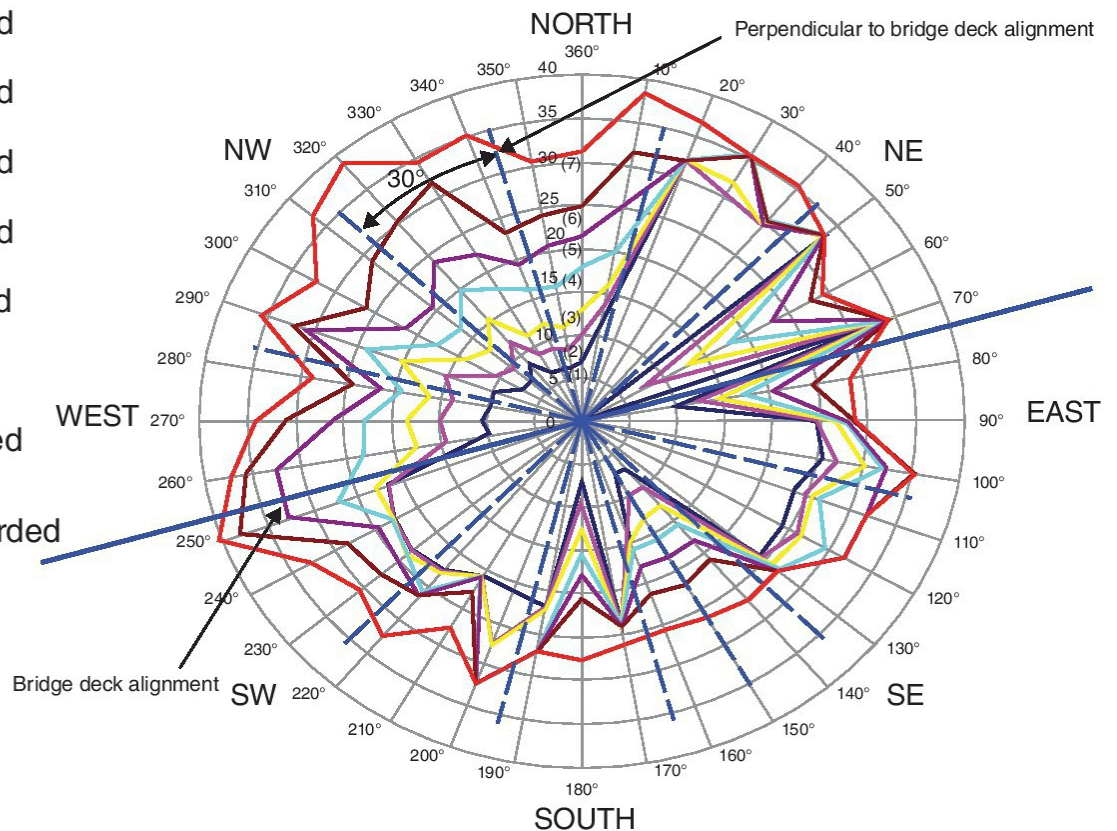
In case of collisions, an exchange of kinetic energy to deformation energy occurs, and the load effect is often dynamic and nonlinear. Thus, the load generally cannot be separated from the structural response, and requires suitable models for determination (Rücker et al. 2006b). A starting point is the use of the models of elastic and plastic action effects with measured dynamic values.

9.2.3 Monitoring of Environmental Factors

Environmental factors such as temperature and wind may have significant effects on a civil engineering structure, thus it is important to monitor these factors during construction and service phases. Thermal effects due to change in temperature may cause much higher strains in comparison to traffic loads. Thermal effects also cause constraint forces and residual stresses if not linearly distributed. They generate deformation and can lead to irreversible damage (e.g. cracks in concrete due to tensile stress). In general, strains caused by thermal effects can be estimated by numerical studies, only if temperature distribution is available. Therefore, measurements of temperature from the installed sensors are necessary for determining temperature distribution and variation over time on the structure (Rücker et al. 2006b). Through the crosssectional temperature distributions and the associated models, load effects can be obtained.

Wind as a natural factor can excite civil engineering structures, in particular highrise buildings and longspan bridges. The measurements of dynamic response (e.g. accelerations) through monitoring systems provide critical data for operational modal analysis to extract modal parameters. The quality of the extracted modal parameters may depend on the wind speed to excite the structure, and stronger wind conditions generally offer better quality of modal parameters. Thus, the characteristics of wind, including speed and direction, have to be recorded through monitoring systems. Furthermore, the recorded wind data can be used to develop wind load models for the specific structure. By analysing long term measurements, wind load models can be calibrated for particular locations. These models can then be used as a basis for a refined estimation of the expected wind loading. The simultaneous monitoring of the weather conditions is necessary. Typical wind monitoring results, such as wind velocities, directions and occurrence (Wong and Ni 2009), are illustrated in [Figure 9.2](#).

- (1) 80% ER wind speed
- (2) 60% ER wind speed
- (3) 40% ER wind speed
- (4) 20% ER wind speed
- (5) 10% ER wind speed
- (6) 5% ER wind speed
- (7) 2.5% ER wind speed



ER: Exceedance Recorded

Figure 9.2 Monitoring of wind velocities, directions and occurrence at tower top of Tsing Ma Bridge.

Besides the mechanical quantities described above, a variety of other physical and chemical processes exist in a civil structure during its service life. For example, corrosion of steel rebar leads to an early deterioration of reinforced concrete structures and reduces the safe service life. Reinforcement corrosion consumes the original steel rebar, accumulates rust products and creates an expansive layer at the bond interface. As corrosion progresses, the expansive displacement at the interface causes tensile stress in the hoop direction over the surrounding concrete cover, leading to radial splitting cracks in the concrete. As a result, the bond strength of corroding rebar starts decreasing, and the performance of the concrete structure deteriorates gradually to an unacceptable level for the serviceability and safety of the structure (Chen and Alani 2013, Chen and Nepal 2016). The main reasons of reinforcement corrosion in concrete structures are chloride contamination and concrete carbonation. The corrosion penetration rate within concrete structures depends substantially on the environmental factors, such as humidity, electric conductivity, temperature and carbon dioxide concentration. Therefore, sensors need to be applied to concrete structures for measuring these environmental quantities.

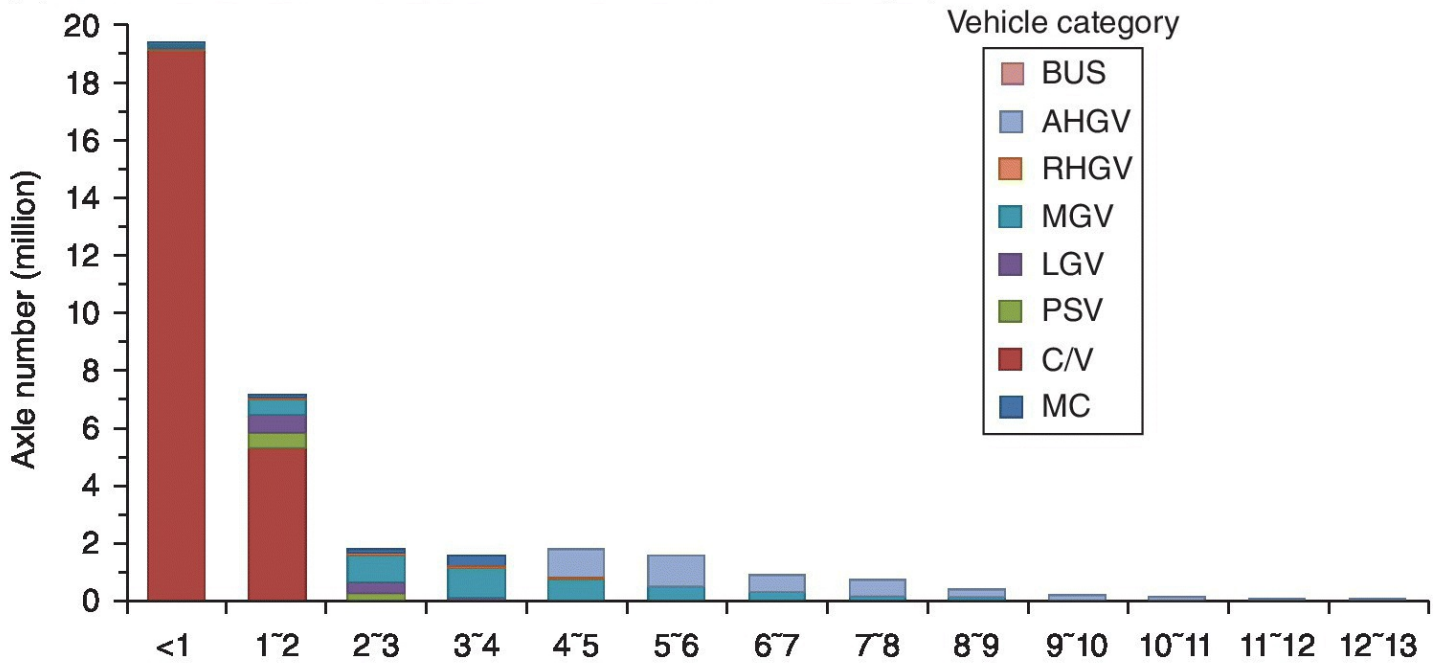
9.2.4 Example for Usage Monitoring – a Suspension Bridge (VI)

The longspan suspension Tsing Ma Bridge, as described in [Section 2.3.5](#) and [Section 7.3.7](#), is used here again to study the highway traffic loading from one year monitoring data. The knowledge of traffic monitoring is beneficial to the bridge managers for assessing the bridge safety and scheduling proper inspection and maintenance activities. As a part of the longterm SHM system, the monitored data was acquired by a weighinmotion (WIM) system, as

shown in [Figure 2.6](#). Seven dynamic weigh-in-motion stations were installed in the seven lanes of the carriageways to monitor road traffic condition and highway loading on the bridge. There are three weigh-in-motion stations in the airport-bound direction and four weigh-in-motion stations in the Kowloon-bound direction. Each weigh-in-motion station consists of two parts: two bending path pads located on the left and right sides of the lane for vehicle weight detection and two magnetic loop detectors placed in the front and rear of the road for determining vehicle characteristics. For every passing vehicle, weigh-in-motion stations generate a line of raw data accordingly. Thus, the weigh-in-motion system generates various measurements, including vehicle class, number of axles and axle weight.

The parameter of axle load is very important for both the bridge structure and the pavement. According to the vehicle classification system, the percentage of axle load in various loading ranges at one-ton intervals can be determined (Ni et al. 2015). On the basis of the data acquired from the weigh-in-motion stations in year 2007, the distributions of axle load are obtained, as shown in [Figure 9.3\(a\)](#) for different vehicle categories. From the results, the axle number decreases with increase in axle load. Over half vehicle axles have an axle load lower than 1 ton, and only around 10% of the total vehicle axles have an axle load higher than 5 tons. With the obtained diagrams of axle loads and the categories of vehicle classification, the number of axles falling into individual load ranges can be determined in ascending series to give an axle load spectrum. Here, two reference axle load spectra are considered for comparison: the load spectrum stipulated in BS 5400 Part 10 (BSI 1980) and the design load spectrum for the bridge. The axle load spectrum from the weigh-in-motion data on the slow lane (for the airport-bound direction) is presented in [Figure 9.3\(b\)](#), together with the two reference load spectra. According to the road traffic regulation set by the government, the maximum allowable axle load is 10 tons, thus the percentage of overloaded axles is 1.27% in the airport-bound direction. The spectrum of axle loads on the slow lanes of the bridge is quite in agreement with that provided in BS 5400 Part 10. The spectrum from real measurements is safer than that given by BS 5400 Part 10. Both of them are on the safe side as compared with the design spectrum.

(a) Axle load distribution versus axle number and vehicle category



(b) Axle load spectrum for airport-bound slow lane

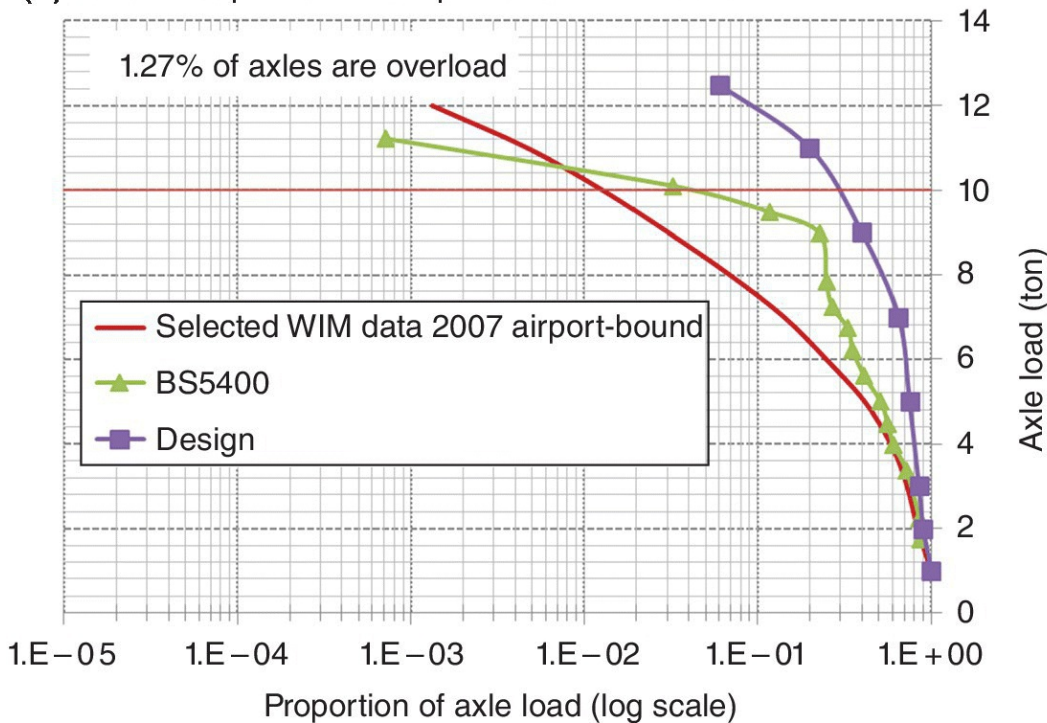
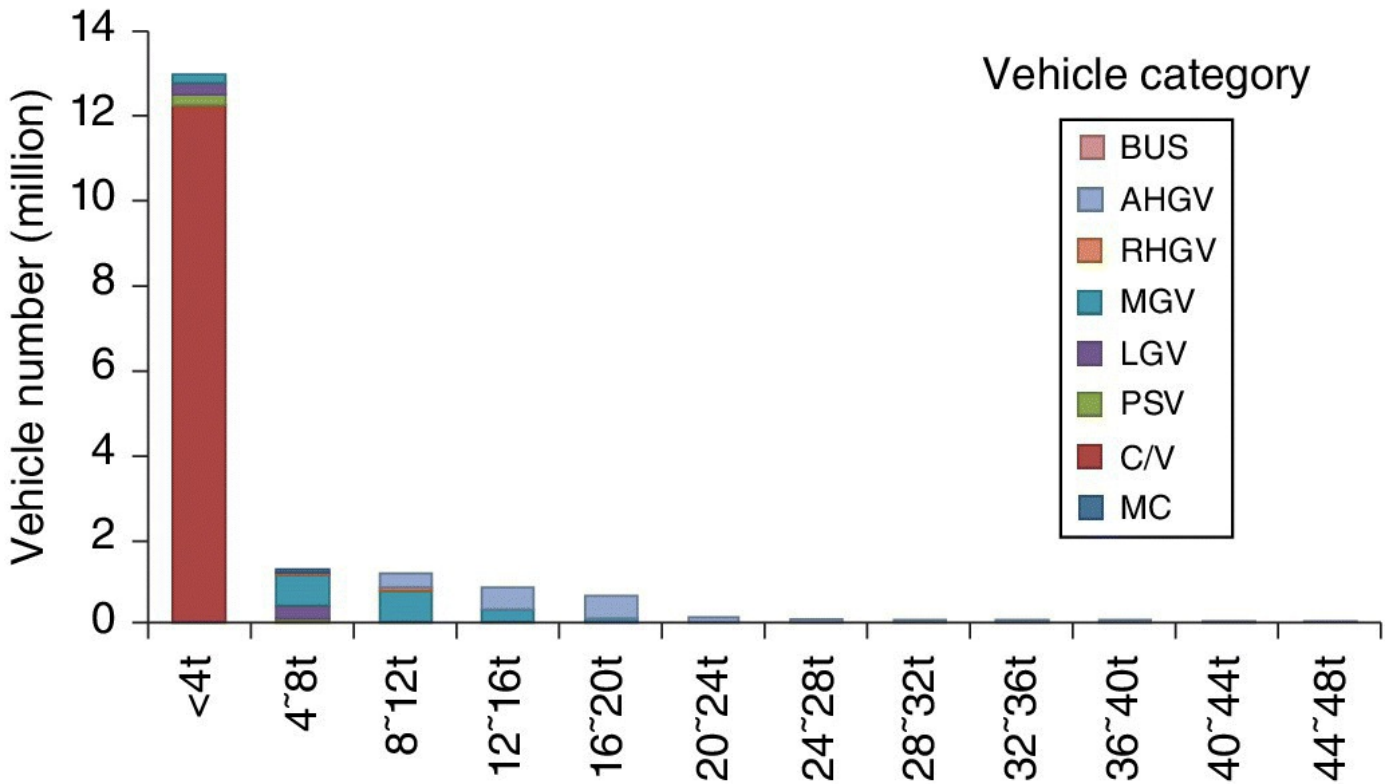


Figure 9.3 Axle load distribution and spectrum from the weighinmotion data.

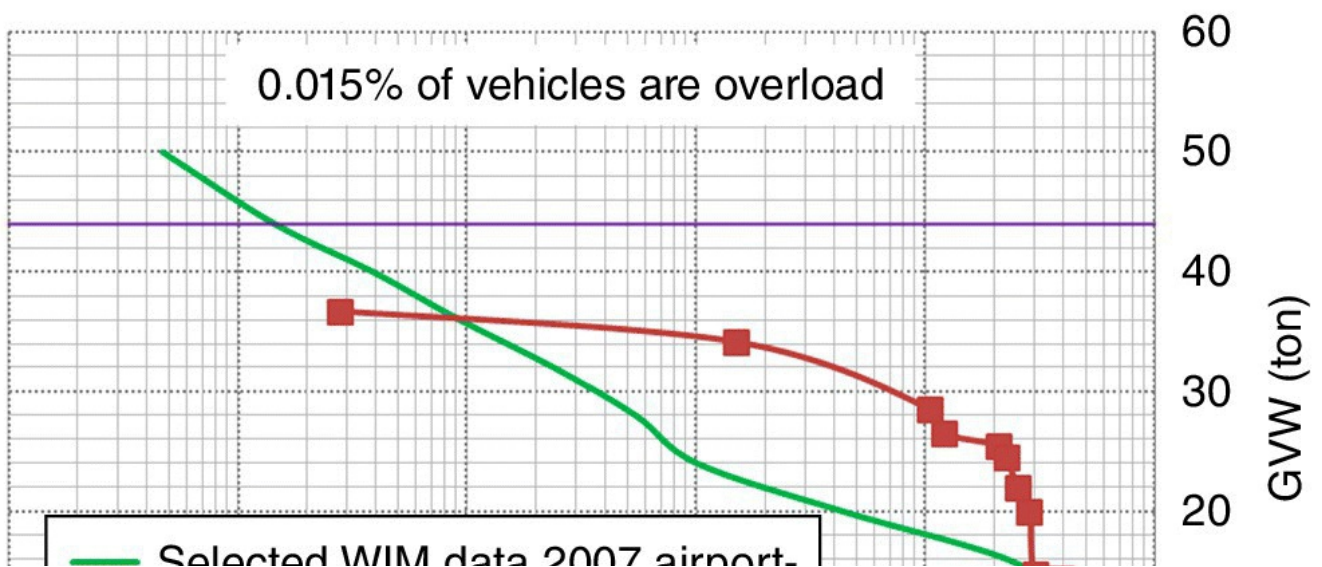
The parameter of gross vehicle weight (GVW) is also important. The percentage of vehicles in gross vehicle weight is calculated at the 4 tons interval according to the vehicle classification system. With the recorded weighinmotion data, the distributions of gross vehicle weight are shown in [Figure 9.4\(a\)](#) in terms of vehicle category. From the results, the vehicle number is inversely proportional to the gross vehicle weight. More than three quarters of the total vehicles have a gross vehicle weight lower than 4 tons, and only 4.8% of the total vehicles

have a gross vehicle weight over 16 tons. The gross vehicle weight spectrum can be developed in a similar way on the basis of the recorded gross vehicle weight data, as shown in [Figure 9.4\(b\)](#). The gross vehicle weight spectrum given by BS 5400 is also plotted in the figure for comparison. The parameter of the lower bound threshold of gross vehicle weight is set as 4 tons, and the allowable maximum gross vehicle weight is 44 tons, according to government regulations. Results show that the measured spectrum is on the safe side, compared with the reference spectrum specified in BS 5400. There is a small proportion (0.015%) of overloaded vehicles on the airportbound slow lane.

(a) Gross vehicle weight distribution versus vehicle number and category



(b) Gross vehicle weight spectrum for airport-bound slow lane



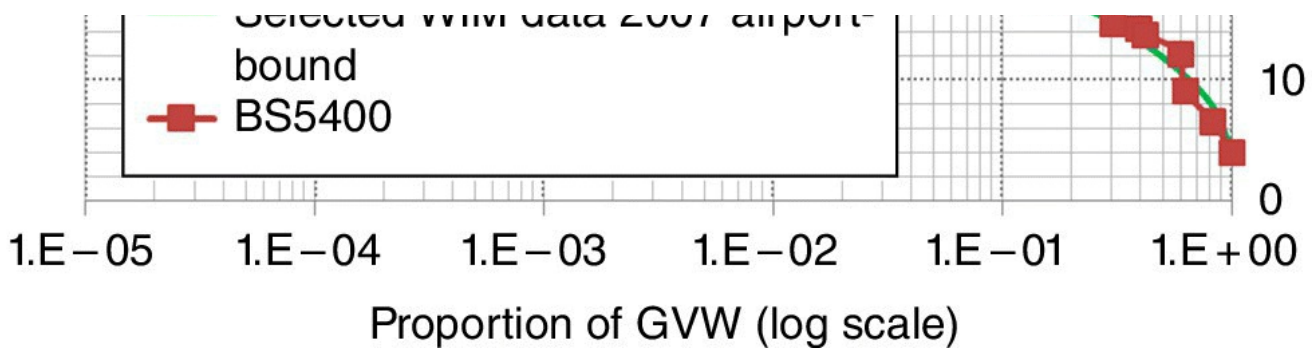


Figure 9.4 Gross vehicle weight distribution and spectrum from the weighinmotion data.

9.3 Probabilistic Deterioration Modelling

As civil engineering structures are aging due to various causes, it is essential to understand the realistic state of health and the rate of deterioration at an early stage. The current and future states of a civil structure, however, are associated with various degrees of uncertainty. Thus, a probabilistic approach is necessary for deterioration modelling with uncertainty. Typical probabilistic approaches for deterioration modelling of civil infrastructure include failure rate function, Markov process and gamma process.

9.3.1 Sources of Deterioration

Sources of deterioration vary, depending on the operational and environmental conditions of the existing civil structures. These sources can be broadly categorised into two groups: natural sources and manmade sources. Natural sources include short term and long term effects. The short term effects are such as earthquake, wind or flood. The long term effects include corrosion, fatigue, thermal effects, freezethaw, chemical process (e.g. carbonation), creep, shrinkage and settlement of foundations or supports. Also, manmade sources can include sudden effects, such as overload, fire and vehicle collision, as well as long term effects, such as inadequate design and construction defects (e.g. improper assembly or misfits). Effects of these sources are cumulative, and quantitative evaluation of these effects is difficult. Models are often used to describe the resulting deterioration over time. However, there are always uncertainties in these deterioration models, since it is almost impossible to use a mathematical description for the deterioration process in practice.

The evolution over time of the deterioration process of civil infrastructure can be simply described by deterministic models of timevariant deterioration rate (Biondini and Frangopol 2016). Empirical deterministic models can be adopted in some cases to estimate the deterioration over time $d(t)$, initiated at time t_i :

$$d(t) = a(t - t_i)^b, t \geq t_i \quad (9.1)$$

where a and b are parameters to be determined from regression of available data. In the cases where data is available over time, these parameters could be also considered as timevariant, and estimated by timevariant regression procedures.

The above deterministic deterioration model has many limitations due to uncertainties in the deterioration process of civil structures. Therefore, a probabilistic approach is necessary to account for the relevant uncertainties associated with natural randomness, errors in modelling and prediction of reality.

9.3.2 Modelling and Parameter Uncertainty

In assessing the performance of existing civil engineering structures, two types of uncertainties have to be considered: aleatoric and epistemic (Frangopol and Messervey 2009). Aleatoric uncertainty describes the inherent randomness of phenomena being observed and cannot be reduced, for example, natural variations in temperature. Epistemic uncertainty describes the error associated with imperfect models of reality due to insufficient or inaccurate knowledge, for example, errors in stresses predicted by an analytical model as material properties, geometry and loads are never deterministic. Both types of uncertainty are critical in the monitoring and modelling of civil structures. Model updating, that is, adjusting structural parameters through experimental data, can reduce epistemic uncertainty by improving the accuracy of model parameters. In general, the consideration of aleatoric uncertainty significantly improves the assessment and prediction of structural performance. For example, temperature effects need to be considered in a physical model, as temperature greatly contributes to variations in strain or modal parameters.

Modelling uncertainty can be introduced during the physical modelling process (Farrar et al. 2003). Many uncertainties in physical modelling can be classified as epistemic uncertainty. Modelling uncertainty can arise from approximations or errors in the form of the model equations, the applied loads and the boundary and initial conditions. Uncertainties in modelling are inevitable, since it is difficult to model large and complex civil engineering structures in reality. The fidelity of the models is often limited and is usually application dependent in predicting the outcome of real world situations. There are few methods available for the systematic treatment of uncertainty in physical modelling. When the uncertainty is caused by the known but not modelled physics, either the model can be adjusted to include the physics or an attempt can be made to characterise the uncertainty induced by its exclusion. However, when the excluded physics is not known, little can be done to characterise the associated uncertainty.

Parametric uncertainty exists in the input parameters of a model. In physical models, these parameters may be geometric or material properties, or they may be selected to characterise the applied loads, or boundary or initial conditions. When test data is available on a real structure, the uncertainty can be reduced by improving the accuracy of model parameters through a model updating procedure, as described in [Chapter 6](#). In addition, there are many other methods available to deal with this type of uncertainty, such as stochastic approaches, probabilistic methods and reliability based methods. Among these methods, the probabilistic methods are powerful and commonly used tools for treating parametric uncertainty.

9.3.3 Probabilistic Deterioration Models

For proper maintenance of a civil structure, it is necessary to estimate the future state of the

structure. A deterioration model is then used to approximate and predict the actual process over time. To consider uncertainties in the deterioration model, probabilistic approaches can be used for deterioration modelling, such as failure rate function, Markov process and gamma process.

9.3.3.1 Failure Rate Function

A lifetime distribution represents the uncertainty in the time to failure of a structural system or its components. Assuming the lifetime distribution has a cumulative probability distribution $F(t)$ with probability density function $f(t)$, the failure rate (or hazard rate) function $r(t)$ over time t is defined (van Noortwijk 2009) as

$$r(t) = \frac{f(t)}{1 - F(t)}, t \geq 0 \quad (9.2)$$

A probabilistic interpretation of the failure rate function is that $r(t)dt$ indicates the probability that a component of age t will fail in the time interval $[t, t + dt]$. For a deteriorating structural system or its components, the failure rate increases over time. Lifetime distributions and failure rate functions are especially useful in mechanical and electrical engineering. The equipment can be assumed either at the functioning state or at the failed state. However, a structure or component can be in a range of states depending on its degrading condition.

Failure rates have a major disadvantage that they cannot be observed or measured for a particular component. Due to lack of failure data generally, a reliability approach solely based on lifetime distributions and their unobservable failure rates is unsatisfactory. Therefore, it is more useful to model deterioration in terms of a timevariant stochastic process such as a Markov process or gamma process.

9.3.3.2 Markov Process

A Markov process is a stochastic timevariant process to estimate the future event as a random outcome. The Markov process is governed by three features: (a) the process is discrete in time, (b) the process has a countable and finite statespace, (c) the future state of the process depends on its present state, but not on its past state (van Noortwijk and Frangopol 2004). The Markov process is a suitable model for a state based approach and has been extensively applied for predicting the future conditions of civil infrastructure such as flood defences (Nepal et al. 2015). Mathematically, a Markov process is considered as a series of transitions between certain condition states. Generating an accurate and reliable transition probability matrix is a critical step in the process. When the Markov process is used to model deterioration of a system in state i , a fixed probability p_{ij} exists when a system changes from state i to state j during a certain period. The general form of transition probability matrix \mathbf{P} with condition states $\{i, j = 1, 2, \dots, m\}$ is expressed as

$$\mathbf{P} = \{p_{ij}\} \text{ and } p_{ij} = \Pr\{X_{n+1} = j \mid X_n = i\} \quad (9.3)$$

The transition probability has the property $\sum_{j=1}^m p_{ij} = 1$ for $i = 1, 2, \dots, m$. The probability that a process in state i will be in state j after n transitions is defined as n step transition probability. To satisfy the homogeneity assumption of a Markov process, a zoning concept is applied. A zone is a certain period of time assumed to produce constant transition probabilities. The period for a zone is based on engineering judgement or inspection intervals. The transition probability matrix \mathbf{P} for n transitions can be obtained by minimising the difference between the observed and the predicted condition states of the structure.

The Markov process is popular approach for stochastic modelling of deteriorating civil engineering structures. This process is relatively simple and has been applied in practice with many successful applications. However, the Markov process has several disadvantages: (a) the constant transition probability matrix is not realistic, (b) the condition state is not continuous, but discrete and finite, (c) the Markovian assumption of no memory and independent of past history is not accurate in some cases, (d) the potential interaction of deterioration between two components is not considered. The Markov process model is purely a condition model, and the model is very well suited to incorporate information from visual inspections, but it cannot be used to assess the reliability of a structure in terms of strengths and stresses.

9.3.3.3 Gamma Process

The gamma process has been increasingly utilised for modelling a stochastic deterioration process to evaluate the deterioration of aging civil engineering structures (Chen and Alani 2012). A comprehensive review on the application of gamma process in the maintenance and management of deteriorating civil infrastructure is provided in van Noortwijk (2009). In mathematical terms, the gamma process with a random quantity $\{Y(t), t \geq 0\}$ is a continuous stochastic process with independent nonnegative increments of a gamma distribution. The gamma process has the following properties: (a) $Y(t)$ has a probability value of one at initial time $t = 0$, (b) $Y(t)$ has independent increments, (c) the increment at a time interval follows a gamma distribution. Thus, the gamma process can be an appropriate model for the gradual monotonically accumulated damage in a structure occurring random in time by continuous use, for example wear, fatigue, corrosion, crack growth, erosion, creep or a degrading health index. In the gamma process, the deterioration process is assumed to be independent and considered as the sequences of the deterioration increments.

From the definition of the gamma process, the probability density function of the deterioration increments Δy occurring at time t ($t \geq 0$) can be described as

$$f_{\Delta y(t)}(\Delta y) = Ga(\Delta y | \eta(t), \lambda) = \begin{cases} \frac{\lambda^{\eta(t)}}{\Gamma(\eta(t))} \Delta y^{\eta(t)-1} e^{-\lambda \Delta y}, & \text{for } \Delta y \geq 0 \\ 0, & \text{elsewhere} \end{cases} \quad (9.4)$$

where $\Gamma(\eta(t)) = \int_0^{\infty} v^{\eta(t)-1} e^{-v} dv$ for $\eta(t) > 0$ is the gamma function. The scale parameter λ

with $\lambda > 0$ and the shape function $\eta(t)$ can be estimated from the maximum likelihood method by using in situ measurements about the deterioration processes, expressed as

$$\lambda = \mu / \sigma^2, \eta(t) = \mu^2 t / \sigma^2 \quad (9.5)$$

in which μ and σ are the mean value and standard deviation for the average deterioration rate, respectively. Empirical studies show that the expected deterioration at time t is often proportional to a power law (van Noortwijk 2009):

$$\mu(t) = at^b \quad (9.6)$$

where $a > 0$ and $b > 0$ are physical constants. There is often engineering knowledge available about the shape of the expected deterioration in terms of the parameter b in the equation.

As the gamma process is well suited for modelling the temporal variability of deterioration, it can be adopted for reliability analysis and maintenance decision making problems. The gamma process is often used together with statistical estimation techniques, such as maximum likelihood, method of moments, Bayesian updating and expert judgement. As a result, the gamma process is satisfactorily fitted to real life data on many civil engineering problems, including creep of concrete, fatigue crack growth, corrosion of steel or reinforcement, corrosion induced thinning and chloride ingress into concrete (Chen and Alani 2013, van Noortwijk, 2009). So far, the gamma process has mainly been applied to deterioration modelling for individual components rather than for a system. There are many less developed aspects in gamma process deterioration modelling, such as spatial variability and dependence, as well as multicomponent and multifailure mode models including their statistical dependencies.

9.3.4 Example for Fatigue Cracking Modelling – a Steel Bridge (I)

Fatigue in members of a steel bridge is the process of initiation and growth of cracks under the action of repeated traffic loading. Fatigue crack propagation in a steel structural component can be modelled by the popular Paris–Erdogan law. In order to account for uncertainty in fatigue crack growth, the stochastic gamma process is used for modelling the fatigue crack evolution of the steel bridge members under cyclic loading (Huang et al. 2016).

Assume that the necessary physical parameters are available for the numerical study: annual cycles of 10^6 times per year, initial fatigue crack length of 0.5 mm and material parameters in the Paris–Erdogan law $C = 3.54 \times 10^{-12}$, $m = 2.54$ and $Y(a) = 1$. [Figure 9.5](#) shows the results for the simulated fatigue crack growth curve using the gamma process model, together with the deterministic curve predicted by the Paris–Erdogan law. From the results, the simulated fatigue crack growth generally matches the prediction by the Paris–Erdogan law, although the simulated curve does not appear smooth due to uncertainties in the parameters. From the results, when the service life is less than 20 years, the fatigue crack growth is slow. The growth rate increases sharply after the service life of over 20 years.

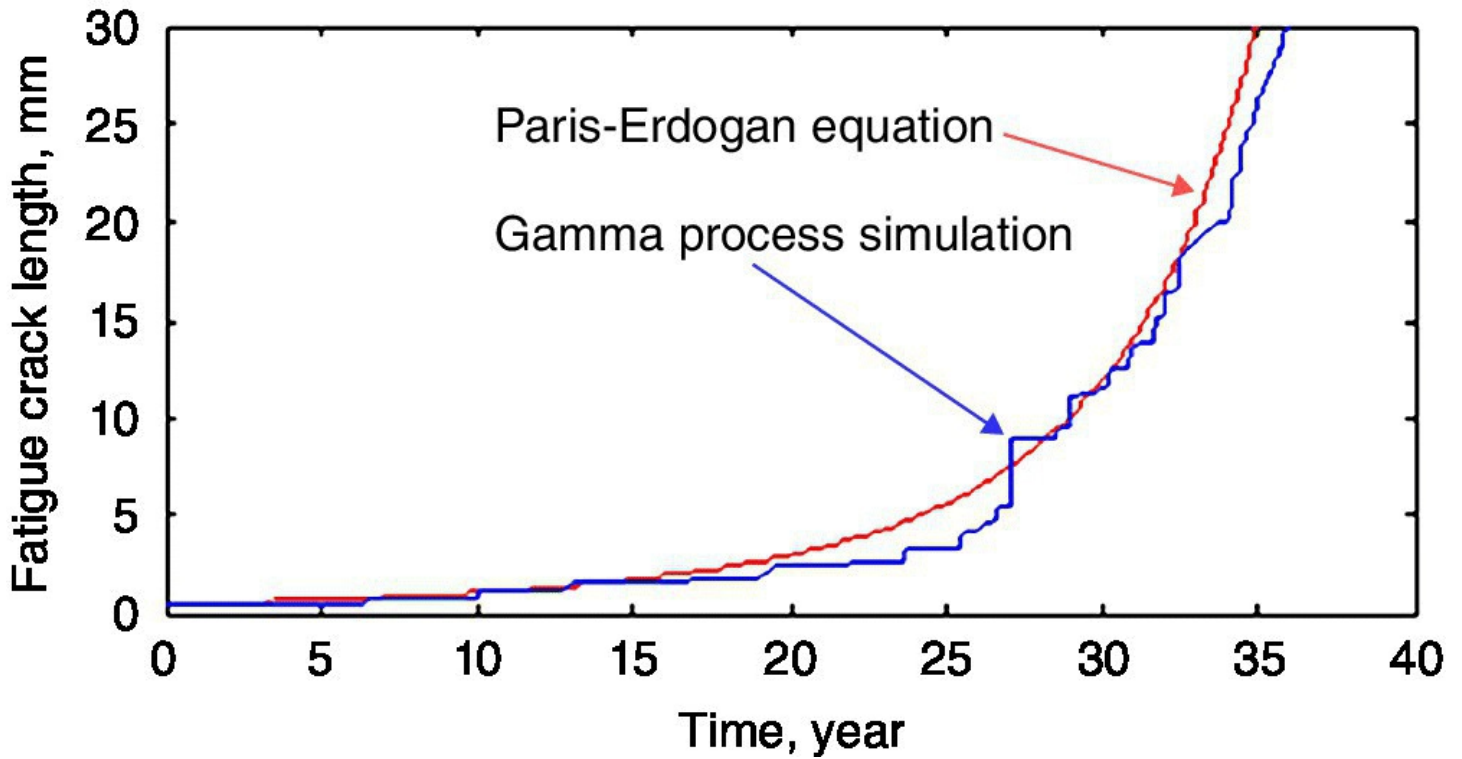


Figure 9.5 Fatigue crack growth curves simulated by the gamma process model and predicted by the Paris–Erdogan law.

9.4 Lifetime Distribution Analysis

Lifetime distributions are representation of the time of failure of a system by using a continuous and nondecreasing probability distribution of lifetime with consideration of time to failure of the system as a random variable. Lifetime distributions consider the combined effect of all uncertainties on the system by using an explicit life model, such as the gamma process model and the Weibull model. The lifetime distributions can be updated by Bayesian updating after inspection and repair.

9.4.1 Stochastic Gamma Process

For a civil engineering structure, its component is said to fail when the chosen quantity $Y(t)$ (e.g. crack width) exceeds a certain allowable value Y_L (e.g. allowable crack width) for a limit state problem at time T_L . From the gamma distributed deterioration in [Equation \(9.4\)](#), the lifetime distribution of time to failure is given by

$$p_f = \Pr\{t \geq T_L\} = \Pr\{Y(t) \geq Y_L\} = \int_{y=Y_L}^{\infty} f_{Y(t)}(y) dy = \frac{\Gamma(\eta(t), Y_L \lambda)}{\Gamma(\eta(t))} \quad (9.7)$$

where $\Gamma(\eta, x) = \int_{v=x}^{\infty} v^{\eta-1} e^{-v} dv$ for $x \geq 0$ and $\eta > 0$ is the incomplete gamma function. This

formulation provides a useful relationship between probability of time to failure and lifetime, thus making the gamma process model suitable for lifetime distribution analysis.

The results for the simulated fatigue crack growth, as shown in [Figure 9.5](#), are now used for lifetime distribution analysis using the stochastic gamma process model (Huang et al. 2016). [Figure 9.6](#) provides the results for the probability of time to failure for different values of critical crack length: $a_{cr} = 5$ mm, 10 mm and 15 mm. At the beginning of service, since the fatigue crack length grows slowly, the probability of time to failure is very small and close to zero. As the service time increases, fatigue crack length increases gradually, until it reaches the critical threshold. After the service time nears the time corresponding to the critical fatigue crack threshold, the probability of time to failure increases significantly and quickly approaches unity. From the results, in the case with larger threshold of fatigue crack, the probability of time to failure experiences faster growth before failure. As a result, proper inspection and maintenance should be carried out before the fatigue crack length reaches the predefined critical value in order to keep the structure safe.

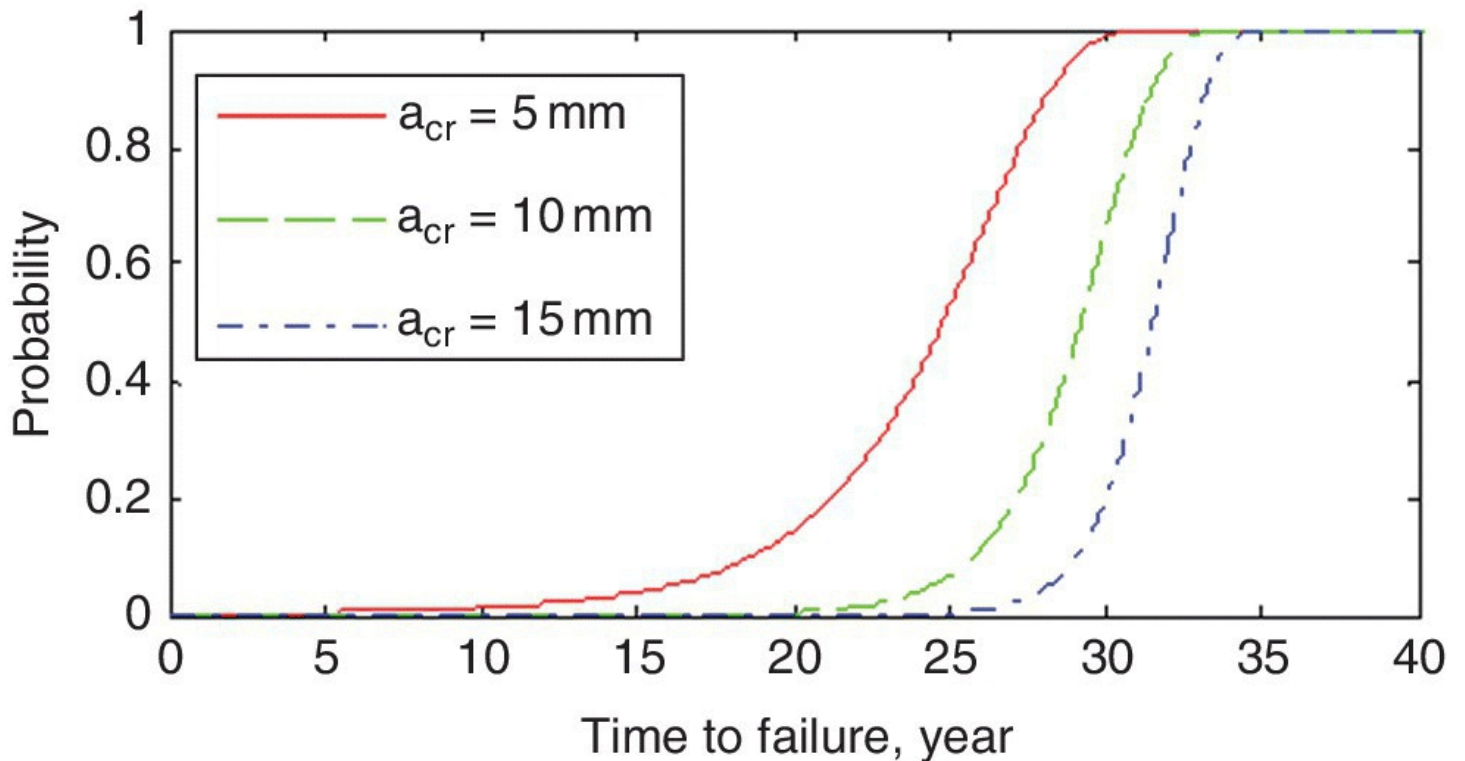


Figure 9.6 Probability distribution of time to failure using the gamma process model under different critical thresholds of fatigue crack length (a_{cr}).

9.4.2 Weibull Life Distribution Model

For civil infrastructure, measurable quantities, such as cracking, fatigue, erosion and structural capacity deterioration, can be chosen as random variables (symptoms) for lifetime distribution analysis. When a symptom exceeds a given limit value, the system fails to meet the designed requirements. Thus, the symptom reliability (survival function) can be assumed to be dependent on the symptom and the associated failure rate function for deterioration. It is well

known that the Weibull model is a very flexible life distribution model and widely used for undertaking symptom reliability analysis (Chen and Xiao 2015, Cempel et al. 2000). Thus, the Weibull life distribution model is adopted for the evolution of the symptom Y (e.g. concrete crack width) caused by the damage parameter x (e.g. corrosion penetration) and the probability density function (PDF) is expressed by

$$f(Y) = \frac{\beta}{Y} \left(\frac{Y}{Y_b} \right)^{\beta} \exp \left[- \left(\frac{Y}{Y_b} \right)^{\beta} \right] \quad (9.8)$$

where $Y_b = vY_L$ and v is the scale factor to be determined by design requirements with respect to allowable limit Y_L , and $\beta > 0$ is the shape parameter to be determined by fitting the predicted results to the Weibull model, estimated from

$$\beta = \frac{\sum_i \left\{ \ln \left[-\ln \left(1 - \frac{x_i}{x_b} \right) \right] \right\}^2}{\sum_i \left\{ \ln \left[-\ln \left(1 - \frac{x_i}{x_b} \right) \right] \right\} \ln \left(\frac{Y_i}{Y_b} \right)} \quad (9.9)$$

in which x_b is the damage parameter corresponding to Y_b . Then the probability distribution of time to failure (i.e. cumulative distribution function, CDF) as a function of the damage parameter $x(t)$ over time t is obtained from

$$p_f(Y(t)) = 1 - \exp \left[- \left(\frac{Y(t)}{Y_b} \right)^{\beta} \right] \quad (9.10)$$

From the calculated probability of failure, the symptom reliability (survival function) for the symptom Y as a function of damage parameter $x(t)$ is given as

$$R(Y(t)) = \int_{Y(t)}^{\infty} f(y) dy = \exp \left[- \left(\frac{Y(t)}{Y_b} \right)^{\beta} \right] \quad (9.11)$$

The expected remaining life T_{rul} , associated with the symptom of the system that is still surviving at service age of T_m , is estimated from

$$T_{rul} = \int_{T_m}^{\infty} R(Y(t)) dt \quad (9.12)$$

The expected remaining life T_{rul} depends on the predefined allowable limit Y_L for the

symptom.

9.4.3 Data Informed Updating

Monitoring and inspection data can be used to update the condition assessment of the structures concerned. In general, there exists some prior belief about the reliability or random variables from expert experience, numerical simulations or experimental tests. New information from these investigations then needs to be combined with existing information in a reasonable manner. Two different approaches are often used: direct updating of the probability of failure and updating of the probability distribution of the basic variables. For direct updating, the probability of failure can be directly updated using Bayesian theorem from the following conditional probability

$$P_f'' = \Pr(F | I) = \frac{\Pr(F \cap I)}{\Pr(I)} \quad (9.13)$$

where F represents local or global structural failure, and I represents the information obtained from investigation.

Alternatively, the probability distribution of the basic variables can be updated using new information available. Assume that $f'(\theta)$ is an existing (prior) belief of a random variable. The use of monitoring provides sample data that defines the same random variable with a different distribution $f(x)$. The combined (posterior) distribution $f''(\theta)$ is expressed (Frangopol and Messervey 2009) as

$$f''(\theta) = g(\theta) f'(\theta) / \lambda \quad (9.14)$$

where the likelihood $g(\theta)$ represents the conditional probability of observing $f(x)$ given $f'(\theta)$, expressed as $g(\theta) = f(x | \theta)$, and λ is a normalised factor to ensure that the area under the

probability density function (PDF) is unity, defined as $\lambda = \int_{-\infty}^{\infty} g(\theta) f'(\theta) d\theta$.

In the special case where the Weibull life distribution model is used for analysing probability distribution of time to failure, as discussed in [Section 9.4.2](#), the PDF in [Equation \(9.8\)](#) can be updated using the new data available. When condition assessment is undertaken at symptom $Y = Y^a$, a likelihood function $g(Y, Y^a)$ is introduced for the Bayesian updating of the probability density function, defined as

$$g(Y, Y^a) = f(Y - Y^a) = \frac{\beta}{(Y - Y^a)} \left(\frac{Y - Y^a}{v' Y_L} \right)^{\beta} \exp \left[- \left(\frac{Y - Y^a}{v' Y_L} \right)^{\beta} \right] \quad (9.15)$$

where v' is the updated scale factor. The PDF after Bayesian updating needs to be multiplied by lifetime reliability at $Y = Y^a$, that is, $R(Y^a)$, to keep the updated cumulative distribution function (CDF) not exceeding unity (Orcesi and Frangopol 2011). Consequently, the updated

PDF after the assessment at $Y = Y^a$ is given as

$$f^a(Y) = \frac{g(Y, Y^a) f(Y)}{\int_0^{\infty} g(Y, Y^a) f(Y) dY} R(Y^a) \quad (9.16)$$

The survival function (symptom reliability) after assessment is calculated from [Equation \(9.11\)](#), in which the updated PDF in [Equation \(9.16\)](#) has to be used. In general, structural maintenances are necessary to keep structures safe and reliable during their service life. The symptom reliability profiles of the structure will be changed after the structural repair and essential maintenance (Okasha and Frangopol 2009). The PDF given in [Equation \(9.8\)](#) after repair at symptom $Y = Y^r$ is written as

$$f^r(Y) = f(Y - Y^r) R(Y^r) = \frac{\beta}{(Y - Y^r)} \left(\frac{Y - Y^r}{\nu Y_L} \right)^\beta \exp \left[- \left(\frac{Y - Y^r}{\nu Y_L} \right)^\beta \right] R(Y^r) \quad (9.17)$$

where $R(Y^r)$ is the symptom reliability associated with the repair at symptom $Y = Y^r$. The symptom reliability by Bayesian updating and the associated probability distribution of time to failure can then be used for optimising the maintenance strategy.

9.4.4 Example for Lifetime Distribution Analysis – a Concrete Bridge

A reinforced concrete Tgirder bridge exposed to aggressive environments is utilised for lifetime distribution analysis using the Weibull model. The bridge is designed for a service life of 60 years, operating in aggressive environments with mean annual corrosion current per unit length $i_{corr} = 5 \mu\text{A} / \text{cm}^2$. The detailed description of the problem as well as the data for the calculations are given in Chen (2017). The lifetime evolution of corrosion-induced concrete cracking (the symptom) is modelled by the Weibull life distribution. The allowable crack width is assumed to be $Y_L = 1.0 \text{ mm}$ for the failure in spalling of concrete cover. The scale parameter $\nu = 1.1$ and shape parameter $\beta = 3.3$ is estimated by fitting the analytical predictions and/or experimental data to the Weibull model. [Figure 9.7](#) shows the results for the probability distribution of time to failure of the reinforced concrete Tgirder as a function of equivalent concrete crack width. The probability of time to failure increases as concrete crack width increases.

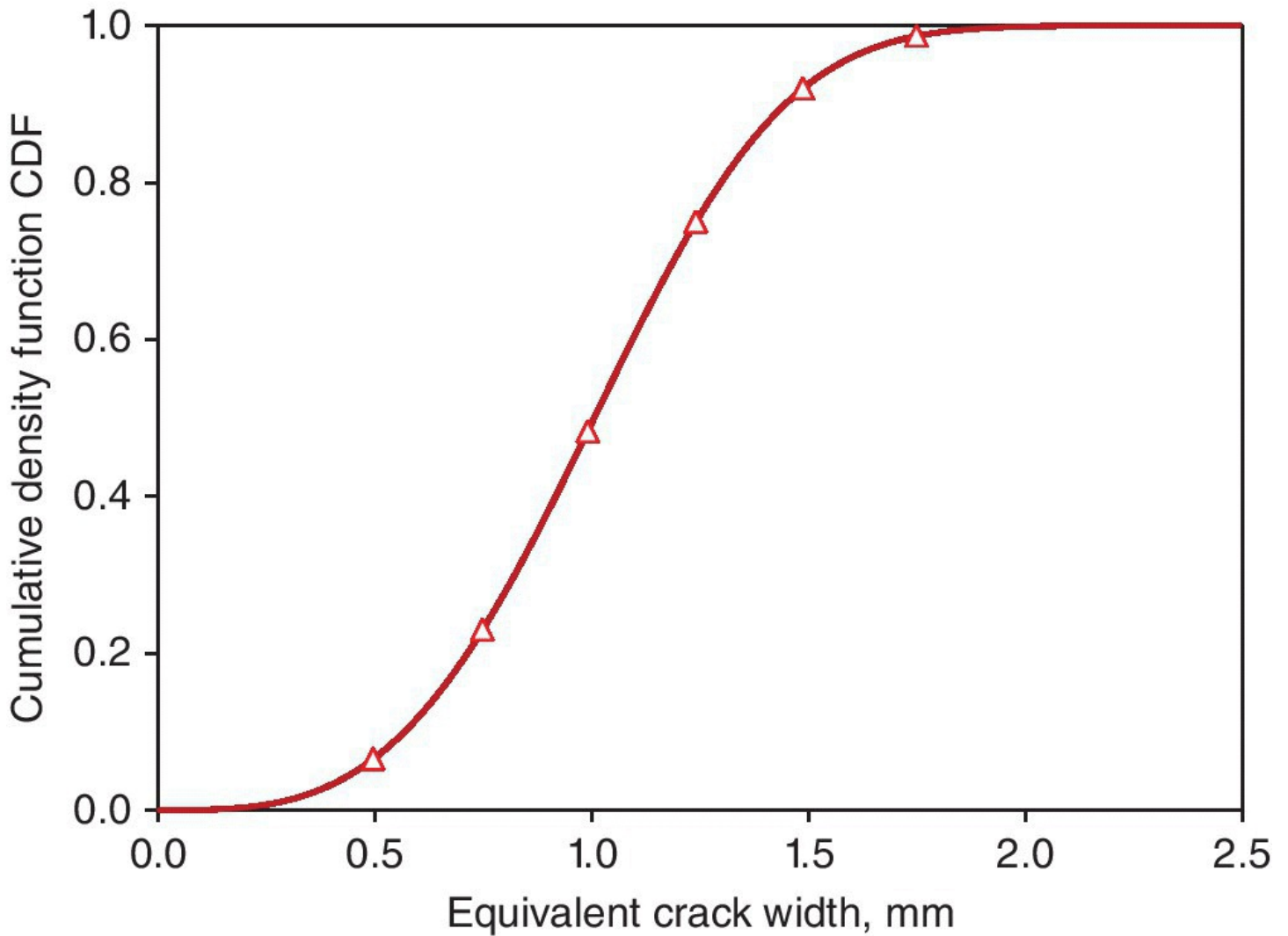


Figure 9.7 Lifetime distribution (CDF) as a function of concrete crack width.

Figure 9.8 shows the results for the effect of inspection and repair on the symptom reliability by Bayesian updating. Assume that an inspection and a repair are undertaken at concrete crack widths $Y^a = 0.8$ mm and at $Y^r = 1.2$ mm, respectively. The symptom reliability increases immediately after inspection at $Y^a = 0.8$ mm, comparing with the corresponding prior symptom reliability. The risk of condition failure is then reduced after the inspection. Also, the symptom reliability is significantly affected by the structural repair at $Y^r = 1.2$ mm. The symptom reliability increases from the corresponding prior symptom reliability, after the structural repair has taken place during the service life of the reinforced concrete Tgirder.

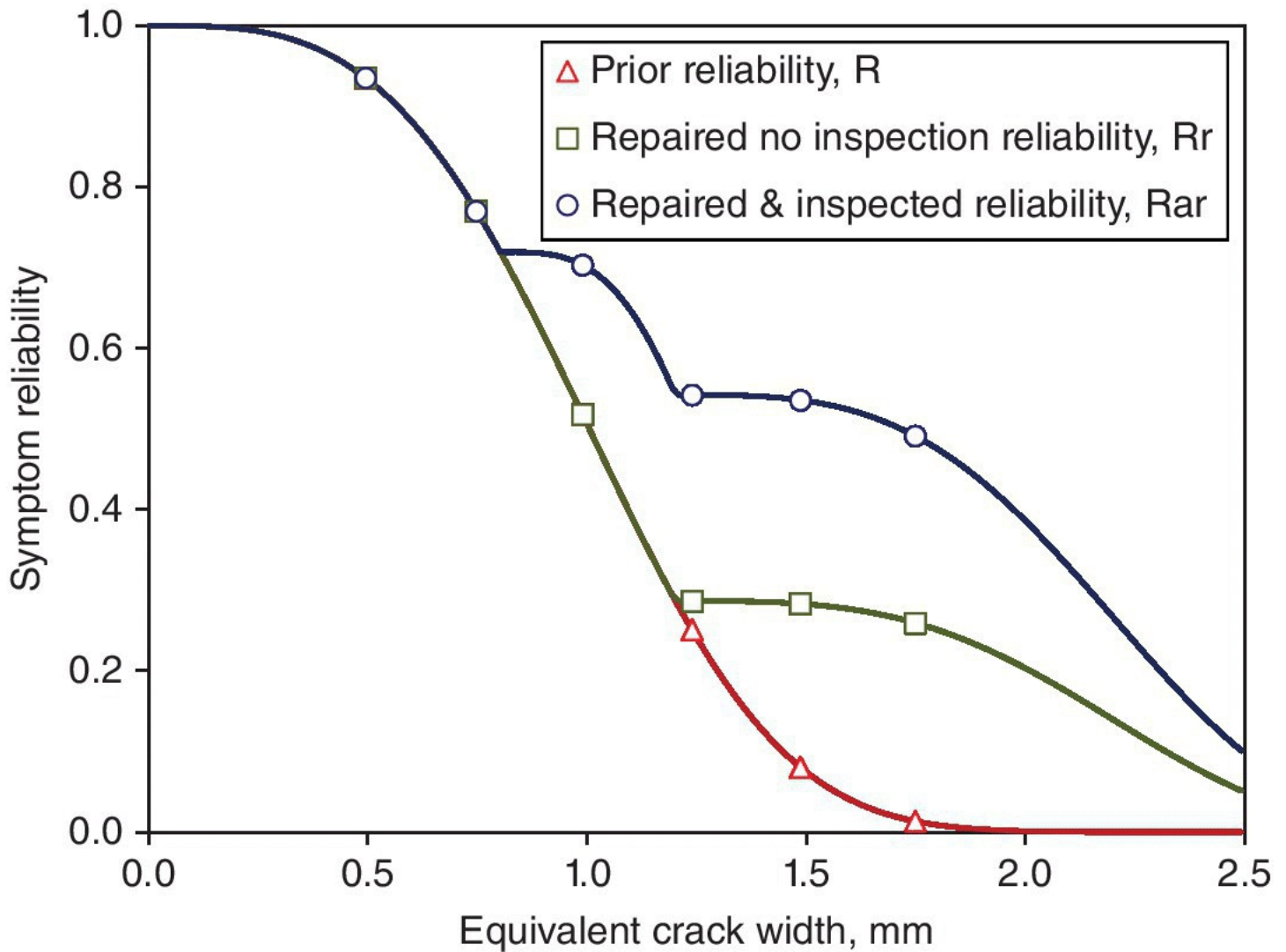


Figure 9.8 Symptom reliability (survival function) by Bayesian updating due to inspection and repair.

9.5 Structural Reliability Analysis

The advantage of lifetime distribution analysis using a stochastic process or a life distribution model is simple and straightforward, which is appropriate for assessing the condition of a structure. However, lifetime distribution analysis cannot include the specific resistance and load effects as well as their changes with time. On the other hand, structural reliability analysis is based on the limit state equations associated with failure modes of a structure, by considering both resistance and load effects. For civil engineering structures, the loading condition and structural capacity often change with time. Timevariant reliability analysis is therefore necessary for assessing the safety and estimating the remaining useful life of the deteriorating civil structure and its components.

9.5.1 Limit States and Reliability Analysis

In structural reliability analysis, the probability of failure or the equivalent reliability index of

a structure or a structural member needs to be calculated. The probability of failure for a defined limit state largely depends on the uncertainties in the load and resistance parameters. Very often, the uncertainties are modelled using appropriate probability distribution functions for each basic variable in the defined limit state. Typical uncertainties in structural reliability analysis include inherent random variability or uncertainty, uncertainty due to inadequate knowledge and statistical uncertainty. From the probability distribution functions for basic variables, the probability of failure associated with the failure modes of a civil structure is calculated. The calculated probability of failure is then used for comparison with acceptance criteria to assess safety and serviceability of the structure or structural member.

The critical failure modes of the structure or structural member need be determined in the reliability analysis process. For each identified failure mode, the associated limit state equation can be expressed as $g = R - S = 0$, where R and S are the resistance and load effects, respectively. In general, the probability of failure p_f is defined by the limit state $R - S \leq 0$:

$$p_f = \Pr(R - S \leq 0) = \iint_{R \leq S} f_{R,S}(r, s) dr ds \quad (9.18)$$

where $f_R(r)$ and $f_S(s)$ are the probability density functions (PDFs) of resistance effect R and load effect S , as indicated in [Figure 9.9](#), and $f_{R,S}(r, s)$ is their joint PDF. For civil engineering structures, the resistance R and load S are usually functions of many random variables. Thus, the limit state equation is rewritten as $g(\mathbf{x}) = R(\mathbf{x}) - S(\mathbf{x}) = 0$ where \mathbf{x} is the vector of basic variables.

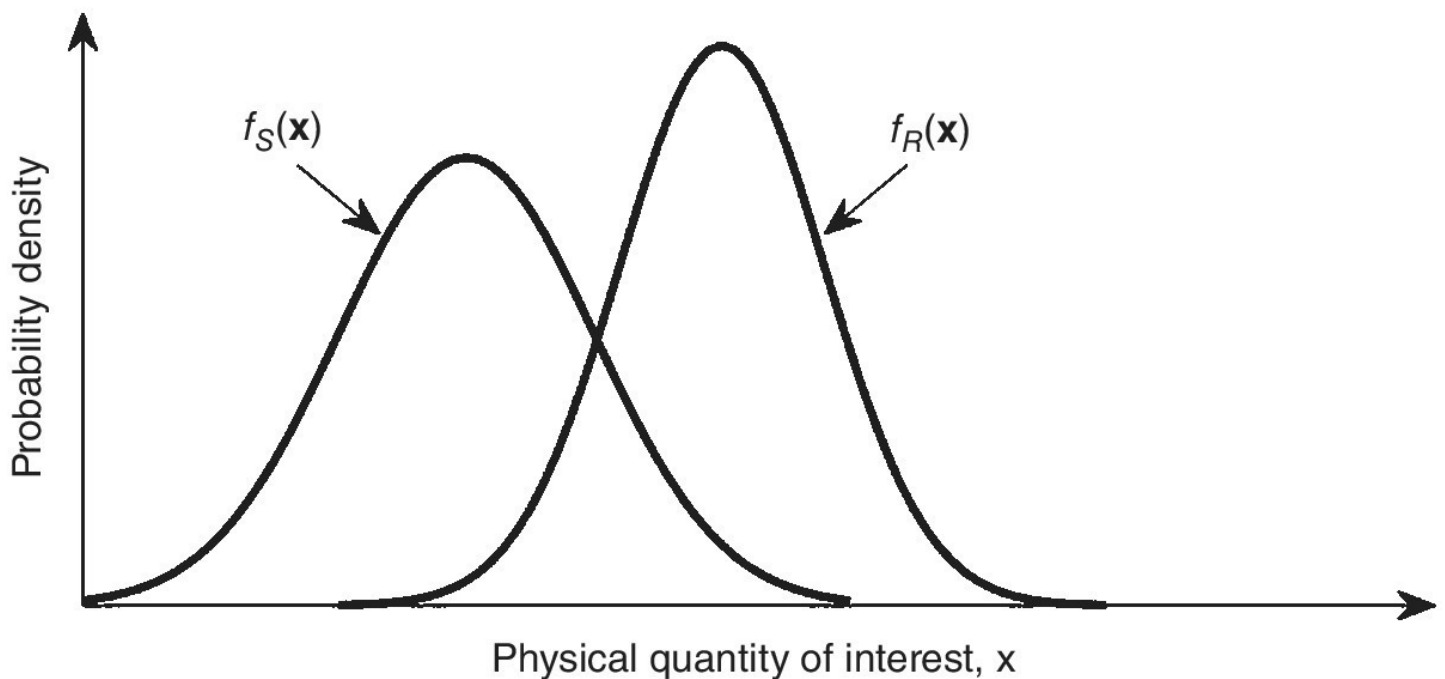


Figure 9.9 Probability density functions (PDFs) of resistance effect R and load effect S .

All basic variables related to load and resistance should be modelled as stochastic variables on the basis of knowledge available. Information on the identified location and extent of

structural damage or deterioration should be considered in the resistance modelling. Since the limit state equation defines the boundary between safe domain $g(\mathbf{x}) > 0$ and failure domain $g(\mathbf{x}) \leq 0$, the probability of failure is now calculated from

$$p_f = \Pr(g(\mathbf{x}) \leq 0) = \int_{g(\mathbf{x}) \leq 0} f_{\mathbf{x}}(\mathbf{x}) d\mathbf{x} \quad (9.19)$$

which is the volume integral of $f_{\mathbf{x}}(\mathbf{x})$, that is, PDF of \mathbf{x} , over the failure domain $g(\mathbf{x}) \leq 0$.

Several methods have been developed to compute the probability of failure P_f , including exact analytical methods, approximate analytical methods, numerical integration methods and simulation methods (e.g. Monte Carlo simulation, importance sampling). The calculations of probability of failure often require tremendous computational efforts for civil engineering structures. The approximate methods such as the firstorder reliability method (FORM) and the secondorder reliability method (SORM) may be adopted in the calculations. Details of these methods can be found in the book by Melchers (1999).

For a civil engineering structure, the probability of failure often has a very small value and is usually reported in terms of reliability index β . When the resistance R and load S are independent and normally distributed, the relationship between the reliability index and the probability of failure can be expressed as

$$p_f = \Phi(-\beta), \text{ and } \beta = \frac{\mu_R - \mu_S}{\sqrt{\sigma_R^2 + \sigma_S^2}} \quad (9.20)$$

where $\Phi(\bullet)$ is standard normal cumulative probability function, μ_R and μ_S are the mean values of the resistance and load effects, respectively, and σ_R and σ_S are their standard deviations.

Finally, the calculated structural reliability is compared to the safety requirements for the reliability index.

9.5.2 TimeVariant Reliability

For existing civil engineering structures, the resistance and load will change with time due to operational and environmental effects, as shown in [Figure 9.10](#). In the cases with no structural maintenance actions taken, structural resistance usually deteriorates over time due to various factors (e.g. corrosion, fatigue, cracking), while loads on the structure often increase, leading to an increase in probability of failure of the structure. Thus, structural reliability analysis has to consider time variance in basic variables related to load and/or resistance effects. The limit state function for an identified potential failure mode is expressed in relation to time t as

$g(\mathbf{x}(t)) = R(\mathbf{x}(t)) - S(\mathbf{x}(t))$ for t within time reference period $[0, T]$. The probability of failure over time is then calculated from

$$p_f(t) = \Pr(g(\mathbf{x}(t)) \leq 0) \quad (9.21)$$

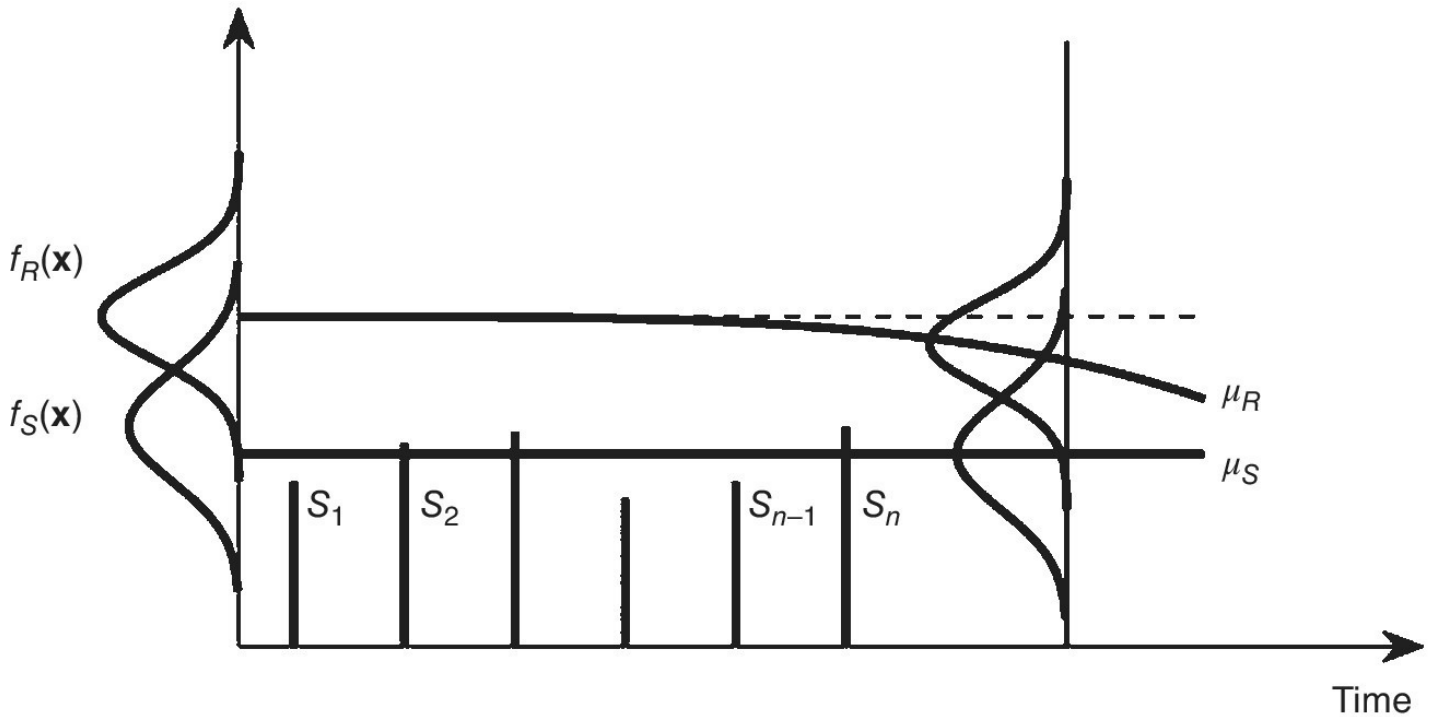


Figure 9.10 Schematic representation of load processes and resistance deterioration (after Melchers 1999).

The above formulation represents the probability that the limit state is crossed for the first time during the reference period, that is, first passage probability. Several methods are available for estimating the probability of failure at specific points in time, with consideration of the time dependence of load effect and/or resistance effect. Typical methods include the time integrated approach for the whole lifetime and the discrete approach for shorter periods (e.g. earthquakes, storms).

Timevariant reliability analysis is discussed in Melchers (1999). When a load process is replaced by a random variable with a mean value equal to its expected maximum value over a chosen reference period, the timevariant problems can be transformed into timeinvariant problems. This approach can be used for solving the problems such as overload failures and cumulative failures (e.g. fatigue, corrosion). In special cases where the resistance in the limit state equation is deterministic and the loading is a Gaussian process, the probability of failure of the structure can be estimated from the integral of mean timevariant outcrossing rate over the reference period.

9.5.3 Remaining Useful Life

Timevariant structural reliability analysis can be further used for estimating the lifetime T of a civil engineering structure (Biondini and Frangopol 2016), when load effect S exceeds resistance effect R , namely

$$T = \min\{(t - t_0) | R(t) < S(t)\} \quad (9.22)$$

where t_0 is time instant at the end of the construction phase. For a given allowable value of reliability index β^* or probability of failure p_f^* , as shown in [Figure 9.11](#), the corresponding threshold T^* of the random variable T can be directly estimated from

$$T^* = \min\{(t - t_0) | p_f(t) > p_f^*\} = \min\{(t - t_0) | \beta(t) < \beta^*\} \quad (9.23)$$

Similarly, the remaining useful life T_{rul} associated with a target reliability index or probability of failure after service time t_s can be evaluated from

$$T_{rul} = \min\{(t - t_s - t_0) | p_f(t) > p_f^*\} = \min\{(t - t_s - t_0) | \beta(t) < \beta^*\} \quad (9.24)$$

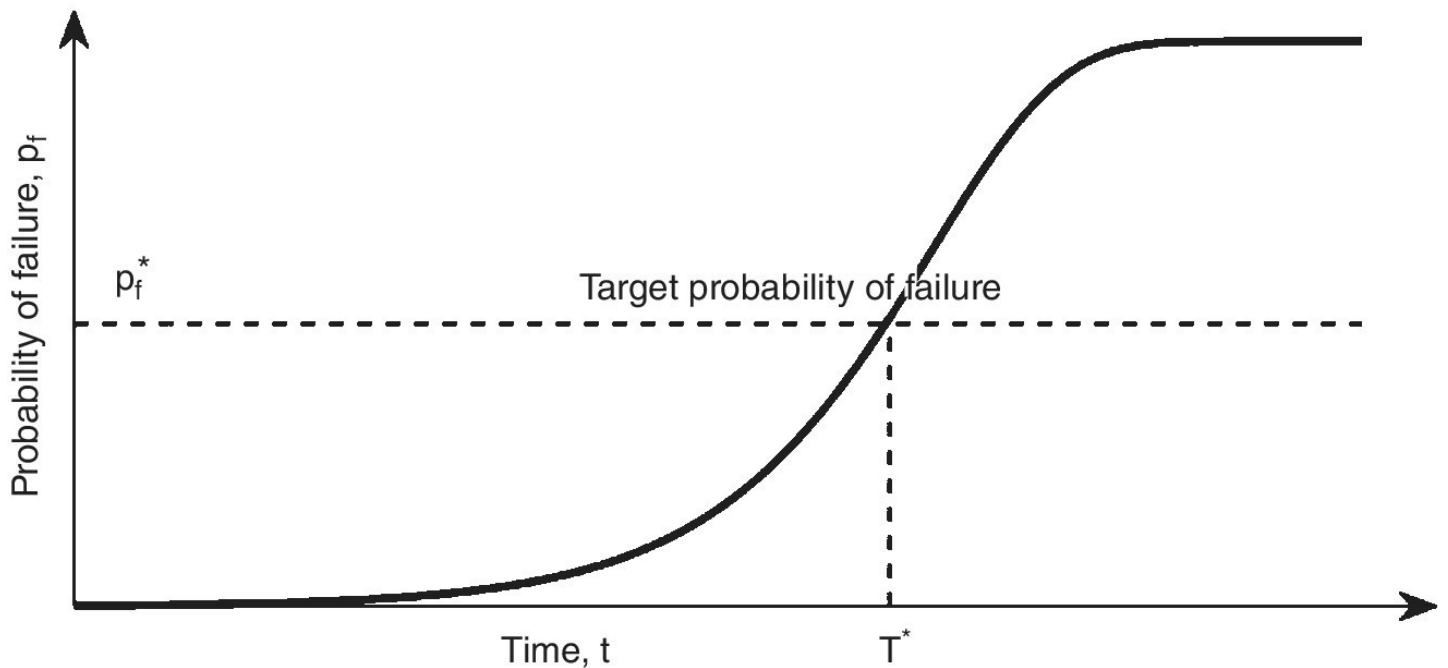


Figure 9.11 Structural lifetime T^* associated with a target probability of failure p_f^* .

Proper management of existing structures under timevariant performance deterioration requires frequent inspections and maintenance actions. The application of timevariant reliability analysis and lifecycle cost analysis can play a significant role in optimising maintenance strategy for existing civil infrastructure to balance risk of structural failure and costs for maintenance.

9.5.4 Example for Fatigue Reliability Analysis – a Suspension Bridge (VII)

The Tsing Ma Bridge, as described in [Section 2.3.5](#) and [Section 7.3.7](#), is used here to investigate the fatigue reliability of its structural components (Ye et al. 2012). As part of the

structural monitoring system, 110 weldable foiltype strain gauges were installed to measure dynamic strains at critical positions of deck crosssections and bearings. One year's monitoring data (the year of 1999) was acquired from the strain gauges for strainbased fatigue and condition assessment. Here, the monitoring data from the strain gauge SPTLS16 located at the deck crosssection CH24662.5, as Detail H in [Figure 9.12](#), is used for fatigue reliability assessment.

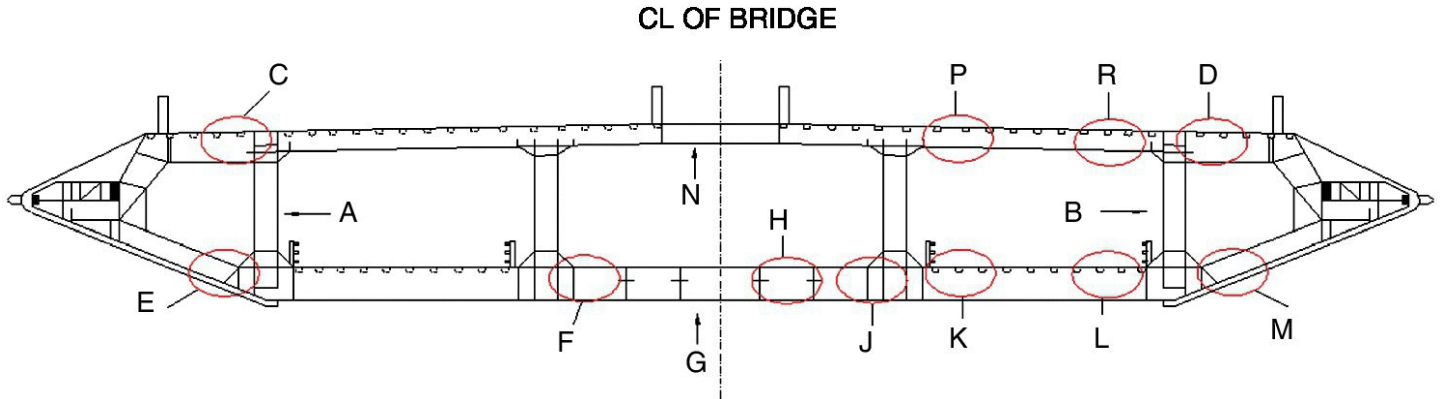
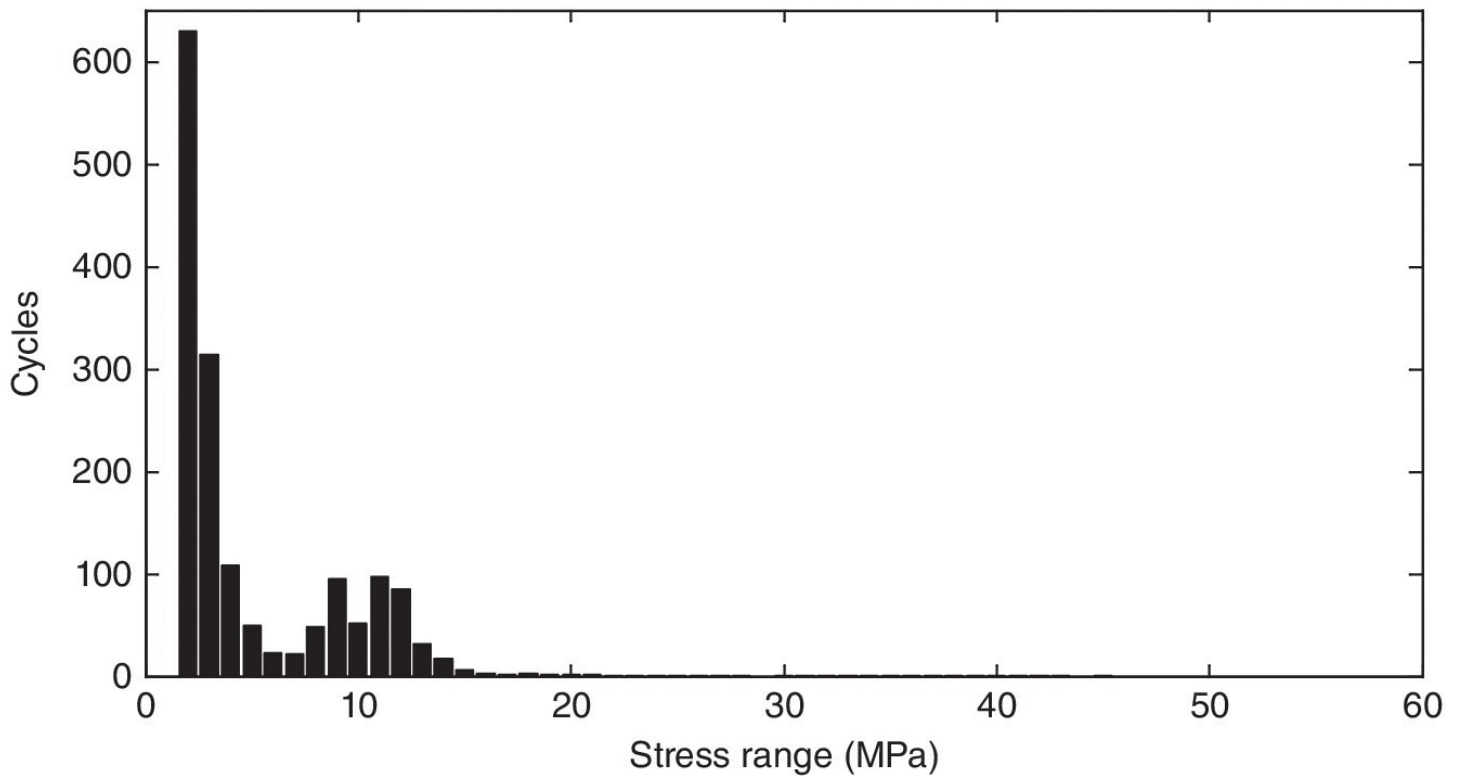


Figure 9.12 Deck crosssection CH24662.5 and strain gauge SPTLS16 at Detail H of Tsing Ma Bridge.

From monitoring data of the strain gauge SPTLS16, the daily stress spectra are similar for different days under normal traffic and monsoon conditions. It is therefore reasonable to average a number of daily stress spectra resulting from different days to obtain a 'standard daily stress spectrum'. Data acquired from 20 days including one day under typhoon condition is chosen to construct a representative data sample. [Figure 9.13\(a\)](#) illustrates the obtained standard daily stress spectrum using the 20day daily stress spectra in consideration of highway traffic, railway traffic and typhoon effects. The rainflowcounted stress that ranges from 2 to 30 MPa is extracted for modelling the probability density function (PDF) of the stress range measured by the strain gauge SPTLS16. The total observation number of the 20day stress range data is 30,986, and the number of classes is obtained as 16 according to the Sturges classification rule.

(a) Histogram of standard daily stress spectrum



(b) Mixed PDFs of 20 days' stress range data

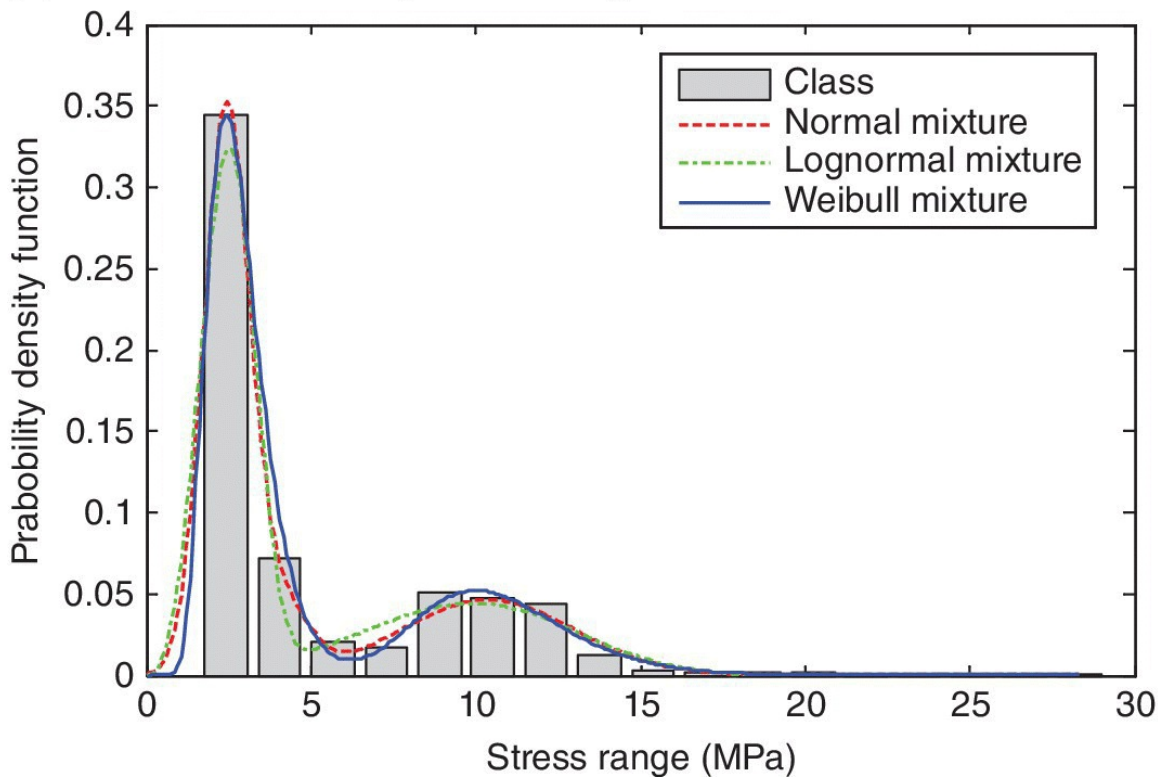


Figure 9.13 Monitoring data of dynamic stresses collected from strain gauge SPTLS16.

Figure 9.13(b) shows the finite mixed PDFs of the 20day stress range data, where normal, lognormal and Weibull distributions are used, respectively. From the results, the scatter of the

stress ranges is well modelled by the finite mixture distributions and easily extrapolated to the region beyond the measured stress ranges. Also, the predicted stress range distribution is a twomodel PDF separated at 6 MPa. The stress ranges less than 6 MPa are caused by highway traffic, and the stress ranges larger than 6 MPa are mainly attributed to train traffic. From comparison of the results, the Weibull distribution is taken as the component distribution for modelling the measured stress ranges.

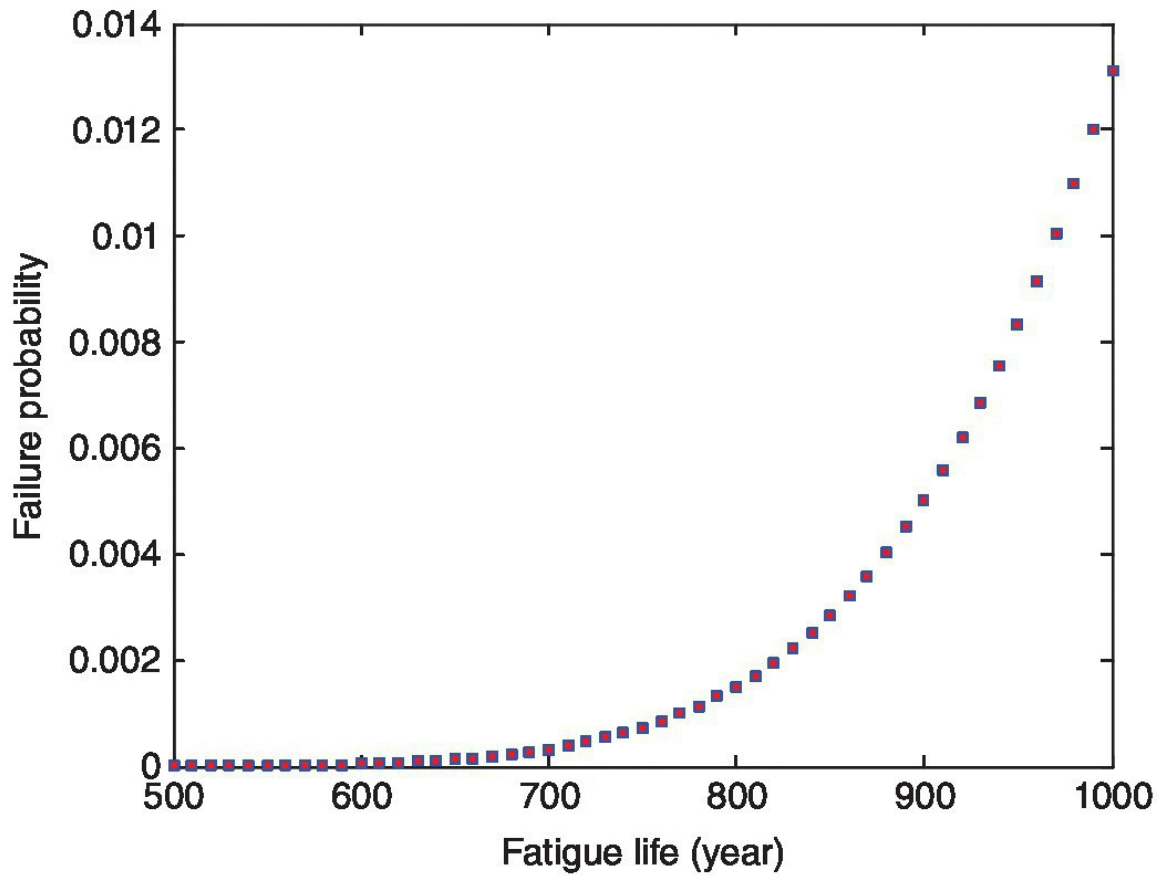
To analyse the fatigue reliability, the limit state function for fatigue damage $g(\sigma, \tau)$, in terms of nominal stress range (σ) and stress concentration factor (τ), can be expressed as

$$g(\sigma, \tau) = D_f - \iint_{\Sigma T} \frac{N_{tot} f(\sigma) f(\tau)}{N_f} d\sigma d\tau \quad (9.25)$$

where D_f is the fatigue damage at failure, N_{tot} is total number of stress cycles, N_f is the stress cycles at failure and $f(\sigma)$ and $f(\tau)$ are the PDFs of nominal stress range and stress concentration factor, respectively. From the limit state function, the probability of failure as well as the corresponding reliability index can be calculated.

[Figure 9.14](#) shows the results for the probability of failure and reliability index versus fatigue life, where the range of the counted stress is between 2 and 30 MPa and the coverage of stress concentration factor is from 1 to 2. The reliability index in the range between 2 and 4 is used to establish code safety margins. Fatigue life is then determined for a given target reliability index or probability of failure. From the results, the predicted fatigue life is 796 years if the value of target reliability index is taken as 3. The results also indicate that the service fatigue life directly affects the probability of failure or reliability index of the structural component. When the requirement for service life increases, the corresponding probability of fatigue failure increases, and reliability index decreases sharply.

(a) Probability of failure versus fatigue life



(b) Reliability index versus fatigue life

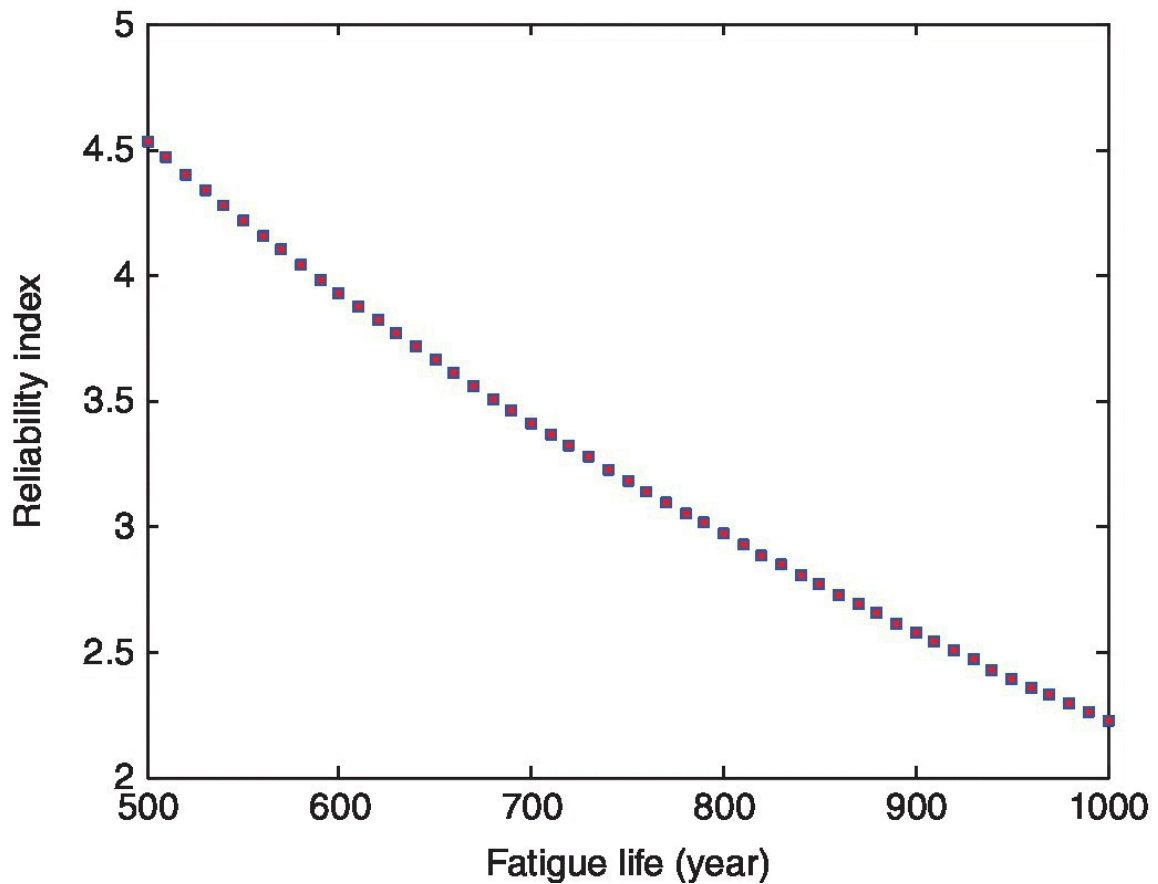


[Figure 9.14](#) Probability of failure and reliability index as a function of fatigue life.

9.6 Optimum Maintenance Strategy

The results of lifetime deterioration modelling and timevariant reliability analysis can be used to determine an optimal maintenance strategy. The advances in lifetime reliability assessment and lifecycle cost analysis provide critical information to establish guiding policies and support decision making processes for rational management of existing civil structures.

9.6.1 Lifetime Costs

Optimum planning of inspection, monitoring, maintenance and repairs of existing civil structures in a costeffective manner relies on lifecycle cost analysis. This optimisation problem consists of minimising total expected lifecycle cost, including costs for inspection, maintenance and repair (Orcesi and Frangopol 2011). For an existing civil structure, the expected total cost over the remaining life span C_{total} can be expressed as

$$C_{total} = C_{insp} + C_{main} + C_{rep} + C_{fail} + C_{mon} \quad (9.26)$$

The total expected cost of performing inspections C_{insp} for a total of N_i structural inspections over the remaining service life span T is calculated from

$$C_{insp}(T) = \sum_{i=1}^{N_i} \frac{C_{insp,i}}{(1 + d_r)^{t_i}} \quad (9.27)$$

where $C_{insp,i}$ is reference cost for the i th structural inspection at time t_i and d_r is annual discount rate.

The total expected cost of maintenance C_{main} includes costs for preventive or routine maintenance over the remaining service life span T , depending on specific scheduling. The total expected cost of repair C_{rep} for a total of N_j structural repairs over the remaining service life span T is

$$C_{rep}(T) = \sum_{j=1}^{N_j} \frac{C_{rep,j}}{(1 + d_r)^{t_j}} \quad (9.28)$$

where $C_{rep,j}$ is the reference cost for the j th structural repair at time t_j .

The maintenance strategy including structural inspection and repair will change the profiles of the probability of failure. The expected cost of structural failure C_{fail} over the remaining service life span T is calculated from

$$C_{fail}(T) = C_f p_f(0) + \sum_{t=1}^T \frac{C_f [p_f(t) - p_f(t-1)]}{(1 + d_r)^t} \quad (9.29)$$

where C_f is the cost of structural failure at the present time and $p_f(0)$ and $p_f(t)$ are the probability of failure at the present time and at year t , respectively.

In the cases where a monitoring system has been installed on the structure, the expected cost of monitoring C_{mon} should be included in the expected total cost. The cost of monitoring depends on monitoring times and durations. The monitoring cost is composed of fixed cost due to the preparation and analysis of monitoring (e.g. installation, wiring of sensors and data acquisition system) and variable cost that depends on the duration of monitoring (Orcesi and Frangopol 2011). The expected cost of monitoring C_{mon} over the remaining service life span T is estimated from

$$C_{mon}(T) = \sum_{j=1}^{Mm} \sum_{k=1}^{Njt} \frac{C_{mon,ref}^j \frac{d_k}{d_0} + C_{mon}^{f,j}}{(1 + d_r)^{t_k}} \quad (9.30)$$

where $C_{mon,ref}^j$ is reference cost of monitoring component j during d_0 days, d_k is length of monitoring (in days), $C_{mon}^{f,j}$ is fixed cost of monitoring component j , Mm is number of components that are monitored, Njt is the number of monitoring times for the component j until t and t_k is time of the k th monitoring of component j .

9.6.2 Decision Based on Lifetime Deterioration

Structural performance deterioration over time can be modelled using various stochastic process models, such as failure rate function, Markov process, gamma process and Weibull model, as discussed in [Sections 9.3](#) and [9.4](#). On the basis of these stochastic deterioration models, an optimal maintenance policy with or without performance constraints can be determined.

9.6.2.1 Failure Rate Function Model

In the cases where a failure rate function is used for lifetime deterioration modelling, an optimal maintenance policy can then be determined using the age replacement model and the block replacement model. The age replacement model provides an optimal maintenance policy for replacement upon failure (corrective replacement) or upon reaching a predetermined age k (preventive replacement), whichever occurs first. The block replacement model gives an optimal policy for replacement upon failure and periodically at the times (e.g. $k, 2k, 3k \dots$). The age replacement model is one of the most frequently used maintenance optimisation models in practice. Details of these replacement methods are discussed in Barlow and Proschan (1965).

9.6.2.2 Markov Process Model

To determine an optimal policy for maintenance actions, a finite set of actions A and costs $C(i,a)$ are introduced (Frangopol et al. 2004). When the process is currently in state i and an action a is taken, the process moves into state j with probability

$p_{ij} = \Pr\{X_{n+1} = j \mid X_n = i, a_n = a\}$. This transition probability does not depend on the state history. If a stationary policy is selected, then this process is called a Markov decision process. The state of the structure over time with or without performing maintenance actions can be modelled. Thus, an optimised decision on inspection and/or maintenance policies can be determined.

When the structure is in state i , the expected discounted costs over an unbounded horizon are expressed as the recurrent relation

$$C_\alpha(i) = C(i,a) + \alpha \sum_{j=1}^m p_{ij}(a) C_\alpha(j) \quad (9.31)$$

where $\alpha = (1 + d_r)^{-1}$ is annual discount factor, C_α is the discounted value function. Starting from state i , $C_\alpha(i)$ represents the cost of performing an action a given by $C(i, a)$ plus the expected discounted costs of moving into another state with probability $p_{ij}(a)$. The discounted costs over an unbounded horizon associated with a start in state j are given by $C_\alpha(j)$.

Therefore, [Equation \(9.31\)](#) is a recursive equation. The choice for the action a is determined by the maintenance policy and also includes no repair.

A costoptimal decision can be found by minimising [Equation \(9.31\)](#) with respect to the action a . Many approaches are available to find this optimal solution. A typical policy improvement algorithm can be used to calculate the expected discounted costs for increasingly better policies until no more improvement can be made (Frangopol et al. 2004). Some issues arise in the use of Markov decision processes for maintenance optimisation. For example, this method works well for visual inspections, but it is not suitable for continuous monitoring. The reason for that is the condition state is not continuous, but discrete and finite. The Markovian assumption of no memory may not be true in some practical cases. Also, the transition probabilities are often estimated from the use of expert judgement, thus they are difficult to assess and are quite subjective.

9.6.2.3 Gamma Process Model

The gamma deterioration process was successfully applied to model time based or condition based preventive maintenance (van Noortwijk 2009, Frangopol et al. 2004). Time based preventive maintenance is undertaken at regular intervals of time. By contrast, condition based maintenance is undertaken at times based on inspecting or monitoring condition of a structure. In general, cost based criteria, such as the expected discounted cost over an unbounded horizon, are used for optimising maintenance policy in terms of repair time. These cost based criteria are computed on the basis of renewal theory, assuming that renewals bring a

component or structure back to its original condition. From renewal theory with discounting, the expected discounted cost over an unbounded horizon is expressed as

$$C_{\alpha}(t) = \lim_{t \rightarrow \infty} E(K(t, \alpha)) = \frac{\int_0^{\infty} \alpha^t c(t) dF(t)}{1 - \int_0^{\infty} \alpha^t dF(t)} \quad (9.32)$$

where $E(K(t, \alpha))$ represents the expected discounted cost in the bounded time interval $(0, t)$ with annual discount factor α , $c(t)$ is the cost associated with a renewal at time t and $F(t)$ is the cumulative probability distribution of the time of renewal.

For civil structures, maintenance can often be modelled as a discrete-time renewal process, since the planned lifetime of most structures is very long compared with the possible renewal cycle length. Two typical types of maintenance are often used in practice: preventive maintenance before failure and corrective maintenance after failure. A preventive replacement involves a cost c_P , whereas for a corrective replacement the cost is c_F , where $c_F \geq c_P > 0$. By using discrete-time renewal theory, the expected discounted cost of age replacement over an unbounded horizon is

$$C_{\alpha}(k) = \lim_{k \rightarrow \infty} E(K(k, \alpha)) = \frac{\left(\sum_{i=1}^k \alpha^i p_{fi} \right) c_F + \alpha^k \left(1 - \sum_{i=1}^k p_{fi} \right) c_P}{1 - \left[\left(\sum_{i=1}^k \alpha^i p_{fi} \right) + \alpha^k \left(1 - \sum_{i=1}^k p_{fi} \right) \right]} \quad (9.33)$$

where $k = 1, 2, 3, \dots$ represents the number of time intervals to be determined and p_{fi} represents the failure probability of a renewal in unit time i . The optimal maintenance time interval k^* is then obtained by minimising the expected discounted cost over lifetime.

9.6.2.4 Survival Function

The evolution in time of the safety of an existing civil engineering structure can be described by a survival function such as the Weibull model (Orcesi and Frangopol 2011). The survival function $R(t)$ represents the probability that the structure will not fail before time t , as discussed in [Section 9.4.2](#). From the selected survival function, an optimal maintenance policy of the structure can be determined by minimising the total cost during the service life under constraints of specific safety requirement. Very often, the main objective of civil infrastructure management is to spend the minimum possible amount of financial resources, while keeping the structures safe and serviceable.

When no monitoring is performed, the optimal solution is found by minimising both cumulative expected cost of repair C_{rep} at the end of service life T_f in [Equation \(9.28\)](#) and the expected

cost of structural failure C_{fail} at the end of service life T_f in [Equation \(9.29\)](#). The minimisation of the two objective functions is then

$$\text{Min } C_{rep}(T_f) \text{ and Min } C_{fail}(T_f) \quad (9.34)$$

When monitoring is performed, monitored data can update reliability knowledge of the structure, which affects the maintenance planning. In this case, the cumulative expected cost at the end of service life T_f includes the monitoring cost C_{mon} in [Equation \(9.30\)](#) and the repair cost C_{rep} in [Equation \(9.28\)](#). The minimisation of the two objective functions in [Equation \(9.34\)](#) is then rewritten as

$$\text{Min } [C_{rep}(T_f) + C_{mon}(T_f)] \text{ and Min } C_{fail}(T_f) \quad (9.35)$$

Multiobjective optimisation methods, such as nondominated sorting genetic algorithms (Orcesi and Frangopol 2011), can be used to find the optimal solution set of this biobjective optimisation problem.

9.6.3 Decision Based on Structural Reliability

The proper maintenance decision under safety constraints required for existing civil structures should be made based on both cost and reliability. In order to minimise the lifecycle cost within acceptable risk of structural failure, optimal reliability based maintenance strategy needs to be used in the process of infrastructure management. For existing civil structures without monitoring system installed, from [Equation \(9.26\)](#) the expected total cost over the remaining life span is expressed as

$$C_{total} = C_{insp} + C_{main} + C_{rep} + C_{fail} \quad (9.36)$$

where the expected total cost includes costs for inspections C_{insp} , preventive maintenances C_{main} , repairs C_{rep} and structural failure cost C_{fail} over the remaining life span.

The optimisation problem for existing civil structures consists of minimising expected total cost in [Equation \(9.36\)](#) under reliability constraints (Onoufriou and Frangopol 2002), expressed as

$$\text{Min } C_{total} \text{ subject to } \beta_{RL} \geq \beta_{RL}^* \quad (9.37)$$

where β_{RL} and β_{RL}^* are the structural lifetime reliability index and target reliability index associated with the remaining service life of the structure, respectively.

The optimisation in [Equation \(9.37\)](#) can also be undertaken under constraints of probability of failure

$$\text{Min } C_{total} \text{ subject to } p_f \leq p_f^* \quad (9.38)$$

where p_f and p_f^* are the lifetime probability of failure and target probability of failure associated with the remaining service life, respectively. Many methods are available for finding an optimal solution for the constrained optimisation problem with inequality constraints (Bazaraa et al. 2006).

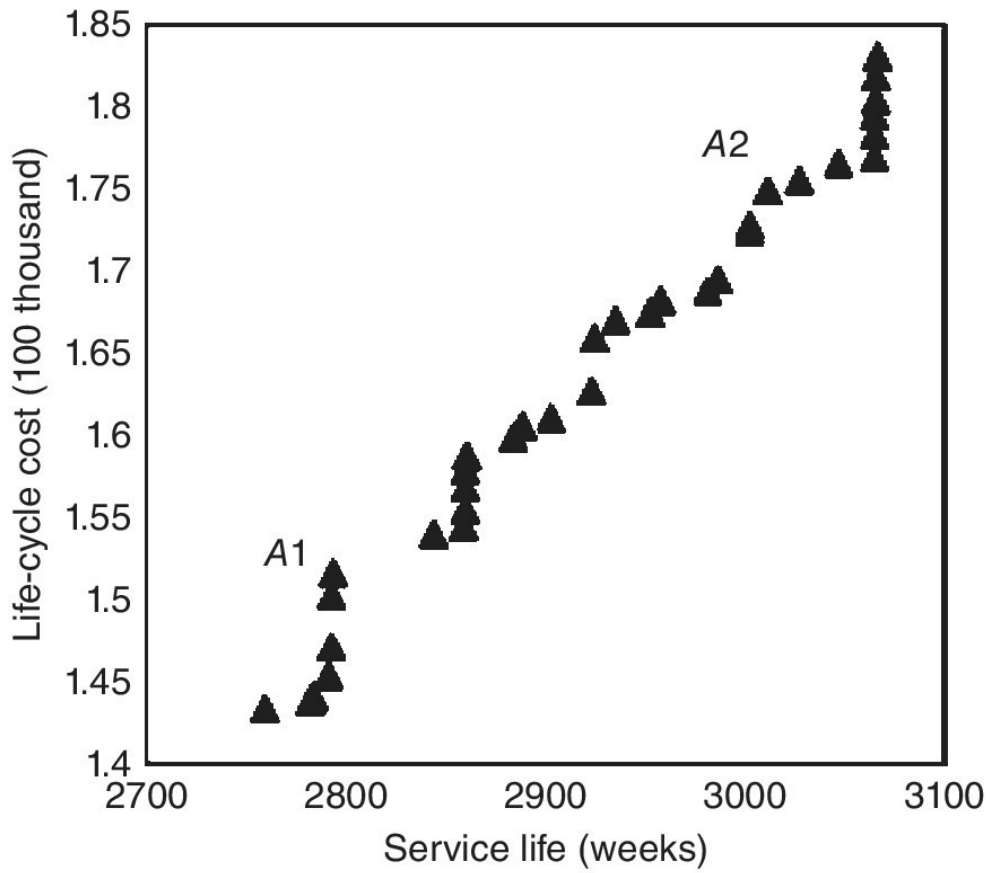
9.6.4 Example for Optimal Maintenance – a Steel Bridge (II)

Fatigue cracks often exist and develop in the welded Utype stiffening ribs and/or in the deck plates of a steel bridge under the action of cyclic loads. The stochastic gamma process can be used for the fatigue crack evolution modelling of the structural components (Huang et al. 2016), as discussed in [Section 9.3.4](#). During the lifecycle of the steel bridge affected by fatigue cracking, a series of inspection and maintenance actions may be required. In order to minimise lifecycle cost, the inspection and maintenance strategy needs to be optimised. The optimisation problem of inspection and maintenance actions is to find an optimal inspection time and repair planning represented by a repair coefficient that indicates the reduction of fatigue crack length after repair. The multiple objectives of the optimisation problem are to maximise the service life after inspections and repairs and to minimise the total cost for inspections and repairs.

Assume the critical threshold value of fatigue crack length $a_{cr} = 15$ mm, inspection cost $C_{insp} = 20$ k\$, maintenance cost $C_{main} = 100$ k\$, and initial failure risk cost $C_{fail}^0 = 500$ k\$. The inspection time interval is assumed at least one year and the repair coefficient is assumed to be between 0.1 and 0.9. A genetic algorithm (GA) is adopted to solve the multiobjective optimisation problem for maximising the service life and minimising the maintenance cost.

[Figure 9.15](#) shows the results for the optimal inspection and repair planning for the fatigue crack in the stiffing ribs of the steel bridge. The number of inspections is assumed to be once in [Figure 9.15\(a\)](#) and twice in [Figure 9.15\(b\)](#), respectively. Every point in the results shown in the figures represents a specific inspection and repair planning. Both the service life after the intervention and the total cost of the inspections and repairs are provided in the results. As expected, the required cost for the inspections and repairs increases, as the expected service life is extended.

(a) Single intervention



(b) Double intervention

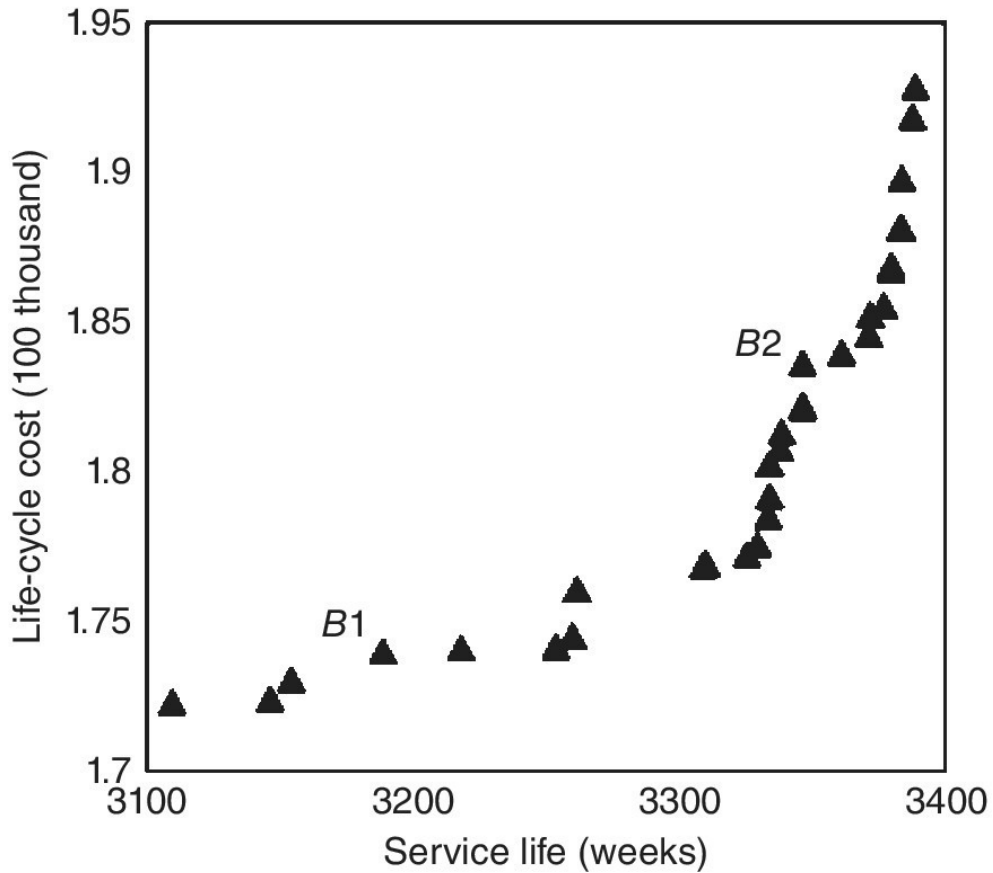


Figure 9.15 Pareto optimum solution sets with single and double interventions for inspection and maintenance.

9.7 Case Study

A bridge health monitoring system has been installed and operated on the Tsing Ma Bridge to monitor four major categories of parameters: environments, traffic loads, bridge features and bridge responses, as described in Wong and Ni (2011) and discussed in [Section 2.3.5](#). The sensory systems used for stress and traffic loads monitoring include dynamic strain gauges, dynamic weighinmotion stations and servotype accelerometers. [Table 9.1](#) summarises the types of structural components, instrumented structural components and monitoring parameters required for the monitoring system of the bridge.

Table 9.1 List of instrumented structural components and monitoring parameters.

Group name	Component name	Monitoring parameters
Suspension cables	Main cables; strand shoes; shoe anchor rods; anchor bolts; cable clamps & bands	<ul style="list-style-type: none"> • Servotype accelerometers in main cables • Fourier analysis of time series acceleration data • Cable force estimation
Suspenders	Hangers; hanger connections; stiffeners; hanger connections; bearing plates	<ul style="list-style-type: none"> • ServoType accelerometers in hangers and following the same method and procedure as above
Outer longitudinal trusses	Top chord; diagonal chord; vertical post; bottom chord	<ul style="list-style-type: none"> • Dynamic strain gauges – single gauges, pair gauges and rosette gauges • Dynamic weigh inmotion stations • Statistical processing of
Inner longitudinal trusses	Top chord; diagonal chord; vertical post; bottom chord	
Main cross	Top web; sloping web; bottom web; bottom chord	

frames		strain/stress history
Intermediate cross frames	Top web; Sloping web; Bottom web; Bottom chord	<ul style="list-style-type: none"> • Stress influence coefficients derivation
Plan bracings	Upper deck bracings; lower deck bracings	<ul style="list-style-type: none"> • Stress demand ratios computation
Deck	Deck troughs; deck plates	<ul style="list-style-type: none"> • Highway traffic loads estimation
Railway waybeams	Tsections; top flanges; connections	<ul style="list-style-type: none"> • Railway traffic loads estimation • Fatigue life estimation
Bearings	Rocker (R.) bearings at Ma Wan Tower; PTFE (P.) bearings at Tsing Yi Tower; P. bearings at pier T1; P. bearings at pier T2; P. bearings at pier T3; P. bearings at Tsing Yi anchorage; R. bearing at M2; P. bearings at M1; Hinged bearing at Ma Wan anchorage	<ul style="list-style-type: none"> • Dynamic strain gauges in Ma Wan rocker bearings only and following the same method and procedure as above.

[Figure 9.16](#) shows the related sensors in longitudinal stiffening truss for highway traffic monitoring of the bridge. In this stress and traffic loads monitoring, the three categories of monitoring parameters are: traffic loads monitoring, cable force monitoring and stiffening deck system stress monitoring. The sensory systems for stress and traffic loads monitoring generate three types of timeseries data of strain, axleweight and axlespeed and acceleration, respectively. This data is then processed and analysed in accordance with the requirements of the monitored parameters. The monitored parameters and related components in each category are discussed as follows.

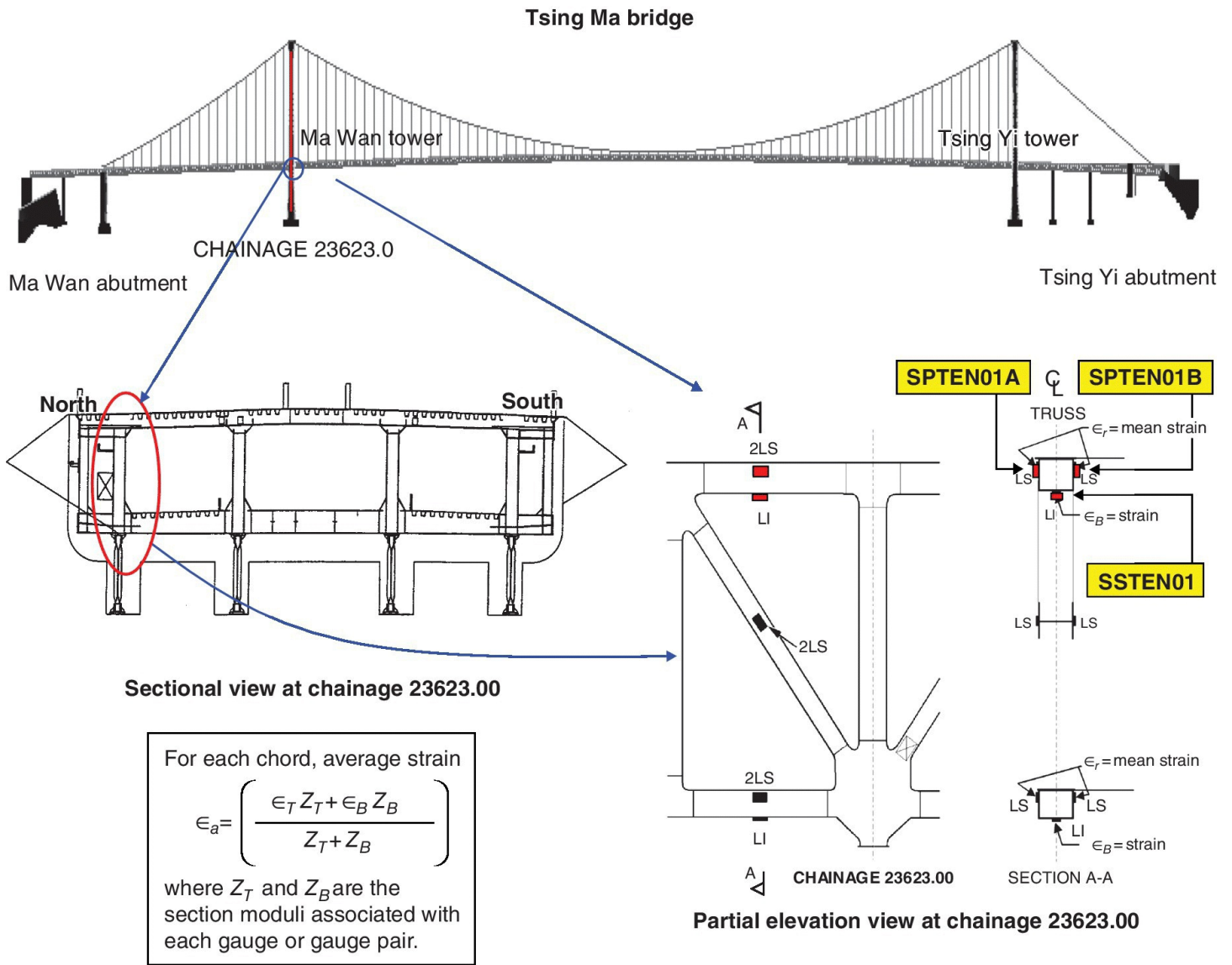


Figure 9.16 Dynamic strain gauges in longitudinal stiffening truss for highway traffic monitoring.

9.7.1 Traffic Loads Monitoring

The highway traffic data obtained from the dynamic weighinmotion stations is first processed in accordance with the vehicular classification required by the Transport Department. The details of vehicular classification are then simplified in accordance with BS 5400:Part 10:1980, Clause 8.4.3 (BSI 1980). The data from dynamic weighinmotion stations is used to monitor the potential rates of fatigue damage, due to highway traffic in selected parts or components sensitive to passages of individual commercial vehicles. The theoretical relationships (influence lines) between stress range and typical vehicular loads are derived by finite element analysis, and the potential fatigue damage related to those ranges is based on the SN curves as given by BS 5400:Part 10:1980. By repeating this process for each typical type of commercial vehicle, the cumulative fatigue damage rate over the prescribed periods is then monitored and compared to that obtained from the design rules and from measurement results.

The railway waybeam on Tsing Ma Bridge is composed of two inverted Tbeams welded to a top flange plate. At the section of the instrumented waybeam, 50 mm from the midway between the cross frames, the dynamic strain gauges are installed. In order to avoid the uncertainties of the effective width of the top flange under wheel loads, the effective section properties should best be calibrated under the passage of bogies of known loads. [Figure 9.17](#) shows the results for the bogie loads for each line of a train, computed from the measured strain and the elastic modulus of structural steel.

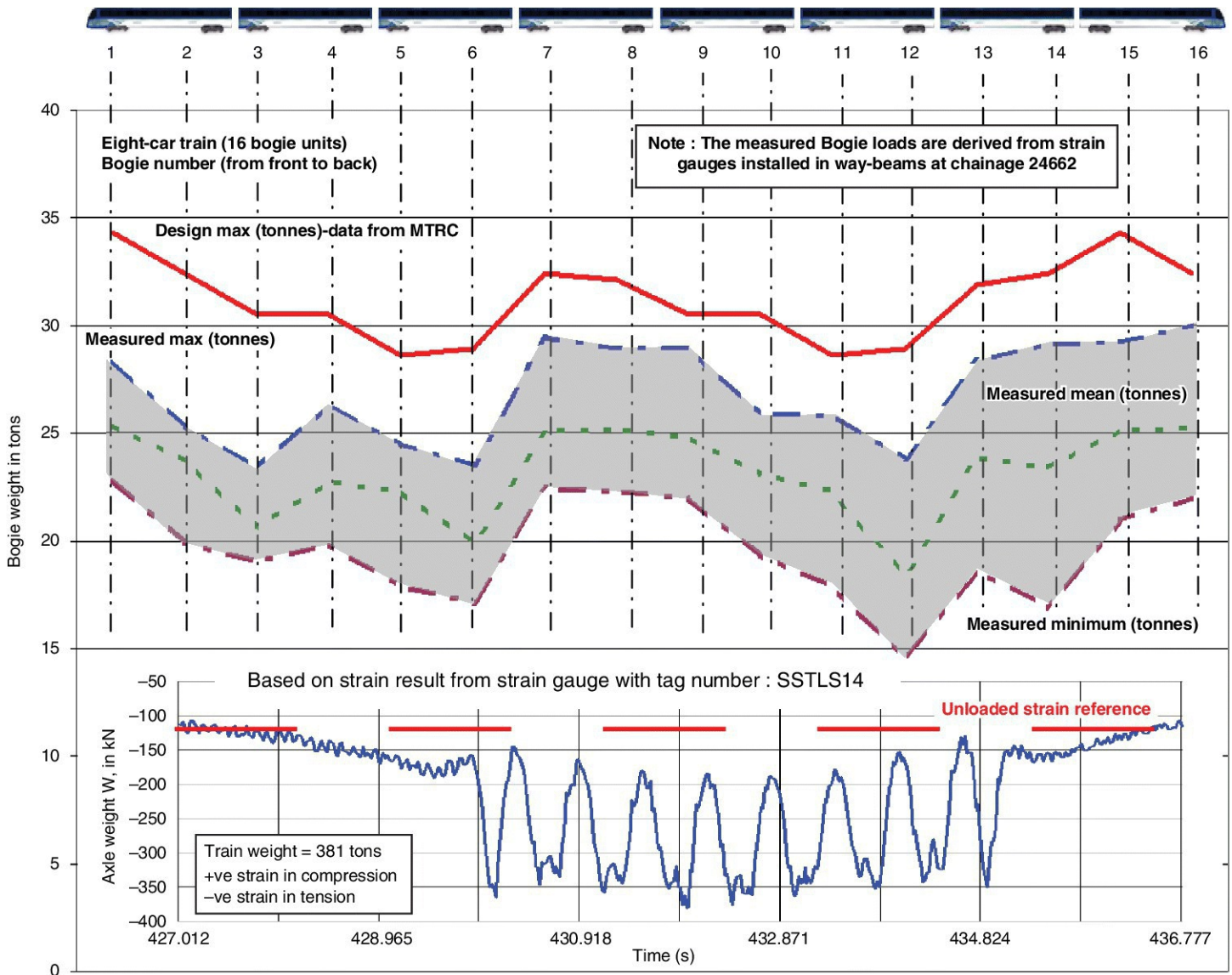


Figure 9.17 Estimates of railway loading based on strain results in waybeams.

9.7.2 Cable Force Monitoring

Cable force monitoring on the Tsing Ma Bridge is composed of main cable monitoring and suspender monitoring. Servotype accelerometers are installed to monitor the tension forces in cables and suspenders, based on the cable and suspender frequencies extracted from the stationary and ergodic timeseries acceleration data. For main cables, the timeseries of acceleration data on the Tsing Yi side span is used, because the influence due to suspenders is

minimum. In the monitoring of tension force in suspenders, since there is no fixed servotype accelerometers installed in the 95 groups of suspenders, field ambient vibration measurements on each group of suspenders are required. In the first two years of monitoring system operation, the field ambient vibration measurements on all the 95 groups of suspenders were completed. Then, around 10% of the measurements are selected each year for calibration and/or updating. [Figure 9.18](#) shows the results for the variation of the tension force in the 95 groups of suspenders.

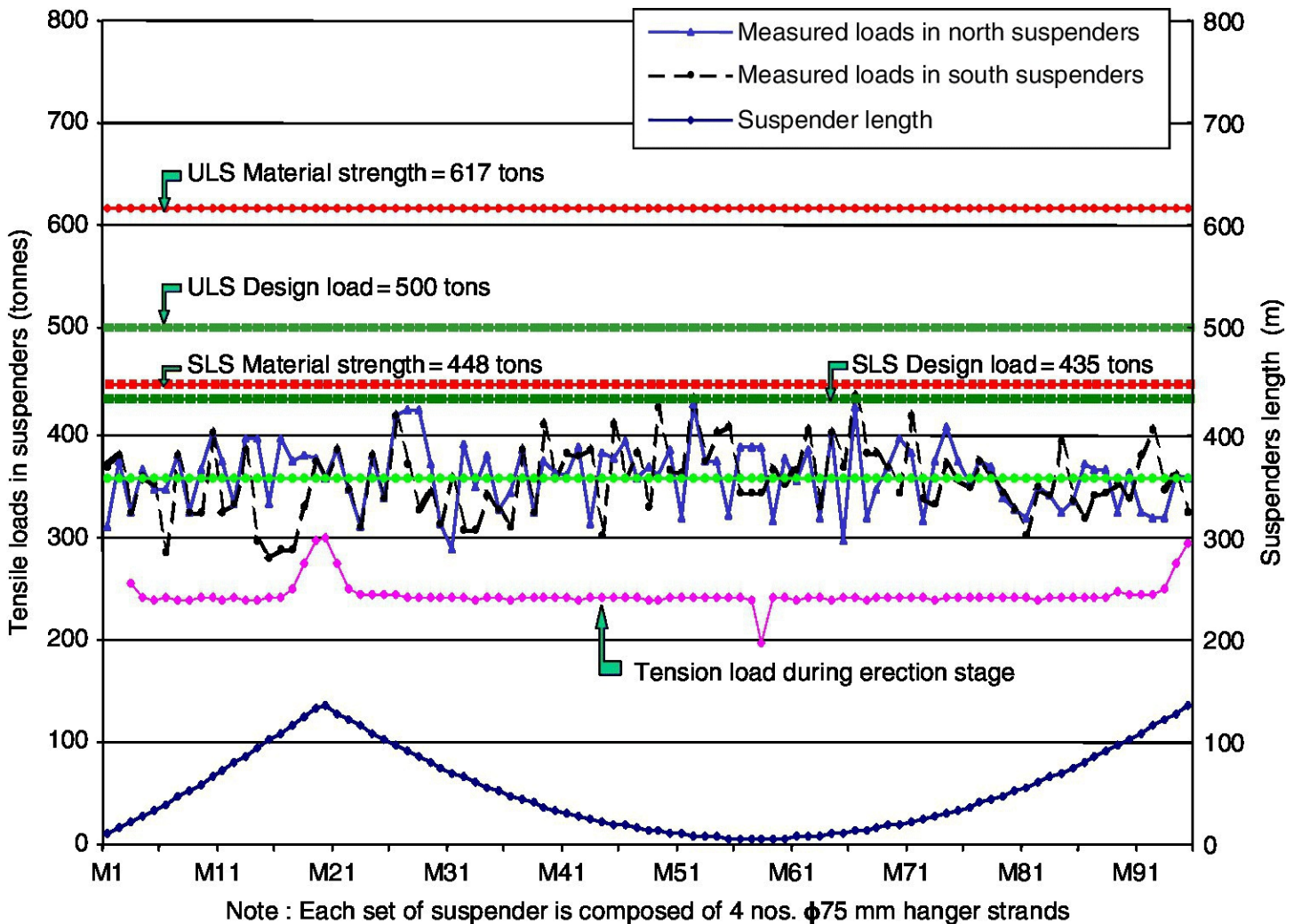


Figure 9.18 Comparison of measured and designed suspender forces.

9.7.3 Stiffening Deck System Stress Monitoring

The three limit states that dominate the design process of steel bridges are tensile fracture, compression buckling and fatigue. Traditionally fatigue has always come last. This is because, in practice, the governing design factor in the majority of components of highway bridges has always been fracture or buckling. In general, there are comparatively few components in which fatigue requires heavier components or heavier connections than demanded by static limit states. Furthermore, fatigue risk of failure by definition needs time to reveal itself. Thus, in stiffening deck system stress monitoring, priority is given to monitoring the current and historical strain/stress status of the component and its stress demand ratios, and then the

estimation of stress influence coefficients and component/connection fatigue life. [Figure 9.19](#) shows the results for statistical processing of strain/stress history in the top chord of outer longitudinal truss on the north side. When sufficient data is collected and processed, the strain/stress variation trend of the component in the future can be predicted.

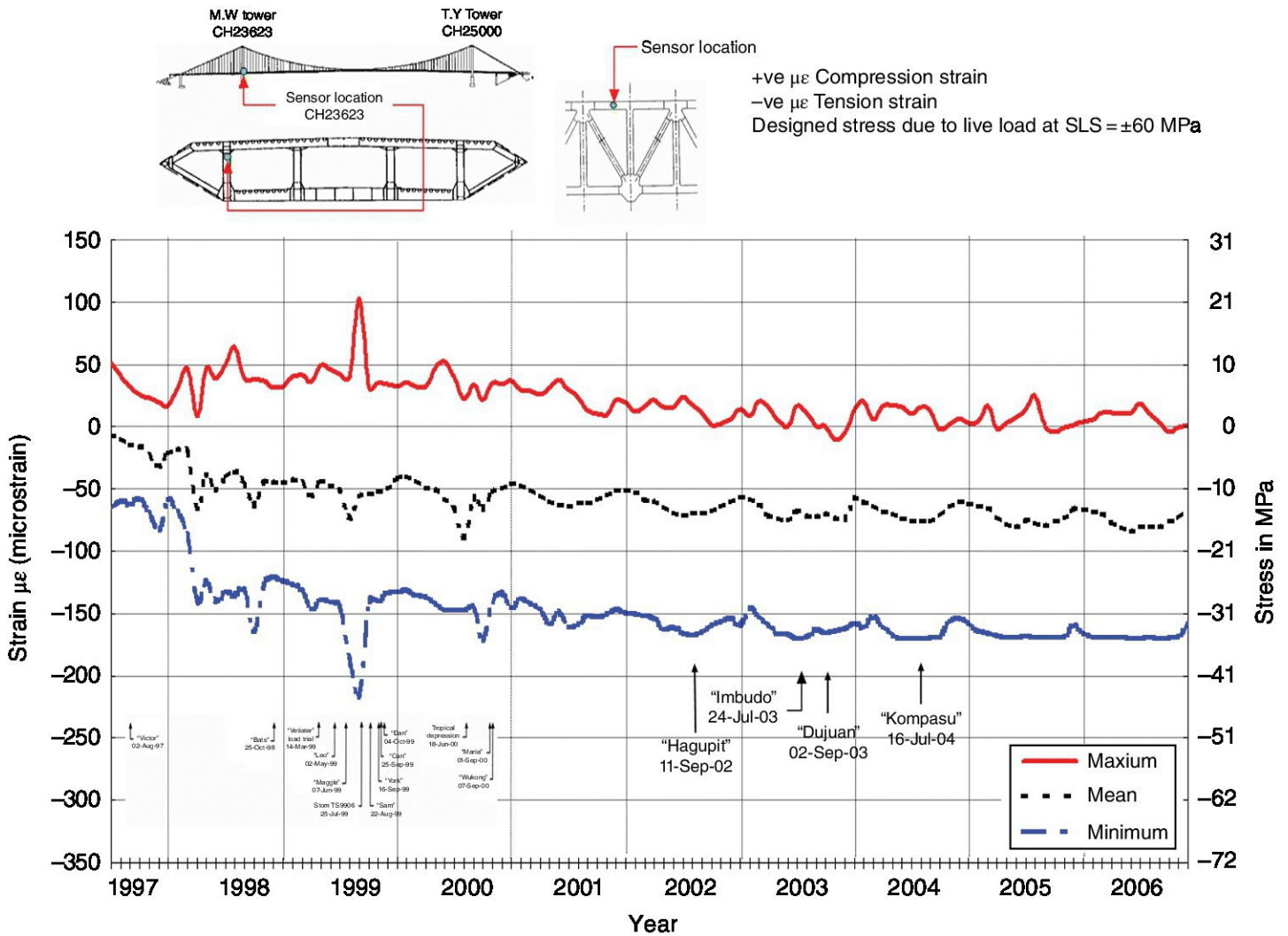
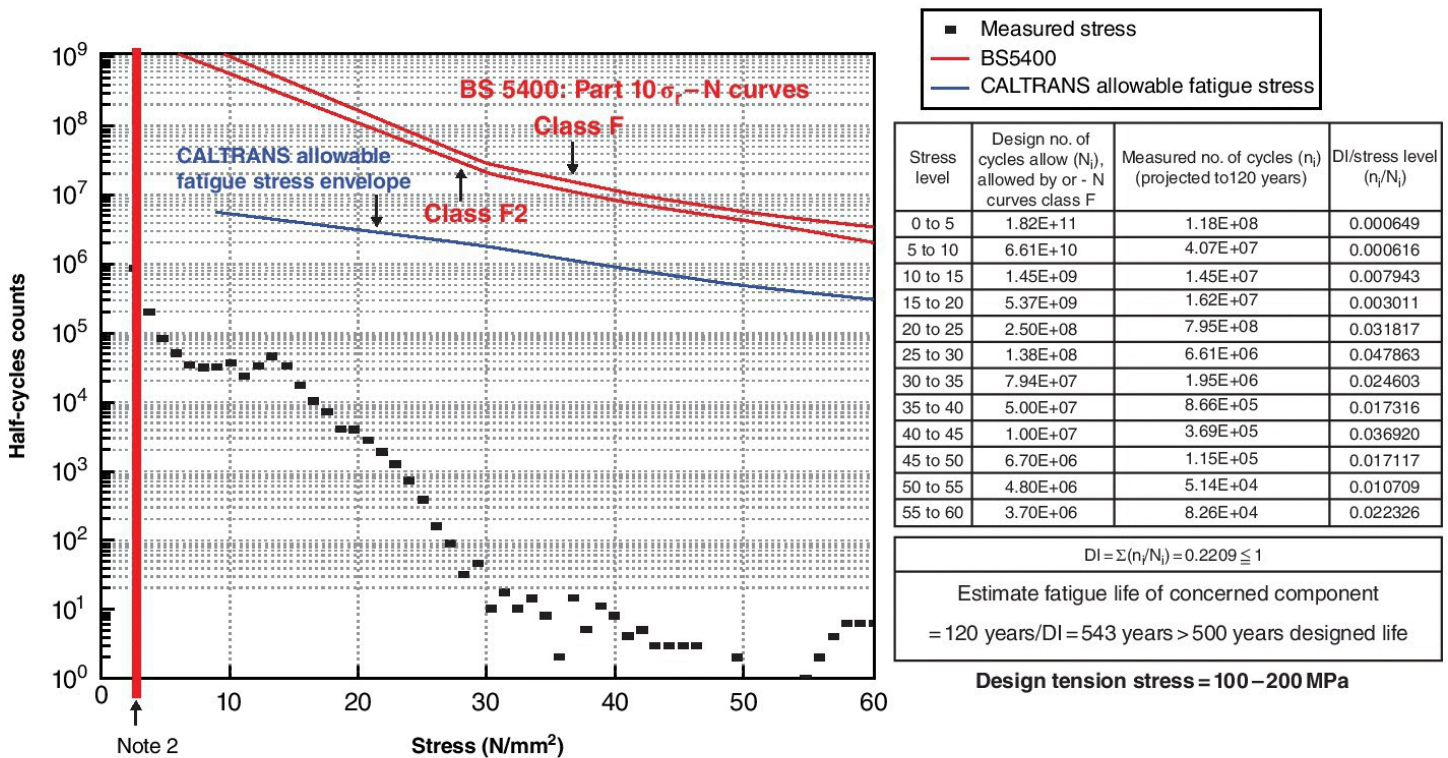


Figure 9.19 Stress history in top chord of outer longitudinal truss (North).

Fatigue life estimation from dynamic strain results of the truss component/connection of Tsing Ma Bridge is carried out in accordance with the requirements, as stated in Clauses 11.1–11.5 and Appendices A and H of BS 5400:Part 10:1980. Fatigue life estimations of the connection between top chord and vertical strut of the outer longitudinal truss, as shown in [Figure 9.16](#), are then undertaken. From the monitored data, the accumulated damage is estimated by the Palmgren–Miner rule. The bridge design life is 120 years. The fatigue life of the connection between the top chord and vertical strut is then estimated from dividing the bridge design life by the predicted accumulated damage. [Figure 9.20](#) shows the results for rainflow counting and fatigue life estimation, with an estimated fatigue life of 543 years.

Histogram of strain half-cycles
Cycles from histogram data from SSTEN01 and SPTEN01. (Cycle ranges above 1000 $\mu\epsilon$ have been discarded.)



Note 1: Based on the palmgren-miner's rule, total fatigue damage (projected to 120 years) = $\sum_{i=1}^i \frac{n_i}{N_i}$

Note 2: Stress level below 2.1N/mm² (or 10 $\mu\epsilon$) is not considered in the analysis

Note 3: Fatigue concentration factor = 1.4

Figure 9.20 Fatigue life estimation for top chord of outer longitudinal truss (North).

9.8 Concluding Remarks

The usage monitoring, including operational load monitoring and environment monitoring, is of great importance for assessing structural performance deterioration, to analyse structural reliability over lifetime and to determine optimal maintenance strategy. From the monitored data and numerical simulations, deterioration of existing civil structures can be modelled with uncertainties using probabilistic approaches. Deterioration processes may involve different types of damage mechanisms with different consequences on the structural performance. In any case, the parameters adopted in modelling of deterioration processes are always affected by uncertainties. Thus, reliable and effective modelling of structural deterioration mechanisms is essential for probabilistic assessment of structural performance over lifetime.

Typical probabilistic approaches for structural deterioration modelling include the failure rate function, Markov process and gamma process. No single approach has yet proven to be generally applicable, and each model has its advantages and disadvantages. For example, deterioration modelling using failure rate functions may be unsatisfactory due to the usual lack of failure data and unobservable failure rates. The Markov process model is purely a condition model and is very well suited to incorporating information from visual inspections, but the

model is not suitable for continuously monitored data. The stochastic gamma processes are well suited for modelling the temporal variability of deterioration. Up to now, the gamma processes have mainly been applied to deterioration and maintenance decision problems for individual components rather than for systems. The gamma processes cannot be used to assess the reliability of a structure in terms of strengths and stresses.

Lifetime distributions take into consideration the combined effect of all the uncertainties in the system by using a stochastic process or an explicit life distribution model, such as the gamma process model or the Weibull model. Lifetime distributions are simple and efficient methods of determining probability distribution of time to failure by considering the time to failure of the system and its components as a random variable. However, lifetime distributions are generally very sensitive to change of the input random variables. It is often very difficult to calibrate and validate the lifetime distributions for a specific structure because of the limited availability of data. Inspection and monitoring activities can provide a powerful aid to reduce the level of epistemic uncertainty and to improve the accuracy of predictive probabilistic models.

Structural reliability analysis associated with the limit states of a civil engineering structure is often used for assessing the safety of the structure at design and operation stages. The probability of failure of a structural system and its components is typically calculated from the limit state equations associated with structural failure modes. Both changes in structural resistance and loading conditions over lifetime can be implemented into timevariant reliability analysis of an existing civil structure. As a result, the remaining useful life of the structure can be estimated from the timevariant reliability analysis. However, this approach has a major disadvantage of computational inefficiency, and it often gives approximate solutions.

Risk and cost optimised maintenance strategy of existing civil structures can be determined on the basis of lifetime reliability analysis and lifecycle cost analysis. These reliability based approaches can be extremely useful to support the decision making process involved in the maintenance and repair of existing civil structures. Among these methods, reliability based multiobjective optimisation methods are particularly useful for evaluating optimal maintenance strategy. However, their computational cost is generally high and can rapidly become prohibitive, when the number of variables, objective functions and necessary constraints become excessive.

For more costeffective management of existing civil structures, further investigations are necessary to collect relevant data from the monitoring systems, to improve the modelling capability and to formulate probabilistic decision problems (Frangopol et al. 2004), including

- developing a generally acceptable and consistent methodology for probabilistic modelling of deterioration processes of structural performance in terms of both condition and reliability
- improving the incorporation of measurement data from SHM systems into the deterioration models and lifetime reliability analysis
- improving the understanding of the influence of maintenance actions on structural

performance, extended service life and their probabilistic modelling

- using optimisation for finding the optimal maintenance strategy with multiple objectives by balancing the risk of structural failure and the costs for maintenance.

References

- Barlow, R.E. and Proschan, F. (1965) *Mathematical Theory of Reliability*. John Wiley & Sons, New York, USA.
- Bazaraa, M.S., Sherali, H.D. and Shetty, C.M. (2006). *Nonlinear programming: Theory and algorithms*. 3rd Edition, John Wiley & Sons, New York, USA.
- Biondini, F. and Frangopol, D.M. (2016) Lifecycle performance of deteriorating structural systems under uncertainty: review. *Journal of Structural Engineering ASCE* **142**(9), F4016001 (1–17).
- British Standards Institution (BSI) (1980) *Code of Practice for Fatigue*. BS 5400, London, UK.
- Catbas, F.N., Susoy, M. and Frangopol, D.M. (2008) Structural health monitoring and reliability estimation: Long span truss bridge application with environmental monitoring data. *Engineering Structures*, **30**(9), 2347–2359.
- Cempel, C., Natke, H.G., Yao, J.T.P. (2000) Symptom reliability and hazard for systems condition monitoring. *Mechanical Systems and Signal Processing*, **14**(3), 495–505.
- Chen, H.P. (2017) Monitoring based reliability analysis of aging concrete structures by Bayesian updating. *Journal of Aerospace Engineering ASCE*, **30**(2), B40150041–8.
- Chen, H.P. and Alani, A.M. (2012) Reliability and optimised maintenance for sea defences. *Proceedings of the ICE: Maritime Engineering* **165**(2), 51–64.
- Chen, H.P. and Alani, A.M. (2013) Optimised repair strategy for cracking concrete structures caused by reinforcement corrosion. *ACI Structural Journal* **110**(2), 229–238.
- Chen, H.P. and Nepal, J. (2016) Analytical model for residual bond strength of corroded reinforcement in concrete structures. *Journal of Engineering Mechanics ASCE* **142**(2), 040150791–8.
- Chen, H.P. and Xiao N. (2015) Symptombased reliability analyses and performance assessment of corroded reinforced concrete structures. *Structural Mechanics and Engineering* **53**(6) 1183–1200.
- Farrar, C.R., Sohn, H., Hemez, F.M., Anderson, M.C., Bement, M.T., Cornwell, P.J., Doebling, S.W., Lieven, N., Robertson A.N. and Schultze J.F. (2003) *Damage Prognosis: Current Status and Future Needs*. Los Alamos National Laboratory report LA14051MS.

- Frangopol, D.M. and Messervey, T.B. (2009) Maintenance principles for civil structures. *Encyclopaedia of Structural Health Monitoring*, Boller, Chang and Fujino (ed.), John Wiley & Sons, Chichester, UK.
- Frangopol, D.M., Kallen, M.J. and van Noortwijk, J.M. (2004) Probabilistic models for lifecycle performance of deteriorating structures: review and future directions. *Progress in Structural Engineering and Materials* **6**(4),197–212.
- Huang, T.L., Zhou, H., Chen, H.P. and Ren, W.X. (2016) Stochastic modelling and optimum maintenance strategy for steel bridge members affected by fatigue damage. *Smart Structures and Systems* **18**(3), 569–584.
- Melchers, R.E. (1999) *Structural Reliability Analysis and Prediction*. 2nd Edition, John Wiley & Sons, Chichester, UK.
- Miyamoto, A. (2009) Usage management of civil structures. *Encyclopaedia of Structural Health Monitoring*, Boller, Chang and Fujino (ed.), John Wiley & Sons, Chichester, UK.
- Nepal, J., Chen, H.P., Gouldby, B., Simm, J. and Tarrant, O. (2015) State based stochastic performance deterioration modelling of flood defence assets. *Proceedings of the 7th International Conference on Structural Health Monitoring of Intelligent Infrastructure (SHMII7)*, Turin, Italy.
- Ni, Y.Q., Wang, Y.W. and Xia, Y.X. (2015) Using weighinmotion data to identify traffic loading on a longspan suspension bridge. *Proceedings of the 7th International Conference on Structural Health Monitoring of Intelligent Infrastructure (SHMII7)*, Turin, Italy.
- Okasha, N.M. and Frangopol, D.M. (2009) Redundancy of structural systems with and without maintenance: an approach based on lifetime functions. *Reliability Engineering and System Safety* **95**(5), 520–533.
- Onoufriou, T. and Frangopol, D.M. (2002). Reliabilitybased inspection optimization of complex structures: a brief retrospective. *Computers and Structures* **80**, 1133–1144.
- Orcesi, A.D. and Frangopol, D.M. (2011) Optimization of bridge maintenance strategies based on structural health monitoring information. *Structural Safety* **33**(1), 26–41.
- Rücker, W., Hille, F. and Rohrman, R. (2006a) *Guideline for the Assessment of Existing Structures F08a*, SAMCO Final Report, Berlin, Germany.
- Rücker, W., Hille, F. and Rohrman, R. (2006b) *Guideline for Structural Health Monitoring F08b*, SAMCO Final Report, Berlin, Germany.
- van Noortwijk, J.M. and Frangopol, D.M. (2004) Two probabilistic lifecycle maintenance models for deteriorating civil infrastructures. *Probabilistic Engineering Mechanics* **19**(4), 345–359.
- van Noortwijk, M. (2009) A survey of the application of gamma processes in maintenance.

Reliability Engineering and System Safety **94**(1), 2–21.

Wong, K.Y. and Ni, Y.Q. (2009) Structural health monitoring of cablesupported bridges in Hong Kong. In book: *Structural Health Monitoring of Civil Infrastructure Systems*, Karbhari and Ansari (ed.), Woodhead Publishing, Cambridge, UK.

Wong, K.Y. and Ni, Y.Q. (2011) Structural health monitoring of a suspension bridge. In book: *Monitoring Technologies for Bridge Management*, Bakht and Mufti and Wegner (ed.), Multi Science Publishing, Essex, UK.

Ye, X., Ni, Y., Wong, K. and Ko, J. (2012) Statistical analysis of stress spectra for fatigue life assessment of steel bridges with structural health monitoring data. *Engineering Structures* **45**, 166–176.

10

Applications of SHM Strategies to Large Civil Structures

10.1 Introduction

The principles of structural health monitoring (SHM) strategies have been discussed in previous chapters. In this chapter, these principles are applied to real civil engineering structures, such as bridges, buildings, tunnels, rails and water mains. In order to achieve the aims of health monitoring of a civil engineering structure, it is necessary to utilise an appropriate SHM strategy on the structure. A good monitoring strategy can offer useful results for making rational decisions with a relatively limited resource. In the design of an SHM system for a civil structure, the selection of sensors and sensing network for structural monitoring depends on many factors, including type of structure, operational loads and environments, possible sources of damage and deterioration mechanisms expected to occur during lifetime of the structure.

Monitoring safe and reliable existing large civil engineering structures is of great importance owing to its economic and social effects. Knowing the integrity and health of civil structures during their construction and operation is essential. Civil engineering structures, such as long span bridges, highrise buildings, underground tunnels and high speed rails, are often large and are subjected to complex loads and harsh environments. Since different structures experience different in-construction and in-service conditions, a universal solution that will be suitable for all possible cases does not exist. Thus, an appropriate SHM strategy needs to be chosen for effective assessment of a specific civil structure.

This chapter provides several case studies on applications of various SHM strategies to real large civil engineering structures. These case studies present engineering practice of structural monitoring, including a wind and SHM system for a cablestayed bridge, wireless sensing networks for in-construction monitoring of a highrise building, fibre optic sensors for monitoring tunnel construction and water pipelines and acoustic emissions for safety monitoring of rails. The applications of data interpretation algorithms, operational modal analysis techniques and damage identification methods are also discussed in the case studies.

10.2 SHM System and Damage Identification of a CableStayed Bridge

The Ting Kau Bridge is a threetower cablestayed bridge with two main spans of 448 m and 475 m respectively, and two side spans of 127 m each, as shown in [Figure 10.1](#) and pictured in [Figure 5.8](#). The bridge deck is divided into two carriageways with a width of 18.8 m each and

a gap of 5.2 m, linked at 13.5 m intervals by Ishape main cross girders. The bridge deck is supported in the transverse direction at the three towers, on the northern end pier and on the southern Tsing Yi abutment. The deck is supported by 384 stay cables in four cable planes. A unique feature of the bridge is its arrangement of the three singleleg towers that are strengthened by longitudinal and transverse stabilising cables. In order to reduce the vibration of the longitudinal stabilising cables, damping devices are installed near the lower anchorage between the stabilising cables and the deck.



Figure 10.1 Threetower cablestayed Ting Kau Bridge.

10.2.1 Sensors and Sensing Network

After the completion of the bridge construction, a sophisticated longterm monitoring system, called wind and structural health monitoring system (WASHMS), was devised to monitor the structural health and performance of the bridge under inservice condition. The monitoring system includes six modules: sensory system, data acquisition and transmission system, data processing and control system, structural health evaluation system, portable data management system and portable inspection and maintenance system (Ni et al. 2011), as illustrated in [Figure 10.2](#).

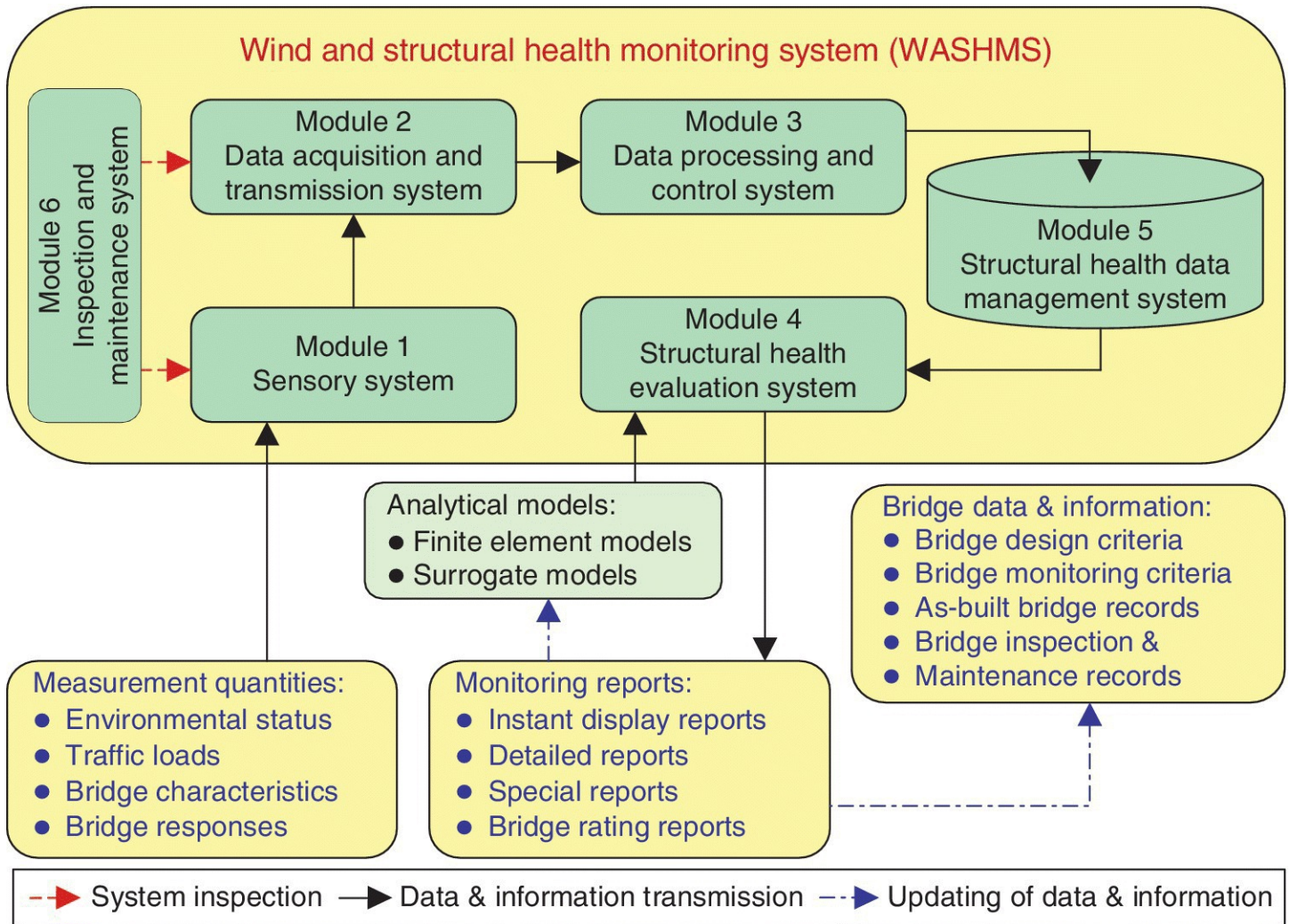


Figure 10.2 Modular architecture of structural monitoring systems for Ting Kau Bridge.

The monitoring system consists of a total number of 232 sensors permanently installed on the bridge (Wong 2004, Wong et al. 2000), as illustrated in [Figure 10.3](#). A total of 45 accelerometers (24 uniaxial, 20 biaxial and one triaxial) accelerometers were installed at the decks, cables, towers and central tower base to measure the dynamic characteristics of the bridge. Seven anemometers (four ultrasonic type and three propeller type) were installed at the deck level and at the top of the three towers to measure the wind velocity and direction. A total of 83 temperature sensors were installed on the deck and on the central tower to measure the temperature at various locations. Two displacement transducers were installed at the road expansion joints at the abutments to measure the deck longitudinal movement. A total of 88 strain gauges (66 linear and 22 rosette) were installed on the deck girders, deck plates and bearings to measure the stress and bearing performance. A weighinmotion sensing system (bending plate type with six sensors) was installed at the carriageways to measure the traffic flow and traffic loading. In addition, a global positioning system (one reference station and seven rover stations) was installed to measure bridge deflection.

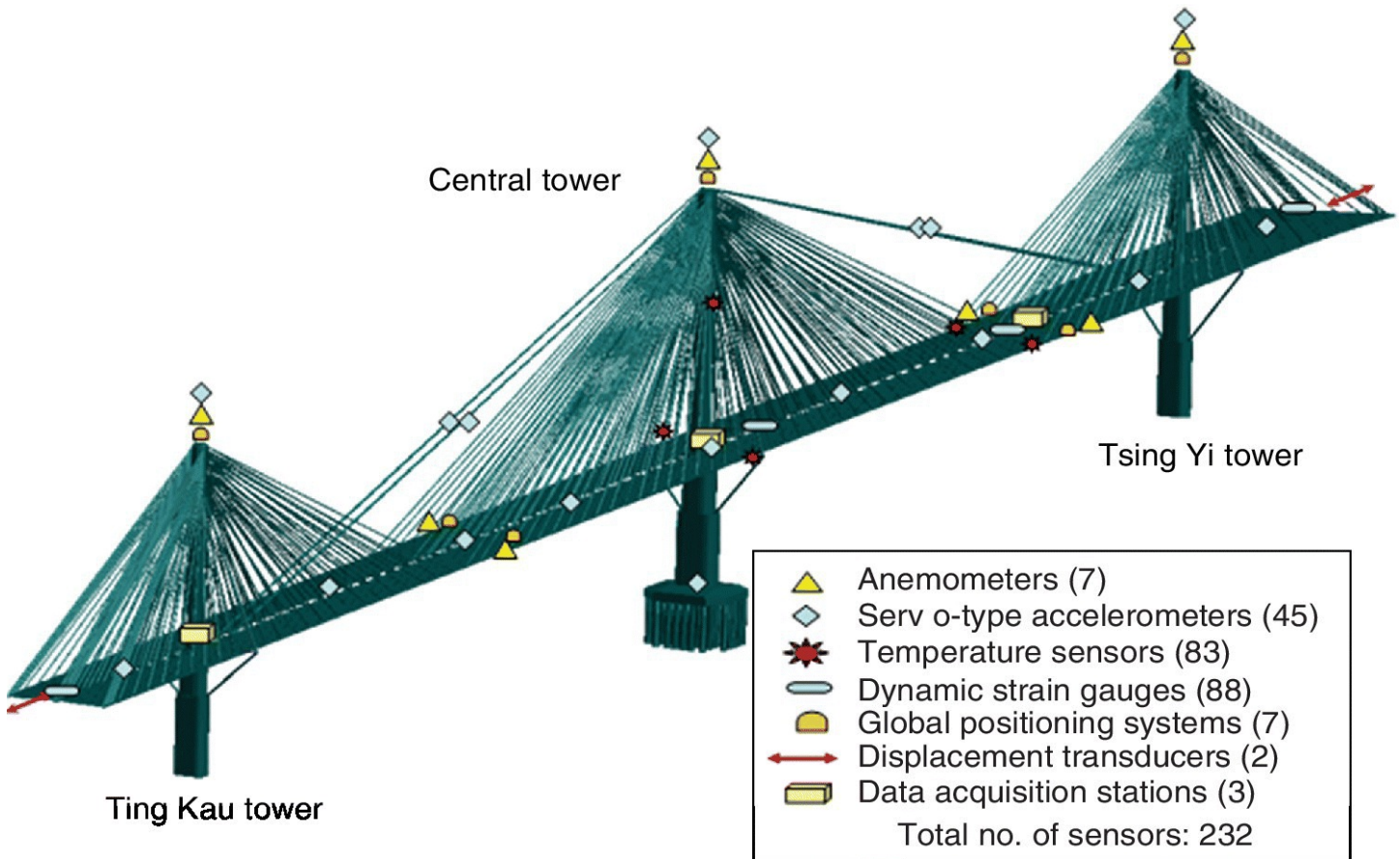


Figure 10.3 Sensory system of SHM strategy for Ting Kau Bridge.

10.2.2 Data Management System

An indexing system for historic raw data management and a database system for current monitoring data management were developed for managing the data from the bridge (Ko et al. 2009). Both the indexing system and the database system adopt a relational database approach. The indexing system greatly facilitates the data probing work and provides a useful method for the management of historic data, because of the limited storage capacity of the database system and the host computer. The database system for current monitoring data management is developed with two modules: an Oracle-driven database system for nonspatial data management and a geographic information system (GIS) software system for spatial data management. The raw data is then preprocessed, including data classification, data filtering etc., before being reorganised into a general purpose dynamic database. The data in the dynamic database can be either automatically updated at regular intervals or manually updated by users.

A client/server architecture running on the internet is adopted for communication between the database system and endusers. The system can provide online information of the bridge and monitoring data to authorised endusers. The web based geographic information system software is installed on the server of the database system. The database system offers functions at three levels: regional level, bridge level and sensor level. A preliminary preprocessing of the retrieved data is made, and the preliminary analysis results can be displayed and exported

to a temporal database for future retrieval. The endusers can also export the data to other software programs for advanced analysis, such as operational modal analysis.

10.2.3 Operational Modal Analysis and Mode Identifiability

The timedomain operational modal analysis method, such as the covariancedriven stochastic subspace identification (SSICOV) technique described in [Section 5.4.2](#), is adopted to identify the modal parameters from ambient acceleration measurements of the Ting Kau Bridge. To investigate the influence of wind speed conditions on the mode identifiability, a total of six data samples of acceleration measurements collected from these 24 accelerometers, as shown in [Figure 5.8](#), with known wind conditions, are used, as listed in [Table 10.1](#). The duration of these acceleration data samples is one hour, and this data was recorded in 1999. These data samples can be classified into three groups: weak wind, typhoon and critical wind speed (around 7.5 m/s), depending on the mean hourly wind speed calculated from the anemometers installed on the bridge deck.

Table 10.1 Recorded ambient acceleration data samples under different wind conditions.

Wind condition	Sample	Time duration	Mean hourly wind speed (m/s)	Note
Weak wind	S1	15:00–16:00, 28 Dec 1999	2.00	
	S2	15:00–16:00, 24 Jul 1999	6.17	
Typhoon	S3	02:00–03:00, 23 Aug 1999	15.62	Sam
	S4	15:00–16:00, 16 Sep 1999	15.91	York2
Critical (wind speed around 7.5 m/s)	S5	08:00–09:00, 07 Jun 1999	7.36	
	S6	22:00–23:00, 16 Sep 1999	7.77	

[Table 10.2](#) summarises the results for the identified frequencies of first eight modes under different wind speed conditions using the SSICOV technique (Huang and Chen 2016). The identified frequencies range between 0.15 Hz and 0.40 Hz. In the typhoon condition (S3 and S4), all the first eight frequencies are clearly identified and consistent. However, in weak wind conditions (S1 and S2), the 2nd and 5th frequencies are unable to be identified. When the wind speed is critical (S5 and S6), the 2nd frequency is clearly identified in both data samples. However, the 3rd frequency in sample S5 and the 5th frequency in sample S6 are unable to be identified. From the results, the identification of modal parameters can be affected by the excitation intensity (e.g. magnitude of wind speed), as well as by the excitation sources (e.g. wind and traffic) and the excitation direction (e.g. wind direction). The mode identifiability is

not only related to the ambient excitation intensity, but also depends on their modal contributions to the measured vibration data (Huang and Chen 2017).

Table 10.2 Identified frequencies (Hz) of first eight modes under various wind speed conditions.

Mode No.	Weak wind		Typhoon		Critical wind		Mode description
	S1	S2	S3	S4	S5	S6	
1	0.162	0.164	0.164	0.166	0.168	0.165	Predominantly vertical mode
2	—	—	0.227	0.226	0.228	0.229	Coupled torsional & lateral mode
3	0.255	0.253	0.264	0.260	—	0.264	Predominantly lateral mode
4	0.289	0.287	0.293	0.289	0.282	0.292	Predominantly lateral mode
5	—	—	0.301	0.302	0.303	—	Predominantly vertical mode
6	0.309	0.316	0.323	0.317	0.315	0.322	Coupled torsional & lateral mode
7	0.358	0.357	0.361	0.359	0.360	0.361	Predominantly vertical mode
8	0.373	0.371	0.372	0.373	0.374	0.379	Predominantly vertical mode

10.2.4 Finite Element Modelling

A three-dimensional finite element model was developed for the Ting Kau Bridge by use of the commercial software package ABAQUS (Ko et al. 2009), as shown in [Figure 10.4](#). The model involves 2901 nodes and 5581 elements. The bridge deck is modelled by membrane/shell elements to account for the horizontal thrust ability, and its bending stiffness is represented as nominal flanges of the longitudinal girders and cross girders. The monoleg towers are modelled as Timoshenko’s beam elements. The geometric distances between cable ends and the crosssection centroids of the deck and towers are represented by rigid bars. For the 456 cables, the longitudinal stabilising cables are modelled by a multielement system and the other cables are modelled by a singleelement system.

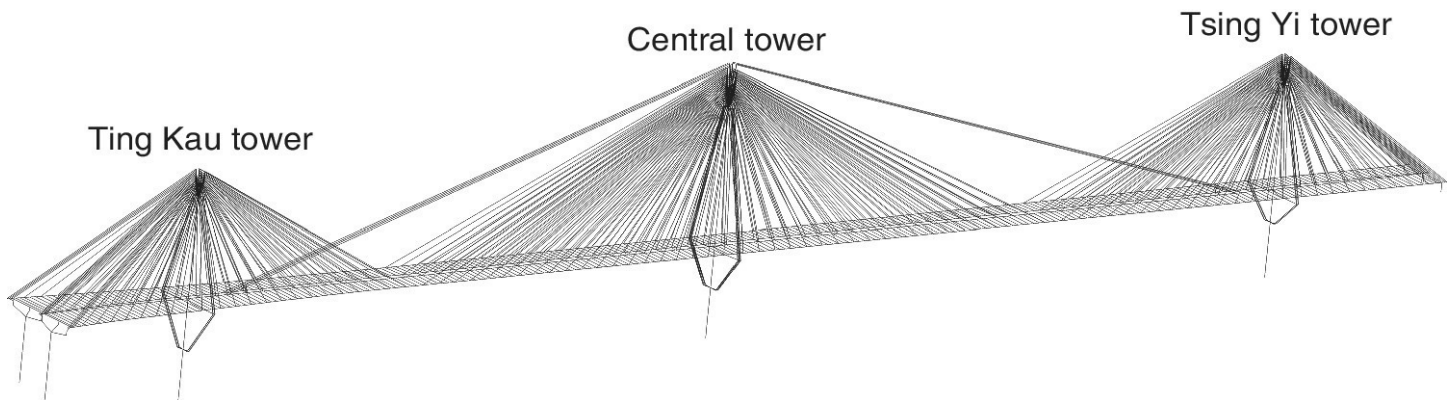


Figure 10.4 Threedimensional finite element model of Ting Kau Bridge.

The finite element model was validated by comparing the modal properties predicted by the finite element numerical model and those identified from the monitored data. A framework for

finite element model updating using monitored data is illustrated in [Figure 10.5](#) (Wong and Ni 2009). In this framework, both measurement data and finite element analysis data in the structural health data management system (SHDMS) module are used for modal analysis and model updating in the structural health evaluation system (SHES) module.

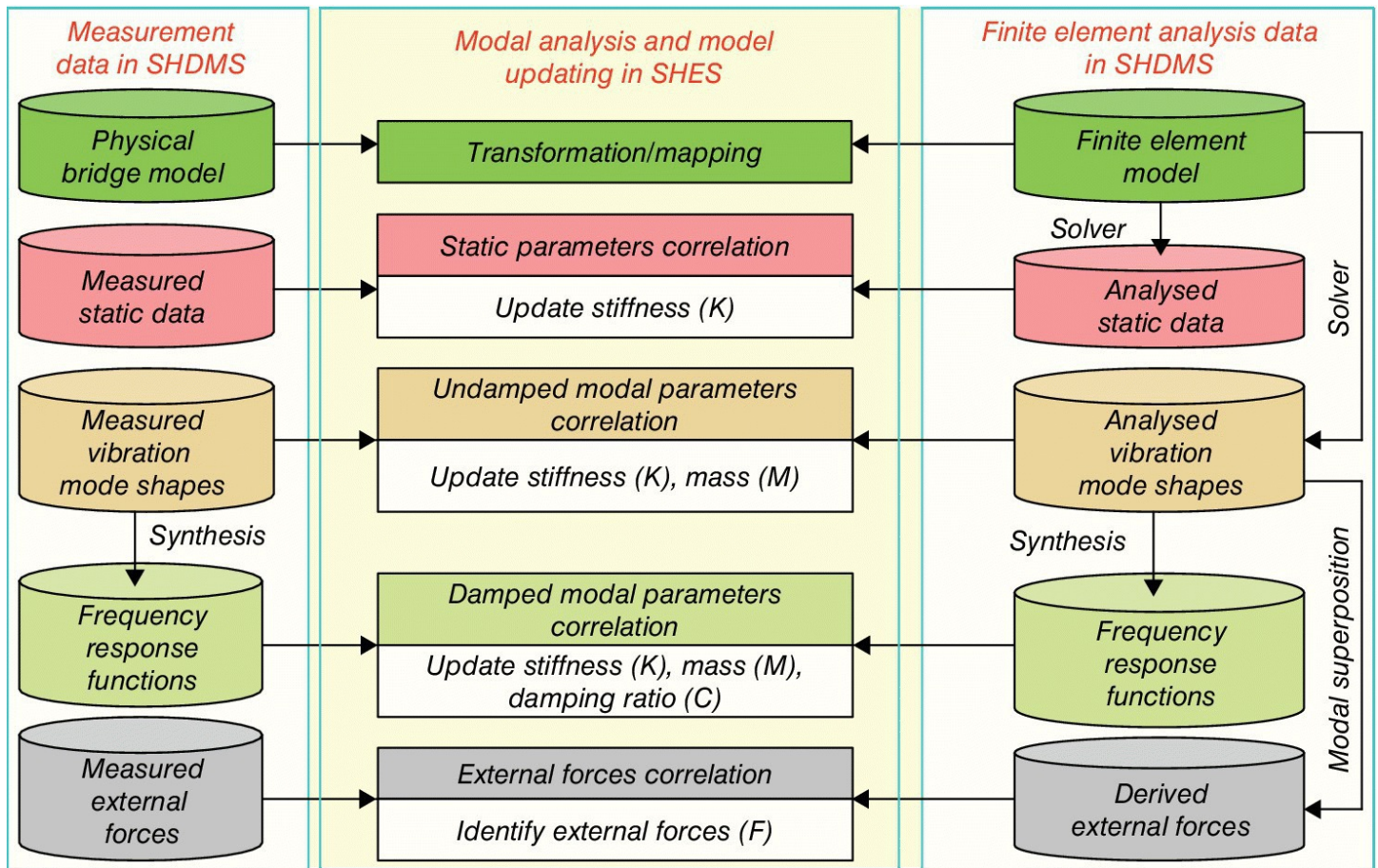


Figure 10.5 Framework for finite element model updating by measurement data.

From finite element modal analysis, more than 200 modes, either global modes or local modes, are found in the frequency range 0–1.5 Hz. The global modes are defined as those with participation of the deck and/or towers, whereas the local modes refer to those where vibration occurs only in the cables. The difference between the predicted and measured frequencies is 0.86% for the first mode with frequency of 0.164 Hz, and the maximum difference is 6.82% for the first 12 global modes. This shows the accuracy of the finite element model after model updating.

10.2.5 Damage Localisation Using Mode Shape Curvature Index

The applicability of vibrationbased damage identification methods, such as the mode shape curvature index, to the Ting Kau Bridge is investigated here. Five damage scenarios with a total of 11 damage cases are assumed in the simulation studies (Ko et al. 2009, Ni et al. 2008), as listed in [Table 10.3](#). The damage occurs at various locations of the bridge, including the longitudinal stabilising cables, stay cables, bearings, longitudinal girders and cross girders.

Table 10.3 Simulated damage cases for damage detection studies of Ting Kau Bridge.

Scenario No.	Case No.	Description
1	a	Damage of longitudinal stabilising cable: 20% tension reduction of cable no. 8414
	b	Damage of longitudinal stabilising cable: 20% tension reduction of cables nos. 8414 & 8412
2	a	Damage of main stay cable: 90% tension loss of cable no. 1073
	b	Damage of main stay cable: 90% tension loss of cables nos. 1073 & 4073
	c	Damage of main stay cable: 90% tension loss of cables nos. 1070, 1071, 1072 & 1073
3	a	Damage of bearing: 90% stiffness deterioration of a longitudinal bearing at central tower
	b	Damage of bearing: 90% stiffness deterioration of an anchorage bearing at Tsing Yi abutment
4	a	Damage of main girder: rotational stiffness of element no. EL6372 on longitudinal girder is lost
	b	Damage of main girder: rotational stiffness of all elements connecting to node no. 6073 is lost
5	a	Damage occurring at the connecting cross girder between cable nodes nos. 1073 & 2073
	b	Damage occurring at two cross girders between cable nodes nos. 1073 & 2073, and between cable nodes nos. 1074 & 2074

The mode shape curvature method is adopted for detecting the assumed damage cases using the mode shapes of the undamaged structure and the correlated mode shapes of the damaged structure, as discussed in detail in [Section 7.3.3](#). For each correlated mode pair, the modal curvature change rate index is a function of location. Because the modal curvature suffers from relatively large change in the vicinity of damage location, it is expected that for some related modes the modal curvature change rate index will have the highest value at the damage location. In order to clearly indicate the damage location, the damage index for the i th mode at the j th node $\beta_i(j)$ defined in [Equation \(7.10\)](#) is normalised to get its Z value for the i th mode as

$$Z_j^{(i)} = \frac{\beta_i(j) - \mu_\beta}{\sigma_\beta} \quad (10.1)$$

where μ_β and σ_β are the mean and standard deviation of the index sequence, respectively. The Neyman—Pearson criterion is adopted to evaluate the damage state, i.e. if $Z_j^{(i)} \geq 3$, damage is

identified at deck section j , otherwise, no damage is detected at location j .

The Z value defined in [Equation \(10.1\)](#) is adopted in damage location identification for the Ting Kau Bridge. Deck section j is represented by the cable nodes from 5 to 101. To identify the damage location, a total of 11 global modes – the first five vertical bending modes, the first four lateral bending modes and the first two torsional modes – are analysed. The Z values of these 11 modes are checked with respect to the modal vectors in the y and z directions, respectively. [Table 10.4](#) summarises the identified results for all 11 simulated damage cases. It is found that the Z values from some modes lead to false identification. In addition, some clear peaks can be noted, although the Z values of those peaks are less than 3. Some of those peaks indicate the correct damage location and some do not. Thus, the Ting Kau Bridge has some regions that are sensitive to modal curvature change, for example, supports at abutments, connecting region at the central tower, region close to the middle of the Ting Kau main span (Nos. 26 and 27). In general, the modal sensitivity by means of Z values using vertical bending modes is more sensitive than that using lateral or torsional modes.

Table 10.4 Damage location identification using mode shape curvature index Z values.

Damage case	Identified Location from damage index					Damage location (deck section)
	1st mode	2nd mode	23rd mode	24th mode	25th mode	
1a	86	0	86,87	26,27	27	Between 86 & 87
1b	86	0	86,87	26,27	27	Between 86 & 87
2a	0	0	0	26,27	0	73
2b	73	0	0	27	27	73
2c	71,72,73	0	0	27	26,27	70,71,72,73
	<u>0*</u>	<u>0*</u>	<u>70,71,72,73*</u>	<u>72,73,74*</u>	<u>5*</u>	
3a	54,55	0	54,55	54,55	54,55	Between 50 & 54
	<u>0*</u>	<u>50,54*</u>	<u>0*</u>	<u>50,54*</u>	<u>50,54*</u>	
3b	100,101	0	100,101	100,101	0	Close to 101
4a	73	0	73	73	73	73
	<u>0*</u>	<u>0*</u>	<u>5,72,74*</u>	<u>5*</u>	<u>5,73*</u>	
4b	72,73	73	73	73,74	72,74	73
	<u>0*</u>	<u>0*</u>	<u>73*</u>	<u>73*</u>	<u>73*</u>	
5a	0	0	73	73	73	73
5b	0	0	73,74	73,74	73,74	73,74

Note: '0' denotes no available identification;

* denotes the identified results from modal vectors in z direction.

10.2.6 Damage Detection Using Neural Network

A neural network based on the novelty detection technique is now used to investigate the applicability for structural damage alarming for the Ting Kau Bridge (Ko et al. 2009). The novelty detector is realised by using an autoassociative neural network, as discussed in detail in [Section 7.5.2](#). The neural network is a multilayer feedforward perception with a ‘bottleneck’ configuration. When the autoassociative neural network is adopted for anomaly detection or damage alarming, a series of measurement data from the healthy structure under normal conditions is used as both input and output to train the network. Five assumed damage scenarios with a total of 11 damage cases are used here again for damage alarming, as listed in [Table 10.3](#).

For comparison, two sets of modal parameters – natural frequencies and modal flexibility vector – are used as input features to train autoassociative neural networks for damage alarming. When using only natural frequencies, the noisy ‘measured’ natural frequencies for both the intact bridge and the damaged bridge are obtained by corrupting the computed natural frequencies in the intact and damage stages with Gaussian random noise of zero mean and 0.005 variance (+1.5% maximum error). [Table 10.5](#) shows the damage alarming results when using only natural frequencies and the damagecaused frequency change ratios for all 11 cases. From the results, when only natural frequencies are used and random noise of variance 0.005 (+1.5% maximum error) is introduced, the novelty detector can unambiguously give an alarming indication for the assumed damage states, if the damagecaused frequency change ratio is greater than 1.0%. When the frequency change ratio ranges from 0.4% to 1.0%, the damage is just detectable with a weak alarming signature. Damage occurrence cannot be detected if the frequency change ratio is below 0.4%.

[Table 10.5](#) Damagecaused frequency change and damage detectability.

Damage case no.	Frequency change ratio (%)	Detectability
1a	3.701	Unambiguously detectable
1b	3.793	Unambiguously detectable
2a	0.027	Undetectable
2b	0.054	Undetectable
2c	0.135	Undetectable
3a	6.452	Unambiguously detectable
3b	2.953	Unambiguously detectable
4a	0.397	Undetectable
4b	0.704	Just detectable
5a	0.375	Undetectable
5b	0.957	Just detectable

The probabilistic neural network (PNN) is a powerful tool for pattern classification, as

discussed in [Section 7.6.3](#). Because the probabilistic neural network describes measurement data in a Bayesian probabilistic approach, it shows great promise for structural damage detection in noisy conditions. In this study, a total of 2000 training vectors, containing the frequency change ratios for simulated damage with Gaussian random noise, have been generated (Ni et al. 2000). After the noisepolluted training vectors of all pattern classes are entered as weights between the input and pattern layers, the probabilistic neural network for the damage localisation is then configured. By entering the 4000 sets of ‘measured’ testing vectors into the configured probabilistic neural network in turn, the damage type and region corresponding to each set of the testing vectors are identified.

[Table 10.6](#) summarises the damage identification results under 11 different noise levels from $\epsilon = 0.01$ to $\epsilon = 1.00$ (Ko et al. 2009). Here, the identification accuracy is defined as the ratio of the total number of correct identifications for all testing damage scenarios to the total number of the testing samples (4000). As expected, the identification accuracy decreases with increase of the noise level corrupted in the training and test samples. The identification accuracy significantly increases when more natural frequencies are used. Therefore, when the first 20 natural frequencies are used and the noise level ϵ is less than 0.1, the damage type and location can be identified with a high confidence (i.e. the probability of identifiability greater than 85%).

[Table 10.6](#) Summary of correct damage identification using probabilistic neural network (PNN) technique.

Noise level (standard deviation)	Identification accuracy		
	Using 20 frequencies	Using 10 frequencies	Using 5 frequencies
$\epsilon = 1.00$	46.23%	33.35%	27.90%
$\epsilon = 0.80$	57.08%	45.25%	33.05%
$\epsilon = 0.60$	62.55%	51.85%	43.40%
$\epsilon = 0.40$	78.15%	62.90%	51.33%
$\epsilon = 0.20$	84.33%	71.70%	58.75%
$\epsilon = 0.10$	86.42%	73.53%	60.83%
$\epsilon = 0.08$	87.63%	75.08%	63.15%
$\epsilon = 0.06$	88.90%	76.85%	65.80%
$\epsilon = 0.04$	89.32%	77.23%	67.58%
$\epsilon = 0.02$	89.97%	77.35%	67.33%
$\epsilon = 0.01$	90.00%	80.05%	67.70%

10.3 InConstruction Monitoring of a HighRise Building

The new headquarters of the Shenzhen Stock Exchange is a highrise building with a height of 228 m. There are 45 storeys above the ground and three basement storeys, as shown in [Figure 10.6\(a\)](#). The main tower is a tube-in-tube structure consisting of an inner reinforced concrete core and an outer shaped steel and reinforced concrete composite frame. The inner structure has a rectangular cross-section of 28 m × 32 m, and the outer structure has a 54 m × 54 m square cross-section. A distinct feature of this highrise building is its huge floating platform. This floating platform is a steel truss structure with an overall plan dimension of 98 m × 162 m and a total height of 24 m, as shown in [Figure 10.6\(b\)](#). The platform consists of 14 steel trusses divided into six types. The outrigger truss storeys have the outrigger component of 22 m in the south–north direction and 36 m in the east–west direction at a height of 36 m above the ground (Ni et al. 2013a). This makes the floating platform the biggest span cantilever civil structure in the world.

(a) View under construction



(b) Floating platform

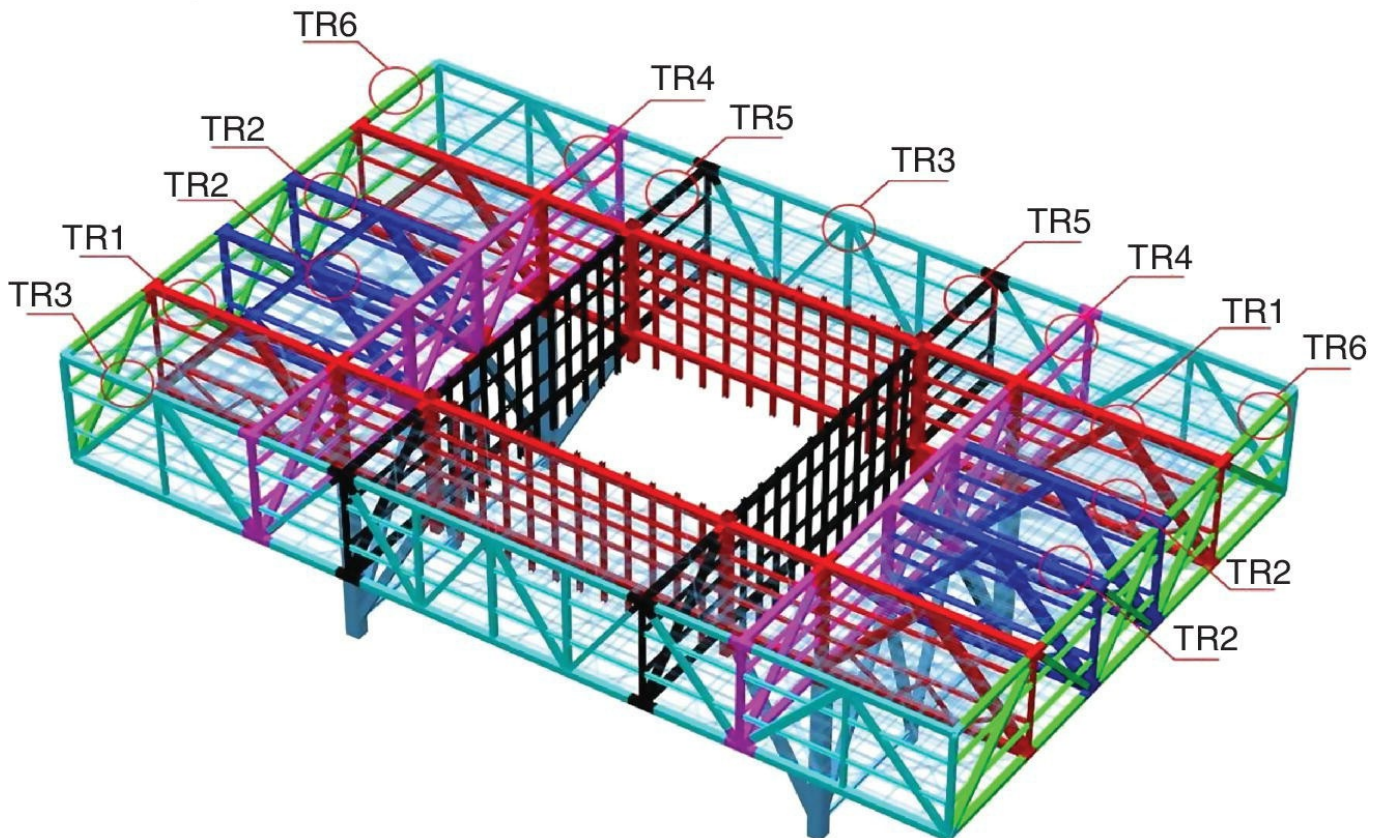


Figure 10.6 New Headquarters of Shenzhen Stock Exchange, a highrise building with a floating platform.

10.3.1 LongTerm SHM System

A longterm SHM system was designed and implemented to monitor the cantilever truss of the highrise building in both construction and service stages. The strain and deflection of the cantilever truss are of the utmost concern in designing the SHM system. A total of 224 vibratingwire strain gauges were installed permanently to measure the strains. A vision based displacement tracking system was also employed to monitor the deflections (Ni et al. 2013a). The SHM system for the building consists of the following modules:

- Module 1: Sensory system. This system includes strain gauges, temperature sensors, accelerometers and a vision based displacement tracking system.
- Module 2: Data acquisition and transmission system. This system is composed of four standalone data acquisition units (DAUs) and two wireless LAN bridges for monitoring of strains. The four DAUs are used to collect the signals from the surrounding strain gauges, digitise the analogue signals and transmit the data into a central room. The signals from the strain gauges are first transmitted to the data loggers inside the structure through coaxial wires, and then sent to the server PC at a site office in a wireless way through a pair of wireless access points for realtime monitoring in construction stage.
- Module 3: Data processing and control system. This system comprises highperformance servers and dataprocessing software. The system is used for routine data processing, structural and system status monitoring and prewarning, as well as display of the data.
- Module 4: Structural health evaluation system. This system is composed of a high performance server and structural health evaluation software. It is used for processing and analysing the monitoring data, evaluating and diagnosing the structural condition and carrying out analysis.
- Module 5: Data management system. This system consists of a highperformance server, relational database system and data management software.

A total of 56 critical crosssections of structural members were selected for monitoring. The deployment locations of strain gauges are predetermined through finite element analysis. Each instrumented crosssection has several strain gauges, and their deployment complies with the following criteria: (a) type of crosssection, e.g. rectangle or Isection, (b) properties of loadings, e.g. axial force, bending or bidirectional bending, etc., (c) limitations due to construction and inaccessibility. The sampling rate for each strain gauge was set as one reading per second during the process of removing the temporary shoring, and switched to one reading per 90 seconds in normal service circumstances. The sampling rate can be adjusted as required for different purposes.

10.3.2 Monitoring During Shoring Dismantlement

In the erection of the floating platform, the tower cranes were used to hoist the steel framework, and a temporary brace frame was used to support the cantilever truss. To keep the stability of the supporting shoring, two-tier connecting trusses were added to strengthen it. After completing the erection of the floating platform, the supporting shoring was dismantled. It was a difficult job to create a rational plan for the unloading process, due to the specific features of this project and the massive unloading of up to 16,000 tons. To ensure the safety of the floating platform and the main tower as well as to maintain consistent deformation, it was necessary to make all the control points subside uniformly. Thus, the procedure for unloading the braces simultaneously in patches and stage by stage was adopted to effect the transition of structural stress and configuration in a steady and successive way. The temporary braces are divided into three groups: TJO, TJM and TJI, as shown in [Figure 10.7](#). The sequence of unloading was from the outer positions to the inner positions, and each step was executed simultaneously to prevent the occurrence of uneven settlement.

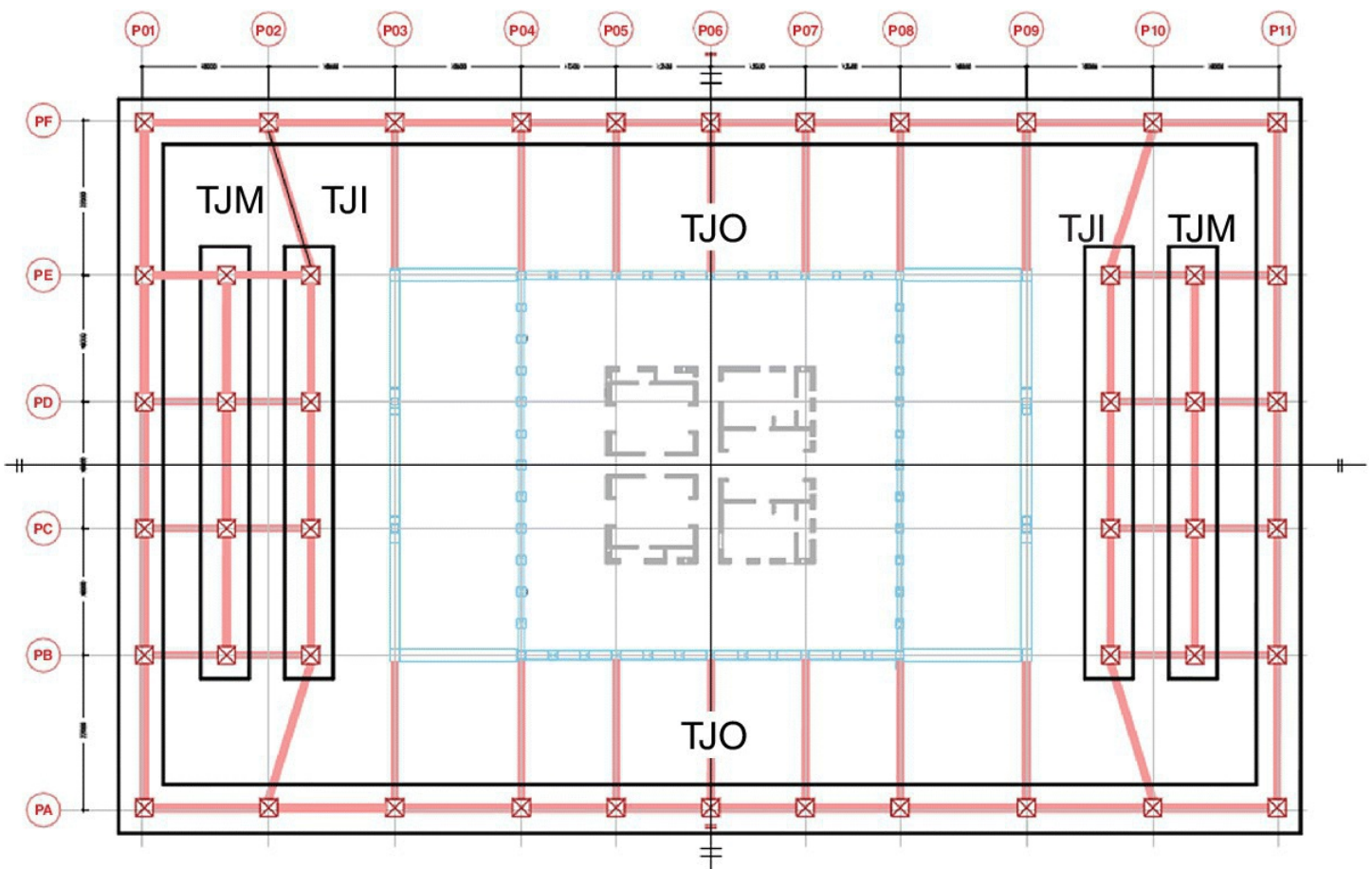


Figure 10.7 Layout of temporary braces of the highrise building.

During the unloading process, the SHM system is highly desirable for detecting potential anomalies such as any sudden significant increase in the stress. As soon as such an anomaly happens, the unloading work is suspended. [Figure 10.8](#) presents the development of structural stresses in the process of dismantling temporary shoring, which was displayed in real time at the site office. As expected, the stresses grew step by step synchronously with the unloading process. Through the realtime SHM system, the duration of dismantling temporary shoring was shortened to less than six hours from the originally scheduled three days.

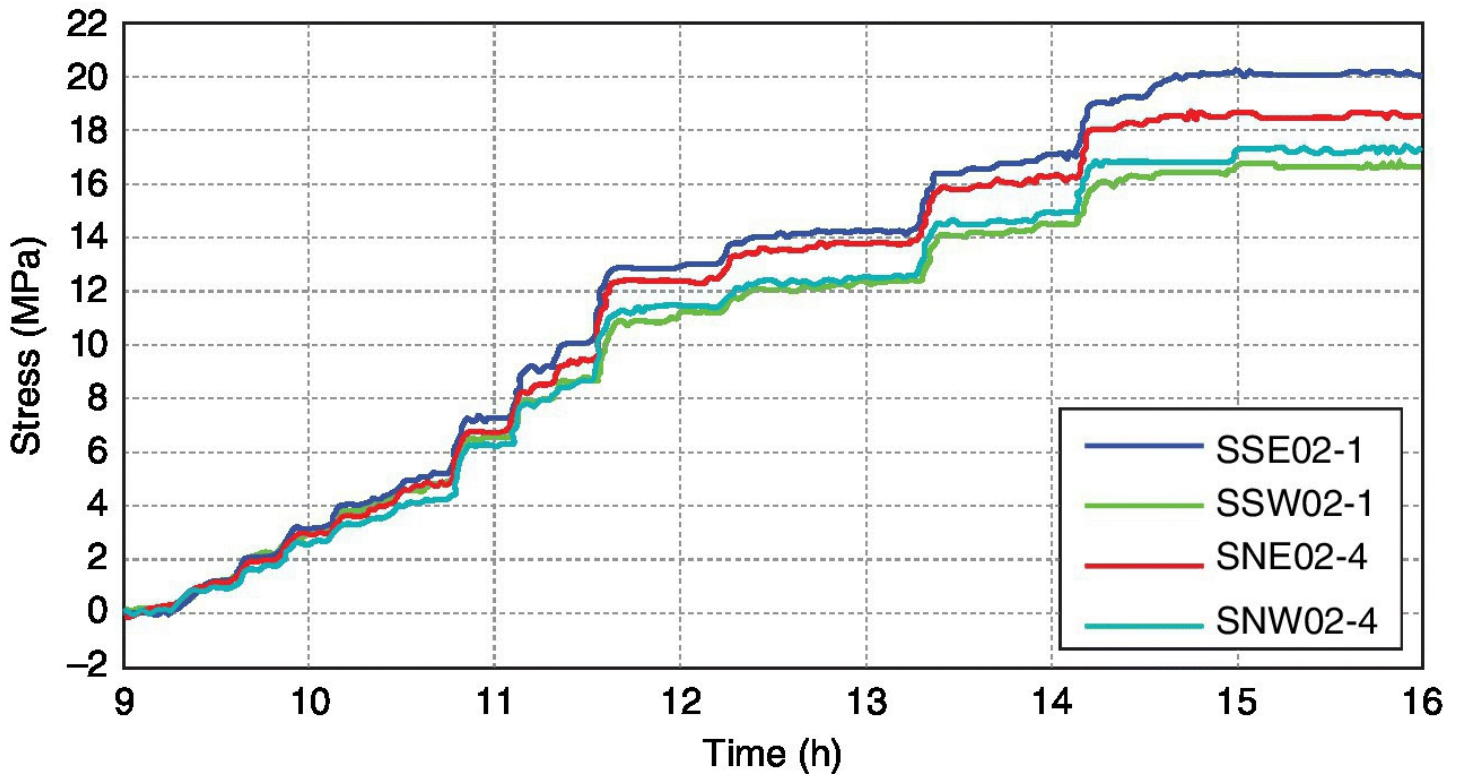


Figure 10.8 Growth of stresses measured in the process of dismantling temporary supports.

For prediction and comparison, a finite element model was established, using the commercial software SAP2000, to simulate the alteration of structural stresses of the building in the process of dismantling the supporting shoring. [Figure 10.9](#) shows a comparison of stress increments during the unloading process obtained from field monitoring measurements and computed by finite element simulations. It is found that the structure is under biaxial symmetry loading which is in agreement with reality.

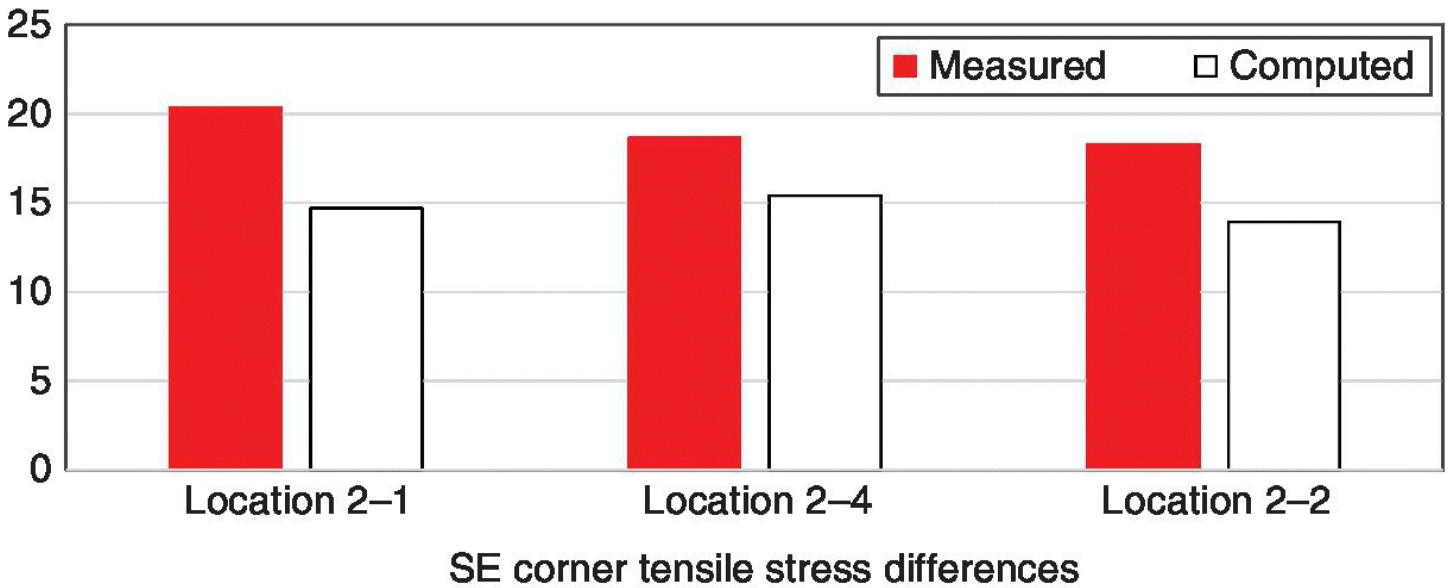


Figure 10.9 Comparison of measured and computed stress increments during unloading process.

10.3.3 Wireless Sensing Network for Vibration Monitoring

In addition, accelerometers and a wireless sensing network were implemented to realtime monitor the ambient vibration responses and identify the modal properties of the highrise building (Ni et al. 2013a). The wireless monitoring prototype system assumes a single data server working with multiple wireless sensors in a startopology network. It comprises multiple wireless sensing units in the network and one base station coordinating the activities of the network. In the prototype implementation, the base station can be a computer connected to a compatible wireless transceiver through RS232 serial communication or USB communication. Through the associated wireless transceiver, the base station can communicate with the wireless sensing units that are allocated throughout the structure. The wireless sensing units are responsible for acquiring sensor output signals, analysing data and transferring data to the base station for storage and further data analysis. A wireless sensor unit consists of three functional modules: sensing interface, computational core and wireless communication channel, as were shown in [Figure 2.12](#)(b). The sensor signal digitisation is responsible for converting analogue sensor signals into digital data, and for transferring the data to the computational core through a high speed serial peripheral interface (SPI) port. The main part of the sensor signal digitisation module is a fourchannel 16bit analoguetodigital (A/D) converter. In order to make the signal ready for A/D conversion, a special low noise signal conditioning module was designed to amplify and filter the sensor signal prior to A/D conversion, as shown in [Figure 10.10](#)(a).

(a) Low-noise high-gain signal conditioning module.

(b) Modem of station.

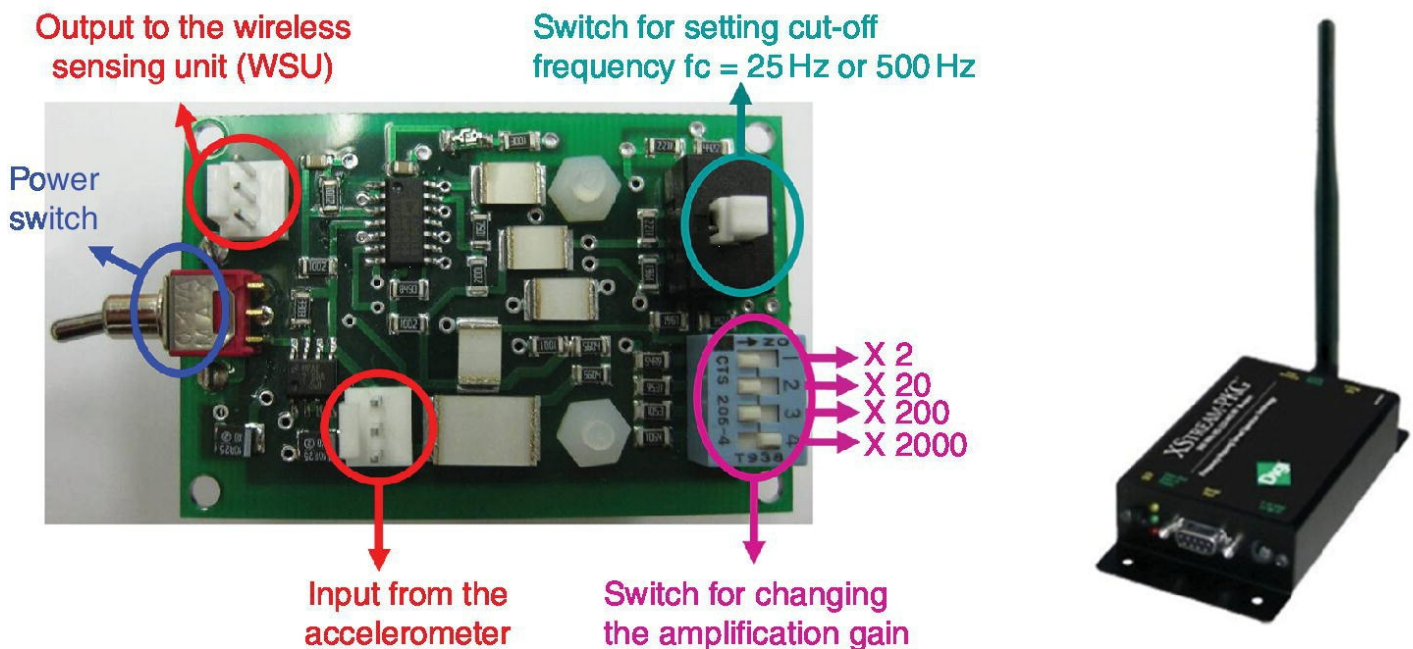


Figure 10.10 Wireless monitoring system for the highrise building.

The wireless sensing unit is designed to operate with two different wireless transceivers: 900 MHz MaxStream 9XCite and 2.4 GHz MaxStream 24XStream. Pintopin compatibility between these two wireless transceivers makes it possible for the two modules to share the same hardware connections in the wireless unit. The 24XStream transceiver was employed in

this project. The 24XStream is expected to have a communication range of 5 km at line of sight, but the effective communication range may vary depending on field conditions. The XStreamPKG 2.4 GHz RS232/485 shown in [Figure 10.10\(b\)](#) was selected as the modem of station. The wireless transmit module embedded in the modem is also 24XStream (2.4 GHz). In the whole system, the modem is the hub of the system. The modem has two tasks: to exchange data with the units distributed in measured points, and to send the commands to the wireless sensing units and transfer the data from units to computer. The accelerometers used in this project are KD1300C with a frequency range of 0.2–1000 Hz, a measurement range of 300 m/s^2 and a sensitivity of 250–300 $\text{pc}/(\text{m/s}^2)$. This type of accelerometer performs well in measuring large structures especially with low frequency vibration. To make the signal comfortable for A/D conversion, a charge amplifier (KD5008) was used, since it can be easily adjusted with a desired amplification factor.

10.3.4 Ambient Vibration Tests and Results

In the ambient vibration tests, the vertical accelerations of the floating platform along the longer edge were measured by the wireless monitoring system. To obtain the mode shapes with good resolution along the length of the longer edge, nine acceleration measurement points were selected along the longer edge, as P1 to P9 illustrated in [Figure 10.11](#). The measurement points are located on the columns in order to facilitate the installation of accelerometers using a magnetic base. After the signal conditioning by the charge amplifier, the analogue signal (voltage) was acquired and digitised by the A/D module of the wireless sensing unit. In the tests, the data was sampled at a frequency of 100 Hz. The digitised acceleration data was wirelessly sent to the base station, a laptop computer connected with a 24XStream transceiver. The sequences were repeated throughout the length of the longer edge of the floating platform. Therefore, modal parameters, including the natural frequencies and mode shapes of the floating platform, were obtained.

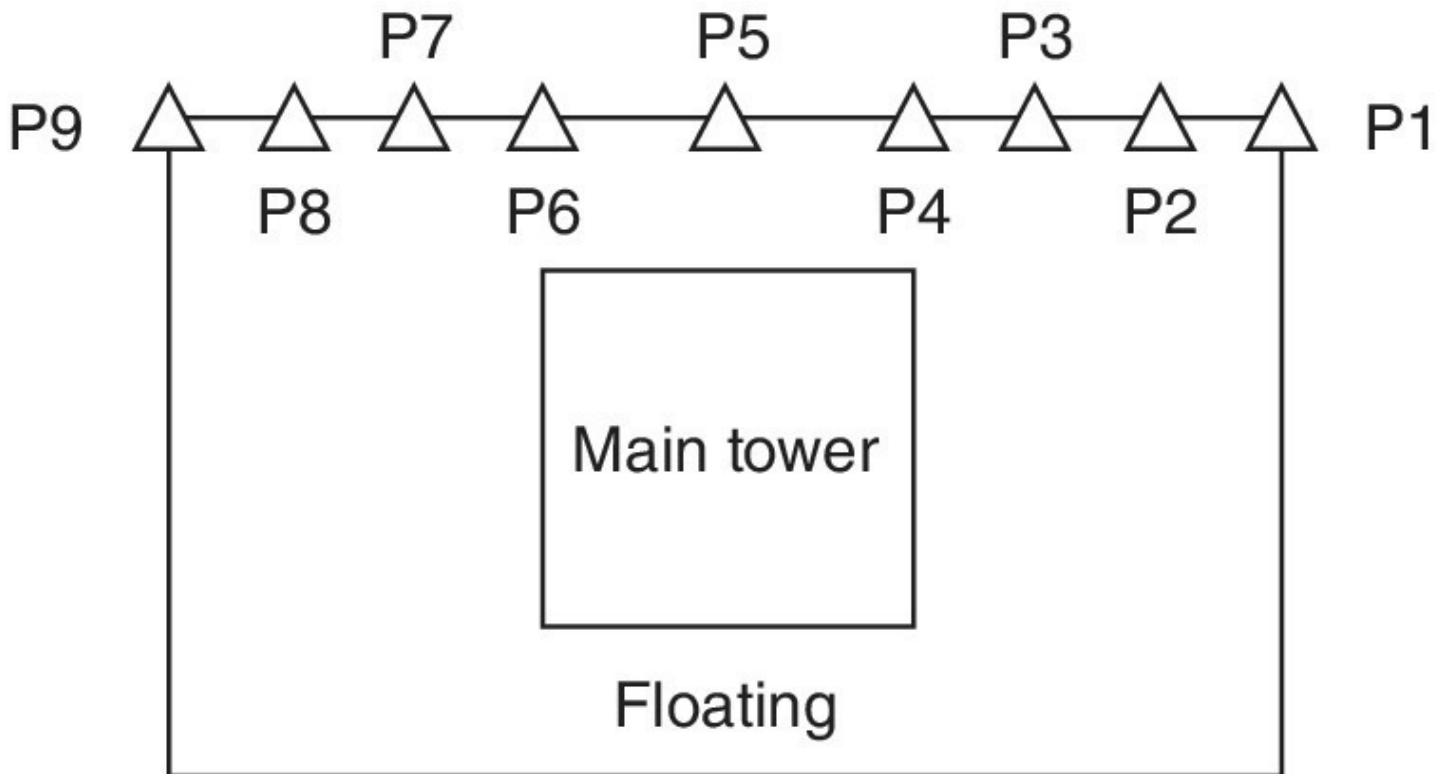
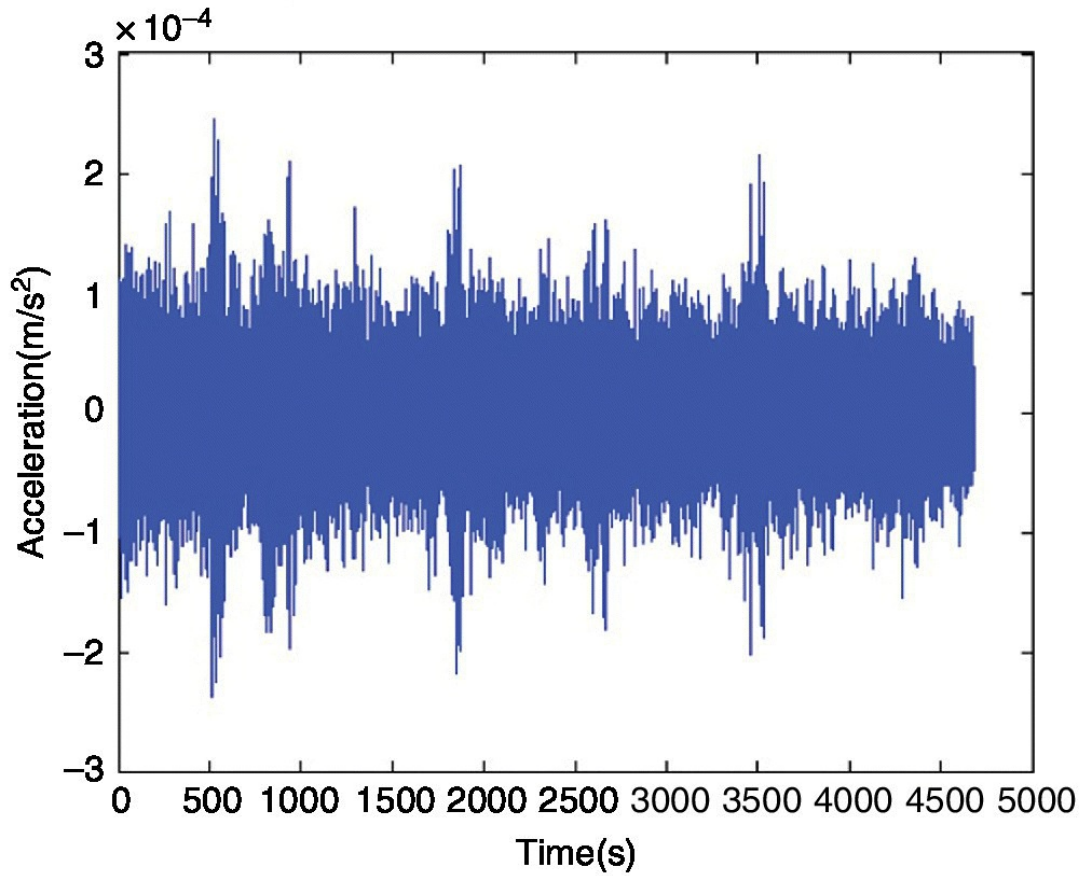


Figure 10.11 Distribution of accelerometers on the floating platform.

From the three tests, the vertical acceleration responses of the longer edge of the floating platform under ambient vibration environment were obtained. Each test lasted for about 80 to 100 minutes. [Figure 10.12\(a\)](#) shows the timehistory of the vertical acceleration at sensor location P9. With the timehistory data, the power spectral density of the vertical acceleration responses is obtained, as illustrated in [Figure 10.12\(b\)](#). From the results, the natural frequencies of the floating platform were identified by the peakpicking method.

(a) Time-history of vertical acceleration



(b) Power spectral density

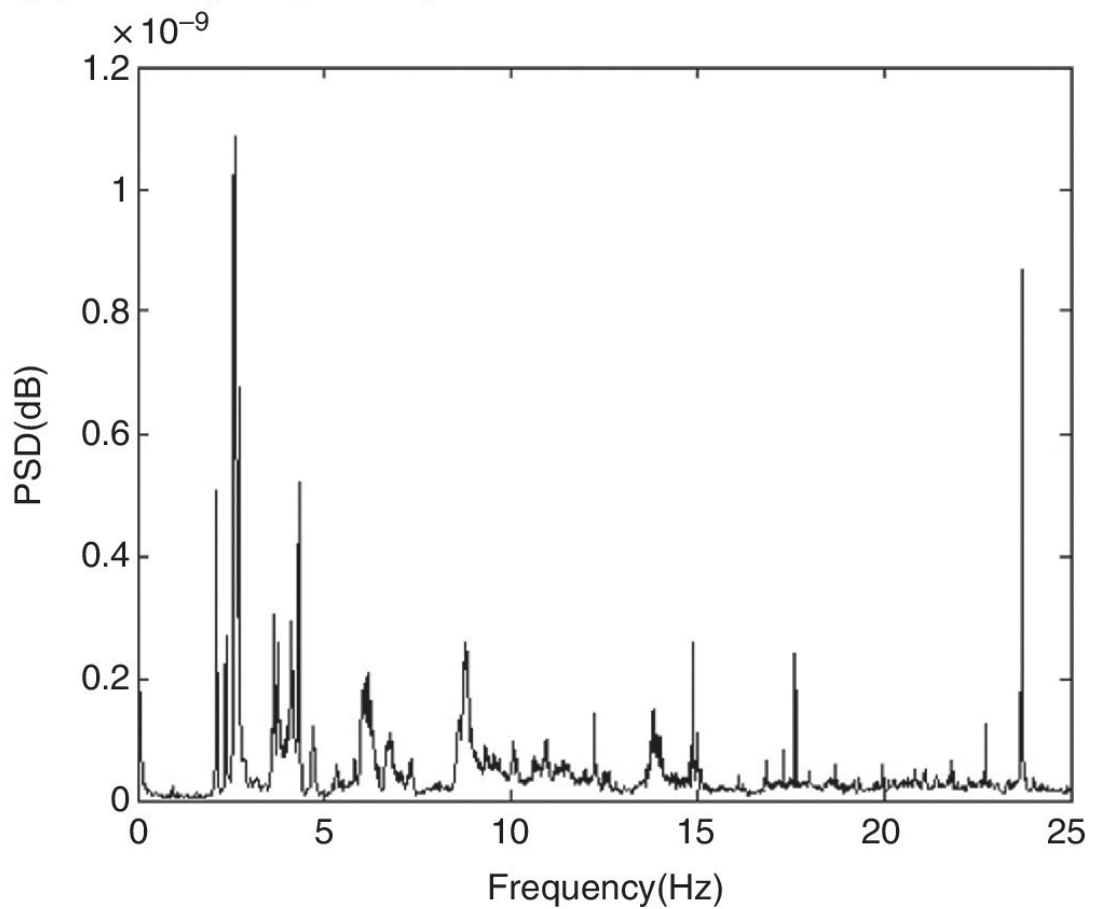


Figure 10.12 Vertical dynamic response of floating platform at sensor location P9.

In addition to the identified natural frequencies and mode shapes by the wireless monitoring system, the modal parameters of the highrise building are also predicted by the finite element dynamic analysis. [Table 10.7](#) provides a comparison between the identified and predicted natural frequencies. The largest discrepancy between the two sets of the results is 5.18% in relative error for the third mode. From the field tests, the wireless system is able to perform favourably in longterm ambient vibration monitoring for the huge floating platform.

Table 10.7 Comparison between identified and predicted natural frequencies (Hz).

Mode No.	Mode 1	Mode 2	Mode 3	Mode 4
Identified frequencies	2.112	2.368	2.583	2.730
Predicted frequencies	2.075	2.390	2.724	2.879
Relative error	1.78%	0.92%	5.18%	5.17%

10.4 Monitoring of Tunnel Construction Using FBG Sensors

Fibre Bragg grating (FBG) sensing technology is used for safety monitoring of railway tunnels during construction stage, including realtime temperature monitoring of the frozen soils during freezing construction and automatic subgrade settlement monitoring of a high speed rail line segment during construction.

10.4.1 Temperature Monitoring of Tunnel Cross Passage Construction

Wuhan Metro Line 2 is characterised by its deeply buried doubleline shield tunnels under the Yangtze River, as shown in [Figure 10.13\(a\)](#). The length of the metro tunnel beneath the Yangtze River is about 1400 m. A total of five cross passages are distributed along the metro tunnel to meet the requirements for regional disaster prevention and drainage. Cross passage 3 beneath the river is selected as a testbed for FBG based instrumentation and realtime temperature monitoring during the freezing construction (Ye et al. 2013). As illustrated in [Figure 10.13\(b\)](#), the distance between the central lines of the left and right metro tunnels at the location of cross passage 3 is 13 m. The tunnel segments of cross passage 3 are steel tube slices with a thickness of 0.35 m. The inner and external diameters of the metro tunnel are 5.5 m and 6.2 m, respectively. The average burial depth of the metro tunnels at the location of cross passage 3 is 20.29 m.

(a) Tunnel during construction



(b) Cross-section of cross passage and freezing hole arrangement

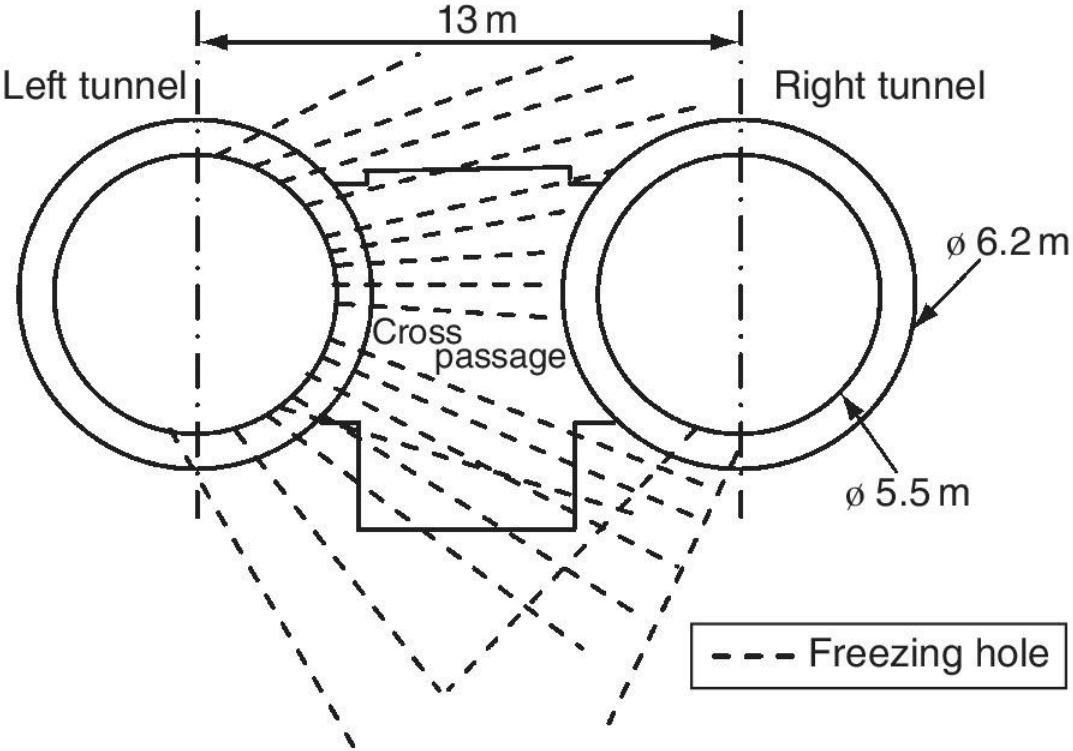
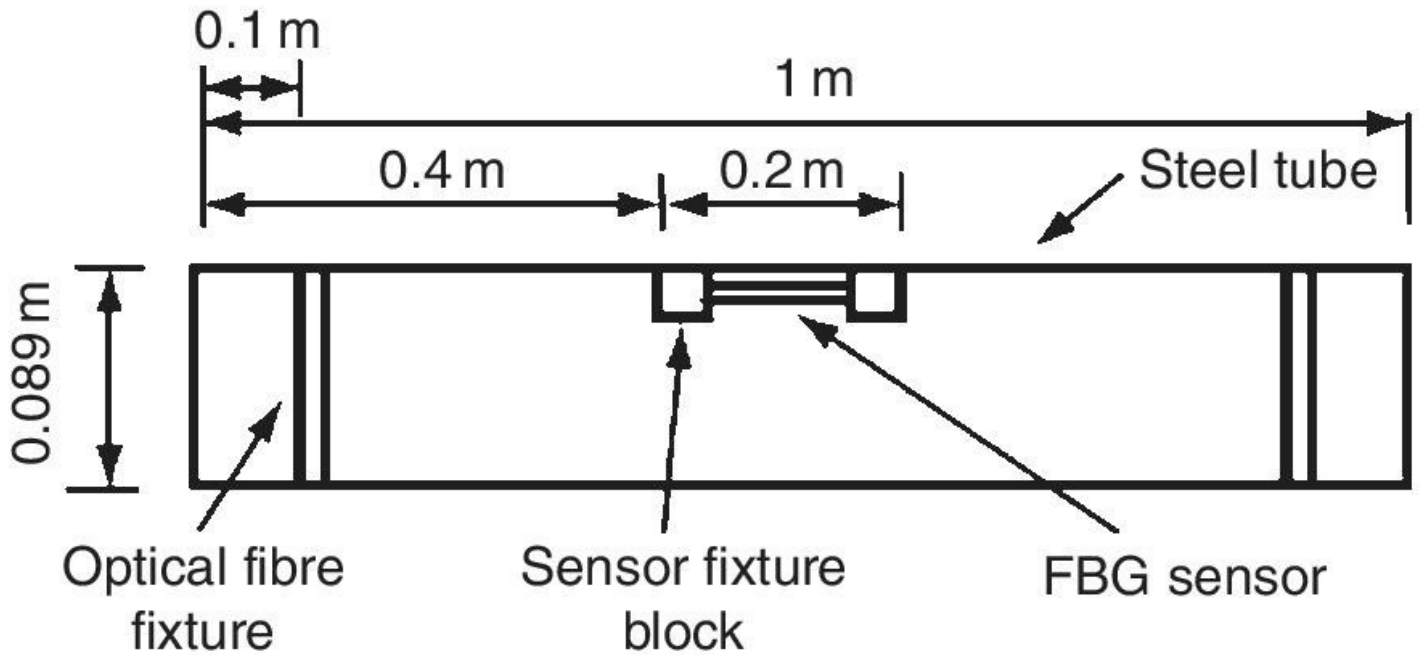


Figure 10.13 Rivercrossing metro tunnel during freezing construction.

Cross passage 3 is located at the soil layers of silty fine sand and mediumcoarse sand with gravel. The deformation resistant capability of the soils is unsatisfactory under the action of the external loads. In addition, the pore water pressure is relatively large since cross passage 3 is surrounded by a waterbearing layer with a high water head. Problems can arise due to soil layer migration and waterbursting in sand layers during shield construction, leading to instability of the excavated surfaces. Thus, an artificial ground freezing method was employed to consolidate the surrounding soil layers around the metro tunnels. As shown in [Figure 10.13\(b\)](#), a total of 112 freezing holes were drilled in the soil layers to strengthen the soils. Then, a frozen soil wall with high strength and good tightness was formed for safety excavation of the cross passage.

To protect the instrumented FBG sensors in harsh environments, a freezing monitoring device was adopted by integrating the FBG sensor with the freezing steel tube (Ye et al. 2013), as illustrated in [Figure 10.14](#). The fabrication process of the freezing monitoring tube mainly includes: (a) FBG sensor together with the fixed blocks, inserted into the freezing steel tube and screwed at a designated position, (b) optical fibre fixtures mounted inside on both ends of the freezing steel tube, (c) sealing protective measure made for the optical fibre connector by use of silicone gel and tinfoil papers.

(a) Front view



(b) Photo of the appliance

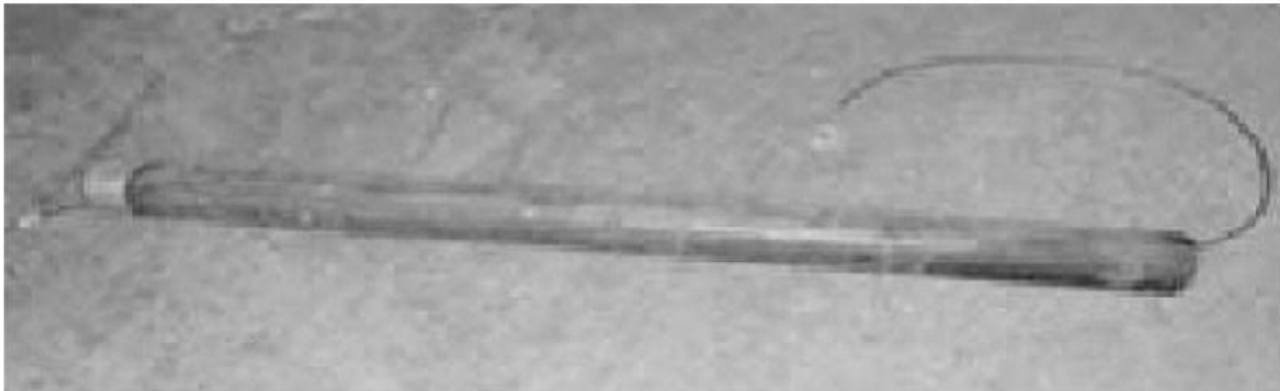


Figure 10.14 Freezing monitoring tube accommodating a FBG sensor.

The developed freezing monitoring tubes were used for realtime temperature monitoring of the frozen soils during cross passage construction. A total of five freezing monitoring tubes with seven working FBG sensors were installed into the soil layers around the right metro tunnel at the location of cross passage 3, as shown in [Figure 10.15](#). The measurement data of the Bragg wavelengths was obtained from all the workable FBG sensors with a sampling frequency of 100 Hz. The temperature at the sensor deployment locations during freezing construction can then be estimated from the relationship between the temperature variation and temperatureinduced wavelength variation. Temperature monitoring data during the 65day period (from 18 January 2012 to 22 March 2012) from all the workable FBG sensors has been acquired during freezing construction of cross passage 3.

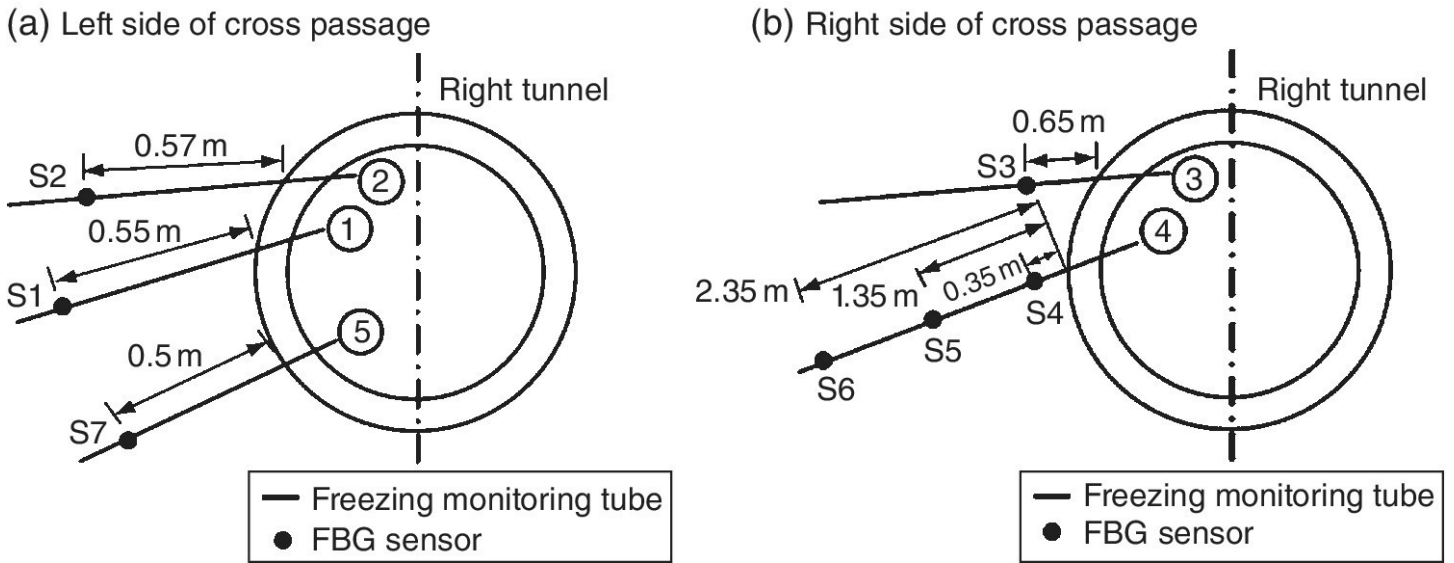


Figure 10.15 Deployment locations of FBG sensors in the frozen soils.

Figure 10.16 provides the temperature time histories obtained from FBG sensors S1 to S7 after eliminating the high frequency noise. The results reveal that the temperatures of the frozen soils decrease sharply at the early stage of freezing construction (aggressive freezing phase) and then gradually become steady (stable freezing phase). With such a continuous temperature evolution profile of the frozen soils, the strength of the frozen curtain can be estimated accurately in real time. This effectively provides useful information for the subsequent excavation construction of the cross passage and thus reduces the risk of construction.

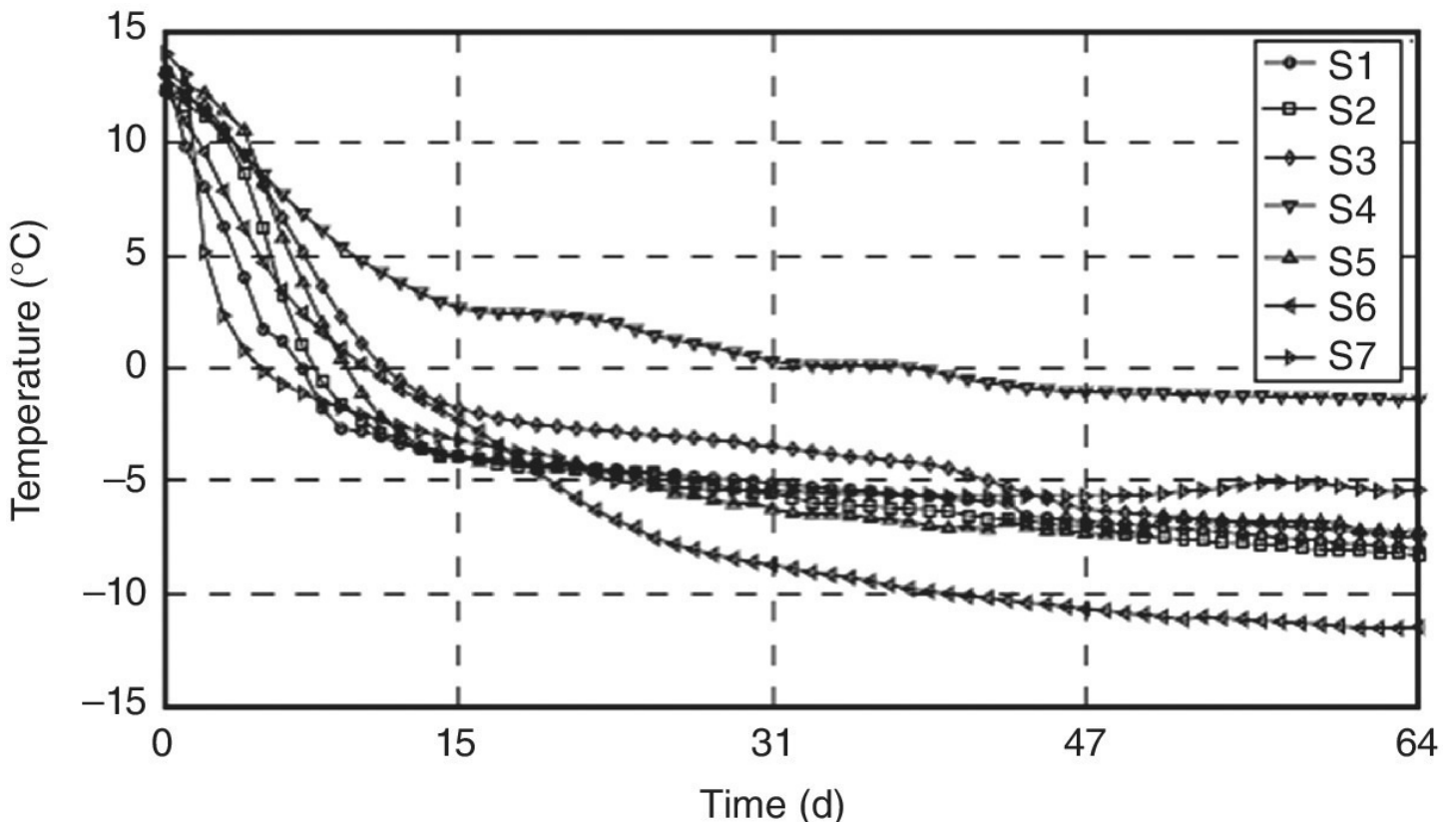


Figure 10.16 Measured temperature time histories during freezing construction.

10.4.2 Settlement Monitoring of Undercrossing Tunnel Construction

Realtime and continuous monitoring of the postconstruction settlement of high speed rail subgrade is necessary for safety surveillance and condition assessment of the high speed rail superstructures and substructures. The Beijing–Shanghai HighSpeed Rail is the world’s longest high speed rail, and started its official operation in June 2011. To construct an undercrossing road, a tunnel excavation was carried out beneath the subgrade of a segment of the high speed rail. In order to accurately assess the effect of the tunnel excavation construction on the subgrade settlement of the rail, an automatic settlement monitoring system on the subgrade surface was deployed (Ye et al. 2013), as shown in [Figure 10.17](#). A total of 12 FBG based liquidlevel sensors were installed along the rail tracks at various intervals. Two liquidlevel sensors were used for the reference points (Nos. 1 and 12) where the settlements can be ignored.

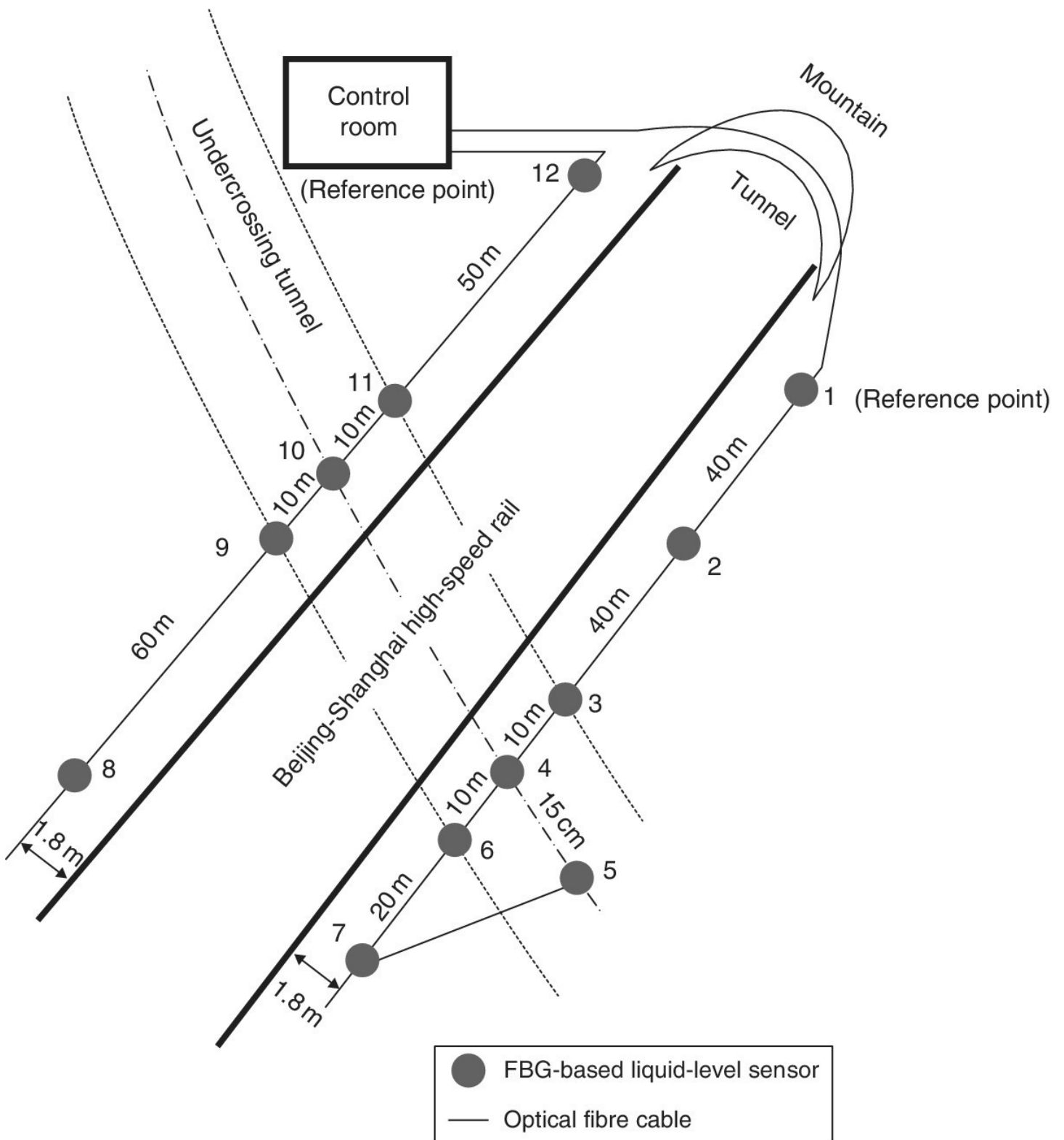


Figure 10.17 Deployment of FBG based liquidlevel sensors on subgrade surface of the railway line.

The Bragg wavelength data from all the deployed liquidlevel sensors was acquired at a sample frequency of 1 Hz from 28 February 2011 to 31 August 2011. This data covers the periods of tunnel excavation construction as well as trial operation and two months of official operation of the rail. On the basis of a calibrated relationship between the Bragg wavelength and the settlementinduced liquid level variation, the subgrade settlement at the locations of

deployed liquidlevel sensors then can be estimated from the measured Bragg wavelength data, as illustrated in [Figure 10.18](#).

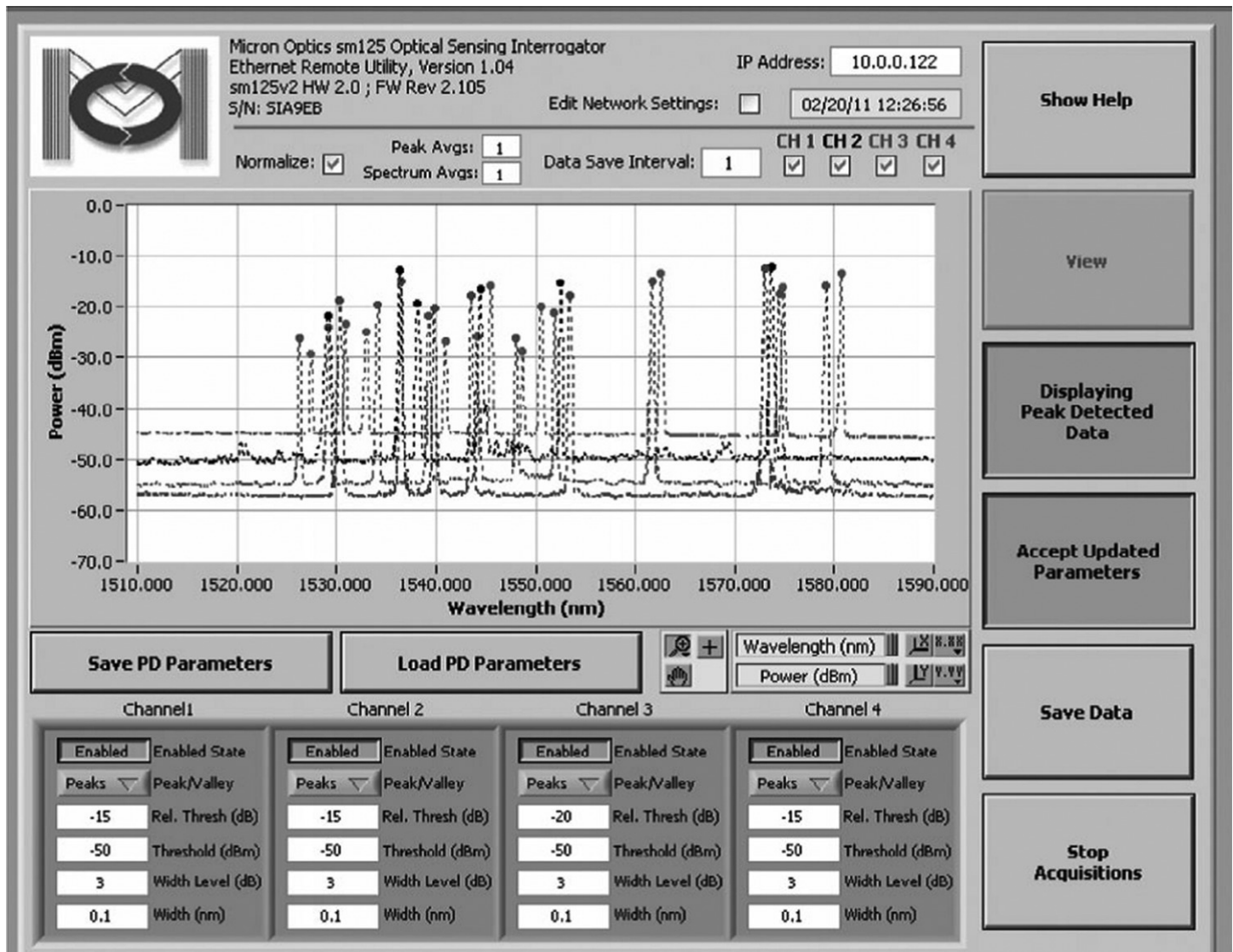


Figure 10.18 Measured Bragg wavelengths by liquidlevel sensors for estimating subgrade settlement.

10.5 Safety Monitoring of Rail Using Acoustic Emission

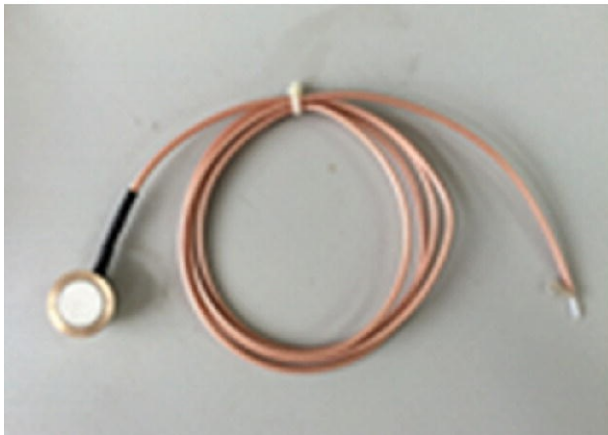
Railway turnouts (railroad switches or ‘points’) are an indispensable part of a railway system. They are the weakest components of the track structure. The operating environment at turnouts is much more complex and harsher than at other parts of a railway line. Due to the particular geometry of wheel–rail contact and the sudden variation of track flexibility, severe cyclic impact loads act on the turnout during train passage. This can cause cracks or even damage to the switch rail, resulting in unexpected structural failure. Without suitable detection, the damaged railway turnout on the network may not be immediately found and replaced, leading to potential safety threat to railway operation. Thus, it is of huge importance to continuously monitor the health condition of railway turnouts and to promptly detect damage once it starts.

10.5.1 Rail Track Damage Detection System

Acoustic emission (AE) occurs as a result of transient elastic waves generated when strain energy is suddenly released within or on the surface of a material. This is due to microstructure changes such as crack generation and propagation. Such changes can be generated internally or externally and cover a broad frequency range between 20 kHz and 1 MHz. Thus, acoustic emission is widely used for crack detection in static structures, such as rail track defect detection. The undamaged rail track usually generates structural vibration under 50 Hz. When there is crack damage in the structure, it will generate high frequency AE bursts. This can be reflected on the AE burst chart in the time domain with the presentation of increased AE bursts, or on the power spectrum density (PSD) chart in the frequency domain with the presentation of highly concentrated energy. The existence of crack damage at rail turnouts will lead to an energy concentration at high frequency when it is excited by a passing train. Therefore, by analysing the corresponding charts, it is possible to assess whether there is any crack damage around the railway turnouts.

The system for damage detection of rail track uses acoustic emissions. The system has been examined and calibrated for warning triggers in laboratory tests (Ni et al. 2014a), as shown in [Figure 10.19](#). Both methods for counting AE bursts and for observing power spectrum density extents were evaluated in the test. By using damage thresholds based on both methods, the system gives the most effective warnings. The effective sensing distance could be as long as 10 m. Therefore, the system is designed to give damage warnings for rail turnouts, when the signal surpasses both thresholds of AE bursts and power spectrum density.

(a) PZT based sensor



(b) System components



Figure 10.19 Piezoelectric (PZT) based acoustic emission sensing system for damage detection of rail turnouts.

Acoustic emission sensors are usually made of sensitive piezoelectric (PZT) materials. They can sense signals from the low kHz up to 1 MHz, and they can be mounted using a coupling set on the surface of the structure to be evaluated. As such, the PZT based sensor for damage detection is made of a PZT disk with a diameter of 22 mm and thickness of 0.8 mm, as shown in [Figure 10.19](#)(a). The sensor is suitable for both signal generating and receiving and works stably under a wide temperature range (from $-40\text{ }^{\circ}\text{C}$ to $80\text{ }^{\circ}\text{C}$). To minimise electronic noise

from the railway environment, the PZT sensor is insulated and packaged twice during manufacture. The procedure shields most electromagnetic noise and improves the quality of signals acquired by the sensor. The data acquisition system has a commercial data acquisition card NI9223 with four channels and sampling rate up to 10 MHz. The system uses Labview software to perform data collecting and analysis. The damage detection system consists of PZT based transducers, damage trigger components, and data acquisition system. The last two parts are integrated into a package box shown in [Figure 10.19\(b\)](#). The system uses passage trains as exciting loads. The sensors generate signals once external loads are applied. If damage occurs in rail turnout parts, warning signals will be generated, and the data will be collected and passed through cables to the central analysis system installed in the nearby control room.

Four PZT transducers are arranged symmetrically on two sides of the internal rail, at 4 m and 3 m away from the rail turnouts, as shown in [Figure 10.20\(a\)](#). Each transducer is secured with a mechanical clamp on the base of the rail, as shown in [Figure 10.20\(b\)](#), with an initial clamping load of 200 N. Four channels were used to collect data, with channels 1 and 2 at 4 m away from the rail turnouts and channels 3 and 4 at 3 m away from the turnouts, respectively. The sampling rates used are 600 kHz to 1 MHz.

(a) Location of PZT transducers



(b) Transducers with mechanical clamps

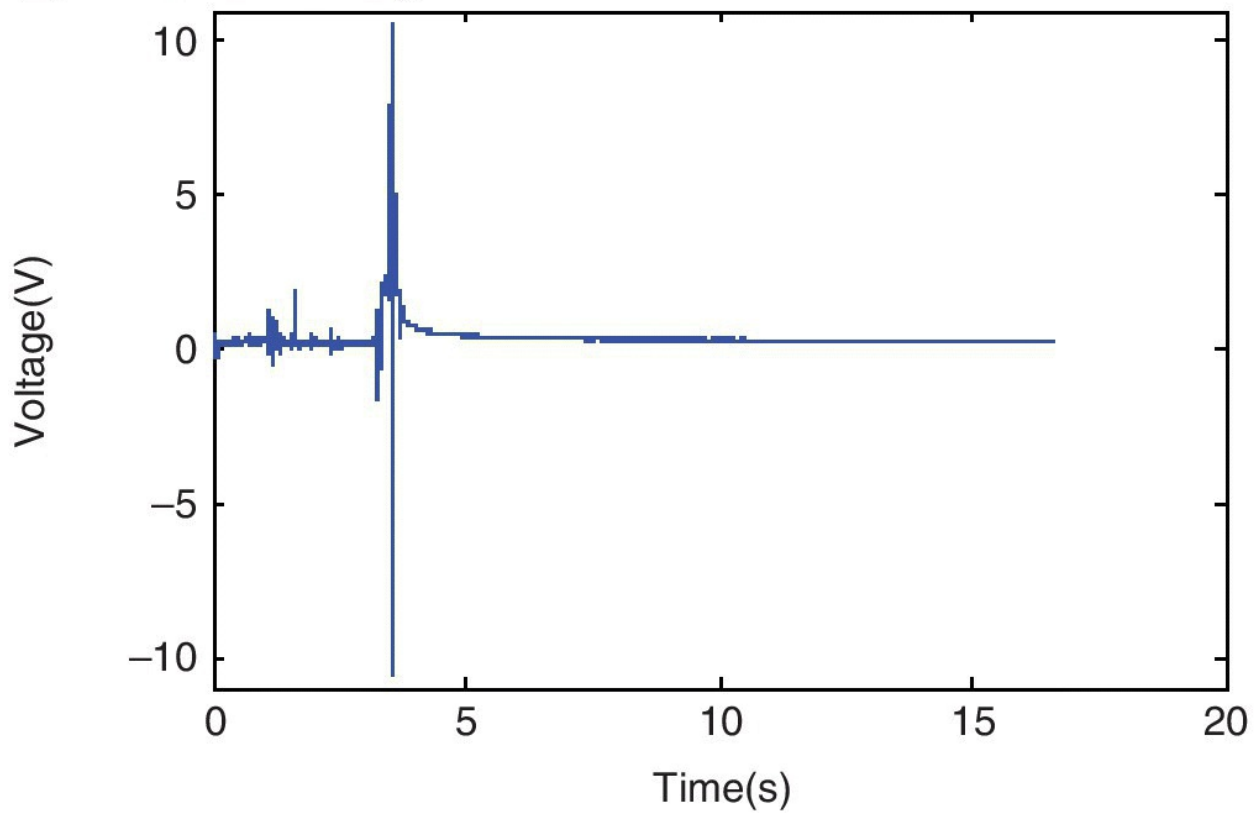


Figure 10.20 Undamaged rail turnouts and arrangement of PZT transducers on railway switch area.

10.5.2 OnSite Monitoring Data

The damage detection system was installed at the rail turnouts in February 2013. The baseline signals (e.g. from undamaged rail turnouts) were collected in both time domain and frequency domain. The collected baseline signals for channel 1 are plotted in [Figures 10.21\(a\)](#) and (b). The sampling rate used was 1 MHz. From the results for all channels, there is very limited AE bursts in time domain, and the power spectrum density (PSD) curves from the sensors are very smooth.

(a) Time domain signal



(b) Power spectrum density

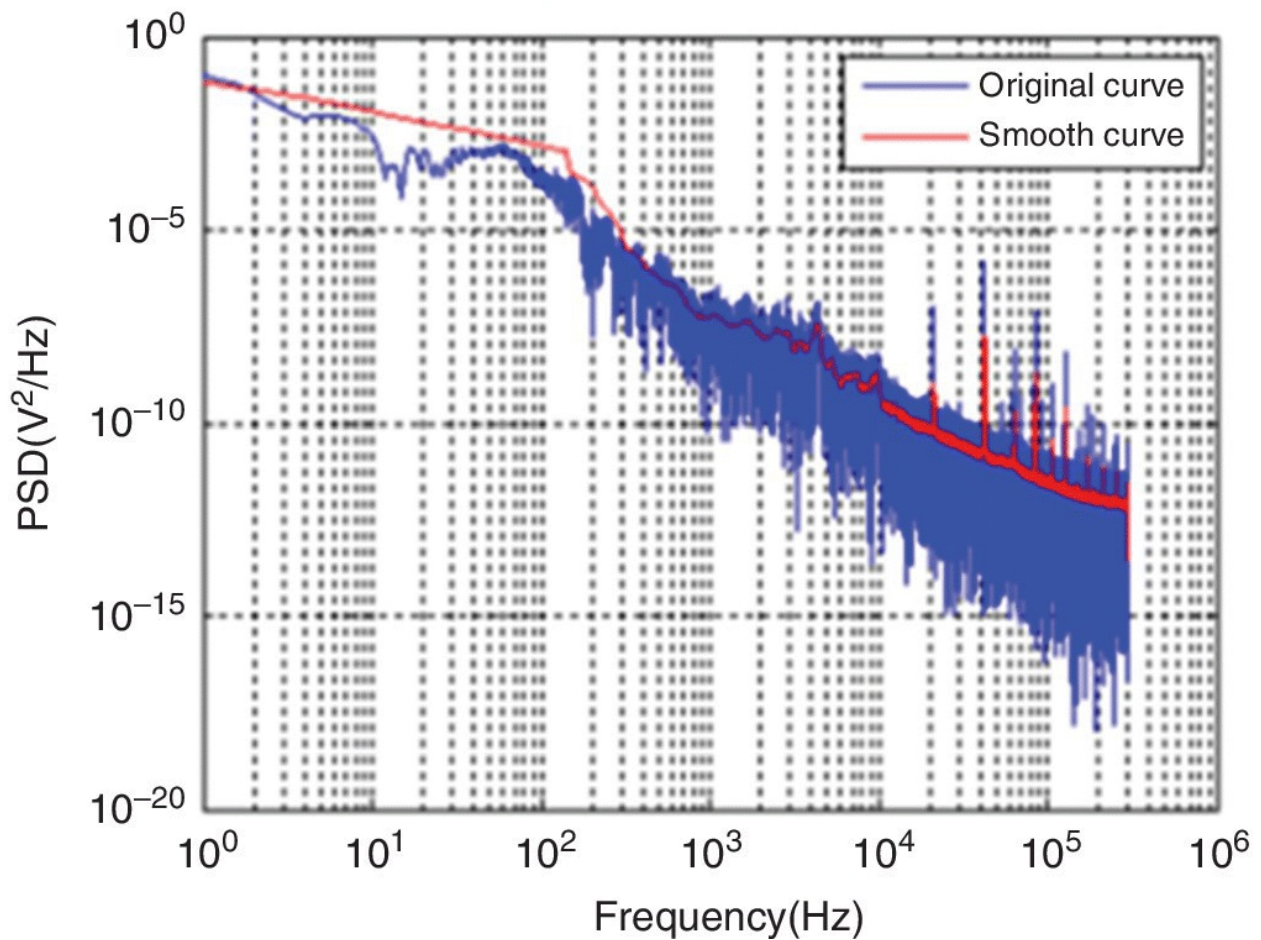


Figure 10.21 Signals collected from PZT transducer 1 for undamaged rail turnout.

In June 2013, the damage detection system was triggered by the warning signals and successfully recorded the data associated with the damaged rail turnouts, as shown in [Figure 10.22](#). In the damaged rail turnout, part of the turnout is lost. The damaged rail turnout was on the side of PZT transducers 1 and 3. The recorded timedomain signals and their power spectrum density curves for transducer 1 are shown in [Figure 10.23](#). Sampling rate used was 600 kHz. The damaged rail part was replaced immediately to avoid any potential accidents.

(a) Damaged rail turnout

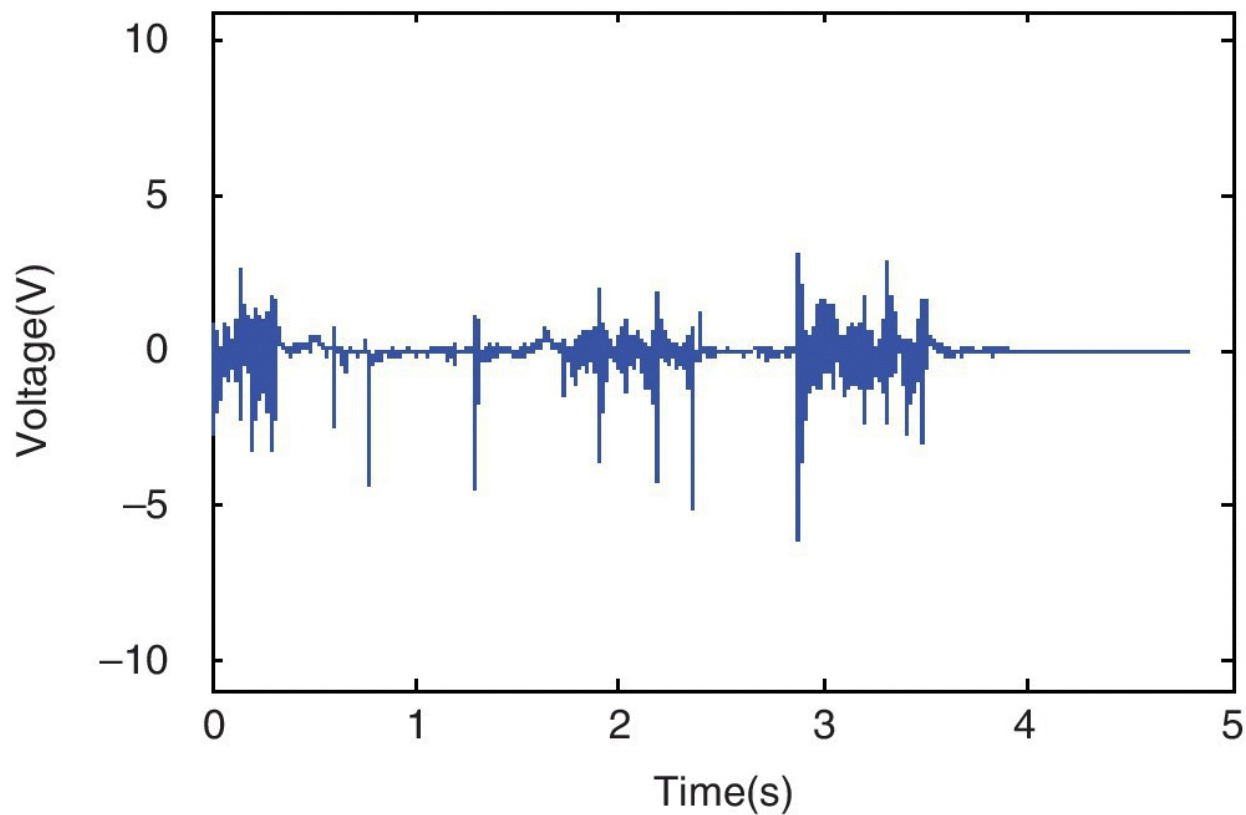


(b) Passage train



Figure 10.22 Damaged rail turnout and passage train.

(a) Time domain signal



(b) Power spectrum density

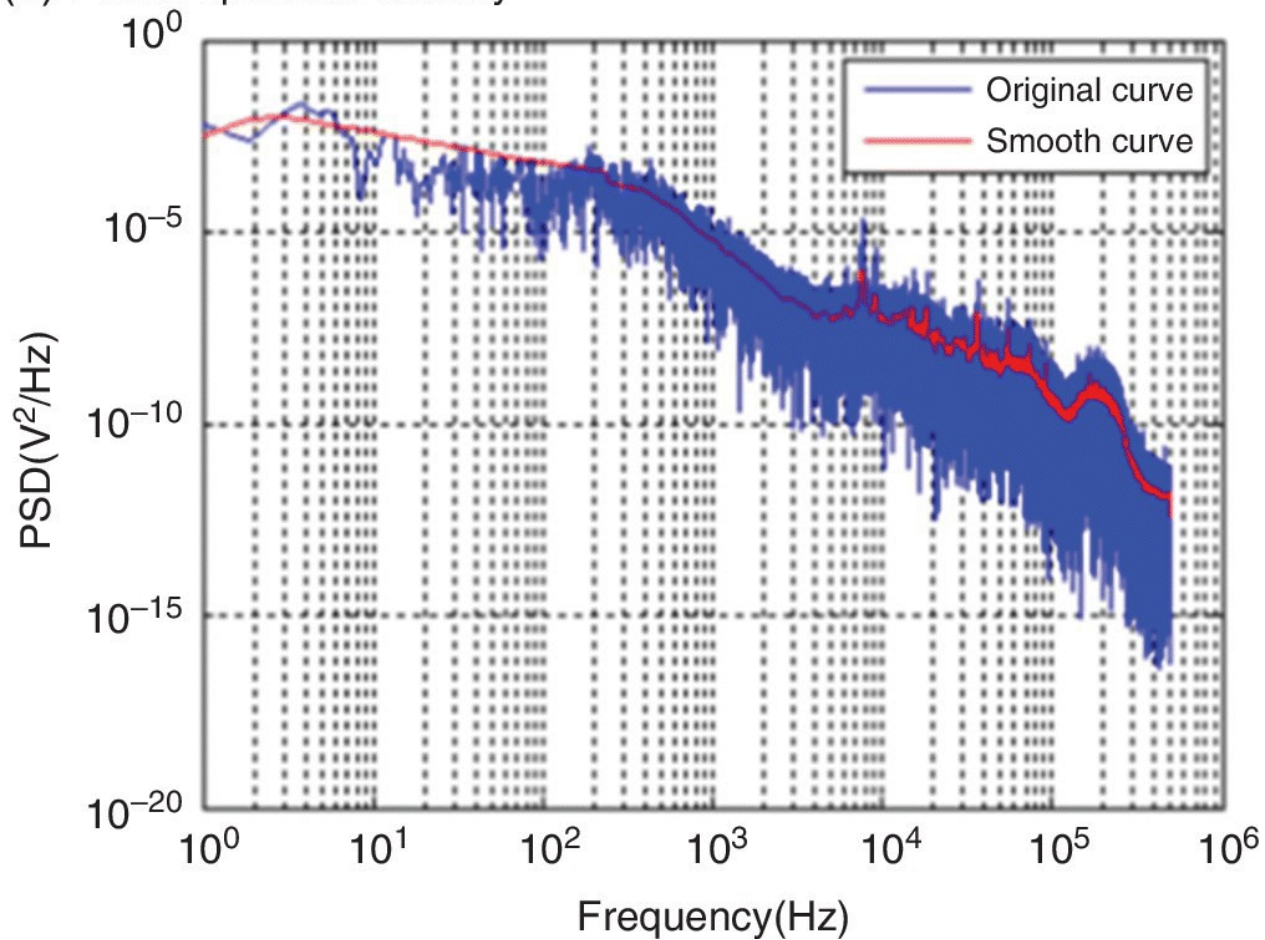
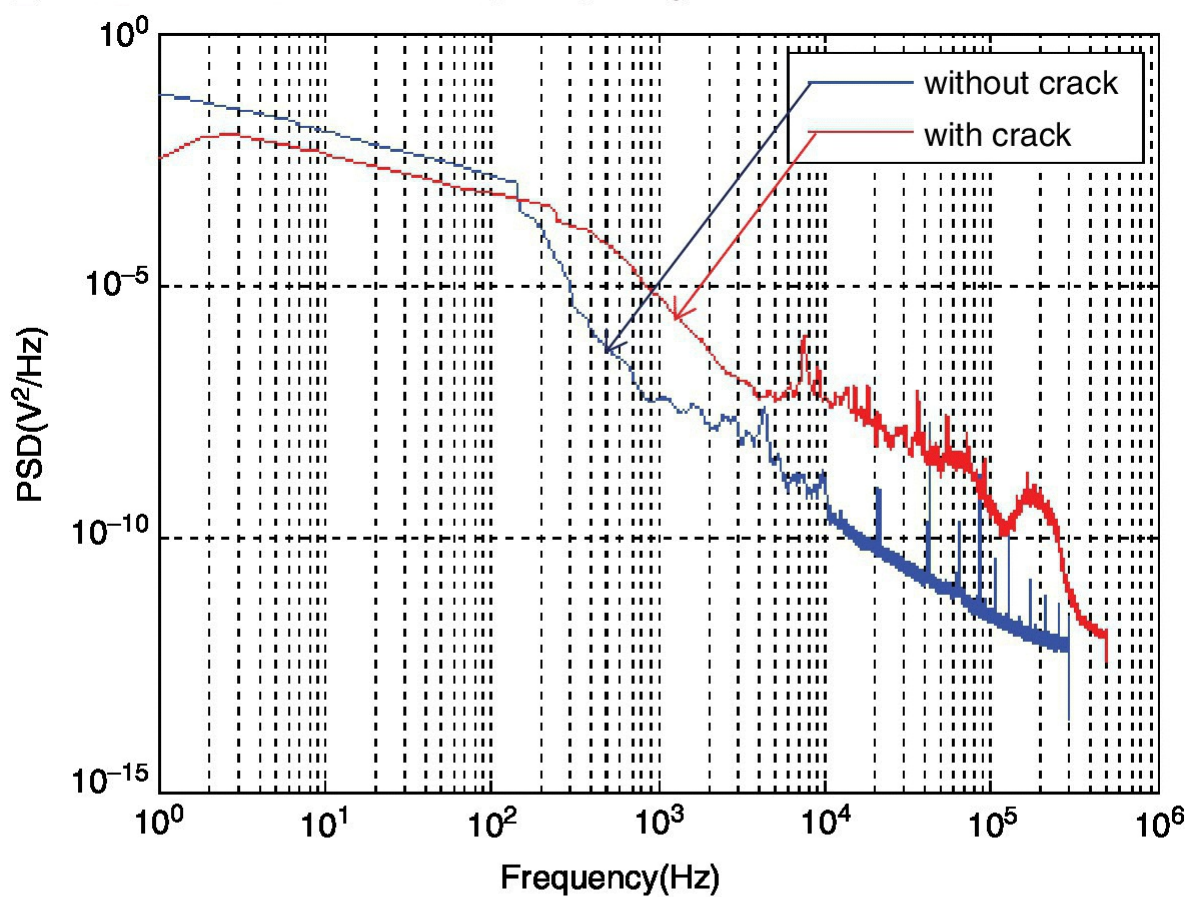


Figure 10.23 Signals collected from PZT transducer 1 for damaged rail turnout.

By comparing the undamaged charts in the time domain in [Figure 10.21\(a\)](#) with the corresponding damaged charts in [Figure 10.23\(a\)](#), more AE high frequency bursts are found in the damaged chart of PZT transducer 1. Similarly, the damaged power spectrum density curve shows higher energy than the undamaged one, as shown in [Figure 10.24\(a\)](#). Moreover, there is an obvious energy peak (concentration) within the 100–300 kHz frequency range for the damaged power spectrum density curve. [Figure 10.24\(b\)](#) gives clearer results of the power spectrum density charts for the undamaged and damaged rail turnout within this high frequency range (Ni et al. 2014a). This confirms the concept that the crack damage is related to the strain energy released at the crack opening at high frequencies. From the analysis of the data acquired from the onsite damage detection system, both AE transient bursts and PSD spectrum at high frequency could be used to detect the crack damage of railway turnouts.

(a) PSD curves over wide frequency range



(b) PSD curves at high frequency range

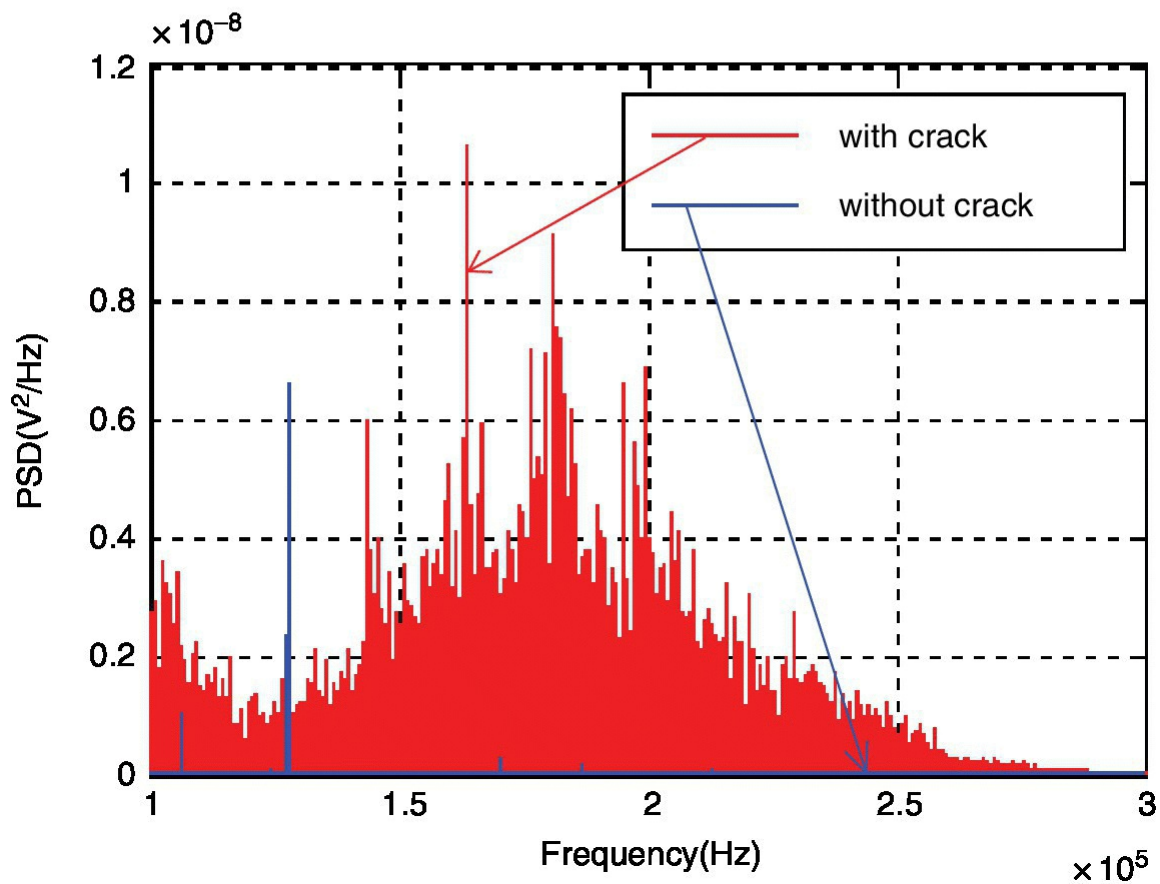


[Figure 10.24](#) Comparisons of power spectrum density (PSD) from PZT transducer 1 for undamaged and damaged rail turnout.

10.6 Structural Integrity Monitoring of Water Mains

The burst/leak of mains water can cause disruption to the raw water supply and may affect neighbouring areas. The structural integrity of water supply pipelines is critical due to its significant influence, such as high environmental impact, severe interruptions in service, substantial time consumption and considerable financial cost. Since water supply pipelines are often buried underground and the diameter of the pipes is very large, ordinary sensors can hardly survive these surrounding environments. A pilot study on the use of fibre Bragg grating (FBG) sensors for monitoring the structural integrity of the glass reinforced plastic (GRP) pipes of the Dongjiang water mains in Hong Kong has been carried out.

10.6.1 FBG Sensory System

This pilot project monitors a 200 metre long segment of GRP underground pipe of the water mains of diameter 2.1 m (Ni et al. 2013b). The FBG sensory system consists of 300 FBG strain sensors, 300 FBG temperature sensors, six FBG water pressure sensors, optical cable for signal/data transmission, data logger, multiplexer, computer and other facilities, as shown in [Figure 10.25](#). As the integrity monitoring system is expected to work continuously for several years at a maximum flow velocity of 3 m/s, all the sensors are specially designed to be waterproof, anticorrosive and suitable in contact with potable water.

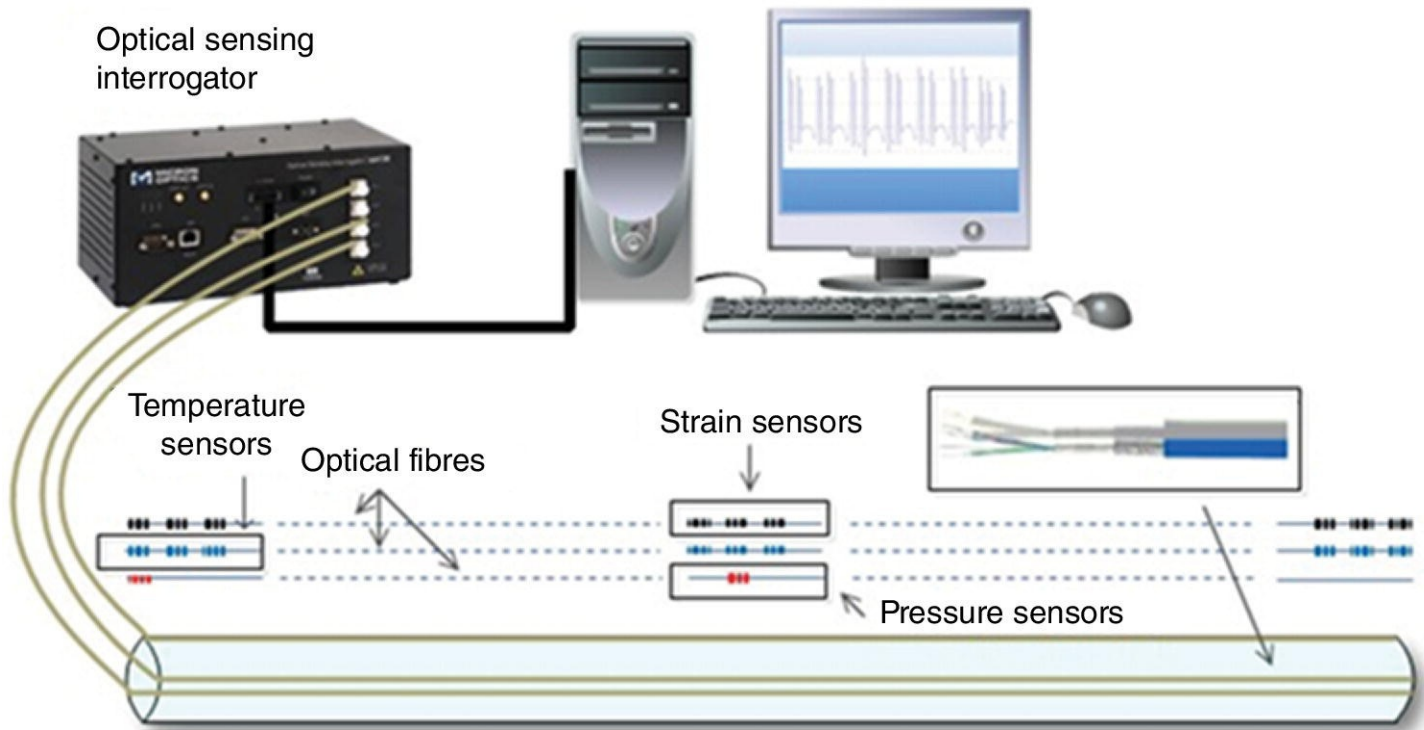
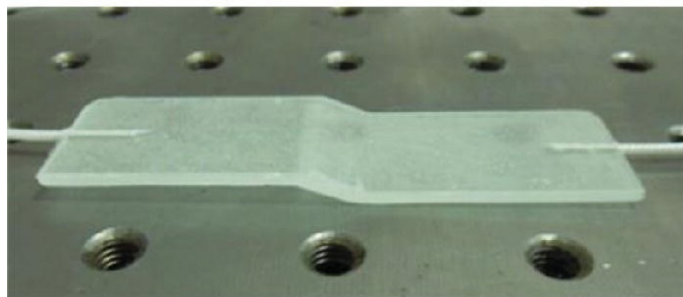


Figure 10.25 Schematic of FBG sensory system for structural integrity monitoring of water mains.

Various types of sensors are used in the monitoring system. The fibre reinforced plastic encapsulated FBG strain sensors with temperature compensation sensors are adopted, as shown in [Figure 10.26\(a\)](#). Two FBG sensors with different wavelengths – the strain sensor and the temperature compensation sensor – are embedded tightly into a lamina in order to make the sensor much more compact. Food grade stainless steel packed water pressure sensors are used in the monitoring system, as shown in [Figure 10.26\(b\)](#). The special water pressure sensor is designed for easy installation on the pipe, vertical pressure measurement and suitability in contact with potable water. Also, a fibre glass braid sleeve coated optical cable is selected to be waterproof and suitable for contact with potable water.

(a) FBG strain sensor with temperature compensation sensor



(b) The stainless steel packed water pressure sensor

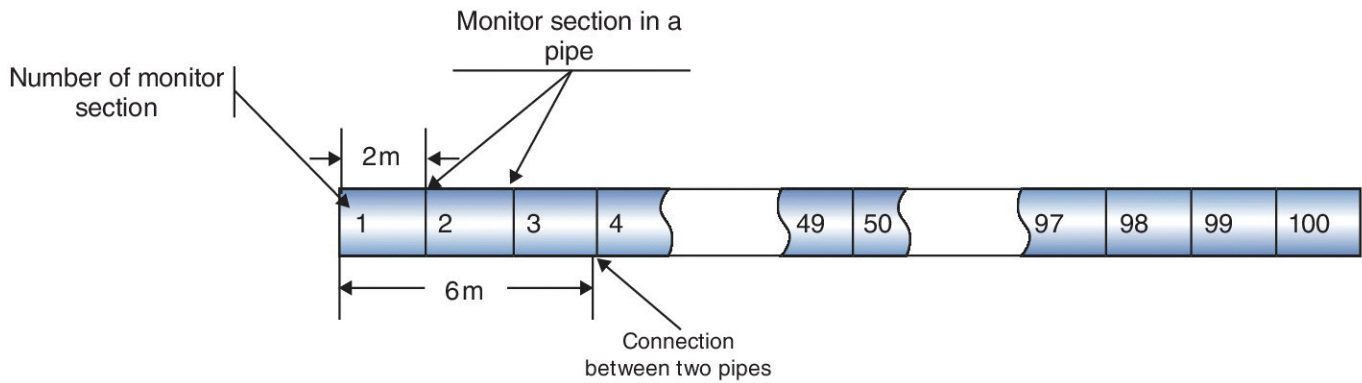


Figure 10.26 FBG sensors for monitoring water mains.

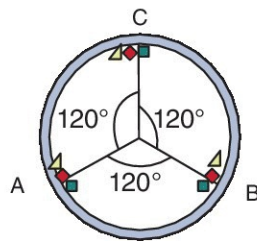
The 200 metre long GRP pipes are monitored at 100 monitoring sections. The spacing of the sections is 2 m. The distribution diagram of the monitoring sections is shown in [Figure 10.27\(a\)](#). The installation spacing of the FBG pressure sensors is 100 m and each installation

section has three sensors. The three FBG pressure sensors in each section are installed at points A, B and C near the strain and temperature sensors, respectively, as shown in [Figure 10.27\(b\)](#). A total of three FBG strain sensors and three FBG temperature sensors are used in each installation section, and are divided into three groups. Each group has one FBG strain sensor and one FBG temperature sensor. The three groups of sensors are installed at points A, B and C in the monitoring section, as shown in [Figs. 10.27\(b\)](#) and (c).

(a) Distribution of monitoring sections



(b) Monitoring sections of 1 and 50



(c) Other monitoring sections

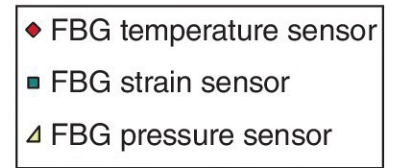
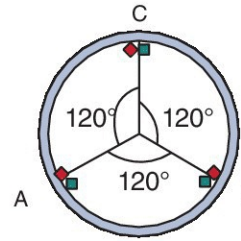


Figure 10.27 Distribution of strain, temperature and pressure sensors.

10.6.2 Implementation of Monitoring System

The monitored underground pipe is under the footpath or road. There are extremely complex railway traffic conditions: e.g. about 1–2 pairs of east line trains in one minute, 12 pairs of through trains running daily and thousands of passengers every day. The system topology (Ni et al. 2013b) is shown in [Figure 10.28](#). The deployment of the sensory system mainly consists of three steps:

- Connection between cables on ground and inner pipes, as shown in [Figure 10.28\(c\)](#). This part is specially designed for waterproof and pressure-tight under water pressure of 12 bar.
- Cable installation inside the pipe. There are two kinds of materials inside the underground pipe: steel and GRP. A small diameter galvanised steel tube was employed to protect and fix the signal transmission cables, as shown in [Figure 10.28\(d\)](#). And the glass fibre mesh preimpregnated into epoxy resin was employed to protect and fix the signal transmission cable to the surface of the GRP pipe, as shown in [Figure 10.28\(e\)](#). Glass fibre mesh and epoxy resin were used to repair the GRP pipe wall of the water mains.

- Sensor installation on the surface of the GRP pipe. The 300 strain sensors and 300 temperature compensation sensors are divided into 30 arrays and interrogated as one channel. Each array consists of 10 strain sensors and 10 temperature compensation sensors. The 30 arrays are divided into three groups, installed at points A, B and C in each section, as shown in [Figs. 10.27\(b\)](#) and (c). Each sensor was attached to the surface of the pipe with epoxy resin and protected by a stainless steel box for water pressure protection. Finally, all the sensors and cables are protected and fixed by the glass fibre mesh, pre impregnated into epoxy resin.

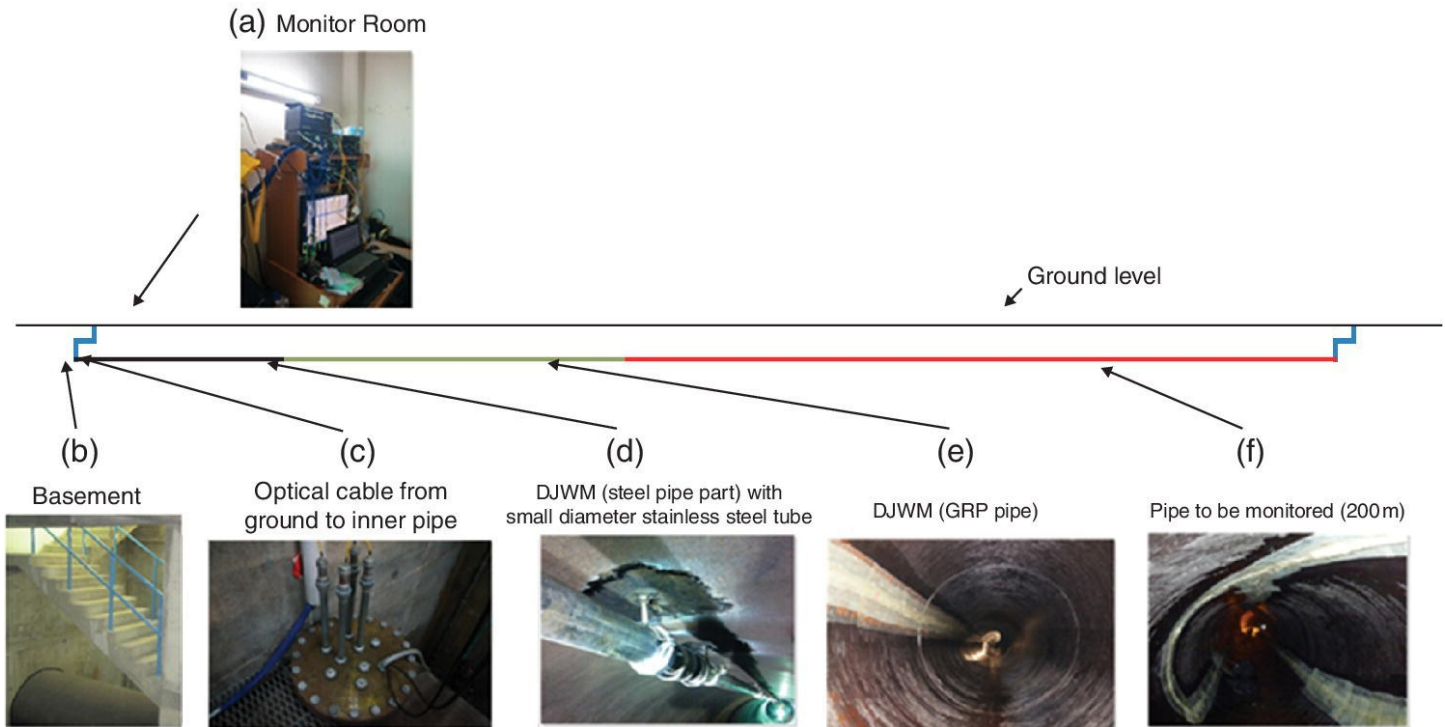
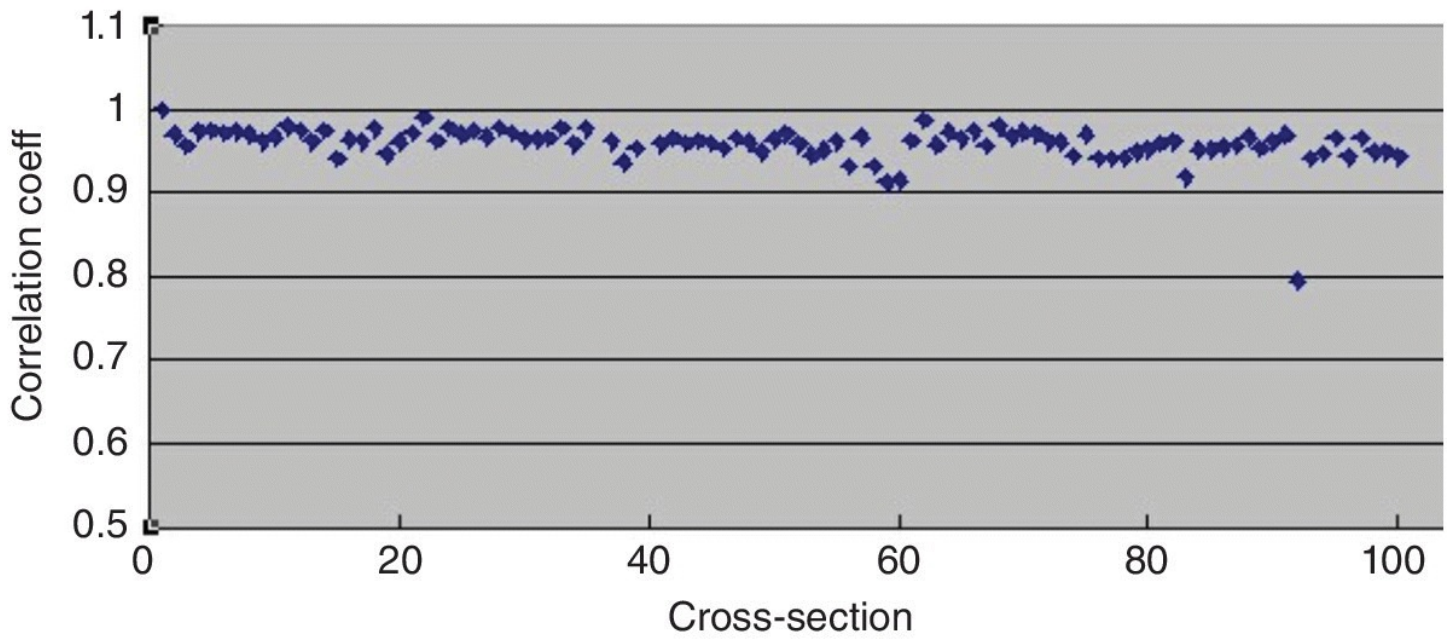


Figure 10.28 Topology of the sensory system for structural monitoring of water mains.

10.6.3 Measurements Under Different Operational Conditions

The water mains were monitored under different operational conditions: with water flow (17 April 2014) and with water cutoff (2 December 2013). Firstly, correlations between the first crosssection and all other crosssections are analysed under different operational conditions. The correlation coefficients of strain and temperature change of measurement point A between crosssection #1 and crosssections #1 to #100 are plotted in [Figure 10.29](#) and [Figure 10.30](#) for cases with water flow and with water cutoff, respectively (Ni et al. 2014b).

(a) Strain variation



(b) Temperature variation

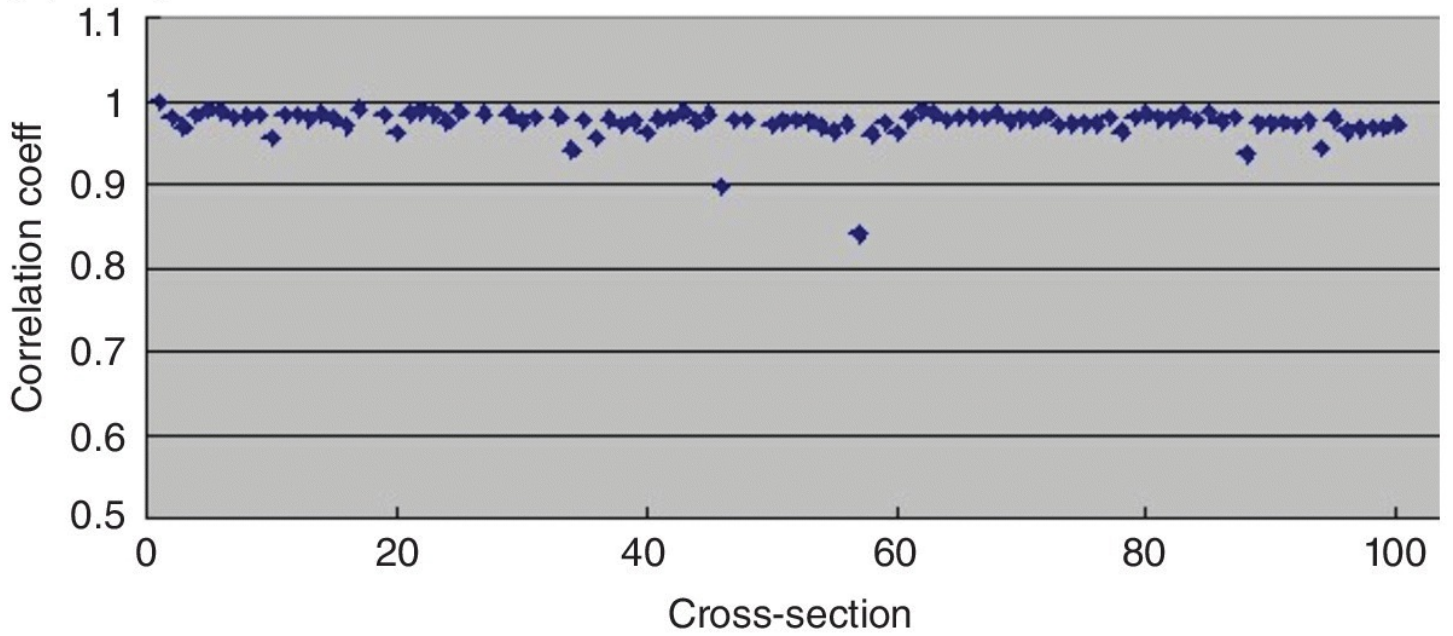
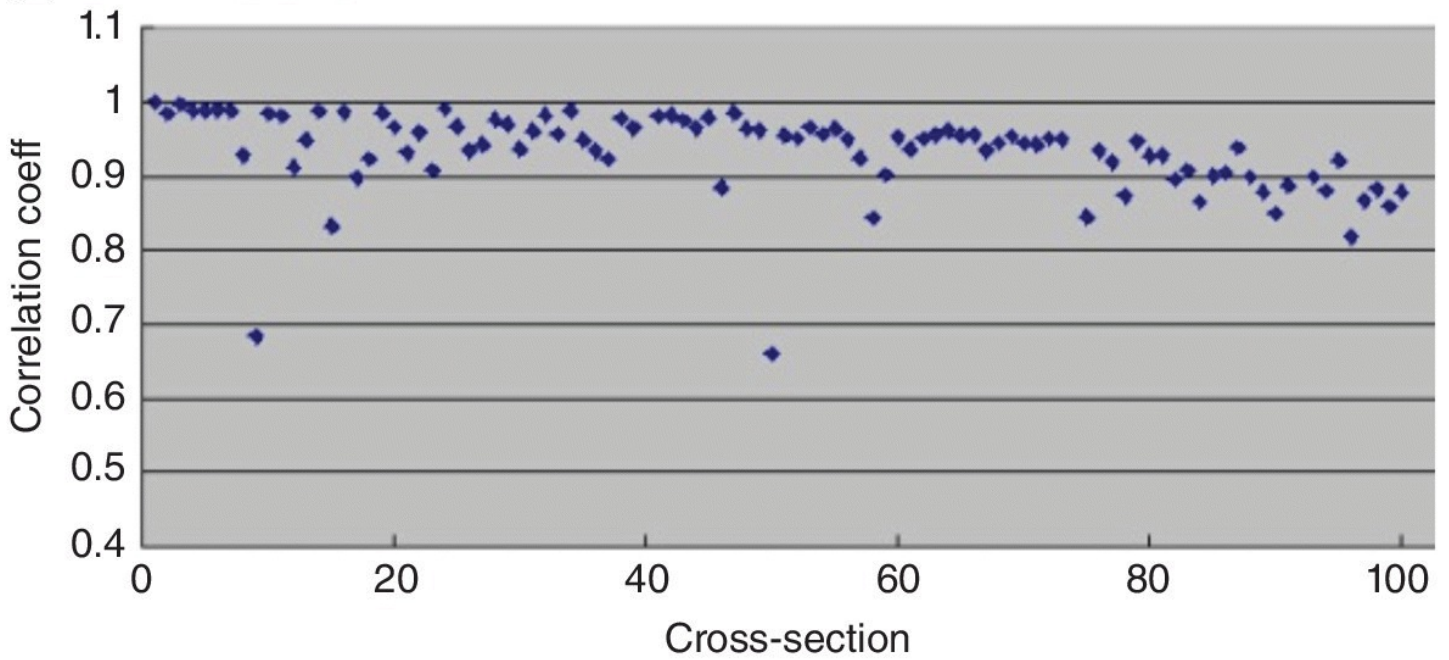


Figure 10.29 Correlation of strain and temperature variation at measurement point A with water flow.

(a) Strain variation



(b) Temperature variation

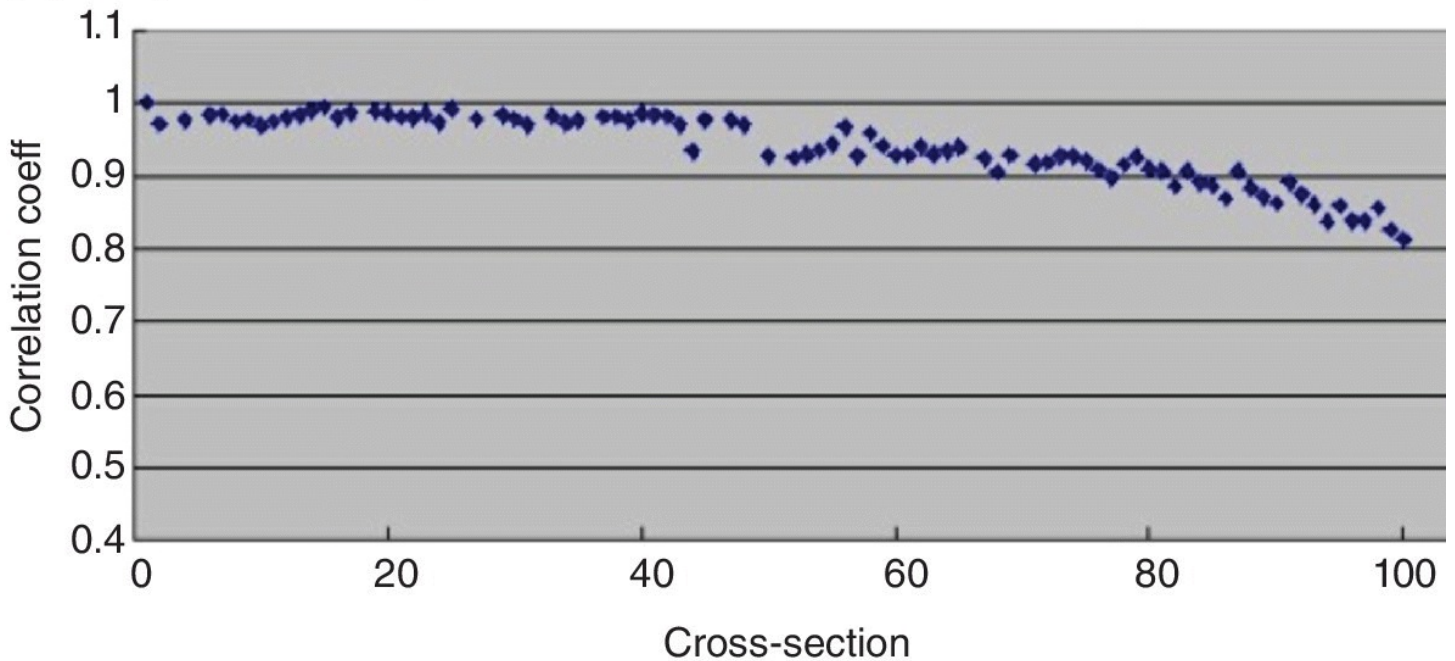


Figure 10.30 Correlation of strain and temperature variation at measurement point A with water cutoff.

[Figure 10.29](#) shows that, in the case with water flow, section #1 and sections #1–100 generally indicate high correlation (close to 1), and the correlation coefficients decrease gradually by a small amount with the increase of the section number. The lowest correlation coefficient is about 0.8. The point associated with this low correlation coefficient is AS92, at the end of the third turn of the GRP pipeline. Besides, several crosssections, namely sections #06, #12, #21, #35, #41, #45, #62, #68, #81 and #95, display a high correlation with the first cross

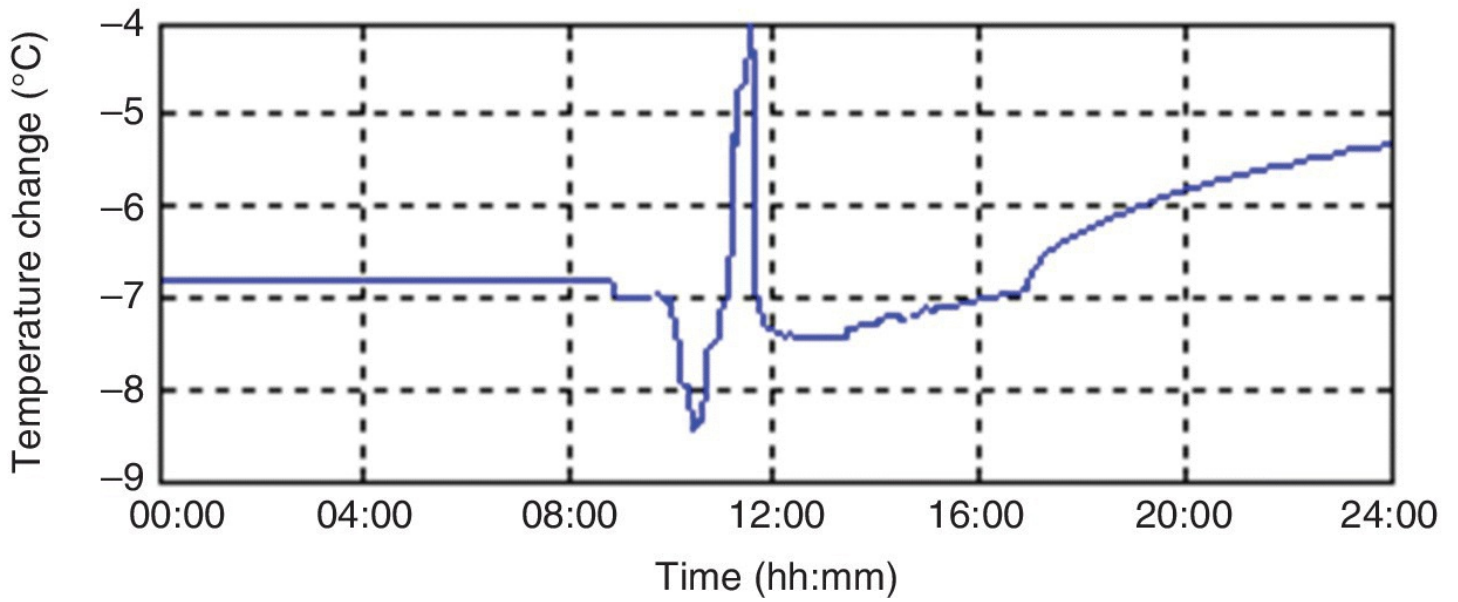
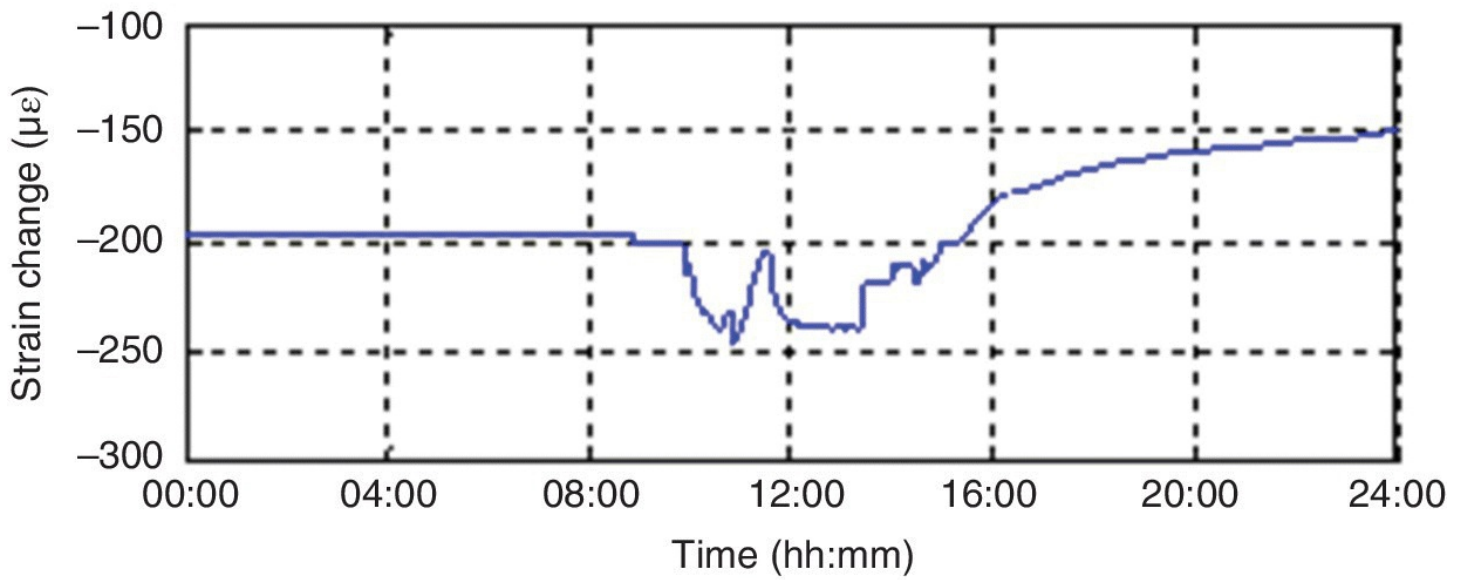
section, which implies their suitability for the analysis of structural integrity.

[Figure 10.30](#) provides results for the case with water cutoff, section #1 and sections #1–100 generally indicate slightly lower correlation (but still close to 1), and the correlation coefficients of temperature and strain variations experience relatively large decrease. Also, the points with the lowest coefficients are AS15 and AS50. Both sections are located near or at the turns of the GRP pipeline, and thus easily affected by the change of water flow by the cutoff. However, several crosssections, namely sections #06, #20, #21, #31, #35, #45, #62, #68, #81, and #83, still display a high correlation with the first crosssection in this unsteady situation. This indicates their suitability for the analysis of structural integrity.

Based on above analyses of the two different operational conditions, in the cases with water flow, nearly all correlation coefficients are close to 1, the highest correlation. This indicates that the GRP pipeline and the sensory system are healthy. In the case with water cutoff, the correlation coefficients show relatively large decrease, particularly those of strain variation. Almost all points with low coefficients are associated with the turns in the GRP pipeline.

[Figure 10.31](#) shows the monitored data in the case with water cutoff for strain and temperature changes at the points A and C of crosssection #35. The results of data analyses at cross section #35 are discussed, since this crosssection shows very high correlations with the first crosssection in both operational cases. Significant variations in strain and temperature were recorded due to the water cutoff. In response to this temporary disturbance, the water pressures indicate significant change between 10 am and 4 pm during the water cutoff, as shown in [Figure 10.32](#). The recorded water pressures at point B are very similar to those at point A.

(a) Strain and temperature changes at measurement point A



(b) Strain and temperature changes at measurement point C

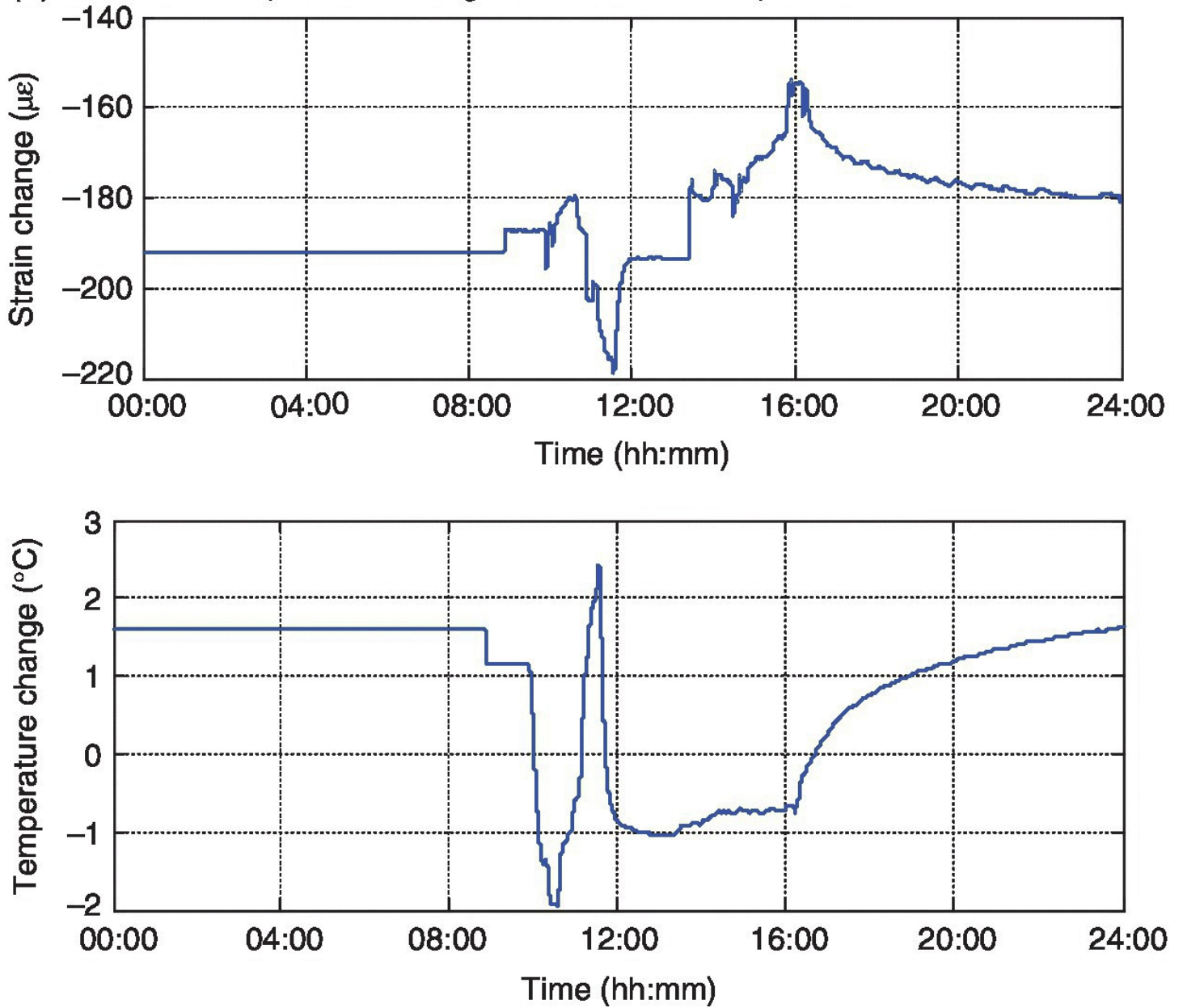
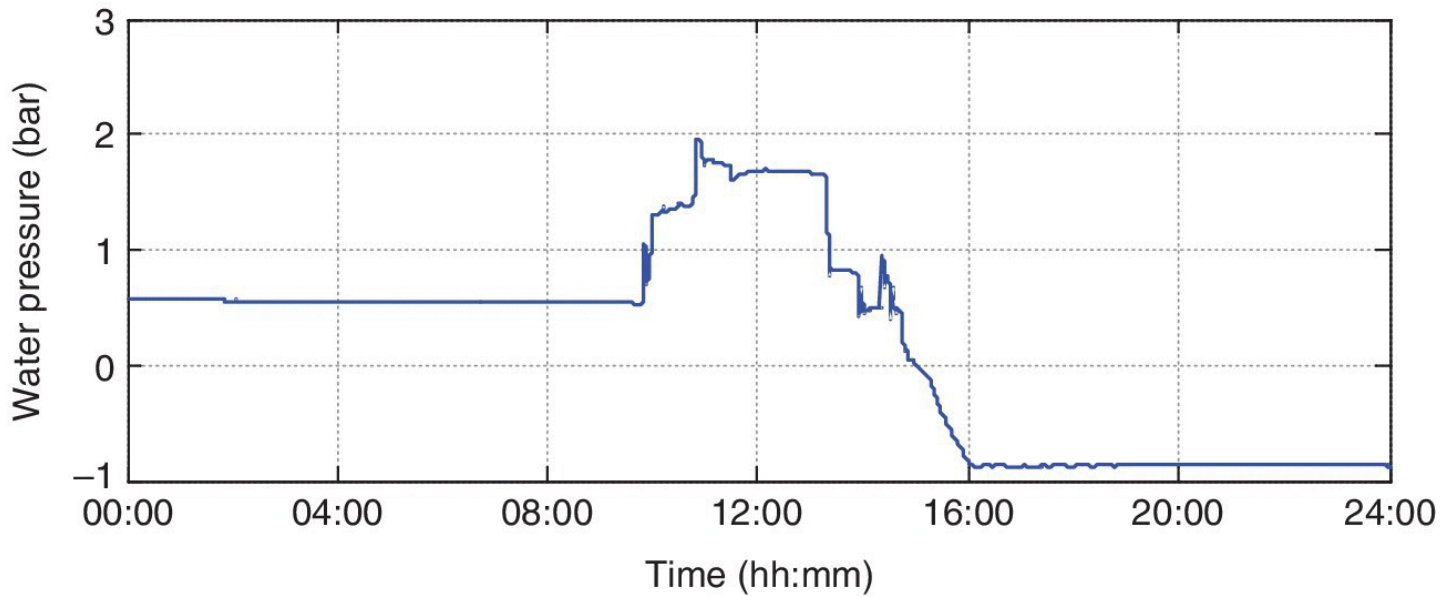


[Figure 10.31](#) Strain and temperature changes at crosssection #35 with water cutoff.

(a) Near measurement point A



(b) Near measurement point C

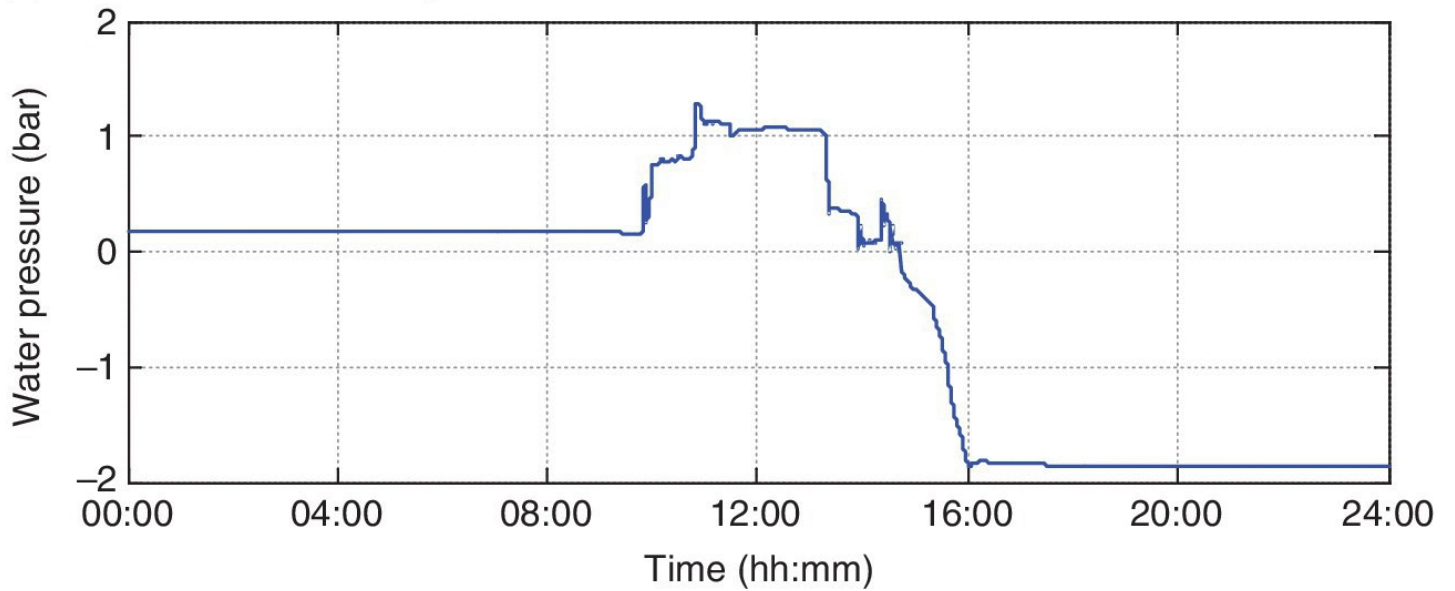


Figure 10.32 Water pressures at the middle of the GRP pipeline with water cutoff.

The crosscorrelation between each pair of temperature and strain sensors is now examined. The crosscorrelation between the temperature variation and strain variation minus their mean values is calculated and then normalised by the maximum crosscorrelation values. The normalised correlation between each pair of temperature and strain sensors at crosssection #35 is plotted in [Figure 10.33](#). This correlation analysis is performed for two cases, steady water flow and water cutoff. From the results in [Figure 10.33\(a\)](#), the blue solid line almost coincides with the green dashed line, indicating the similarity of responses at points A and B. Moreover, the crosscorrelation curves of point C (red dot lines) and the two curves of points A and B are approximately symmetrical with respect to the axis. This indicates their oscillations are characterised by the reversed phase relationship. However, when the GRP pipeline experienced a water cutoff lasting for several hours, this symmetrical relationship is

destroyed and the values of correlation on the curves are decreased, as shown in [Figure 10.33\(b\)](#).

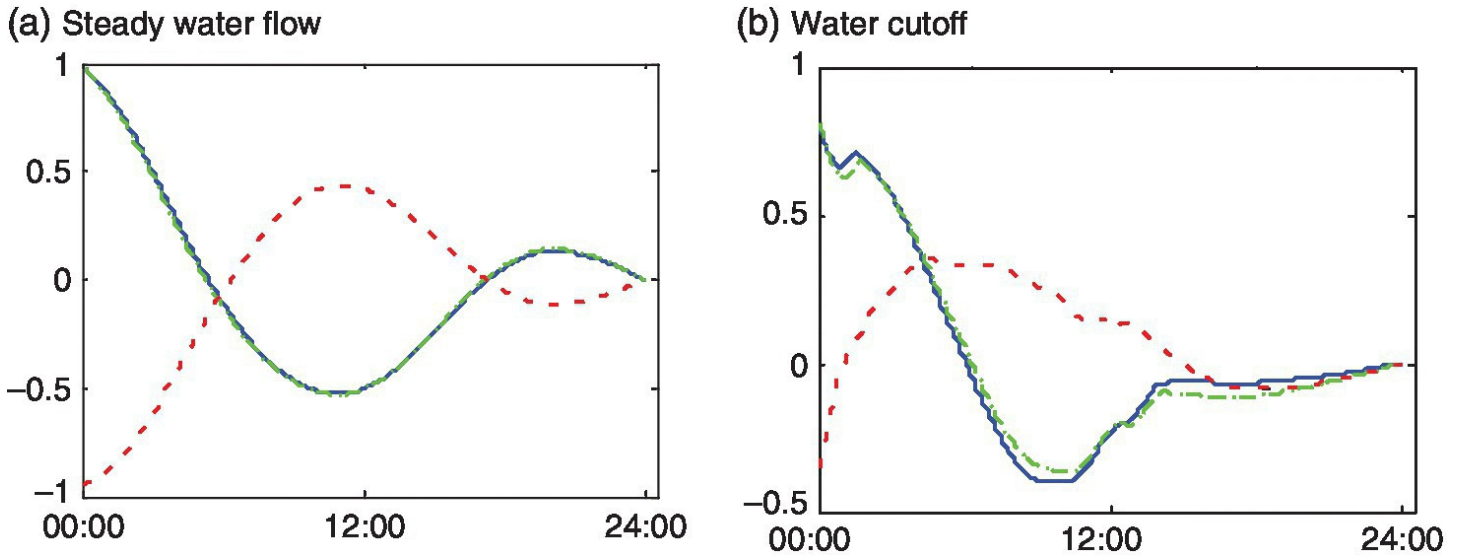


Figure 10.33 Normalised crosscorrelation between each pair of temperature and strain sensors at crosssection #35, where blue (solid) line for point A; green (dashed) line for point B; red (dotted) line for point C.

10.7 Concluding Remarks

The use of advanced SHM systems allows continuous monitoring and effective management of large civil engineering structures, such as longspan bridges, highrise buildings, underground tunnels, high speed railway lines and buried water mains. The structural health monitoring strategies increase the safety of these existing civil structures, and allow the infrastructure operators to make informed decisions on the maintenance and management of the structures. Various monitoring systems are introduced in these real case studies, including the wind and SHM system, wireless sensing networks, acoustic emissions and fibre optic sensing systems.

The application examples of these monitoring systems in the case studies demonstrate how it is possible to obtain different types of information on the states and conditions of various civil engineering structures. From the case studies, local monitoring techniques are much more likely to locate structural damage in local regions. Global monitoring methods should be combined with the use of local monitoring techniques to obtain a better understanding of structural damage. When longterm monitoring data of both structural responses and operational factors (e.g. loads, temperature, wind, etc.) are available, it is possible to quantitatively assess the current condition and even predict the future performance of the existing civil engineering structures using the continuous measurements.

For civil engineering structures, continuous structural monitoring requires the use of robust sensors that can withstand the damaging effects of the aggressive environments. These sensors are expected to operate for the service life of the structures which is often over 50 years.

Robust sensors are expected to perform reliably during the lifecycle of the structures. Also, the number of sensors on a civil structure should be sufficient to make an effective global monitoring approach on a large scale. When structural monitoring is implemented on large civil engineering structures, the density of sensors requires a wireless sensing network (Chang et al. 2003). The structural monitoring systems need to be inexpensive and easy to deploy, so that the systems can be attached to existing civil structures with little effort.

Although successful applications of SHM strategies are demonstrated in these case studies, further works on SHM of large civil engineering structures are needed: (a) advanced sensing systems with improved and optimised placement of networkable sensors, (b) reliable wireless sensors and data transmission systems, (c) advanced signal processing techniques to increase signal-to-noise ratios, (d) software and hardware integration, (e) effective methods for data interpretations and damage feature extractions, (f) predictive damage model for a structure and its components, (g) reliability-based and monitoring-informed optimal maintenance strategies.

References

Chang, P.C., Flatau, A. and Liu, S.C. (2003) Review paper: Health monitoring of civil infrastructure. *Structural Health Monitoring*2(3), 257–267.

Huang, T.L. and Chen, H.P. (2016) Investigation of the robustness of identified dynamic modes of a cablestayed bridge using modal contribution index. *Proceedings of the 6th Workshop on Civil Structural Health Monitoring*, Belfast, UK.

Huang, T.L. and Chen, H.P. (2017) Mode identifiability of a cablestayed bridge using modal contribution index. *Smart Structures and Systems*, in press.

Ko, J.M., Ni, Y.Q., Zhou, H.F., Wang, J.Y. and Zhou, X.T. (2009) Investigation concerning structural health monitoring of an instrumented cablestayed bridge. *Structure and Infrastructure Engineering*5(6), 497–513.

Ni, Y.Q., Li, Z.G., Wu, F. and Liu, X.Z. (2014a) Crack detection of railway turnouts using PZT sensors. *Proceedings of the 2014 SPIE Smart Structures/NDE Conference on Health Monitoring of Structural and Biological Systems VIII*, San Diego, California, USA.

Ni, Y.Q., Su, J. and Lam, K.C. (2013b) Development of an optical FBG based sensory system for monitoring structural integrity of water mains. *Proceedings of the 6th International Conference on Structural Health Monitoring of Intelligent Infrastructure (SHMII6)*, Hong Kong.

Ni, Y.Q., Wang, J., Xie, Q.L. and Lam, K.C. (2014b). A fibre Bragg grating sensing network for structural integrity monitoring of underground water pipes: Analysis of monitoring data. *Proceedings of the 5th International Forum on Optoelectronic Sensorbased Monitoring in Geoenvironment*, Nanjing, China.

- Ni, Y.Q., Wong, K.Y. and Xia, Y. (2011) Health checks through landmark bridges to skyhigh structures. *Advances in Structural Engineering***14**(1), 103–119.
- Ni, Y.Q., Xia, Y.X. and Ye, X.W. (2013a) Structural health monitoring of a tall building with huge floating platform. *Advances in Science and Technology***83**, 177–187.
- Ni, Y.Q., Zhou, H.F., Chan, K.C. and Ko, J.M. (2008) Modal flexibility analysis of cable stayed Ting Kau Bridge for damage identification. *ComputerAided Civil and Infrastructure Engineering***23**(3), 223–236.
- Ni, Y.Q., Zhou, X.T., Ko, J.M. and Wang, B.S. (2000) Vibrationbased damage localization in Ting Kau Bridge using probabilistic neural network. In: *Advances in Structural Dynamics*, Vol. **II**, Ko and Xu (eds.), Elsevier Science Ltd., Oxford, UK.
- Wong, K.Y. (2004). Instrumentation and health monitoring of cablesupported bridges. *Structural control and health monitoring***11**, 91–124.
- Wong, K.Y., Lau, C.K. and Flint, A.R. (2000). Planning and implementation of the structural health monitoring system for cablesupported bridges in Hong Kong. In: *Nondestructive evaluation of highways, utilities, and pipelines IV*. Aktan and Gosselin (eds.), Bellingham, Washington, SPIE, 3995.
- Wong, K.Y. and Ni, Y.Q. (2009) Structural health monitoring of cablesupported bridges in Hong Kong. In book: *Structural Health Monitoring of Civil Infrastructure Systems*, Karbhari and Ansari (ed.), Woodhead Publishing, Cambridge, UK.
- Ye, X.W., Ni, Y.Q. and Yin, J.H. (2013) Safety monitoring of railway tunnel construction using FBG sensing technology. *Advances in Structural Engineering***16**(8), 1401–1409.

Index

a

accelerometer
acoustic emission
age replacement model
aleatoric uncertainty
anemometer
annual discount factor

b

backpropagation neural network
Bayesian updating
bridge monitoring

c

cable force monitoring
Canton Tower
capacitive method
civil engineering SHM character
complex mode indication function
condition based maintenance
coordinate modal assurance criterion (COMAC)
costoptimal decision
covariancedriven stochastic subspace identification (SSICOV)

d

damage

assessment

characterisation

at critical point level

at element level

classification

in continuum

definition

detectability

detection

diagnosis

in frame

identification

index

indicator

localisation

locating vector

location assurance criterion

model

prognosis

signature index

damping identification

data acquisition

data analysis

databased technique

data compression

datadriven stochastic subspace identification (SSIDATA)

data management system

data preprocessing

data processing system

data storage

data transmission

deterioration

 modelling

 process

 source

deterministic deterioration model

dynamic mode expansion

dynamic perturbation governing equation

dynamic perturbation method

e

eigenvalue problem

electromagnetic method

enhanced coordinate modal assurance criterion (ECOMAC)

environmental factor

environmental quantity

epistemic uncertainty

f

Fabry–Pérot interferometric sensor

failure mode

failure rate function

fatigue reliability

fibre Bragg grating (FBG) sensor

fibre optic sensor

file management

finite element modelling

flexibility matrix

Fourier transform

framed building

frequencydomain method

frequency response function (FRF)

frequency response function curvature

g

gamma process

global monitoring

global positioning system (GPS)

guided wave

Guyan static mode expansion

h

highrise building

Hilbert–Huang transform

i

Ibrahim timedomain

incomplete mode

inconstruction monitoring

inservice monitoring

iterative solution procedure

l

laser Doppler vibrometer (LDV)

Lcurve criterion

lifetime cost

lifetime distribution

lifetime model

limit state

load monitoring

local monitoring

m

Markov process

mass matrix
matrix update method
measurand
minimum rank update
modal assurance criterion (MAC)
modal data
modal parameter
modal scale factor (MSF)
modal strainbased damage index
modal strain energy
modal testing
 equipment
 procedure
modelbased technique
modelling error
modelling uncertainty
model reduction
model updating
 at element level
 at integration point level
mode participation factor
mode shape
 curvatures
 expansion
 orthogonality
monitoring cost
multiobjective optimisation

n

natural frequency
neural network

noise

nondestructive testing (NDT) technique

novelty detection

novelty index

o

operational modal analysis

operational monitoring

operational quantity

optimal maintenance

optimal matrix updating

optimal sensor placement

outputonly modal identification

p

parameter estimation

parametric uncertainty

peakpicking

performance deterioration

perturbed force mode expansion

piezoelectric sensor

pipeline monitoring

pressure monitoring

probabilistic deterioration model

probabilistic neural network

probability of failure

r

rail track

railway monitoring

rational fraction polynomial

regularisation parameter

regularised solution
reliability analysis
reliability index
remaining useful life
residual force vector

s

sensing method
sensing system
sensitivity based method
sensitivity of eigenvalue
sensitivity of eigenvector
sensitivity of FRF
sensitivity of input force
sensor measurement
sensors
sensor selection
sensor type
settlement monitoring
signal processing
singular value decomposition (SVD)
SOFO interferometric sensor
statistical pattern recognition
stiffness matrix
strain energy based damage index
strain gauge
stress monitoring
structural damage

structural health monitoring (SHM)

architecture

benefit

challenge

component

definition

development

framework

further work

level

method

strategy

system

structural monitoring system

structural parameter

structural reliability

structural response

survival function

system equivalent reduction expansion process

t

temperature effect

temperature monitoring

thermography

Tikhonov regularisation

timedomain method

timevariant reliability

Ting Kau Bridge

traffic load

Tsing Ma Bridge

tunnel monitoring

u

ultrasound

updating parameter

usage monitoring

v

vibration based damage detection

vibrationbased SHM advantage

vibrationbased SHM limitation

visual inspection

w

wavelet transform

Weibull model

wind monitoring

wired transmission system

wireless sensor

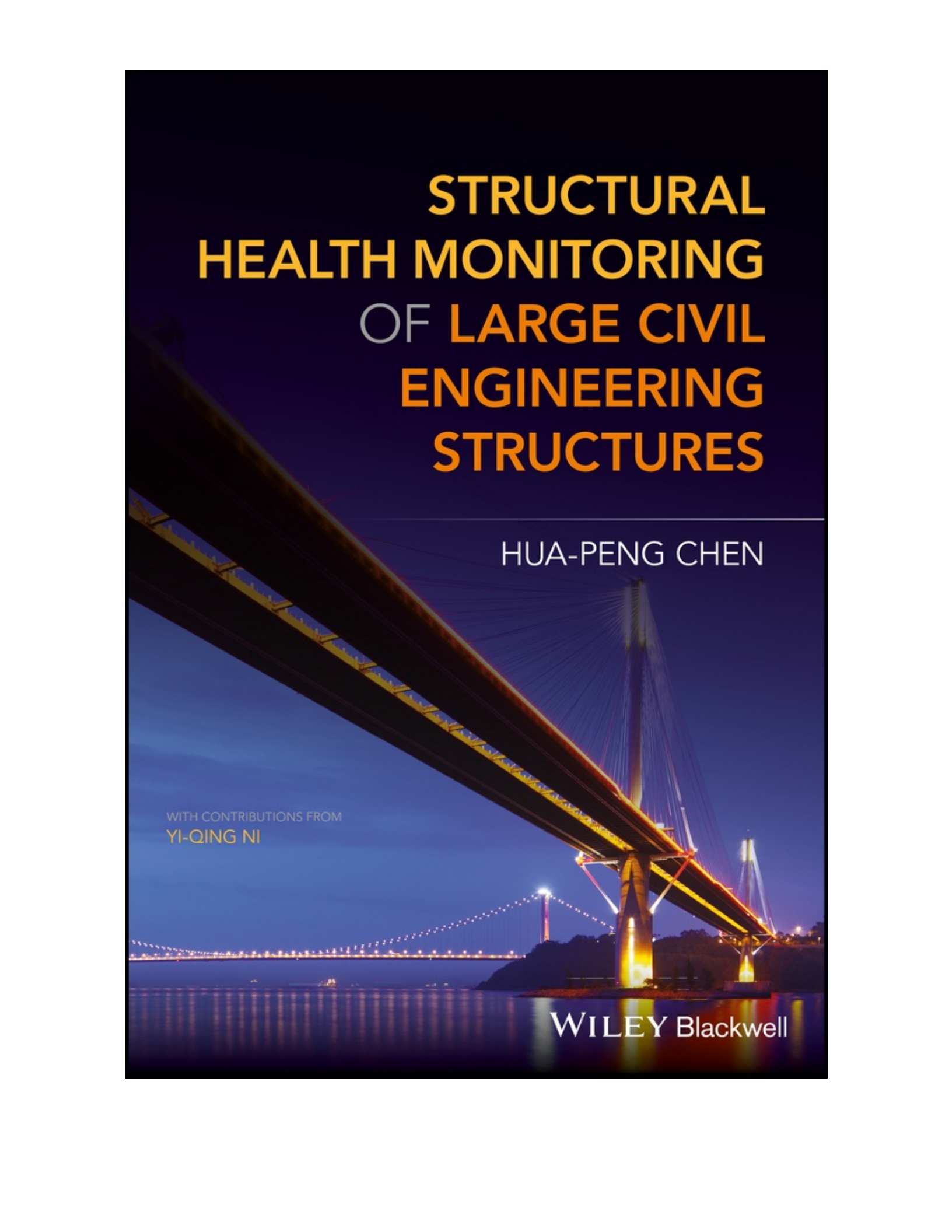
wireless sensor application

wireless sensor component

wireless transmission system

WILEY END USER LICENSE AGREEMENT

Go to www.wiley.com/go/eula to access Wiley's ebook EULA.



STRUCTURAL HEALTH MONITORING OF LARGE CIVIL ENGINEERING STRUCTURES

HUA-PENG CHEN

WITH CONTRIBUTIONS FROM
YI-QING NI

WILEY Blackwell